Phototherapies and Materials Photoprocessing

CePOF paper collection

CEPOF
CENTRO DE PESQUISAS EM ÓPTICA E FOTÔNICA

Laser Phys. **23** (2013) 055601 (8pp) doi:10.1088/1054-660X/23/5/055601

Biostimulatory effects of low-level laser therapy on epithelial cells and gingival fibroblasts treated with zoledronic acid

F G Basso[1], T N Pansani[2], A P S Turrioni[2], C Kurachi[3], V S Bagnato[3], J Hebling[2] and C A de Souza Costa[2,4]

[1] UNICAMP—Universidade de Campinas, Piracicaba School of Dentistry, Piracicaba, SP, 13414-903, Brazil
[2] UNESP—Universidade Estadual Paulista, Araraquara School of Dentistry, Araraquara, SP, 14801-903, Brazil
[3] USP—Universidade de São Paulo, Physics Institute, São Carlos, SP, Brazil

E-mail: casouzac@foar.unesp.br

Received 18 November 2012, in final form 14 February 2013
Accepted for publication 15 February 2013
Published 4 April 2013
Online at stacks.iop.org/LP/23/055601

Abstract
Low-level laser therapy (LLLT) has been considered as an adjuvant treatment for bisphosphonate-related osteonecrosis, presenting positive clinical outcomes. However, there are no data regarding the effect of LLLT on oral tissue cells exposed to bisphosphonates. This study aimed to evaluate the effects of LLLT on epithelial cells and gingival fibroblasts exposed to a nitrogen-containing bisphosphonate—zoledronic acid (ZA). Cells were seeded in wells of 24-well plates, incubated for 48 h and then exposed to ZA at 5 μM for an additional 48 h. LLLT was performed with a diode laser prototype—LaserTABLE (InGaAsP—780 nm $\pm$ 3 nm, 25 mW), at selected energy doses of 0.5, 1.5, 3, 5, and 7 J cm^{-2} in three irradiation sessions, every 24 h. Cell metabolism, total protein production, gene expression of vascular endothelial growth factor (VEGF) and collagen type I (Col-I), and cell morphology were evaluated 24 h after the last irradiation. Data were statistically analyzed by Kruskal–Wallis and Mann–Whitney tests at 5% significance. Selected LLLT parameters increased the functions of epithelial cells and gingival fibroblasts treated with ZA. Gene expression of VEGF and Col-I was also increased. Specific parameters of LLLT biostimulated fibroblasts and epithelial cells treated with ZA. Analysis of these *in vitro* data may explain the positive *in vivo* effects of LLLT applied to osteonecrosis lesions.

1. Introduction

Bisphosphonate-related osteonecrosis was recently described as a condition that affects from 1% to 10% of patients receiving bisphosphonate treatment. This condition is mainly observed in patients subjected to nitrogen-containing bisphosphonates, which present strong adhesion to bone tissue and higher potency [1–3].

It has been reported that the etiopathogenesis of osteonecrosis is related to factors such as type, dose, and duration of bisphosphonate treatment, as well as to local factors such as local inflammation, biofilm formation, and trauma [2–4]. Several researchers have shown that bisphosphonate-related osteonecrosis occurs due to the toxic effects of this drug on oral mucosal cells like fibroblasts and keratinocytes [3, 5, 6].

In addition to the topical and systemic administration of antibiotics, as well as surgical treatment [7, 8], LLLT has been proposed as an adjuvant therapy for osteonecrosis, with positive clinical outcomes [9–13]. *In vitro* and *in vivo*

[4] Address for correspondence: Departamento de Fisiologia e Patologia, Faculdade de Odontologia de Araraquara, Universidade Estadual Paulista, Rua Humaitá, 1680. Centro, Caixa Postal: 331 Cep: 14801903 Araraquara, SP, Brazil.

Table 1. LLLT parameters for cell irradiation.

Wavelength (nm)	Optical power (W)	Area (cm^2)	Energy doses (J cm^{-2})	Time (s)
780	0.025	2.0	0.5, 1.5, 3, 5, 7	40, 120, 240, 400, 560

studies have demonstrated that LLLT causes biostimulatory effects on different cell types, characterized by increase in cell proliferation, metabolism, migration, and protein and gene expression [14–16]. It has also been shown that specific LLLT can penetrate tissues, promoting local biostimulation [17–19]. In addition, numerous investigations have reported the efficacy of LLLT in the treatment of osteonecrosis lesions, demonstrating that this therapy accelerates tissue repair and promotes faster wound healing of exposed bone areas [9–13]. However, data about the effects of LLLT on cells previously exposed to bisphosphonates are missing. Therefore, the aim of this study was to evaluate the effects of specific parameters of LLLT applied on cultures of epithelial cells and gingival fibroblasts treated with ZA.

2. Materials and methods

2.1. Cell culture

Experiments were performed with immortalized human epithelial cells (HaCaT—CLS 300493) and human gingival fibroblasts (continuous cell line; Ethics Committee 64/99-Piracicaba Dental School, UNICAMP, Brazil). Cells were seeded in 24-well plates in plain DMEM (Invitrogen, Carlsbad, CA, USA), containing 10% fetal bovine serum (FBS) (Invitrogen) for 48 h, as previously described [15, 16]. After this period, the culture medium was replaced by DMEM without FBS for 24 h.

2.2. Zoledronic acid (ZA)

Zoledronic acid at 5 μM was added to the culture medium and maintained in contact with the cells for an additional 48 h. This concentration was chosen based upon results from a previous study in which the authors determined the concentrations of ZA in saliva and bone of patients being treated with this drug and presenting with oral osteonecrosis [20].

2.3. Irradiations

Cells were subjected to three LLL irradiations (every 24 h) via a diode laser prototype, LaserTABLE (InGaAsP—780 nm $\pm$ 3 nm, 25 mW) [15, 16, 18, 21–23], at selected energy doses of 0.5, 1.5, 3, 5, and 7 J cm^{-2} (table 1).

Twenty-four hours after the last irradiation, the cells were analyzed for metabolism, total protein production, gene expression, and morphology.

2.4. Cell metabolism

The cell metabolism of the epithelial cells and gingival fibroblasts was analyzed by MTT assay, as previously described [24].

2.5. Total protein production

The total protein production by the epithelial cells and gingival fibroblasts was determined as reported by Basso *et al* [15].

2.6. Gene expression

Gene expression of vascular endothelial growth factor (VEGF) and collagen type I (Col-I) was analyzed by real-time PCR, with specific primer and probe sets for each evaluated gene [15].

2.7. Scanning electron microscopy (SEM)

Cell morphology analysis after cell treatments was carried out as described by Oliveira *et al* [23]. This was a protocol that allowed us to observe the characteristics of those treated cells that still adhered to the glass substrate. After preparation, samples were analyzed by scanning electron microscopy (Inspect Scanning Electron Microscope S50, FEI, Hillsboro, OR, USA), in which photomicrographs representative of each experimental and control group were obtained.

2.8. Statistical analysis

The data from both cell lines were analyzed for normal distribution. Since the numerical data did not fit this condition, they were subjected to statistical analysis by Kruskal–Wallis complemented by Mann–Whitney tests, with 5% considered significant. Each cell line was analyzed individually, and the effects of each variable, ZA treatment and LLLT, were determined.

3. Results

3.1. Effect of zoledronic acid and LLLT on the metabolism of epithelial cells and gingival fibroblasts

Both cell lines exposed to ZA presented decreased metabolism, as shown in tables 2 and 3.

For the LLLT-treated groups, energy doses of 1.5, 3, 5, and 7 J cm^{-2} promoted an increase in epithelial cell metabolism. However, only the gingival fibroblasts irradiated with 3 J cm^{-2} presented increased metabolism. Conversely, this effect was not observed when LLLT was applied to ZA-treated cells, for both cell lines.

Table 2. Cell metabolism of epithelial cells after LLLT, with or without ZA treatment. (Note: values indicate median (25th–75th percentile), $n = 8$. A, a: capital and lower-case letters allow for columns and rows, respectively, to be compared. The same letters indicate no statistical difference (Mann–Whitney, $p > 0.05$).)

	Energy dose (J cm^{-2})					
ZA	0	0.5	1.5	3	5	7
+	25 (22–26) B, ab	18 (17–19) B, c	24 (23–27) B, ab	21 (19–21) B, bc	26 (25–28) B, a	21 (19–21) B, bc
−	102 (96–105) A, b	105 (100–108) A, bc	108 (106–110) A, ab	120 (113–121) A, a	113 (111–113) A, ac	117 (116–119) A, a

Table 3. Cell metabolism of gingival fibroblasts after LLLT, with or without ZA treatment. (Note: values indicate median (25th–75th percentile), $n = 8$. A, a: capital and lower-case letters allow for columns and rows, respectively, to be compared. The same letters indicate no statistical difference (Mann–Whitney, $p > 0.05$).)

	Energy dose (J cm^{-2})					
ZA	0	0.5	1.5	3	5	7
+	28 (24–31) B, a	30 (28–34) B, a	28 (25–30) B, a	29 (27–31) B, a	27 (26–28) B, a	27 (24–29) B, a
−	100 (96–104) A, bc	110 (107-113) A, b	96 (93–101) A, bc	114 (112–121) A, a	99 (83–108) A, bc	92 (91–96) A, c

Table 4. Total protein production by epithelial cells after LLLT, with or without ZA treatment. (Note: values indicate median (25th–75th percentile), $n = 8$. A, a: capital and lower-case letters allow for columns and rows, respectively, to be compared. The same letters indicate no statistical difference (Mann–Whitney, $p > 0.05$).)

	Energy dose (J cm^{-2})					
ZA	0	0.5	1.5	3	5	7
+	84.47 (79.11–81.96) B, b	81.57 (77.96–84.06) B, b	87.80 (84.66–92.09) B, ab	76.48 (71.79–81.10) B, b	114.52 (109.00–22.55) B, a	80.00 (77.78–82.54) A, b
−	102.74 (95.90–104.12) A, ab	90.88 (85.80–103.33) A, b	93.24 (90.79–100.38) A, ab	87.64 (86.74–91.05) A, b	144.01 (132.75–149.40) A, a	86.95 (81.77–90.06) A, b

Table 5. Total protein production by gingival fibroblasts after LLLT, with or without ZA treatment. (Note: values indicate median (25th–75th percentile), $n = 8$. A, a: capital and lower-case letters allow for columns and rows, respectively, to be compared. The same letters indicate no statistical difference (Mann–Whitney, $p > 0.05$).)

	Energy dose (J cm^{-2})					
ZA	0	0.5	1.5	3	5	7
+	81.42 (79.61–85.71) B, b	79.88 (78.78–82.21) B, b	85.26 (81.93–91.66) A, ab	88.05 (81.06–90.98) B, ab	127.00 (212.49–129.74) A, a	83.64 (80.88–86.10) A, b
−	101.23 (93.89–109.18) A, ab	87.02 (83.83–90.31) A, ac	98.99 (90.03–100.50) A, ab	96.84 (93.19–97.64) A, ab	105.57 (101.03–108.92) B, a	72.22 (68.38–74.25) B, c

3.2. Total protein production of cells treated with zoledronic acid and LLLT

As observed for cell metabolism, ZA caused a reduction in total protein production for epithelial cells and gingival fibroblasts (tables 4 and 5).

Epithelial cells treated with LLLT at 5 J cm^{-2} showed an increase in total protein production. This result was also observed for ZA-treated epithelial cells. Similarly, this dose of LLLT also increased the production of gingival fibroblasts.

3.3. Gene expression of Col-I and VEGF by epithelial cells and gingival fibroblasts after zoledronic acid treatment and LLLT

In terms of gene expression, different patterns were obtained according to cell line and evaluated gene. Expression of Col-I by epithelial cells was not affected by ZA treatment (table 6). None of the selected low-power laser energy doses interfered with the expression of this specific gene. However, for ZA-treated epithelial cells, LLLT at 1.5, 3, 5, and 7 J cm^{-2} significantly increased Col-I expression.

Table 6. Gene expression of Col-I by epithelial cells after LLLT, with or without ZA treatment. (Note: values indicate median (25th–75th percentile), $n = 8$. A, a: capital and lower-case letters allow for columns and rows, respectively, to be compared. The same letters indicate no statistical difference (Mann–Whitney, $p > 0.05$).)

	Energy dose (J cm^{-2})					
ZA	0	0.5	1.5	3	5	7
+	0.926 (0.826–1.011) A, b	1.289 (1.011–1.782) A, ab	2.918 (1.550–3.496) A, a	2.157 (1.630–2.431) A, a	2.274 (2.190–2.715) A, a	2.149 (1.680–2.741) A, a
−	1.370 (0.833–1.836) A, a	0.875 (0.656–1.033) A, a	0.769 (0.660–0.958) B, a	0.993 (0.929–1.068) B, a	0.980 (0.504–1.170) B, a	1.096 (1.002-1.136) B, a

Table 7. Gene expression of Col-I by gingival fibroblasts after LLLT, with or without ZA treatment. (Note: values indicate median (25th–75th percentile), $n = 8$. A, a: capital and lower-case letters allow for columns and rows, respectively, to be compared. The same letters indicate no statistical difference (Mann–Whitney, $p > 0.05$).)

	Energy dose (J cm^{-2})					
ZA	0	0.5	1.5	3	5	7
+	0.567 (0.517–0.619) B, a	0.517 (0.517–0.519) B, a	0.518 (0.517–0.522) B, a	0.518 (0.515–0.521) B, a	0.517 (0.513–0.522) B, a	0.514 (0.512–0.517) B, a
−	1.020 (0.919–1.084) A, a	0.957 (0.931–1.006) A, ab	0.902 (0.746–0.931) A, ab	0.877 (0.774–0.981) A, ab	0.802 (0.724–0.906) A, ab	0.649 (0.620–0.701) A, b

Table 8. Gene expression of VEGF by epithelial cells after LLLT, with or without ZA treatment. (Note: values indicate median (25th–75th percentile), $n = 8$. A, a: capital and lower-case letters allow for columns and rows, respectively, to be compared. The same letters indicate no statistical difference (Mann–Whitney, $p > 0.05$).)

	Energy dose (J cm^{-2})					
ZA	0	0.5	1.5	3	5	7
+	0.704 (0.688–0.708) B, c	3.018 (2.849–3.527) A, b	3.587 (3.049–4.302) A, ab	3.795 (3.548–4.058) A, ab	4.187 (4.085–4.302) A, a	3.375 (3.130–3.769) A, b
−	1.011 (0.852–1.147) A, b	1.564 (1.518–1.873) B, ab	1.197 (1.035–1.373) B, ab	1.865 (1.394–2.340) B, ab	2.089 (1.868–2.539) B, a	2.038 (1.796–2.533) B, a

For gingival fibroblasts, ZA significantly decreased Col-I expression. No differences in Col-I expression were observed for LLLT-treated fibroblasts, with or without previous exposure to ZA (table 7).

The expression of VEGF by epithelial cells was negatively affected by ZA. However, when LLLT was applied at 5 and 7 J cm^{-2}, a significant increase in VEGF expression was observed. When associated with ZA, all energy doses promoted positive effects regarding the expression of VEGF (table 8).

The expression of VEGF by gingival fibroblasts was decreased by ZA. No increase in this expression was observed for all energy doses of LLLT (table 9).

3.4. Morphology evaluation of epithelial cells and gingival fibroblasts treated with zoledronic acid and LLLT

Cells subjected only to LLLT presented morphology similar to that of control group cells (figures 1 and 3). For gingival fibroblasts, energy doses of 0.5, 1.5, 3, and 5 J cm^{-2} appeared to promote increased cell numbers. SEM analysis of ZA-treated cells demonstrated that this drug decreased the numbers of fibroblasts and epithelial cells that remained attached to the glass substrate. This negative effect caused by ZA was counteracted when epithelial cells and gingival fibroblasts were treated with LTTT at 0.5, 1.5, and 3 J cm^{-2} (figures 2 and 4).

4. Discussion

The cytotoxicity of bisphosphonates to different cell types has been used to explain, at least in part, the occurrence of osteonecrosis in patients subjected to treatment with this kind of drug [5, 6, 20, 25]. Several *in vivo* investigations have reported a decrease in local vascularization, bone remodeling, and delayed tissue repair, which are directly related to oral osteonecrosis [26, 27].

Among the different types of bisphosphonates available, a nitrogen-containing bisphosphonate, ZA, has been widely prescribed, in spite of its significant cytotoxicity, which is

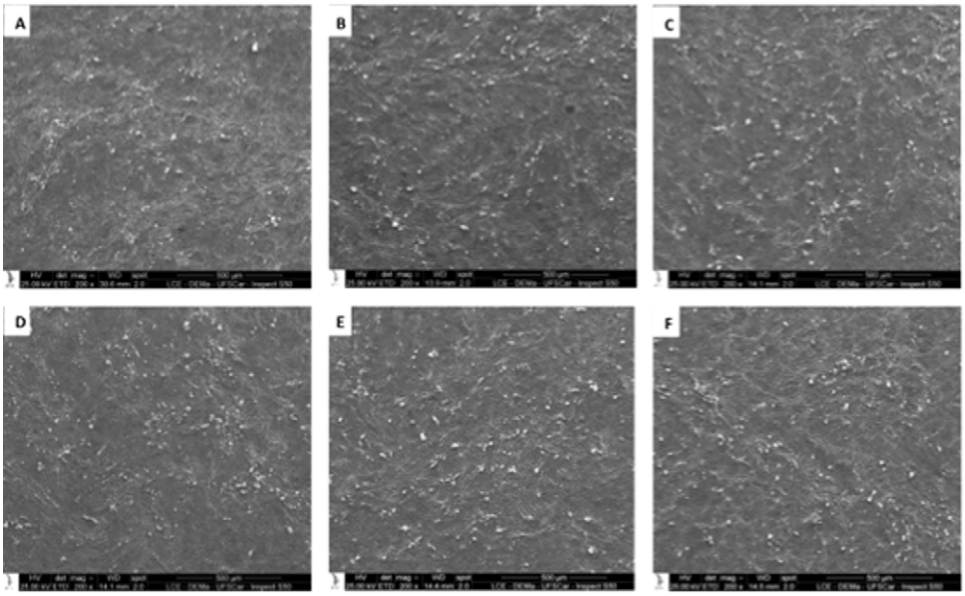

Figure 1. Morphology of epithelial cells subjected to LLLT at different energy doses (A—control group; B—0.5 J cm^{-2}; C—1.5 J cm^{-2}; D—3 J cm^{-2}; E—5 J cm^{-2}; F—7 J cm^{-2}). No significant difference was observed between LLLT-treated cells and the control group. All images show adherent and confluent cells. MEV, original magnification 200× .

Table 9. Gene expression of VEGF by gingival fibroblasts after LLLT, with or without ZA treatment. (Note: values indicate median (25th–75th percentile), $n = 8$. A, a: capital and lower-case letters allow for columns and rows, respectively, to be compared. The same letters indicate no statistical difference (Mann–Whitney, $p > 0.05$).)

	Energy dose (J cm^{-2})					
ZA	0	0.5	1.5	3	5	7
+	0.532 (0.530–0.548) B, ab	0.499 (0.410–0.530) B, ab	0.352 (0.352–0.408) B, b	1.060 (1.050–1.060) B, a	0.832 (0.676–0.972) A, ab	0.353 (0.352–0.378) A, b
−	0.944 (0.882–1.120) A, a	1.019 (0.932–1.058) A, a	0.872 (0.822–0.892) A, ab	0.699 (0.611–0.794) A, ab	0.689 (0.601–0.706) A, ab	0.487 (0.398–0.546) B,b

related to the development of osteonecrosis [5, 6, 20, 25, 28]. To minimize the negative effects of bisphosphonates on oral mucosal cells, several researchers have recommended the use of LLLT as an adjuvant procedure to treat bisphosphonate-related osteonecrosis of the jaw [11–13]. However, only limited data have been published concerning the effects of LLLT on ZA-treated bone or oral mucosal cells. Therefore, the effects of distinct parameters of LLLT on cultured epithelial cells and gingival fibroblasts previously exposed to ZA at 5 μM were evaluated in the present investigation. In general, it was shown that this drug reduced the metabolism of both cell lines, which is in accordance with reports from previous studies [6, 20, 29]. Total protein production by the cultured cells was also decreased after ZA treatment, showing that a 5 μM solution of this drug causes direct cytotoxic effects, which were confirmed by the SEM evaluation.

LLLT at 5 J cm^{-2} was capable of stimulating the metabolism of epithelial cells, even when they were previously exposed to ZA. In terms of Col-I and VEGF expression, ZA caused significant reduction in this cell activity, suggesting that, in clinical situations, this drug may affect local repair and wound healing. Similar data were previously reported by Scavelli *et al* [30]. Conversely, LLLT at 5 and 7 J cm^{-2} significantly increased Col-I and VEGF expression by both cell lines, even when they had been exposed to ZA.

It is well known that VEGF plays an important role in the tissue repair process and in tissue regeneration [31]. Therefore, as demonstrated in this study, LLLT can promote or accelerate tissue healing by stimulating VEGF expression, which is fundamental to cell migration, proliferation, and local neovascularization [31].

It was also demonstrated in this study that all LLLT parameters increased the Col-I expression by cultured epithelial cells. This positive effect was not observed for gingival fibroblasts. The analysis of these data contradicts reports from prior investigations such as that published by Damante *et al* [32]. However, these authors evaluated different LLLT parameters, which clearly led to different results for cell biostimulation or inhibition [33–36].

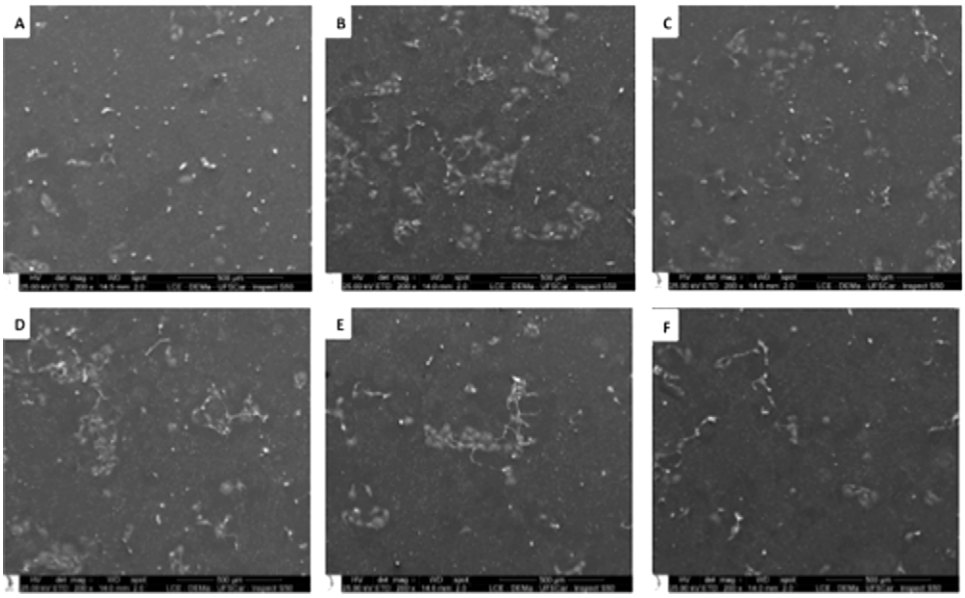

Figure 2. Morphology of epithelial cells subjected to ZA treatment and LLLT at different energy doses (A—ZA; B—ZA + 0.5 J cm^{-2}; C—ZA + 1.5 J cm^{-2}; D—ZA + 3 J cm^{-2}; E—ZA + 5 J cm^{-2}; F—ZA + 7 J cm^{-2}). All groups subjected to ZA treatment show intense morphological alterations and a decrease in the number of adherent cells. For groups B–D, where LLLT was applied, an increase in adherent cells can be observed, compared with the ZA-treated group (A). MEV, original magnification 200×.

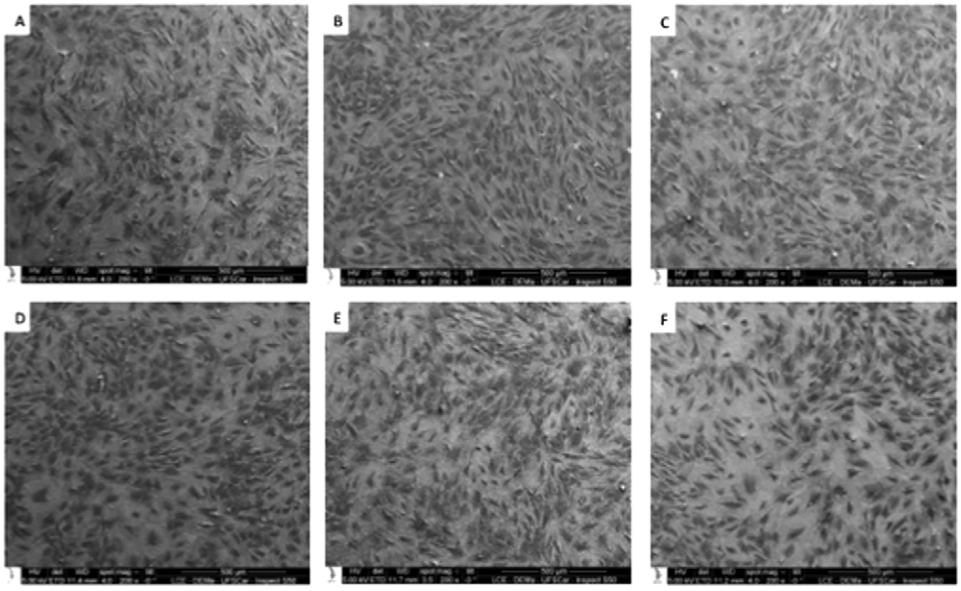

Figure 3. Morphology of gingival fibroblasts subjected to LLLT at different energy doses (A—control group; B—0.5 J cm^{-2}; C—1.5 J cm^{-2}; D—3 J cm^{-2}; E—5 J cm^{-2}; F—7 J cm^{-2}). No alterations in the morphology of the LLLT-treated cells were observed when compared with the control group (A). For groups B–D, and F, more adherent cells can be observed. MEV, original magnification 200×.

As shown in previous studies [15, 16], the LLLT used in the present investigation promoted biostimulatory effects on epithelial cells and gingival fibroblasts, mainly at 5 J cm^{-2} and 0.5 J cm^{-2}, respectively. It is interesting to note that different energy doses of LLLT promoted distinct patterns of biostimulation on cultured cells, even when the cells were previously exposed to ZA. Analysis of these scientific data has led workers in this research field to attempt to standardize the LLLT protocols for each specific oral disease and cell biostimulation. Despite the fact that *in vitro* data obtained from laboratory studies cannot be directly extrapolated to clinical situations, the results of this investigation suggest specific LLLT parameters to be applied to fibroblasts and epithelial cells present in human oral mucosa cells treated with ZA. Thus, in a general way, analysis of the data from this study may explain, at least in part, the positive clinical effects of LLLT on osteonecrosis lesions [10–13, 37]. However, further studies are needed to evaluate the *in vitro* effects

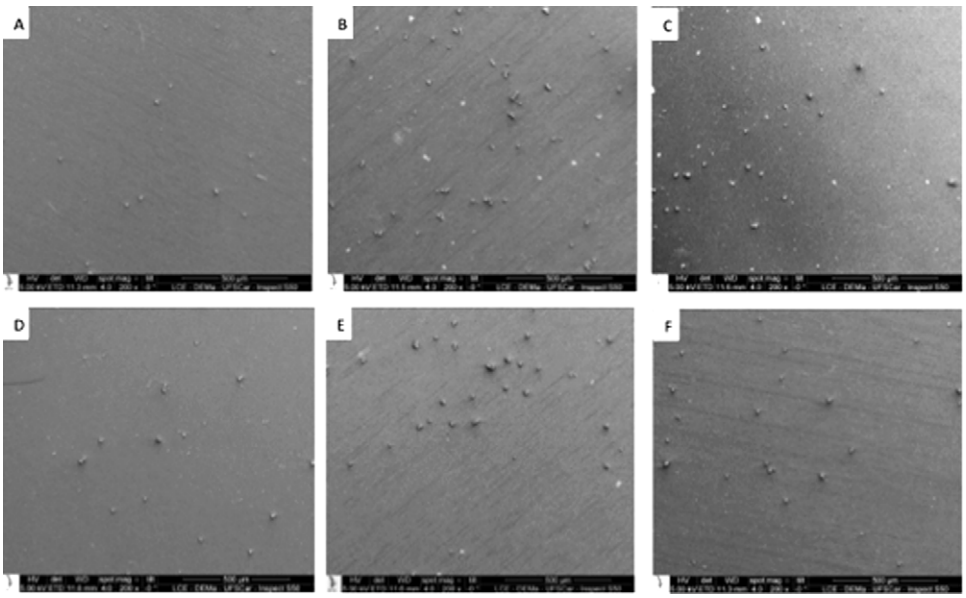

Figure 4. Morphology of gingival fibroblasts subjected to ZA treatment and LLLT at different energy doses (A—ZA; B—ZA + 0.5 J cm^{-2}; C—ZA + 1.5 J cm^{-2}; D—ZA + 3 J cm^{-2}; E—ZA + 5 J cm^{-2}; F—ZA + 7 J cm^{-2}). All groups subjected to ZA treatment show intense effects on cell morphology and reduction of adherent cells. For groups B, C, and E, subjected to LLLT, an increase in adherent cells was observed compared with the ZA-treated group (A). MEV, original magnification 200×.

of LLLT applied to co-cultures of different oral mucosal cells, as well as the biostimulatory effects of LLLT on oral osteonecrosis induced by bisphosphonates.

Acknowledgments

The authors acknowledge the Fundação de Amparo à Pesquisa do Estado de São Paulo—FAPESP (grants 2009/54722-1 and BP.DR 2009/52326-1) and the Conselho Nacional de Desenvolvimento Científico e Tecnológico—CNPq (grant 301029/2010-1) for the financial support.

References

[1] Badros A *et al* 2006 *J. Clin. Oncol.* **24** 945
[2] Badros A, Terpos E, Katodritou E, Goloubeva O, Kastritis E, Verrou E, Zervas K, Bae M R, Meiller T and Dimopoulos M A 2008 *J. Clin. Oncol.* **26** 5904
[3] Allen M R and Burr D B 2009 *J. Oral Maxillofac. Surg.* **67** 61
[4] Otto S, Pautke C, Opelz C, Westphal I, Drosse I, Schwager J, Bauss F, Ehrenfeld M and Schieker M 2010 *J. Oral Maxillofac. Surg.* **68** 2837
[5] Scheper M A, Badros A, Chaisuparat R, Cullen K J and Meiller T F 2009 *Br. J. Haematol.* **144** 667
[6] Ravosa M J, Ning J, Liu Y and Stack M S 2011 *Arch. Oral Biol.* **56** 491
[7] Diel I J, Fogelman I, Al-nawas B, Hoffmeister B, Migliorati C, Gligorov J, Väänänen K, Pylkkänen L, Pecherstorfer M and Aapro M S 2007 *Crit. Rev. Oncol. Hematol.* **63** 198
[8] Chiu C, Changi W, Chuang C and Chang S 2010 *J. Oral Maxillofac. Surg.* **68** 1055
[9] Vescovi P, Merigo E, Manfredi M, Meleti M, Fornaini C, Bonanini M, Rocca J P and Nammour S 2008 *Photomed. Laser Surg.* **26** 37
[10] Scoletta M, Arduino P G, Reggio L, Dalmasso P and Mozatti M 2010 *Photomed. Laser Surg.* **28** 179
[11] Romeo U, Galanakis A, Marias C, Del Vecchio A, Tenore G, Palaia G, Vescovi P and Polimeni A 2011 *Photomed. Laser Surg.* **29** 447
[12] Vescovi P, Manfredi M, Merigo E, Guidotti R, Meleti M, Pedrazzi G, Fornaini C, Bonanini M, Ferri T and Nammour S 2012 *Photomed. Laser Surg.* **30** 5
[13] Vescovi P, Merigo E, Meleti M, Manfredi M, Fornaini C and Nammour S 2013 *J. Osteoporos.* at press
[14] AlGhamdi K M, Kumar A and Moussa N A 2011 *Lasers Med. Sci.* **27** 237
[15] Basso F G, Oliveira C F, Kurachi C, Hebling J and Costa C A 2013 *Lasers Med. Sci.* at press
[16] Basso F G, Pansani T N, Turrioni A P, Bagnato V S, Hebling J and de Souza Costa C A 2013 *Int. J. Dent.* at press
[17] Scheler E E, Rohde E, Minet O, Muller G and Bindig U 2008 *Laser Phys. Lett.* **5** 70
[18] Fontana C R, Kurachi C, Marcantonio R A C, Costa C A S and Bagnato V S 2009 *Laser Phys.* **19** 2204
[19] Longo L 2010 *Laser Phys. Lett.* **7** 771
[20] Scheper M A, Badros A, Salama A R, Warburton G, Cullen K J, Weikel D S and Meiller T F 2009 *Support. Care Cancer* **17** 1553
[21] Oliveira C F, Basso F G, Lins E C, Kurachi C, Hebling J, Bagnato V S and de Souza Costa C A 2010 *Laser Phys.* **20** 1659
[22] Tagliani M M, Oliveira C F, Lins E M M, Kurachi C, Hebling J, Bagnato V S and de Souza Costa C A 2010 *Laser Phys. Lett.* **7** 247
[23] Oliveira C F, Basso F G, Lins E C, Kurachi C, Hebling J, Bagnato V S and de Souza Costa C A 2011 *Laser Phys. Lett.* **8** 155
[24] Oliveira C F, Hebling J, Souza P P C, Sacono N T, Lessa F R, Lizarelli R F Z and Costa C A S 2008 *Laser Phys. Lett.* **5** 680
[25] Agis H, Blei J, Watzek G and Gruber R 2010 *J. Dent. Res.* **89** 40
[26] Landersberg R, Cozin M, Cremers S, Woo V, Kousteni S, Sinha S, Garret-Sinha L and Raghavan S 2008 *J. Oral Maxillofac. Surg.* **66** 839

[27] Allen M R 2011 *Odontology* **99** 8
[28] Woo S, Hellstein J W and Kalmar J R 2006 *Ann. Int. Med.* **144** 753
[29] Walter C, Klein M O, Pabst A, Al-Nawas B, Duschner H and Ziebart T 2010 *Clin. Oral Invest.* **14** 35
[30] Scavelli C *et al* 2007 *Mol. Cancer Ther.* **6** 3256
[31] Bates D O and Jones R O P 2003 *Int. J. Lower Extremity Wounds* **2** 107
[32] Damante C A, De Micheli G, Miyagi S P H, Feist I S and Marques M M 2009 *Lasers Med. Sci.* **24** 885
[33] Almeida-Lopes L, Rigau J, Zângaro R A, Guidugli-Neto J and Jaeger M M M 2001 *Lasers Surg. Med.* **29** 179
[34] Hawkins-Evans D and Abrahamse H 2008 *Photodermatol. Photoimmunol. Photomed.* **24** 199
[35] Ankri R, Lubart R and Taitelbaum H 2010 *Lasers Surg. Med.* **42** 760
[36] Schartinger V H, Galvan O, Riechelmann H and Dudás J 2012 *Support. Care Cancer* **20** 523
[37] Atalay B, Yalcin S, Emes Y, Aktas I, Aybar B, Issever H, Mandel N M, Cetin O and Oncu B 2011 *Lasers Med. Sci.* **26** 815

Laser Phys. **23** (2013) 055604 (10pp) doi:10.1088/1054-660X/23/5/055604

In vitro transdentinal effect of low-level laser therapy

C F Oliveira[1], F G Basso[2], R I dos Reis[3], L T Parreiras-e-Silva[3], E C Lins[4], C Kurachi[5], J Hebling[6], V S Bagnato[5] and C A de Souza Costa[6,7]

[1] Laboratory of Genetics, Butantan Institute/Department of Morphology of Federal University of Sao Paulo (UNIFESP), Sao Paulo, SP, Brazil
[2] UNICAMP—Universidade de Campinas, Piracicaba School of Dentistry, Piracicaba, SP, 13414-903, Brazil
[3] USP—Universidade de São Paulo, Biochemical Institute of Ribeirão Preto, Ribeirão Preto, SP, 13560-970, Brazil
[4] UFABC—Universidade Federal do ABC, Engineering Center, Modeling and Applied Social Science, Santo André, SP, 09210-170, Brazil
[5] USP—Universidade de São Paulo, Physics Institute of São Carlos, São Carlos, SP, 13560-970, Brazil
[6] UNESP—Universidade Estadual Paulista, Araraquara School of Dentistry, Araraquara, SP, 14801-903, Brazil

E-mail: casouzac@foar.unesp.br

Received 22 March 2012, in final form 13 August 2012
Accepted for publication 4 January 2013
Published 4 April 2013
Online at stacks.iop.org/LP/23/055604

Abstract
Low-level laser therapy (LLLT) has been used for the treatment of dentinal hypersensitivity. However, the specific LLL dose and the response mechanisms of these cells to transdentinal irradiation have not yet been demonstrated. Therefore, this study evaluated the transdentinal effects of different LLL doses on stressed odontoblast-like pulp cells MDPC-23 seeded onto the pulpal side of dentin discs obtained from human third molars. The discs were placed in devices simulating *in vitro* pulp chambers and the whole set was placed in 24-well plates containing plain culture medium (DMEM). After 24 h incubation, the culture medium was replaced by fresh DMEM supplemented with either 5% (simulating a nutritional stress condition) or 10% fetal bovine serum (FBS). The cells were irradiated with doses of 15 and 25 J cm^{-2} every 24 h, totaling three applications over three consecutive days. The cells in the control groups were removed from the incubator for the same times as used in their respective experimental groups for irradiation, though without activating the laser source (sham irradiation). After 72 h of the last active or sham irradiation, the cells were evaluated with respect to succinic dehydrogenase (SDH) enzyme production (MTT assay), total protein (TP) expression, alkaline phosphatase (ALP) synthesis, reverse transcriptase polymerase chain reaction (RT-PCR) for collagen type 1 (Col-I) and ALP, and morphology (SEM). For both tests, significantly higher values were obtained for the 25 J cm^{-2} dose. Regarding SDH production, supplementation of the culture medium with 5% FBS provided better results. For TP and ALP expression, the 25 J cm^{-2} presented higher values, especially for the 5% FBS concentration (Mann–Whitney $p < 0.05$). Under the tested conditions, near infrared laser irradiation at 25 J cm^{-2} caused transdentinal biostimulation of odontoblast-like MDPC-23 cells.

(Some figures may appear in colour only in the online journal)

1. Introduction

The effects of low-level laser therapy (LLLT) on different cell cultures have been extensively investigated over recent years,

[7] Address for correspondence: Departamento de Fisiologia and Patologia, Faculdade de Odontologia de Araraquara, Universidade Estadual Paulista, Rua Humaitá, 1680 Centro, Caixa Postal: 331 Cep: 14801903 Araraquara, SP, Brazil.

but the specific therapeutic window of LLLT for each cell type has not yet been determined [1, 2].

Studies using several cell lines, such as keratocytes, endothelial cells, osteoblasts and hamster mucosa cells, have shown that near infrared laser irradiation is capable of inducing cell proliferation [3–5] and differentiation [6], increase of DNA [7] and bone protein synthesis [8–10], increase of mitochondrial alkaline phosphatase (ALP) levels and cellular adhesion in HeLa tumor cells [11, 12], and bone tissue formation, without causing genotoxic or cytotoxic damage [13].

In an *in vivo* study, the application of an infrared laser in rat molars induced the production of reactionary dentin matrix, without causing significant damage to the pulp tissue [14]. In humans, the biostimulatory effect of LLLT resulted in an increase in the synthesis of collagen type III, tenastin and fibronectin by odontoblasts related to the cavity floor [15]. However, the possible mechanism of odontoblast-like cell response to LLLT at a molecular level remains unclear [4].

Regarding the treatment of dentinal hypersensitivity, it may be suggested that the odontoblasts, which underlie the dentin in areas with exposed dentinal tubules, are under continuous chemical (bacterial products and others) and/or mechanical (outward dentin fluid movement from the pulp inside the tubules) stress conditions. In this way, the positive clinical results of LLLT could be related to the transdentinal stimulus of these odontoblasts, which would participate effectively in the repair process by means of the synthesis and expression of some dentin matrix proteins, resulting in sclerosis of dentinal tubules and/or deposition of intrapulpal reactive tertiary dentin.

It has been demonstrated that transdentinal laser propagation occurs by light dispersion through the microstructure of dentinal tubules [16]. Nevertheless, scientific data that characterize the transdentinal propagation of LLL and its relationship with the decrease of dentinal hypersensitivity by the increase of odontoblastic metabolic activity as well as the molecular response mechanism of cells with odontoblast-like phenotype to near infrared laser irradiation have not yet been demonstrated [9, 17].

The aim of this *in vitro* study was to evaluate the transdentinal effects of different LLL doses on stressed odontoblast-like pulp cells (MDPC-23) seeded onto dentin discs.

2. Material and methods

2.1. Preparation of dentin discs

Sixty sound human third molars were obtained from the Human Tooth Bank of UNESP—Universidade Estadual Paulista, Araraquara School of Dentistry, after approval of the research protocol by the institutional ethics committee (protocol 41/06). After being scaled for removal of periodontal tissue remnants and other debris, the teeth were mounted individually in a metallographic cutting machine (Isomet 1000; Buehler Ltda., Lake Bluff, IL, USA) with a diamond saw (11–4254, 4″ × 0.012″/ series 15LC, diamond wafering blade, Buehler Ltda., Lake Bluff, IL, USA) and one 0.4 mm thick dentin disc was cut transversally from the central portion of the crown of each tooth. The dentin surface was flattened and polished with wet 400- and 600-grit silicon carbide paper (T469-SF; Norton, Saint-Gobain Abrasivos Ltda., Jundiaí, SP, Brazil) [18]. A 0.5 M ethylenediaminetetraacetic acid (EDTA) solution, pH 7.2, was applied on dentin surface for 2 min [19] for removal of the smear layer and the discs were thoroughly rinsed with sterile deionized water. The discs were adapted to *in vitro* pulp chambers, modified from the initial project developed by Hanks *et al* [20] in order to determine dentin permeability by the analysis of the hydraulic conductance (Lp), which is the facility of a fluid to move through a surface with known area (0.28 cm^2) and under a certain pressure within a specific period of time. This measure reduces the interference of dentin permeability due to anatomic variations in dentin and permits a homogeneous distribution of the discs in the experimental and control groups. Statistical analysis of the hydraulic conductance data by the Kruskal–Wallis test confirmed similar ($p > 0.05$) dentin permeability among the groups.

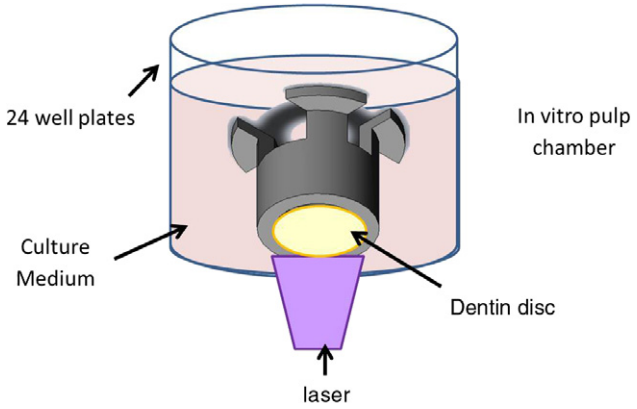

Figure 1. Illustration showing the irradiation of the occlusal surface of the dentin disc adapted in the *in vitro* pulp chamber. The MDPC-23 cells were seeded on the occlusal surface of the dentin discs.

2.2. Experimental conditions

Disc refinement was carried out with a cylindrical diamond bur (No 1095; KG Sorensen, Barueri, SP, Brazil) at high speed under water cooling and then at low speed to obtain discs with final diameter of 8 mm. Each enamel/dentin disc was placed in an *in vitro* pulp chamber, which has an upper and a lower compartment. The discs were positioned in the upper compartment of the *in vitro* pulp chamber with their occlusal side turned upwards, and were maintained between two silicone rings that promoted a tight seal between the two compartments.

The *in vitro* pulp chambers containing the discs were individually placed upside down in wells (figure 1) of sterile 24-well plates (Costar Corp., Cambridge, MA, USA) with Dulbecco's modified Eagle's medium (DMEM; Sigma

Table 1. LLLT dose, irradiation time and FBS concentrations used in the study. ($N = 20$—total samples per group. FBS, fetal bovine serum; LLLT, low-level laser therapy.)

Energy dose (J cm^{-2})	Active/sham irradiation time (s)	FBS concentration	
		5%	10%
15	698	G1	G2
25	930	G3	G4
0	698	G1-control	G2-control
0	930	G3-control	G4-control

Chemical Co., St Louis, MO, USA), which were maintained in a humidified incubator (Isotemp; Fisher Scientific, Pittsburgh, PA, USA) with 5% CO_2 and 95% air at 37 °C for 24 h. Then, the odontoblast-like cells MDPC-23 were seeded (30,000 cells cm^{-2}) on the pulpal side of the discs. After 24 h, the culture medium was aspirated and fresh DMEM supplemented with either 5% (simulating a nutritional stress condition) or 10% fetal bovine serum (FBS) was applied to the cells for an additional 24 h.

The LLL device used in this study was a near infrared indium gallium arsenide phosphide (InGaAsP) diode laser prototype (LASERTable; 808 ± 3 nm wavelength, 100 mW maximum output) specifically designed to provide a uniform irradiation of the occlusal side of the discs (figure 1), simulating the clinical conditions.

Due to the presence of the dentin barrier (disc), the energy losses during irradiation were equivalent to ten times the output value. Therefore, the laser parameters were adjusted to permit the preset energy density to reach the cells after transdentinal irradiation.

The cells in the control groups received the same treatment as those in the experimental groups. The 24-well plates containing the control cells were removed from the incubator and maintained in the LASERTable for the same times as used in the respective experimental groups for irradiation, though without activating the laser source (sham irradiation). One control group was established for each experimental group. The laser parameters and FBS concentrations used in the study are summarized in table 1.

The cells were subjected to transdentinal irradiation every 24 h, totaling three applications over three consecutive days. Immediately after the last active or sham irradiation, the cells were incubated for 72 h and then evaluated with respect to production of succinic dehydrogenase (SDH) enzyme (cell viability—MTT assay), total protein (TP) expression, ALP synthesis, reverse transcriptase polymerase chain reaction (RT-PCR) for collagen type 1 (Col-I) and ALP, and morphology (scanning electron microscopy—SEM).

2.3. SDH production (MTT assay)

Twelve specimens of each experimental and control groups were used for analysis of cell metabolism 72 h after the last active or sham irradiation, respectively. Cell metabolic activity was evaluated by SDH production, which is a measure of the mitochondrial respiration of the cells. The methyltetrazolium (MTT) assay was used for this purpose [21].

The dentin discs with the cells attached to the pulpal surface were carefully removed from the pulp chamber and placed in wells of 24-well plates containing 900 μl of DMEM in combination with 100 μl of MTT solution (5 mg ml^{-1} sterile PBS). The cells were incubated at 37 °C for 4 h. Thereafter, the culture medium (DMEM) with the MTT solution was aspirated and replaced by 700 μl of acidified isopropanol solution (0.04 N HCl) in each well to dissolve the violet formazan crystals resulting from the cleavage of the MTT salt ring by the SDH enzyme present in the mitochondria of viable cells. Three 100 μl aliquots of each well were transferred to a 96-well plate (Costar Corp., Cambridge, MA, USA). Cell viability was evaluated by spectrophotometry as being proportional to the absorbance measured at 570 nm wavelength with an ELISA plate reader (Multiskan, Ascent 354, Labsystems CE, Les Ulis, France). The values obtained from the three aliquots were averaged to provide a single value, and the inhibitory effect of the different groups on cell mitochondrial activity was calculated and expressed as medians.

2.4. Analysis of cell morphology by SEM

Four specimens of each experimental and control group were used for analysis of cell morphology by SEM 72 h after the last active or sham irradiation. The dentin discs carefully removed from the pulp chambers were placed at the bottom of the wells of 24-well plates. Then, the MDPC-23 cells that remained attached to the pulpal surface of the dentin discs were fixed in 1 ml of buffered 2.5% glutaraldehyde for 24 h and post-fixed with 1% osmium tetroxide for 1 h. The cells were dehydrated in a series of increasing ethanol concentrations (30, 50, 70, 95 and 100%) and immersed in 1,1,1,3,3,3-hexamethyldisilazane (HMDS; Acros Organics, Springfield, NJ, USA) for 90 min and maintained in a desiccator for 24 h. The dentin discs with the pulpal surface upward were mounted on metallic stubs and sputter-coated with gold, and the morphology of the surface-adhered MDPC-23 cells was examined with a scanning electron microscope (JEOL-JMS-T33A, Tokyo, Japan).

2.5. TP expression

TP expression was analyzed according to the Read–Northcote [22] protocol, using 20 specimens of each experimental and control group. The culture medium was aspirated and the cells on the dentin discs were washed three times with 1 ml PBS heated at 37 °C. An amount of 1.1 ml of 0.1% sodium lauryl sulfate (Sigma Chemical Co., St Louis, MO, USA) was added to each well and left for 30 min at room temperature to produce cell lysis. The samples were homogenized and 1 ml from each well was transferred to labeled Falcon tubes (Corning Inc., Corning, NY, USA). One milliliter of distilled water was added to the blank tube. Next, 1 ml of Lowry reagent solution (Sigma Chemical Co., St Louis, MO, USA) was added to all tubes, which were agitated for 10 s in a tube agitator (Phoenix AP 56, Araraquara, SP, Brazil). After 20 min at room temperature, 500 μl of Folin–Ciocalteau

phenol reagent solution (Sigma Chemical Co., St Louis, MO, USA) were added to each tube followed by 10 s agitation. Twenty minutes later, three 100 μl aliquots from each tube were transferred to a 96-well plate and the absorbance of the test and blank tubes was measured at 655 nm wavelength in a spectrophotometer (Micronal B328, São Paulo, SP, Brazil). TP expression was calculated by multiplying the absorbance obtained in the test by the calibration factor.

2.6. ALP synthesis

In each group, the same 20 specimens as used for TP expression were employed for analysis of ALP synthesis at 3 and 72 h after the last irradiation using a colorimetric endpoint assay (ALP Kit; Labtest Diagnóstico S.A., Lagoa Santa, MG, Brazil) with a thymolphthalein monophosphate substrate. This is a phosphoric acid ester substrate that is hydrolyzed by ALP and releases thymolphthalein, which gives a bluish color to the solution. The intensity of the resulting color is directly proportional to the enzymatic activity and is analyzed by spectrophotometry [23].

The culture medium was aspired and the cells attached to the dentin discs were washed three times with sterile PBS at 37 °C. An amount of 1.1 ml of 0.1% sodium lauryl sulfate (Sigma Chemical Co., St Louis, MO, USA) was added to each well and maintained for 30 min at room temperature to produce cell lysis. Next, Falcon tubes (test, standard and blank) were properly labeled and 50 μl of substrate (thymolphthalein monophosphate 22 mmol l^{-1}—Kit's reagent No 1) and 500 μl of buffer (300 mmol l^{-1}, pH 10.1—Kit's reagent No 2) were added to each tube. An amount of 50 μl of the standard solution, 45 U l^{-1} (Kit's reagent No 4), was added only to the standard tube. Thirty minutes after cell lysis, the tubes were placed in a double boiler (Fanem, Guarulhos, SP, Brazil) at 37 °C for 2 min. The samples were homogenized and 50 μl from each plate were transferred to the test tubes and maintained in the double boiler under gentle agitation. After 10 min incubation, 2 ml of color reagent (sodium carbonate 94 mmol l^{-1} and sodium hydroxide 250 mmol l^{-1}—Kit's reagent No 3) were added. The absorbances of the test, standard and blank tubes were measured at 590 nm wavelength with a spectrophotometer (Micronal B382, São Paulo, SP, Brazil). ALP activity was calculated by multiplying the absorbance values by the calibration factor and the final values were normalized.

2.7. Reverse transcriptase polymerase chain reaction (RT-PCR)

2.7.1. RNA extraction. The culture medium in contact with the irradiated and non-irradiated cells that remained attached to the pulpal surface of the dentin discs was aspirated and RNA was extracted using 1 ml of TRIzol (Invitrogen, Carlsbad, CA, USA) for each 10 cm^2 of cultured area, according to the manufacturer's instructions. The extracted RNA was eluted in 10 μl of ultra-pure water treated with diethylpyrocarbonate (DEPC) (BioAgency Ltda., São Paulo, SP, Brazil) by the 'up and down' technique.

Table 2. Primer sequences and applications.

Sequences of primers	Application
S: 5′-AGC CAT GTA CGT AGC CAT CC-3′ AS: 5′-CT CTC AGC TGT GGT GGT GAA-3′	β-actin amplification
S: 5′-GCT GAT CAT TCC CAC GTT TT-3′ AS: 5′-CTG GGC CTG GTA GTT GTT GT-3′	ALP amplification
S: 5′-ACG TCC TGG TGA AGT TGG TC-3′ AS: 5′-CAG GGA AGC CTC TTT CTC CT-3′	Col-I amplification

Total RNA was then quantified at 260/280 nm wavelength with a spectrophotometer (Eppendorf, model RS-232C, Hamburg, Germany) and its integrity was confirmed by electrophoresis in 1% agarose gel. Subsequently, cDNA was synthesized from 1 μg total RNA using the Superscript II enzyme (Invitrogen, Carlsbad, CA, USA), following the manufacturer's recommendations.

2.7.2. qPCR. After synthesis of cDNA, the expression of the genes was evaluated by qPCR. The primer pairs used to evaluate the expression of the genes encoding for ALP, Col-I and β-actin as a '*housekeeping gene*' were determined from the mRNA sequences available in the GENBANK database and are described in table 2.

The reactions were prepared with standard reagents for real-time PCR, Platinum SYBR Green qPCR SuperMix-UDG with ROX (Invitrogen). The fluorescence readings were performed using the Step One Plus System (Applied Biosystems, Foster City, CA, USA) at each amplification cycle, and were analyzed subsequently using the Step One Software 2.1 (Applied Biosystems, Foster City, CA, USA). All reactions were subjected to the same analytical conditions. The result, expressed in CT values, refers to the number of PCR cycles necessary for the fluorescent signal to reach the detection threshold. The individual results expressed in CT values were recorded in worksheets, grouped according to the irradiated groups and using β-actin as reference for normalization. Then, the mRNA concentrations of each target gene were analyzed statistically.

2.8. Statistical analysis

The control groups were first compared with each other to determine the influence of the sham irradiation time on their metabolism. As sham irradiation time had a statistically significant influence on results, the data for this test were transformed into percentages of the control, considering the mean of each control as 100%. The Kruskal–Wallis test complemented by the Mann–Whitney test for pairwise comparisons was applied to all collected data. A significance level of 5% was set for all analyses.

3. Results

3.1. Effect of irradiation dose on SDH production

The values of SDH enzyme production obtained in the irradiated and control groups after transformation into percentages are presented in table 3.

Table 3. Production of SDH enzyme detected by the MTT assay in the non-irradiated (control[a]) and irradiated groups of cell culture according to the laser dose (J cm^{-2}) and fetal bovine serum concentration (%FBS). (Note: values are medians (percentile 25 − percentile 75), $n = 12$ (except for the control groups, $n = 24$). Groups identified by the same lowercase letters in columns and uppercase letters in rows do not differ significantly (Mann–Whitney, $p > 0.05$).)

Energy dose (J cm^{-2})	%FBS	
	5%	10%
15	113.6 (101.9–123.0)a A	106.8 (102.1–117.2)b A
25	104.5 (83.4–129.5)ab A	129.1 (124.8–135.6)a A
0[a] (control)	100.0 (96.7–109.1)b A	100.1 (93.2–111.2)b A

[a] Represents the sham irradiation (0 J cm^{-2}), that is, the control cells were maintained in the LASERTable for the same irradiation times used in the experimental groups, though without activating the laser source. After transformation into percentages, the controls were compiled into a single control group ($n = 80$).

Table 4. Total protein expression (Lowry's method) in the non-irradiated (control[a]) and irradiated groups, according to the irradiation dose (J cm^{-2}) and fetal bovine serum concentration (%FBS). (Note: values are medians (percentile 25 − percentile 75), $n = 12$ (except for the control groups, $n = 24$). Groups identified by the same lowercase letters in columns and uppercase letters in rows do not differ significantly (Mann–Whitney, $p > 0.05$).)

Irradiation dose (J cm^{-2})	%FBS	
	5%	10%
15	93.6 (72.9–102.1)b A	100.2 (93.2–105.7)b A
25	111.0 (103.8–119.0)a A	110.8 (102.7–116.6)a A
0[a] (control)	100.0 (96.5–105.1)b A	100.1 (90.4–104.8)b A

[a] Represents the sham irradiation (0 J cm^{-2}), that is, the control cells were maintained in the LASERTable for the same irradiation times as used in the experimental groups, though without activating the laser source. After transformation into percentages, the controls were compiled into a single control group ($n = 80$).

No significant effect of the FBS concentrations (5% or 10%) was seen within the same energy dose or for the control group (table 3, rows). Conversely, comparing the different doses within each concentration of FBS, a significant effect was observed. When the culture medium was supplemented with 5% FBS and the cells were irradiated with 15 J cm^{-2} statistically higher production of SDH was observed when compared with the control group, while the same was not detected for the dose of 25 J cm^{-2} (table 3, columns). The opposite was seen when 10% FBS was used. The dose of 25 J cm^{-2} was superior to the dose of 15 J cm^{-2}, which did not differ from the control (table 3, columns).

3.2. Effect of laser dose on TP expression

As the sham irradiation time had a significant effect on TP expression (table 4), all data were transformed into percentages, considering the median of each control as 100% of TP expression. The data expressed as percentages of the control are shown in table 4.

No statistically significant difference was observed between the FBS concentrations for the same laser dose applied on the MDPC-23 cells (table 4, rows). However, for the same FBS concentration, higher TP expression was observed when the cells were irradiated with 25 J cm^{-2}. For both FBS concentrations, the irradiated groups did not differ significantly from the control groups when the cells were irradiated with the dose of 15 J cm^{-2}.

Table 5. ALP synthesis in the non-irradiated (control[a]) and irradiated groups after 9 days of cell culture according to the laser dose (J cm^{-2}) and fetal bovine serum concentration (%FBS). (Note: values are medians (percentile 25 − percentile 75), $n = 12$ (except for the control groups, $n = 24$). Groups identified by the same lowercase letters in columns and uppercase letters in rows do not differ significantly (Mann–Whitney, $p > 0.05$).)

Energy dose (J cm^{-2})	%FBS	
	5%	10%
15	99.2 (80.7–128.3)b A	100.0 (74.8–124.4)a A
25	116.8 (108.0–148.0)a A	110.1 (104.7–123.0)a A
0[a] (control)	100.0 (84.3–117.9)b A	100.2 (90.6–114.1)a A

[a] Represents the sham irradiation (0 J cm^{-2}), that is, the control cells were maintained in the LASERTable for the same irradiation times as used in the experimental groups, though without activating the laser source. After transformation into percentages, the controls were compiled into a single control group ($n = 80$).

3.3. Effect of laser irradiation dose on ALP synthesis

The values of ALP synthesis transformed into percentages of the control are presented in table 5. The effect of the FBS concentration incorporated into the culture medium did not vary for the same laser dose applied to the MDPC-23 cells (table 5, rows). However, when the different irradiated groups were compared for the same FBS concentration, greater ALP synthesis could be observed for the combination of irradiation at 25 J cm^{-2} and 5% FBS concentration. The same FBS concentration combined with an irradiation dose of 15 J cm^{2} did not result in significant difference from the controls. However, when the culture medium was supplemented with 10% FBS, no significant difference was observed among the groups irradiated with either 15 J cm^{-2} or 25 J cm^{-2} (table 5, columns).

3.4. Analysis of cell morphology by SEM

The MDPC-23 cells seeded on the pulpal side of the dentin discs were subjected to nutritional stress condition (5% FBS) and irradiated with the laser at 15 J cm^{-2} appeared organized in well defined epithelioid nodules and covering the entire dentin surface (figure 2(C)). The same pattern of cell morphology and distribution of cells on the discs was observed in the group in which the cells were maintained in culture medium supplemented with 10% FBS (figure 2(D)). In both situations (normal or stress condition), mitoses were frequent in all specimens. When compared with the control groups in which the cells were cultivated in DMEM with 5% (stress) or 10% FBS and maintained for 750 s out of the incubator (sham irradiation), a similar morphological cell pattern was observed. Dense epithelioid

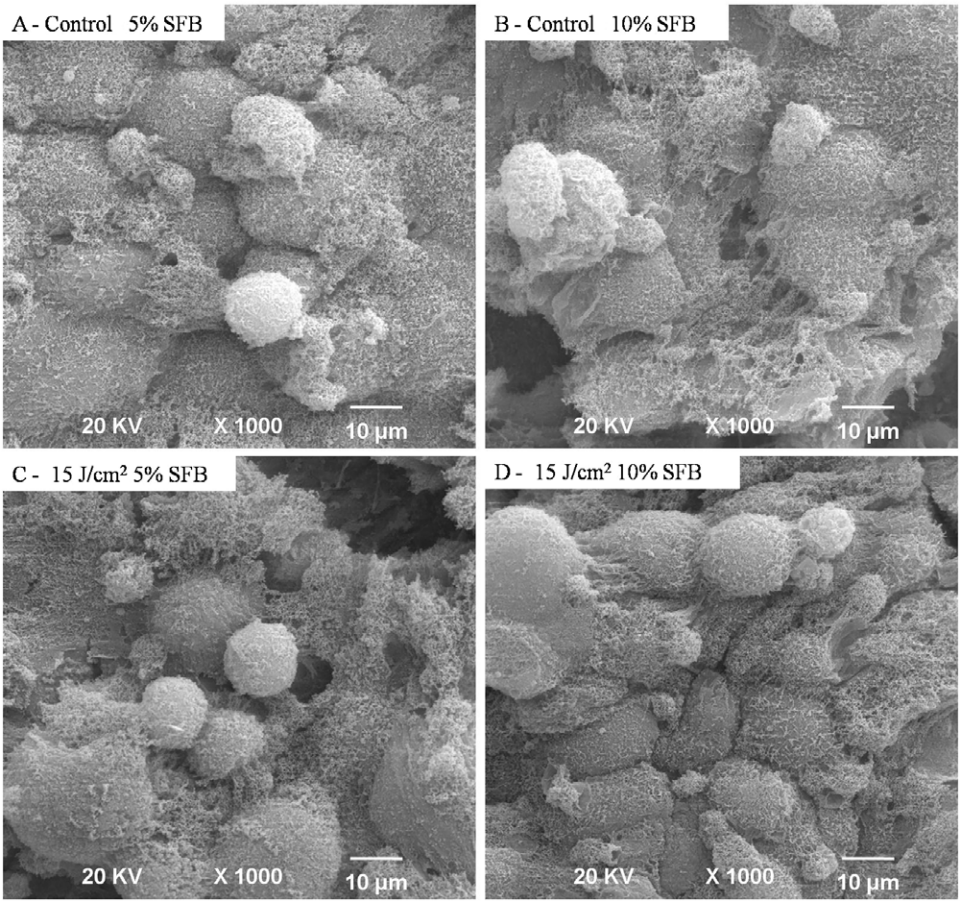

Figure 2. (A) (Control) MDPC-23 cells with normal morphology covering the pulpal side of the dentin disc. (B) Large number of odontoblast-like cells with numerous thin cytoplasmic processes, characterizing the formation of an epithelioid nodule on the dentin surface. (C) The morphological and cell distribution pattern is very similar to that of (B). (D) Dentin surface completely covered by MDPC-23 cells, which seem to be compacted. SEM, original magnification 1000×.

nodules were formed by compacted MDPC-23 cells that exhibited numerous cytoplasmic processes originated from the cytoplasm membrane (figures 2(A) and (B)).

In the control groups in which the cells were cultivated in culture medium with 5% (stress) or 10% FBS and maintained for 1250 s out of the incubator (sham irradiation), a number of cells organized in epithelioid nodules could be seen on dentin substrate (figures 3(A) and (B)). The irradiated cells exhibited a similar aspect to that of the control group, also presenting well defined dense epithelioid nodules (figures 3(C) and (D)). In both situations (normal or stress condition), mitoses were frequently observed in all specimens, and the MDPC-23 cells did not present morphological alterations or reduction in their number on dentin substrate. A discrete increase in the number of cells that remained adhered to the dentin surface was observed after irradiation at 25 J cm^{-2}.

3.5. RT-PCR (ALP expression and Col-I expression)

Overall, the analysis of gene expression in the odontoblast-like MDPC-23 cell cultures nine days after irradiation with a laser dose of 15 J cm^{-2} did not reveal alterations in the levels of ALP mRNA expression, comparing the irradiated groups with their respective controls (figure 4).

It was also observed that the transdentinal irradiation of the cells cultivated in DMEM supplemented with 10% FBS and irradiated with laser dose of 25 J cm^{-2} caused a onefold decrease of ALP synthesis compared with its respective control. However, for the 5% FBS concentration, no change in ALP expression was observed when the cells were irradiated with the same laser dose (figure 5).

Based on the results obtained after irradiation of the cells with the dose of 15 J cm^{-2}, it was possible to identify a discrete increase in the levels of Col-I mRNA expression when the odontoblast-like cells were maintained in culture medium supplemented with 5% FBS compared with its respective control (figure 6).

The analysis of cDNA samples after irradiation with 25 J cm^{-2} revealed a discrete increase of Col-I mRNA expression when the culture medium was supplemented with 5% FBS. However, supplementation with 10% FBS caused a onefold decrease of Col-I mRNA expression compared with its respective control (figure 7).

4. Discussion

The actual direct or indirect mechanisms of action of LLLT on cells are not yet well known [12, 24]. It is speculated

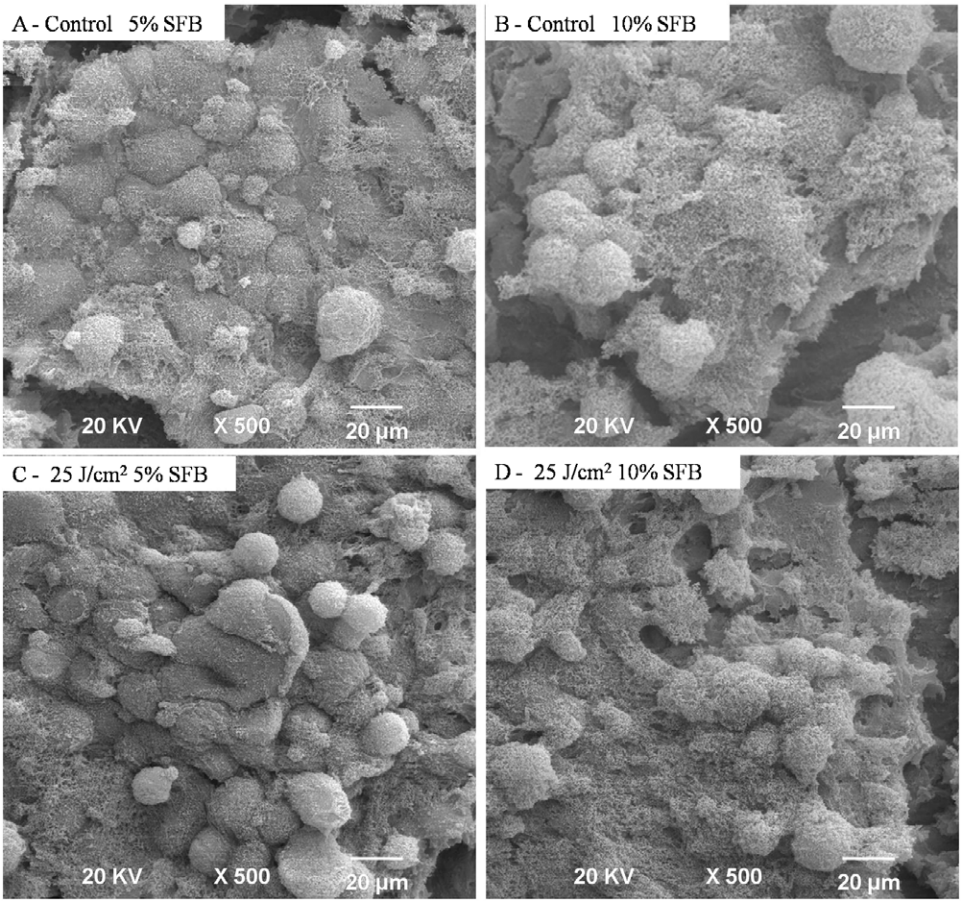

Figure 3. (A) Control—5% FBS: MDPC-23 cells organized in a dense epithelioid nodule on the dentin surface. (B) Control—10% FBS: the cells exhibit a wide irregular cytoplasmic membrane from which numerous cytoplasmic processes originate. (C) Dense epithelioid nodule formed by a large group of compacted odontoblast-like cells with normal morphology. (D) In the same way as observed for the other control groups, a great portion of the dentin disc is covered by numerous cells. SEM, original magnification 500×.

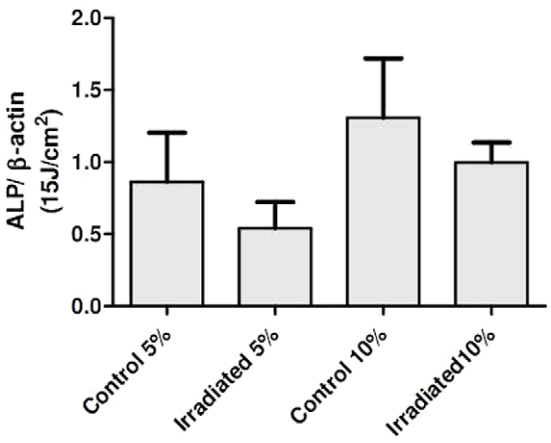

Figure 4. Levels of ALP mRNA expression after laser treatment at 15 J cm^{-2}. Columns represent the means and the error bars represent the standard deviations ($n = 6$).

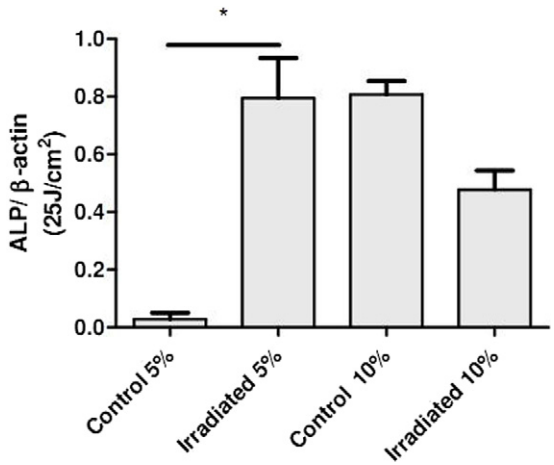

Figure 5. Levels of ALP mRNA synthesis after laser treatment at 25 J cm^{-2}. Columns represent the means and the error bars represent the standard deviations ($n = 6$).

that, in a first moment, the laser light is absorbed by the tissue and, in a second moment, this energy is transferred to intracellular components, promoting photoelectric effects that regulate the cell system by means of a process known as biomodulation [10, 25].

The present study investigated the possible transdentinal effect of LLLT on pulp odontoblasts, using an immortalized odontoblast-like MDPC-23 cell line seeded onto dentin discs. Odontoblasts are highly specialized cells, which have the neural crest cells as precursors. After differentiation, these

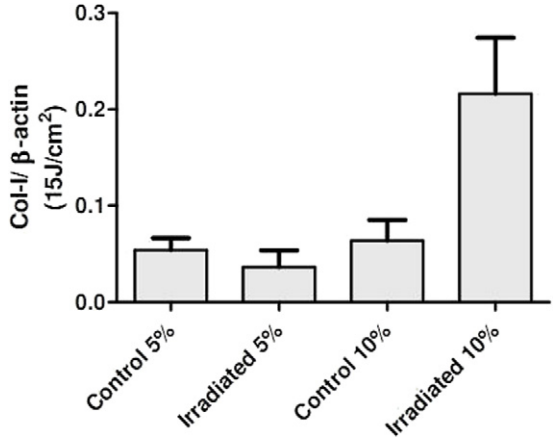

Figure 6. Levels of Col-I mRNA expression after laser treatment at 15 J cm^{-2}. Columns represent the means and the error bars represent the standard deviations ($n = 6$).

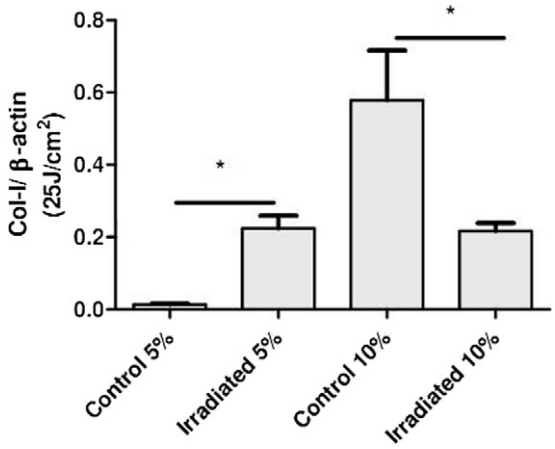

Figure 7. Levels of Col-I mRNA expression after laser treatment at 25 J cm^{-2}. Columns represent the means and the error bars represent the standard deviations ($n = 6$).

pulp cells become mainly responsible for the synthesis and secretion of products of the dentin matrix, which is mineralized at a later time [26]. This process is specifically controlled and regulated by such cells [27].

Certain conditions, such as incorrect toothbrushing, gingival recession, inadequate diet [14] and eccentric occlusal forces [28], either alone or in combination, may cause loss and/or wear of part of the enamel layer of the cervical region of the teeth, exposing the subjacent dentinal tubules. This exposure leads to movement (exudation) of dentinal fluid through the tubules, which may cause depolarization of the intratubular nerve endings and consequent dentinal hypersensitivity associated or not with damage of varied intensity to the underlying pulp tissue [29, 30].

LLLT has been widely used to accelerate tissue healing, treat dentinal hypersensitivity and stimulate bone regeneration as well as for an auxiliary therapy on the formation of reparative dentin [31]. Thus, studies employing cell cultures and animal models as well as clinical investigations have been carried out to elucidate the molecular mechanisms of LLLT–pulp interaction [32].

In order to simulate a clinical condition of dentin exposure, regardless of the etiology, the present study proposed an indirect irradiation of cells by interposing a dentin disc between the light source and the cell culture, using *in vitro* pulp chambers.

Tate *et al* [14] demonstrated *in vivo* that the deposition of reparative dentin occurred in a dose-dependent manner, and the presence of this dentin pattern was more evident 30 days after laser irradiation. Villa *et al* [33] reported a positive effect of the laser, characterized by the formation of reparative dentin when porcine teeth were irradiated with a laser dose of 12.8 J cm^{-2}. In the present study, an increase in the metabolism of MDPC-23 cells was observed with both light doses used (15 and 25 J cm^{-2}). These results confirm that, regardless of possible alterations in the pattern of the light that reached the cells after transdentinal propagation, the irradiation was capable of biostimulating the immortalized MDPC-23 cells in the same way as observed by Oliveira *et al* [34] when this cell line was directly irradiated. Allied to this positive biostimulatory effect on cell metabolism, in this study, there was an expressive increase in TP synthesis, especially at the dose of 25 J cm^{-2}. From a clinical standpoint, such an effect is of paramount importance, as the odontoblasts, which underlie the dentin, need to be stimulated by laser irradiation to synthesize and deposit typical matrix proteins, such as Col-I, ALP and fibronectin, which are involved in pulp tissue repair. In a concomitant manner, different types of matrix metalloproteinase (MMP) are synthesized with the aim of remodeling the matrix that is being deposited. For such a process to proceed after a non-lethal stimulus to odontoblasts, a sequence of events is triggered and culminates with the mineralization of this matrix. Therefore, hydroxyapatite nuclei are deposited close to the source of mineralization; however, cleavage of phosphate ions for local mineralization only starts after alkalinization of the medium. For mineralization to be complete, great deposition of calcium ions is necessary. This is achieved through several transmembrane mechanisms, which permit the creation of calcium transport systems through the inter-odontoblastic spaces up to the dentin matrix [35–39].

The mineralization of a recently deposited protein matrix requires the presence of ALP, which has also been recognized and described as an important marker for odontoblasts. Ueda and Shimizu [40] applied a GaAlAs laser on odontoblast-like cell cultures and observed an increase of ALP synthesis and expression. However, other authors found that laser irradiation did not influence ALP synthesis [1, 4]. In the present study, in the same way as demonstrated by Ueda and Shimizu [40], the dose of 25 J cm^{-2} significantly stimulated ALP synthesis. These *in vitro* results are paramount considering that this protein is the main component of the matrix vesicles responsible for the calcification process, although not all its functions are entirely known yet [41]. However, in the present study, no alteration in ALP mRNA expression was detected when the odontoblast-like cells were irradiated with the laser at either of the doses. The discrepancy between

ALP synthesis and ALP mRNA expression might be due to the time of evaluation of the real-time PCR assay or to production of protein without necessarily an increase in its mRNA expression. Protein synthesis requires two steps: transcription (mRNA synthesis from the gene that encodes the protein) and translation (protein synthesis from mRNA). In the present study, when ALP synthesis was evaluated in the culture medium, it was possible to determine the activity of all protein secreted until that moment, but not its transcription or translation. Therefore, as two mechanisms may occur, namely increase of mRNA expression and increase of translation, other evaluation times of mRNA expression levels should be considered to confirm the conduction of these stages. Therefore, the findings of the present study indicate that laser irradiation at a dose of 25 J cm^{-2} is capable of increasing ALP synthesis. Other stimulation periods should be investigated in order to determine whether this increase is dependent or not on mRNA transcription of this enzyme.

Collagen is another typical protein of dentin, and it is responsible for the highly fibrous nature of dentin and bone matrices, on which the apatite crystals are deposited [1, 42, 15]. During pulp repair, there is an intense synthesis of dentin matrix, which is basically composed by Col-I. This dentin matrix rich in collagen can be synthesized by fibroblasts, odontoblasts and/or osteoblasts [15]. Although a few authors have reported an increase in *in vitro* fibroblast proliferation after infrared laser irradiation [2, 43], Kreisler *et al* and Marques *et al* [32, 42] stated that the increase in cell number does not mean an increase in cell synthesis activity. Those authors also demonstrated that application of high energy density on cells such as cultured fibroblasts, in spite of activating cell proliferation, may reduce collagen synthesis. In the present study, Col-I expression was slightly increased in the groups irradiated with 15 and 25 J cm^{-2} and supplemented with 5% FBS. However, when the dose of 25 J cm^{-2} was used in combination with 10% FBS supplementation, Col-I expression decreased, which is in accordance with previous studies [32, 42].

In the present laboratory study, both Col-I and ALP were evaluated by mRNA expression. The electronic signal originated from irradiation exciting the photoreceptor molecules located in the mitochondria. Such a signal is amplified and transduced in the nucleus by means of biochemical reactions [12], resulting in the production of enzymes, such as Na^+-ATPase, K^+-ATPase and Na^+/K^+ exchangers (NHEs). All these enzymes play important roles in gene regulation and transduction signals [12]. These photobiological reactions end in the nucleus, which may cause an increase in DNA and RNA synthesis [44]. Hamajima *et al* [8] irradiated odontoblast-like cell cultures with a laser at 7.64 J cm^{-2} and observed a 2.3-fold increase in osteoglycin expression. In the present study, the analysis of the genes that encode for Col-I and ALP did not reveal a statistically significant increase in the levels of ALP mRNA and Col-I expression. However, this does not mean that the level of protein expression was not increased, as the other experiments compared the increase of ALP synthesis; it only indicates that there was no increase in mRNA expression.

The findings of the present study suggest that, under nutritional stress condition (5% FBS), laser doses of 15 and 25 J cm^{-2} were capable of stimulating the odontoblast-like MDPC-23 cells. The presence of the dentin disc was not a limiting factor to the stimulus, but adjustments in laser output were necessary because the structural characteristics of dentin blocked in part the passage of light and its action on the cells. Future research is necessary because, in an *in vivo* dentinopulpar complex model, LLLT may interact with different cells at the same time and trigger different pathways related to biostimulation and/or tissue repair. The development of *in vivo* studies will permit a safe application of LLLT in different clinical situations.

Acknowledgment

The authors acknowledge the Fundação de Amparo à Pesquisa do Estado de São Paulo—FAPESP (grants: 2007/50646-3, 2008/08424-6 and 2008/54785-0) for financial support.

References

[1] Coombe A R, Ho C T G and Darendeliler M A 2001 *Clin. Orthod.* **4** 3
[2] Almeida-Lopes L, Rigau J, Zângaro R A, Guidugli-Neto J and Jaeger M M M 2001 *Lasers Surg. Med.* **29** 179
[3] Grossman N, Schneid N, Reuveni H, Halevy S and Lubart R 1998 *Lasers Surg. Med.* **22** 212
[4] Khadra M, Kasem N, Lyngstadaas S P, Haanæs H R and Mustafa K 2005 *Clin. Oral Implants Res.* **16** 168
[5] Moore P, Ridgway T D, Higbee R G, Howard E W and Lucroy M D 2005 *Lasers Surg. Med.* **36** 8
[6] Aihara N, Yamaguchi M and Kasai K 2006 *Lasers Med Sci.* **21** 24
[7] Yamada K 1991 *Nippon Seik. Gak. Zass.* **65** 787
[8] Hamajima S, Hiratsuka K, Kiyama-Kishikawa M, Tagama T, Kawahara M, Ohta M, Sasahara H and Abiko Y 2003 *Lasers Med. Sci.* **18** 78
[9] Khadra M, Lyngstadaas P S, Haanæs R H and Mustafa K 2005 *Biomaterials* **26** 3503
[10] Stein A, Benayahu D, Maltz D and Oron U 2005 *Photomed. Laser Surg.* **23** 161
[11] Karu T I, Pyatibrat L V and Kalendo G S 1995 *J. Photochem. Photobiol. Biol.* **27** 219
[12] Karu T I, Pyatibrat L V, Kalendo G S and Esenaliev R O 1996 *Lasers Surg. Med.* **18** 171
[13] Kujawa J, Zavodnik I B, Lapshina A, Labieniec M and Bryszewska M 2004 *Photomed. Laser Surg.* **22** 504
[14] Tate Y, Yoshiba K, Yoshiba N and Iwaku M 2006 *Eur. J. Oral Sci.* **114** 50
[15] Ferreira A N S, Silveira L, Genovese W J, de Araújo V C, Frigo L, de Mesquita R A and Guedes E 2006 *Photomed. Laser Surg.* **24** 358
[16] Kienle A and Hibst R 2006 *Phys. Rev. Lett.* **97** 018104
[17] Oliveira C F, Hebling J, Souza P P C, Sacono N T, Lessa F R, Lizarelli R F Z and de Souza Costa C A 2008 *Laser Phys. Lett.* **5** 680
[18] Lanza C R, de Souza Costa C A, Furlan M, Alécio A and Hebling J 2009 *Cell Biol. Toxicol.* **25** 533
[19] Jacques P and Hebling J 2005 *Dent. Mater.* **21** 103
[20] Hanks C T, Sun Z L, Fang D N, Edwards C T, Ritchie H H and Butler W T 1998 *Connect. Tissue Res.* **37** 233
[21] Mosmann T 1983 *J. Immunol. Methods* **65** 55
[22] Read S M and Northcote D H 1981 *Anal. Biochem.* **116** 53

[23] Roy A V 1970 *Clin. Chem.* **16** 431
[24] Jia Y L and Guo Z Y 2004 *Lasers Surg. Med.* **34** 323
[25] Tuby H, Maltz L and Oron U 2007 *Lasers Surg. Med.* **39** 373
[26] Goldberg M and Smith A J 2004 *Crit. Rev. Oral Biol. Med.* **15** 13
[27] Linde A and Goldberg M 1993 *Crit. Rev. Oral Biol. Med.* **4** 679
[28] Kimura Y, Wilder-Smith P, Yonaga K and Matsumoto K 2000 *J. Clin. Periodontol.* **27** 715
[29] Friedmann H, Lubart R and Laulicht I 1991 *J. Photochem. Photobiol. Biol.* **11** 87
[30] Dababneh R H, Khouri A T and Addy M 1999 *Br. Dent. J.* **187** 606
[31] Godoy B M, Arana-Chavez V E, Núñez S C and Ribeiro M S 2007 *Arch. Oral Biol.* **52** 899
[32] Kreisler M, Christoffer A B, Willerstausen B and d'Hoedt B 2003 *J. Clin. Periodontol.* **30** 353
[33] Villa G E P, Catirse A B C E B, Lia R C C and Lizarelli R F Z 2007 *Laser Phys. Lett.* **4** 690
[34] Oliveira C F, Basso F G, Lins E C, Kurachi C, Hebling J, Bagnato V S and de Souza Costa C A 2011 *Laser Phys. Lett.* **8** 155
[35] Butler W T and Ritchie H 1995 *Int. J. Dev. Biol.* **39** 169
[36] Butler W T 1998 *Eur. J. Oral Sci.* **106** 204
[37] Butler W T, Brunn J C, Qin C and McKee M D 2002 *Connect. Tissue Res.* **43** 301
[38] Butler W T, Brunn J C and Qin C 2003 *Connect. Tissue Res.* **44** 171
[39] Butler W T 2008 *Connect. Tissue Res.* **49** 383
[40] Ueda Y and Shimizu N 2003 *J. Clin. Laser Med. Surg.* **21** 271
[41] Simão A M, Beloti M M, Cezarino R M, Rosa A L, Pizauro J M and Ciancaglini P 2007 *Comput. Biochem. Physiol.* A **146** 679
[42] Marques M M, Pereira A N, Fujihara N A, Nogueira F N and Eduardo C P 2004 *Lasers Surg. Med.* **34** 260
[43] Pereira S N, Eduardo C P, Matson E and Marques M M 2002 *Lasers Surg. Med.* **31** 263
[44] Karu T I, Pyatibrat L V and Kalendo G S 2004 *Photochem. Photobiol. Sci.* **3** 211

Lasers Med Sci (2013) 28:415–422
DOI 10.1007/s10103-012-1062-y

ORIGINAL ARTICLE

Infrared LED irradiation applied during high-intensity treadmill training improves maximal exercise tolerance in postmenopausal women: a 6-month longitudinal study

Fernanda Rossi Paolillo · Adalberto Vieira Corazza · Audrey Borghi-Silva · Nivaldo Antonio Parizotto · Cristina Kurachi · Vanderlei Salvador Bagnato

Received: 22 September 2011 / Accepted: 6 February 2012 / Published online: 2 March 2012

Abstract Reduced aerobic fitness is associated with an increased risk of cardiovascular diseases among the older population. The aim of this study was to investigate the effects of LED irradiation (850 nm) applied during treadmill training on the maximal exercise tolerance in postmenopausal women. At the beginning of the study, 45 postmenopausal women were assigned randomly to three groups, and 30 women completed the entire 6 months of the study. The groups were: (1) the LED group (treadmill training associated with phototherapy, $n=10$), (2) the exercise group (treadmill training, $n=10$), and (3) the sedentary group (neither physical training nor phototherapy, $n=10$). The training was performed for 45 min twice a week for 6 months at intensities between 85% and 90% maximal heart rate (HR_{max}). The irradiation parameters were 39 mW/cm^2, 45 min and 108 J/cm^2. The cardiovascular parameters were measured at baseline and after 6 months. As expected, no significant differences were found in the sedentary group ($p\geq0.05$). The maximal time of tolerance (Tlim), metabolic equivalents (METs) and Bruce stage reached significantly higher values in the LED group and the exercise group ($p<0.01$). Furthermore, the HR, double product and Borg score at isotime were significantly lower in the LED group and in the exercise group ($p<0.05$). However, the time of recovery showed a significant decrease only in the LED group ($p=0.003$). Moreover, the differences between before and after training (delta values) for the Tlim, METs and HR at isotime were greater in the LED group than in the exercise group with a significant intergroup difference ($p<0.05$). Therefore, the infrared LED irradiation during treadmill

F. R. Paolillo · C. Kurachi · V. S. Bagnato
Optics Group, Instituto de Física de São Carlos (IFSC),
University of São Paulo (USP),
São Carlos, SP, Brazil

C. Kurachi
e-mail: cristina@ifsc.usp.br

V. S. Bagnato
e-mail: vander@ifsc.usp.br

F. R. Paolillo · N. A. Parizotto · C. Kurachi · V. S. Bagnato
Biotechnology Program,
Federal University of São Carlos (UFSCar),
São Carlos, SP, Brazil

N. A. Parizotto
e-mail: parizoto@ufscar.br

A. V. Corazza
Department of Morphology, Faculty of Dentistry of Piracicaba,
State University of Campinas (UNICAMP),
Piracicaba, SP, Brazil
e-mail: avcorazza@gmail.com

A. Borghi-Silva
Cardiopulmonary Physiotherapy Laboratory,
Department of Physical Therapy,
Federal University of São Carlos (UFSCar,
São Carlos, SP, Brazil
e-mail: audrey@ufscar.br

N. A. Parizotto
Electrothermophototherapy Laboratory,
Department of Physical Therapy,
Federal University of São Carlos (UFSCar,
São Carlos, SP, Brazil

F. R. Paolillo (✉)
University of São Paulo (USP),
Av. Trabalhador Sãocarlense, 400 – Centro,
CEP 13560-970, São Carlos, SP, Brazil
e-mail: fer.nanda.rp@hotmail.com

training can improve maximal performance and post-exercise recovery in postmenopausal women.

Keywords Infrared LED · Treadmill training · Aerobic capacity · Postmenopausal women

Introduction

Sedentariness and reduced aerobic fitness [1] associated with an increased cardiac sympathetic stimulation [2], hypertension [3] and/or obesity seem to play a critical role in the onset and/or progression of cardiovascular diseases (mainly coronary heart disease), especially in postmenopausal women, as they are subject to a decline in estrogen production [4]. Physical exercise combined with phototherapeutic technologies [5] might be more efficient in preventing cardiovascular diseases, because physical training is known to increase metabolic, cardiovascular and osteomuscular function [6, 7], while phototherapy applied before [8, 9], during [5] or after [10] physical exercise has been shown to enhance muscle performance.

Phototherapy can result in biochemical adaptation of the mitochondria with changes in the redox state resulting in a conversion of electromagnetic to biochemical energy with an increase in the oxygen binding, respiration rate and production of ATP [11–13]. Structural changes may also occur, such as the formation of giant mitochondria [13]. At the same time, it is a well-known fact that physical training also results in biochemical and structural changes in the mitochondria [14, 15]. Therefore, phototherapy together with exercise may help enhance the effects of physical training. Lastly, infrared radiation shows better skin penetration than red radiation, infrared radiation has been used in several studies [5, 8, 10, 16] to improve physical performance, and we have done the same.

Only one study [16] has investigated the immediate effects of phototherapy applied before a treadmill exercise on cardiorespiratory parameters in young people. However, long-term cardiovascular adaptations to exercise performance need to be investigated. In this context, we apply phototherapy during exercise, instead of at rest, because we postulated that phototherapy during an intense metabolic stage caused by physical exercise may be more efficient [5]. Metabolic, cardiovascular, respiratory and osteomuscular stress during exercise results in a breakdown of the body's homeostasis requiring adjustments to this stress or momentary imbalance, and this occurs mostly in middle-age to elderly people. Under these conditions, the interaction between phototherapy and the physiological responses to exercise triggering a cascade of biochemical reactions via the mitochondria that can enhance physical performance and reflect the general health of the individual, especially cardiovascular health.

The objective of our study was to evaluate the effects of infrared radiation emitted from LEDs during treadmill training on the maximal exercise tolerance in postmenopausal women. Our hypothesis was that the infrared LED irradiation during treadmill training would be able to enhance physical performance in these women, as evaluated by a progressive aerobic exercise test on a treadmill.

Materials and methods

The current research was approved by the National Ethics Committee of the Ministry of Health in Brasilia, Brazil, and by the Ethics Committee of the Federal University of São Carlos (UFSCar) in São Carlos, Brazil. All subjects provided written informed consent and agreed to participate in the study.

Subjects

A prospective randomized trial was conducted. Following screening of 321 subjects, 45 subjects were included and randomly allocated by a computer program. For inclusion a subject had to be a healthy postmenopausal Caucasian women between 50 and 60 years of age. Postmenopausal was defined as the absence of menstruation for more than 12 months. The exclusion criteria were: signs and symptoms of any neurological, metabolic, inflammatory, pulmonary, oncological or cardiac disease or endocrinopathy, musculotendinous or articular injuries, cigarette smoking, and the use of any hormone replacement therapy. It is important to note that we excluded diseases, disorders or injuries which would have limited the execution of high-intensity exercise. Moreover, women who failed to participate in more than 70% training sessions or who had started physical exercise during the study were also excluded. The 45 postmenopausal women were assigned to three groups at the beginning of the study. However, five women in each group (n=15) were unable to continue the program. We therefore evaluated 30 women who completed the entire 6 months of the study. These 30 women had a body mass index of 28±6 kg/cm^2. The three groups were: (1) the LED group (treadmill training associated with phototherapy, n=10), (2) the exercise group (only treadmill training, n=10), and (3) the sedentary group (neither physical training nor phototherapy, n=10). The clinical characteristics of the women are listed in Table 1.

Phototherapy and treadmill training

In order to perform the phototherapy during the treadmill training, the Optics Group from Instituto de Física de São Carlos (IFSC), University of São Paulo (USP), developed a system based on infrared LEDs (850 nm) for use during the physical exercises (Fig. 1). To measure the power in the

Table 1 Clinical characteristics (mean and standard deviation)

Characteristic	LED group	Exercise group	Sedentary group
Age (years)	56±2	55±2	55±2
Duration of menopause (years)	8±6	9±6	7±6
Estradiol (pg/ml)	18±10	15±9	19±10
TSH (μIU/ml)	3±2	3±2	3±2
Urea (mg/dl)	34±6	32±10	34±9
Creatinine (mg/dl)	0.7±0.09	0.8±0.09	0.7±0.09
Heart rate during training (bpm)	148±7	140±8	–

The groups were not significantly different (one-way ANOVA, $p \geq 0.05$)

milliwatt range, a FieldMaster power meter and a photodetector (Coherent, Portland, OR) were used. The average power and power density on the women's skin were 100 mW and 39 mW/cm^2, respectively. The treatment time was 45 min bilaterally in both thighs. These parameters led to an approximate fluence of 108 J/cm^2. The volunteers wore safety glasses and swimwear to ensure infrared absorption through the bare skin during the treadmill training with the infrared LED irradiation [5, 17].

Treadmill training with and without the application of the phototherapy was performed twice a week for 6 months, each session lasting 45 min at intensities between 85% and 90% maximal heart rate (HR_{max}) during the progressive aerobic exercise test. According to the American College of Sports Medicine [18] and the American Heart Association (AHA) [19], high-intensity endurance training is when HR values are between 70% and 90% of HR_{max} [20]. In addition, according to Enoksen et al. [21], training in the intensity zone 65% to 82% of HR_{max} is recommended as a training regime, whereas training from 82% to 92% is considered a high-intensity training regime above the anaerobic or lactate threshold. The accumulation of lactate beyond the lactate threshold provides an indication that the mechanisms of lactate removal are failing to keep pace with lactate production. Lactate threshold training is important to help improve the endurance performance and induce beneficial metabolic adaptations for cardiovascular health [22]. To monitor the HR during training, a Cardiofrequencemetre (Polar A3; Polar Electro, Woodbury, NY) was used. A period of 1 month was allowed for adaptation to the intensity of the training. Training and evaluation were carried out in a laboratory at an air temperature between 22°C and 24°C and a relative humidity between 50% and 60%, always at the same time of day at the School Health Unit of the Federal University of São Carlos.

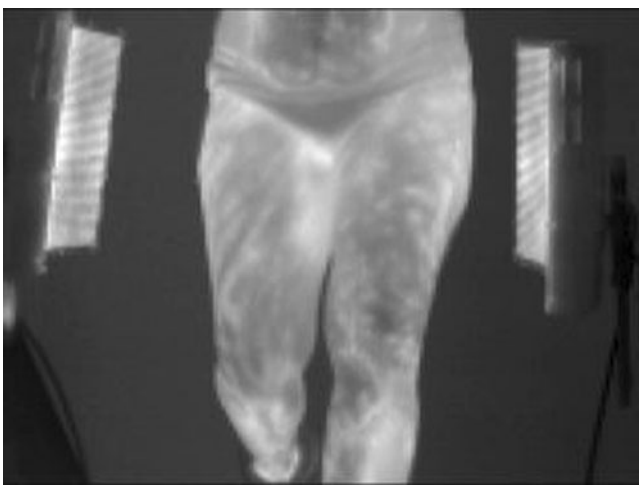

Fig. 1 Thermographic image of the infrared LED irradiation during treadmill training

Clinical characteristics

The biochemical tests performed included thyroid stimulating hormone (TSH), urea and creatinine. The women were asked to fast in the morning before the basal blood test was done. This test was carried out according to the standard laboratory procedures of the Medical Hospital School of São Carlos.

HR and blood pressure assessment at rest and during aerobic exercise testing

Prior to aerobic exercise testing a resting 12-lead ECG (Ergo; HeartWare, Belo Horizonte, MG, Brazil) was obtained. The women then underwent a progressive aerobic exercise test on a treadmill (using the modified Bruce protocol) [5]. The test was stopped once the patient showed signs and/or limiting symptoms such as fatigue of the lower limbs, general physical fatigue, dizziness, nausea, cyanosis, arrhythmias, excessive sweating, increased or sudden drop in BP or angina, or when the patient reached the HR_{max} relative to age. The criteria for terminating the aerobic assessment followed the AHA guidelines established for exercise testing [23].

The ECG signal was obtained using a cardiac monitor and an analogue-to-digital converter, the latter being the interface between the monitor and a computer (Ergo; HW Systems, HeartWare). The HR and the R–R interval were recorded for each heart beat. The Cardiofrequencemetre was used simultaneously. The systolic BP and diastolic BP were measured by the auscultatory method using an aneroid sphygmomanometer and a stethoscope during rest, during each stage of the test and during the recovery period.

The volunteers carried out the exercise up to the maximal time of tolerance (Tlim). The metabolic equivalents (METs) were determined as oxygen consumption (VO_2)/3.5. The concept of METs is used to assign an intensity value to a specific activity (1 MET=oxygen consumption of 3.5 ml/kg/min) [24].

Estimated maximal oxygen consumption (VO_{2max}) achieved at peak exercise was determined from the following

equation: VO_2 (ml/kg/min)=(V×0.1)+(V×I×1.8)+3.5, if the patient finished the test at a speed between 3.2 km and 6.4 km/h (walking) or VO_2 (ml/kg/min)=(V×0.2)+(V×I×0.9)+3.5 if the patient finished the test at a speed above 8 km/h (running), V is the speed in meters per minute, and I is the inclination in percent, according to the AHA [19, 24].

The double product (DP) was determined as HR×systolic BP (bpm×mmHg) at peak effort. At the beginning and at the end of the test the volunteers were evaluated using the Borg scale 0–10 score which is a simple method to rate perceived exertion, sensation of physical tiredness or possible breathing difficulties (dyspnea) [25]. The HR, DP and Borg scale score obtained during the peak of the exercise of the pretreatment measurement and during the isotime (the same intensity time) were analyzed. The recovery time was considered ended when the HR and the BP reached the pre-exercise values.

Statistical analysis

The data are expressed as means and standard deviations. The Shapiro-Wilk test was used to determine the normality of the data. One-way ANOVA was used to evaluate the differences in clinical characteristics between the groups. Repeated measures ANOVA with Bonferroni adjustments were used to compare values before and after training. The delta (Δ) values (differences between the values before and after training) were used to compare groups via a one-way ANOVA with Bonferroni adjustments. Statistica for Windows release 7 software (Statsoft, Tulsa, Ok) was used for the statistical analysis and the significance level was set at 5% ($p<0.05$).

Results

The results of maximal exercise testing are shown in Table 2. There were significant differences between before and after training in the women who performed the exercises with or without infrared LED irradiation. As expected, there was no significant difference in the results for the sedentary group ($p\geq0.05$). There were significant increases in Tlim, METs and Bruce stage in the both the LED group and the exercise group ($p<0.01$)] after 6 months of training. The results at isotime showed a significant reduction in HR, DP and Borg score in the LED group and the exercise group ($p<0.05$). The recovery time for HR and BP significantly decreased in the LED group ($p=0.003$), but did not show any significant difference in the exercise group ($p\geq0.05$).

No significant difference was found between the groups in the delta values between the before and after training ($p\geq0.05$), except for Tlim (Δ=432±180 s vs. 186±118s, $p=0.002$; Fig. 2), METs (Δ=4.3±1.4 vs. 2.7±0.9, $p=0.02$; Fig. 3) and HR at isotime (Δ=−39±9bpm vs. −29±11 bpm, $p=0.03$; Fig. 4) in the LED group which showed a greater variation than the exercise group with significant intergroup differences.

Discussion

Postmenopausal women who performed exercise with or without infrared LED irradiation showed an improvement in aerobic fitness after 6 months of training. However, the main findings of this study were that women in the LED group showed an improvement in maximal exercise performance as

Table 2 Cardiovascular parameters during rest, ergometric testing and recovery

Time point	Parameter	LED group		Exercise group		Sedentary group	
		Baseline	Study end	Baseline	Study end	Baseline	Study end
Before exercise	HR (bpm)	73±9	69±8	73±10	71±8	71±8	74±12
	Systolic BP (mmHg)	122±17	126±18	116±12	121±6	131±15	137±19
	Diastolic BP (mmHg)	75±12	81±10	72±7	76±9	85±8	87±10
During exercise peak	Tlim (s)	788±131	1,219±128**	790±99	976±75**	751±189	722±177
	METs reached	9±2	13±2**	8±1	11±1**	7±1	8±2
	Modified Bruce (last stage)	2.5±0.5	4.5±0.5**	2.5±0.5	3.5±0.5**	2.5±0.5	2.5±1
During exercise at isotime	HR (bpm)	165±9	126±12**	155±14	127±4**	157±15	157±20
	Double product (bpm.mmHg)	26,238±3,394	19,885±2,587**	23,985±2,912	19,729±2,424**	26,810±4,874	28,968±5,563
	Borg score (0-10)	7±2	3±1**	8±2	5±1**	8±1	9±1
After exercise	Recovery time for HR and BP (s)	426±107	336±42**	384±31	330±51	406±56	364±51

*$p<0.05$, **$p<0.01$, before vs. after training (repeated measures ANOVA with Bonferroni adjustments).

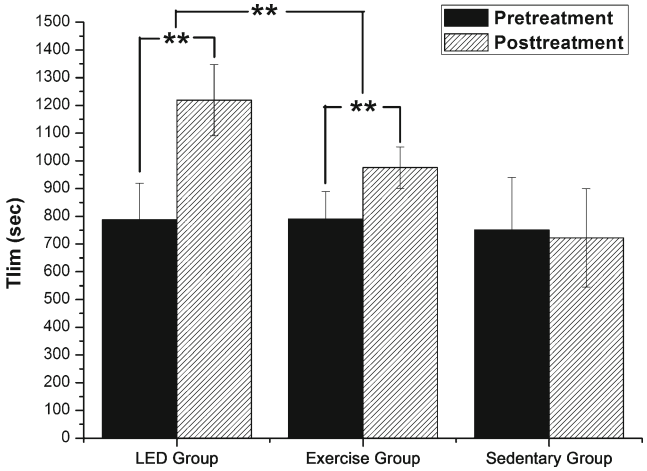

Fig. 2 Tlim obtained during maximal exercise testing. The values obtained are significantly higher in the LED group and the exercise group ($p<0.01$, repeated measures ANOVA with Bonferroni adjustments). The difference between before and after training (delta value) is greater in the LED group than in the exercise group ($\Delta=432\pm180$ s vs. 186 ± 118 s) with a significant intergroup difference ($p=0.002$, one-way ANOVA with Bonferroni adjustments; $^{**}p<0.01$)

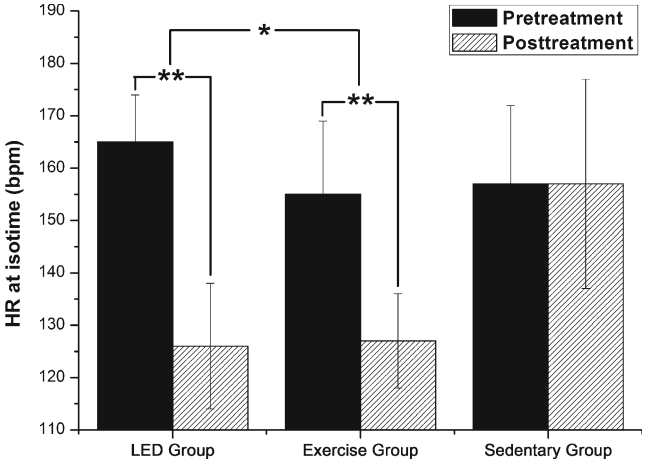

Fig. 4 HR at isotime during maximal exercise testing. The values obtained are significantly lower in the LED group and the exercise group ($p<0.01$, repeated measures ANOVA with Bonferroni adjustments). The difference between before and after training (delta value) is greater in the LED group than in the exercise group ($\Delta=-39\pm9$ bpm vs. -29 ± 11 bpm) with a significant intergroup difference ($p=0.03$, one-way ANOVA with Bonferroni adjustments; $^{*}p<0.05$, $^{**}p<0.01$)

indicated by the increase in Tlim and METs, as well as by a decrease in HR at isotime as evidenced by the difference in delta values between the groups. Moreover, an accelerated recovery time of HR and BP only occurred in the LED group. As expected, in the sedentary group, no significant differences were found in the cardiovascular variables during rest, ergometric testing and recovery between baseline and the study end. The increase in Tlim indicates that these women performed the physical exercise for longer, the increase in METs indicates that they performed the physical exercise with greater

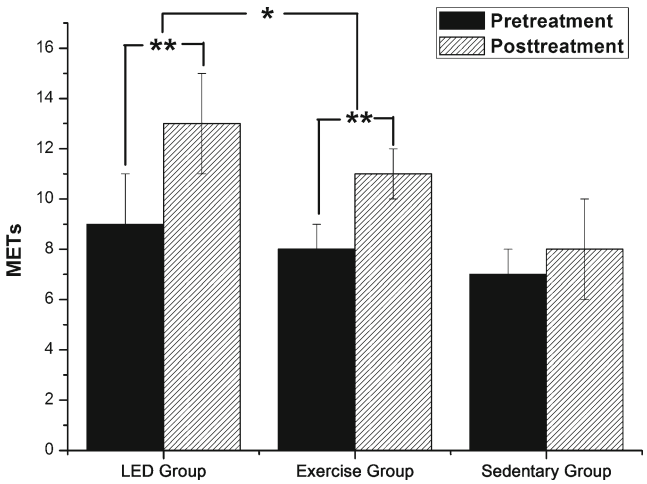

Fig. 3 METs achieved during exercise peak. The values obtained are significantly higher in the LED group and the exercise group ($p<0.01$, repeated measures ANOVA with Bonferroni adjustments). The difference between before and after training (delta value) is greater in the LED group than in the exercise group ($\Delta=4.3\pm1.4$ vs. 2.7 ± 0.9) with a significant intergroup difference ($p=0.02$, one-way ANOVA with Bonferroni adjustments; $^{*}p<0.05$, $^{**}p<0.01$)

intensity [24, 25], the reduction in HR at isotime indicates a lower cardiovascular effort [25], which can lead to an accelerated recovery of HR and BP after exercise, possibly as a result of better adaptation to autonomic modulation of the HR as well as baroreflex activity [26, 27]. All of these beneficial physiological adaptations reflect an increase in maximal exercise tolerance [25, 28] and a higher fatigue resistance after the physical training program combined with infrared LED irradiation.

According to Lynch et al. [1], postmenopausal women have both a lower VO_{2max} and a greater risk of cardiovascular disease compared to perimenopausal women. The increase in METs (multiples of resting VO_2) found in the LED group therefore indicates an important improvement in the health of these postmenopausal women. In a recent study in young untrained male subjects [16], phototherapy applied 5 min before a progressive intensity running protocol on a treadmill had immediate effects on exercise performance. Compared to the results in a placebo group, the subjects who received phototherapy performed the exercise for longer with a greater VO_{2max}. In addition, they also showed decreases in exercise-induced oxidative stress. The authors suggested that modulation of the redox system delays the onset of muscle fatigue and protects against exercise-induced damage [16].

Postmenopausal women experience changes in body composition, such as increased fat mass and intramuscular fat [4], which creates a biological barrier to the penetration of light into the muscle. The infrared spectrum has been used in several studies investigating the association between phototherapy and physical exercise because the radiation penetrates more deeply. The wavelengths most commonly used in clinical studies with phototherapy and physical exercise are 655 nm [29], 660 nm [30], 808 nm [10, 31], 810 nm [9, 16, 32] and

830 nm [8, 30] for laser irradiation, and 660 nm [33, 34] and 850 nm for LED irradiation [5, 33, 34]. Another important consideration involves the optical properties of tissue. Both the absorption and scattering of light in tissue are wavelength-dependent and tissue chromophores such as hemoglobin and melanin have high absorption bands at wavelengths shorter than 600 nm. In addition, water begins to absorb significantly at wavelengths greater than 1,150 nm. The optical window is primarily limited by absorption, due to blood at short wavelengths and water at long wavelengths [35]. We consider the total energy per unit of area reaching the surface as the delivered dose, but this is not necessarily absorbed.

Our first study with LED irradiation plus treadmill training showed that exercises with or without LED improved submaximal exercise performance, as shown by an increase in Tlim in both groups [5]. In that study the physical training was performed over 3 months twice a week for 30 min, and the irradiation parameters were 31 mW/cm^2 and 55.8 J/cm^2 of fluence. That protocol also resulted in improvements in muscle power and delayed leg fatigue in the LED group [5]. Now, in the current study we found that the women in the LED group showed an improvement in their maximal exercise performance, probably because of the higher amount of physical training and phototherapy dose. In the first study [5], we chose the applied dose based on typical doses used in regular practice (around 60 J/cm^2 seemed reasonable). In a subsequent study [17], we chose an optimal dose (around 100 J/cm^2). Pöntinen [36] showed that a normal irradiance (dose) of 4 J/cm² at the skin level will maintain an effective irradiance at depths in the range 0.5–2.5 cm. When irradiating larger joints and muscles, the initial irradiance of 100–300 J/cm² at the skin level is attenuated to 2 J/cm^2 and effective irradiance can be maintained to depths in the range 5–10 cm [36]. In this context, several studies of phototherapy associated with physical exercise have shown that fluences above 100 J/cm^2 result in much more accentuated photobiomodulatory effects in muscle [9, 10, 16].

Although Almeida et al. [30] found a greater muscle force in a group that received phototherapy compared to a placebo group, they considered that the performance enhancement could not have been due to thermal effects in the irradiated area. The authors suggest that an intense modulation of the redox system may have occurred and also improvement in mitochondrial activity and ATP synthesis [30]. However, we believe that the improvement in physical performance can also be explained by thermal effects. Paolillo et al. [17] found differences between the thermal effects during physical exercise with and without LED irradiation. Thermal images in those performing physical exercise with LED irradiation showed significantly increased the skin temperature during exercise, and increased metabolic activity was indicated by the improved microcirculation via the vasodilator reflex [17, 37]. However, the images in those performing physical exercise without LED irradiation showed decreases in temperature, indicating a cutaneous vasoconstrictor response [38]. Therefore, the higher circulation may improve oxygen supply as well as the transport and utilization of metabolic substrates, such as lactic acid, enhancing exercise tolerance [39].

It is a well-known fact that physical training is beneficial for the cardiovascular system, especially in postmenopausal women. Several studies have confirmed these advantages [6, 7, 20]. At the same time, phototherapy has effects on cell regeneration, for example skeletal and cardiac muscle cells [40]. Oron et al. [41] have shown a reduction in infarct size in dogs following phototherapy with the Ga-As laser at 803 nm indicating a cardioprotective effect of this irradiation. Moreover, phototherapy can improve vasodilatation and angiogenesis as a result of the action of infrared and red radiation on nitric oxide [42, 43] and it can improve circulation due to thermal effects [17, 37].

A reduction in HR at isotime, which was observed in the LED group, is an important factor in reducing the risk of cardiovascular disease, because during aging a decrease in vagal modulation and an increase in sympathetic modulation can result in an increase in HR, and therefore an increase in the risk of myocardial infarction [2]. The recovery times for HR and BP were reduced only in the LED group, which indicates an improved physical condition. Studies mainly in athletes have shown that physical training reduces the recovery time as a result of physiological adaptation to exercise, such as autonomic modulation [26, 27]. Several studies investigating the use of phototherapy before exercise have shown an accelerated recovery after exercise as indicated by a decrease in blood lactate levels [8, 33].

The hemodynamic parameters in the postmenopausal women in this study were not influenced by the kidney or thyroid systems, as the groups showed normal values for urea, creatinine and TSH. Future studies including the determination of cardiorespiratory parameters using gas analysis and HR variability should be performed to investigate any possible respiratory and cardiovascular adaptations due to phototherapy associated with physical exercise.

Conclusion

This is the first study evaluating the long-term effects of LED phototherapy (6 months of LED irradiation during treadmill training) on cardiovascular adaptations and exercise performance in postmenopausal women. As expected, the subjects performed physical exercise with or without phototherapy showed an improvement in their aerobic fitness. However, infrared LED irradiation combined with treadmill training led to both a higher increase of the maximal exercise tolerance, as shown by an increase in Tlim and METs and reduced HR at isotime, and shorter HR and BP recovery times after exercise. Thus the study demonstrated that the application of

infrared LEDs potentiated the effects of physical training. These benefits are important in postmenopausal women, because they could contribute to reducing the risk of cardiovascular disease.

Acknowledgments We would like to thank the Fundação de Amparo à Pesquisa do Estado de São Paulo (FAPESP, grant nos. 98/14270-8 and 09/01842-0), the Conselho Nacional de Desenvolvimento Científico e Tecnológico (CNPq, grant no. 150949/2011-1) and the Coordenação de Aperfeiçoamento de Pessoal de Nível Superior (CAPES) for financial support. We also acknowledge the valuable technical assistance graciously provided by Ms. Juliana Cristina Milan (physical therapist) and Ms. Isabela Verzola Aniceto (medical doctor).

References

1. Lynch NA, Ryan AS, Berman DM, Sorkin JD, Nicklas BJ (2002) Comparison of VO2max and disease risk factors between perimenopausal and postmenopausal women. Menopause 9(6):456–462
2. Meersman RE, Stein PK (2007) Vagal modulation and aging. Biol Psychol 74:165–173
3. Pal GK, Pal P, Nanda N, Amudharaj D, Karthik S (2009) Spectral analysis of heart rate variability (HRV) may predict the future development of essential hypertension. Med Hypotheses 72:183–185
4. Gorodeski GI (2002) Update on cardiovascular disease in postmenopausal women. Best Pract Res Clin Obstet Gynaecol 16:329–355
5. Paolillo FR, Milan JC, Aniceto IV, Barreto SG, Rebelatto JR, Borghi-Silva A, Parizotto NA, Kurachi C, Bagnato VS (2011) Effects of infrared-LED illumination applied during high-intensity treadmill training in postmenopausal women. Photomed Laser Surg 29 (9):639–645
6. Di Blasio A, Di Donato F, Mastrodicasa M et al (2010) Effects of the time of day of walking on dietary behaviour, body composition and aerobic fitness in post-menopausal women. J Sports Med Phys Fitness 50(2):196–201
7. Kemmler W, Lauber D, Weineck J, Hensen J, Kalender W, Engelke K (2004) Benefits of 2 years of intense exercise on bone density, physical fitness, and blood lipids in early postmenopausal osteopenic women. Arch Intern Med 164:1084–1091
8. Leal Junior ECP, Lopes-Martins RAB, Barone BM et al (2009) Effect of 830 nm Low-Level Laser Therapy Applied Before High-Intensity Exercises on Skeletal Muscle Recovery in Athletes. Lasers Med Sci 24:857–863
9. Leal Junior ECP, Lopes-Martins RAB, Baroni BM et al (2009) Comparison between single-diode low-level laser therapy (LLLT) and LED multi-diode (cluster) therapy (LEDT) applications before high-intensity exercise. Photomed Laser Surg 27:617–623
10. Ferraresi C, Oliveira TB, Zafalon LO et al (2011) Effects of low level laser therapy (808 nm) on physical strength training in humans. Lasers Med Sci 26:349–358
11. Amat A, Rigau J, Waynant RW, Ilev IK, Tomas J, Anders JJ (2005) Modification of the intrinsic fluorescence and the biochemical behavior of ATP after irradiation with visible and near-infrared laser light. J Photochem Photobiol B 81:26–32
12. Karu TI, Piatybrat LV, Afanasyeva NI (2004) A novel mitochondrial signaling pathway activated by visible-to-near infrared radiation. Photochem Photobiol 80:366–372
13. Bakeeva LE, Manteifel VM, Rodichev EB, Karu TI (1993) Formation of gigantic mitochondria in human blood lymphocytes under the effect of an He-Ne laser. Mol Biol (Mosk) 27:608–617
14. Lumini-Oliveira J, Magalhães J, Pereira CV, Aleixo I, Oliveira PJ, Ascensão A (2009) Endurance training improves gastrocnemius mitochondrial function despite increased susceptibility to permeability transition. Mitochondrion 9:454–462
15. Irrcher I, Adhihetty PJ, Joseph AM, Ljubicic V, Hood DA (2003) Regulation of mitochondrial biogenesis in muscle by endurance exercise. Sports Med 33:783–793
16. De Marchi T, Leal Junior EC, Bortoli C, Tomazoni SS, Lopes-Martins RA, Salvador M (2012) Low-level laser therapy (LLLT) in human progressive-intensity running: effects on exercise performance, skeletal muscle status, and oxidative stress. Lasers Med Sci 27:231–236
17. Paolillo FR, Borghi-Silva A, Parizotto NA, Kurachi C, Bagnato VS (2011) New treatment of cellulite with infrared-LED illumination applied during high-intensity treadmill training. J Cosmet Laser Ther 13:166–171
18. American College of Sports Medicine (2006) Guidelines for exercise testing and prescription, 7th edn. Lippincott, Williams & Wilkins, Philadelphia
19. Fletcher GF, Balady GJ, Amsterdam EA et al (2011) Exercise standards for testing and training: a statement for healthcare professionals from the American Heart Association. Circulation 104:1694–1740
20. King AC, Haskell WL, Young DR, Oka RK, Stefanick ML (1995) Long-term effects of varying intensities and formats of physical activity on participation rates, fitness, and lipoproteins in men and women aged 50 to 65 years. Circulation 91:2596–2604
21. Enoksen E, Shalfawi SA, Tønnessen E (2011) The effect of high- vs. low-intensity training on aerobic capacity in well-trained male middle-distance runners. J Strength Cond Res 25:812–818
22. Riedl I, Yoshioka M, Nishida M et al (2010) Regulation of skeletal muscle transcriptome in elderly men after 6 weeks of endurance training at lactate threshold intensity. Exp Gerontol 45:896–903
23. Gibbons RJ, Balady GJ, Bricker JT et al (2002) ACC/AHA 2002 guideline update for exercise testing: summary article: a report of the American College of Cardiology/American Heart Association Task Force on Practice Guidelines (Committee to Update the 1997 Exercise Testing Guidelines). Circulation 106:1883–1892
24. Haskell WL, Lee IM, Pate RR (2007) Physical activity and public health: updated recommendation for adults from the American College of Sports Medicine and the American Heart Association. Med Sci Sports Exerc 39:1423–1434
25. Borghi-Silva A, Baldissera V, Sampaio LM et al (2006) L-carnitine as an ergogenic aid for patients with chronic obstructive pulmonary disease submitted to whole-body and respiratory muscle training programs. Braz J Med Biol Res 39:465–474
26. Ostojic SM, Markovic G, Calleja-Gonzalez J, Jakovljevic DG, Vucetic V, Stojanovic MD (2010) Ultra short-term heart rate recovery after maximal exercise in continuous versus intermittent endurance athletes. Eur J Appl Physiol 108:1055–1059
27. Lamberts RP, Swart J, Capostagno B, Noakes TD, Lambert MI (2010) Heart rate recovery as a guide to monitor fatigue and predict changes in performance parameters. Scand J Med Sci Sports 20:449–457
28. Zoll J, Ponsot E, Dufour S et al (2006) Exercise training in normobaric hypoxia in endurance runners. III. Muscular adjustments of selected gene transcripts. J Appl Physiol 100:1258–1266
29. Leal Junior EC, Lopes-Martins RA, Dalan F et al (2008) Effect of 655 nm low-level laser therapy on exercise-induced skeletal muscle fatigue in humans. Photomed Laser Surg 26:419–424
30. Almeida P, Lopes-Martins RA, De Marchi T et al (2011) Red (660 nm) and infrared (830 nm) low-level laser therapy in skeletal muscle fatigue in humans: what is better? Lasers Med Sci (Epub ahead of print). doi:10.1007/s10103-011-0957-3.
31. Gorgey AS, Wadee AN, Sobhi NN (2008) The effect of low-level laser therapy on electrically induced muscle fatigue: a pilot study. Photomed Laser Surg 26:501–506
32. Baroni BM, Leal Junior ECP, De Marchi T, Lopes AL, Salvador M, Vaz MA (2010) Low level laser therapy before eccentric

exercise reduces muscle damage markers in humans. Eur J Appl Physiol 110:789–796
33. Leal Junior ECP, Lopes-Martins RAB, Rossi RP et al (2009) Effect of cluster multi-diode light emitting diode therapy (LEDT) on exercise-induced skeletal Muscle fatigue and skeletal muscle recovery in humans. Lasers Surg Med 41:572–577
34. Baroni BM, Leal Junior ECP, Geremia JM, Diefenthaeler F, Vaz FM (2010) Effect of light-emitting diodes therapy (LEDT) on knee extensor muscle fatigue. Photomed Laser Surg 28:653–658
35. Svanberg S (2002) Tissue diagnostics using lasers. In: Waynant RW (ed) Lasers in medicine. CRC Press, Boca Raton, FL, pp 135–169
36. Pöntinen PJ (2000) Laseracupuncture. In: Simunovic Z (ed) Lasers in medicine and dentistry: basic and up-to-date clinical application of low-energy-level laser therapy (LLLT). Vitgraf, Rijeka, Croatia, pp 455–475
37. Makihara E, Makihara M, Masumi SI, Sakamoto E (2005) Evaluation of facial thermographic changes before and after low level laser irradiation. Photomed Laser Surg 23:191–195
38. Merla A, Mattei PA, Donato L, Romani GL (2010) Thermal imaging of cutaneous temperature modifications in runners during graded exercise. Ann Biomed Eng 38:158–163
39. Paolillo FR, Paolillo AR, Cliquet A Jr (2005) Cardiorespiratory responses of patients with spinal cord injuries. Acta Ortop Bras 13 (3):148–151
40. Oron U (2006) Photoengineering of tissue repair in skeletal and cardiac muscles. Photomed Laser Surg 24(2):111–120
41. Oron U, Yaakobi T, Oron A (2001) Low-energy laser irradiation reduces formation of scar tissue after myocardial infarction in rats and dogs. Circulation 103: 296–301
42. Karu TI, Piatybrat LV, Afanasyeva NI (2005) Cellular effects of low power laser therapy can be mediated by nitric oxide. Lasers in Surgery and Medicine 36:307–314
43. Yu SY, Chiu JH, Yan SD, Hsu YC, Lui WY, Wu CW (2006) Biological effect of far-infrared therapy on increasing skin microcirculation in rats. Photodermatol Photoimmunol Photomed 22:78–86

LED light attenuation through human dentin: A first step toward pulp photobiomodulation after cavity preparation

ANA PAULA S. TURRIONI, DDS, MS, JULIANA R. L. ALONSO, FERNANDA G. BASSO, DDS, PHD, LILIAN T. MORIYAMA, PHD, JOSIMERI HEBLING, DDS, PHD, VANDERLEI S. BAGNATO, PHD & CARLOS A. DE SOUZA COSTA, DDS, PHD

ABSTRACT: **Purpose:** To evaluate the transdentinal light attenuation of LED at three wavelengths through different dentin thicknesses, simulating cavity preparations of different depths. **Methods:** Forty-two dentin discs of three thicknesses (0.2, 0.5 and 1 mm; n = 14) were prepared from the coronal dentin of extracted sound human molars. The discs were illuminated with a LED light at three wavelengths (450 ±10 nm, 630 ±10 nm and 850 ±10 nm) to determine light attenuation. Light transmittance was also measured by spectrophotometry. **Results:** In terms of minimum (0.2 mm) and maximum (1.0 mm) dentin thicknesses, the percentage of light attenuation varied from 49.3% to 69.9% for blue light, 42.9% to 58.5% for red light and 39.3% to 46.8% for infrared. For transmittance values, an increase was observed for all thicknesses according to greater wavelengths, and the largest variation occurred for the 0.2 mm thickness. All three wavelengths were able to pass through the dentin barrier at different thicknesses. Furthermore, the LED power loss and transmittance showed wide variations, depending on dentin thickness and wavelength. (*Am J Dent* 2013;26:319-323).

CLINICAL SIGNIFICANCE: Determining light attenuation through the dentin barrier as a function of the wavelength is a first step toward establishing the ideal window for the biostimulation of pulpal tissue previously injured by caries lesion progression and cavity preparation.

✉: Prof. Dr. Carlos Alberto de Souza Costa, Department of Physiology and Pathology, School of Dentistry of Araraquara, Univ. Estadual Paulista, Rua Humaitá, 1680. Centro, Caixa Postal: 331 CEP: 14801903 Araraquara, SP, Brazil. E-✉: casouzac@foar.unesp.br

Introduction

Phototherapy with light-emitting diodes (LEDs) may cause intracellular photobiochemical reactions,[1] producing positive effects on different cell cultures. In recent years, several in vitro and in vivo studies have demonstrated the benefits of phototherapy at different wavelengths, such as the inhibition of cyclooxygenase I (COX-1) expression,[2,3] stimulation of collagen production,[4] increased cell proliferation[5] and accelerated wound healing.[6]

The application of light to pulp cells exposed or not to some kind of aggressive stimuli may favor pulp healing by the predictable bioinduction of reparative dentin formation.[7-9] The use of LED for pulp photobiomodulation may be an inexpensive and effective technique in clinical dentistry. Therefore, this study is a first step toward defining parameters for this type of light application.

As the carious process progresses, bacteria and/or their byproducts may penetrate the dentin tubules to reach the pulp cells.[10] This process, as well as the mechanical procedure of caries removal, may cause pulpal inflammation. It has been reported that aggressive stimuli applied to dentin also unchain the modulation of odontoblast activity, stimulating the production of reparative dentin and local sclerosis.[11] Such stimuli may result in pain and exacerbate the inflammatory pulp reaction. In this context, several dental materials and different treatment techniques have been proposed to attenuate pain of pulpal origin and control the progress of local inflammatory processes. Promising results have been achieved with phototherapy.[12]

Despite encouraging reports in the literature, controlled studies are needed to establish effective clinical protocols. Numerous factors—namely, wavelength, power density, energy dose, exposure area and irradiation time - may contribute to the validity of an irradiation protocol as effective in obtaining certain effects, whether biostimulatory or not.[13,14] Among these factors, wavelength is of paramount importance because it determines the depth of light penetration into the target tissue.[15] It has been demonstrated that distinct wavelengths result in different coefficients of absorption, depths of penetration and scattering in the same tissue.[15,16]

The physical and chemical constituents of the tissues are also important factors to be considered in photobiostimulation, because tissues are heterogeneous from an optical standpoint, and thus absorb and reflect energy differently.[15] The importance of this difference in light absorption relies on the fact that, for each wavelength, different extinction coefficients affect the penetration depth through tissues.[15] Once absorbed by the cell, luminous energy is converted into photochemical energy. Depending on its irradiance (power/area), light can stimulate molecules by activating several biochemical cascades, such as the cell respiratory chain, while for longer wavelengths excitation seems to occur through the cell membrane.[16]

Despite its positive clinical effects, little is known about the mechanisms of LED light transmission through dentin and the ideal energy dose required to cause biostimulation of pulp cells of teeth previously subjected to an aggressive stimulus. This study may help determine parameters for pulp cell biostimulation. Therefore, our aim was to evaluate the transdentinal light attenuation of LED at three wavelengths through different dentin thicknesses.

Materials and Methods

Forty-two dentin discs were cut transversely from the middle portion of the tooth crowns of sound human third molars, by means of a precision cutting machine (Isomet 1000[a]). The teeth were free of surface-adhering debris, cracks,

American Journal of Dentistry, Vol. 26, No. 6, December, 2013

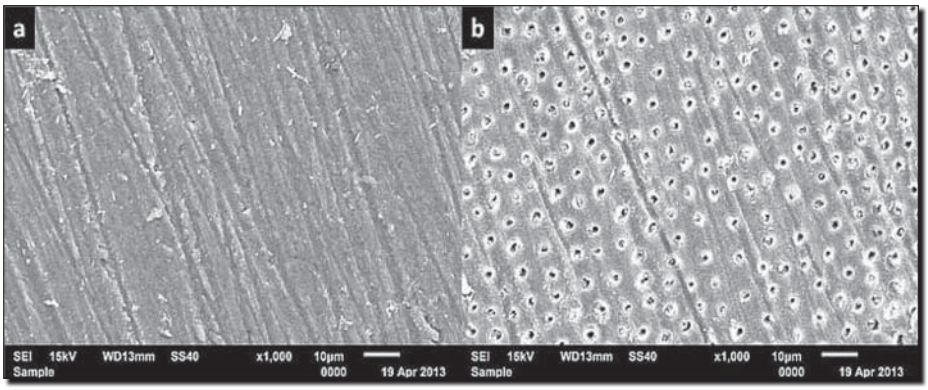

Fig. 1. (a) Surface of a dentin disc covered by smear layer. (b) Surface of a dentin disc subjected to EDTA treatment. Note that the smear layer removal allowed observing a number of dentin tubules. SEM, original magnification ×1000.

defects or morphological alterations and were obtained from the Human Tooth Bank of Araraquara School of Dentistry, UNESP, Brazil, after approval of the research project by the University Research Ethics Committee (Protocol 26/09). Disc refinement was made with a water-cooled cylindrical diamond bur (#1095[b]) in a high-speed handpiece to obtain discs with a final diameter of 8 mm. The discs were cut from mid-crown dentin as close as possible to the pulp region but without the presence of pulp horns or any other structures that could interfere with light transmission.

The dentin discs were divided into three groups (n = 14), according to thickness (0.2 mm, 0.5 mm and 1 mm), to simulate the clinical conditions of irradiation of the floor of, respectively, very deep, deep and medium cavities prepared in human teeth. A 0.5 M ethylenediaminetetraacetic acid (EDTA) solution (pH 7.2) was applied to the surfaces of the discs (occlusal and pulpal) for 2 minutes for superficial cleaning and removal of the smear layer,[17] after which the discs were thoroughly rinsed with sterile deionized water for 60 seconds and then immersed in 1 mL of the same solution for 72 hours. Therefore, wet dentin discs were used for all light transmittal evaluations. Figure 1 shows scanning electron microscopy images of a dentin disc before and after EDTA application.

The transdentinal light attenuation was measured at 450 ±10 nm (blue), 630 ±10 nm (red) and 850 ±10 nm (infrared) wavelengths by illuminating the discs in the occlusal-to-pulpal direction via a light power sensor (LM-2 VIS[c]). These wavelengths were selected because they have been used in other study protocols and in clinical applications like photopolymerization (blue light), photodynamic therapy[3] (blue and red light) and tissue or cell biostimulation/wound healing[6,14,18,19] (blue, red and infrared light).

Fourteen samples were used in each group, and this was considered statistically representative for this in vitro study. Each sample was measured only once for each wavelength. According to the manufacturer, the high-sensitivity sensor used in these experiments has a resolution of 1 nW and can detect light at wavelengths ranging from 400 to 1060 nm. This sensor was coupled to a power meter (Field Master[c]) set to measure light power at the specific wavelengths used.

This test determined the light attenuation that could occur through the dentin structure during the irradiation of discs of different thicknesses for each wavelength. The pulpal side of the disc was in contact with the light power sensor, while the light beam of the LED source (λ = 450, 630 and 850 ±10 nm) was directed to the occlusal side of the disc at a fixed distance (6 cm) such that the disc could be illuminated uniformly.[20] The time of LED application in each disc was 3 seconds. An acrylic cylinder was attached to the LED light guide tip to collimate the light and direct it to the disc-sensor set area. The diameter of the active area of the sensor (6 mm) was smaller than that of the dentin discs (8 mm). The discs were then positioned in the central region of the device containing the sensor and were not manipulated during irradiation. The LED source was regulated to reach maximum power of 30 mW, which is the detection limit of the light power sensor used. The percent light attenuation in each disc was calculated by the ratio between illumination with and without interposition of the 0.2, 0.5 and 1 mm-thick dentin discs.

In addition to the measurement of light attenuation, five dentin discs of each thickness (0.2, 0.5 and 1 mm) were randomly selected for measurement of light transmittance (three readings for each sample) in the region of the spectrum from 400 nm to 850 nm. Each disc was individually adapted to a metallic device, and the disc-device set was viewed spectrophotometrically (Varian Cary 50 Bio - UV-VIS[d]), which generated light transmittance readings from which a graph was prepared showing percent values of the light transmitted through dentin.

The transdentinal light attenuation (%) data were subjected to two-way ANOVA (wavelength × dentin thickness) and Tukey's test for pairwise multiple comparisons of groups (SPSS 13.0 for Windows[e]). A significance level of 5% was set for all analyses.

Results

The transdentinal light attenuation values (%) during illumination of the discs with LEDs at the three wavelengths are shown in Table 1. Both factors (wavelength and dentin thickness) significantly influenced light attenuation. When each variable was considered alone, greater light attenuation occurred with 450 ±10 nm (blue) (58.1 ± 9.8; n = 42), followed by 630 ±10 nm (red) (50.9 ± 7.1; n = 42) and 850 ±10 nm (infrared) (44.9 ± 5.7; n = 42), with a statistically significant difference ($P < 0.05$) among them. For dentin thickness, greater light attenuation occurred with 1 mm-thick discs (58.4 ± 10.0; n = 14), followed by thicknesses of 0.5 mm (52.0 ± 5.2; n = 14) and 0.2 mm (43.5 ± 5.3; n = 13), with a statistically significant

Table. Light attenuation (%) according to LED wavelength and dentin disc thickness.

	Dentin disc thickness (mm)		
LED wavelength (nm)	0.2	0.5	1.0
450 ±10 (blue)	48.3 (4.0) cd*	56.0 (4.2) e	69.9 (3.9) f
630 ±10 (red)	42.9 (3.2) ab	51.4 (3.8) d	58.5 (2.1) e
850 ±10 (infrared)	39.3 (4.2) a	48.6 (4.9) cd	46.8 (3.2) bc

*Values represent mean (standard deviation) of light attenuation for each dentin thickness (n= 14). Means followed by same letters do not differ significantly (Tukey, P> 0.05).

difference among all thicknesses (P< 0.05).

For factor interaction, the lowest light attenuation was obtained from the irradiation of 0.2 mm-thick discs with LED of 850 ±10 nm (infrared) (39.3 ± 4.2) and 630 ±10 nm (red) (42.9 ± 3.2) wavelengths, while the greatest light attenuation was obtained from the irradiation of 1 mm-thick discs with blue LED (450 ±10 nm wavelength) (69.9 ± 3.9). These values were significantly different from each other and from the values obtained for all other groups (P< 0.05).

We also measured the mean values of light transmittance in the region of the spectrum from 400 nm to 850 nm for each dentin thickness (Fig. 2). We observed that light transmittance values decreased with increased dentin thickness. In addition, we observed that for all dentin thicknesses, the longer the wavelength, the greater the transdentinal light transmittance.

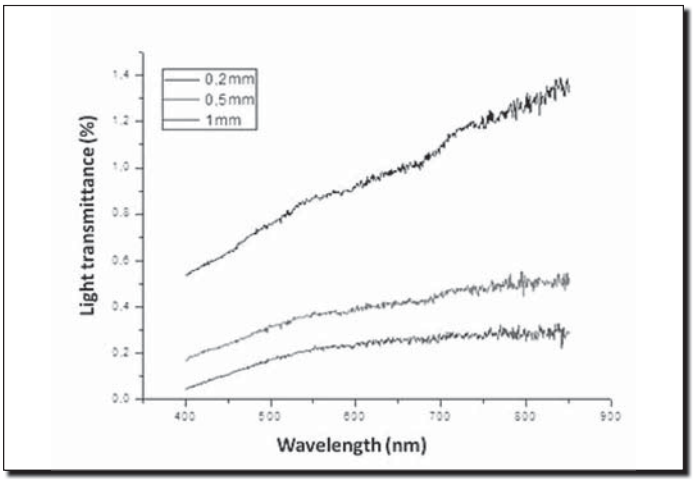

Fig. 2. Mean values of light transmittance in the region of the spectrum from 400 nm to 850 ± 10 nm for dentin thicknesses of 0.2 mm, 0.5 mm and 1 mm.

Discussion

Phototherapy with LED light has been used in dentistry for the treatment of several different conditions, including oral mucositis,[6,21] candidiasis,[22] and dentin hypersensitivity[23] as well as for the decontamination of carious cavities.[24] Particularly for the biostimulation of pulpal tissue, a recent study reported that LED irradiation can stimulate the metabolism and proliferation of cells as well as increase the mineral deposition by human dental pulp cells.[25]

It has been reported that the effects of light in reducing dentin hypersensitivity seems to be due to its capacity to increase the excitation threshold of the free nerve endings in the pulp, stimulating the differentiation of mesenchymal stem cells into osteoblasts, and activating these cells for synthesizing and producing the collagen-rich reparative dentin matrix.[7,26] However, to obtain any beneficial effect on the pulp, the light must be transmitted across the dentin structure to reach the pulp cells with sufficient energy to cause biostimulation. Therefore, in the present study, we evaluated the transdentinal transmission of LEDs at three wavelengths, varying the dentin thicknesses. Dentin discs with different thicknesses were used in this study in order to simulate clinical situations in which variable dentin thickness may remain between the cavity floor and the pulp cells after a dental cavity preparation. Our results revealed that both the wavelength and the dentin thickness significantly influenced the propagation of LED light through the tubular dentin structure.

The discs with 0.2 mm thickness allowed for the greater transmission of light, followed by thicknesses of 0.5 and 1 mm. It is known that dentin has a tubular structure (Fig. 1b) and that the relative numbers (tubular density) and diameters of tubules increase from the outer to the inner layers of dentin and close to the pulp tissue.[27] In addition, due to the anisotropic property of dentin, variable light propagation in this tissue occurs according to the aligned microstructure of this tubular structure.[27] In this way, the transdentinal transmission of LED light is different depending on the dentin region, resulting in non-homogeneous irradiation.[28,29] In the present study, all discs were obtained from the same tooth region (middle portion of the tooth crown, close to the pulp), to reduce any possible interference caused by variations in the dentin structure. Additionally, at the moment of irradiation, the discs were positioned with their occlusal side faced upward.

Kienle et al[27] investigated the optical magnification/reduction effects of dentin and concluded that transdentinal light propagation is due to multiple scattering by the dental microstructure. According to this theory, although the tubules are the main scatterers of light in dentin, part of the incident light is also reflected through the peritubular dentin, and part is transmitted through the adjacent intertubular dentin. Therefore, it may be considered that the lack of structural homogeneity of dentin interferes with light transmission through the tubular structure of this tissue. In addition to the influence of different dentin thicknesses, we also found a direct relationship among the different wavelengths and light transmission.

Illumination of the discs with infrared light (850 ±10 nm) resulted in greater transdentinal light transmission, followed by red light (630 ±10 nm) and blue light (450 ±10 nm). Wavelength is important because it defines the depth of light penetration into the target tissue.[30] It has been demonstrated that distinct wavelengths present different absorption coefficients in the same tissue.[30] In other words, since ultraviolet radiation has a high absorption coefficient, it has low penetration capacity, and its absorption occurs in the most superficial layers, while the low absorption coefficient of infrared radiation results in deeper penetration.

The light transmittance values shown in Fig. 2 for dentin thickness and LED wavelength reinforce the concept that the thinner the irradiated tissue and the longer the LED wavelength, the more the transdentinal light transmission is increased. Arikawa et al[31] evaluated light attenuation in dentin discs irradiated with xenon lamps in the wavelength region of 380 to 550 nm, which covers the range of absorption wavelengths of the catalyst system of conventional light-activated restorative res-

ins. As in the present study, those authors demonstrated that the longer the wavelength, the greater the transdentinal light transmittance. However, they evaluated only light in the blue band of the electromagnetic spectrum applied to 1 mm-thick dentin discs. In the present study, three wavelengths corresponding to different bands in the light spectrum (blue, red and infrared) were applied to dentin discs with thicknesses ranging from 0.2 mm to 1 mm.

It is interesting to observe that the spectrophotometric measurements provided transmittance values two orders of magnitude lower than those of transdentinal light attenuation with LED. This can be justified by the fact that the spectrophotometer contains a filament lamp and two diffraction gratings. During measurements, the gratings are rotated automatically, and, as a result, each wavelength (every 0.5 nm) is measured individually; that is, a small bundle passes through the specimen, and only the specific wavelength is considered for measurement. However, for measurement of the transdentinal light attenuation of LED, the entire spectral band is considered.

It is thus relevant to investigate light propagation in different dentin thicknesses and wavelengths. Wavelengths between 400 and 500 nm have a positive effect on tissues due to high absorption by flavins, while wavelengths above 500 nm are better absorbed by cytochrome c oxidase, which is the terminal enzyme in the respiratory chain.[32,33] This difference is important because cascades activated by the different wavelengths may generate different cell responses. Activation of cytochrome c oxidase leads to a greater synthesis of ATP by the cells, with a consequent increase in energy by oxidative phosphorylation.[1] Conversely, flavins are small, water-soluble molecules known to initiate free-radical reactions when excited by light at wavelengths below 500 nm.[33] These reactions may produce positive or negative effects on the cells, depending on the intensity of the stimulus.[14]

In the present study, LED irradiation at 850 ± 10 nm and 450 ± 10 nm wavelengths facilitated increased and reduced transmission of light through the dentin structure, respectively. It is important to emphasize that, to date, specific parameters for the use of LED in research studies have not yet been established, especially in studies investigating the transdentinal effect of irradiation on pulp cell cultures. Therefore, the methodology used in the present study and the obtained results may help guide future investigations. Knowing the light attenuation that occurred during irradiation of different dentin thicknesses with a specific LED wavelength will make it possible to determine ideal parameters for the biostimulation of pulp cells in vivo, thus improving the healing of injured dental pulp. However, although it is essential to know light attenuation as a function of wavelength, it is also important to know the action spectrum for the desired effect. It is possible that a wavelength with lower attenuation will be more effective if it coincides with a peak of the action spectrum. Therefore, determining light attenuation through the dentin barrier as a function of wavelength is a first step toward establishing the ideal window for biostimulation of the pulp. A wavelength with low light attenuation could be the most effective for the biostimulatory effect desired.

The results of our experimental study indicated that all wavelengths were able to pass through the dentin barrier at different thicknesses. Furthermore, the power loss and transmittance of LED irradiation were directly influenced by dentin thickness and wavelength. Further studies are indicated to define the optimal parameters for pulp photobiomodulation in teeth subjected to cavity preparation.

a. Buehler Ltd., Lake Bluff, IL, USA.
b. KG Sorensen, Barueri, SP, Brazil.
c. Coherent, Santa Clara, CA, USA.
d. Varian Indústria e Comércio Ltda, São Paulo, SP, Brazil.
e. SPSS Inc., Chicago, IL, USA.

Acknowledgement: To the Institute of Physics of the University of São Paulo for making its laboratories available to the authors.

Disclosure statement: The authors declared no conflict of interest. State of São Paulo Research Foundation – FAPESP (grants #2011/13895-0) and the National Council for Scientific and Technological Development – CNPq (grant # 301291/2010-1) for financial support.

Dr. Turrioni is a PhD student, Ms. Alonso is a predoctoral dental student, Dr. Basso is a Post-Doctoral Researcher, Dr. Hebling is Associate Professor and Dr. de Souza Costa is Full Professor, Araraquara School of Dentistry, UNESP – Univ. Estadual Paulista, Araraquara, São Paulo, Brazil. Dr. Moriyama is Senior Researcher and Dr. Bagnato is Full Professor, University of São Paulo, São Carlos, São Paulo, Brazil.

References

1. Karu TI, Kolyakov SF. Exact action spectra or cellular responses relevant to phototherapy. *Photomed Laser Surg* 2005;23:355-361.
2. Lim W, Lee S, Kim I, Chung M, Kim M,, Lim H, Paark J, Kim O, Choi H. The anti-inflammatory mechanism of 635 nm light-emitting-diode irradiation compared with existing COX inhibitors. *Lasers Surg Med* 2007;39:614-621.
3. Machado AH, Pacheco Soares C, da Silva NS, Moraes KC. Cellular and molecular studies of the initial process of the photodynamic therapy in HEp-2 cells using LED light source and two different photosensitizers. *Cell Biol Int* 2009;33:785-795.
4. Huang PJ, Huang YC, Su MF, Yang TY, Huang JR, Jiang CP. In vitro observations on the influence of copper peptide aids for the LED photoirradiation of fibroblast collagen synthesis. *Photomed Laser Surg* 2007;25:183-190.
5. Hawkins D, Abrahamse H. How long after laser irradiation should cellular responses be measured to determine the laser effect? *J Laser Appl* 2007;19:74-83.
6. Sacono NT, Costa CA, Bagnato VS, Abreu-e-Lima FC. Light-emitting diode therapy in chemotherapy-induced mucositis. *Lasers Surg Med* 2008;40:625-633.
7. Romanos GE, Pelekanos S, Strub JR. Effects of Nd:YAG laser on wound healing processes: Clinical and immuno-histochemical findings in rat skin. *Lasers Surg Med* 1995;16:368-379.
8. Tate Y, Yoshiba K, Yoshiba N, Iwaku M. Odontoblast responses to GaAIAs laser irradiation in rat molars: An experimental study using heat-shock protein-25 immunohistochemistry. *Eur J Oral Sci* 2006;114:50-57.
9. Ferreira AN, Silveira S, Genovese WJ, Cavalcante de Araújo V, Frigo L, de Mesquita RA, Guedes E. Effect of GaAIAs laser on reactional dentinogenesis induction in human teeth. *Photomed Laser Surg* 2006; 24:358-365.
10. Wambier DS, dos Santos FA, Guedes-Pinto AC, Jaeger RG, Simionato MR. Ultrastructural and microbiological analysis of the dentin layers affected by caries lesions in primary molars treated by minimal intervention. Pediatr Dent 2007;29:228-234.
11. Nakamura Y, Hammarström L, Matsumoto K, Lyngstadaas SP. The induction of reparative dentine by enamel proteins. *Int Endod J* 2002;35:407-417.
12. Villa GEP, Catirse ABCED, Lia RCC, Lizarelli RFZ. In vivo analysis of low-power laser effects irradiation at stimulation of reactive dentine. *Laser Phys Lett* 2007;4:690-695.
13. Almeida-Lopes L, Rigau J, Zângaro RA, Guidugle-Neto J, Jaeger MMM. Comparison of the low level laser therapy effects on cultured human gingival fibroblasts proliferation using different irradiance and same fluence. *Lasers Surg Med* 2001;29:179-184.
14. Silveira PC, Silva LA, Freitas TP, Latini A, Pinho RA. Effects of low-power laser irradiation (LPLI) at different wavelengths and doses on oxi-

dative stress and fibrogenesis parameters in an animal model of wound healing. *Lasers Med Sci* 2011;26:125-131.
15. Neupane J, Ghimire S, Shakya S, Chaudhary L, Shrivastava VP. Effect of light emitting diodes in the photodynamic therapy of rheumatoid arthritis. *Photodiagnosis Photodyn Ther* 2010;7:44-49.
16. Karu TI. Photobiological fundamentals of low power laser therapy. *IEEE J Quantum Electron* 1987;23:1703-1717.
17. de Souza PPC, Hebling J, Scalon MG, Aranha AM, Costa CAS. Effects of intrapulpal temperature change induced by visible light units on the metabolism of odontoblast-like cells. *Am J Dent* 2009;22:151-156.
18. Gritsch K, Ponsonnet L, Schembri C, Farge P, Pourreyron L, Grosgogea B. Biological behaviour of buccal cells exposed to blue light. *Mater Sci Eng C* 2008;28:805-810.
19. Lewis JB, Wataha JC, Messer RL, Caughman GB, Yamamoto T, Hsu SD. Blue light differentially alters cellular redox properties. *J Biomed Mater Res B Appl Biomater* 2005;72:223-229.
20. Turrioni APS, Oliveira CF, Basso FG, Moriyama LT, Kurachi C, Hebling J, Bagnato VS, Costa CA. Correlation between light transmission and permeability of human dentin. *Lasers Med Sci* 2012;27:191-196.
21. Corti L, Chiarion-Sileni V, Aversa S, Ponzoni A, D'Arcais R, Pagnutti S, Fiore D, Sotti G. Treatment of chemotherapy-induced oral mucositis with light-emitting diode. *Photomed Laser Surg* 2006;24:207-213.
22. Mima EG, Pavarina AC, Dovigo LN, Vergani CE, Costa CA, Kurachi C, Bagnatto VS. Susceptibility of Candida albicans to photodynamic therapy in a murine model of oral candidosis. *Oral Surg Oral Med Oral Pathol Oral Radiol Endod* 2010;109:392-401.
23. Lizarelli RFZ, Miguel FAC, Villa GEP, Carvalho Filho E, Pelino JEP, Bagnato VS. Clinical effects of low intensity laser vs light-emitting diode therapy on dentin hypersensitivity. *J Oral Laser Appl* 2007;7:129-136.
24. Araujo PV, Cortes ME, Poletto LTA. Photodynamic therapy of cariogenic agents: A systematic review. *J Laser Appl* 2010;22:13-21.
25. Holder MJ, Milward MR, Palin WM, Hadis MA, Cooper PR. Effects of red light-emitting diode irradiation on dental pulp cells. *J Dent Res* 2012;91:961-966.
26. Gerschman JA, Ruben J, Gebart-Eaglemont J. Low level laser therapy for dentinal tooth hypersensitivity. *Aust Dent J* 1994;39:353-357.
27. Kienle A, Michels R, Hibst R. Magnification: A new look at a long-known optical property of dentin. *J Dent Res* 2006;85:955-959.
28. Vaarkamp J, ten Bosch JJ, Verdonschot EH. Propagation of light through human dental enamel and dentine. *Caries Res* 1995;29:8-13.
29. Zolotarev VM, Grisimov VN. Architectonics and optical properties of dentin and dental enamel. *Opt Spectrosc* 2001;90:753-759.
30. Meglinski IV, Matcher SJ. Quantitative assessment of skin layers absorption and skin reflectance spectra simulation in the visible and near-infrared spectral regions. *Physiol Meas* 2002;23:741-753.
31. Arikawa H, Kanie T, Fujii K, Ban S, Takahashi H. Light-attenuating effect of dentin on the polymerization of light-activated restorative resins. *Dent Mater J* 2004;23:467-473.
32 Laloraya MM, Pradeep KG, Laloraya M. Photochemical reaction sequences of blue light activated flavins: Sensory transduction through free radical messengers. *Biochem Mol Biol Int* 1994;33:543-551.
33. Eichler M, Lavi R, Shainberg A, Lubart R. Flavins are source of visible-light-induced free radical formation in cells. *Lasers Surg Med* 2005; 37:314-319.

Lasers Med Sci (2013) 28:1271–1280
DOI 10.1007/s10103-012-1223-z

ORIGINAL ARTICLE

Low-level laser therapy (LLLT) combined with swimming training improved the lipid profile in rats fed with high-fat diet

Antonio E. Aquino Jr. · Marcela Sene-Fiorese · Fernanda R. Paolillo · Fernanda O. Duarte · Jorge C. Oishi · Airton A. Pena Jr. · Ana C. G. O. Duarte · Michael R. Hamblin · Vanderlei S. Bagnato · Nivaldo A. Parizotto

Received: 6 June 2012 / Accepted: 25 October 2012 / Published online: 14 November 2012

Abstract Obesity and associated dyslipidemia is the fastest growing health problem throughout the world. The combination of exercise and low-level laser therapy (LLLT) could be a new approach to the treatment of obesity and associated disease. In this work, the effects of LLLT associated with exercises on the lipid metabolism in regular and high-fat diet rats were verified. We used 64 rats divided in eight groups with eight rats each, designed: SC, sedentary chow diet; SCL, sedentary chow diet laser, TC, trained chow diet; TCL, trained chow diet laser; SH, sedentary high-fat diet; SHL, sedentary high-fat diet laser; TH, trained high-fat diet; and THL, trained high-fat diet laser. The exercise used was swimming during 8 weeks/90 min daily and LLLT (GA-Al-As, 830 nm) dose of 4.7 J/point and total energy 9.4 J per animal, applied to both gastrocnemius muscles after exercise. We analyzed biochemical parameters, percentage of fat, hepatic and muscular glycogen and relative mass of tissue, and weight percentage gain. The statistical test used was ANOVA, with post hoc Tukey–Kramer for multiple analysis between groups, and the significant level was $p<0.001$, $p<0.01$, and $p<0.05$. LLLT decreased the total cholesterol ($p<0.05$), triglycerides ($p<0.01$), low-density lipoprotein cholesterol

A. E. Aquino Jr. · M. Sene-Fiorese · F. R. Paolillo · V. S. Bagnato
Optics Group from Institute of Physics of São Carlos (IFSC),
University of São Paulo (USP),
São Carlos, Brazil

A. E. Aquino Jr. · F. O. Duarte · J. C. Oishi · A. A. Pena Jr. · A. C. G. O. Duarte
Laboratory of Nutrition and Metabolism Applied to Exercise,
Physical Education and Motor Human Department,
Federal University of São Carlos (UFSCar),
São Carlos, Brazil

A. E. Aquino Jr. · V. S. Bagnato · N. A. Parizotto
Biotechnology Post Graduation Program,
Federal University of São Carlos (UFSCar),
São Carlos, Brazil

M. Sene-Fiorese
Physical Education Department,
University Camilo Castelo Branco,
AV: Hilário da Silva Passos,
13690-970 Descalvado, São Paulo, Brazil

M. R. Hamblin · N. A. Parizotto
Wellman Center for Photomedicine,
Massachusetts General Hospital,
Boston, MA, USA

M. R. Hamblin · N. A. Parizotto
Department of Dermatology, Harvard Medical School,
Boston, MA, USA

M. R. Hamblin
Harvard-MIT Division of Health Sciences and Technology,
Cambridge, MA, USA

N. A. Parizotto
Electrothermophototherapy Laboratory, Department of Physical Therapy, Federal University of São Carlos (UFSCar),
São Carlos, Brazil

A. E. Aquino Jr. (✉) · N. A. Parizotto (✉)
Federal University of São Carlos (UFSCar),
Via Washington Luis, km 235, Monjolinho,
13565-905 São Carlos, São Paulo, Brazil
e-mail: spydera@ig.com.br
e-mail: parizoto@ufscar.br

($p<0.05$), and relative mass of fat tissue ($p<0.05$), suggesting increased metabolic activity and altered lipid pathways. The combination of exercise and LLLT increased the benefits of exercise alone. However, LLLT without exercise tended to increase body weight and fat content. LLLT may be a valuable addition to a regimen of diet and exercise for weight reduction and dyslipidemic control.

Keywords Exercise · Metabolism · LLLT · Photobiomodulation · Obesity · Dyslipidemia.

Introduction

The pathogenesis of obesity is complex and not well understood. It is fundamentally a problem of energy balance, which can develop only when energy intake is in excess of energy expenditure. This fact has led to a major focus on the mechanisms controlling food intake and the components and regulatory mechanisms of energy expenditure [1]. Eating high-fat or high-calorie food associated with a sedentary lifestyle facilitates the development of a positive energy balance [1]. Obesity is strongly associated with many chronic diseases, such as hypertension, diabetes, coronary heart disease, cancer, nonalcoholic fatty liver disease, and dyslipidemias [2, 3]

Physical activity is already established as an important nonpharmacological strategy for control of obesity or high body-fat percentage and for the treatment of associated diseases [4]. Several clinical and experimental studies have demonstrated that a moderate exercise regimen combined with a normocaloric diet resulted in the reduction of adiposity and improved lipid profile [5, 6]. However, due to the increased incidence of obesity in the world, it becomes necessary to seek new noninvasive and nonpharmacological strategies to increase the physiological effects of exercises.

Several studies have investigated low-level laser therapy (LLLT) or light-emitting diode (LED) therapy and have made advances in the understanding of the underlying mechanisms LLLT in biological systems [7–9]. The main characteristics of photobiomodulation or photobiostimulation are the induction and stimulation of many aspects of cellular processes. According to Karu [10], the cellular redox state is an important determinant of the final response, and there are three signaling pathways that operate relating to cell attachment, mitochondrial respiratory chain, and Na, K-ATPase. Moreover, results suggest that specific wavelengths, such as red and near-infrared radiation, can create, regulate, or activate enzymatic processes in cells to improve metabolism [8].

There is still much to elucidate about the mechanisms underlying LLLT and how it acts on cells and tissues, but there is evidence that the response usually exhibit a biphasic dose–response profile [11]. In the adipose tissues, some authors have attempted to modify their metabolism using LLLT, and some clinical studies [12, 13] tried to explain how there could be the reduction of body contours promoted by the LLLT, including the transitory induction of pores in the membranes of the adipocytes and consequently liberation of intracellular constituents (fat) and its removal and metabolism; however, the mechanisms still remain unclear.

For this reason, parameters such as quantity hepatic and muscle glycogen, the percentage of lipids in different tissues, as well as triglycerides, total cholesterol, high-density lipoprotein (HDL) cholesterol and low-density lipoprotein (LDL) cholesterol may provide the state of health of individuals, as well as can be used to monitor the systemic of conditions, which are distributed the products of the metabolism of fat and sugar [5, 14, 15].

Nevertheless, only a few studies have described LLLT combined with exercise training, for example, in young males [8], postmenopausal women [9], or overweight individuals [16]. Thus, our goal was to perform a randomized controlled trial to investigate the effects of the LLLT associated with exercise training on lipid profile in rats fed with different diets. Our hypothesis was that combined exercise with LLLT could control the serum lipids and modify the lipid metabolism in animals with normocaloric and hypercaloric diet. If successful, this combination could play an important role in control of diseases associated with obesity.

Methods and procedures

Animals

All animal procedures were performed according to the principles in the Guide for the Care and Use of Laboratory Animals and were approved by the Institutional Animal Ethics Committee (number 067/2010). Sixty-four male Wistar rats (90 days old and weight of 317.00±19.16 g) were included in this study. Before beginning the experimental protocol, all of the groups [except for the normocaloric groups (N)] were fed ad libitum with the hyperlipidic diet (H) for 3 weeks [14] for the development of obesity and dyslipidemia. The animals were randomized according to diet into eight groups with eight rats each ($n=8$): normocaloric diet (N) groups—sedentary normal diet (SN), trained normal diet (TN), sedentary normal diet plus laser (SNL), and trained normal diet plus laser (TNL); hypercaloric high-fat diet (H) groups—sedentary high-fat diet (SH), trained high-fat diet (TH), sedentary high-fat diet plus laser (SHL), and trained high-fat diet plus laser (THL). Rats were kept

one per cage with food and water ad libitum (8 weeks), on a 12:12-h light–dark cycle at 23±1 °C.

Diet

The experimental groups received the following diet: the normocaloric diet (N)—MP-77 standard rat chow diet provided in pellet form (Primor®, São Paulo, Brazil) containing 23 g of protein, 49 g of carbohydrate, 4 g of total fat, 5 g of fiber, 7 g of ash, and 6 g of vitamins per 100 g diet. The hypercaloric diet consisted of the same commercial rat chow plus peanuts, milk chocolate, and sweet biscuit in a proportion of 3:2:2:1. It contained 5.12 kcal/g (35 % of calories as fat) for the hypercaloric high-fat diet and 4.07 kcal/g for the normocaloric diet [14].

Exercise and LLLT protocols

The exercise program consisted of swimming in individual tanks (Fig. 1) filled with water, maintained at 28–32 °C. The animals of the trained groups swam for 30, 60, and 90 min on the first, second, and third days to adapt. The swimming period was then increased to 90 min/day, during 5 days/week. All rats swam with a load of 3–5 % body mass attached to the trunk by a jacket. The exercise protocols were performed for 5 days/week during 8 weeks. This program is considered to be of moderate intensity [5].

The LLLT parameters are shown in Table 1. It was irradiated transcutaneously on the muscles of the rat's paw (one point on quadriceps and other point on gastrocnemius). The energy density of laser irradiation and the anatomical points were chosen based on previous studies [8]. We decided not to use sham group because we have a positive control (hypercaloric diet and treated with LLLT), a negative control (hypercaloric diet and not treated with LLLT), as well as positive (hypercaloric) and negative (normocaloric) controls for the factor diet, with or without laser treatment.

The laser was applied after the exercises because the advantage of using the stress induced to get the maximum of absorption and effects on metabolism. It was used the same protocol before in different papers from our laboratory [17].

Fig. 1 The training of swimming in individual tanks at controlled temperature (T=30 °C)±2. It is possible to see the jacket attached to the trunk during the training session

Experimental procedure

At the end of 8 weeks of training and after a 24-h rest period, analysis was performed. All animals were euthanized by decapitation. The collected blood was immediately centrifuged and frozen at −80 °C. The heart (H), liver (L), gastrocnemius muscle (GAST), soleus muscle (SOL), the white adipose tissues (epididymal (EPI) retroperitoneal (RET), visceral (VIS)), and the interscapular brown adipose tissue (BAT) were immediately removed, weighted, and frozen at −20 °C.

Hepatic and muscular glycogen and percentage of lipids of tissues

The muscle and liver glycogen was determined by colorimetric method, which assesses the concentration of glycosyl-glucose using a standard of 100 nmol of glucose and determined using a ultraviolet/visible spectrophotometer Biospectro® SP220 [18]. The percentage of lipid content in the tissue was determined by the gravimetric method [6].

Serum analysis

Total cholesterol (CHOL-total), triacylglycerol (TG), and high-density lipoprotein cholesterol (HDL-c) in the serum were determined enzymatically (Laborlab® kits) using a spectrophotometer [6]. The low-density lipoprotein (LDL-c) was calculated by Friedewald equation [19].

Statistical analysis

All data were expressed as a mean and standard deviation. The Kolmogorov–Smirnov test was used to analyze the normality. For statistical evaluation of the metabolic parameters, a one-way ANOVA test with post hoc analysis (Tukey–Kramer multiple comparisons) was used between groups. Instat 3.0 for Windows 7 (Graph Pad, San Diego, CA, USA, 1998) was used for the statistical analysis and the significance level was given as $p<0.001$, $p<0.01$, and $p<0.05$.

Table 1 Characteristics of the laser used in the experimental procedures

These are the characteristics of equipment and wavelength used during the study. All applications were realized to the same person (Theralase, DMC, Equipment, São Carlos, SP, Brazil)

Type	Ga-Al-As	Treatment time	47 s
Wavelength	830 nm (infrared)	Number of points	2 points
Frequency	Continuous wave (CW)	Total energy delivered	9.4 J
Optical output	100 mW	Application mode: probe held stationary in skin contact with a 90º angle and slight pressure. Used always after the training session.	
Spot diameter	0.6 mm		
Power density	35.36 W/cm^2		
Energy per point	4.7 J/point		
Energy density	1,662 J/cm^2		

Results

Body mass and relative mass of tissues

Effects of type diet and exercise

The body mass gain differences are shown in Fig. 2 as the percentage of gain depending on diet used and treatments. High-fat diet promoted in the sedentary group an increase in EPI, RET, and BAT relative weight compared with as observed in the sedentary rats fed with chow diet group (SN), but the relative weight of liver, VIS, GAST, SOL, and heart was not significantly affected by this diet (Table 2). In the TH group, there was a significant reduction in relative weight of RET when compared with SH group. In the same comparison, the EPI declined 18 % in their relative weight. In contrast, no difference was observed in relative weight of tissues when comparing SN and TN groups (Table 2).

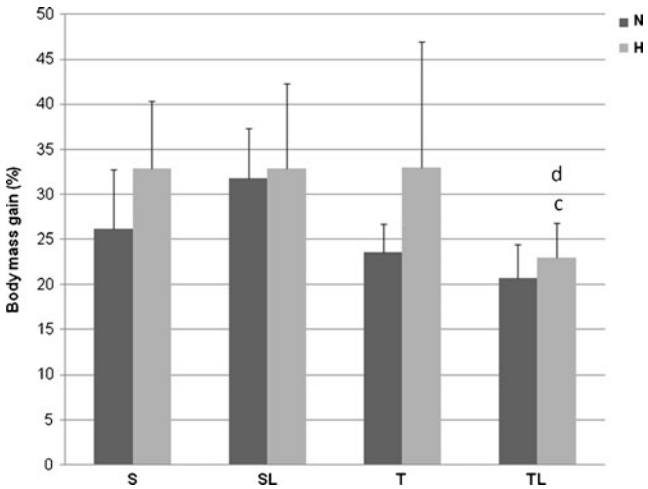

Fig. 2 Values of weight gain in percentage of two series of animals: normocaloric diet (N) and hypercaloric diet (H). Different superscripts (*a* S versus SL; *b* S versus T; *c* SL versus TL; *d* T versus TL; *e* effects of high-fat diet in the different protocols) are significantly different (Tukey–Kramer multiple comparisons for $p<0.05$ except the specific comparisons: SHL×THL $p<0.05$, TH×THL $p<0.05$). The groups are designed: *S* sedentary; *SL* sedentary laser; *T* trained; *TL* trained laser

Effects of LLLT combined with diet and exercise

In the LLLT sedentary groups (SNL and SHL), the relative weight of EPI was greater than respective controls (SN and SH). In the SCL group, the relative weight of RET also showed an increase compared with the SN group (Table 2). Exercise associated with LLLT promoted a significant reduction in the relative weight of adipose tissues (EPI, RET) in rats fed with chow diet when compared with the sedentary (SNL). In the THL group, EPI declined 12 % in relative weight, and the relative weight of RET was lower than SHL group (Table 2). In the other tissues, no difference was observed in the relative weight in SHL, SNL, THL, and TNL groups (Table 2).

Glycogen content and percentage of lipid in the tissues

Effects of type diet and exercise

The glycogen content in liver, GAST, and SOL did not differ significantly across sedentary and exercise groups during the experimental period when compared with respective control groups (Table 3). Nevertheless, exercise increased the glycogen content in the liver of the groups TN and TH by 32 and 28 %, respectively. In the TH group, the SOL glycogen content was 40 % smaller when compared with SH group (Table 3). High-fat diet promoted a significant increase in fatty liver of the sedentary rats. On the other hand, exercise promoted a significant reduction in the fat content in liver in TH group. No significant differences occurred in lipid content in GAST in the SN, SH, TN, and TH groups.

Effects of LLLT combined with diet and exercise

In rats fed with chow diet, LLLT did not promote changes in the glycogen and lipid content in the tissues. The same effect was observed in the fat content of the gastrocnemius muscle in SHL and THL groups (Table 3). SHL showed higher GAST glycogen content when compared with SNL and SH groups. Exercise and LLLT in rats fed with high-fat diet showed

Table 2 Relative mass of tissues in rat fed with normocaloric or hypercaloric diet (g/100 g of body weight)

Mass of	SN	SNL	TN	TNL	SH	SHL	TH	THL
Heart	0.28±0.10	0.35±0.02	0.36±0.01	0.38±0.04	0.33±0.03	0.33±0.02	0.35±0.04	0.36±0.02
Liver	2.66±0.29	2.52±0.34	2.28±0.32	2.54±0.20	2.28±0.32	2.54±0.20	2.28±0.18	2.48±0.12
GAST	0.45±0.10	0.49±0.03	0.55±0.03	0.52±0.04	0.49±0.03	0.47±0.01	0.52±0.02	0.51±0.02
SOL	0.04±0.00	0.04±0.00	0.04±0.01	0.04±0.00	0.04±0.00	0.04±0.00	0.04±0.00	0.04±0.00
BAT	0.07±0.02	0.06±0.01	0.09±0.01	0.09±0.02	0.11[e]±0.04	0.08±0.01	0.10±0.01	0.10±0.01
EPI	0.78±0.11	1.13[a]±0.26	0.79±0.12	0.67[c]±0.09	1.38[e]±0.23	1.47±0.07	1.13±0.14	1.29[e]±0.21
RET	0.74±0.16	1.37[a]±0.26	1.04±0.29	0.77[c]±0.17	2.09[e]±0.50	2.19[e]±0.37	1.47[b]±0.19	1.53[ce]±0.12
VIS	0.69±0.16	0.81±0.11	0.70±0.25	0.83±0.29	0.99±0.16	1.14±0.58	1.00±0.18	1.05±0.35

Values are expressed as mean±standard deviation (n=8/group). Different superscripts ([a] S versus SL; [b] S versus T; [c] SL versus TL; [d] T versus TL; [e] effects of hypercaloric diet in the different protocols) are significantly different (Tukey–Kramer multiple comparisons for $p<0.001$ except the specific comparisons: Brown adipose tissue, SC×SH $p<0.05$; epididymal, SN×SNL $p<0.05$; retroperitoneal, SH×TH and TH×THL $p<0.05$.

The groups are designed: *SN* sedentary normocaloric diet; *SNL* sedentary normocaloric diet laser; *TN* trained normocaloric diet; *TNL* trained normocaloric diet laser; *SH* sedentary hypercaloric diet; *SHL* sedentary hypercaloric diet laser; *TH* trained hypercaloric diet; *THL* trained hypercaloric diet laser. The variables are the mass for: heart; liver; *GAST* gastrocnemius muscle; *SOL* soleus muscle; *BAT* brown Adipose Tissue; EPI: Epididymal adipose tissue; RET: Retroperitoneal adipose tissue; *VIS* Visceral adipose tissue

higher glycogen content in the liver when compared with SHL, TH and TNL groups. Exercise and LLLT, in rats fed with high-fat diet, also promoted an increase in glycogen content in SOL when compared with the TH group. On the other hand, in the GAST, exercise and LLLT promoted a significant decrease in glycogen content when compared with its respective control group (SHL) (Table 3). Fatty liver in THL was 32 % smaller when compared with the SHL group.

Lipid profile

Effects of type diet and exercise

The consumption of a high-fat diet, compared to a chow diet, in sedentary rats promoted an increase in the total amount of plasma cholesterol (CHOL-total), TG and low density lipoprotein cholesterol (LDL-c). HDL-c concentrations did not show a statistically significant difference. On the other hand, exercise promoted a significant reduction in the CHOL-total, TG, HDL-c, and LDL-c concentrations in both diets (Fig. 3a–d).

Effects of LLLT combined with diet and exercise

No difference was observed in this parameter in the group SLC. However, in the sedentary rats fed with high-fat diet (SHL), LLLT promoted a significant decrease in CHOL-total, TG, and LDL-c concentrations when compared with SH group. HDL-c concentrations do not change in the same comparison. Exercise and LLLT in both diets promoted a significant reduction in CHOL-total, TG, LDL-c, and HDL-c concentrations when compared with the respective control

Table 3 Glycogen hepatic/muscle (μml/g) and percentage of fat in the tissues of rats fed with normocaloric or hypercaloric diet

	SN	SNL	TN	TNL	SH	SHL	TH	THL
Glycogen content								
Liver	0.80±0.41	0.87±0.23	1.06±0.42	1.04±0.23	0.78±0.13	0.87±0.13	1.00±0.08	1.68[cde]±0.34
GAST	0.29±0.03	0.31±0.02	0.31±0.02	0.28±0.03	0.30±0.02	0.39[ea]±0.06	0.29±0.03	0.30[c]±0.02
SOL	0.38±0.09	0.35±0.16	0.36±0.05	0.35±0.08	0.37±0.07	0.38±0.14	0.22±0.04	0.57[d]±0.17
Percentage of fat								
Liver	1.43±0.26	1.56±0.23	1.67±0.17	1.63±0.32	2.74[e]±1.39	2.74[e]±0.43	1.47[b]±0.25	1.87±0.32
Gast	0.36±0.11	0.37±0.11	0.34±0.07	0.37±0.06	0.43±0.10	0.43±0.15	0.39±0.10	0.37±0.09

Values are expressed as mean±standard deviation (n=8/group). The differences are highlighted in italics. Different superscripts ([a] S versus SL; [b] S versus T; [c] SL versus TL; [d] T versus TL; [e] effects of hypercaloric diet in the different protocols) are significantly different (Tukey–Kramer multiple comparisons for $p<0.001$ except the specific comparisons for glycogen: liver, TH×THL $p<0.01$ and TNL×THL $p<0.05$; gastrocnemius muscle, SNL×SHL $p<0.01$ and SHL×THL $p<0.01$; for percentage of fat: liver, SN SH $p<0.01$, SNL×SHL $p<0.05$ and SH×TH $p<0.01$).

The groups are designed: *SN* sedentary normocaloric; *SNL* sedentary normocaloric laser; *TN* trained normocaloric; *TNL* trained normocaloric laser; *SH* sedentary hypercaloric; *SHL* sedentary hypercaloric laser; *TH* trained hypercaloric; *THL* trained hypercaloric laser. The variables are: *GAST* gastrocnemius muscle; *SOL* soleus muscle

groups. THL in rats fed with high-fat diet also showed a significant decrease in serum cholesterol and TG concentrations compared with the TH group (Fig. 3a–d).

Discussion

This is the first randomized controlled experimental study evaluating effects of combined LLLT and training exercise on lipid pathways. We found a decreased lipid profile, and these results suggest that this LLLT with exercise training as a new alternative for dyslipidemic control.

Recent research has discussed the effects of high-fat diet consumption on fatty liver, intramuscular fat, lipid profile, glycogen concentration in the muscle or liver, and their relation to the development of chronic diseases and obesity [20, 21]. Moreover, there is recent interest in the role of physical exercise combined with LLLT as an adjunct approach to reduce the adverse effects of high-fat diet and sedentary life-style. However, the intensity, frequency, and duration of the exercise and the kind of diet promote different metabolic adaptations [15, 22, 23]. It is questionable whether all models of physical exercise have the same beneficial effects on adiposity, fatty liver, lipid profile, and glycogen concentration. Several studies have reported that moderate swimming exercise in animals (90 min) promotes reduction in adiposity, fatty liver, and increase in glycogen concentration and improvement in lipid profile [2, 5, 24–26].

In relation to the high-fat diet (SH group), experimental studies demonstrated that the intake of this diet was related to the dyslipidemic profile and was observed in our results by an increase in total cholesterol, TG, and LDL-c concentrations (see Fig. 3a–d) [5, 6, 14, 25]. Besides, due to the higher energy content of the high-fat diet compared with the chow diet, this diet induced increases in adiposity and fatty liver [2, 5, 6]. These alterations were observed in the present study (see Table 2 and 3).

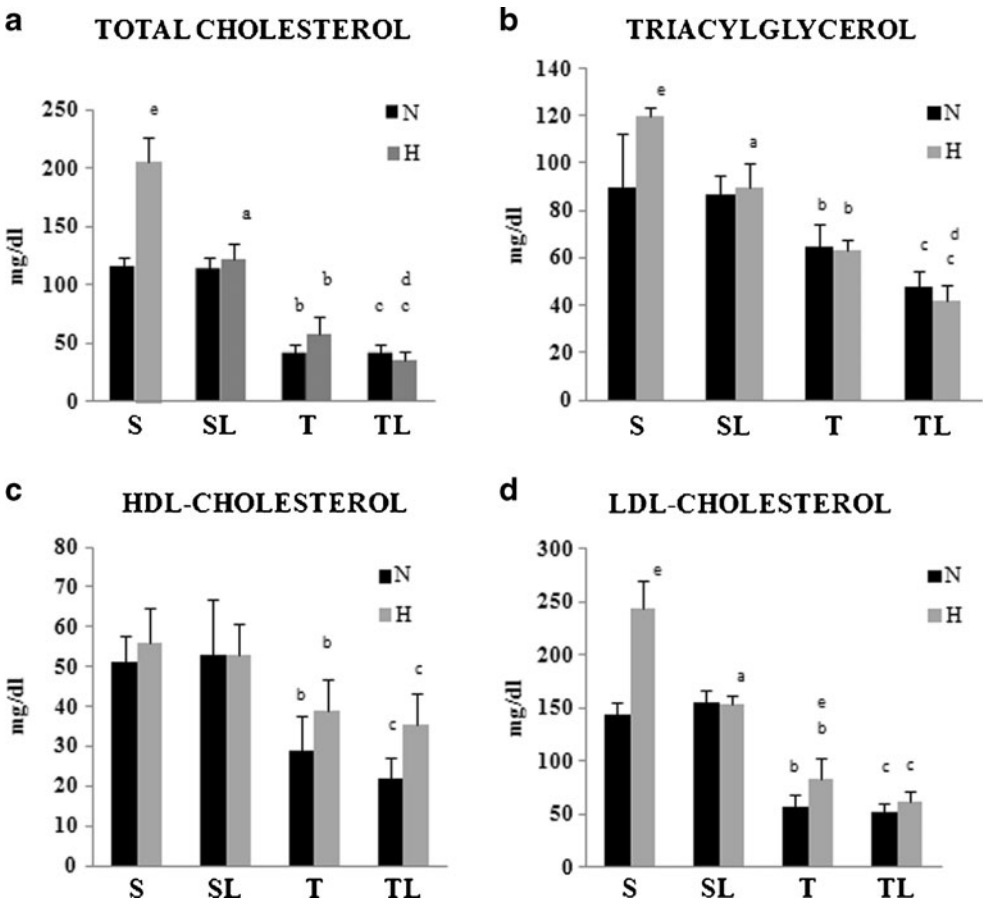

Fig. 3 Blood lipid analysis. C denotes normocaloric diet and H denotes hypercaloric diet. The groups are designated: *S* sedentary; *SL* sedentary laser; *T* trained; *TL* trained laser. Values are expressed as mean±standard deviation (n=8/group). Different superscripts (*a* S versus SL; *b* S versus T; *c* SL versus TL; *d* T versus TL; *e* effects of hypercaloric diet in the different protocols) are significantly different (Tukey–Kramer multiple comparisons for $p<0.001$ except the specific comparisons for cholesterol total: TH×THL $p<0.05$; for triglycerides: SN×TN $p<0.01$; and TH×THL $p<0.01$; for HDL-cholesterol: SN×TN $p<0.01$, SHL×THL $p<0.05$ and SH×TH $p<0.05$; LDL-cholesterol: TN×TH $p<0.05$). **a** Total cholesterol. **b** Triacylglycerol. **c** HDL-cholesterol. **d** LDL-cholesterol

A high-fat diet has been associated with a decrease in the rate of glycolysis and glycogen synthesis, leading to a lower content of glycogen in tissues [15, 22, 23]. However, this fact was not observed in our results when the glycogen content in the muscle and liver did not differ significantly from the control group (see Table 3). Several studies have reported that moderate exercise promotes reduction in body adiposity, dyslipidemia and fatty liver in rats [5, 24–26]. It has been reported that high-fat diets result in an increase in lipid oxidation during exercise [27]. It is known that both increased lipolysis and the consequent increase in plasma fatty acids during exercise facilitate this change [28]. However, these same two factors act in an opposite direction with respect to the metabolism of carbohydrates. Physical training increases the glycogen content stored, while the high-fat diet has been associated with a decreased rate of glycolysis and glycogen synthesis [29]. Thus, our finding agrees with that those found in the literature demonstrated by improvement in lipid profile in trained groups (see Fig. 3a, b), reduction in relative weight of EPI, RET (see Table 2), and fatty liver and glycogen content (see Table 3). In Fig. 4 we give a summary of our key findings related to kind of diet and training.

It is known that exercise improves the lipid profile and lipid metabolism. However, the effect of LLLT on the metabolic activity is not yet established. Jackson et al. [12] performed a noncontrolled and nonrandomized pilot clinical study that investigated the effects of the LLLT (635 nm) on lipid parameters. The individuals were able to maintain a regular diet and exercise regimen during the study. The LLLT was applied around the patient abdomen (five independent diode lasers with power output of 17 mW each was applied for 20 min leading to 6.6 J/cm^2 fluence) during 2 weeks (three sessions per week with duration of 20 min each) with the subject at rest. Their results showed a significant reduction in cholesterol and triglyceride levels.

In a similar, but this time-controlled and randomized study, Rushdi [30] showed that LLLT (four laser pads with 38 diodes laser at each pad, 650–660 nm and 1.3 W) of total energy applied on the abdomen, for 55 min, two times per week for 2 weeks, could reduce cholesterol and triglyceride

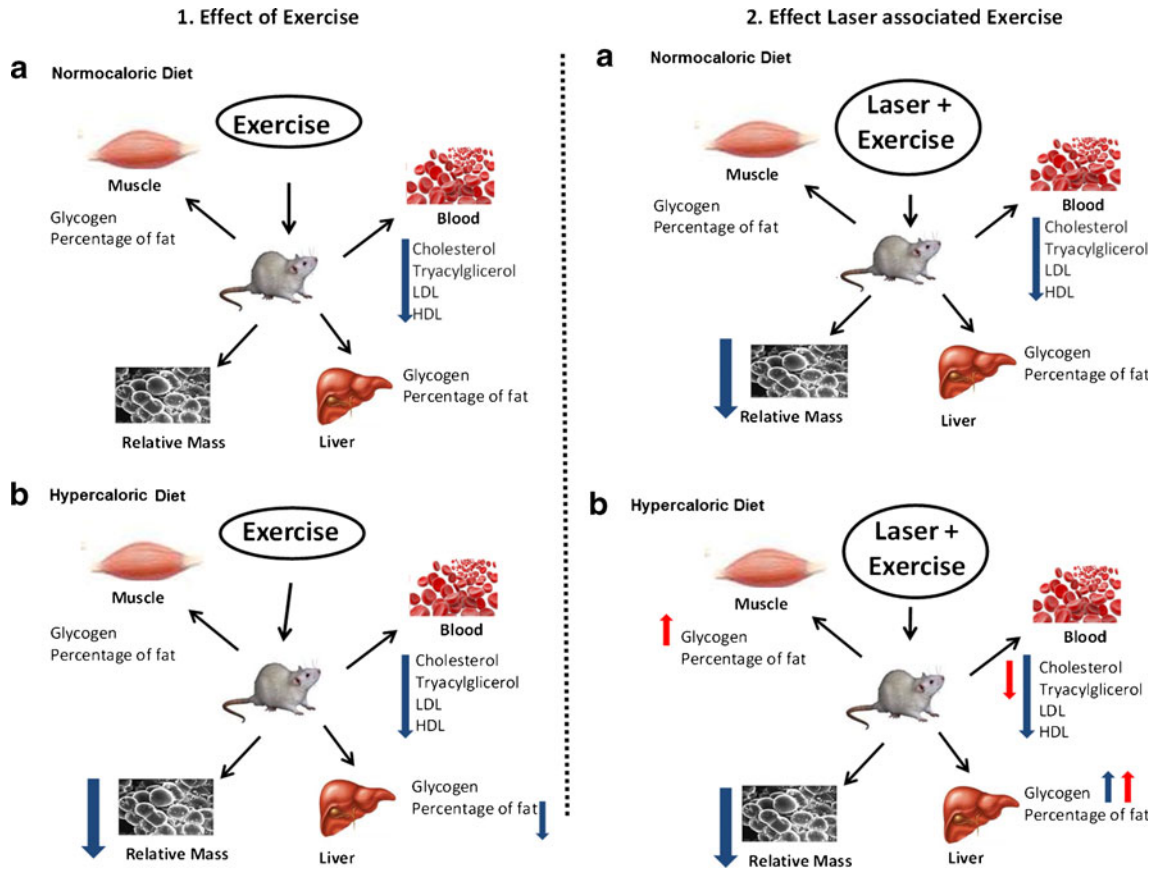

Fig. 4 The summary of key findings related to kind of diet and training. The *blue arrows* showed the comparisons control groups× trained and the *red arrows* the comparisons with trained groups× trained and laser groups. The comparison with laser effects associated to exercise for hypercaloric groups showed a *red arrow* and a *blue arrow* for the variables of blood. The *red arrow* includes the variables cholesterol, and tryacylglicerol as the *blue arrow* includes all variables

levels as well as reduce LDL levels while preserving HDL levels.

The hypothesis proposed by authors [30, 31] was that the LLLT could alter the mitochondrial membrane potential and the intracellular redox state with a resultant increase in ADP-ATP exchange rate. These mitochondrial changes may suppress cholesterologenesis by altering the transcription factors responsible for the expression of essential genes involved in the biosynthetic process.

We agree partly with this hypothesis. Our results showed that the LLLT did not suppress cholesterol synthesis, but caused a redirection of serum lipids to fat reserves (in sedentary conditions) and an improved supply of substrate for energy expenditure (in trained conditions). In addition, we believe that the exercise training combined with LLLT could have increased mitochondrial metabolism, as well as increased mitochondrial number and/or caused the fusion of smaller mitochondria to form giant mitochondria [32]. These effects could increase physical performance [7, 33–35].

Cytochrome c oxidase is unit IV of the electron transport chain of mitochondria and is also a chromophore for LLLT. It had been speculated that LLLT increases the rate at which cytochrome c oxidase transfers electrons and could cause the reduction of the catalytic center of cytochrome c oxidase, thus making more electrons available for the reduction of dioxygen [36, 37]. This mechanism of action of LLLT causes an increase in the electron and proton transfer, an increased quantity of ATP, and an initially increased production of reactive oxygen species (ROS). Elevated ROS concentration increases the lipid peroxidation, and this event occurs where ROS reacts with lipids found within cell membranes, temporarily damaging them [38]. Transitory pores created on adipocytes' membrane have been shown on several studies through scanning electron microscopy and transmission electron microscopy [39]. In addition to this, when irradiated adipocytes were cultured, they were shown to be able to recover to their original cell membrane structure and remain alive or viable.

A controlled and randomized trial showed that LLLT combined with aerobic or strength training in humans had long-lasting effects with improvement of muscle performance over three months [7]. Leal Junior et al. [33] and De Marchi et al. [7] showed that LLLT applied before exercise had acute effects with reduction of blood lactate, creatine kinase, and C-reactive protein levels with accelerated postexercise recovery in athletes, and showed that inflammation was reduced.

There is an extensive literature showing a high correlation between obesity and inflammatory activity [40]. Many of these papers correlate various adipokines as responsible for this pathophysiologic state [41]. Adiponectin is one of the adipokines that is responsible for response to exercise, leading to upregulation of its receptors, apparently related to increased mitochondrial metabolism [42]. It is a hypothesis that may explain how LLLT interacts with mitochondria, especially when combined with exercise [43]. LLLT is known to have a modulatory effect on inflammation, which could in turn affect the action of adiponectin on fat metabolism.

Several studies have demonstrated that LLLT alters cyclic adenosine monophosphate (cAMP) levels [44]. One mechanism to explain reduction in fat levels through the action of LLLT is that the adipocyte membrane is activated by raised cAMP concentrations that stimulate, in turn, cytoplasmic lipase that triggers the conversion of triglycerides into fatty acids and glycerol, both elements that can easily pass through the cell membrane. On the other hand, epinephrine is known to exert antilopolytic effects through its action on adrenergic receptors via increasing cAMP levels [45]. In addition to this, variations in types of adrenergic receptors and adrenergic receptor sensitivity on adipocytes of the abdominal and femoral regions in both males and females have been previously reported [39]. Based on these findings, it can be speculated that LLLT through increasing levels of cAMP might have enhancing effects on lipolysis and different amounts of fat reduction in different regions in the body might be explained by this hypothesis, which further confirms our results that showed variations in fat reduction among different regions.

Results of lipid profile can be changed by alteration in dietary habits and when patients perform exercise training. However, the studies discussed [30, 31] did not measure the aerobic fitness and dietary variables. In this context, our study is important because there was control of both diet and training.

Thus LLLT can improve pathways of energetic metabolism, mainly lipid metabolism, potentiating the effects of LLLT and, when combined with exercise of moderated intensity, could be used as a new approach to control dyslipidemia and consequently have a role in treatment of diseases related to dyslipidemia and obesity [2, 15]. The summary of our key findings of this study is shown in Fig. 4.

Acknowledgments We are grateful to Dr. Pinar Avci for the interesting discussion about the mechanisms involved in the lipid metabolism.

References

1. Tock L, Prado WL, Caranti DA, Cristofalo DM, Lederman H, Fisberg M, Siqueira KO, Stella SG, Antunes HK, Cintra IP, Tufik S, de Mello MT, Damaso AR (2006) Nonalcoholic fatty liver disease decrease in obese adolescents after multidisciplinary

therapy. Eur J Gastroenterol Hepatol 18(12):1241–1245. doi:10.1097/01.meg.0000243872.86949.95 00042737-200612000-00001 [pii]
2. Gauthier MS, Couturier K, Latour JG, Lavoie JM (2003) Concurrent exercise prevents high-fat-diet-induced macrovesicular hepatic steatosis. J Appl Physiol 94(6):2127–2134. doi:10.1152/japplphysiol.01164.2002.01164.2002 [pii]
3. Linsel-Nitschke P, Tall AR (2005) HDL as a target in the treatment of atherosclerotic cardiovascular disease. Nat Rev Drug Discov 4 (3):193–205. doi:10.1038/nrd1658
4. Pappachan JM, Chacko EC, Arunagirinathan G, Sriraman R (2011) Management of hypertension and diabetes in obesity: non-pharmacological measures. Int J Hypertens 2011:398065. doi:10.4061/2011/398065
5. Sene-Fiorese M, Duarte FO, Scarmagnani FR, Cheik NC, Manzoni MS, Nonaka KO, Rossi EA, de Oliveira Duarte AC, Damaso AR (2008) Efficiency of intermittent exercise on adiposity and fatty liver in rats fed with high-fat diet. Obesity (Silver Spring) 16 (10):2217–2222. doi:oby2008339 [pii] 10.1038/oby.2008.339
6. Duarte FO, Sene-Fiorese M, Manzoni MS, de Freitas LF, Cheik NC, de Oliveira G, Duarte AC, Nonaka KO, Damaso A (2008) Caloric restriction and refeeding promoted different metabolic effects in fat depots and impaired dyslipidemic profile in rats. Nutrition 24(2):177–186. doi:S0899-9007(07)00318-8 [pii] 10.1016/j.nut.2007.10.012
7. De Marchi T, Leal Junior EC, Bortoli C, Tomazoni SS, Lopes-Martins RA, Salvador M (2012) Low-level laser therapy (LLLT) in human progressive-intensity running: effects on exercise performance, skeletal muscle status, and oxidative stress. Lasers Med Sci 27(1):231–236. doi:10.1007/s10103-011-0955-5
8. Ferraresi C, de Brito OT, de Oliveira ZL, de Menezes Reiff RB, Baldissera V, de Andrade Perez SE, Matheucci Junior E, Parizotto NA (2011) Effects of low level laser therapy (808 nm) on physical strength training in humans. Lasers Med Sci 26(3):349–358. doi:10.1007/s10103-010-0855-0
9. Paolillo FR, Milan JC, Aniceto IV, Barreto SG, Rebelatto JR, Borghi-Silva A, Parizotto NA, Kurachi C, Bagnato VS (2011) Effects of infrared-LED illumination applied during high-intensity treadmill training in postmenopausal women. Photomed Laser Surg 29(9):639–645. doi:10.1089/pho.2010.2961
10. Karu TI, Pyatibrat LV, Afanasyeva NI (2005) Cellular effects of low power laser therapy can be mediated by nitric oxide. Lasers Surg Med 36(4):307–314. doi:10.1002/lsm.20148
11. Huang YY, Sharma SK, Carroll J, Hamblin MR (2011) Biphasic dose response in low level light therapy—an update. Dose-Response 9(4):602–618. doi:10.2203/dose-response.11-009.Hamblin drp-09-602 [pii]
12. Jackson RF, Dedo DD, Roche GC, Turok DI, Maloney RJ (2009) Low-level laser therapy as a non-invasive approach for body contouring: a randomized, controlled study. Lasers Surg Med 41 (10):799–809. doi:10.1002/lsm.20855
13. Jackson RF, Stern FA, Neira R, Ortiz-Neira CL, Maloney J (2012) Application of low-level laser therapy for noninvasive body contouring. Lasers Surg Med 44(3):211–217. doi:10.1002/lsm.22007
14. Duarte FO, Sene-Fiorese M, Cheik NC, Maria AS, de Aquino AE Jr, Oishi JC, Rossi EA, de Oliveira Duarte AC G, Damaso AR (2012) Food restriction and refeeding induces changes in lipid pathways and fat deposition in the adipose and hepatic tissues in rats with diet-induced obesity. Exp Physiol 97(7):882–894. doi: doi:10.1113/expphysiol.2011.064121
15. Horowitz JF (2003) Fatty acid mobilization from adipose tissue during exercise. Trends Endocrinol Metab 14(8):386–392. doi:Doi 10.1016/S1043-2760(03)00143-7
16. Caruso-Davis MK, Guillot TS, Podichetty VK, Mashtalir N, Dhurandhar NV, Dubuisson O, Yu Y, Greenway FL (2011) Efficacy of low-level laser therapy for body contouring and spot fat reduction. Obes Surg 21(6):722–729. doi:10.1007/s11695-010-0126-y
17. Vieira WH, Ferraresi C, Perez SE, Baldissera V, Parizotto NA (2012) Effects of low-level laser therapy (808 nm) on isokinetic muscle performance of young women submitted to endurance training: a randomized controlled clinical trial. Lasers Med Sci 27(2):497–504. doi:10.1007/s10103-011-0984-0
18. Moraes G, Altran AE, Avilez IM, Barbosa CC, Bidinotto PM (2005) Metabolic adjustments during semi-aestivation of the marble swamp eel (Synbranchus marmoratus, Bloch 1795)—a facultative air breathing fish. Braz J Biol 65(2):305–312. doi:S1519-69842005000200015 [pii]
19. Friedewald WT, Levy RI, Fredrickson DS (1972) Estimation of the concentration of low-density lipoprotein cholesterol in plasma, without use of the preparative ultracentrifuge. Clin Chem 18(6):499–502
20. Marchesini G, Bugianesi E, Forlani G, Cerrelli F, Lenzi M, Manini R, Natale S, Vanni E, Villanova N, Melchionda N, Rizzetto M (2003) Nonalcoholic fatty liver, steatohepatitis, and the metabolic syndrome. Hepatology 37(4):917–923. doi:10.1053/jhep.2003.50161 S0270913903001216 [pii]
21. Liao CC, Su TC, Chien KL, Wang JK, Chiang CC, Lin CC, Lin RS, Lee YT, Sung FC (2009) Elevated blood pressure, obesity, and hyperlipidemia. J Pediatr 155(1):79–83. doi:doi:10.1016/j.jpeds.2009.01.036, 83 e71
22. Ruby BC, Robergs RA (1994) Gender differences in substrate utilization during exercise. Sports Med 17(6):393–410
23. Even PC, Rieth N, Roseau S, Larue-Achagiotis C (1998) Substrate oxidation during exercise in the rat cannot fully account for training-induced changes in macronutrients selection. Metabolism 47(7):777–782. doi:S0026-0495(98)90111-1 [pii]
24. Schrauwen P, Westerterp KR (2000) The role of high-fat diets and physical activity in the regulation of body weight. Br J Nutr 84 (4):417–427. doi:S0007114500001720 [pii]
25. Do Nascimento CMO, Estadella D, Oyama LM, Damaso AR, Ribeiro EB (2004) Effect of palatable hyperlipidic diet on lipid metabolism of sedentary and exercised rats. Nutrition 20(2):218–224. doi:DOI 10.1016/j.nut.2003.10.008
26. Novelli ELB, Burneiko RCM, Diniz YS, Galhardi CM, Rodrigues HG, Ebaid GMX, Faine LA, Padovani CR, Cicogna AC (2006) Interaction of hypercaloric diet and physical exercise on lipid profile, oxidative stress and antioxidant defenses. Food Chem Toxicol 44(7):1167–1172. doi:DOI 10.1016/j.fct.2006.01.004
27. Helge JW, Watt PW, Richter EA, Rennie MJ, Kiens B (2001) Fat utilization during exercise: adaptation to a fat-rich diet increases utilization of plasma fatty acids and very low density lipoprotein-triacylglycerol in humans. J Physiol-London 537(3):1009–1020
28. Helge JW (2002) Long-term fat diet adaptation effects on performance, training capacity, and fat utilization. Med Sci Sport Exer 34 (9):1499–1504. doi:Doi 10.1249/01.Mss.0000027691.95763.B5
29. Lee KU, Kim CH, Youn JH, Park JY, Hong SK, Park KS, Park SW, Suh KI (2000) Effects of high-fat diet and exercise training on intracellular glucose metabolism in rats. Am J Physiol-Endoc M 278(6):E977–E984
30. Rushdi TA (2010) Effect of low-level laser therapy on cholesterol and triglyceride serum levels in icu patients: a controlled, randomized study. EJCTA 4(2):5
31. Jackson RF, Roche GC, Wisler K (2010) Reduction in cholesterol and triglyceride serum levels following low-level laser irradiation: a noncontrolled, nonrandomized pilot study. Am J Cosmet Surg 27 (4):177–184
32. Bakeeva LE, Manteifel VM, Rodichev EB, Karu TI (1993) [Formation of gigantic mitochondria in human blood lymphocytes under the effect of an He–Ne laser]. Mol Biol (Mosk) 27(3):608–617
33. Leal Junior EC, Lopes-Martins RA, Baroni BM, De Marchi T, Taufer D, Manfro DS, Rech M, Danna V, Grosselli D, Generosi RA, Marcos RL, Ramos L, Bjordal JM (2009) Effect of 830 nm

low-level laser therapy applied before high-intensity exercises on skeletal muscle recovery in athletes. Lasers Med Sci 24(6):857–863. doi:10.1007/s10103-008-0633-4
34. Sussai DA, Carvalho Pde T, Dourado DM, Belchior AC, dos Reis FA, Pereira DM (2010) Low-level laser therapy attenuates creatine kinase levels and apoptosis during forced swimming in rats. Lasers Med Sci 25(1):115–120. doi:10.1007/s10103-009-0697-9
35. Paolillo FR, Corazza AV, Borghi-Silva A, Parizotto NA, Kurachi C, Bagnato VS (2012) Infrared LED irradiation applied during high-intensity treadmill training improves maximal exercise tolerance in postmenopausal women: a 6-month longitudinal study. Lasers Med Sci. doi:10.1007/s10103-012-1062-y
36. Brunori M, Giuffre A, Sarti P (2005) Cytochrome c oxidase, ligands and electrons. J Inorg Biochem 99(1):324–336. doi:S0162-0134(04)00316-2 [pii] 10.1016/j.jinorgbio.2004.10.011
37. Chen CH, Hung HS, Hsu SH (2008) Low-energy laser irradiation increases endothelial cell proliferation, migration, and eNOS gene expression possibly via PI3K signal pathway. Lasers Surg Med 40 (1):46–54. doi:10.1002/lsm.20589
38. Geiger PG, Korytowski W, Girotti AW (1995) Photodynamically generated 3-beta-hydroxy-5 alpha-cholest-6-ene-5- hydroperoxide: toxic reactivity in membranes and susceptibility to enzymatic detoxification. Photochem Photobiol 62(3):580–587
39. Neira R, Arroyave J, Ramirez H, Ortiz CL, Solarte E, Sequeda F, Gutierrez MI (2002) Fat liquefaction: effect of low-level laser energy on adipose tissue. Plast Reconstr Surg 110(3):912–922, discussion 923–915
40. Athyros VG, Tziomalos K, Karagiannis A, Anagnostis P, Mikhailidis DP (2010) Should adipokines be considered in the choice of the treatment of obesity-related health problems? Curr Drug Targets 11 (1):122–135
41. Koh EH, Park JY, Park HS, Jeon MJ, Ryu JW, Kim M, Kim SY, Kim MS, Kim SW, Park IS, Youn JH, Lee KU (2007) Essential role of mitochondrial function in adiponectin synthesis in adipocytes. Diabetes 56(12):2973–2981. doi:db07-0510 [pii] 10.2337/db07-0510
42. Huang H, Iida KT, Sone H, Yokoo T, Yamada N, Ajisaka R (2006) The effect of exercise training on adiponectin receptor expression in KKAy obese/diabetic mice. J Endocrinol 189(3):643–653. doi:189/3/643 [pii] 10.1677/joe.1.06630
43. de Almeida P, Lopes-Martins RA, Tomazoni SS, Silva JA Jr, de Carvalho PT, Bjordal JM, Leal Junior EC (2011) Low-level laser therapy improves skeletal muscle performance, decreases skeletal muscle damage and modulates mRNA expression of COX-1 and COX-2 in a dose-dependent manner. Photochem Photobiol 87(5):1159–1163. doi:10.1111/j.1751-1097.2011.00968.x
44. Franco W, Leite RS, Parizotto NA (2003) Effects of low intensity infrared laser radiation on the water transport in the isolated toad urinary bladder. Lasers Surg Med 32(4):299–304. doi:10.1002/lsm.10166
45. Khan MH, Victor F, Rao B, Sadick NS (2010) Treatment of cellulite: part II. advances and controversies. J Am Acad Dermatol 62(3):373–384. doi:doi:10.1016/j.jaad.2009.10.041, quiz 385–376

Published in final edited form as:
Lasers Med Sci. 2013 September ; 28(5): 1271–1280. doi:10.1007/s10103-012-1223-z.

Low-level laser therapy (LLLT) combined with swimming training improved the lipid profile in rats fed with high-fat diet

Antonio E. Aquino Jr.
Optics Group from Institute of Physics of São Carlos (IFSC), University of São Paulo (USP), São Carlos, Brazil

Laboratory of Nutrition and Metabolism Applied to Exercise, Physical Education and Motor Human Department, Federal University of São Carlos (UFSCar), São Carlos, Brazil

Biotechnology Post Graduation Program, Federal University of São Carlos (UFSCar), São Carlos, Brazil

Federal University of São Carlos (UFSCar), Via Washington Luis, km 235, Monjolinho, 13565-905 São Carlos, São Paulo, Brazil

Marcela Sene-Fiorese
Optics Group from Institute of Physics of São Carlos (IFSC), University of São Paulo (USP), São Carlos, Brazil

Physical Education Department, University Camilo Castelo Branco, AV: Hilário da Silva Passos, 13690-970 Descalvado, São Paulo, Brazil

Fernanda R. Paolillo
Optics Group from Institute of Physics of São Carlos (IFSC), University of São Paulo (USP), São Carlos, Brazil

Fernanda O. Duarte
Laboratory of Nutrition and Metabolism Applied to Exercise, Physical Education and Motor Human Department, Federal University of São Carlos (UFSCar), São Carlos, Brazil

Jorge C. Oishi
Laboratory of Nutrition and Metabolism Applied to Exercise, Physical Education and Motor Human Department, Federal University of São Carlos (UFSCar), São Carlos, Brazil

Airton A. Pena Jr.
Laboratory of Nutrition and Metabolism Applied to Exercise, Physical Education and Motor Human Department, Federal University of São Carlos (UFSCar), São Carlos, Brazil

Ana C. G. O. Duarte
Laboratory of Nutrition and Metabolism Applied to Exercise, Physical Education and Motor Human Department, Federal University of São Carlos (UFSCar), São Carlos, Brazil

Michael R. Hamblin
Wellman Center for Photomedicine, Massachusetts General Hospital, Boston, MA, USA

Department of Dermatology, Harvard Medical School, Boston, MA, USA

Harvard-MIT Division of Health Sciences and Technology, Cambridge, MA, USA

Vanderlei S. Bagnato

spydera@ig.com.br. parizoto@ufscar.br.

Optics Group from Institute of Physics of São Carlos (IFSC), University of São Paulo (USP), São Carlos, Brazil

Biotechnology Post Graduation Program, Federal University of São Carlos (UFSCar), São Carlos, Brazil

Nivaldo A. Parizotto
Biotechnology Post Graduation Program, Federal University of São Carlos (UFSCar), São Carlos, Brazil

Wellman Center for Photomedicine, Massachusetts General Hospital, Boston, MA, USA

Department of Dermatology, Harvard Medical School, Boston, MA, USA

Electrothermophototherapy Laboratory, Department of Physical Therapy, Federal University of São Carlos (UFSCar), São Carlos, Brazil

Federal University of São Carlos (UFSCar), Via Washington Luis, km 235, Monjolinho, 13565-905 São Carlos, São Paulo, Brazil

Abstract

Obesity and associated dyslipidemia is the fastest growing health problem throughout the world. The combination of exercise and low-level laser therapy (LLLT) could be a new approach to the treatment of obesity and associated disease. In this work, the effects of LLLT associated with exercises on the lipid metabolism in regular and high-fat diet rats were verified. We used 64 rats divided in eight groups with eight rats each, designed: SC, sedentary chow diet; SCL, sedentary chow diet laser, TC, trained chow diet; TCL, trained chow diet laser; SH, sedentary high-fat diet; SHL, sedentary high-fat diet laser; TH, trained high-fat diet; and THL, trained high-fat diet laser. The exercise used was swimming during 8 weeks/90 min daily and LLLT (GA-Al-As, 830 nm) dose of 4.7 J/point and total energy 9.4 J per animal, applied to both gastrocnemius muscles after exercise. We analyzed biochemical parameters, percentage of fat, hepatic and muscular glycogen and relative mass of tissue, and weight percentage gain. The statistical test used was ANOVA, with post hoc Tukey–Kramer for multiple analysis between groups, and the significant level was $p<0.001$, $p<0.01$, and $p<0.05$. LLLT decreased the total cholesterol ($p<0.05$), triglycerides ($p<0.01$), low-density lipoprotein cholesterol ($p<0.05$), and relative mass of fat tissue ($p<0.05$), suggesting increased metabolic activity and altered lipid pathways. The combination of exercise and LLLT increased the benefits of exercise alone. However, LLLT without exercise tended to increase body weight and fat content. LLLT may be a valuable addition to a regimen of diet and exercise for weight reduction and dyslipidemic control.

Keywords

Exercise; Metabolism; LLLT; Photobiomodulation; Obesity; Dyslipidemia

Introduction

The pathogenesis of obesity is complex and not well understood. It is fundamentally a problem of energy balance, which can develop only when energy intake is in excess of energy expenditure. This fact has led to a major focus on the mechanisms controlling food intake and the components and regulatory mechanisms of energy expenditure [1]. Eating high-fat or high-calorie food associated with a sedentary lifestyle facilitates the development of a positive energy balance [1]. Obesity is strongly associated with many chronic diseases, such as hypertension, diabetes, coronary heart disease, cancer, nonalcoholic fatty liver disease, and dyslipidemias [2, 3]

Physical activity is already established as an important nonpharmacological strategy for control of obesity or high body-fat percentage and for the treatment of associated diseases [4]. Several clinical and experimental studies have demonstrated that a moderate exercise regimen combined with a normocaloric diet resulted in the reduction of adiposity and improved lipid profile [5, 6]. However, due to the increased incidence of obesity in the world, it becomes necessary to seek new noninvasive and nonpharmacological strategies to increase the physiological effects of exercises.

Several studies have investigated low-level laser therapy (LLLT) or light-emitting diode (LED) therapy and have made advances in the understanding of the underlying mechanisms LLLT in biological systems [7–9]. The main characteristics of photobiomodulation or photobiostimulation are the induction and stimulation of many aspects of cellular processes. According to Karu [10], the cellular redox state is an important determinant of the final response, and there are three signaling pathways that operate relating to cell attachment, mitochondrial respiratory chain, and Na, K-ATPase. Moreover, results suggest that specific wavelengths, such as red and near-infrared radiation, can create, regulate, or activate enzymatic processes in cells to improve metabolism [8].

There is still much to elucidate about the mechanisms underlying LLLT and how it acts on cells and tissues, but there is evidence that the response usually exhibit a biphasic dose–response profile [11]. In the adipose tissues, some authors have attempted to modify their metabolism using LLLT, and some clinical studies [12, 13] tried to explain how there could be the reduction of body contours promoted by the LLLT, including the transitory induction of pores in the membranes of the adipocytes and consequently liberation of intracellular constituents (fat) and its removal and metabolism; however, the mechanisms still remain unclear.

For this reason, parameters such as quantity hepatic and muscle glycogen, the percentage of lipids in different tissues, as well as triglycerides, total cholesterol, high-density lipoprotein (HDL) cholesterol and low-density lipoprotein (LDL) cholesterol may provide the state of health of individuals, as well as can be used to monitor the systemic of conditions, which are distributed the products of the metabolism of fat and sugar [5, 14, 15].

Nevertheless, only a few studies have described LLLT combined with exercise training, for example, in young males [8], postmenopausal women [9], or overweight individuals [16]. Thus, our goal was to perform a randomized controlled trial to investigate the effects of the LLLT associated with exercise training on lipid profile in rats fed with different diets. Our hypothesis was that combined exercise with LLLT could control the serum lipids and modify the lipid metabolism in animals with normocaloric and hypercaloric diet. If successful, this combination could play an important role in control of diseases associated with obesity.

Methods and procedures

Animals

All animal procedures were performed according to the principles in the Guide for the Care and Use of Laboratory Animals and were approved by the Institutional Animal Ethics Committee (number 067/2010). Sixty-four male Wistar rats (90 days old and weight of 317.00±19.16 g) were included in this study. Before beginning the experimental protocol, all of the groups [except for the normocaloric groups (N)] were fed ad libitum with the hyperlipidic diet (H) for 3 weeks [14] for the development of obesity and dyslipidemia. The animals were randomized according to diet into eight groups with eight rats each (n=8): normocaloric diet (N) groups—sedentary normal diet (SN), trained normal diet (TN),

sedentary normal diet plus laser (SNL), and trained normal diet plus laser (TNL); hypercaloric high-fat diet (H) groups—sedentary high-fat diet (SH), trained high-fat diet (TH), sedentary high-fat diet plus laser (SHL), and trained high-fat diet plus laser (THL). Rats were kept one per cage with food and water ad libitum (8 weeks), on a 12:12-h light–dark cycle at 23±1 °C.

Diet

The experimental groups received the following diet: the normocaloric diet (N)—MP-77 standard rat chow diet provided in pellet form (Primor®, São Paulo, Brazil) containing 23 g of protein, 49 g of carbohydrate, 4 g of total fat, 5 g of fiber, 7 g of ash, and 6 g of vitamins per 100 g diet. The hypercaloric diet consisted of the same commercial rat chow plus peanuts, milk chocolate, and sweet biscuit in a proportion of 3:2:2:1. It contained 5.12 kcal/g (35 % of calories as fat) for the hypercaloric high-fat diet and 4.07 kcal/g for the normocaloric diet [14].

Exercise and LLLT protocols

The exercise program consisted of swimming in individual tanks (Fig. 1) filled with water, maintained at 28–32 °C. The animals of the trained groups swam for 30, 60, and 90 min on the first, second, and third days to adapt. The swimming period was then increased to 90 min/day, during 5 days/week. All rats swam with a load of 3–5 % body mass attached to the trunk by a jacket. The exercise protocols were performed for 5 days/week during 8 weeks. This program is considered to be of moderate intensity [5].

The LLLT parameters are shown in Table 1. It was irradiated transcutaneously on the muscles of the rat's paw (one point on quadriceps and other point on gastrocnemius). The energy density of laser irradiation and the anatomical points were chosen based on previous studies [8]. We decided not to use sham group because we have a positive control (hypercaloric diet and treated with LLLT), a negative control (hypercaloric diet and not treated with LLLT), as well as positive (hypercaloric) and negative (normocaloric) controls for the factor diet, with or without laser treatment.

The laser was applied after the exercises because the advantage of using the stress induced to get the maximum of absorption and effects on metabolism. It was used the same protocol before in different papers from our laboratory [17].

Experimental procedure

At the end of 8 weeks of training and after a 24-h rest period, analysis was performed. All animals were euthanized by decapitation. The collected blood was immediately centrifuged and frozen at −80 °C. The heart (H), liver (L), gastrocnemius muscle (GAST), soleus muscle (SOL), the white adipose tissues (epididymal (EPI) retroperitoneal (RET), visceral (VIS)), and the interscapular brown adipose tissue (BAT) were immediately removed, weighted, and frozen at −20 °C.

Hepatic and muscular glycogen and percentage of lipids of tissues

The muscle and liver glycogen was determined by colorimetric method, which assesses the concentration of glycosyl-glucose using a standard of 100 nmol of glucose and determined using a ultraviolet/visible spectrophotometer Biospectro® SP220 [18]. The percentage of lipid content in the tissue was determined by the gravimetric method [6].

Serum analysis

Total cholesterol (CHOL-total), triacylglycerol (TG), and high-density lipoprotein cholesterol (HDL-c) in the serum were determined enzymatically (Laborlab® kits) using a spectrophotometer [6]. The low-density lipoprotein (LDL-c) was calculated by Friedewald equation [19].

Statistical analysis

All data were expressed as a mean and standard deviation. The Kolmogorov–Smirnov test was used to analyze the normality. For statistical evaluation of the metabolic parameters, a one-way ANOVA test with post hoc analysis (Tukey–Kramer multiple comparisons) was used between groups. Instat 3.0 for Windows 7 (Graph Pad, San Diego, CA, USA, 1998) was used for the statistical analysis and the significance level was given as $p<0.001$, $p<0.01$, and $p<0.05$.

Results

Body mass and relative mass of tissues

Effects of type diet and exercise—The body mass gain differences are shown in Fig. 2 as the percentage of gain depending on diet used and treatments. High-fat diet promoted in the sedentary group an increase in EPI, RET, and BAT relative weight compared with as observed in the sedentary rats fed with chow diet group (SN), but the relative weight of liver, VIS, GAST, SOL, and heart was not significantly affected by this diet (Table 2). In the TH group, there was a significant reduction in relative weight of RET when compared with SH group. In the same comparison, the EPI declined 18 % in their relative weight. In contrast, no difference was observed in relative weight of tissues when comparing SN and TN groups (Table 2).

Effects of LLLT combined with diet and exercise—In the LLLT sedentary groups (SNL and SHL), the relative weight of EPI was greater than respective controls (SN and SH). In the SCL group, the relative weight of RET also showed an increase compared with the SN group (Table 2). Exercise associated with LLLT promoted a significant reduction in the relative weight of adipose tissues (EPI, RET) in rats fed with chow diet when compared with the sedentary (SNL). In the THL group, EPI declined 12 % in relative weight, and the relative weight of RET was lower than SHL group (Table 2). In the other tissues, no difference was observed in the relative weight in SHL, SNL, THL, and TNL groups (Table 2).

Glycogen content and percentage of lipid in the tissues

Effects of type diet and exercise—The glycogen content in liver, GAST, and SOL did not differ significantly across sedentary and exercise groups during the experimental period when compared with respective control groups (Table 3). Nevertheless, exercise increased the glycogen content in the liver of the groups TN and TH by 32 and 28 %, respectively. In the TH group, the SOL glycogen content was 40 % smaller when compared with SH group (Table 3). High-fat diet promoted a significant increase in fatty liver of the sedentary rats. On the other hand, exercise promoted a significant reduction in the fat content in liver in TH group. No significant differences occurred in lipid content in GAST in the SN, SH, TN, and TH groups.

Effects of LLLT combined with diet and exercise—In rats fed with chow diet, LLLT did not promote changes in the glycogen and lipid content in the tissues. The same effect was observed in the fat content of the gastrocnemius muscle in SHL and THL groups (Table

3). SHL showed higher GAST glycogen content when compared with SNL and SH groups. Exercise and LLLT in rats fed with high-fat diet showed higher glycogen content in the liver when compared with SHL, TH and TNL groups. Exercise and LLLT, in rats fed with high-fat diet, also promoted an increase in glycogen content in SOL when compared with the TH group. On the other hand, in the GAST, exercise and LLLT promoted a significant decrease in glycogen content when compared with its respective control group (SHL) (Table 3). Fatty liver in THL was 32 % smaller when compared with the SHL group.

Lipid profile

Effects of type diet and exercise—The consumption of a high-fat diet, compared to a chow diet, in sedentary rats promoted an increase in the total amount of plasma cholesterol (CHOL-total), TG and low density lipoprotein cholesterol (LDL-c). HDL-c concentrations did not show a statistically significant difference. On the other hand, exercise promoted a significant reduction in the CHOL-total, TG, HDL-c, and LDL-c concentrations in both diets (Fig. 3a–d).

Effects of LLLT combined with diet and exercise—No difference was observed in this parameter in the group SLC. However, in the sedentary rats fed with high-fat diet (SHL), LLLT promoted a significant decrease in CHOL-total, TG, and LDL-c concentrations when compared with SH group. HDL-c concentrations do not change in the same comparison. Exercise and LLLT in both diets promoted a significant reduction in CHOL-total, TG, LDL-c, and HDL-c concentrations when compared with the respective control groups. THL in rats fed with high-fat diet also showed a significant decrease in serum cholesterol and TG concentrations compared with the TH group (Fig. 3a–d).

Discussion

This is the first randomized controlled experimental study evaluating effects of combined LLLT and training exercise on lipid pathways. We found a decreased lipid profile, and these results suggest that this LLLT with exercise training as a new alternative for dyslipidemic control.

Recent research has discussed the effects of high-fat diet consumption on fatty liver, intramuscular fat, lipid profile, glycogen concentration in the muscle or liver, and their relation to the development of chronic diseases and obesity [20, 21]. Moreover, there is recent interest in the role of physical exercise combined with LLLT as an adjunct approach to reduce the adverse effects of high-fat diet and sedentary life-style. However, the intensity, frequency, and duration of the exercise and the kind of diet promote different metabolic adaptations [15, 22, 23]. It is questionable whether all models of physical exercise have the same beneficial effects on adiposity, fatty liver, lipid profile, and glycogen concentration. Several studies have reported that moderate swimming exercise in animals (90 min) promotes reduction in adiposity, fatty liver, and increase in glycogen concentration and improvement in lipid profile [2, 5, 24–26].

In relation to the high-fat diet (SH group), experimental studies demonstrated that the intake of this diet was related to the dyslipidemic profile and was observed in our results by an increase in total cholesterol, TG, and LDL-c concentrations (see Fig. 3a–d)[5, 6, 14, 25]. Besides, due to the higher energy content of the high-fat diet compared with the chow diet, this diet induced increases in adiposity and fatty liver [2, 5, 6]. These alterations were observed in the present study (see Table 2 and 3).

A high-fat diet has been associated with a decrease in the rate of glycolysis and glycogen synthesis, leading to a lower content of glycogen in tissues [15, 22, 23]. However, this fact

was not observed in our results when the glycogen content in the muscle and liver did not differ significantly from the control group (see Table 3). Several studies have reported that moderate exercise promotes reduction in body adiposity, dyslipidemia and fatty liver in rats [5, 24–26]. It has been reported that high-fat diets result in an increase in lipid oxidation during exercise [27]. It is known that both increased lipolysis and the consequent increase in plasma fatty acids during exercise facilitate this change [28]. However, these same two factors act in an opposite direction with respect to the metabolism of carbohydrates. Physical training increases the glycogen content stored, while the high-fat diet has been associated with a decreased rate of glycolysis and glycogen synthesis [29]. Thus, our finding agrees with that those found in the literature demonstrated by improvement in lipid profile in trained groups (see Fig. 3a, b), reduction in relative weight of EPI, RET (see Table 2), and fatty liver and glycogen content (see Table 3). In Fig. 4 we give a summary of our key findings related to kind of diet and training.

It is known that exercise improves the lipid profile and lipid metabolism. However, the effect of LLLT on the metabolic activity is not yet established. Jackson et al. [12] performed a noncontrolled and nonrandomized pilot clinical study that investigated the effects of the LLLT (635 nm) on lipid parameters. The individuals were able to maintain a regular diet and exercise regimen during the study. The LLLT was applied around the patient abdomen (five independent diode lasers with power output of 17 mW each was applied for 20 min leading to 6.6 J/cm^2 fluence) during 2 weeks (three sessions per week with duration of 20 min each) with the subject at rest. Their results showed a significant reduction in cholesterol and triglyceride levels.

In a similar, but this time-controlled and randomized study, Rushdi [30] showed that LLLT (four laser pads with 38 diodes laser at each pad, 650–660 nm and 1.3 W) of total energy applied on the abdomen, for 55 min, two times per week for 2 weeks, could reduce cholesterol and triglyceride levels as well as reduce LDL levels while preserving HDL levels.

The hypothesis proposed by authors [30, 31] was that the LLLT could alter the mitochondrial membrane potential and the intracellular redox state with a resultant increase in ADP-ATP exchange rate. These mitochondrial changes may suppress cholesterologenesis by altering the transcription factors responsible for the expression of essential genes involved in the biosynthetic process.

We agree partly with this hypothesis. Our results showed that the LLLT did not suppress cholesterol synthesis, but caused a redirection of serum lipids to fat reserves (in sedentary conditions) and an improved supply of substrate for energy expenditure (in trained conditions). In addition, we believe that the exercise training combined with LLLT could have increased mitochondrial metabolism, as well as increased mitochondrial number and/or caused the fusion of smaller mitochondria to form giant mitochondria [32]. These effects could increase physical performance [7, 33–35].

Cytochrome c oxidase is unit IV of the electron transport chain of mitochondria and is also a chromophore for LLLT. It had been speculated that LLLT increases the rate at which cytochrome c oxidase transfers electrons and could cause the reduction of the catalytic center of cytochrome c oxidase, thus making more electrons available for the reduction of dioxygen [36, 37]. This mechanism of action of LLLT causes an increase in the electron and proton transfer, an increased quantity of ATP, and an initially increased production of reactive oxygen species (ROS). Elevated ROS concentration increases the lipid peroxidation, and this event occurs where ROS reacts with lipids found within cell membranes, temporarily damaging them [38]. Transitory pores created on adipocytes'

membrane have been shown on several studies through scanning electron microscopy and transmission electron microscopy [39]. In addition to this, when irradiated adipocytes were cultured, they were shown to be able to recover to their original cell membrane structure and remain alive or viable.

A controlled and randomized trial showed that LLLT combined with aerobic or strength training in humans had long-lasting effects with improvement of muscle performance over three months [7]. Leal Junior et al. [33] and De Marchi et al. [7] showed that LLLT applied before exercise had acute effects with reduction of blood lactate, creatine kinase, and C-reactive protein levels with accelerated postexercise recovery in athletes, and showed that inflammation was reduced.

There is an extensive literature showing a high correlation between obesity and inflammatory activity [40]. Many of these papers correlate various adipokines as responsible for this pathophysiologic state [41]. Adiponectin is one of the adipokines that is responsible for response to exercise, leading to upregulation of its receptors, apparently related to increased mitochondrial metabolism [42]. It is a hypothesis that may explain how LLLT interacts with mitochondria, especially when combined with exercise [43]. LLLT is known to have a modulatory effect on inflammation, which could in turn affect the action of adiponectin on fat metabolism.

Several studies have demonstrated that LLLT alters cyclic adenosine monophosphate (cAMP) levels [44]. One mechanism to explain reduction in fat levels through the action of LLLT is that the adipocyte membrane is activated by raised cAMP concentrations that stimulate, in turn, cytoplasmic lipase that triggers the conversion of triglycerides into fatty acids and glycerol, both elements that can easily pass through the cell membrane. On the other hand, epinephrine is known to exert antilopolytic effects through its action on adrenergic receptors via increasing cAMP levels [45]. In addition to this, variations in types of adrenergic receptors and adrenergic receptor sensitivity on adipocytes of the abdominal and femoral regions in both males and females have been previously reported [39]. Based on these findings, it can be speculated that LLLT through increasing levels of cAMP might have enhancing effects on lipolysis and different amounts of fat reduction in different regions in the body might be explained by this hypothesis, which further confirms our results that showed variations in fat reduction among different regions.

Results of lipid profile can be changed by alteration in dietary habits and when patients perform exercise training. However, the studies discussed [30, 31] did not measure the aerobic fitness and dietary variables. In this context, our study is important because there was control of both diet and training.

Thus LLLT can improve pathways of energetic metabolism, mainly lipid metabolism, potentiating the effects of LLLT and, when combined with exercise of moderated intensity, could be used as a new approach to control dyslipidemia and consequently have a role in treatment of diseases related to dyslipidemia and obesity [2, 15]. The summary of our key findings of this study is shown in Fig. 4.

Acknowledgments

We are grateful to Dr. Pinar Avci for the interesting discussion about the mechanisms involved in the lipid metabolism.

References

1. Tock L, Prado WL, Caranti DA, Cristofalo DM, Lederman H, Fisberg M, Siqueira KO, Stella SG, Antunes HK, Cintra IP, Tufik S, de Mello MT, Damaso AR. Nonalcoholic fatty liver disease decrease in obese adolescents after multidisciplinary therapy. Eur J Gastroenterol Hepatol. 2006; 18(12):1241–1245. doi:10.1097/01.meg.0000243872.86949.95 00042737-200612000-00001 [pii]. [PubMed: 17099371]
2. Gauthier MS, Couturier K, Latour JG, Lavoie JM. Concurrent exercise prevents high-fat-diet-induced macrovesicular hepatic steatosis. J Appl Physiol. 2003; 94(6):2127–2134. doi:10.1152/japplphysiol.01164.2002.01164.2002 [pii]. [PubMed: 12547845]
3. Linsel-Nitschke P, Tall AR. HDL as a target in the treatment of atherosclerotic cardiovascular disease. Nat Rev Drug Discov. 2005; 4(3):193–205. doi:10.1038/nrd1658. [PubMed: 15738977]
4. Pappachan JM, Chacko EC, Arunagirinathan G, Sriraman R. Management of hypertension and diabetes in obesity: non-pharmacological measures. Int J Hypertens. 2011; 2011:398065. doi:10.4061/2011/398065. [PubMed: 21629871]
5. Sene-Fiorese M, Duarte FO, Scarmagnani FR, Cheik NC, Manzoni MS, Nonaka KO, Rossi EA, de Oliveira Duarte AC, Damaso AR. Efficiency of intermittent exercise on adiposity and fatty liver in rats fed with high-fat diet. Obesity (Silver Spring). 2008; 16(10):2217–2222. doi:oby2008339 [pii] 10.1038/oby.2008.339. [PubMed: 18719640]
6. Duarte FO, Sene-Fiorese M, Manzoni MS, de Freitas LF, Cheik NC, de Oliveira G, Duarte AC, Nonaka KO, Damaso A. Caloric restriction and refeeding promoted different metabolic effects in fat depots and impaired dyslipidemic profile in rats. Nutrition. 2008; 24(2):177–186. doi:S0899-9007(07)00318-8 [pii] 10.1016/j.nut.2007.10.012. [PubMed: 18068950]
7. De Marchi T, Leal EC Junior, Bortoli C, Tomazoni SS, Lopes-Martins RA, Salvador M. Low-level laser therapy (LLLT) in human progressive-intensity running: effects on exercise performance, skeletal muscle status, and oxidative stress. Lasers Med Sci. 2012; 27(1):231–236. doi:10.1007/s10103-011-0955-5. [PubMed: 21739259]
8. Ferraresi C, de Brito OT, de Oliveira ZL, de Menezes Reiff RB, Baldissera V, de Andrade Perez SE, Matheucci E Junior, Parizotto NA. Effects of low level laser therapy (808 nm) on physical strength training in humans. Lasers Med Sci. 2011; 26(3):349–358. doi:10.1007/s10103-010-0855-0. [PubMed: 21086010]
9. Paolillo FR, Milan JC, Aniceto IV, Barreto SG, Rebelatto JR, Borghi-Silva A, Parizotto NA, Kurachi C, Bagnato VS. Effects of infrared-LED illumination applied during high-intensity treadmill training in postmenopausal women. Photomed Laser Surg. 2011; 29(9):639–645. doi:10.1089/pho.2010.2961. [PubMed: 21749263]
10. Karu TI, Pyatibrat LV, Afanasyeva NI. Cellular effects of low power laser therapy can be mediated by nitric oxide. Lasers Surg Med. 2005; 36(4):307–314. doi:10.1002/lsm.20148. [PubMed: 15739174]
11. Huang YY, Sharma SK, Carroll J, Hamblin MR. Biphasic dose response in low level light therapy—an update. Dose-Response. 2011; 9(4):602–618. doi:10.2203/dose-response.11-009.Hamblin drp-09-602 [pii]. [PubMed: 22461763]
12. Jackson RF, Dedo DD, Roche GC, Turok DI, Maloney RJ. Low-level laser therapy as a non-invasive approach for body contouring: a randomized, controlled study. Lasers Surg Med. 2009; 41(10):799–809. doi:10.1002/lsm.20855. [PubMed: 20014253]
13. Jackson RF, Stern FA, Neira R, Ortiz-Neira CL, Maloney J. Application of low-level laser therapy for noninvasive body contouring. Lasers Surg Med. 2012; 44(3):211–217. doi:10.1002/lsm.22007. [PubMed: 22362380]
14. Duarte FO, Sene-Fiorese M, Cheik NC, Maria AS, de Aquino AE Jr, Oishi JC, Rossi EA, de Oliveira Duarte AC G, Damaso AR. Food restriction and refeeding induces changes in lipid pathways and fat deposition in the adipose and hepatic tissues in rats with diet-induced obesity. Exp Physiol. 2012; 97(7):882–894. doi: doi:10.1113/expphysiol.2011.064121. [PubMed: 22467759]
15. Horowitz JF. Fatty acid mobilization from adipose tissue during exercise. Trends Endocrinol Metab. 2003; 14(8):386–392. doi:Doi 10.1016/S1043-2760(03)00143-7. [PubMed: 14516937]

16. Caruso-Davis MK, Guillot TS, Podichetty VK, Mashtalir N, Dhurandhar NV, Dubuisson O, Yu Y, Greenway FL. Efficacy of low-level laser therapy for body contouring and spot fat reduction. Obes Surg. 2011; 21(6):722–729. doi:10.1007/s11695-010-0126-y. [PubMed: 20393809]

17. Vieira WH, Ferraresi C, Perez SE, Baldissera V, Parizotto NA. Effects of low-level laser therapy (808 nm) on isokinetic muscle performance of young women submitted to endurance training: a randomized controlled clinical trial. Lasers Med Sci. 2012; 27(2):497–504. doi:10.1007/s10103-011-0984-0. [PubMed: 21870127]

18. Moraes G, Altran AE, Avilez IM, Barbosa CC, Bidinotto PM. Metabolic adjustments during semi-aestivation of the marble swamp eel (Synbranchus marmoratus, Bloch 1795)—a facultative air breathing fish. Braz J Biol. 2005; 65(2):305–312. doi:S1519-69842005000200015 [pii]. [PubMed: 16097734]

19. Friedewald WT, Levy RI, Fredrickson DS. Estimation of the concentration of low-density lipoprotein cholesterol in plasma, without use of the preparative ultracentrifuge. Clin Chem. 1972; 18(6):499–502. [PubMed: 4337382]

20. Marchesini G, Bugianesi E, Forlani G, Cerrelli F, Lenzi M, Manini R, Natale S, Vanni E, Villanova N, Melchionda N, Rizzetto M. Nonalcoholic fatty liver, steatohepatitis, and the metabolic syndrome. Hepatology. 2003; 37(4):917–923. doi:10.1053/jhep. 2003.50161 S0270913903001216 [pii]. [PubMed: 12668987]

21. Liao CC, Su TC, Chien KL, Wang JK, Chiang CC, Lin CC, Lin RS, Lee YT, Sung FC. Elevated blood pressure, obesity, and hyperlipidemia. J Pediatr. 2009; 155(1):79–83. 83, e71. doi:doi:10.1016/j.jpeds.2009.01.036. [PubMed: 19446850]

22. Ruby BC, Robergs RA. Gender differences in substrate utilization during exercise. Sports Med. 1994; 17(6):393–410. [PubMed: 8091048]

23. Even PC, Rieth N, Roseau S, Larue-Achagiotis C. Substrate oxidation during exercise in the rat cannot fully account for training-induced changes in macronutrients selection. Metabolism. 1998; 47(7):777–782. doi:S0026-0495(98)90111-1 [pii]. [PubMed: 9667220]

24. Schrauwen P, Westerterp KR. The role of high-fat diets and physical activity in the regulation of body weight. Br J Nutr. 2000; 84(4):417–427. doi:S0007114500001720 [pii]. [PubMed: 11103212]

25. Do Nascimento CMO, Estadella D, Oyama LM, Damaso AR, Ribeiro EB. Effect of palatable hyperlipidic diet on lipid metabolism of sedentary and exercised rats. Nutrition. 2004; 20(2):218–224. doi:DOI 10.1016/j.nut.2003.10.008. [PubMed: 14962690]

26. Novelli ELB, Burneiko RCM, Diniz YS, Galhardi CM, Rodrigues HG, Ebaid GMX, Faine LA, Padovani CR, Cicogna AC. Interaction of hypercaloric diet and physical exercise on lipid profile, oxidative stress and antioxidant defenses. Food Chem Toxicol. 2006; 44(7):1167–1172. doi:DOI 10.1016/j.fct.2006.01.004. [PubMed: 16516366]

27. Helge JW, Watt PW, Richter EA, Rennie MJ, Kiens B. Fat utilization during exercise: adaptation to a fat-rich diet increases utilization of plasma fatty acids and very low density lipoproteintriacylglycerol in humans. J Physiol-London. 2001; 537(3):1009–1020. [PubMed: 11744773]

28. Helge JW. Long-term fat diet adaptation effects on performance, training capacity, and fat utilization. Med Sci Sport Exer. 2002; 34(9):1499–1504. doi:Doi 10.1249/01.Mss.0000027691.95763.B5.

29. Lee KU, Kim CH, Youn JH, Park JY, Hong SK, Park KS, Park SW, Suh KI. Effects of high-fat diet and exercise training on intracellular glucose metabolism in rats. Am J Physiol-Endoc M. 2000; 278(6):E977–E984.

30. Rushdi TA. Effect of low-level laser therapy on cholesterol and triglyceride serum levels in icu patients: a controlled, randomized study. EJCTA. 2010; 4(2):5.

31. Jackson RF, Roche GC, Wisler K. Reduction in cholesterol and triglyceride serum levels following low-level laser irradiation: a noncontrolled, nonrandomized pilot study. Am J Cosmet Surg. 2010; 27(4):177–184.

32. Bakeeva LE, Manteifel VM, Rodichev EB, Karu TI. [Formation of gigantic mitochondria in human blood lymphocytes under the effect of an He-Ne laser]. Mol Biol (Mosk). 1993; 27(3):608–617. [PubMed: 8316242]

33. Leal EC Junior, Lopes-Martins RA, Baroni BM, De Marchi T, Taufer D, Manfro DS, Rech M, Danna V, Grosselli D, Generosi RA, Marcos RL, Ramos L, Bjordal JM. Effect of 830 nm low-level laser therapy applied before high-intensity exercises on skeletal muscle recovery in athletes. Lasers Med Sci. 2009; 24(6):857–863. doi:10.1007/s10103-008-0633-4. [PubMed: 19057981]
34. Sussai DA, Carvalho Pde T, Dourado DM, Belchior AC, dos Reis FA, Pereira DM. Low-level laser therapy attenuates creatine kinase levels and apoptosis during forced swimming in rats. Lasers Med Sci. 2010; 25(1):115–120. doi:10.1007/s10103-009-0697-9. [PubMed: 19554361]
35. Paolillo FR, Corazza AV, Borghi-Silva A, Parizotto NA, Kurachi C, Bagnato VS. Infrared LED irradiation applied during high-intensity treadmill training improves maximal exercise tolerance in postmenopausal women: a 6-month longitudinal study. Lasers Med Sci. 2012 doi:10.1007/s10103-012-1062-y.
36. Brunori M, Giuffre A, Sarti P. Cytochrome c oxidase, ligands and electrons. J Inorg Biochem. 2005; 99(1):324–336. doi: S0162-0134(04)00316-2 [pii] 10.1016/j.jinorgbio.2004.10.011. [PubMed: 15598510]
37. Chen CH, Hung HS, Hsu SH. Low-energy laser irradiation increases endothelial cell proliferation, migration, and eNOS gene expression possibly via PI3K signal pathway. Lasers Surg Med. 2008; 40(1):46–54. doi:10.1002/lsm.20589. [PubMed: 18220263]
38. Geiger PG, Korytowski W, Girotti AW. Photodynamically generated 3-beta-hydroxy-5 alpha-cholest-6-ene-5- hydroperoxide: toxic reactivity in membranes and susceptibility to enzymatic detoxification. Photochem Photobiol. 1995; 62(3):580–587. [PubMed: 8570716]
39. Neira R, Arroyave J, Ramirez H, Ortiz CL, Solarte E, Sequeda F, Gutierrez MI. Fat liquefaction: effect of low-level laser energy on adipose tissue. Plast Reconstr Surg. 2002; 110(3):912–922. discussion 923-915. [PubMed: 12172159]
40. Athyros VG, Tziomalos K, Karagiannis A, Anagnostis P, Mikhailidis DP. Should adipokines be considered in the choice of the treatment of obesity-related health problems? Curr Drug Targets. 2010; 11(1):122–135. [PubMed: 20017725]
41. Koh EH, Park JY, Park HS, Jeon MJ, Ryu JW, Kim M, Kim SY, Kim MS, Kim SW, Park IS, Youn JH, Lee KU. Essential role of mitochondrial function in adiponectin synthesis in adipocytes. Diabetes. 2007; 56(12):2973–2981. doi:db07-0510 [pii] 10.2337/db07-0510. [PubMed: 17827403]
42. Huang H, Iida KT, Sone H, Yokoo T, Yamada N, Ajisaka R. The effect of exercise training on adiponectin receptor expression in KKAy obese/diabetic mice. J Endocrinol. 2006; 189(3):643–653. doi:189/3/643 [pii] 10.1677/joe.1.06630. [PubMed: 16731794]
43. de Almeida P, Lopes-Martins RA, Tomazoni SS, Silva JA Jr, de Carvalho PT, Bjordal JM, Leal EC Junior. Low-level laser therapy improves skeletal muscle performance, decreases skeletal muscle damage and modulates mRNA expression of COX-1 and COX-2 in a dose-dependent manner. Photochem Photobiol. 2011; 87(5):1159–1163. doi:10.1111/j.1751-1097.2011.00968.x. [PubMed: 21749398]
44. Franco W, Leite RS, Parizotto NA. Effects of low intensity infrared laser radiation on the water transport in the isolated toad urinary bladder. Lasers Surg Med. 2003; 32(4):299–304. doi:10.1002/lsm.10166. [PubMed: 12696098]
45. Khan MH, Victor F, Rao B, Sadick NS. Treatment of cellulite: part II. advances and controversies. J Am Acad Dermatol. 2010; 62(3):373–384. doi:doi:10.1016/j.jaad.2009.10.041, quiz 385-376. [PubMed: 20159305]

Fig. 1.
The training of swimming in individual tanks at controlled temperature (T=30 °C)±2. It is possible to see the jacket attached to the trunk during the training session

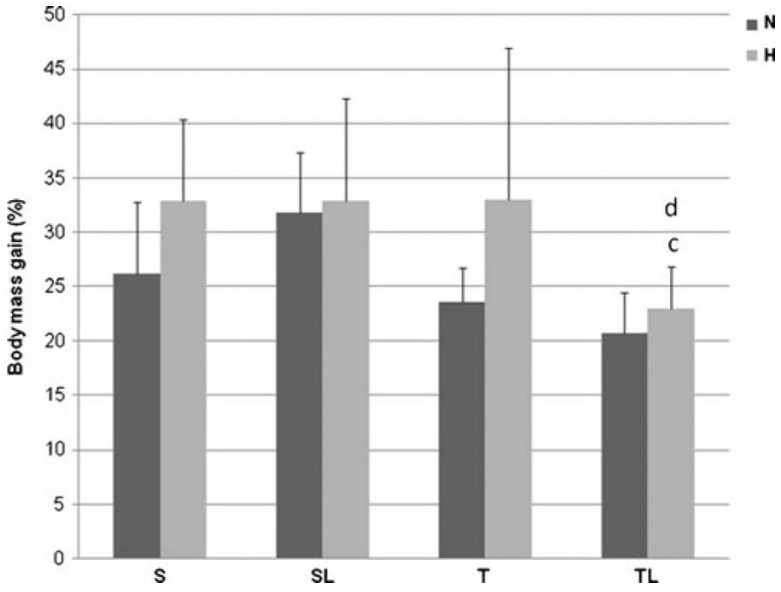

Fig. 2.

Values of weight gain in percentage of two series of animals: normocaloric diet (N) and hypercaloric diet (H). Different superscripts (*a* S versus SL; *b* S versus T; *c* SL versus TL; *d* T versus TL; *e* effects of high-fat diet in the different protocols) are significantly different (Tukey-Kramer multiple comparisons for $p<0.05$ except the specific comparisons: SHL×THL $p<0.05$, TH×THL $p<0.05$). The groups are designed: *S* sedentary; *SL* sedentary laser; *T* trained; *TL* trained laser

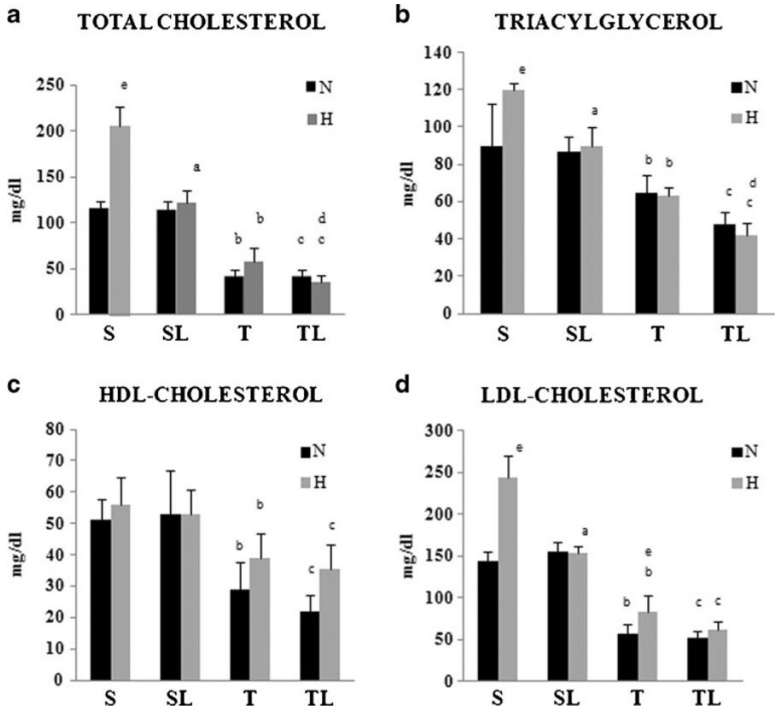

Fig. 3.

Blood lipid analysis. C denotes normocaloric diet and H denotes hypercaloric diet. The groups are designated: *S* sedentary; *SL* sedentary laser; *T* trained; *TL* trained laser. Values are expressed as mean±standard deviation (n=8/group). Different superscripts (*a* S versus SL; *b* S versus T; *c* SL versus TL; *d* T versus TL; *e* effects of hypercaloric diet in the different protocols) are significantly different (Tukey–Kramer multiple comparisons for $p<0.001$ except the specific comparisons for cholesterol total: TH×THL $p<0.05$; for triglycerides: SN×TN $p<0.01$; and TH×THL $p<0.01$; for HDL-cholesterol: SN×TN $p< 0.01$, SHL×THL $p<0.05$ and SH×TH $p<0.05$; LDL-cholesterol: TN×TH $p<0.05$). **a** Total cholesterol. **b** Triacylglycerol. **c** HDL-cholesterol. **d** LDL-cholesterol

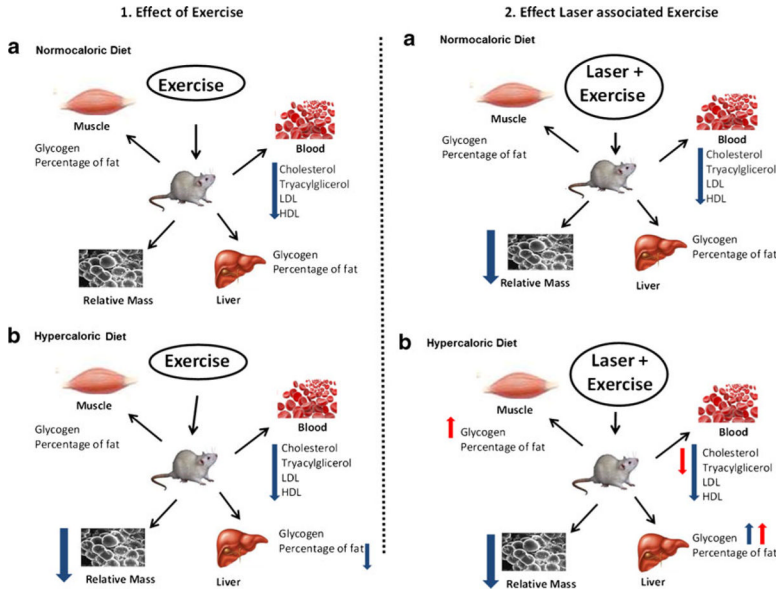

Fig. 4.

The summary of key findings related to kind of diet and training. The *blue arrows* showed the comparisons control groups×trained and the *red arrows* the comparisons with trained groups×trained and laser groups. The comparison with laser effects associated to exercise for hypercaloric groups showed a *red arrow* and a *blue arrow* for the variables of blood. The *red arrow* includes the variables cholesterol, and tryacylglicerol as the *blue arrow* includes all variables

Table 1

Characteristics of the laser used in the experimental procedures

Type	**Ga-Al-As**	**Treatment time**	**47 s**
Wavelength	830 nm (infrared)	Number of points	2 points
Frequency	Continuous wave (CW)	Total energy delivered	9.4 J
Optical output	100 mW		
Spot diameter	0.6 mm		
Power density	35.36 W/cm^2	Application mode: probe held stationary in skin contact with a 90° angle and slight pressure. Used always after the training session.	
Energy per point	4.7 J/point		
Energy density	1,662 J/cm^2		

These are the characteristics of equipment and wavelength used during the study. All applications were realized to the same person (Theralase, DMC, Equipment, São Carlos, SP, Brazil)

Table 2

Relative mass of tissues in rat fed with normocaloric or hypercaloric diet (g/100 g of body weight)

Mass of	SN	SNL	TN	TNL	SH	SHL	TH	THL
Heart	0.28±0.10	0.35±0.02	0.36±0.01	0.38±0.04	0.33±0.03	0.33±0.02	0.35±0.04	0.36±0.02
Liver	2.66±0.29	2.52±0.34	2.28±0.32	2.54±0.20	2.28±0.32	2.54±0.20	2.28±0.18	2.48±0.12
GAST	0.45±0.10	0.49±0.03	0.55±0.03	0.52±0.04	0.49±0.03	0.47±0.01	0.52±0.02	0.51±0.02
SOL	0.04±0.00	0.04±0.00	0.04±0.01	0.04±0.00	0.04±0.00	0.04±0.00	0.04±0.00	0.04±0.00
BAT	0.07±0.02	0.06±0.01	0.09±0.01	0.09±0.02	0.11^{e}±0.04	0.08±0.01	0.10±0.01	0.10±0.01
EPI	0.78±0.11	1.13^{a}±0.26	0.79±0.12	0.67^{c}±0.09	1.38^{e}±0.23	1.47±0.07	1.13±0.14	1.29^{e}±0.21
RET	0.74±0.16	1.37^{a}±0.26	1.04±0.29	0.77^{c}±0.17	2.09^{e}±0.50	2.19^{e}±0.37	1.47^{b}±0.19	1.53^{ce}±0.12
VIS	0.69±0.16	0.81±0.11	0.70±0.25	0.83±0.29	0.99±0.16	1.14±0.58	1.00±0.18	1.05±0.35

Values are expressed as mean±standard deviation (n=8/group). Different superscripts

The groups are designed: *SN* sedentary normocaloric diet; *SNL* sedentary normocaloric diet laser; *TN* trained normocaloric diet; *TNL* trained normocaloric diet laser; *SH* sedentary hypercaloric diet; *SHL* sedentary hypercaloric diet laser; *TH* trained hypercaloric diet; *THL* trained hypercaloric diet laser. The variables are the mass for: heart; liver; *GAST* gastrocnemius muscle; *SOL* soleus muscle; *BAT* brown Adipose Tissue; EPI: Epididymal adipose tissue; RET: Retroperitoneal adipose tissue; *VIS* Visceral adipose tissue

^{a}S versus SL;

^{b}S versus T;

^{c}SL versus TL;

^{d}T versus TL;

^{e}effects of hypercaloric diet in the different protocols are significantly different (Tukey–Kramer multiple comparisons for p <0.001 except the specific comparisons: Brown adipose tissue, SC × SH p<0.05; epididymal, SN × SNL p<0.05; retroperitoneal, SH × TH and TH × THL p<0.05.

Table 3

Glycogen hepatic/muscle (μml/g) and percentage of fat in the tissues of rats fed with normocaloric or hypercaloric diet

	SN	SNL	TN	TNL	SH	SHL	TH	THL
Glycogen content								
Liver	0.80±0.41	0.87±0.23	1.06±0.42	1.04±0.23	0.78±0.13	0.87±0.13	1.00±0.08	1.68^{cde}±0.34
GAST	0.29±0.03	0.31 ±0.02	0.31 ±0.02	0.28±0.03	0.30±0.02	0.39^{ea}±0.06	0.29±0.03	0.30^{c}±0.02
SOL	0.38±0.09	0.35±0.16	0.36±0.05	0.35 ±0.08	0.37±0.07	0.38±0.14	0.22±0.04	0.57^{d}±0.17
Percentage of fat								
Liver	1.43±0.26	1.56±0.23	1.67±0.17	1.63 ±0.32	2.74^{e}±1.39	2.74^{e}±0.43	1.47^{b}±0.25	1.87±0.32
Gast	0.36±0.11	0.37±0.11	0.34±0.07	0.37±0.06	0.43±0.10	0.43±0.15	0.39±0.10	0.37±0.09

Values are expressed as mean± standard deviation (n=8/group). The differences are highlighted in italics. Different superscripts

The groups are designed: *SN* sedentary normocaloric; *SNL* sedentary normocaloric laser; *TN* trained normocaloric; *TNL* trained normocaloric laser; *SH* sedentary hypercaloric; *SHL* sedentary hypercaloric laser; *TH* trained hypercaloric; *THL* trained hypercaloric laser. The variables are: *GAST* gastrocnemius muscle; *SOL* soleus muscle

^{a}S versus SL;

^{b}S versus T;

^{c}SL versus TL;

^{d}T versus TL;

^{e}effects of hypercaloric diet in the different protocols are significantly different (Tukey–Kramer multiple comparisons for p<0.001 except the specific comparisons for glycogen: liver, TH × THL p<0.01 and TNL × THL p<0.05; gastrocnemius muscle, SNL × SHL p<0.01 and SHL × THL p<0.01; for percentage of fat: liver, SN SH p<0.01, SNL × SHL p<0.05 and SH × TH p<0.01).

Lasers Med Sci. Author manuscript; available in PMC 2014 September 01.

THE JOURNAL OF ALTERNATIVE AND COMPLEMENTARY MEDICINE
Volume 19, Number 4, 2013, pp. 376–382

DOI: 10.1089/acm.2011.0531

Case Reports

Low-Level Laser Therapy in Pediatric Bell's Palsy: Case Report in a Three-Year-Old Child

Carla Raquel Fontana, PhD,[1] and Vanderlei Salvador Bagnato, PhD[2]

Abstract

Objectives: The objective of this study was to apply low-level laser therapy (LLLT) to accelerate the recovery process of a child patient with Bell's palsy (BP). *Design:* This was a prospective study.
Subject: The subject was a three-year-old boy with a sudden onset of facial asymmetry due to an unknown cause.
Materials and methods: The low-level laser source used was a gallium aluminum arsenide semiconductor diode laser device (660 nm and 780 nm). No steroids or other medications were given to the child. The laser beam with a 0.04-cm^2 spot area, and an aperture with approximately 1-mm diameter, was applied in a continuous emission mode in direct contact with the facial area. The duration of a laser session was between 15 and 30 minutes, depending on the chosen points and the area being treated. Light was applied 10 seconds per point on a maximum number of 80 points, when the entire affected (right) side of the face was irradiated, based on the small laser beam spot size. According to the acupuncture literature, this treatment could also be carried out using 10–20 Chinese acupuncture points, located unilaterally on the face. In this case study, more points were used because the entire affected side of the face (a large area) was irradiated instead of using acupuncture points.
Outcome measures: The House-Brackmann grading system was used to monitor the evolution of facial nerve motor function. Photographs were taken after every session, always using the same camera and the same magnitude. The three-year-old boy recovered completely from BP after 11 sessions of LLLT. There were 4 sessions a week for the first 2 weeks, and the total treatment time was 3 weeks.
Results: The result of this study was the improvement of facial movement and facial symmetry, with complete reestablishment to normality.
Conclusions: LLLT may be an alternative to speed up facial normality in pediatric BP.

Introduction

Facial nerve paralysis may be congenital or neoplastic or may result from trauma, toxic exposures, iatrogenic causes, autoimmune inflammation, vascular ischemia, or infections.[1,2] This problem can also be caused by a degenerative cerebral disease, the Guillain-Barré syndrome, or other diseases that affect the nerves and any associated tissues.[3]

The most frequent nontrauma-related etiologies in otherwise neurologically intact patients is the idiopathic dysfunction of the cranial nerve VII, called Bell's palsy (BP), which has a good prognosis. The facial nerve has motor, sensory, and parasympathetic fibers. Among its functions are the vital control of the facial expression, taste to the anterior two thirds of the tongue, and salivary and lachrymal-gland secretion. The main sign for BP is a distorted facial expression, but patients can experience symptoms (e.g., taste loss, pain around the ear, or hearing problems[1,4]). One of the main differential diagnoses for central paralysis versus BP is that only the voluntary movement of the lower face is affected, without any loss of taste, salivary, and lachrymal secretions. Patients with those characteristics should immediately be referred to a neurologist.[1,4,5]

Warning signs for a serious underlying cause are otitis media (osteomyelitis), hearing loss, lymphadenopathy, tonsillar enlargement (parotid tumor), mastoid enlargement, frontal sparing, and motor function of tongue/fingers for a duration of longer than 1 month. Physical examination, including otoscopy, and examination of the parotid and cranial nerves are important in order to determine the cause and the location of facial nerve injury. The involvement of other cranial nerves can be a sign of polyneuropathy or malignancy and a concomitant involvement of the VI pair reveals a pathology of the brainstem, V, VI, and VIII, pathology of

[1]Department of Clinical Analysis, School of Pharmaceutical Sciences, Univ Estadual Paulista (UNESP), Araraquara, SP, Brazil.
[2]Institute of Physics of São Carlos, University of São Paulo (USP), São Carlos, SP, Brazil.

the petrous apex, and the IX, X, and XI, pathology of the skull base.[1,5,6]

Although most cases of facial palsy are idiopathic, their diagnosis can be determined only after having ruled out all other possible etiologies.[7,8]

The prevalence of BP is about four times lower for those patients who are up to 10 years old compared to adults; no significant difference between the sexes has been observed.[9] The right or left side of the face is equally affected, and less than 1% of cases are bilateral.[10] Diabetes and pregnancy can increase the risk of developing Bell's palsy.[8,11]

Most people with BP (about 69%) show a spontaneous complete recovery. However, patients who did not receive an appropriate treatment may suffer from incomplete recovery and continue to show certain symptoms for life.[12] Residual facial muscle weakness with complications such as synkinesis, hyperkinesis, and/or contracture can occur. The latter may cause secondary psychologic sequels. Conventional treatment may include use of steroid or antiviral medications. A surgical decompression of the nerve is subject to debate in medicine.[13]

Although there is a controversy about the role of alternative treatment methods (e.g., physical therapy, acupuncture, local superficial heat therapy, massage, exercises, electrical stimulation, and laser therapy), all of these have been used with different degrees of success.[14]

Currently, each method has its indication in the treatment of lower motor facial palsy. A lot of attention has paid to improve the outcome of the treatments, and to decrease the incidence of complications in BP.

This report describes the complete recovery of a three-year-old boy from BP after 11 sessions of low-level laser treatment (LLLT). This case report will present a therapeutic option for treating BP and fully rehabilitating to normal.

Table 1. House-Brackmann System to Grade the Degree of Nerve Damage in a Facial Nerve Palsy

Grade 1: Normal
Normal symmetrical function in all areas
Grade 2: Slight
General: slight weakness noticeable only on close inspection
Forehead: good to moderate function
Eye: complete eye closure with minimal effort
Mouth: Slight asymmetry of smile with maximal effort
Synkinesis barely noticeable, contracture or spasm absent
Grade 3: Moderate
General: Obvious weakness but not disfiguring
Difference between sides, synkinesis and/or hemifacial spasm noticeable but not severe
May not be able to lift eyebrow
Forehead: slight to moderate movement
Eye: complete eye closure with effort,
Mouth: asymmetrical mouth movement with maximal effort
Obvious but not disfiguring synkinesis, mass movement or spasm
Grade 4: Moderately Severe
General: Obvious disfiguring weakness
Inability to lift brow
Forehead: no movement
Eye: Incomplete eye closure
Mouth: asymmetry of mouth with maximal effort
Severe synkinesis, mass movement, spasm
Grade 5: Severe
General: Motion barely perceptible
Facial asymmetry
Forehead: no movement
Eye: Incomplete eye closure
Mouth: slight movement corner mouth
Synkinesis, contracture, and spasm usually absent
Grade 6: Total
No movement, loss of tone, no synkinesis, contracture, or spasm

Materials and Methods

The methods of assessment of facial nerve function may be classified into two major groups: clinical and electrophysiologic.[15–19] The clinical evaluation of the degree of facial paralysis is a subjective parameter and may differ from examiner to examiner. Several systems have been proposed to standardize a universal scale, and the House-Brackmann (HB) system is the most widely accepted scale, adopted by the American Academy of Otolaryngology.[20]

The HB grading system is quite comprehensive and includes important criteria (e.g., the appearance of the frontal, periorbital, and peribuccal musculature, both at rest and in motion[16–18]). The literature shows rates of agreement for 93% of different evaluators using the HB system to assess the function of the facial nerve).[19,20] In this case study, the HB grading system (Table 1) was used to monitor the evolution of the facial nerve motor function. Photographs were taken after every session using the same camera and the same magnitude. The patient was photographed facing the camera both at rest and in motion.[6,10]

Case history

A three-year-old boy showed a sudden onset of facial asymmetry. The mother, who accompanied her child to the clinic, stated that he had difficulties closing his right eye. She denied excessive eye tearing, fever, cough, vomiting, diarrhea, cold, or recent travel. No signs of gait disturbance, weakness, numbness, hyperacusis, tingling, or taste disturbance were noted. No allergies were known for this patient, and he was taking no medication.

At the emergency room of a public hospital in Sao Carlos, a medical doctor prescribed laser therapy for BP on the child's facial muscles and nerves of the affected side of the face, to be performed by the Optics Group of the University of Sao Paulo. A clinical evaluation of the degree of severity of the facial paralysis on day 1, was evaluated as an HB, Grade 5. Approved informed consent and permission to take pictures of the patient was obtained from the boy's mother, protocol number: BP/2011 at the University of Sao Paulo.

Medical history

There is no medical history for the child. In general, the child appeared to be well nourished and of appropriate height and weight for the stated age. The child had not been in pain, or subject to infections or frequent headaches.

The only unusual situation experienced by the patient was a stress condition with his parents before the rapid onset of BP, presenting irritability at that occasion.

Light Source and Irradiation Procedure

The patient was treated using laser therapy without any other co-intervention. The only other medication used was artificial tears (Refresh® Allergan) to maintain the eye moisture. To document the progress, the patient pictures were captured during each session.

The low-level laser source used was a gallium aluminum arsenide semiconductor diode laser device (Twin-Laser; MmOptics Industry, São Carlos, SP, Brazil), which had the following specifications: wavelength of 780 nm, 70 mW output power; area of beam spot size of 0.04 cm^2, aperture of approximately 1 mm diameter. The time of irradiation was 10 seconds per point, with an energy density of 17.5 J/cm^2 per point, during each of the first 4 sessions.

During the 5th, 7th, 9th, and 11th sessions, the diode laser wavelength was chosen at 660 nm, because according to the literature[21–25] the infrared light (780 nm) has more penetration and can stimulate deeper regions, especially during the early treatment. Once the stimulus has been initiated, however, a 660-nm laser with a low (10 J/cm^2) or moderate (60 J/cm^2) energy density can be helpful to accelerate the neural recovery.[21,23,24,26] For these reasons, from the sixth session onward, the energy density was progressively decreased, based on the patient's report as well as clinical observations. Output power of 60 mW, 50 mW, and 40 mW were applied for sessions 6, 7, and 8. The laser beam was delivered in a continuous emission mode in direct contact with the facial area. LLLT should be used within hours following the onset of BP. The earlier the irradiation is started, the faster and better are the results. This patient received a total of 11 sessions. In the first 2 weeks, there were 4 sessions a week, so a total of 3 weeks of treatment was done in this case.

The length of the laser treatment session varied from 15 to 30 minutes, depending on the number of chosen points and the area being treated. The irradiation can be applied to all the facial muscles and nerves of the lower part of the face or frontalis to treat BP. A maximum of up to 80 points may therefore have to be used to apply the laser beam with a spot area of 0.04 cm^2. Each application included points around the eyes, mouth, maxilla, and other areas penetrated by the facial nerve. The distance between the points treated were very close in the beginning of the treatment and gradually became more distant from each other (after the eighth session). The laser treatment should not be applied close to the eyes without proper eye protection. During the laser therapy, it is recommended to use specific glasses or to cover the eyes with aluminum foil wrapped in cotton gauze, especially if the patient is unable to close the eyelid.

Outcome

An obvious improvement was noted during the course of the treatment: a marked development of the right facial muscle strength and a progressive attenuation of the facial asymmetry. After every session, the overall improvement of different facial expressions were rated and scored (Fig. 1) using the HB grading system.

Discussion

To the best of the authors' knowledge, laser treatment and management of LLLT on BP for children have not yet been evaluated or documented in depth in the literature so far. Neural regeneration and neuromuscular recovery after different types of injury have been explored more deeply in the literature. Several studies have used therapeutic sources (e.g., low-power lasers) in order to promote early nerve regeneration. However, this laser therapy has not gained unanimous acceptance with regard to its methodology, having led to controversial conclusions. Barbosa et al.[21] compared the effects of low-power lasers (660 nm and 830 nm) applied during 21 days to regenerate sciatic nerves following crushing injuries in rats. One source found that the laser application at 660 nm was effective in promoting early functional recovery. In another study, Rochkind et al.[22] examined the effects of composite implants of cultured embryonal nerve cells and the effect of 14 days of laser irradiation (780 nm) on the regeneration and repair of the completely transected spinal cord. The results showed that infrared laser light enhances axonal sprouting and spinal cord repair. Another study[23] using a biodegradable nerve guide conduit and a red laser irradiation applied daily for 21 consecutive days demonstrated that LLLT contributes to accelerate neural repair in rats. Gigo-Benato et al.[24] investigated the effect of 660 nm and 780 nm laser light using different energy densities on neuromuscular and functional recovery as well as on matrix metalloproteinase (MMP) activity after crush injury in sciatic nerves of rats. The data suggest that a 660 nm LLLT with low (10 J/cm^2) or moderate (60 J/cm^2) energy densities can accelerate neuromuscular recovery after nerve crush injuries in rats. Dias et al.[25] reported that low-level laser therapy (780 nm) stimulated the oxidative metabolism and the expression of MMPs of the masseter muscles, which may indicate a matrix remodeling process. However, a high dosage of infrared laser light did not show the best results for oxidative metabolism.

In this case report, both effects of 660 nm and 780 nm laser light were explored, avoiding high dosage based on results reported in the literature. For this patient, both the wavelength selection and point selection were adjusted from time to time, and seemed to contribute to the patient's improvement. In order to balance between beneficial stimulatory and inhibitory effects, the authors suggest alternating use of red and infrared wavelength. During the first five treatment sessions, only infrared laser light (780 nm) was used, while the other sessions were carried out alternating red laser (660 nm) and infrared laser light. This was done in order to avoid plateau effect stimulations due to an extended use of a single wavelength.

Initially, LLLT was mainly used in medicine to assist in wound healing and pain relief. The field of application of LLLT has now been broadened to include use in treatment of diseases such as stroke, myocardial infarction, and neurodegenerative or traumatic brain disorders. In a recent review, Hashmi et al.[26] covered the mechanisms of LLLT that operate both on a cellular and a tissue level. The authors discussed animal studies and human clinical trials of LLLT for indications with relevance to neurology. These studies support the present case application and reinforce the rapidly growing applications of low level laser in physical therapy, acupuncture, chiropractic, sports medicine, and increasingly in mainstream medicine. Hashmi et al.[27] reviewed the studies that compared continuous wave and pulsed light in both animals and patients. There is some evidence that applications using pulsed light do show effects different from

FIG. 1. Clinical evaluation of facial paralysis degree at the first day classified as House-Brackmann (HB) Grade 5 and after the following 11 sessions (in 3 weeks) of treatment classified as HB Grade 1 (normal symmetrical function in all areas). **A.** First session (day 1, Tuesday) Right-sided facial nerve palsy. HB Grade 5 during initial presentation (first week). **B.** Facial asymmetry (day 1) (first week). Eye: Incomplete eye closure. Mouth: slight movement corner of mouth. Muscles: Nasolabial folds away; fall of the labial commissure jaw muscle does not contract on the affected side. **C.** Third session (day 3, Thursday) (first week). The face is asymmetrical both at rest and during mimicry. Patient cannot wrinkle one side of his forehead or jaw or raise the eyebrow, and when attempting to smile, the face is pulled to the opposite side. **D.** Fourth session (day 4, Friday). Finalizing first week of treatment. Labial commissure begins to restore position (not fallen), but the jaw muscles in the area close to right mental foramen are not contracting. **E.** Fifth session (day 7, Monday). HB Grade 3 (initializing the second week of treatment). Difference between sides, noticeable but not severe. Not able yet to easily lift eyebrow. Eye: complete eye closure with effort. Mouth: asymmetrical mouth movement with maximal effort. **F.** Fifth session (second week). HB Grade 3. Application of low-level laser source: red diode laser device, 660 nm, 50 mW, 12.5 J/cm^2. Note especially the nasolabial folds, forehead wrinkles, corner of the mouth, and symmetry of the face starting return to normality. **G.** Sixth session (day 8, Tuesday) (second week). Patient was sleeping. Note the eye closes perfectly on the affected side. Face symmetry reestablished at rest. **H.** Seventh session (day 10, Thursday). HB Grade 2 (second week). Slight weakness noticeable only on close inspection. Mouth: Slight asymmetry of smile with maximal effort. **I.** HB Grade 2, seventh session (day 10, Thursday) (second week). Forehead: good-to-moderate function. Eye: complete eye closure with minimal effort. **J.** HB Grade 1, ninth session. Last week of treatment (third week) (day 15, Tuesday). Normal symmetrical function in all areas. Total ability to move corners of mouth. **K.** HB Grade 1. **L.** Tenth session. HB Grade 1 (day 17 Thursday). Normalized nasolabial folds. Symmetry of the face is normalized. **M.** HB Grade I (day 17). Normal symmetrical function in all areas. **N.** Eleventh session. HB Grade 1 (day 18, Friday). Normal symmetrical function in all areas. **O.** Eleventh session. HB Grade 1 (day 18, Friday). Final session. (Photos printed with parental permission. Since the permission was signed in Portuguese, to facilitate the understanding of "Termo de Consentimento Liver Esclarecido," we also added an English version of this document.)

those using continuous-wave light. However, further work is needed to define these effects for different disease conditions and pulse structures. According to Cruccu et al.,[28] laser pulses excite superficial free nerve endings stimulated by small-myelinated (Adelta) and unmyelinated (C) fibers. The authors reveal that pulsed laser may be useful in patients with lesions affecting the trigeminal thermal pain pathways.

In the present study, the duration of a laser session was between 15 and 30 minutes, depending on the number of chosen points on the treated area. The maximum number of points used was 80. It was necessary to irradiate on 80 spots, when the entire face was treated, as the spot of the laser beam used is small. According to acupuncture literature,[29–31] this treatment could also be carried out using less than 20 Chinese

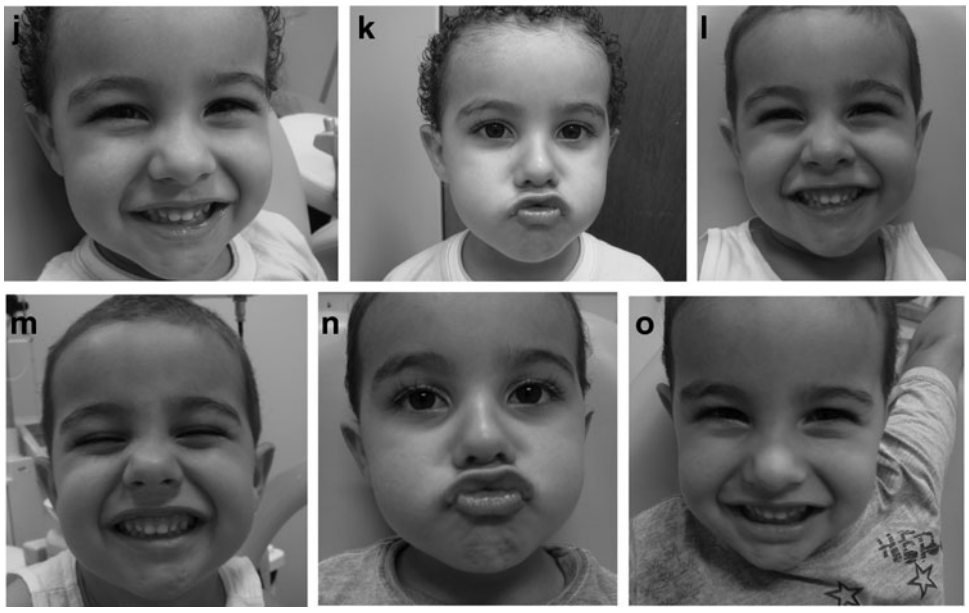

FIG. 1. (Continued).

acupuncture points defined unilaterally on a face. O'Connor and Bensky,[32] Wang and Yang,[33] and other authors[34,35] have used a much smaller number of points (average of 10 acupuncture points) with equally good success. Lei et al.[36] also used few acupuncture points to achieve a complete recovery from BP of a 27-year-old woman, 27 weeks pregnant. After 2 weeks of acupuncture treatment the symptoms had disappeared, her face was restored to normal, and HB returned to grade 1.

In the case reported here, more points were used because the laser device had a laser beam with a spot area of 0.04 cm^2. Furthermore, instead of using acupuncture points, our irradiation protocol covered the entire right side of the face, requiring about 80 points to cover the large irradiation area. Using different laser equipment with a larger "pad" applicator could also lead to the same satisfactory treatment results using fewer irradiation points.[37] In the current study, the laser beam with a spot area of 0.04 cm^2 was delivered in a continuous emission mode in direct contact with the facial area without targeting acupuncture points. A complete recovery was achieved after 3 weeks of treatment.

According to Wong and Wong,[38] acupuncture in a 7-year-old child with chronic BP takes longer to show good results. The patient was given 25 acupuncture treatment sessions in 2 months. The acupuncture points used (apparently on only the affected side, except for midline points) included the following three sets of points: (1) on the face—LI20, ST2,ST3, ST4, ST6, ST7, SI18, BL2, TE17, TE23, GB14, GV26, CV24, EXHN5, and EX-HN16; (2) on the upper extremity—LI11, HT8, SI3, PC8, TE5; and (3) on the lower extremity—ST36, ST40, SP6, SP10, BL67, and LR3. Self-perceived muscle strength when smiling and puffing out cheeks increased from 20% of normal strength to 65%, and the strength when raising eyebrows increased from 10% to 70%. Synkinesis was attenuated. HB scale changed to grade 3 after treatment.

Hou et al.[39] compared therapeutic effects of acupuncture combined with He-Ne laser irradiation to use of Western medicine to treat facial paralysis. After 14 days, the cure rate was 81.8% for the acupuncture with laser group, and 45.20% for the medication group. There was a significant difference concerning the results of the two groups after treatment, showing that the therapeutic effect of acupuncture combined with He-Ne laser on facial paralysis is higher than that of routine medication. Tang et al.,[40] in a retrospective study, reviewed the factors that may influence the treatment outcome for patients with idiopathic facial nerve paralysis. Full recovery was more likely for patients treated with combined acyclovir and prednisolone compared to being treated with prednisolone alone. However, adult patients who were treated with routine medication with concurrent chronic medical illness and facial nerve paralysis HB Grade IV–VI showed a reduced chance of full recovery of facial nerve paralysis. Salman and MacGregor[41] studied the effect of corticosteroids when treating pediatric BP. The pediatric trial did not provide proof of benefit when using corticosteroids. Even though the study was based on a quite heterogeneous population evaluated, based on a subsequent systematic review, the authors do not recommend the routine use of steroids in children with BP. Prescott,[42] evaluating 228 children with BP during a 10-year period, concluded that the children treated with a high dose of steroids did not show any positive effects, neither an improved recovery rate nor a decreased recovery period.

Patients or people responsible for the pediatric patients receiving laser therapy usually asked about the number of sessions needed to obtain an optimal therapeutic effect. Unfortunately, there is no general rule. Each case must be treated individually, and for chronic conditions, patients may receive recommendation to continue lifelong treatment. The patient in this report received the laser therapy promptly after he had the onset of BP. In this case, improvement was initially noted after 5 sessions (of a total of 11 sessions during 3 weeks of treatment), but sometimes the beneficial effect can reach a plateau before complete recovery. If the effect flattens out toward the end of the course after a certain period of continued treatment, it is suggested that the patient stop the treatment temporarily, continuing only after a 2–3-weeks' break in the treatment.

Based on data from the literature, it was determined that combinations of many different laser parameters may influence clinical outcomes. Various types of laser equipment and treatment parameters that need to be considered include the following: continuous wave or pulsed wave, power output, beam spot size, beam diameter, wavelength, pulse frequency, and duty cycle. Additional factors include the irradiation duration, treatment technique, number of points to be treated (or the area of affected tissue to be treated), and the target tissue depth. Patient characteristics such as skin color and tissue type, and whether the condition is acute, subacute, or chronic should also be considered. Even given this limited set of factors, there still remain innumerable combinations of factors to consider when applying laser therapy. The purpose of this study was to present the current LLLT protocol, as an alternative therapy, to routine medication when treating pediatric BP. Other LLLT or light-emitting diode protocols could also be effective.

Conclusions

Common signs of BP are weakness of the muscles, generally on one side of the face, one-sided drooping eyelid or mouth, or drooling from one side of the mouth as presented in this case. After treatment with a low-level diode laser, the patient's symptoms ceased and he completely recovered after 11 sessions during a 3-week treatment period. This study provided clinical evidence to support the early use of LLLT in BP as an effective alternative treatment, which may be considered a noninvasive application especially for pediatric use.

Acknowledgments

The authors acknowledge the financial support provided by Fundacao amparo a Pesquisa do estado de Sao Paulo (Centro pesquisa optica fotonica-centro pesquisa inovação e difusao program) and Conselho nacional desenvolvimento cientifico tecnológico.

Disclosure Statement

The authors affirm no financial affiliation with any commercial organization that might create a conflict of interest in connection with this article.

References

1. Facer GW. Facial nerve paralysis: Is it always Bell's palsy? Postgrad Med 1981;69:206–208, 211–213, 216.
2. Musani MA, Farooqui AN, Usman A, et al. Association of herpes simplex virus infection and Bell's palsy. J Pak Med Assoc 2009;59:823–825.
3. Smith N, Grattan-Smith P, Andrews IP, Kainer G. Acquired facial palsy with hypertension secondary to Guillain-Barre syndrome. J Paediatr Child Health 2010;46:125–127.
4. Sajadi MM, Sajadi MR, Tabatabaie SM. The history of facial palsy and spasm: Hippocrates to Razi. Neurology 2011;77: 174–178.
5. Kanerva M, Jonsson L, Berg T, et al. Sunnybrook and House-Brackmann systems in 5397 facial gradings. Otolaryngol Head Neck Surg 2011;144:570–574.
6. Merino P, Gómez de Liaño P, Villalobo JM, et al. Etiology and treatment of pediatric sixth nerve palsy. J AAPOS 2010; 14:502–505.
7. Linder TE, Abdelkafy W, Cavero-Vanek S. The management of peripheral facial nerve palsy: "Paresis" versus "paralysis" and sources of ambiguity in study designs. Otol Neurotol 2010;31:319–327.
8. Grosheva M, Beutner D, Volk GF, et al. Idiopathic facial palsy HNO. 2010;58:419–425.
9. Wong CL, Wong VC. Effect of acupuncture in a patient with 7-year-history of Bell's palsy. J Altern Complement Med 2008;14:847–853.
10. Smith SA, Ouvrier R. Peripheral neuropathies in children. In: Kenneth F, Swaiman SA, eds. Pediatric Neurology: Principles and Practice. 3rd ed. vol 2. St. Louis, MO: Mosby, 1999: 1178–1181.
11. Fawale MB, Owolabi MO, Ogunbode O. Bell's palsy in pregnancy and the puerperium: A report of five cases. Afr J Med Med Sci 2010;39:147–151.
12. Holland J, Bernstein J. Bell's palsy. Clin Evid (Online) 2011; pii:1204.
13. Browning GG. Bell's palsy: A review of three systematic reviews of steroid and anti-viral therapy. Clin Otolaryngol 2010;35:56–58.
14. Teixeira LJ, Soares BG, Vieira VP, Prado GF. Physical therapy for Bell's palsy (idiopathic facial paralysis). Cochrane Database Syst Rev 2008;3:CD006283.
15. Mackinnon SE, Dellon AL. Surgery of peripheral nerve. 1st ed. New York: Thieme Medical, 1988:638.
16. Yen TL, Driscoll CLW, Lalwani AK. Significance of House-Brackmann facial nerve grading global score in the setting of differential facial nerve function. Otol Neurotol 2003;24:118–122.
17. Satoh Y, Kanzaki J, Yoshihara S. A comparison and conversion table of the House-Brackmann facial nerve grading system and the Yanagihara grading system. Auris Nasus Larynx 2000;27:207–212.
18. Kang TS, Vrabec JT, Giddings N, Terris DJ. Facial nerve grading systems (1985–2002): Beyond the House-Brackmann scale. Otol Neurotol 2002;23:767–771.
19. Evans RA, Harries ML, Baguley DM, Moffat DA. Reliability of the House and Brackmann grading system for facial palsy. J Laryngol Otol 1989;103:1045–1046.
20. House JW, Brackmann DE. Facial nerve grading system. Otolaryngol Head Neck Surg 1985;93:146–147.
21. Barbosa RI, Marcolino AM, de Jesus Guirro RR, et al. Comparative effects of wavelengths of low-power laser in regeneration of sciatic nerve in rats following crushing lesion. Lasers Med Sci 2010;25:423–430.
22. Rochkind S, Shahar A, Amon M, Nevo Z. Transplantation of embryonal spinal cord nerve cells cultured on biodegradable microcarriers followed by low power laser irradiation for the treatment of traumatic paraplegia in rats. Neurol Res 2002; 24:355–360.
23. Shen CC, Yang YC, Liu BS. Large-area irradiated low-level laser effect in a biodegradable nerve guide conduit on neural regeneration of peripheral nerve injury in rats. Injury 2011; 42:803–813.
24. Gigo-Benato D, Russo TL, Tanaka EH, et al. Effects of 660 and 780 nm low-level laser therapy on neuromuscular recovery after crush injury in rat sciatic nerve. Lasers Surg Med 2010;42:673–682.
25. Dias FJ, Issa JP, Vicentini FT, et al. Effects of low-level laser therapy on the oxidative metabolism and matrix proteins in the rat masseter muscle. Photomed Laser Surg 2011;29:677–684.
26. Hashmi JT, Huang YY, Osmani BZ, et al. Role of low-level laser therapy in neurorehabilitation. PMR 2010;2(12 suppl 2):S292–S305.

27. Hashmi JT, Huang YY, Sharma SK, et al. Effect of pulsing in low-level light therapy. Lasers Surg Med 2010;42:450–466.
28. Cruccu G, Pennisi E, Truini A, et al. Unmyelinated trigeminal pathways as assessed by laser stimuli in humans. Brain 2003;126(pt 10):2246–2256.
29. Naeser MA. Acupuncture to treat paralysis due to central nervous system damage. J Altern Complement Med 1996;2: 211–248.
30. Naeser MA. Neurological rehabilitation: Acupuncture and laser acupuncture to treat paralysis in stroke, other paralytic conditions, and pain in carpal tunnel syndrome. J Altern Complement Med 1997;3:425–428.
31. Naeser MA. Acupuncture in the treatment of paralysis due to central nervous system damage. J Altern Complement Med 1996;2:211–248.
32. O'Connor J, Bensky DF. Acupuncture, A Comprehensive Text, Shanghai College of Traditional Chinese Medicine. Chicago: Eastland Press, 1981:609.
33. Wang Y, Yang J. Clinical observation on treatment of acupuncture for different stages of Bell's palsy. Zhongguo Zhen Jiu 2010;30:23–26.
34. Lim S. WHO Standard acupuncture point locations. Evid Based Complement Alternat Med 2010;7:167–168.
35. Qiu T, Li L. Discussion on the Chinese edition of the WHO Standard Acupuncture Point Locations in the Western Pacific Region. Zhongguo Zhen Jiu 2011;31:827–830.
36. Lei H, Wang W, Huang G. Acupuncture benefits a pregnant patient who has Bell's palsy: A case study. J Altern Complement Med 2010;16:1011–1014.
37. Saeki S. Equipment for low reactive level laser therapy including that for light therapy. Masui 2006;55:1104–1111.
38. Wong CL, Wong VC. Effect of acupuncture in a patient with 7-year-history of Bell's palsy. J Altern Complement Med 2008;14:847–853.
39. Hou YL, Li ZC, Ouyang Q, et al. Observation on therapeutic effect of acupuncture combined with He-Ne laser radiation on facial paralysis. Zhongguo Zhen Jiu 2008;28:265–266.
40. Tang IP, Lee SC, Shashinder S, Raman R. Outcome of patients presenting with idiopathic facial nerve paralysis (Bell's palsy) in a tertiary centre: A five year experience. Med J Malaysia 2009;64:155–158.
41. Salman MS, MacGregor DL. Should children with Bell's palsy be treated with corticosteroids? A systematic review. J Child Neurol 2001;16:565–568.
42. Prescott CA. Idiopathic facial nerve palsy in children and the effect of treatment with steroid. Int J Pediatr Otorhinolaryngol 1987;13:257–264.

Address correspondence to:
Carla Raquel Fontana, PhD
Department of Clinical Analysis
School of Pharmaceutical Sciences
Univ Estadual Paulista (UNESP)
Rua Expedicionários do Brasil 1621 Araraquara
SP 14801-960
Brazil

E-mail: fontanacr@fcfar.unesp.br

Lasers Med Sci (2013) 28:1467–1474
DOI 10.1007/s10103-012-1251-8

ORIGINAL ARTICLE

Phototherapy and resistance training prevent sarcopenia in ovariectomized rats

Adalberto Vieira Corazza · Fernanda Rossi Paolillo · Francisco Carlos Groppo · Vanderlei Salvador Bagnato · Paulo Henrique Ferreira Caria

Received: 7 August 2012 / Accepted: 10 December 2012 / Published online: 10 January 2013

Abstract The aim of this study was to histologically and biochemically analyze the effects of light-emitting diode therapy (LEDT) associated with resistance training to prevent sarcopenia in ovariectomized rats. Forty female Wistar rats (12 months old, 295–330 g) were bilaterally ovariectomized and divided into four groups ($n=10$ per group): control–sedentary (C), resistance training (T), LEDT–sedentary (L), and LEDT plus resistance training (LT). Trained rats performed a 12-week water-jumping program (3 days per week) carrying a load equivalent to 50–80 % of their body mass strapped to their back. Depending on the group protocol, the LED device (850 nm, 100 mW, 120 J/cm^2, spot size 0.5 cm^2) was used either as the only method or after the resistance training had been performed. The device was used in the single point contact mode (for 10 min). The irradiated region was the center of the greater trochanter of the right femur and the middle third of the rectus femoris muscle was subsequently analyzed histomorphometrically. Significant increases ($p<0.05$) were noted for the muscle volume of the T (68.1±19.7 %), the L (74.1±5.1 %), and the LT (68.2±11.5 %) groups compared to the C group (60.4±5.5 %). There were also significant increases in the concentrations of IGF-1, IL-1, and TNF-α in the muscles of the treated groups ($p<0.05$). Animals in the LT group showed a significant increase in IL-6 compared to T, L, and C groups ($p<0.05$). These findings suggest that resistance training and LEDT can prevent sarcopenia in ovariectomized rats.

Keywords LEDT · Ovariectomy · Phototherapy · Resistance training · Sarcopenia

A. V. Corazza (✉) · F. C. Groppo · P. H. F. Caria
Department of Morphology, Piracicaba Dental School (FOP), University of Campinas (UNICAMP), Av. Limeira, 901, 13414-903 Piracicaba, SP, Brazil
e-mail: avcorazza@gmail.com

F. C. Groppo
e-mail: fcgroppo@fop.unicamp.br

P. H. F. Caria
e-mail: phcaria@fop.unicamp.br

F. R. Paolillo · V. S. Bagnato
Optics Group from Physics Institute of São Carlos (IFSC), University of São Paulo (USP), Av. Trabalhador Sãocarlense, 400–Centro, 13560-970 São Carlos, SP, Brazil

F. R. Paolillo
e-mail: fer.nanda.rp@hotmail.com

V. S. Bagnato
e-mail: vander@ifsc.usp.br

Introduction

For women, menopause causes metabolic changes, which are related to a reduction of the estrogen production. Estrogen decreases the inflammatory response and accelerates muscle healing, through a proliferation and activation of the muscle fiber satellite cells [1] and expression of the insulin-like growth factor 1 (IGF-1) gene [2].

IGF-1 plays a vital role in regulating somatic growth and cellular proliferation, thereby contributing to human longevity. In aging, somatopause is associated with reduced activity of the hypothalamic–pituitary (growth hormone (GH)–IGF) system that decreases GH production by ~14 % per decade after middle age. This hormone deficit decreases the density of muscle fibers and leads to sarcopenia, a condition characterized by the loss of muscle mass and strength [3].

Resistance training (RT) is recognized as a means of preventing and treating sarcopenia in postmenopausal women by inflammatory cytokines modulation [4] and IGF-1

stimulation [5] with increases in number and activity of satellite cells and consequent muscle hypertrophy [6]. Despite the benefits of RT, the high muscle tension achieved with unusual exercise loads and/or detrimental effects on immune function promote a disturbed skeletal muscle resulting in muscle damage and low-grade inflammatory reaction [7]. These symptoms are accompanied by local glycogen depletion, excessive lactate production, and lymphocytes proliferation which decreases blood pH and causes cell death (apoptosis) [8]. Phenomenon apoptosis and sarcopenia in elderly are associated with an increased generation of reactive oxygen species (ROS) during sustained hyperemia following high-intensity exercise by biochemical and structural changes in the mitochondria [9]. ROS accumulation can promote oxidative stress by the addition of a single electron to the oxygen molecule and are usually generated by an altered function of the mitochondrial respiratory chain and an insufficient functioning of the antioxidant cellular defense mechanisms [10].

In order to regulate the deficiencies in cell activity in young and elderly subjects after physical training, amino acid, myostatin inhibitors, testosterone treatment, calorie restriction [11], and non-invasive physical procedures like ultrasound therapy, electrical current modalities [12], and phototherapy have been used.[13].

Phototherapy is justified in biochemical theory by the increased activity of the mitochondria and changes to the redox state. By the conversion of electromagnetic to biochemical energy with an increase in the oxygen binding, cellular respiration rate and production of adenosine triphosphate [14], avoiding release ROS high levels [15].

Low-level laser therapy (LLLT) is a form of light monochromatic, coherence, and colimation with proprieties to modulate pain and can promote healing in different biological systems [16]. Phototherapy showed excellent therapeutic response in muscle injury, especially in a metabolically weakened environment [17]. The inflammatory phase of muscle microlesion repair can be regulated by LLLT with a reduction of inflammatory cells and their mediators like cytokines as tumor necrosis factor α (TNF-α) [18] as well as photobiomodulation of oxygen-free radicals by modulate of antioxidants [15, 17, 19]. Consequently in the proliferative phase, LLLT stimulates growth factors such as IGF-1 [19], growth of blood vessels (angiogenesis) by signaling vascular endothelial growth factor and stimulated satellite cells of muscle fibers to prevent muscle atrophy [20].

An alternative to LLLT is the light-emitting diode therapy (LEDT), which yields similar results while offering an excellent cost–benefit ratio and short time of application [21] by using probes with large numbers of LEDs [22]. Device-based LED that is not a monochromatic and coherent source nevertheless shows a narrower emission band compared to conventional lamps. Concerning LLLT, LED energy density is distributed in a broader spectrum, possibly interacting with a higher number of specific photoreceptors and wide absorption window in biological tissues [23]. LEDT has been investigated for use in the repair process of tissues [24] and optimize the physical performance of athletes [13] and elderly people [22].

Depending on the fluence delivered on the surface of the tissue, different responses may be observed during the healing process [21] and prevention of muscle atrophy by phototherapy [25]. In this way, scientific research for correct dosimetric determination of wavelength, fluence, and irradiance, as well as each clinical condition and specific cellular modulation is of great relevance to promote the photobiomodulation in muscle tissue.

Given the lack of information regarding the action of LEDT in association with resistance training, and their effects on aging muscles, the aim of this study was to assess the effects of LEDT associated with resistance training protocol to prevent sarcopenia in ovariectomized rats. The hypotheses of this study is that LEDT plus RT can improve skeletal muscle metabolism after physical exercise for a long period, as evaluated by muscle volume fraction, muscle IGF-1, and inflammatory mediators (IL-1, IL-6, and TNF-α).

Materials and methods

Animals

Forty female Wistar rats (12 months old, 295–330 g) were housed in plastic cages (five rats per cage) in a temperature-controlled room (22±2 °C), with lights switched on from 6 AM to 6PM. The experiments were approved by the Ethics Committee for Animal Experimentation (CEUA/UNICAMP, protocol number 2115–1), and were performed in accordance with the ethical guidelines of the Brazilian Society of Laboratory Animal Science.

Ovariectomy

Bilateral ovariectomy was performed via translumbar incisions under ketamine/xylazine anesthesia (47.5 and 12 mg/kg, respectively, i.m.). The uterine tubes were ligated (catgut 4.0) and the ovaries were removed. Intact control groups were sham operated. The efficiency of the surgical procedure was verified by postmortem dissection to confirm the uterine tube atrophy. The rats were randomly divided into four groups (n= 10 per group): control–sedentary (C), resistance training (T), LEDT–sedentary (L), and LEDT plus resistance training (LT).

Training protocol

For high-intensity resistance training, the rats underwent weightlifting sessions every 48 h over a 12-week period in

a container (75 cm high, 30 cm diameter) with water at 30± 2 °C. For training, a small backpack filled with lead balls corresponding to 50–80 % of the body mass was strapped to the back of each animal. Prior to the exercise sessions, the rats underwent an adaptation period (in training groups) during which they were subjected to an increasing number of exercise sets (2–4) and repetitions (5–10; protocol adapted from Cunha et al. [26]) in the water every other day for 1 week (a total of 3 days). The animals were allowed to rest for 30 s between each set of exercises.

The body mass of the animals was measured preoperatively (12 days before the RT), after the adaptation period (1 week) and finally on the last day of each of the 12 weeks of the resistance training. The modified protocol of Hornberger and Farrar [27] was used with load weights that were appropriate for the training cycle. The load weight was proportional to each rat's body mass (Fig. 1) and increased from 50 % of the body mass (weeks 1 and 2) to 60 % (weeks 3–6), 70 % (weeks 7–10), and 80 % (weeks 11 and 12). The water column height started at 30 cm (week 1) and was increased to 35 cm (week 2) and 40 cm (week 3 onwards). The rats were killed 24 h after the end of the protocol and the rectus femoris muscle was removed for biochemical and histological analyses.

LED therapy

The prototype LED device used was developed in the Physics Institute of the University of São Paulo, São Carlos, SP, Brazil. The device was operated at 100 mW using a continuous wavelength of 850 nm with a 200 mW/cm^2 irradiation over an illuminated area of 0.5 cm^2. Phototherapy was started postoperatively on day 12. The fluence of 120 J/cm^2 [22, 25] was performed punctually, through a single point contact mode in the center of the greater trochanter of the right femur for 10 min every 48 h over a 12-week period. The center of the greater trochanter was located by palpation and was relabeled every week. Infrared LED shows a nonlocal energy absorption during this procedure by photography measurement (Fig. 2) using an infra-red digital camera (Seco Eletronics Inc, CCD B/W Ontário, Canada). For the LT group, phototherapy was applied immediately after the training.

Parameters evaluated

Histomorphometry

The middle third of the rectus femoris muscle was removed and placed in 10 % formaldehyde solution for 24 h. The tissue samples were embedded in paraffin blocks and cut into 5 μm sections, stained with hematoxylin and eosin and examined by light microscopy (Axioskop 2 Plus, Zeiss, Jena, Germany) coupled to a digital camera (DFC280, Leica, Germany). The images (×20 magnification) were processed using a IM50 software (Leica). The muscle volume fractions were determined according to the stereological principles of Weibel et al. [28] using an image analysis system (Image-Pro, Media Cybernetics, Silver Spring, MD, USA) and a digital grid with 667 intersections, with one central and two marginal fields in relation to the transverse axis of the middle third of the muscle.

Cytokines and IGF-1

Muscle samples were collected from the right thigh (middle third of the rectus femoris muscle) 24 h after the final training session. The muscles were frozen and stored at −80 °C. Just before performing the analysis, the samples were defrosted and cut into cubes (±1.52 g), with one cube from each animal being macerated in liquid nitrogen and then resuspended in 5 mL of phosphate buffer solution. The samples were assayed together in triplicate in the tests described below.

TNF-α, IL-1, and IL-6

Muscle cytokine concentrations were assayed using ELISA kits (Peprotech Inc.) with the absorbance being measured at

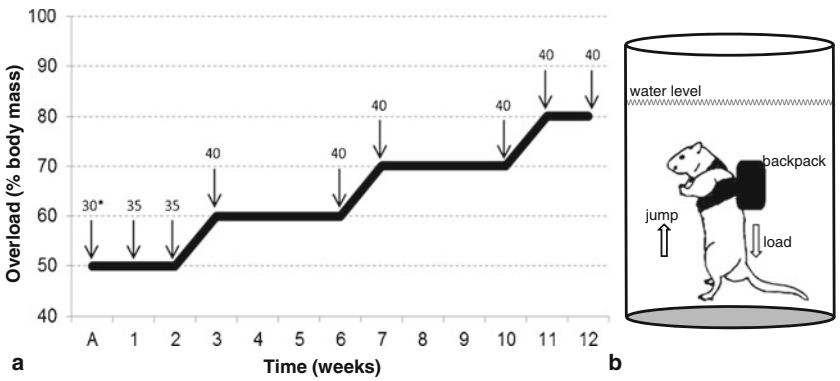

Fig. 1 Schematic presentation of training protocol. **a** Increase in exercise overload (expressed as a percentage of the body mass) during resistance training. The training protocol lasted 12 weeks and was preceded by a period of adaptation (**a**). *Water level (in centimeters) in the container used to train the rats. **b** Training container

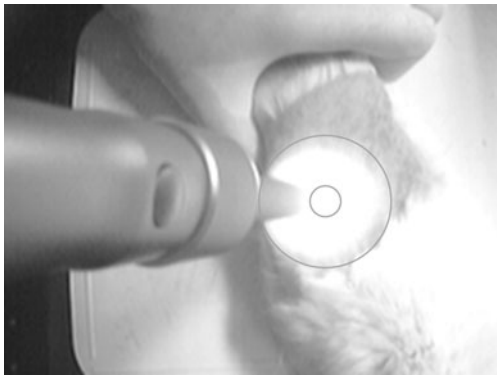

Fig. 2 LEDT illuminated muscle volume during the procedure. The central point contact irradiation was 0.5 cm^2 and showed light scattering in the rat's thigh after transmitted to the skin

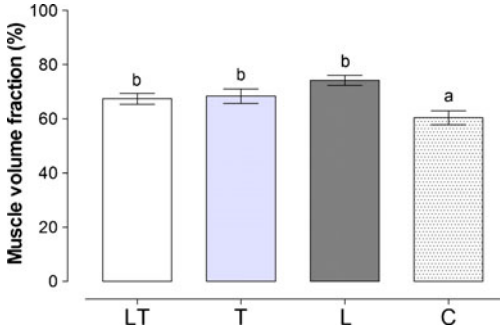

Fig. 3 Total muscle volume fraction for the four groups of rats studied. *C* Control–sedentary, *L* LEDT sedentary, *LT* LEDT and resistance training, *T* resistance training. *Columns* with different letters (*a–c*) show significant differences ($p<0.05$)

450 nm in a microplate reader (ELX 800, Bio-Tek Instruments, Winooski, Vermont, USA). The concentration ranges for the sandwich ELISAs were 63–3,000, 16–1,000, 62–8,000 pg/mL and for TNF-α, IL-1, and IL-6, respectively.

IGF-1

The IGF-1 concentration in rectus femoris muscle was measured using a quantitative, high sensitivity (range, 62–6,000 pg/mL) ELISA kit (Peprotech Inc., Rock Hill, NJ, USA) according to the manufacturer's instructions.

Statistical analysis

The Levene and Shapiro–Wilk tests were used to analyze the data variance and distribution, respectively. The Kruskal–Wallis test was used to compare the muscle volume fraction, IGF-1 and cytokine, and the data of the four groups. BioEstat 5.0 software (Fundação Mamirauá, Bélem, PA, Brazil) was used for all statistical analyses, with the level of significance set at 5 %.

Results

Muscle volume fraction

The treated groups showed a significant increase ($p<0.05$) in the volume fraction of the rectus femoris muscle compared to the control group (Fig. 3) as illustrated in muscle histology (Fig. 4).

Cytokines

The muscle TNF-α concentrations for the LT, T, and L groups were also significantly higher than for C group, although the concentration for the LT group was significantly lower than for T and L groups (Fig. 5). The muscle IL-1 concentrations of the LT, T, and L groups were significantly higher ($p<0.05$) than for C group (Fig. 6). The IL-6 concentration in muscles of the LT group was significantly greater than in T, L, and C groups (Fig. 7).

IGF-1

There was a significant increase ($p<0.05$) in the muscle IGF-1 concentration for the LT, T, and L groups compared to C group (Fig. 8).

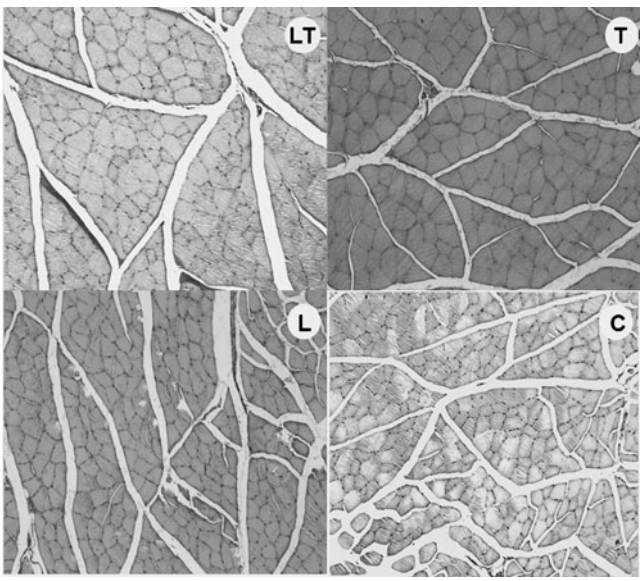

Fig. 4 Photomicrograph (HE) of rectus femoris muscle after 14 weeks of rats ovariectomy. *LT* LED therapy plus resistance training group applied in rats showing increase diameter of muscle fibers transverse section. *T* resistance training performed in rats showing increase muscle fibers transverse section. *L* LED therapy irradiated in rats showing increase diameter of muscle fibers transverse section. *C* control–sedentary group with absence treatment in rat's presenting decrease and irregular fiber sizes

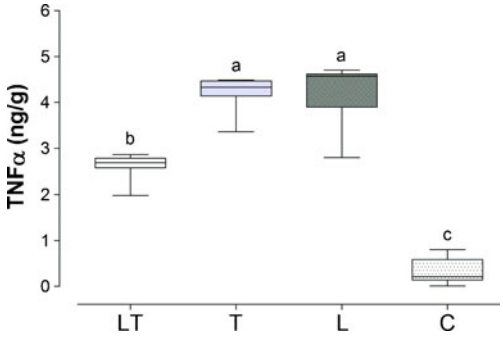

Fig. 5 Muscle TNF-α concentrations for rats after 12 weeks of resistance training. *C* control–sedentary, *L* LEDT–sedentary, *LT* LEDT and resistance training, *T* resistance training. *Columns with different letters* (*a–c*) show significant differences ($p<0.05$)

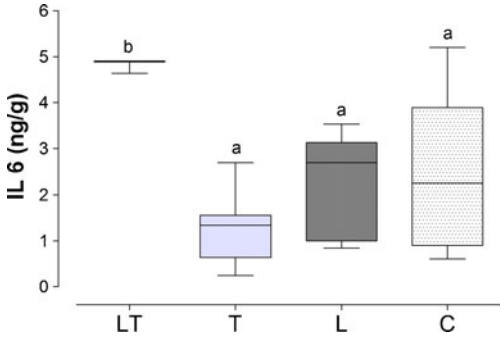

Fig. 7 Muscle IL-6 concentrations for rats after 12 weeks of resistance training. *C* control–sedentary, *L* LEDT–sedentary, *LT* LEDT and resistance training, *T* resistance training. *Columns with different letters* (*a–c*) show significant differences ($p<0.05$)

Discussion

The association of resistance training to LEDT showed to prevent muscle fiber atrophy of ovariectomized rats, but did not supplemented muscle volume compared to T group. However, the LT group demonstrated low TNF-α concentration in high-intensity exercise protocol. Scientific studies indicate that high intensity training stimulates TNF-α and leads to an activation of caspase-3 and caspase-8 (cysteine–aspartic acid proteases) which induces muscle apoptosis and sarcopenia [29]. Thus, photobiomodulation inflammatory mediator TNF-α can collaborate in preventive action of sarcopenia for RT long periods.

RT overtraining in hormonal deficient subjects can promote biochemical alterations of mitochondrial structures with an increased unbalance in ROS production and depletion of the body's antioxidant reserve, leading to increased fragility of muscle that accompanies mechanical injury and subsequent inflammation. Therefore, these factors can contribute to oxidative stress stem and reduced regenerative potential of muscle fibers due to a reduction of satellite cells [8].

When we used protocol training of a long period of RT on rats with an absent of estrogen associated with advanced age (15 months old in protocol completed) was with objective of collaborate in metabolic deficits. In this regard, LEDT was applied immediately after RT demonstrating the reduction of inflammatory mediator TNF-α in longitudinal training ovariectomized rats. Similarly, phototherapy applied during [22] and after exercise [30] showed optimized physical performance in longitudinal training program. On the other hand, other studies showed results in muscle performance with phototherapy applied before exercise to reducing markers of fatigue, oxidative stress, and muscle damage but only in athletes and transversal exercise protocols [13, 25]. In this sense, the photobiomodulation can improve inflammatory modulation after RT because RT overload in the elderly accentuates muscle fragility [8] and phototherapy showed better biomodulation when applied in metabolic deficit [15, 17, 19].

The decrease in the TNF-α concentration in the LT group compared to L and T groups was possibly influenced by the increase in the IL-6. Exercise stimulates an IL-6 secretion by the muscles and this mediator attenuates the production of both IL-1β and TNF-α while also increasing the levels of the anti-inflammatory cytokines such as IL-10 [4]. Despite the conflicting behavior of IL-6 as both an anti-inflammatory and

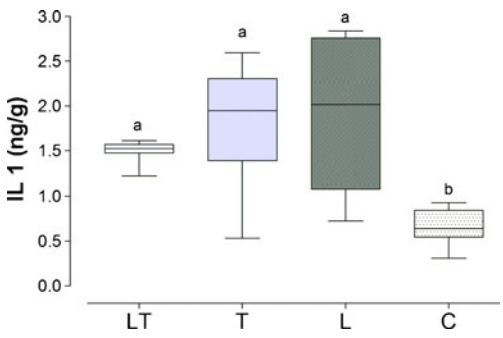

Fig. 6 Muscle IL-1 concentrations for rats after 12 weeks of resistance training. *C* control–sedentary, *L* LEDT–sedentary, *LT* LEDT and resistance training, *T* resistance training. *Columns with different letters* (*a–c*) show significant differences ($p<0.05$)

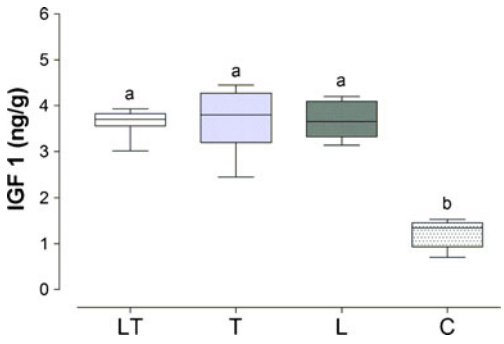

Fig. 8 Muscle IGF-1 concentrations for rats after 12 weeks of resistance training. *C* control–sedentary, *L* LEDT–sedentary, *LT* LEDT and resistance training, *T* resistance training. *Columns* with *different letters* (*a–c*) show significant differences ($p<0.05$)

a pro-inflammatory marker [31], we suggest that the LEDT increased in the muscle IL-6 formation facilitated and enhanced the physical recovery after RT, as reported in another study regarding IL-6 and post-training recovery [4]. The positive result observed in the LT group was the IL-6 signaling to IGF-1 synthesis [3], which can be stimulated to avoid atrophy muscle volume in middle-age rats ovariectomized.

When irradiance of 120 J/cm^2 was used in the rats there was photobiomodulator effects on TNF-α and IL-6 concentration post-training, suggesting the prevention in the loss muscle due to an increase of IGF-1 concentration. Similarly, Sussai et al. [25] when using LLLT (λ, 660 nm) with fluence of 133.3 J/cm^2 before high intensity exercise in the rats gastrocnemius muscle prevented apoptosis of muscle cells. On the other hand, Wu et al. [32] irradiated with a He–Ne laser for 10 min under a fluence of 120 J/cm^2 human lung adenocarcinoma cells (ASTC-a-1) and in an African green monkey SV40-transformed kidney fibroblast cells (COS-7) showed an increase of ROS and apoptose cellular evolution. In this context, when fluence is applied in cell culture, experimental, and clinical studies show variations in the absorption of energy, which answers phototherapeutics distinct need for adjustments in the therapeutic window as phototherapeutic goals differ in each type of body tissue.

LEDT (λ, 850 nm) with fluence of 120 J/cm^2 applied in muscle tissue was regarded as high as related by Huangh et al. [33]. However, the light interacted with several interfaces of skin, adipose, muscle, and bone volume around of irradiance central point, allowing higher number of specific photoreceptors and wide absorption window in tissues [24]. Tunner and Hode [34] related that the usage of high fluences in the skin promotes light attenuation throughout the deep tissue volume, resulting in a dose within the therapeutic window. Other author comment that initial fluence of 100–300 J/cm^2 on surface tissues is attenuated to 20 J/cm^2 to the depth of 5–10 cm [35]. Nakano et al. [20] suggest that LLLT irradiation (λ, 830 nm) with power output of 60 mW can promote recovery of muscle atrophy, from disuse, by proliferation of satellite cells and angiogenesis, but the power was reduced to 20 and 5 mW by in rat skin penetration and rat skin plus gastrocnemius muscle penetration, respectively. Despite difficulties involved in complying energy dose simulation to be used in the present study, the fluence was distributed to the rat's thigh muscle, which suggests that light attenuation in the tissue layer promotes fluence within range of the therapeutic window. Therefore, it demonstrated a preventive action in the rectus femoris muscle volume loss in 14 weeks after rat's ovariectomy.

The higher IGF-1 concentration for the L group compared to C group indicated the prevention of sarcopenia, possibly through the stimulation of pathways in the hormonal IGF-1/GH axis, same without influencing estrogen in the production of IGF-1 [1]. As reported by other authors, phototherapy can help prevent muscle atrophy by angiogenesis stimulation [36], increase IGF-I [37] with signalizing to protein synthesis similar to intracellular concentrations of cytoprotective heat shock proteins (HSP-70i), and consequent satellite cell proliferation [38]. Different to our results, in an in vivo study, LLLT (at 830 nm) did not stimulate IGF-1 production in the gastrocnemius muscle of rats irradiated with a fluence of 0.6 J/cm^2 (per point) on a total of 60 points (3.6 J total energy) [20]. This finding suggests that LEDT with an energy density of 120 J/cm^2 applied at a single point, as used in our study, was highly effective in stimulating the IGF-1 production and to maintain muscle volume.

Beside the fluence, the wavelengths and light type influences in the energy distribution. Our study used infrared LED (λ, 830 nm) due to scatter of light with elliptic shape [34], to compensate the scattering of LED light after skin transmitted (Fig. 2), due low coherence in relation to laser low level [13], thus ensure more light penetration efficiency [15].

In the T group, the exercise frequency (48 h intervals) may have contributed to the benefits observed in the anti-atrophic action. An interval of 48 h shows a positive effect on the protein synthesis during recovery from inflammation following an overload resistance training [39]. Another study, however, found that resistance training for five times per week led to atrophy in rat plantaris muscles [40]. A functional overload of physical exercise could decrease the protein synthesis [41], with increased rates of catabolism/anabolism and a reduction in muscle volume. Furthermore, an RT with adequate intervals between exercises can increase mitochondrial content and decrease oxidative stress in older adults [42].

Physical exercise promoting an increase in cytokines may be pro-inflammatory (IL-1β, TNF-α, and IL-6), anti-inflammatory (IL-6, IL-10, IL-4, IL-5, IL-13, and IL-1rα), or may contribute to a biomodulation of the inflammation [31]. In this study, it was observed that despite an increasing IL-1 and TNF-α for the T and L groups there was no impairment in the IGF-1 synthesis when compared to the sedentary group. These results are in agreement with previous work in which the optimization of the IGF-1 production during a high-intensity resistance training was associated with an enhanced signaling of the inflammatory cytokines [43].

Another response to the positive effects of the sarcopenia prevention by means of RT arises from the increase in IGF-1, and consequently this may be added to the effect of estrogen deficiency developed by the ovariectomy done on the rats. Enhanced IGF-1 production in response to resistance exercises [5] inhibits protein degradation in myotubes by stimulating the phosphatidylinositol-3 kinase/protein kinase B pathway [44] and improves muscle hypertrophy [7]. It is therefore possible that the RT for 12 weeks provided sufficient anabolic signaling to avoid sarcopenia for the rats in this study. Suetta et al. [45] showed that RT in elderly postoperative patients helps regulate muscle hypertrophy by

IGF-1 regarding electrical stimulation and functional training. When transposing this experiment to humans, we may expect to find that the gradual increase of the load during the training promotes the prevention of sarcopenia and develops muscle hypertrophy as has been reported by other authors [5]. Clinical studies are needed to establish the mechanisms by which LEDT may prevent sarcopenia in elderly women subjected to resistance training.

Conclusion

Our results indicate that both the RT and the LEDT can enhance the anabolic activity by stimulating the IGF-1 production, thereby increasing the muscle volume of middle-aged ovariectomized rats. Despite the increased muscle volume being similar for all treated groups we can report that the phototherapy may also regulate the TNF-α and IL-6 concentrations and can optimize the metabolic recovery of the rats after high-intensity resistance training.

Acknowledgments The authors would like to thank Felippe Furlan, Júlio César Domingues, Luis Vaz de Lima Júnior, and Mariana Sabino Bortolozzo for valuable technical assistance. We would also like to thank the Conselho Nacional de Desenvolvimento Científico e Tecnológico (CNPq) for their financial support.

References

1. Enns DL, Tiidus PM (2008) Estrogen influences satellite cell activation and proliferation following downhill running in rats. J Appl Physiol 104(2):347–353
2. Goldspink G (2007) Loss of muscle strength during aging studied at the gene level. Rejuvenation Res 10:397–405
3. Yang J, Anzo M, Cohen P (2005) Control of aging and longevity by IGF-1 signaling. Exp Gerontol 40(11):867–872
4. de Salles BF, Simão R, Fleck SJ, Dias I, Kraemer-Aguiar LG, Bouskela E (2010) Effects of resistance training on cytokines. Int J Sports Med 31(7):441–450
5. Adamo ML, Farrar RP (2006) Resistance training and IGF involvement in the maintenance of muscle mass during the aging process. Ageing Res Rev 5(3):310–331
6. Lee S, Barton ER, Sweeney HL, Farrar RP (2004) Viral expression of insulin-like growth factor-I enhances muscle hypertrophy in resistance-trained rats. J Appl Physiol 96(3):1097–1104
7. Izquierdo M, Ibañez J, Calbet JA, Navarro-Amezqueta I, González-Izal M, Idoate F, Häkkinen K, Kraemer WJ, Palacios-Sarrasqueta M, Almar M, Gorostiaga EM (2009) Cytokine and hormone responses to resistance training. Eur J Appl Physiol 107:397–409
8. Yarrow JF, Borsa PA, Borst SE, Sitren HS, Stevens BR, White LJ (2007) Neuroendocrine responses to an acute bout of eccentric-enhanced resistance exercise. Med Sci Sports Exerc 39:941–947
9. Peterson CM, Johannsen DL, Ravussin E (2012) Skeletal muscle mitochondria and aging: a review. J Aging Res. doi:10.1155/2012/194821
10. Fulle S, Protasi F, Di Tano G, Pietrangelo T, Beltramin A, Boncompagni S, Vecchiet L, Fanò G (2004) The contribution of reactive oxygen species to sarcopenia and muscle ageing. Exp Gerontol 39(1):17–24
11. Sakuma K, Yamaguchi A (2010) Molecular mechanisms in aging and current strategies to counteract sarcopenia. Curr Aging Sci 3 (2):90–101
12. Cheung K, Hume P, Maxwell L (2003) Delayed onset muscle soreness: treatment strategies and performance factors. Sports Med 33(2):145–164
13. Leal Junior EC, Lopes-Martins RA, Baroni BM, De Marchi T, Rossi RP, Grosselli D, Generosi RA, de Godoi V, Basso M, Mancalossi JL, Bjordal JM (2009) Comparison between single-diode low-level laser therapy (LLLT) and LED multi-diode (cluster) therapy (LEDT) applications before high-intensity exercise. Photomed Laser Surg 27(4):617–623
14. Karu TI, Piatybrat LV, Afanasyeva NI (2004) A novel mitochondrial signaling pathway activated by visible to-near infrared radiation. Photochem Photobiol 80(2):366–372
15. De Marchi T, Leal Junior EC, Bortoli C, Tomazoni SS, Lopes-Martins RA, Salvador M (2012) Low-level laser therapy (LLLT) in human progressive-intensity running: effects on exercise performance, skeletal muscle status, and oxidative stress. Lasers Med Sci 27(1):231–236
16. Reddy GK (2004) Photobiological basis and clinical role of low-intensity lasers in biology and medicine. J Clin Laser Med Surg 22 (2):141–150
17. Servetto N, Cremonezzi D, Simes JC, Moya M, Soriano F, Palma JA, Campana VR (2010) Evaluation of inflammatory biomarkers associated with oxidative stress and histological assessment of low-level laser therapy in experimental myopathy. Lasers Surg Med 42(6):577–583
18. Mesquita-Ferrari RA, Martins MD, Silva JA Jr, da Silva TD, Piovesan RF, Pavesi VC, Bussadori SK, Fernandes KP (2011) Effects of low-level laser therapy on expression of TNF-α and TGF-β in skeletal muscle during the repair process. Lasers Med Sci 26(3):335–340
19. Luo L, Sun Z, Zhang L, Li X, Dong Y, Liu TC (2012) Effects of low-level laser therapy on ROS homeostasis and expression of IGF-1 and TGF-β1 in skeletal muscle during the repair process. Lasers Med Sci. doi:10.10007/s10103-0/2-1133-0
20. Nakano J, Kataoka H, Sakamoto J, Origuchi T, Okita M, Yoshimura T (2009) Low-level laser irradiation promotes the recovery of atrophied gastrocnemius skeletal muscle in rats. Exp Physiol 94 (9):1005–1015
21. Corazza AV, Jacks J, Kurachi C, Bagnato VS (2007) Photobiomodulation on the angiogenesis of skin wounds in rats using different light sources. Photomed Laser Surg 25(2):102–106
22. Paolillo FR, Corazza AV, Borghi-Silva A, Parizotto NA, Kurachi C, Bagnato VS (2012) Infrared LED irradiation applied during high-intensity treadmill training improves maximal exercise tolerance in postmenopausal women: a 6-month longitudinal study. Lasers Med Sci. doi:10.1007/s10103-012-1062-y
23. DaCosta RS, Andersson H, Wilson BC (2003) Molecular fluorescence excitation–emission matrices relevant to tissue spectroscopy. Photochem Photobiol 78:384–392
24. Whelan HT, Buchmann EV, Dhokalia A, Kane MP, Whelan NT, Wong-Riley MT, Eells JT, Gould LJ, Hammamieh R, Das R, Jett M (2003) Effect of NASA light-emitting diode irradiation on molecular changes for wound healing in diabetic mice. J Clin Laser Med Surg 21(2):67–74
25. Sussai DA, Carvalho Pde T, Dourado DM, Belchior AC, dos Reis FA, Pereira DM (2010) Low-level laser therapy attenuates creatine kinase levels and apoptosis during forced swimming in rats. Lasers Med Sci 25(1):115–120
26. Cunha TS, Tanno AP, Moura MJCS, Marcondes FK (2005) Influence of high-intensity exercise training and anabolic steroid treatment on rat tissue glycogen contents. Life Sci 77(9):1030–1043

27. Hornberger TA, Farrar RP (2004) Physiological hypertrophy of the FHL muscle following 8 weeks of progressive resistance exercise in the rat. Can J Appl Physiol 29(1):16–31
28. Weibel ER, Kistler GS, Scherle WF (1966) Practical stereological methods for morphometric cytology. J Cell Biol 30(1):23–38
29. Phillips T, Leeuwenburgh C (2005) Muscle fiber specific apoptosis and TNF-α signaling in sarcopenia are attenuated by life-long calorie restriction. FASEB J 19(6):668–670
30. Ferraresi C, de Brito Oliveira T, de Oliveira Zafalon L, de Menezes Reiff RB, Baldissera V, de Andrade Perez SE, Matheucci Júnior E, Parizotto NA (2011) Effects of low level laser therapy (808 nm) on physical strength training in humans. Lasers Med Sci 26(3):349–358
31. Smith C, Kruger MJ, Smith RM, Myburgh KH (2008) The inflammatory response to skeletal muscle injury: illuminating complexities. Sports Med 38(11):947–969
32. Wu S, Xing D, Wang F, Chen T, Chen WR (2007) Mechanistic study of apoptosis induced by high-fluence low-power laser irradiation using fluorescence imaging techniques. J Biomed Opt 12 (6):064015
33. Huang YY, Chen AC, Carroll JD, Hamblin MR (2011) Biphasic dose response in low-level light therapy—an update. Dose-Response 9(4):602–618
34. Tunér J, Hode L (2002) Laser therapy—clinical practice and scientific background. UP Print, Tallinn, 571
35. Pöntinen PJ (2000) Laser acupuncture. In: Simunovic Z (ed) Lasers in medicine and dentistry: basic and up-to-date clinical application of low-energy-level laser therapy (LLLT). Vitgraf, Rijeka, pp 455–475
36. Lakyová L, Toporcer T, Tomečková V, Sabo J, Radoňak J (2010) Low-level laser therapy for protection against skeletal muscle damage after ischemia–reperfusion injury in rat hind limbs. Lasers Surg Med 42(9):665–672
37. Saygun I, Karacay S, Serdar M, Ural AU, Sencimen M, Kurtis B (2008) Effects of laser irradiation on the release of basic fibroblast growth factor (bFGF), insulin like growth factor-1 (IGF-1), and receptor of IGF-1 (IGFBP3) from gingival fibroblasts. Lasers Med Sci 23(2):211–215
38. Oron U (2006) Photoengineering of tissue repair in skeletal and cardiac muscles. Photomed Laser Surg 24(2):111–120
39. Karagounis LG, Yaspelkis BB III, Reeder DW, Lancaster GI, Hawley JA, Coffey VG (2010) Contraction-induced changes in TNF-α and Akt-mediated signalling are associated with increased myofibrillar protein in rat skeletal muscle. Eur J Appl Physiol 109(5):839–848
40. de Souza RWA, Aguiar AF, Carani FR, Campos GER, Padovani CR, Silva MDP (2011) High-intensity resistance training with insufficient recovery time between bouts induce atrophy and alterations in myosin heavy chain content in rat skeletal muscle. Anat Rec (Hoboken) 294(8):1393–1400
41. Seene T, Kaasik P, Alev K, Pehme A, Riso EM (2004) Composition and turnover of contractile proteins in volume-overtrained skeletal muscle. Int J Sports Med 25(6):438–445
42. Forbes SC, Little JP, Candow DG (2012) Exercise and nutritional interventions for improving aging muscle health. Endocrine 42 (1):29–38
43. Petersen AMW, Pedersen BK (2005) The anti-inflammatory effect of exercise. J Appl Physiol 98(4):1154–1162
44. Stitt TN, Drujan D, Clarke BA, Panaro F, Timofeyva Y, Kline WO, Gonzalez M, Yancopoulos GD, Glass DJ (2004) The IGF-1/PI3K/Akt pathway prevents expression of muscle atrophy-induced ubiquitin ligases by inhibiting FOXO transcription factors. Mol Cell 14(3):395–403
45. Suetta C, Clemmensen C, Andersen JL, Magnusson SP, Schjerling P, Kjaer M (2010) Coordinated increase in skeletal muscle fiber area and expression of IGF-I with resistance exercise in elderly post-operative patients. Growth Horm IGF Res 20(2):134–140

Lasers Med Sci (2015) 30:279–286
DOI 10.1007/s10103-014-1659-4

ORIGINAL ARTICLE

Synergic effects of ultrasound and laser on the pain relief in women with hand osteoarthritis

Alessandra Rossi Paolillo · Fernanda Rossi Paolillo · Jessica Patrícia João · Herbert Alexandre João · Vanderlei Salvador Bagnato

Received: 8 June 2014 / Accepted: 9 September 2014 / Published online: 20 September 2014

Abstract Patients with pain avoid movements, leading to a gradual impairment of their physical condition and functionality. In this context, the use of ultrasound (US) and low-level laser therapy (LLLT) show promising results for nonpharmacological and noninvasive treatment. The aim of this study was evaluated the synergistic effects of the US and the LLLT (new prototype) with or without therapeutic exercises (TE) on pain and grip strength in women with hand osteoarthritis. Forty-five women with hand osteoarthritis, aged 60 to 80 years, were randomly assigned to one of three groups, but 43 women successfully completed the full study. The three groups were as follows: (i) the placebo group which did not perform TE, but the prototype without emitting electromagnetic or mechanical waves was applied (n=11); (ii) the US + LLLT group which carried out only the prototype (n=13); and (iii) the TE + US + LLLT group which performed TE before the prototype is applied (n=13). The parameters of US were frequency 1 MHz; 1.0 W/cm^2 intensity, pulsed mode 1:1 (duty cycle 50 %). Regarding laser, the output power of the each laser was fixed at 100 mW leading to an energy value of 18 J per laser. Five points were irradiated per hand, during 3 min per point and 15 min per session. The prototype was applied after therapeutic exercises. The treatments are done once a week for 3 months. Grip strength and pressure pain thresholds (PPT) were measured. Grip strength did not differ significantly for any of the groups ($p \geq 0.05$). The average PPT between baseline and 3 months shows significant decrease of the pain sensitivity for both the US + LLLT group (Δ=30±19 N, p 0.001) and the TE + US + LLLT group (Δ=32±13 N, $p<0.001$). However, there were no significant differences in average PPT for placebo group (Δ=−0.3±9 N). There was no placebo effect. The new prototype that combines US and LLLT reduced pain in women with hand osteoarthritis.

Keywords Ultrasound · Laser · Pain · Osteoarthritis · Hand · Women

A. R. Paolillo · F. R. Paolillo · J. P. João · H. A. João · V. S. Bagnato
Optics Group from Physics Institute of São Carlos (IFSC), University of São Paulo (USP), Av. Trabalhador Sãocarlense, 400-Centro, CEP 13560-970 São Carlos, SP, Brazil

F. R. Paolillo
e-mail: fer.nanda.rp@hotmail.com

J. P. João
e-mail: jessicapatriciaj@hotmail.com

H. A. João
e-mail: herbert@ifsc.usp.br

V. S. Bagnato
e-mail: vander@ifsc.usp.br

A. R. Paolillo (✉)
Department of Occupational Therapy, Federal University of São Carlos (UFSCar), Rodovia Washington Luiz, Km. 235, CEP 13565-905 São Carlos, SP, Brazil
e-mail: arpaolillo@gmail.com

Introduction

Osteoarthritis (OA) is the most common joint disorder and with fastest growing public health concern, reflecting the aging of the population [1]. The clinical symptoms and consequences of hand OA are, for example, pain, reduced joint range, and deformity with interference in grip and fine precision pinch, muscle weakness, and dissatisfaction with cosmetic appearance [2].

Patients with pain, especially chronic pain, avoid movements. This in turn results in a gradual impairment of their physical condition, reducing, for example, strength, flexibility, physical functionality, and occupational activity. All of the recent guidelines recommend therapeutic exercise for chronic, subacute, and postsurgical OA for improvement of physical functionality and life quality [2, 3]. Previous studies from our

group observed the potential effects of exercise associated with phototherapy to improve muscle function and health-related outcomes [4–7].

Low-level laser therapy (LLLT) is a form of phototherapy with application of low-power monochromatic or quasimonochromatic and coherent electromagnetic radiation in the therapeutic optical region of ~600–1,000 nm. The light is absorbed by mitochondria and alters cell metabolism without any thermal damage or destructive effects [8]. In parallel, ultrasound (US) is a source of mechanical wave. The energy is transmitted by the vibrations of molecules through the medium such as a solid, liquid, or gas with absorption of mechanical energy by body tissues. Then, the vibrational energy is converted into molecular energy with both thermal and cavitation effects [9].

There are several therapeutic effects of the US or LLLT, including pain relief, increase of microcirculation, enzymatic activity, and collagen synthesis, as well as a modulation of inflammatory response and accelerated tissue repair, e.g., skin, muscle, tendon, nerve, cartilage, and bone [10]. In this context, a combination of US, LLLT, and therapeutic exercise [11] may maximize clinical outcome.

Several studies investigated the effects of US [12, 13] or LLLT [14, 15] on pain relief, range of motion, and grip strength, but few clinical trials were performed with hands OA [16]. In addition, the effects of US together with LLLT for treatment of hand OA, to our knowledge, have not been investigated.

The aim of this study was evaluated the synergistic effects of the US and LLLT (prototype) with or without therapeutic exercises (TE) on grip strength and pain in women with hands OA. We hypothesized that the new prototype associated with TE may help relieve pain and improve grip strength.

Materials and methods

The current research has been approved by the National Ethics Committee of Ministry of Health in Brasilia, Brazil (approval no. 362.789) and by the Ethics Committee of Federal University of São Carlos (UFSCar) in São Carlos, Brazil (approval no. 143.392). The study was registered with NIH clinical trials (NCT02154893). All subjects signed written informed consents before their participation in the study.

This study was performed on 45 Caucasian women with hand osteoarthritis, aged between 60 and 80 years. Exclusion criteria were signs and symptoms of any psychiatric disorder, neurological, metabolic, pulmonary, cardiac disease, thrombosis, and/or cancer. We performed simple randomization by a computer program. Then, the subjects were randomly divided into three groups (15 per group), but 43 women successfully completed the full study: (i) the placebo group (n=11) which did not perform TE, but the device with US and LLLT without emitting electromagnetic or mechanical waves was applied (null dose); (ii) the US + LLLT group (n=13) which carried out only the prototype; and (iii) the TE + US + LLLT group (n=13) which performed TE before the prototype is applied.

Development of the prototype and clinical protocol

To perform physical treatments, a prototype device was developed by researchers of the Technological Support Laboratory (LAT) of the Optics Group from the Physics Institute of São Carlos (IFSC), University of São Paulo (USP), together with the company MM Optics Ltda. The device includes four diode laser beams (808 nm) around of the one US transducer (Fig. 1). The shape of each diode laser beam is elliptical, and four laser beams form a square around the transducer.

The output power of each laser was fixed at 100 mW [17, 18]. A FieldMaster TO-II optical power meter (Coherent Inc., Santa Clara, CA, USA) linked to a photodetector was used to calibrate this device and revaluated ~40 mW/cm^2 average optical power density. The treatment time was 3 min per point, leading to an energy value of 18 J and a fluence of 7 J/cm^2 per laser or 72 J and 28 J/cm^2 per point. Five points were irradiated per hand, leading to a total energy of 360 J and a fluence delivered close to 142 J/cm^2 per hand. The volunteers wore safety glasses.

The US includes 1–3 MHz frequency and 3.5 cm^2 effective radiation area (ERA). The parameters used were as follows: frequency 1 MHz, 1.0 W/cm^2 intensity, pulsed mode 1:1 (duty cycle 50 %), 0.5 W/cm^2 spatial average-temporal average (SATA) for 3 min per point, a total of five points per hand, and 15 min per hand per session, leading to 3.150 J total energy [12, 13, 19]. Transparent conductive gel was used. The interaction of transparent gel with radiation was investigated by the Cary-17 Spectrophotometer Conversion, OLIS (OnLine Instruments Systems Inc., Bogart, GA). The percent transmittance (% T) was defined as $100 \times I/I_0$, where I_0 is the intensity of light entering the sample, and I is the intensity of light leaving the sample. The results showed ~80 % of transmittance for the wavelengths between 600 and 1,000 nm. There was only small loss of intensity. It shows that the transparent gel does not appear to interfere negatively in treatment.

The prototype application techniques were identical for all groups, but the null dose was applied in the placebo group. The two hands were treated. The movements of the device were circular, continuous, slow, and smooth, contemplating all hand (left and right). The landmarks are not indicated by colored paint on the bare skin, because it can lead to loss of energy delivered from the laser to the skin. In addition, we do not use hand immersed in water or bladder application procedure, because these methods are appropriate for US; however, it also can lead to loss of laser energy. Then, we performed US

Fig. 1 Prototype with four diode laser beams around one US transducer, points of application on the hand, and US plus laser during therapeutic session

and LLLT for all hand with safety, mainly on bony protuberances and smaller muscles. The points of applications of the device on the hand are indicated in Fig. 1.

The prototype was applied after therapeutic exercises to prevent delayed onset muscle soreness (DOMS) or joint pain post-exercise in the TE + US + LLLT group. The therapeutic exercises consisted of two sensorimotor exercises with ball tennis, two stretching exercises for upper limb and resistance training using hand training device, DigiFlex® (IMC Products Corp., Hicksville, NY) [20], as seen in Fig. 2. The resistance levels 5, 10, 16, and 23 lbs per hand were used. The load was progressively increased over 2 months. Each load was maintained for 15 days. The patients performed ten grip movements at each session. After 2 months, the patients performed efforts (maximal number of grip movements) for 1 min per session with maximal load (23 lbs).

The prototype with or without therapeutic exercise was applied once a week for 3 months. Hand evaluations were performed on the baseline and after 3 months in a laboratory always at controlled air temperature (22–24 °C) and relative humidity (50–60 %).

Clinical characteristics

Clinical characteristics (Table 1) were measured as previously described [21]. Anthropometric data were used to determine the body mass index [BMI: body weight (in kg) divided by height (in m^2)] and the waist-to-hip ratio [WHR: waist circumference (in cm) divided by hip circumference (in cm)]. The body fat and hydration were measured by the bipolar electrical bioimpedance of the upper limbs (OMRON®, Kyoto, Japan).

Grip strength testing

Grip strength of the dominant limb was measured by the hand dynamometer (JAMAR Hydraulic Hand Dynamometer, Sammons Preston Inc, Bolingbrook, IL, USA) with patients sitting with the shoulder in a neutral position and the elbow flexed at 90°. The average force of three consecutive trials was calculated [22].

PPT measurement and topographical pressure pain sensitivity maps of the hand

A pressure pain threshold (PPT) is defined as the amount of pressure where a sense of pressure changes to pain. An electronic algometer (Wagner Instruments, Greenwich, CT, USA) was used to measure the PPT. The algometer consists of a 1 cm^2 rubber-tipped plunger mounted on a force transducer. The pressure was applied at a rate of approximately 1 $N/cm^2/s$ and the algometer scores are stated as newtons per square centimeter (N/cm^2) in all reported results [23]. The individual was instructed to ask to say "stop" when the sensation changed from pressure to pain. Thus, PPT represents the intensity at which a stimulus (amount of force or pressure) begins to evoke pain. Three PPT measurements (intraexaminer reliability) were taken at each point with a 20 s interval between two consecutive points to avoid effects of temporal summation [24].

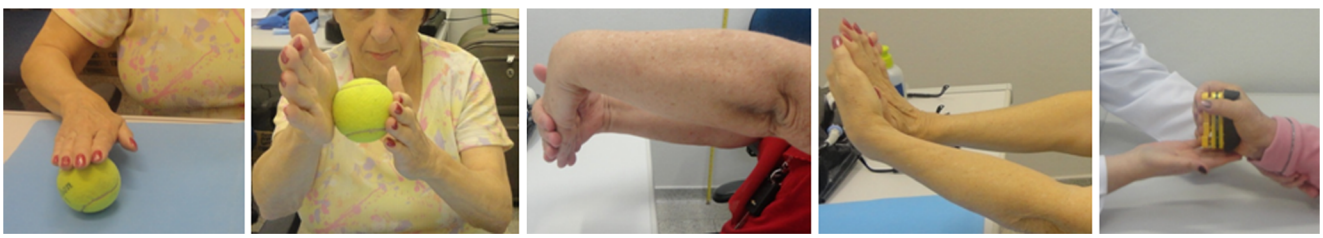

Fig. 2 Exercise protocol: sensorimotor exercises with ball tennis, stretching, and therapeutic exercise with DigiFlex®

Table 1 Clinical characteristics of the women with hand osteoarthritis

	Placebo group	US + LLLT group	TE + US + LLLT group
Age (years)	72±6	69±5	68±6
Body mass (kg)	70±16	68±11	76±14
Body height (m)	1.57±0.06	1.57±0.06	1.57±0.06
BMI (kg/m^2)	28±5	28±5	31±5
Waist (cm)	99±13	95±10	101±11
Hip (cm)	104±9	95±12	112±11
WHR	0.94±0.05	0.91±0.04	0.89±0.04
Fat (%)	38±9	41±9	43±9
Hydration (%)	43±6	39±8	39±6

No significant differences were found between the groups ($p \geq 0.05$)

The participants were instructed not to exercise on the previous day and not allowed to take analgesics or a muscle relaxant through the 72 h prior to the measurements. Subjects were asked to take a seated position, and PPT levels were measured at 30 locations on dominant hand as previously described [24]. The locations were as follows: distal phalanx (point 1), proximal phalanx (point 2), and thenar eminency (point 3); index finger—distal phalanx (point 4), middle phalanx (point 5), and proximal phalanx (point 6); middle finger—distal (point 7), middle (point 8), and proximal (point 9) phalanx; fourth finger—distal (point 10), middle (point 11), and proximal (point 12) phalanx; fifth finger—distal (point 13), middle (point 14), and proximal (point 15) phalanx; and head of the fifth (point 16), fourth (point 17), third (point 18), and second (point 19) metacarpal bones. For points 20–27, 2 cm equidistant points over each metacarpal bone were marked (20–24 over the second metacarpal bone, 21–25 over the third metacarpal bone, 22–26 over the fourth metacarpal bone, and 23–27 over the fifth metacarpal bone). Finally, one point over the lower end of the hypothenar eminency (point 28), over the carpal tunnel (point 29), and over the lower end of the thenar eminency (point 30) were also assessed.

Three measurements were performed at each location to obtain an average as previously described [24]. Averaged PPT values over the 30 locations were interpolated using an inverse distance weighted interpolation for the PPT distribution [24] over dominant hand of patients with OA. The Origin 8.0 software (OriginLab Corporation, Northampton, MA) was used to create the color schemes from average PPT values measured at 30 points on hand.

Statistical analysis

The Shapiro-Wilk test was used to analyze data normality and the homogeneity of variances using Levene's test. Two-way ANOVA with repeated measures was used to compare changes before and after the treatment. The independent factors were group (with three levels: TE + US + LLLT group, US + LLLT group, and Placebo group) and time (with two levels: pretreatment and posttreatment). The delta (post-pre=Δ) between the situations before and after the treatment was used to compare groups using a one-way ANOVA with pos hoc Tukey tests. The Statistica for Windows Release 7 software (Statsoft Inc., Tulsa, OK) was used for the statistical analysis, and the significance level was set at 5 % ($p<0.05$).

Results

The mean value of the grip strength did not differ significantly for any of the groups [placebo group—from 19±3 to 19±4 kgf; US + LLLT group—from 19±5 to 19±4 kgf and; TE + US + LLLT group—from 16±4 to 17±3 kgf ($p \geq 0.05$)]. The results of PPT and topographical maps can be seen in the Figs. 3 and 4, respectively. The average PPT shows significant decrease of the pain sensitivity for both the US + LLLT group and the TE + US + LLLT group.

Discussion

This is the first study evaluating the long-term synergic effects of US and LLLT in women with hand osteoarthritis. The main finding of this study was an increase of the pain threshold after 3 months of treatment. There was no placebo effect.

US alone generates pain relief [12, 13], through modulation of nerve conduction velocity and increasing a nociceptive threshold. The US also changes the muscular contractility and reduces spasms [9]. These factors may increases hand function [13]. In parallel, phototherapy alone also induces pain relief via alteration in the mitochondrial membrane potential, modulation of nociception, changing in nerve conduction velocity with decreased number of sensory impulses per unit of time, increasing production of serotonin and beta-endorphins, generating antioxidant effects, and reducing inflammatory mediators such as prostaglandin E2 and cytokines. In addition, the modulations of the synaptic transmission generate effects of muscle relaxation [25, 26].

The effective results depend of clinical trial's protocol. Brosseau et al. [16] investigated the effects of LLLT on pain, stiffness, and grip strength in hand osteoarthritis, but there was no significant difference for these parameters between LLLT and placebo groups. Meireles et al. [27] also found no significant difference for pain and range of motion after treatment with LLLT on the hands of patients with rheumatoid arthritis. However, Ekim et al. [28] show that LLLT was effectives for pain and hand function in patients with rheumatoid arthritis with carpal tunnel syndrome. Other studies show that LLLT

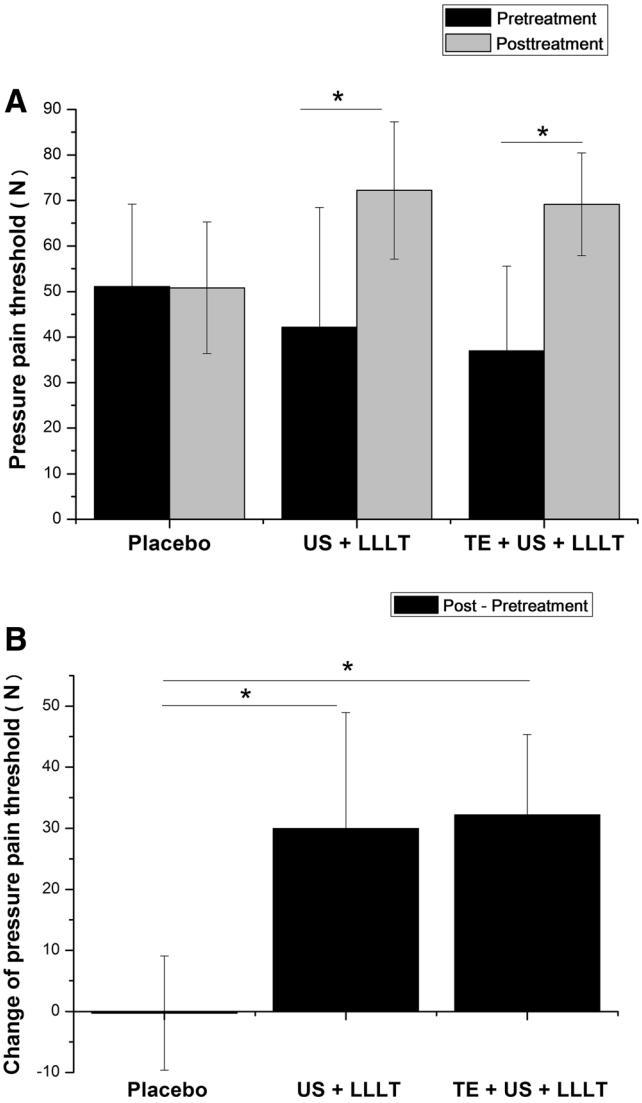

Fig. 3 Average pressure pain threshold (PPT). Results obtained for the PPT are significantly higher for both the US + LLLT and TE + US + LLLT groups (intragroup differences) (**a**). The changes in the average PPT between baseline and 3 months showed significant intergroup differences (**b**). *$p<0.001$

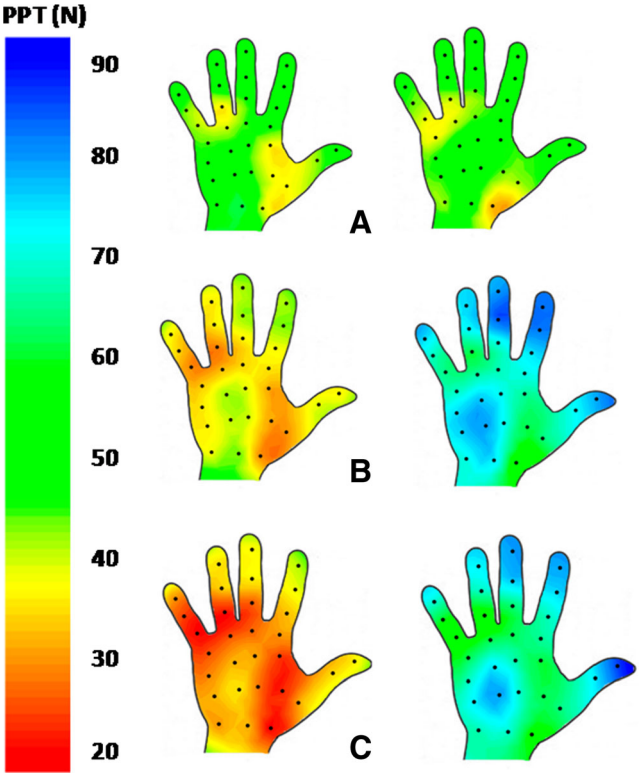

Fig. 4 Pressure pain sensitivity topographical maps. Pretreatment (*right*) and posttreatment (*left*) for placebo group (**a**), US + LLLT group (**b**), and TE + US + LLLT group (**c**). The color schemes for PPT values measured at 30 points on dominant hand can be observed. The *red to yellow color schemes* (lower PPT levels) indicated pressure hyperalgesia and the *green to blue color schemes* (PPT levels increased) indicated less sensitivity to pain after 3 months, mainly for both the US + LLLT group and the TE + US + LLLT group

have also been effective for treatment of carpal tunnel syndrome [14, 15].

These results are controversial and may be related to laser parameters used. The lack of understanding of dose (J/cm^2) and energy (J), as well as types of laser and wavelength may lead to error in the parameters used, and no effect of treatment for rheumatic diseases [29, 30]. The dosage recommendations of the World Association for Laser Therapy (WALT) states a total of 4 J per finger joint and total of 8 J for a wrist (www.walt.nu). On the other hand, new geometries of devices may explain the differences in the adopted parameters, especially when the parameters are compared with the dosage recommendations of the WALT. Although we applied high energy, the scanning mode (noncontact) was used, leading to small energy loss. However, deep penetration of infrared radiation in biological tissue is well known. It is estimated that the infrared laser irradiation on skin may show a 1/e penetration over 2 cm [31, 32]. This kind of penetration adequate assures quantity of light reaching the inflammation spots during treatment. Moreover, study that used US plus laser suggested the improvement of light penetration by US [33]. Photoacoustic diagnostic systems show laser and US at 90° [34] or 360° [35] or positioned side by side [36] also to improve light penetration and image quality. Al-Habib et al. [33] measured the amount of infrared laser power that passed the skin, muscle, and bone of rats with or without US effect using the Beer-Lambert law equation. The results showed power output of the laser increased when US was added to various tissue thicknesses indicating light deep penetration. Although this recent study has showed that ultrasonic irradiation together with infrared irradiation may increase light penetration, this is a topic out of the scope of our current study.

Regarding our protocol, the prototype has simple manipulation and great effectiveness reducing the time of therapeutic session and leading to economical advantages, because it

includes US together with LLLT. For these reasons, we do not use US and after, LLLT.

In addition, US plus LLLT may potentiate therapeutic effects, as evidenced by bone healing accelerated [33, 37]. In the study of Otadi et al. [11], the therapeutic effects were more evidenced when US and LLLT were associated with exercise for the management of shoulder tendonitis. However, in our study, the therapeutic exercise did not provide additional effect in grip strength of the women with hand osteoarthritis. Probably, both exercise load and training volume were lower and insufficient to improve grip strength. In contrast, US or LLLT has been effective to promote anti-inflammatory effect [9, 17] with analgesia alleviating symptoms of OA [11, 12, 14, 15], and so, therapeutic exercises can be performed without difficulties. Futures studies should include measurements of range of motion (ROM) and hand functionality to develop a better understanding of rehabilitation process in hand osteoarthritis.

Regarding to US, Akinbo et al. [38] applied US plus anti-inflammatory drugs (phonophoresis) and physical exercise for treatment of knee osteoarthritis. The authors found significant improvements in pain, stiffness, and physical function. However, Akinbo et al. [38] used continuous ultrasonic waves (predominant thermal effects), but we choose pulsed ultrasonic waves (predominant nonthermal effects), because according to in vitro [39] and animal models [40], as well as clinical trials [12, 13, 19, 41], the pulsed mode generates improvement of cartilage repair as well as anti-inflammatory and analgesic actions without damaging the patients with acute joint inflammation due to thermal effects.

For pain analysis, we used mechanically evoked pain by algometer to determine PPT measures. This is a useful popular model for inducing acute experimental pain and provides highly reliable measures of PPT [42]. According to Fernández-de-Las-Peñas et al. [24], PPT mapping is a new imaging modality of pain sensitivity that enables visualization of nonuniformity in pressure pain sensitivity and consequently, deep tissue hyperalgesia in a specific location of the body.

The PPT increased for both US + LLLT and TE + US + LLLT groups indicate desensitization of mechanonociceptors caused by pain modulation [43]. The current results about pain relief might be due to the effects of US plus LLLT prototype. Then, this prototype may induce its antinociceptive effect through central neuromodulatory mechanisms (central desensitization). Some factors can influence in antinociceptive effect [44], such as physiologic (biochemical and electrochemical), spinal (segmental), and supraspinal mechanisms. Temporal summation of pain in humans is presented as an increased pain perception in response to repetitive stimulation of the same stimulus intensity, including skin, muscle, and joint structures [45]. Several therapeutic modalities or physical agents may induce temporal summation of somatic pain, for example, neuromuscular electrical stimulation, LLLT, thermotherapy (cold, superficial heat, or contrast) [46], microwaves [47], radiofrequency [48], US [44], and body vibration [49]. In this context, the synergic effects of US and LLLT may generate temporal summation of pain and analgesia for long term.

Regarding the limitations of this study, we did not perform other control groups with individual treatments, for example, US alone and LLLT alone used in a scanning mode, both applied with the same parameters of our prototype. Moreover, the penetration of light in the presence of the US was also not investigated in our study. Future studies should be done to investigate (i) the penetration of light with and without US effect through a phantom, ex vivo, or in vivo studies and (ii) the effects of the US and LLLT, separately, on the pain relief and hand rehabilitation.

Conclusion

The new device combines the therapeutic effects of both US and LLLT. These positive effects lead to an increase of the pain threshold in women with hand osteoarthritis. Then, there was long-term decrease in pain sensitivity. Moreover, there was no placebo effect. In this context, we considered that the US associated with LLLT can be potentially used for physical rehabilitation and sports protocols where the main objective is a pain relief.

Acknowledgments We would like to thank the Fundação de Amparo à Pesquisa do Estado de São Paulo (FAPESP)—grant no. 2013/07276-1 and 2013/14001-9, Conselho Nacional de Desenvolvimento Científico e Tecnológico (CNPq)—grant no. 573587/2008.

References

1. Zhang Y, Jordan JM (2010) Epidemiology of osteoarthritis. Clin Geriatr Med 26(3):355–369
2. Zhang W, Doherty M, Leeb BF, Alekseeva L, Arden NK, Bijlsma JW, Dinçer F, Dziedzic K, Häuselmann HJ, Herrero-Beaumont G, Kaklamanis P, Lohmander S, Maheu E, Martín-Mola E, Pavelka K, Punzi L, Reiter S, Sautner J, Smolen J, Verbruggen G, Zimmermann-Górska I (2007) EULAR evidence based recommendations for the management of hand osteoarthritis: report of a Task Force of the EULAR Standing Committee for International Clinical Studies Including Therapeutics (ESCISIT). Ann Rheum Dis 66(3):377–388
3. Bennell K, Hinman R (2005) Exercise as a treatment for osteoarthritis. Curr Opin Rheumatol 17(5):634–640
4. Vieira WH, Ferraresi C, Perez SE, Baldissera V, Parizotto NA (2012) Effects of low-level laser therapy (808 nm) on isokinetic muscle performance of young women submitted to endurance training: a randomized controlled clinical trial. Lasers Med Sci 27(2):497–504
5. Aquino AE Jr, Sene-Fiorese M, Paolillo FR, Duarte FO, Oishi JC, Pena AA Jr, Duarte AC, Hamblin MR, Bagnato VS, Parizotto NA (2012) Low-level laser therapy (LLLT) combined with swimming training improved the lipid profile in rats fed with high-fat diet. Lasers Med Sci 28(5):1271–1280

6. Corazza AV, Paolillo FR, Groppo FC, Bagnato VS, Caria PH (2013) Phototherapy and resistance training prevent sarcopenia in ovariectomized rats. Lasers Med Sci 28(6):1467–1474
7. Paolillo FR, Corazza AV, Paolillo AR, Borghi-Silva A, Arena R, Kurachi C, Bagnato VS (2014) Phototherapy during treadmill training improves quadriceps performance in postmenopausal women. Climacteric 17(3):285–293
8. Karu TI (2008) Mitochondrial signaling in mammalian cells activated by red and near-IR radiation. Photochem Photobiol 84(5):1091–1099
9. Haar D (1999) Therapeutic ultrasound. Eur J Ultrasound 9:3–9
10. Huang YY, Chen ACH, Carroll JD, Hamblin MR (2009) Biphasic dose response in low level light therapy. Dose Response 7:358–383
11. Otadi K, Hadian MR, Olyaei G, Jalaie S (2012) The beneficial effects of adding low level laser to ultrasound and exercise in Iranian women with shoulder tendonitis: a randomized clinical trial. J Back Musculoskelet Rehabil 25(1):13–19
12. Ebenbichler GR, Resch KL, Nicolakis P, Wiesinger GF, Uhl F, Ghanem AH, Fialka V (1998) Ultrasound treatment for treating the carpal tunnel syndrome: randomised "sham" controlled trial. BMJ 7;316(7133):731–735
13. Bakhtiary AH, Rashidy-Pour A (2004) Ultrasound and laser therapy in the treatment of carpal tunnel syndrome. Aust J Physiother 50(3): 147–151
14. Chang WD, Wu JH, Jiang JA, Yeh CY, Tsai CT (2008) Carpal tunnel syndrome treated with a diode laser: a controlled treatment of the transverse carpal ligament. Photomed Laser Surg 26(6):551–557
15. Fusakul Y, Aranyavalai T, Saensri P, Thiengwittayaporn S (2014) Low-level laser therapy with a wrist splint to treat carpal tunnel syndrome: a double-blinded randomized controlled trial. Lasers Med Sci 29(3):1279–1287. doi:10.1007/s10103-014-1527-2
16. Brosseau L, Wells G, Marchand S, Gaboury I, Stokes B, Morin M, Casimiro L, Yonge K, Tugwell P (2005) Randomized controlled trial on low level laser therapy (LLLT) in the treatment of osteoarthritis (OA) of the hand. Lasers Surg Med 36(3):210–219
17. Rosa AS, Dos Santos AF, da Silva MM, Facco GG, Perreira DM, Alves AC, Leal Junior EC, de Carvalho P, De T (2012) Effects of low-level laser therapy at wavelengths of 660 and 808 nm in experimental model of osteoarthritis. Photochem Photobiol 88(1):161–166
18. Paolillo FR, Corazza AV, Borghi-Silva A, Parizotto NA, Kurachi C, Bagnato VS (2013) Infrared LED irradiation applied during high-intensity treadmill training improves maximal exercise tolerance in postmenopausal women: a 6-month longitudinal study. Lasers Med Sci 28(2):415–422
19. Yildiz N, Atalay NS, Gungen GO, Sanal E, Akkaya N, Topuz O (2011) Comparison of ultrasound and ketoprofen phonophoresis in the treatment of carpal tunnel syndrome. J Back Musculoskelet Rehabil 24(1):39–47
20. Olafsdottir HB, Zatsiorsky VM, Latash ML (2008) The effects of strength training on finger strength and hand dexterity in healthy elderly individuals. J Appl Physiol 105(4):1166–1178
21. Paolillo FR, Milan JC, Paolillo AR, Lopes SLB, Kurachi C, Bagnato VS, Borghi-Silva A (2014) Impact of fat distribution on metabolic, cardiovascular and symptomatic aspects in postmenopausal women. Int J Diabetes Dev Ctries 34(1):32–39
22. Moe RH, Garratt A, Slatkowsky-Christensen B, Maheu E, Mowinckel P, Kvien TK, Kjeken I, Hagen KB, Uhlig T (2010) Concurrent evaluation of data quality, reliability and validity of the Australian/Canadian Osteoarthritis Hand Index and the Functional Index for Hand Osteoarthritis. Rheumatology (Oxford) 49(12): 2327–2336
23. Wajed J, Ejindu V, Heron C, Hermansson M, Kiely P, Sofat N (2012) Quantitative sensory testing in painful hand osteoarthritis demonstrates features of peripheral sensitisation. Int J Rheumatol 2012: 703138
24. Fernández-de-Las-Peñas C, Madeleine P, Martínez-Perez A, Arendt-Nielsen L, Jiménez-García R, Pareja JÁ (2010) Pressure pain sensitivity topographical maps reveal bilateral hyperalgesia of the hands in patients with unilateral carpal tunnel syndrome. Arthritis Care Res (Hoboken) 62(8):1055–1064
25. Chow RT, David MA, Armati PJ (2007) 830 nm laser irradiation induces varicosity formation, reduces mitochondrial membrane potential and blocksf axonal flow in small and medium diameter rat dorsal root ganglion neurons: implications for the analgesic effects of 830 nm laser. J Peripher Nerv Syst 12:28–39
26. Hagiwara S, Iwasaka H, Okuda K, Noguchi T (2007) GaAlAs (830 nm) low-level laser enhances peripheral endogenous opioid analgesia in rats. Lasers Surg Med 39:797–802
27. Meireles SM, Jones A, Jennings F, Suda AL, Parizotto NA, Natour J (2010) Assessment of the effectiveness of low-level laser therapy on the hands of patients with rheumatoid arthritis: a randomized double-blind controlled trial. Clin Rheumatol 29(5):501–509
28. Ekim A, Armagan O, Tascioglu F, Oner C, Colak M (2007) Effect of low level laser therapy in rheumatoid arthritis patients with carpal tunnel syndrome. Swiss Med Wkly 16;137(23–24):347–352
29. Tunér J, Hode L (2010) Low-level laser therapy for hand arthritis-fact or fiction? Clin Rheumatol 29(9):1075–1076
30. Meireles SM, Jones A, Natour J (2011) Low-level laser therapy on hands of patients with rheumatoid arthritis. Clin Rheumatol 30(1): 147–148
31. Ohshiro T, Ogata H, Yoshida M, Tanaka Y, Sasaki K, Yoshimi K (1996) Penetration depths of 830 nm diode laser irradiation in the head and neck assessed using a radiographic phantom model and wavelength-specific imaging film. Laser Therapy 8(3):197–203
32. Pöntinen PJ (2000) Laseracupuncture. In: Simunovic Z (ed) Lasers in medicine and dentistry: basic and up-to-date clinical application of low-energy-level laser therapy (LLLT). Vitgraf, Rijeka, Croatia, pp 455–475
33. Al-Habib MF, Salman MO, Faleh FW, Al-Ani IM (2011) Histological observation related to the use of laser and ultrasound on bone fracture healing. Int Med J Malaysia 10(2):29–35
34. Beard P (2011) Biomedical photoacoustic imaging. Interface Focus 1:602–631
35. Wang P, Wang HW, Sturek M, Cheng JX (2012) Bond-selective imaging of deep tissue through the optical window between 1600 and 1850 nm. J Biophotonics 5:25–32
36. Chivukula VS, Shur MS, Ciplys D (2007) Recent advances in application of acoustic, acousto-optic and photoacoustic methods in biology and medicine. Phys Stat Sol 204(10):3209–3236
37. Babuccu C, Keklikoğlu N, Baydoğan M, Kaynar A (2014) Cumulative effect of low-level laser therapy and low-intensity pulsed ultrasound on bone repair in rats. Int J Oral Maxillofac Surg 43(6): 769–776
38. Akinbo S, Owoeye O, Adesegun S (2011) Comparison of the therapeutic efficacy of diclofenac sodium and methyl salicylate phonophoresis in the management of knee osteoarthritis. Turk J Rheumatol 26(2):111–119
39. Korstjens CM, van der Rijt RH, Albers GH, Semeins CM, Klein-Nulend J (2008) Low-intensity pulsed ultrasound affects human articular chondrocytes in vitro. Med Biol Eng Comput 46(12): 1263–1270
40. Naito K, Watari T, Muta T, Furuhata A, Iwase H, Igarashi M, Kurosawa H, Nagaoka I, Kaneko K (2010) Low-intensity pulsed ultrasound (LIPUS) increases the articular cartilage type II collagen in a rat osteoarthritis model. J Orthop Res 28(3):361–369
41. Tascioglu F, Kuzgun S, Armagan O, Ogutler G (2010) Short-term effectiveness of ultrasound therapy in knee osteoarthritis. J Int Med Res 38(4):1233–1242
42. Chesterton LS, Sim J, Wright CC, Foster NE (2007) Interrater reliability of algometry in measuring pressure pain thresholds in healthy humans, using multiple raters. Clin J Pain 23(9):760–766
43. Kosek E, Ekholm J, Hansson P (1996) Modulation of pressure pain thresholds during and following isometric contraction in

patients with fibromyalgia and in healthy controls. Pain 64(3): 415–423
44. Srbely JZ, Dickey JP, Lowerison M, Edwards AM, Nolet PS, Wong LL (2008) Stimulation of myofascial trigger points with ultrasound induces segmental antinociceptive effects: a randomized controlled study. Pain 15;139(2):260–266
45. Finocchietti S, Arendt-Nielsen L, Graven-Nielsen T (2012) Tissue characteristics during temporal summation of pressure-evoked pain. Exp Brain Res 219(2):255–265
46. Ottawa Panel Members (2004) Ottawa Panel evidence-based clinical practice guidelines for electrotherapy and thermotherapy interventions in the management of rheumatoid arthritis in adults. Phys Ther 84(11):1016–1043
47. Giombini A, Di Cesare A, Di Cesare M, Ripani M, Maffulli N (2011) Localized hyperthermia induced by microwave diathermy in osteoarthritis of the knee: a randomized placebo-controlled double-blind clinical trial. Knee Surg Sports Traumatol Arthrosc 19(6):980–987
48. Takahashi K, Kurosaki H, Hashimoto S, Takenouchi K, Kamada T, Nakamura H (2011) The effects of radiofrequency hyperthermia on pain and function in patients with knee osteoarthritis: a preliminary report. J Orthop Sci 16(4):376–381
49. Alentorn-Geli E, Padilla J, Moras G, Lázaro Haro C, Fernández-Solà J (2008) Six weeks of whole-body vibration exercise improves pain and fatigue in women with fibromyalgia. J Altern Complement Med 14(8):975–981

Photomedicine and Laser Surgery
Volume 31, Number 7, 2013

Pp. 349–355
DOI: 10.1089/pho.2013.3505

Thermography Applied During Exercises With or Without Infrared Light-Emitting Diode Irradiation: Individual and Comparative Analysis

Fernanda Rossi Paolillo, PhD,[1] Emery C. Lins, PhD,[2] Adalberto Vieira Corazza, PhD,[1,3] Cristina Kurachi, PhD,[1] and Vanderlei Salvador Bagnato, PhD[1]

Abstract

Objective: The aim of our study was to evaluate the cutaneous temperature during an exercise on a treadmill with or without infrared light-emitting diode (LED) irradiation in postmenopausal women. ***Background data:*** Thermography is an imaging technique in which radiation emitted by a body in the middle and far infrared spectrum is detected and associated with the temperature of the body's surface. ***Materials and methods:*** Eighteen postmenopausal women were randomly divided into two groups: (1) the LED group, which performed the exercises on a treadmill associated with phototherapy ($n=9$) and; (2) the exercise group, which performed the exercises on a treadmill without additional phototherapy ($n=9$). The irradiation parameters for each women's thigh were: array of 2000 infrared LEDs (850 nm) with an area of 1,110 cm^2, 100 mW, 39 mW/cm^2, and 108 J/cm^2 for 45 min. The submaximal constant-speed exercise on the treadmill at intensities between 85% and 90% maximal heart rate ($HR_{max)}$ with or without phototherapy were performed during 45 min, to perform the thermographic analysis. Thermography images were captured before the exercise (t = 0), after 10, 35, and 45 min of exercising (t = 10, t = 35, and t = 45) and at 5 min post-exercising (t = 50). ***Results*:** The LED group showed an increased cutaneous thigh temperature during the exercise (from 33.5 ± 0.8°C to 34.6 ± 0.9°C, $p=0.03$), whereas the exercise group showed a reduced cutaneous temperature (from 33.5 ± 0.6 to 32.7 ± 0.7°C, $p=0.02$). The difference between the groups was significant ($p<0.05$) at t = 35, t = 45, and t = 50. ***Conclusions:*** These data indicate an improved microcirculation, and can explain one possible mechanism of action of phototherapy associated with physical exercises.

Introduction

The human body transforms the chemically bonded energy of adenosine triphosphate (ATP) into mechanical work, as the result of a heat release through the aerobic and anaerobic metabolism. Thermogenesis can occur during muscle work as well as during rest, with the release of vasoconstrictors, such as norepinephrine, and increases the metabolic rate. Thermoregulation occurs to maintain a constant body temperature. Thermoregulation is managed by the hypothalamus through the autonomic nervous system, with its vasoconstriction and vasodilatation of the blood vessels. Heat is exchanged with the environment by means of physical mechanisms (conduction, convection, evaporation, radiation).[1–3] Infrared thermography is an accurate method to measure the cutaneous temperature.

When used in medical diagnostics, thermography[4] reveals anatomic structures under the skin, metabolic information about a patient, or an inflammatory process associated with diseases. Kohler et al.[5] used thermography to pre-clinically detect deep vein thrombosis after proximal femur fractures. In a study by Ohsawa et al.,[6] the amputation level of the limb was determined by thermography, in order to avoid repeat amputation. In another study,[7] thermography was performed to diagnose musculoskeletal disorders of workers' upper extremities during pre-typing and post-typing.

Only one study has investigated the effects of infrared laser (780 nm) irradiation and a stretching exercise program specified for the trapezius or levator scapulae muscles on cutaneous temperature via a thermographic evaluation in patients with myofascial pain syndrome.[8] However, the thermal effects of the infrared light-emitting diode (LED)

[1]Optics Group from Physics Institute of São Carlos (IFSC), University of São Paulo (USP), São Carlos, SP, Brazil.
[2]Center of Engineering, Modeling and Applied Social Sciences, Federal University of ABC (UFABC), Santo André, SP, Brazil.
[3]Department of Morphology, Faculty of Dentistry of Piracicaba, State University of Campinas (UNICAMP), Piracicaba, SP, Brazil.

irradiation during physical exercises need to be investigated. To our knowledge, no previous studies have assessed the synergistic effects of phototherapy on cutaneous temperature during exercises. Previous work from our group has found infrared LED irradiation to significantly improve physical performance[9,10] and body aesthetics[11] in postmenopausal women participating in a high-intensity training program. Therefore, the aim of this study was to evaluate the cutaneous temperature during exercises on treadmill with or without infrared LED irradiation in postmenopausal women. Our hypothesis was that the cutaneous temperature in postmenopausal women would be increased during the physical exercise with or without infrared LED irradiation.

The current research was approved by the National Ethics Committee of the Ministry of Health in Brasilia, Brazil and by the Ethics Committee of the Federal University of São Carlos (UFSCar) in São Carlos, Brazil. The study was registered with the NIH ClinicalTrials (NCT01610232). All subjects signed written informed consents before their participation in the study.

Materials and Methods

A cross-sectional study was conducted. Eighteen postmenopausal Caucasian women between 50 and 60 years of age, who were not users of any hormone replacement therapy, participated in this study. "Postmenopausal" was defined as the absence of menstruation for >12 months. Women who had neurological, metabolic, inflammatory, endocrinopathic, pulmonary, malignant, and heart diseases were excluded from this study. The 18 postmenopausal women were randomly divided into two groups: (1) the LED group, which performed the exercises on a treadmill associated with phototherapy ($n=9$); and (2) the exercise group that performed exercises on a treadmill without any additional phototherapy ($n=9$).

Evaluations were conducted in a laboratory always at the same time of the day (beginning at 8 a.m.) at controlled air temperature (between 22°C and 24°C) and relative humidity controlled between 50% and 60%. Anthropometric data were performed to determine the Body Mass Index (BMI: body weight [in Kg] divided by height [in m] squared).[12] The maximal exercise testing on treadmill using the Modified Bruce Protocol[9,13] was performed to elaborate the submaximal exercise intensity based on the maximal heart rate (HR_{max}). The electrocardiogram system model Ergo (HW Systems; HeartWare Ltda., Belo Horizonte, MG, Brazil) and the cardiofrequencimeter model Polar S830i (Polar Electro Inc., Woodbury, NY) were used to acquire the HR_{max}. Submaximal constant speed exercises on a treadmill[13,14] at intensities between 85% and 90% HR_{max} with or without phototherapy were performed during 45 min for the thermographic analysis. The cardiofrequencimeter model Polar A3 (Polar Electro Inc., Woodbury, NY) was used to monitor the HR.

According to Ferreira et al.,[15] the women were instructed: (1) to eat 2 h before the assessment; (2) not to drink either alcohol or any caffeine; (3) not to practice any kind of physical exercise 24 h prior to the evaluation; (4) not to apply hydrating lotion or any similar product on the lower limbs; and (5) prior to starting the temperature recordings to remain in the examination room for 10 min in order to acclimatize to the room temperature (thermalization). Regarding the acquisition of the thermal images, all the women wore swimwear, which allowed the complete exposure of the lower limbs. Moreover, the women in the LED group wore safety glasses to ensure biosecurity during the phototherapy.

Instrumentation to perform phototherapy and thermography

In order to perform the phototherapy on the patients during the exercise on a treadmill, a homemade system based on near infrared (NIR) LED (array of 2000 LEDs [850 nm ± 15 nm] with an area of 1110 cm^2 to illuminate each the subjects' thigh) was developed by researchers of the Optics Group of the Physics Institute of São Carlos (IFSC), University of São Paulo (USP) as previously described.[9–11] An optical power meter model FieldMaster TO-II (Coherent Inc., Santa Clara, CA) linked to a VIS/NIR sensor (head) was used to calibrate this system, and to reveal a 100 mW average optical power and a 39 mW/cm^2 average optical power density on the patient's skin. Phototherapy was applied bilaterally on both thighs for 45 min, which led to an energy density (radiation dose) delivered close to 108 J/cm/per limb.[9]

To perform imaging, the thermographic camera model IR810 (FLUKE Corp., Washington) was used. This model detects infrared radiation in the spectral range between 8 μm and 14 μm, and composes termographic images with 0.1°C sensibility, and a 0–50°C measuring range was used to perform the thermographic measurements of the cutaneous surface temperature. The camera connected to a the computer and the software Pixel View Play TV Pro v8.01b (ProLink Microsystems Corporation, Taiwan, China) were used for acquisition, screening, and storage of the thermal images. Regarding the calibration procedure, the camera automatically calibrates between two points of temperature (minimal and maximal) for gray scale distribution. The Optics Group of the IFSC, USP, developed a system based on sensors, controllers, and actuators (two peltiers that were placed on each side of the women's bodies) to obtain the temperature values. This system controls two peltiers, which have a fixed temperature at ~30°C and 40°C (minimal and maximal point). The temperatures of each peltier were measured using a digital thermometer (MV 362, MINIPA Co Ltd, Shanghai, China) to compare the temperature values obtained by the camera. Figure 1 shows the schematic representation of the experimental setup.

The camera was maintained at a distance of 180 cm from the women, and at a height of 75 cm from the floor. This position of the camera allowed the subjects' lower limbs to be adequately captured. The measurements were performed during rest in the standing position during a pre-exercise period (0′), during 10, 35, and 45 min of the submaximal constant speed exercise (10′, 35′, and 45′) and after 5 min of the post-exercise recovery period in the standing position (50′). Following Ferreira et al,[15] we did not place any marker around the area of interest, to avoid temperature shifts by conduction or any other possible interference. The regions of interest for cutaneous temperature analyses were: (1) at an equidistant position between the knee and superior limits of the right and left thighs and between the lateral and the medial limits of the right and left thighs (quadriceps); and (2) at an equidistant position between the knee and the half

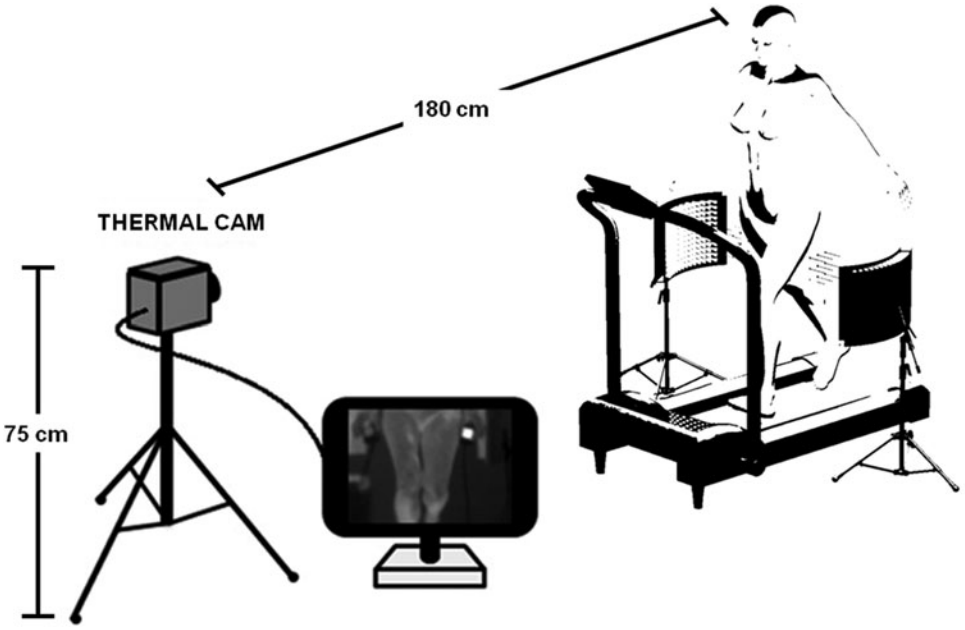

FIG. 1. The schematic representation of the experimental setup used for the measurements. The thermal camera was kept at a fixed position, 75 cm from the floor, 180 cm from the subject, and centered relative to the thighs. The thermal image was displayed on a computer screen and recorded. The thermal image shows (1) the light-emitting diode (LED) devices next to the woman and (2) two peltiers that were placed on each side of the woman's body to obtain the temperature. The distance between the LED devices (modified from Paolillo et al.)[10] and the subject was ~15 cm.

limits of the right and left lower legs and between the lateral and the medial limits of the right and left lower legs (superior half of the tibialis anterior muscle).

A homemade image processing was developed and applied over each of the thermal images. This simple computational routine was developed in Matlab® 7.0.4 - R14 (The MathWorks, Inc., Natick, MA) and allows the user to select a region of interest of the image followed by a calculation of an average and standard deviation of the temperature inside the region of interest. According to Ferreira et al.,[15] the use of the calculated average temperature of the area minimizes positioning errors. This is important, because we performed measurements with the subjects at rest as well as during physical exercises in real time, and the major limitation of thermography is that the acquisitions are a two-dimensional representation of a three-dimensional surface of a three-dimensional structure.[16] The average temperature and standard deviation were plotted as a function of time for the physical exercise with or without infrared LED irradiation, and reveal the dynamic behavior of the cutaneous temperature.

Statistical analysis

The data were expressed as mean and standard deviations. The Shapiro–Wilk test was used to analyze data normality. Repeated measures ANOVA with Bonferroni adjustments was used to compare changes of temperature as a function of time. The temperature was compared to each measurement of the immediately prior period, and all temperatures were compared to the pre-exercise period (0'). One-way ANOVA with Bonferroni adjustments was used to compare the temperatures between the groups. The Statistica for Windows Release 7 software (Statsoft Inc., Tulsa, OK) was used for the statistical analysis, and the significance level was set at 5% ($p < 0.05$).

Results

The clinical characteristics of the postmenopausal women are shown in Table 1. The mean values and standard deviation were 8 ± 5 years for the duration of the menopause. The statistical results of the cutaneous temperature can be seen in the Table 2. The thermal images before, during and after physical exercises with or without infrared LED irradiation can be seen in Figs. 2A and B. The dynamic behavior of the cutaneous temperature of the thighs (Fig. 3A) and of the lower legs (Fig. 3B) before, during, and after physical exercise with or without infrared LED irradiation can also be observed.

Table 1. Values of Mean and Standard Deviation and Statistical Results of the Clinical Characteristics of the Women

	LED group (n = 9)	*Exercise group* (n = 9)
Anthropometry		
Body mass (kg)	70 ± 10	67 ± 9
Height (cm)	153 ± 7	157 ± 5
BMI (kg/m^2)	30 ± 4	27 ± 3
Rest		
HR (bpm)	72 ± 9	73 ± 10
Maximal exercise testing		
HR_{max} (bpm)	161 ± 9	160 ± 13
Bruce (stage)	2.5 ± 0.5	2.5 ± 0.5
Submaximal constant speed exercise		
HR (bpm)	146 ± 11	142 ± 7
Velocity (km/h)	6 ± 1	6 ± 1

The groups were not significantly different ($p \geq 0.05$)
LED, light-emitting diode; BMI, body mass index; HR, heart rate.

Table 2. Cutaneous Temperature of the Thighs and the Lower Legs Before, During, and After Physical Exercise With and Without Infrared LED Irradiation

	Pre-exercise	*Exercise*			*Post-exercise*
	0′	*10′*	*35′*	*45′*	*50′*
Thigh temperature (°C)					
LED group	33.5 ± 0.8	34.1 ± 0.5	34.5 ± 0.9[a]	34.6 ± 0.9[a,b]	34.5 ± 0.9[a]
Exercise group	33.5 ± 0.6	33.7 ± 0.6	32.9 ± 0.9[b,c]	32.7 ± 0.7[b]	33.1 ± 0.5
Lower leg temperature (°C)					
LED group	33.7 ± 0.8	34.3 ± 0.7	34.7 ± 0.9[d]	34.9 ± 0.9[a]	34.7 ± 0.9[d]
Exercise group	33.7 ± 0.7	34.1 ± 0.8	33.7 ± 0.5	33.6 ± 0.6	33.8 ± 0.5

[a]Significant intergroup difference ($p < 0.01$).
[b]Significant intragroup difference compared with instance 0′ ($p < 0.05$).
[c]Significant intragroup difference compared with the period immediately beforehand ($p < 0.05$).
[d]Significant intergroup difference ($p < 0.05$).
LED, light-emitting diode.

No significant difference was found for the temperature of the thighs for each measurement compared with the prior period for the LED group ($p \geq 0.05$), whereas the exercise group showed a significant reduction of the thighs' temperature at instance 35′ compared with instance 10′ ($p = 0.03$). The LED group showed a significant increase of the thighs' temperature at instance 45′ compared with instance 0′ ($p = 0.03$), whereas the exercise group showed significant reduction of the thighs' temperature at instance 35′ ($p = 0.03$) and 45′ ($p = 0.02$) compared with instance 0′. The LED group showed higher values of the thighs' temperature compared with the exercise group at instance 35′ ($p = 0.0003$), 45′ ($p = 0.00005$), and 50′ ($p = 0.006$).

No significant difference was found for the lower leg temperatures for each measurement compared with the prior period or compared with instance 0′ for both the LED group and the exercise group ($p \geq 0.05$). However, the LED group showed significantly higher temperatures compared with the exercise group at instances 35′ ($p = 0.01$), 45′ ($p = 0.006$), and 50′ ($p = 0.04$).

Discussion

The main finding of this study was that the LED group showed an increased cutaneous temperature during the exercises, whereas the exercise group showed a reduced cutaneous temperature. These data are relevant because they can explain one possible mechanisms of action of phototherapy.

The increase of the initial cutaneous temperature observed in our study is similar to the discussion by Reilly and Waterhouse.[17] During the exercises, the set points for heat storage and heat loss have been reported as 3 and 10 min, respectively. The blood flow to the active muscles is increased in order to boost the transport of oxygen to them. The body acts at first as a heat sink, until a portion of the increased cardiac output is shunted to the skin to transfer heat to the environment. As the internal temperature begins to rise, the vasodilatory response is increased by secretion of sweat to the skin surface to produce evaporative cooling.[17] After this period (10 min) the response to exercise differs between the LED group and the exercise group.

The LED group showed an increased cutaneous temperature during the exercises. The infrared radiation is absorbed by water and produces heat. Moreover, Makihara et al.[18] showed that phototherapy applied with a CO_2 laser (1.0 W) positioned 10 cm above the skin, increased the facial temperature because it improved the microcirculation via the vasodilator reflex and warmed the face. Another study Makihara and Masumi[19] showed that phototherapy on one side of the face

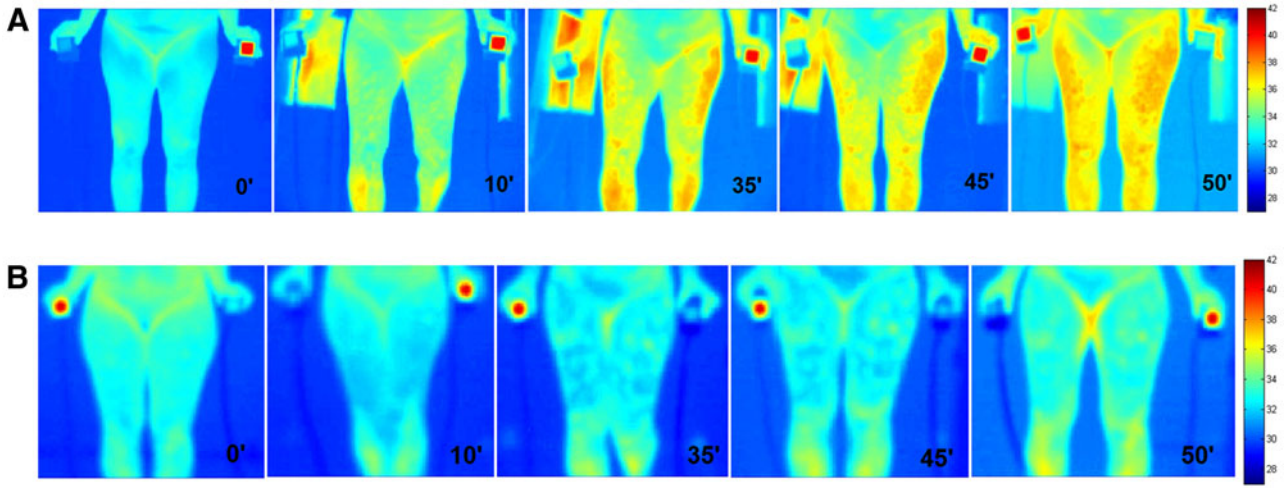

FIG. 2. Thermal images before, during, and after the physical exercises **(A)** with or **(B)** without infrared light-emitting diode (LED) irradiation.

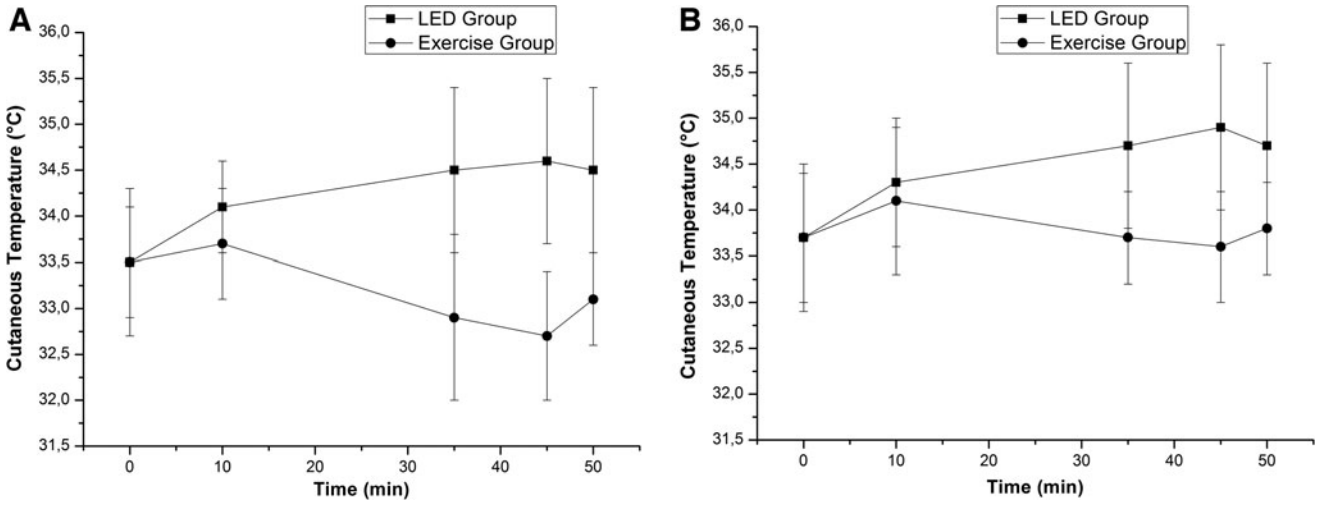

FIG. 3. Dynamic behavior of the cutaneous temperature of the **(A)** thighs and of the **(B)** lower legs before, during, and after physical exercise with or without light-emitting diode (LED) irradiation.

induced a significant increase of the diameter and blood flow volume of superficial temporal artery 10 min after stopping the irradiation, compared with the situation before the irradiation. These changes also occurred on the opposite side of the face.

On the other hand, similar results to those observed in the exercise group were obtained by Merla and collaborators.[16] Their study showed a reduced cutaneous temperature of the thighs, forearms, and trunk during a graded exercise testing, compared with that during rest and post-exercise recovery. The authors suggested a continuous cutaneous vasoconstrictor response, attributable to an increase in catecholamine and other vasoconstrictor hormones released as the exercise intensity increased.[16]

In a study by Zontak et al.,[20] it was shown that the cutaneous temperature of the hands during exercises depended upon the type of exercises (graded vs. constant load). During a graded load exercise, there was increased metabolic demand from the working organs (e.g., leg muscles) and the temperature of the hands continuously decreased throughout the exercise period. During constant load exercise, there was an initial temperature decrease followed by the rewarming of the hands, which reflected a dominance of the thermoregulatory reflexes at a later stage of the exercise.[20]

Our results of the exercise group are different of the results obtained by Zontak et al.,[20] because these evaluated the response thermodynamics of the hands of young men during the exercise on a bicycle ergometer (without weight-bearing effects) performed with different intensities and duration than in the current study. Moreover, the hands are not main actuators during exercise, and have no skeletal muscle pump. Our study, however, evaluated the region related to a presence of the main muscle actuators (legs) of postmenopausal women, during an exercise on a treadmill.

During a post-exercise recovery, our results were similar to those observed in the study of Merla et al.[16] The high cutaneous temperature post-exercise is a consequence of peripheral vasodilatation. This is indicated by the presence of hyperthermal spots. The authors suggested that these spots were indicators for a diffusion of heat from the hyperthermal spots to the surrounding cutaneous tissue, suggesting a possible hemodynamic and thermoregulatory role of the perforator vessels for the transition from exercise to rest.[16]

Although in the current study, the body core temperature (e.g., rectal, tympanic, or esophageal) had not been measured, probably hyperthermia (when a heat production exceeds a loss of heat and results in core temperature of $\sim 40^{\circ}$ C)[21] did not occur because there was no reduction of physical performance. In addition, an artificial heat was applied locally only in the thighs. The infrared LEDs at a power of 100 mW during 45 min produced heat exerting a biological effect, but not a hyperthermic effect, on promoting and improving skin microcirculation. These therapeutic effects can be associated with vasodilatation and angiogenesis caused by action of infrared LEDs on nitric oxide (NO).[22–24]

Human[25] and animal[26] studies have shown increased skin temperatures when phototherapy was applied; however, darker skin showed a higher cutaneous temperature than did lighter skin. According to the authors,[25,26] the heat induced in the skin during application of phototherapy is strongly related to skin color, and the lowest thermal effect in light skin may be caused by light reflection.

Thermal effects can explain the treatment of the pain when phototherapy is applied. Infrared radiation (Ga-As-Al laser, 780 nm) with muscle-stretching exercises had superior significant effects on feeling pain in active myofascial trigger points with thermographic changes 3 weeks after a treatment.[6] Furthermore, Hegedus et al.[27] showed that thermographic measurements had at least a 0.58°C increase in temperature, and, therefore, an improvement in circulation compared with the initial values and improvement of the joint range-of-motion, pain, and pressure sensitivity in patients with knee osteoarthritis who had received phototherapy (Ga-Al-As diode laser, 830 nm), in comparison with a placebo group.

The thermal effect observed in the current study can explain the performance improvement with LED infrared irradiation during treadmill exercises,[9,10] as higher circulation induced by an increasing muscle temperature can improve oxygen supply as well as transport and utilize metabolic substrates, mainly when phototherapy is combined with skeletal muscle contractions during a physical exercise.

This thermal effect also can explain the treatment of cellulite and the reduction of the perimeter of the thighs in both young and middle-aged women who underwent LED infrared irradiation during treadmill exercises.[11] The reduction of the thigh circumference may be related to infrared LED effects, resulting in increased microcirculation and lymphatic drainage,[28] because cellulite is characterized by alterations of the microcirculation and the lymphatic system, in addition to a dysfunction of cutaneous and adipose tissue with a fibrotic reaction.[29]

Future studies should be performed using a large sample size, different ages and genders, and a large post-exercise period in order to investigate cutaneous temperature, body core temperature, and microcirculation in more detail (e.g., diameter and blood flow volume of the femoral artery).

Conclusions

To conclude, the results of our study showed that the LED group showed increases of the cutaneous temperature of the lower limbs during the exercise, whereas the exercise group experienced reduced temperatures. This intergroup difference can explain one of the possible mechanisms of phototherapy associated with physical exercises in improving physical performance, body aesthetic, and health.

Acknowledgments

We thank the Fundação de Amparo à Pesquisa do Estado de São Paulo (FAPESP) – Grant nos. 2008/578588-9 and 98/14270-8, Conselho Nacional de Desenvolvimento Científico e Tecnológico (CNPq) – Grant nos. 573587/2008 and 151008/2012-4, and Coordenação de Aperfeiçoamento de Pessoal de Nível Superior (CAPES) for financial support. We also acknowledge the contributions of Nivaldo Antonio Parizotto and Audrey Borghi-Silva from the Federal University of São Carlos, as well as the valuable technical assistance graciously provided by Juliana Cristina Milan and Cristine Letícia Grandisoli.

Author Disclosure Statement

No competing financial interests exist.

References

1. Miland, A.O., and Mercer, J.B. (2006). Effect of a short period of abstinence from smoking on rewarming patterns of the hands following local cooling. Eur. J. Appl. Physiol. 98, 161–168.
2. Roelands, B., and Meeusen, B. (2010). Alterations in central fatigue by pharmacological manipulations of neurotransmitters in normal and high ambient temperature. Sports Med. 40, 229–246.
3. Schlader, Z.J., Stannard, S.R., and Mündel, T. (2010). Human thermoregulatory behavior during rest and exercise – a prospective review. Physiol. Behav. 99, 269–275.
4. Barnes, R.B. (1963). Thermography of the human body. Infrared-radiant energy provides new concepts and instrumentation for medical diagnosis. Science 140, 870–877.
5. Kohler, A., Holfmann, R., Platz, A., and Bino, M. (1998). Diagnostic value of duplex ultrasound and liquid crystal contact thermography in preclinical detection of deep vein thrombosis after proximal femur fractures. Arch. Orthop. Trauma Surg. 117, 39–42.
6. Ohsawa, S., Inamori, Y., Fukuda, K., and Hirotuji, M. (2001). Lower limb amputation for diabetic foot. Arch. Orthop. Trauma Surg. 121, 186–1901.
7. Gold, J.E., Cherniack, M., Hanlon, A., Dennerlein, J.T., and Dropkin, J. (2009). Skin temperature in the dorsal hand of office workers and severity of upper extremity musculoskeletal disorders. Int. Arch. Occup. Environ. Health 82, 1281–1292.
8. Hakgüder, A., Birtane, M., Gürcan, S., Kokino, S., and Turan, F.N. (2003). Efficacy of low level laser therapy in myofascial pain syndrome: an algometric and thermographic evaluation. Lasers Surg. Med. 33, 339–343.
9. Paolillo, F.R., Corazza, A.V., Borghi–Silva, A., Parizotto, N.A., Kurachi, C., and Bagnato, V.S. (2013). Infrared-LED applied during high-intensity treadmill training improved maximal exercise tolerance in postmenopausal women: a 6-month longitudinal study. Lasers Med. Sci. 28, 415–422.
10. Paolillo, F.R., Milan, J.C., Aniceto, I.V., Barreto, S.G., Rebelatto, J.R., Borghi–Silva, A., Parizotto, N.A., Kurachi, C., and Bagnato, V.S. (2011). Effects of infrared-LED illumination applied during high-intensity treadmill training in postmenopausal women. Photomed. Laser Surg. 29, 639–645.
11. Paolillo, F.R., Borghi–Silva, A., Parizotto, N.A., Kurachi, C., and Bagnato, V.S. (2011). New treatment of cellulite with infrared-LED illumination applied during high-intensity treadmill training. J. Cosmet. Laser Ther. 13, 166–171.
12. Ebrahimpour, P., Fakhrzadeh, H., Heshmat, R., Ghodsi, M., Bandarian, F., and Larijani, B. (2010). Metabolic syndrome and menopause: a population-based study. Diabetes Metab. Syndr. 4, 5–9.
13. Fletcher, G.F., Balady, G.J., Amsterdam, E.A., Chaitman, B., Eckel, R., Fleg, J., Froelicher, V.F., Leon, A.S., Piña, I.L., Rodney, R., Simons–Morton, D.A., Williams, M.A., and Bazzarre, T. (2011). Exercise standards for testing and training: a statement for healthcare professionals from the American Heart Association. Circulation 104, 1694–1740.
14. Noonan, V., and Dean, E. (2000). Submaximal exercise testing: clinical application and interpretation. Phys. Ther. 80, 782–807.
15. Ferreira, J.J.A., Mendonça, L.C.S., Nunes, L.A.O., Andrade Filho, A.C.C., Rebelatto, J.R., and Salvini, T.F. (2008). Exercise-associated thermographic changes in young and elderly subjects. Ann. Biomed. Eng. 36, 1420–1427.
16. Merla, A., Mattei, P.A., Di Donato, L., and Romani, G.L. (2010). Thermal imaging of cutaneous temperature modifications in runners during graded exercise. Ann. Biomed. Eng. 38, 158–163.
17. Reilly, T., and Waterhouse, J. (2009). Circadian aspects of body temperature regulation in exercise. J. Therm. Biol. 34, 161–170.
18. Makihara, E., Makihara, M., Masumi, S.I., and Sakamoto, E. (2005). Evaluation of facial thermographic changes before and after low-level laser irradiation. Photomed. Laser Surg. 23, 191–195.
19. Makihara, E., and Masumi, S.I. (2008). Blood flow changes of a superficial temporal artery before and after low-level laser irradiation applied to the temporomandibular joint area. Nihon Hotetsu Shika Gakkai Zasshi. 52, 167–170.
20. Zontak, A., Sideman, S., Verbitsky, O., and Beyar, R. (1998). Dynamic thermography: analysis of hand temperature during exercise. Ann. Biomed. Eng. 26, 988–993.
21. Brotherhood, J.R. (2008). Heat stress and strain in exercise and sport. J. Sci. Med. Sport 11, 6–19.
22. Yu, S.Y., Chiu, J.H., Yang, S.D., et al. (2006). Biological effect of far-infrared therapy on increasing skin microcirculation in rats. Photodermatol. Photoimmunol. Photomed. 22, 78–86.

23. Karu, T.I., Piatybrat, L.V., and Afanasyeva, N.I. (2004). A novel mitochondrial signaling pathway activated by visible-to-near infrared radiation. Photochem. Photobiol. 80, 366–372.
24. Karu, T.I., Piatybrat, L.V., and Afanasyeva, N.I. (2005). Cellular effects of low power laser therapy can be mediated by nitric oxide. Lasers Surg. Med. 36, 307–314.
25. Joensen, J., Demmink, J.H., Johnson, M.I., Iversen, V.V., Lopes–Martins, R.A.B., and Bjordal, J.M. (2011). The thermal effects of therapeutic lasers with 810 and 904 nm wavelengths on human skin. Photomed. Laser Surg. 29, 145–153.
26. Stadler, I., Lanzafame, R.J., Oskoui, P., Zhang, R.Y., Coleman, J., and Whittaker, M. (2004). Alteration of skin temperature during low-level laser irradiation at 830 nm in a mouse model. Photomed. Laser Surg. 22, 227–231.
27. Hegédus, B., Viharos, L., Gervain, M., and Gálfi, M. (2009). The effect of low-level laser in knee osteoarthritis: a double-blind, randomized, placebo-controlled trial. Photomed. Laser Surg. 27, 577–584.
28. Kaviani, A., Fateh, M., Nooraie, R.Y., Alinagi–Zadeh, M., and Ataie–Fashtami, L. (2006). Low-level laser therapy in management of postmastectomy lymphedema. Lasers Med. Sci. 21, 90–94.
29. Rawlings, A.V. (2006). Cellulite and its treatment. Int. J. Cosmet. Sci. 28, 175–190.

Address correspondence to:
Fernanda Rossi Paolillo
University of São Paulo (USP)
Av. Trabalhador Sãocarlense
400 – Centro
CEP 13560-970
São Carlos, SP
Brazil

E-mail: fer.nanda.rp@hotmail.com

Brazilian Dental Science
Ciência Odontológica Brasileira
unesp
UNIVERSIDADE ESTADUAL PAULISTA "JÚLIO DE MESQUITA FILHO"
Instituto de Ciência e Tecnologia
Campus de São José dos Campos

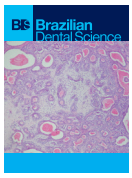

ORIGINAL ARTICLE

Effect of different light-curing techniques on hardness of a microhybrid dental composite resin

Efeito de diferentes técnicas de fotoativação na dureza de uma resina composta dental microhíbrida

Alessandra Nara de Souza RASTELLI[1], Ricardo Scarparo NAVARRO[2], José Roberto Cury SAAD[1], Marcelo Ferrarezi de ANDRADE[1], Vanderlei Salvador BAGNATO[3]

1 – Univ Estadual Paulista – UNESP – Araraquara School of Dentistry – Department of Restorative Dentistry – Araraquara – SP – Brazil.

2 – Camilo Castelo Branco University – UNICASTELO – BEC – Biomedical Engeneering Center – CITE – City of Science Technology and Information – São José dos Campos – SP – Brazil.

3 – University of São Paulo – USP – Physics Institute of São Carlos – Optical Group – Department of Physics and Materials Science – São Carlos – SP – Brazil.

ABSTRACT

Objective: This study assessed the Vickers hardness (VHN) provided by two LCUs when using (1) direct and indirect light-curing techniques, (2) 40 and 60 s and (3) top and bottom surfaces. **Material & Methods:** One halogen Curing Light 2500 (3M Espe) and one LED (MM Optics) were used by direct and indirect (0, 1.0, 2.0 and 3.0 mm of dental structure) techniques during 40 and 60 s. The samples were made with FiltekTM Z250 in a metallic mould with a central orifice (4 mm in diameter, 2 mm in thickness). The samples were stored in dry mean by ± 24 h and the hardness measurements were performed in a testing machine (Buehler MMT-3 digital microhardness tester Lake Bluff, Illinois USA). A 50 gf load was used and the indenter with a dwell time of 30 s. The data were submitted to multiple ANOVA and Newman-Keuls's test ($p < 0.05$). **Results:** Halogen LCU exhibited higher Vickers hardness values than LED mainly because of the power density used. Hardness values were influenced by LCUs, light-curing techniques, irradiation times and surfaces. For both LCUs, hardness values were found to decrease with indirect light-curing technique, mainly for the bottom surface. Samples irradiated for 60 s exhibited higher hardness values when the halogen LCU was used. For 60 s, the VHN values were statistically significant greater than 40 s. Significant differences in top and bottom surfaces Vickers hardness number (VHN) values were observed among different LCUs used 40 and 60 s. **Conclusion:** The LCUs, light-curing techniques, variations of irradiation times, and surfaces (top and bottom) influence the composite resin hardness.

KEYWORDS

Composite resin, LED, Halogen lamp, Hardness, Photo-activation.

RESUMO

Objetivo: Este estudo avaliou a dureza Vickers (VHN) em função de duas fontes de luz quando utilizadas diferentes (1) técnicas de fotoativação, direta e indireta, (2) 40 e 60 s, e (3) superfícies de topo e base. **Material e Métodos:** Uma fonte de luz halógena Curing Light 2500 (3M Espe) e um LED (MM Optics) foram utilizados nas técnicas de fotoativação direta e indireta (0 , 1,0, 2,0 e 3,0 milímetros de estrutura dental), durante 40 e 60 s. As amostras foram feitas utilizando-se FiltekTM Z250 em matriz metálica com orifício central (4 mm de diâmetro, com 2 mm de espessura). As amostras foram armazenadas em meio seco por ± 24 h e as medidas de dureza foram realizadas em microdurômetro (Buehler MMT-3 digital microhardness tester Lake Bluff, Illinois USA). Uma carga de 50 gf durante 30 s foi utilizada. Os dados foram submetidos à análise de variância múltipla e teste de Newman-Keuls ($p < 0,05$). **Resultados:** A fonte de luz halógena promoveu os maiores valores de dureza Vickers, principalmente, em função da densidade de potência utilizada. Os valores de dureza foram influenciados pelas fontes de luz, técnicas de fotoativação, tempos de irradiação e superfícies, topo e base. Para ambas as fontes de luz, os valores de dureza diminuíram com a técnica de fotoativação indireta, principalmente para a superfície de base. Amostras irradiadas por 60 s apresentaram valores de dureza maiores quando a fonte de luz halógena foi utilizada. Durante 60 s , os valores de VHN foram estatisticamente significativos maior do que 40 s. Diferenças significativas foram observadas nos valores dureza Vickers (VHN) para as superfícies de topo e base utilizando 40 e 60 s. **Conclusão:** As fontes de luz, técnicas de fotoativação direta e indireta, tempos de irradiação e superfícies (topo e base) influenciam na dureza da resina composta.

PALAVRAS-CHAVE

Resina composta, LED, Lâmpada halógena, Dureza, Fotoativação.

INTRODUCTION

The generally preferred mode of polymerization in dental composite resins is photo-activation method [1]. Effectiveness of the polymerization is one important meaning to obtain adequate physical properties.

One limitation of photo-activated dental composite resins is that a hard top surface is not an indication of adequate polymerization throughout the depth of restoration [2,3]. Poorly polymerized composite resin can lead to undesirable effects, such as: gap formation, marginal microleakage, recurrent caries, adverse pulpal effects and ultimate failure of restorative procedure [2,3]. Effective polymerization is important not only to ensure optimum physical-mechanical properties, however also to ensure that clinical problems do not arise due to the cytotoxicity of inadequately polymerized material [4, 5-7].

Many factors affect the polymerization effectiveness. These factors can be related to the material's composition, resin chemistry, shade, translucency, catalyst concentration, power density, spectral distribution of the light source, irradiation time, absorption coefficient and placement technique [8].

Now, light-curing units (LCUs) and light curing methods have been in constant evolution. Light curing of composite resins with blue light has proven to be the best photo-activation method and can be made with different light-curing sources [9]. Four light-curing sources have been clinically applied: quartz tungsten halogen (QTH) lamps, light emitting diodes (LED) units, plasma-arc lamps and argon-ion lasers [10,11]. However, halogen lamp and LED LCUs are overwhelmingly applied in daily clinical practice [10]. However, the most widely used light-curing units (LCUs), a low cost technology, are based on quartz tungsten halogen lamps (QTH) [12]. The main radiant output from a QTH LCU is infrared energy, which may be absorbed by dental composite resins and results in an increased molecular vibration and consequently heat generation. Thus, the QTH LCUs need of use of filters to reduce the passage of infrared energy from the LCU to the tooth. However, the filter degrades over time due to high operating temperatures and significant heat produced during curing cycles [13]. Thus, unfiltered infrared energy can result in heat generation at the pulp chamber [14]. In addition, the halogen bulbs have a limited effective lifetime of about 40-100 h and reflectors too degrade over time. Then, the drawbacks of the halogen LCU will reduce the effectiveness of polymerization in composite restoratives.

LED (light-emitting diodes) light-curing units (LCUs) developed to overcome the problems inherent to halogen LCUs, use junctions of doped semi-conductors (p-n-junction) to generate light [15,16]. Under proper forward biased conditions, electrons and holes recombine at the LEDs p-n junction leading, in the case of gallium nitride LEDs, to the emission of blue light. A small polymer lens in front of the p-n junction partially collimates the light. As spectral output of gallium nitride blue LEDs falls within the absorption spectrum of the camphorquinone photo-initiator, no filters are required in LED LCUs. The absorption spectrum of camphorquinone lies in the 450-500 nm wavelength range, with peak absorption at 470 nm [17-19].

The basic composite technique insertion and photo-activation protocol usually recommends the use of increments not thicker than 2 mm to provide an effective polymerization. Further, the light guide should be as close as possible to the composite surface to guarantee the light will not be dissipated. However, some clinical situations present a real challenge to the utilization of these recommended polymerization techniques, such as accessing the floor of Class II proximal boxes where the distance between the light guide and the material surface is generally greater [20]. For such situations, the increase of the light-curing time and the use of photo-activation of

the composite resin through teeth have been strongly recommended [21,22].

It has been reported that the light is not transmitted well through composite resins and through teeth. The photo-activation of the composite resin through teeth which used transdental technique (TDT) or indirect techniques was introduced based on the common belief that the direction of the shrinkage vectors was towards the polymerization light, attempted to change the direction of the vectors towards the bonded walls [23]. However, it was further demonstrated that the shrinkage vectors actually develop toward the bonded walls, irrespective of the light position [24]. Nonetheless, the TDT could be effective in modifying the kinetics of polymerization, as a reduction in light intensity of up to 70 % may occur when light passes through the dental structure [25]. The photo-activation of the composite resins through the dental structure, enamel and/or dentine, is related to the curing depth of these materials and can promote a reduction in hardness values, depending yet on the dental structure thickness [26]. However, little is known about the influence of different light sources when using the TDT.

Effectiveness of polymerization may be assessed directly and indirectly. Indirect techniques have included scraping, visual and surface hardness. However, incremental surface hardness has been used, because surface hardness shown to indicate the degree of conversion of the monomers. Direct methods have included the degree of conversion, such as infrared spectroscopy and laser Raman spectroscopy. However, these techniques are complex, expensive and time-consuming. Hardness testing appears to be the most popular technique for investigating factors that affect effectiveness of polymerization of dental composite resins [13,18,19,27,28].

Thus, the purpose of this study was to evaluate the effectiveness of polymerization of one microhybrid composite resin cured with a halogen lamp or a LED LCUs with two irradiation times by means of Vickers hardness testing when direct or indirect light-curing techniques were used.

MATERIAL & METHODS

Composite resin used

The microhybrid composite resin, FiltekTM Z250 (3M Espe Dental Products Division, St. Paul, MN 55144-1000, USA - batch n°: 1370 – 3WH) at the color A2 was used in the samples preparation. The material was based on bisphenol glycidyl methacrylate (BIS-GMA)/ urethane dimethacrylate (UDMA)/bisphenol ethylene methacrylate (BIS-EMA) resin matrix, with camphorquinone as photoinitiator and 60 vol % inorganic filler content with the medium size of the 0,19 a 3,3 microns. The inorganic filler is based on zirconia/silica. This material is clinically indicated as a universal hybrid composite resin for anterior and posterior restorations.

Photo-activation of the samples

For the photo-activation procedure two different light-curing units (LCUs) were used. The Table 1 shows the LCUs used and their characteristics (Table 1).

The power of the units was measured with a power meter (Fieldmaster, Coherent, model n° FM, set n° WX65, part n° 33-0506, USA) and then the power density was calculated by the equation:

$$I = P/A$$

Where: P = power (mW), A = area of the light tip (cm^2).

Table 1 - Light-curing units, exposure times, power density and peak wavelength that were used in this study

Light-curing units	Manufactures	Power density (mW/cm²)	Tip mm	Peak wavelength nm	Irradiation times s
Halogen Curing Light 2500	3M Espe, Dental Products Division, St. Paul, MN 55144 1000, model 5560AA, serial number 3000552	550	8	487	40 and 60
LED	MMOptics, São Carlos Brazil, model SPL 110F15-A/28	270	10	458	40 and 60

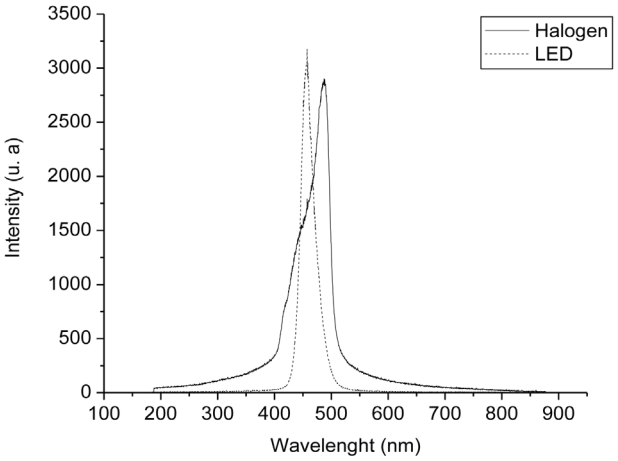

Figure 1 - Spectral distribution emitted by the halogen and LED LCUs.

The Figure 1 shows the spectral range of the LCUs used, as well as its maximum emission peaks obtained by the spectrophotometer USB 2000 (Ocean Optics Inc.), which has a photosensitive cell where the light tip was positioned, registering, in that way, the emission spectrum (Figure 1).

Enamel and Dentin Specimens Preparation

For preparation of enamel and dentin specimens, three recently extracted and caries-free inferior lower third molars were selected (protocol number 38/04 Research Ethic Committee, Araraquara School of Dentistry-UNESP/SP – Brazil). After the extraction, the teeth were stored in 0.5 % chloramine solution for 24 h. After they were rinsed and gross debris was removed, the teeth were again stored in chloramine solution at 0.5 % for seven (7) days. The teeth had their coronary portions separated from their roots to the enamel-cement junction level by the use a diamond disk with 0.3 mm of thickness mounted in a cutting machine Isomet 1000 (Buehler Ltd, Lake Bluff, Illinois). The enamel and dentin specimens were obtained by the cut of the buccal face of the dental crowns. The enamel and dentin specimens (1.0; 2.0 and 3.0 mm) were flattened with wet 1200-grit silicon carbide paper (3M) mounted in a manual polishing machine.

To measure the thickness of enamel and dentin specimens, a digital caliper was used (Brown & Sharpe - *model n°599-571-3*).

Composite Resin Samples Preparation:

The samples (n=80) were made in a metallic mold, with central orifice (2 mm in thickness and 4 mm in diameter) according to IS0 number 4049 [29].

The metallic mold was positioned on a glass plate with 10 mm of thickness where a mylar strip was taken place at the bottom surface of the metallic mold. The composite resin was packed in only increment and then covered with another mylar strip and then pressed with a glass slab to accommodate the material into the matrix and to guarantee the superficial smoothness of the composite for the hardness evaluation. Five samples (n = 5) were made for each Group. The samples were light-

cured by direct (control) and indirect techniques (enamel and dentin specimens) for 40 and 60 s of irradiation times.

Hardness Testing:

The samples were stored in a dark environment for 24 h in dry mean at 37 ºC (± 1 ºC). Following storage, the Vickers Hardness Number (VHN) was recorded in the top and bottom surfaces of the samples with a digital hardness tester (MMT-3 Microhardness Tester - Buehler Lake Bluff, Illinois USA). A 50 gf load was applied through the indentor with a dwell time of 30 s. In each top and bottom surfaces eight impressions were made according to Figure 2 (Figure 2).

Mean values and standard deviations of hardness were calculated for each Group. Statistical analysis was performed with a three-way analysis of variance (ANOVA) regarding light-curing units, power densities and irradiation times. Two-way analysis of variance (ANOVA) was applied regarding light-curing techniques and surfaces (top and bottom) in order to determine their influence. The tests were conducted at a significance level of 5%. In addition, Student-Newman-Keuls range test was used for further comparisons. Statistical significance was considered at the 95% confidence level.

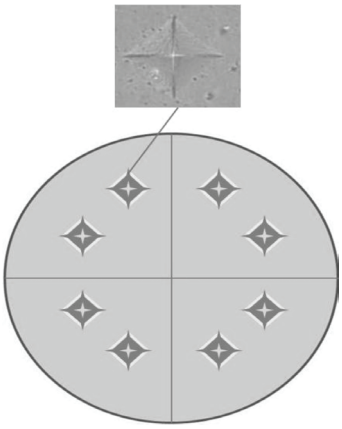

Figure 2 - Esquematic distribution of the indentations on the top and bottom surfaces of the samples.

RESULTS

The Figures 3 and 4 show the results obtained with the hardness test as a function of light-curing units, and indirect (Transdental, TDT) light-curing techniques (0, 1.0, 2.0 and 3.0 mm) and 40 and 60 s of irradiation times for the top and bottom surfaces (Figure 3 and 4).

ANOVA showed that hardness was influenced by light-curing units ($p<0.001$), by light-curing techniques ($p < 0.001$) and by irradiation times (40 or 60 s) ($p<0.001$). Halogen LCU exhibited a statistically higher hardness

Three-way ANOVA revealed significant interaction between direct and indirect light-curing techniques and top and bottom surfaces. Therefore, the effects of the LCUs on hardness were light curing techniques (direct and indirect), surfaces (top and bottom) and irradiation times dependent. At the top and bottom surfaces, VHN mean values after photo-activation with direct light-curing technique were significantly higher than indirect light-curing technique, independently of the irradiation times and LCUs used. There is, therefore, a significant decrease in the effectiveness of polymerization at the bottom surface.

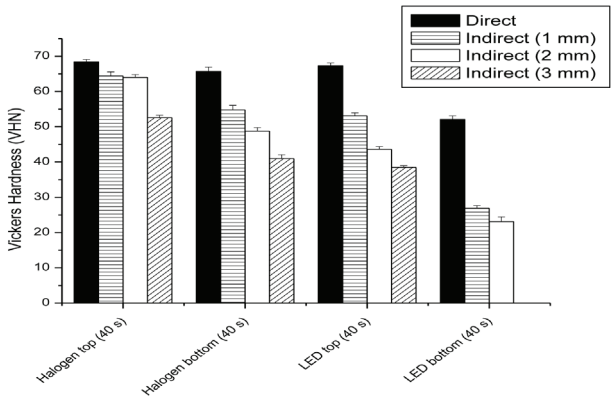

Figure 3 - VHN mean values for halogen and LED LCUs used during 40 s of irradiation time for top and bottom surfaces when direct and indirect (Transdental, TDT) light-curing techniques were used.

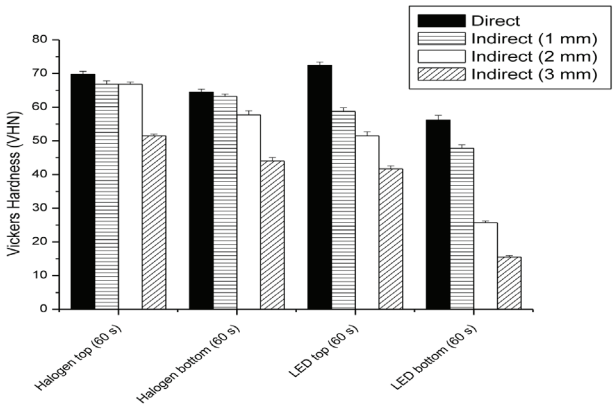

Figure 4 - VHN mean values for halogen and LED LCUs used during 60 s of irradiation time for top and bottom surfaces when direct and indirect (Transdental, TDT) light-curing techniques were used.

DISCUSSION

The polymerization effectiveness can play an important role on physical, chemistry and biological properties [4-6,30]. Problems associated with inadequate polymerization has been associated to the inferior physical properties, solubility in the oral environment, increased microleakage and adverse pulpal response to the free monomers [18,22].

Polymerization effectiveness has been assessed directly or indirectly [31-36]. Direct methods check the degree of conversion, like Fourier transformed infrared spectroscopy (FTIR) and Raman spectroscopy; however, this method is complex, expensive and time-consuming [10,24]. Moreover, the indirect methods, which include the hardness test, have been show to be an indicator of the degree of conversion and there seems to be a good correlation between Vickers hardness and infrared spectroscopy [23,37,38]. The hardness testing appears to be the most popular method for investigating factors that influence the effectiveness of polymerization with relative simplicity. The purpose of micro indentation hardness testing is to obtain a numerical value that distinguishes between the relative ability of materials to resist controlled penetration by a specified type of indenter which is generally much harder than the material being tested [25,37]. In a way of determining degree of polymerization, several studies have compared hardness of dental composite resins [37,39-41].

Now, clinicians face a dilemma when selecting a protocol for light-curing techniques of light-cured dental composite resins. Contemporary choices of LCUs range from conventional, continuous output quartz-tungsten to blue LED. Many authors and manufactures have stated that LED LCUs have similar polymerization effectiveness when compared with QTH LCUs and the advantage of reducing overheating [23].

Adequate physical properties of light-cured dental composite resins are achieved when the LCUs deliver enough light at the appropriate wavelength of the respective photoinitiator systems in dental composite resins. Unlike halogen LCUs, LED emission spectrum is narrow and located close to the absorption maximum of camphorquinone. The polymerization of light-cured dental composite resins depends not only on the power density, but also on its wavelength. In this sense, LCUs based on LED seems to be the best option [30].

LCUs based on blue LED produce light by electroluminescence, while the halogen LCUs produce light by incandescence, when a tungsten filament is heated, causing excitation of atoms over a wide range of energy levels that produce a very broad spectrum. Therefore, a filter is required to restrict the emitted light to the blue region of the spectrum required for curing.

The hardness measurements was used in this study In order to analyze the polymerization effectiveness of halogen and LED LCUs by the direct and indirect (Transdental, TDT) light-curing techniques.. The Figures 2 and 3 show the VHN mean values obtained with halogen and LED LCUs, respectively for microhybrid dental composite resin (top and bottom surfaces) by direct and indirect (TDT) light-curing techniques

during 40 and 60 s of irradiation times. In this study, halogen LCU showed the higher VHN mean values. The amount of energy may be explaining these findings.

The results show that for the direct light-curing technique, the top surface was not as susceptible to the effects of power densities as the bottom surface.

(In the ideal situation, the hardness:thickness ratio of dental composite resins should be equal or very close to 1:1 or very close. However, as light passes through the bulk of the restorative material, its power density is greatly decreased due to the light absorption and scattering by dental composite resins, thus, decreasing the potential for polymerization [42,43].

This scattering of light accounts for the minor differences in hardness between the top and bottom surfaces observed in this study.

In this study, this fact may be also associated with the use of indirect light-curing technique. According to Dietschi et al. and Price et al. the hardness means values decrease when the thickness of dental structure was increased in the indirect technique (TDT) [42,44]. The results observed in this study may be explained by the fact that the light emitted by the LCUs was not well transmitted through the dental structure, mainly through dentine.

In this sense, the exponential decrease in the power density plays an important role on decrease of VHN mean values, mainly for the bottom surface. In general, when the thickness of dental structure was increased a decrease in the VHN mean values was observed [39,45,46]. Frequently, for the top surface, the VHN mean values were equivalent. However, for the bottom surface, the decrease may be high when the LED LCU was used.

Many authors have shown that the presence of external interferences, such as the dental structure during the photo-activation of dental composite resins may influence on the polymerization process [26]. When compared to the other techniques, the radiant exposure for TDT was noticeably lower, as a function of the significant reduction in irradiance for the light transmitted through enamel and dentin, probably leading to a lower degree of conversion [23].

According to Price et al. clinically, the photo-activation of dental composite resin through dental structure, enamel and or dentin, with 2 mm of thickness or plus, produces inadequate polymerization and then, inferior mechanical properties reducing in this way the lifetime of restorative procedure [44]. The reduction in hardness was verified for TDT when compared to the direct light-curing technique. An attempt to explain this outcome considers that the initial exposure at low power density for TDT might result in the formation of short, low-molecular weight polymer chains, with less cross-linking interfering with the mechanical properties of the composite [47,48].

Many authors have shown that the polymerization effectiveness cannot be assessed by top surface hardness alone. According to Rueggeberg et al. for the top surface, only irradiation time is a significant factor that contributes to monomer conversion [24].

The results of this study show that 60 s of irradiation time provided VHN mean values higher than 40 s mainly for the indirect light-curing technique. In general, an increase in VHN mean values was noted with increased irradiation time for both direct and indirect technique.

Despite the marked increase in availability of LED dental LCUs, research comparing composite polymerization associated with halogen LCU and LED LCUs is generally limited. Thus, the polymerization effectiveness using different LCUs by direct and indirect (Transdental, TDT) techniques warrants further investigations. In addition, it is important to

highlight the fact that high-power density lights should be used, as irradiance through the dental structure would be markedly reduced.

CONCLUSION

1. The bottom surface resulted in a significant decrease in hardness mean values for both LCUs used, and direct and indirect techniques.

2. Increased irradiation time resulted in an increase in hardness mean values for both LCUs used, surfaces and direct and indirect techniques.

3. The different light sources (halogen and LED) showed significant influence on the hardness mean values, while the halogen unit yielded greater hardness than LED.

4.The indirect light-curing technique significantly interfering the hardness mean values, regardless of the light-curing units, the irradiation times used and the thickness of dental structure (enamel/dentine) for both, top and bottom surfaces.

5. Maybe when indirect light-curing technique is used will be necessary to change the parameters used during photoactivation and decrease the thickness of composite resin incremente.

ACKNOWLEDGMENTS

This work was supported by CAPES (Coordenadoria de Aperfeiçoamento de Pessoal de Nivel Superior, Brazil).

REFERENCES

1. Discacciati JAC, Neves AD, Orefice RL, Pimenta FJGS, Sander HH. Effect of light intensity and irradiation time on the polymerization process of a dental composite resin. Mater Res. 2004;7:313-8.
2. Pilo R, Cardash HS. Post-irradiation polymerization of different anterior and posterior visible light-activated resin composites. Dent Mater. 1992;8(5):299-304.
3. Hansen EK, Asmussen E. Correlation between depth of cure and surface hardness of a light-activated resin. Scand J Dent Res. 1993;101(1):62-4.
4. Fan PL, Schumacher RM, Azzolin K, Geary R, Eichmiller FC. Curing-light intensity and depth of cure of resin-based composites tested according to international standards. J Am Dent Assoc. 2002;133(4):429-34.
5. Bennett AW, Watts DC. Performance of two blue light-emitting-diodes light curing units with distance and irradiation-time. Dent. Mater. 2004;20(1):72-9.
6. Davidson CL, De Gee AJ. Light-curing units, polymerization, and clinical implications. J Adhes Dent. 2000;2(3):167-73.
7. Sideridou ID, Achilias DS. Elution study of unreacted Bis-GMA, TEGDMA, UDMA, and Bis-EMA from light-cured dental resins and resin composites using HPLC.. J Biomed Mater Res B Appl Biomater. 2005;74(1):617-26.
8. Nomoto R, Asada M, McCabe JF, Hirano S. Light exposure required for optimum conversion of light activated resin systems. Dent Mater. 2006;22(12):1135-42.
9. Correr AB, Sinhoreti MAC, Correr-Sobrinho L, Tango RN, Consani S, Schneider LFJ. Effect of exposure time vs. irradiance on knoop hardness of dental composites. Mater Res. 2006;9:275-80.
10. Hervás-García A, Martínez-Lozano MA, Cabanes-Vila J, Barjau-Escribano A, Fos-Galve P. Composite resins. A review of the materials and clinical indications. Med Oral Patol Oral Cir Bucal. 2006;11(2):E215-20.
11. Vandewalle KS, Roberts HW, Tiba A, Charlton DG. Thermal emission and curing efficiency of LED and halogen curing lights. Oper Dent. 2005;30(2):257-64.
12. Ceballos L, Fuentes MV, Tafalla H, Martínez Á, Flores J, Rodríguez J. Curing effectiveness of resin composites at different exposure times using LED and halogen units. Med Oral Patol Oral Cir Bucal. 2009;14(1):E51-6.
13. Jandt KD, Mills RW, Blackwell GB, Ashworth SH. Depth of cure and compressive strength of dental composites cured with blue light emitting diodes (LEDs). Dent. Mater. 2000;16(1):41-7.
14. Blankenau R, Erickson RL, Rueggeberg F. New light curing options for composite resin restorations. Compend Contin Educ Dent. 1999;20(2):122-515. Nakamura S, Mukai T, Senoh M. Candela-class high-brightness InGaN/AlGaN double-heterostructure blue-light-emitting diodes. Appl Phys Lett. 1994;64:1687-9.
15. Guiraldo RD, Consani S, Consani RL, Bataglia MP, Fugolin AP, Berger SB, et al.. Evaluation of the light energy transmission and bottom/top rate in silorane and methacrylate-based composites with different photoactivation protocols. J Contemp Dent Pract. 2011;12(5):361-7.
16. Nomoto R. Effect of light wavelength on polymerization of light-cured resins. Dent Mater. 1997;16(1):60-73.
17. Uhl A, Siguch BW, Jandt K. Second generation LEDs for the polymerization of oral biomaterials. Dent Mater. 2004;20(1):80-7.
18. Pradhan RD, Melikechi N, Eichmiller F. The effect of irradiation wavelenght bandwidth and spot size on the scraping depth and temperature rise in composite exposed to an argon laser or a conventional quartz-tungsten-halogen source. Dent Mater. 2002;18(3):221-6.
19. Cenci M, Demarco FF, de Carvalho RM. Class II composite resin restorations with two polymerization techniques: relationship between microtensile bond strength and marginal leakage. J Dent. 2005;33(7):603-10.
20. Cefaly DF, Ferrarezi GA, Tapety CM, Lauris JR, Navarro MF. Microhardness of resin-based materials polymerized with LED and halogen curing units. Braz Dent J. 2005;16(2):98-102.

21. Alves EB, Alonso RCB, Correr GM, Correr AB, Moraes RR, Sinhoreti MAC, et al. Transdental photo-activation technique: hardness and marginal adaptation of composite restorations using different light sources. Oper Dent. 2008;33(4):421-5.

22. Peutzfeldt A, Sahafi A, Asmussen E. Characterization of resin composites polymerized with plasma arc curing units. Dent Mater. 2000;16(5):330-6.

23. Rueggeberg FA, Caughman WF, Curtis JW. Effect of light intensity and exposure duration on cure of resin composite. Oper Dent. 1994;19(1):26-32.

24. Vandewalle KS, Ferracane JL, Hilton TJ, Erickson RL, Sakaguchi RL. Effect of energy density on properties and marginal integrity of posterior resin composite restorations. Dent Mater. 2004;20(1):96-106.

25. Yap AU. Effectiveness of polymerization in composite restoratives claiming bulk placement: impact of cavity depth and exposure time. Oper Dent. 2000;25(2):113–20.

26. Price RBT, Felix CA, Andreou P. Knoop hardness of ten resin composites irradiated with high-power LED and quartz-tungsten-halogen lights. Biomater. 2005;26(15):2631-41.

27. Soh MS, Yap AUJ, Siow KS. Effectiveness of composite cure associated with different curing modes of LED lights. Oper Dent. 2003;28(4):707-15.

28. International Organization for Standardization. ISO 4049: 2000. Dentistry: polymer-based filling, restorative and luting materials. 3rd ed. Geneva: ISO; 2000.

29. 30. Orefice RL, Discacciati JAC, Neves AD, Mansur HS, Jansen WC. In situ evaluation of the polymerization kinetics and corresponding evolution of the mechanical properties of dental composites. Polymer Test. 2003;22:77–81.

30. Antonson SA, Antonson DE, Hardigan PC. Should my new curing light be an LED? Oper Dent. 2008;33(4):400-7.

31. Hofmann N, Hugo B, Klaiber B. Effect of irradiation type (LED or QTH) on photo-activated composite shrinkage strain kinetics, temperature rise, and hardness. Eur J Oral Sci. 2002;110(6):471–9.

32. Torno V, Soares P, Martin JMH, Mazur RF, Souza EM, Vieira S. Effects of irradiance, wavelength, and thermal emission of different light curing units on the knoop and vickers hardness of a composite resin. J Biomed Mater Res B Appl Biomater. 2008;85(1):166-71. 34. Yoon TH, Lee YK, Lim BS, Kim CW. Degree of polymerization of resin composites by different light sources. J Oral Rehabil. 2002;29(12):1165-73.

33. Santos GB, Medeiros IS, Fellows CE. Composite depth of cure obtained with QTH and LED units assessed by microhardness and micro-Raman spectroscopy. Oper Dent. 2007;31(1):79-83.

34. Choudhary S, Suprabha BS. Effectiveness of light emitting diode and halogen light curing units for curing microhybrid and nanocomposites. J Conserv Dent. 2013;16(3):233–7.

35. Prati C, Chersoni S, Montebugnoli L, Montanari G. Effect of air, dentin and resin-based composite thickness on light intensity reduction. Am J Dent. 1999;12(5):231-4.

36. Rastelli ANS, Andrade MF, Bagnato VS. Polymerization of composite resin using three different light curing units by direct and indirect techniques. J Oral Laser Appl. 2008;8:175-82.

37. D'Arcangelo C, De Angelis F, Vadini M, Carluccio F, Vitalone LM, D'Amario M. Influence of curing time, overlay material and thickness on three light-curing composites used for luting indirect composite restorations. J Adhes Dent. 2012;14(4):377-84.

38. Topcu FT, Erdemir U, Sahinkesen G, Yildiz E, Uslan I, Acikel C. Evaluation of microhardness, surface roughness, and wear behavior of different types of resin composites polymerized with two different light sources. J Biomed Mater Res B Appl Biomater. 2010;92(2):470-8.

39. Yaman BC, Efes BG, Dörter C, Gömeç Y, Erdilek D, Büyükgökçesu S. The effects of halogen and light-emitting diode light curing on the depth of cure and surface microhardness of composite resins. J Conserv Dent. 2011;14(2):136-9.

40. Dietschi D, Marret N, Krejci I. Comparative efficiency of plasma and halogen light sources on composite micro-hardness in different curing conditions. Dent Mater. 2003;19(6):493-500.

41. Ilie N, Bauer H, Draenert M, Hickel R. Resin-based composite light-cured properties assessed by laboratory standards and simulated clinical conditions. Oper Dent. 2013;38(2):159-67.

42. Price RBT, Murphy DG, Dérand T. Light energy transmission through cured resin composite and human dentin. Quintessence Int. 2000;31(9):659-67.

43. De Paula AB, Tango RN, Sinhoreti MA, Alves MC, Puppin-Rontani RM. Effect of thickness of indirect restoration and distance from the light-curing unit tip on the hardness of a dual-cured resin cement. Braz Dent J. 2010;21(2):117-22.

44. Scotti N, Venturello A, Migliaretti G, Pera F, Pasqualini D, Geobaldo F, et al. New-generation curing units and short irradiation time: the degree of conversion of microhybrid composite resin. Quintessence Int. 2011;42(8):e89-95.

45. Schneider LFJ, Moraes RR, Cavalcante LM, Sinhoreti MAC, Correr-Sobrinho L, Consani S. Cross-link density evaluation through softening tests: Effect of ethanol concentration. Dent Mater. 2008;24(2):199-205.

46. St-Georges AJ, Swift EJ, Thompson JY, Heymann HO. Irradiance effects on the mechanical properties of universal hybrid and flowable hybrid resin composites. Dent Mater. 2003;19(5):406-13.

Profa. Dra. Alessandra Nara de Souza Rastelli
(Corresponding address)
Univ. Estadual Paulista - UNESP,Araraquara School of Dentistry,
Department of Restorative Dentistry, Araraquara, SP, Brazil.
Humaitá St., 1680, Araraquara, SP, Brazil.
MailBox: 331. ZipeCode: 14.801-903.
Telephone: +55 (016) 3301-6524
Fax: +55 (016) 3301-6393.
e-mail address: alrastelli@foar.unesp.br

Date submitted: 2013 Dec 16

Accept submission: 2014 Feb 10

Lasers Med Sci (2014) 29:1533–1538
DOI 10.1007/s10103-013-1309-2

ORIGINAL ARTICLE

Effect of low-level laser therapy on odontoblast-like cells exposed to bleaching agent

Adriano Fonseca Lima · Ana Paula Dias Ribeiro · Fernanda Gonçalves Basso · Vanderlei Salvador Bagnato · Josimeri Hebling · Giselle Maria Marchi · Carlos Alberto de Souza Costa

Received: 29 August 2012 / Accepted: 12 March 2013 / Published online: 23 March 2013

Abstract The aim of the present study was to evaluate the effect of low-level laser therapy (LLLT) on odontoblast-like MDPC-23 cells exposed to carbamide peroxide (CP 0.01 %–2.21 μg/mL of H_2O_2). The cells were seeded in sterile 24-well plates for 72 h. Eight groups were established according to the exposure or not to the bleaching agents and the laser energy doses tested (0, 4, 10, and 15 J/cm^2). After exposing the cells to 0.01 % CP for 1 h, this bleaching solution was replaced by fresh culture medium. The cells were then irradiated (three sections) with a near-infrared diode laser (InGaAsP—780±3 nm, 40 mW), with intervals of 24 h. The 0.01 % CP solution caused statistically significant reductions in cell metabolism and alkaline phosphate (ALP) activity when compared with those of the groups not exposed to the bleaching agent. The LLLT did not modulate cell metabolism; however, the dose of 4 J/cm^2 increased the ALP activity. It was concluded that 0.01 % CP reduces the MDPC-23 cell metabolism and ALP activity. The LLLT in the parameters tested did not influence the cell metabolism of the cultured cells; nevertheless, the laser dose of 4 J/cm^2 increases the ALP activity in groups both with and without exposure to the bleaching agent.

Keywords Odontoblasts · Laser · Low-level laser therapy · Bleaching treatment · Alkaline phosphatase

Introduction

Currently, at-home tooth bleaching may be performed with gels having low concentrations of carbamide peroxide (CP, 10–22 %) or hydrogen peroxide (HP, 6–16 %). On the other

A. F. Lima · G. M. Marchi
Department of Restorative Dentistry, Piracicaba Dental School, University of Campinas—UNICAMP, Avenida Limeira, 901, 13404-903 Piracicaba, Sao Paulo, Brazil

A. F. Lima
Department of Restorative Dentistry, Nove de Julho University, Rua Vergueiro, 235, 01504-000 Sao Paulo, Sao Paulo, Brazil

A. P. D. Ribeiro
Department of Operative Dentistry, University of Brasília-UnB. Campus Universitário Darcy Ribeiro, 70910-900, Brasília, Federal District, Brazil

F. G. Basso
Department of Pathology, Piracicaba Dental School, University of Campinas—UNICAMP, Avenida Limeira, 901, 13404-903 Piracicaba, Sao Paulo, Brazil

V. S. Bagnato
Physics Institute of São Carlos, USP—University of Sao Paulo, C.P. 369, 13560-970 São Carlos, Sao Paulo, Brazil

J. Hebling
Department of Orthodontics and Pediatric Dentistry, Araraquara School of Dentistry, Univ. Estadual Paulista (UNESP), Rua Humaitá, 1680, 14801-903 Araraquara, Sao Paulo, Brazil

C. A. de Souza Costa (✉)
Department of Physiology and Pathology, Araraquara School of Dentistry, Univ. Estadual Paulista (UNESP), Rua Humaitá, 1680, 14801-903 Araraquara, Sao Paulo, Brazil
e-mail: casouzac@foar.unesp.br

hand, high-concentration gels of HP (30–35 %) or CP (35–37 %) have been recommended for in-office bleaching therapy. Studies have shown that tooth bleaching occurs due to the breakdown of pigments located in enamel and/or dentin, by the reactive oxygen species (ROS) released from the bleaching agents, such as hydroxyl radicals (OH^-) and singlet oxygen ($^1O_2$) [1]. These pigments are broken into smaller molecules, which absorb lower light or are diffused from the dentin structure, promoting a clearer aspect of the tooth [1].

Since the tooth-bleaching process is mediated by ROS, which can diffuse through the enamel and dentin, reaching the pulp space [2], these aesthetic procedures can promote pulp alterations, such as mild inflammation or even partial necrosis [3–5]. Due to the deleterious effects caused by components of bleaching agents, which have been demonstrated in both in vitro [6–10] and in vivo studies [3, 5, 11], the evaluation of other bleaching techniques that can prevent or reduce pulp damage is needed. Thus, laser is promising coadjutant treatment that can be used in the photodynamic therapy [12, 13], stimulate cell differentiation, reduction of inflammation, and tissue repair [14–17]. Previous studies demonstrated that the specific parameters of low-level laser therapy LLLT can stimulate the deposition of collagen by fibroblasts [18] and proliferation of osteoblasts [19], as well as increase the mitochondrial activity and synthesis of ATP [20]. Once applied to cultured odontoblast-like cells, the LLLT increased cell metabolism as well as the synthesis of proteins and alkaline phosphate activity [14–16]. The bio-stimulatory effects of LLLT on pulp cells such as odontoblasts are important, since these cells are responsible for dentin matrix deposition and its mineralization. In addition, odontoblasts are the first pulp cells to be reached by products released from dental materials capable of diffusing through enamel/dentin [6, 7]. In this way, it may be suggested that the low-level laser irradiation of odontoblasts, prior to or immediately after tooth-bleaching therapies, may prevent pulp damage or improve the pulpal healing caused by ROS or other sub-products released from bleaching agents. Therefore, the aim of this study was to evaluate the effects of LLLT on odontoblast-like MDPC-23 cells exposed or not to bleaching agents.

Materials and methods

Cell culture, bleaching exposure, and LLL irradiation

Immortalized cells of the MDPC-23 cell line [21, 22] in complete Dulbecco's Modified Eagle's Medium (DMEM; Sigma Chemical Co., St. Louis, MO, USA) were seeded (12,500 cells/cm^2) in wells of sterile 24-well dishes (Costar Corp., Cambridge, MA, USA) and maintained for 72 h in a humidified incubator (Isotemp, Fisher Scientific, Pittsburgh, PA, USA) with 5 % CO_2 and 95 % air at 37 °C.

A 10 % carbamide peroxide (CP) bleaching gel (Whiteness, FGM, Joinville, Santa Catarina, Brazil) was diluted in DMEM without fetal calf serum (FCS) to obtain an extract with 0.01 % of CP (approximately 2.21 μg of hydrogen peroxide) to be applied to the cultured cells [6, 8]. This concentration of bleaching agent was chosen based on previous studies, and represents the amount of hydrogen peroxide that diffuses through enamel and dentin and reaches the pulp chamber after the bleaching procedures [23]. The experimental and control groups are presented in Table 1. After exposing the cells to the extract for 1 h, the DMEM with CP was replaced by fresh culture medium supplemented with 1 % FCS. Thereafter, the cultured cells were irradiated three times with different low-level parameters. The irradiations were performed every 24 h, according to the specific groups shown in Table 1. The low-level laser device (LASERTable) [14–17, 24] used in this study was based on near-infrared indium gallium arsenide phosphide (InGaAsP) diode lasers (LASERTable; 780±3 nm, 0.04 W). Twenty-four hours after the last irradiation, the cell metabolism as well as the alkaline phosphatase activity was evaluated, as described below.

Analysis of cell metabolism (MTT assay)

In each group, ten wells were used to analyze cell metabolism by the cytochemical demonstration of succinic dehydrogenase production, measuring the mitochondrial respiration of the cells by the methyl tetrazolium (MTT) assay, as described in several studies [6, 7, 14–16, 25].

Alkaline phosphatase (ALP) activity

Ten wells per group were also used to evaluate ALP activity. A colorimetric endpoint assay (ALP Kit; Labtest Diagnóstico S.A., Lagoa Santa, Minas Gerais, Brazil) with a thymolphthalein monophosphate substrate was employed for this purpose. This is a phosphoric acid ester substrate that is hydrolyzed by ALP and releases thymolphthalein, which gives a bluish color to the solution. The intensity of the resulting color is directly proportional to the enzymatic activity and is analyzed by spectrophotometry.

The culture medium was aspirated, and the cells were washed with sterile PBS at 37 °C. A 1-mL quantity of 0.1 % sodium lauryl sulfate (Sigma Chemical Co., St. Louis, MO, USA) was added to each well and maintained for 30 min at room temperature to produce cell lysis. Next, Falcon tubes (test, standard, and blank) were properly labeled, and 50 μL of substrate (thymolphthalein monophosphate, 22 mmol/L—Kit's reagent #1) and 500 μL of buffer (300 mmol/L, pH 10.1—Kit's reagent #2) were added to each tube. A 50-μL

Table 1 Experimental and control groups according to the exposure to the bleaching agent and the different energy doses tested

Groups	CP 0.01 %	Energy dose, J/cm^2	Laser	Number of applications
G1 (negative control)	Absent	0	Absent	0
G2 (positive control)	Present	0	Absent	0
G3	Absent	4	Present	3
G4	Absent	10	Present	3
G5	Absent	15	Present	3
G6	Present	4	Present	3
G7	Present	10	Present	3
G8	Present	15	Present	3

quantity of the standard solution 45 U/L (Kit's reagent #4) was added only to the standard tube. Thirty minutes after cell lysis, the tubes were placed in a double boiler (Fanem, Guarulhos, Sao Paulo, Brazil) at 37 °C for 2 min. The samples were homogenized, and a 50-μL quantity from each plate was transferred to the test tubes and maintained in the double boiler under gentle agitation. After 10-min incubation, a 2-mL quantity of color reagent (sodium carbonate, 94 mmol/L, and sodium hydroxide, 250 mmol/L—Kit's reagent #3) was added.

Absorbance was measured by spectrophotometry at a 590-nm wavelength (Thermo Plate, Nanshan District, Shenzhen, China). ALP activity was calculated according to a standard curve, with pre-determined values of the enzyme.

Statistical analysis

After exploratory data analysis to evaluate the homogeneity of variances and normality of errors, the data obtained from MTT assay and ALP activity were subjected to two-way analysis of variance (ANOVA). Multiple comparisons were performed by Tukey's test, at a significance level of 5 %.

Results

The cell metabolism data obtained from the MTT assay are shown in Fig. 1. The exposure to 0.01 % CP solution decreased the cell metabolism, which was statistically different from that observed in the groups not exposed to the bleaching agent (two-way ANOVA and Tukey's test, $p<0.05$). The metabolism of cultured cells was not modulated by the laser irradiation, whether or not they were exposed to carbamide peroxide.

The ALP activity of cells exposed to the bleaching agent was reduced compared with that in the groups without exposure of cultured cells to 0.01 % CP solution. The laser dose of 4 J/cm^2 increased the ALP activity on the cells exposed or not to the carbamide peroxide, which was statistically different from that in the other groups ($p<0.05$). The results of ALP activity are shown in Table 2.

Discussion

Researchers have worked hard to obtain dental bleaching protocols that provide an effective aesthetic clinical outcome without causing collateral deleterious effects to pulp cells [8, 9, 26]. In a current study, Lima et al. [8, 9] demonstrated that the administration of sodium ascorbate before the dental bleaching treatment may reduce the cell damage caused by toxic sub-products released from bleaching agents. In the present study, low-level laser irradiation of 0.01 % CP-treated odontoblast-like cells was assessed to determine if specific laser parameters positively modulated the metabolism of cells damaged by a bleaching agent widely used in dentistry for tooth whitening.

In the present investigation, the MDPC-23 cells exposed to the CP bleaching agent had their metabolism reduced in about 35 %. Previous studies demonstrated that components released from bleaching agents, such as HP and other ROS molecules, are capable of breaking down the double bonds in the fatty acids present in the plasma membrane of cells, which activate endonucleases and proteases as well as increase cell permeability [27, 28]. In this study, a solution (extract) with a very low concentration of bleaching agent was obtained after diluting the 10 % CP gel directly in culture medium without FCS. In this way, different factors beyond the HP by itself, such as the pH of the final solution as well as the presence of other CP bleaching agent components may be responsible, at least in part, for the cytotoxicity observed in the cultured MDPC-23 cells. Nevertheless, since previous studies using similar methodology showed that the toxic effects were reversed after concomitant use of an antioxidizing agent [8, 9], the authors may suggest that the HP released from the 10 % CP bleaching agent in the culture medium played the main role in the cytotoxicity observed in the present study. However, further investigations are needed to clarify this matter.

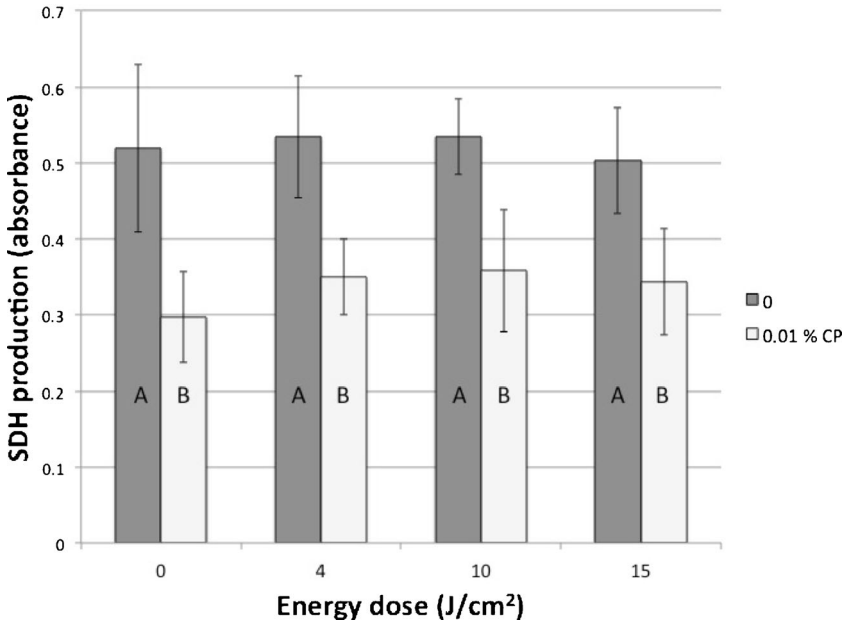

Fig. 1 Graphic representation of the reduction in cell metabolism (*absorbance*) as a function of the different treatments. *Different letters* indicate statistical differences (Tukey; $p<0.05$)

In the current study, different parameters of low-level laser irradiation (4, 10, and 15 J/cm^2) were applied to bio-stimulate ROS-damaged pulp cells. However, the laser protocols tested were not capable of influencing the metabolism of previously damaged odontoblast-like cells. These data were not corroborated by results from in vitro studies in which osteoblasts, odontoblasts, or even fibroblasts exposed to bleaching agents were positively modulated by low-level laser irradiation [26, 29, 30]. The differences observed when results of these investigations were compared with those from the present study may be at least partly due to the variable parameters of the laser protocols tested (wavelength, potency, energy density). In addition, different cultured cell types subjected to specific therapies may provide distinct responses [31].

The bleaching agent evaluated in this study decreased MDPC-23 cell metabolism as well as ALP activity. This last negative collateral effect may have been caused by the interaction among the ROS released from the bleaching agents and the cell protein chains, breaking down the sequence of amino acids near the active center, inactivating this molecule by protein fragmentation [32]. However, in spite of the lack of LLLT influence on cell metabolism, the dose of 4 J/cm^2 was capable of increasing the activity of ALP on the cells, whether or not they were exposed to the CP bleaching agent. It may be explained due to the fact that LLLT may affect cell activity in various ways and different factors can induce specific cell responses after laser irradiation [33]. It has been widely accepted that the action of the LLLT starts in the mitochondria [33]. These organelles play a critical role in calcium homeostasis and storage, sequestering calcium ions from the endoplasmic reticulum or across the plasma membrane, to activate several processes through releasing Ca^{2+} in subcellular regions [34]. After the irradiation and light absorption by a photo acceptor, a cascade of cellular signaling—such as dissociation of the nitric oxide of the catalytic center of the cytochrome C oxidase, and the increase of ATP synthesis—occurs, allied to an increase in intracellular Ca^{2+} [35, 36]. Particularly in osteoblast-like cell line (MC3T3-E1), high concentration of free ionized calcium (Ca^{2+}) may stimulate chemotaxis, proliferation, and matrix maturation [37]. Other studies have shown that extracellular Ca^{2+} increased the mineralization of osteoblasts and mesenchymal stem cells [38, 39]. In addition, the extracellular free ionized Ca^{2+} may promote an increase in intracellular Ca^{2+} through the calcium channels, resulting in the activation of numerous targets [40]. In a current study, Gabusi et al. [41] reported that a high concentration of Ca^{2+} intracellular increased ALP activity as well as collagen-I, osteocalcin, and sialoprotein expression in human osteoblasts. Therefore, based on all these data, it may be speculated that, in the present study, a laser dose of 4 J/cm^2 was able to sensitize the photo acceptor of the MDPC-23 cells, increase ATP synthesis, promoting higher levels of intracellular Ca^{2+}, and, consequently, increase ALP activity in those groups, whether or not they were exposed

Table 2 Results of the alkaline phosphatase activity according to the different experimental and control groups

	Bleaching agent	
Energy dose	0	0.01 % CP
0 J/cm^2	1.97 (0.37) Ab	0.78 (0.31) Bb
4 J/cm^2	2.26 (0.48) Aa	1.38 (0.3) Ba
10 J/cm^2	1.74 (0.5) Ab	0.81 (0.14) Bb
15 J/cm^2	1.46 (0.3) Ab	0.79 (0.22) Bb

Capital letters compare the bleaching treatment and lower case letters compare the LLLT parameters (ANOVA two-way and Tukey's test; $\alpha=0.05$)

to bleaching agents. However, further studies are needed to determine the mechanisms involved in the increase of ALP activity caused by the specific parameter of cell laser irradiation.

In the present study, the positive result regarding ALP cell activity was obtained only with the laser irradiation of cells with 4 J/cm^2. Nevertheless, doses of 10 and 15 J/cm^2 were not capable of producing any effect on the activity of the protein evaluated. These results may be explained, at least in part, by a specific phenomenon known as "biphasic dose response" or "hormesis" (the Arndt–Schulz law) [42]. In this law, it is proposed that weak stimuli can promote positive cell effects. Thus, relatively low doses of laser irradiation, such as 4 J/cm^2, can positively biomodulate MDPC-23 cell behavior; however, when the peak is reached, stronger stimuli can inhibit the positive effects or even, in some situations, promote a negative response.

Analysis of the data obtained in the present study, and other previous investigation [26] , indicated that low-level laser irradiation may represent an alternative therapy for the modulation of pulp cell responses against the toxic effects caused by bleaching agent components capable of diffusing across dental hard tissues, i.e., enamel and dentin. Nevertheless, other factors, such as the number of laser irradiations and the energy doses used, need to be evaluated in further studies.

Conclusions

Based on the methodology used and the results obtained in the present study, it can be concluded that the concentration of 0.01 % carbamide peroxide causes toxic effects in odontoblast-like MDPC-23 cells, characterized by reductions in cell metabolism and ALP activity. Specific doses of low-level laser therapy (4, 10, and 15 J/cm^2) are incapable of modulating cell metabolism positively; however, the laser dose of 4 J/cm^2 increased the ALP activity of bleaching-agent-treated cultured MDPC-23 cells.

Acknowledgments This work is part of a thesis submitted to the Piracicaba Dental School in partial fulfillment of the requirements for the PhD degree. This study was supported by the Fundação de Amparo à Pesquisa do Estado de São Paulo—FAPESP (grants: 2009/08992-7 - 8 and 2010/ 00645–3) and Conselho Nacional de Desenvolvimento Científico e Tecnológico—CNPq (grant: 301291/2010-1).

References

1. Kawamoto K, Tsujimoto Y (2004) Effects of the hydroxyl radical and hydrogen peroxide on tooth bleaching. J Endod 30(1):45–50
2. Gokay O, Mujdeci A, Algin E (2005) In vitro peroxide penetration into the pulp chamber from newer bleaching products. Int Endod J 38(8):516–520
3. Robertson WD, Melfi RC (1980) Pulpal response to vital bleaching procedures. J Endod 6(7):645–649
4. Costa CAS, Ribeiro AP, Giro EM, Randall RC, Hebling J (2011) Pulp response after application of two resin modified glass ionomer cements (rmgics) in deep cavities of prepared human teeth. Dent Mater 27(7):e158–170
5. Kina JF, Huck C, Riehl H, Martinez TC, Sacono NT, Ribeiro AP, Costa CAS (2010) Response of human pulps after professionally applied vital tooth bleaching. Int Endod J 43(7):572–580
6. de Lima AF, Lessa FC, Gasparoto Mancini MN, Hebling J, de Souza Costa CAS, Marchi GM (2009) Cytotoxic effects of different concentrations of a carbamide peroxide bleaching gel on odontoblast-like cells MDPC-23. J Biomed Mater Res B Appl Biomater 90(2):907–912
7. Dias Ribeiro AP, Sacono NT, Lessa FC, Nogueira I, Coldebella CR, Hebling J, de Souza Costa CA (2009) Cytotoxic effect of a 35 % hydrogen peroxide bleaching gel on odontoblast-like MDPC-23 cells. Oral Surg Oral Med Oral Pathol Oral Radiol Endod 108(3):458–464
8. Lima AF, Lessa FC, Hebling J, de Souza Costa CA, Marchi GM (2010) Protective effect of sodium ascorbate on MDPC-23 odontoblast-like cells exposed to a bleaching agent. Eur J Dent 4(3):238–244
9. Lima AF, Lessa FC, Mancini MN, Hebling J, Costa CAS, Marchi GM (2010) Transdentinal protective role of sodium ascorbate against the cytopathic effects of H_2O_2 released from bleaching agents. Oral Surg Oral Med Oral Pathol Oral Radiol Endod 109(4):e70–76
10. Hanks CT, Fat JC, Wataha JC, Corcoran JF (1993) Cytotoxicity and dentin permeability of carbamide peroxide and hydrogen peroxide vital bleaching materials, in vitro. J Dent Res 72(5):931–938
11. Costa CAS, Riehl H, Kina JF, Sacono NT, Hebling J (2010) Human pulp responses to in-office tooth bleaching. Oral Surg Oral Med Oral Pathol Oral Radiol Endod 109(4):e59–64
12. Campos GN, Pimentel SP, Ribeiro FV, Casarin RC, Cirano FR, Saraceni CH, Casati MZ (2013) The adjunctive effect of photodynamic therapy for residual pockets in single-rooted teeth: a randomized controlled clinical trial. Lasers Med Sci. doi:10.1007/s10103-012-1159-3
13. Marotti J, Tortamano P, Cai S, Ribeiro MS, Franco JE, de Campos TT (2013) Decontamination of dental implant surfaces by means of photodynamic therapy. Lasers Med Sci. doi:10.1007/s10103-012-1148-6
14. Tagliani MM, Oliveira CF, Lins EMM, Kurachi C, Hebling J, Bagnato VS, Costa CAS (2010) Nutritional stress enhances cell viability of odontoblast-like cells subjected to low level laser irradiation. Laser Phys Lett 7(3):247–251
15. Oliveira CF, Basso FG, Lins EC, Kurachi C, Hebling J, Bagnato VS, Costa CAS (2010) Increased viability of odontoblast-like cells subjected to low-level laser irradiation. Laser Phys 20(7):1659–1666
16. Oliveira CF, Basso FG, Lins EC, Kurachi C, Hebling J, Bagnato VS, Costa CAD (2011) In vitro effect of low-level laser on odontoblast-like cells. Laser Phys Lett 8(2):155–163
17. Basso FG, Oliveira CF, Kurachi C, Hebling J, Costa CAS (2013) Biostimulatory effect of low-level laser therapy on keratinocytes in vitro. Lasers Med Sci. doi:10.1007/s10103-012-1057-8
18. Romanos GE, Pelekanos S, Strub JR (1995) Effects of nd:Yag laser on wound healing processes: clinical and immunohistochemical findings in rat skin. Lasers Surg Med 16(4):368–379
19. Khadra M, Lyngstadaas SP, Haanaes HR, Mustafa K (2005) Effect of laser therapy on attachment, proliferation and differentiation of human osteoblast-like cells cultured on titanium implant material. Biomaterials 26(17):3503–3509

20. Karu TI, Pyatibrat LV, Kalendo GS, Esenaliev RO (1996) Effects of monochromatic low-intensity light and laser irradiation on adhesion of hela cells in vitro. Lasers Surg Med 18(2):171–177
21. Hanks CT, Fang D, Sun Z, Edwards CA, Butler WT (1998) Dentin-specific proteins in MDPC-23 cell line. Eur J Oral Sci 106(Suppl 1):260–266
22. Sun ZL, Fang DN, Wu XY, Ritchie HH, Begue-Kirn C, Wataha JC, Hanks CT, Butler WT (1998) Expression of dentin sialoprotein (dsp) and other molecular determinants by a new cell line from dental papillae, mdpc-23. Connect Tissue Res 37(3–4):251–261
23. Gokay O, Yilmaz F, Akin S, Tuncbilek M, Ertan R (2000) Penetration of the pulp chamber by bleaching agents in teeth restored with various restorative materials. J Endod 26(2):92–94
24. Basso FG, Oliveira CF, Fontana A, Kurachi C, Bagnato VS, Spolidorio DM, Hebling J, de Souza Costa CA (2011) In vitro effect of low-level laser therapy on typical oral microbial biofilms. Braz Dent J 22(6):502–510
25. Oliveira CF, Hebling J, Souza PP, Sacono NT, Lessa FR, Lizarelli RF, Costa CA (2008) Effect of low-level laser irradiation on odontoblast-like cells. Laser Phys Lett 5(9):680–685
26. Dantas CM, Vivan CL, Ferreira LS, Freitas PM, Marques MM (2010) In vitro effect of low intensity laser on the cytotoxicity produced by substances released by bleaching gel. Braz Oral Res 24(4):460–466
27. Bellomo G, Mirabelli F (1987) Oxidative stress injury studied in isolated intact cells. Mol Toxicol 1(4):281–293
28. Halliwell B (2006) Reactive species and antioxidants. Redox biology is a fundamental theme of aerobic life. Plant Physiol 141(2):312–322
29. Aleksic V, Aoki A, Iwasaki K, Takasaki AA, Wang CY, Abiko Y, Ishikawa I, Izumi Y (2010) Low-level er:Yag laser irradiation enhances osteoblast proliferation through activation of mapk/erk. Lasers Med Sci 25(4):559–569
30. Schwartz-Filho HO, Reimer AC, Marcantonio C, Marcantonio E Jr, Marcantonio RA (2011) Effects of low-level laser therapy (685 nm) at different doses in osteogenic cell cultures. Lasers Med Sci 26(4):539–543
31. Moore P, Ridgway TD, Higbee RG, Howard EW, Lucroy MD (2005) Effect of wavelength on low-intensity laser irradiation-stimulated cell proliferation in vitro. Lasers Surg Med 36(1):8–12
32. Koyama I, Yakushijin M, Goseki M, Iimura T, Sato T, Sonoda M, Hokari S, Komoda T (1998) Partial breakdown of glycated alkaline phosphatases mediated by reactive oxygen species. Clin Chim Acta 275(1):27–41
33. Karu TI (2010) Multiple roles of cytochrome c oxidase in mammalian cells under action of red and ir-a radiation. IUBMB Life 62(8):607–610
34. Karu TI (2008) Mitochondrial signaling in mammalian cells activated by red and near-IR radiation. Photochem Photobiol 84(5):1091–1099
35. Karu T (2004) High-tech helps to estimate cellular mechanisms of low power laser therapy. Lasers Surg Med 34(4):298–299
36. Sarti P, Giuffre A, Barone MC, Forte E, Mastronicola D, Brunori M (2003) Nitric oxide and cytochrome oxidase: reaction mechanisms from the enzyme to the cell. Free Radic Biol Med 34(5):509–520
37. Godwin SL, Soltoff SP (1997) Extracellular calcium and platelet-derived growth factor promote receptor-mediated chemotaxis in osteoblasts through different signaling pathways. J Biol Chem 272(17):11307–11312
38. Ahlstrom M, Pekkinen M, Riehle U, Lamberg-Allardt C (2008) Extracellular calcium regulates parathyroid hormone-related peptide expression in osteoblasts and osteoblast progenitor cells. Bone 42(3):483–490
39. McCullen SD, Zhan J, Onorato ML, Bernacki SH, Loboa EG (2010) Effect of varied ionic calcium on human adipose-derived stem cell mineralization. Tissue Eng Part A 16(6):1971–1981
40. Tada H, Nemoto E, Kanaya S, Hamaji N, Sato H, Shimauchi H (2010) Elevated extracellular calcium increases expression of bone morphogenetic protein-2 gene via a calcium channel and erk pathway in human dental pulp cells. Biochem Biophys Res Commun 394(4):1093–1097
41. Gabusi E, Manferdini C, Grassi F, Piacentini A, Cattini L, Filardo G, Lambertini E, Piva R, Zini N, Facchini A, Lisignoli G (2012) Extracellular calcium chronically induced human osteoblasts effects: specific modulation of osteocalcin and collagen type xv. J Cell Physiol 227(8):3151–3161
42. AlGhamdi KM, Kumar A, Moussa NA (2012) Low-level laser therapy: a useful technique for enhancing the proliferation of various cultured cells. Lasers Med Sci 27(1):237–249

Int. J. Oral Maxillofac. Surg. 2014; 43: 1030–1034
http://dx.doi.org/10.1016/j.ijom.2014.02.011, available online at http://www.sciencedirect.com

International Journal of Oral & Maxillofacial Surgery

Research Paper
Wound Healing

Effects of low-level laser therapy on the proliferation and apoptosis of gingival fibroblasts treated with zoledronic acid

T. Nogueira Pansani[1], F. Gonçalves Basso[1], A. P. Silveira Turirioni[1], C. Kurachi[2], J. Hebling[1], C. A. de Souza Costa[1]
[1]Araraquara School of Dentistry, UNESP – Universidade Estadual Paulista, Araraquara, SP, Brazil; [2]Physics Institute, USP – Universidade de São Paulo, São Carlos, SP, Brazil

T. Nogueira Pansani, F. Gonçalves Basso, A. P. Silveira Turirioni, C. Kurachi, J. Hebling, C. A. de Souza Costa: Effects of low-level laser therapy on the proliferation and apoptosis of gingival fibroblasts treated with zoledronic acid. Int. J. Oral Maxillofac. Surg. 2014; 43: 1030–1034.

Abstract. Low-level laser therapy (LLLT) has been indicated as an adjuvant therapy for bisphosphonate-induced osteonecrosis. However, the effects of LLLT on bisphosphonate-treated cells are not yet clear. This study evaluated the effects of LLLT on the proliferation and apoptosis of gingival fibroblasts treated with zoledronic acid (ZA). Cells were exposed to ZA at 5 μM for 48 h. Irradiation was performed using a laser diode prototype (LaserTABLE, InGaAsP; 780 nm ± 3 nm, 25 mW) at 0.5 or 3 J/cm^2, three times every 24 h. Cell proliferation and apoptosis were evaluated by fluorescence microscopy. Data were analyzed by Mann–Whitney test at the 5% level of significance. ZA decreased cell proliferation to 47.62% (interquartile range (IQR) 23.80–57.14%; $P = 0.007$) and increased apoptosis of gingival fibroblasts to 27.7% (IQR 20.9–33.4%; $P = 0.0001$). LLLT increased cell proliferation compared with non-irradiated cells, at 0.5 J/cm^2 (57.14%, IQR 57.14–71.43%; $P = 0.003$) and at 3 J/cm^2 (76.19%, IQR 61.90–76.19%; $P = 0.0001$), but did not increase cell proliferation in ZA-treated cells. Irradiated fibroblasts presented lower apoptosis rates than the ZA-treated cells, but apoptosis was no different in ZA-treated cells compared to those that were ZA-treated and also irradiated.

Keywords: bisphosphonates; cell culture; cell death; cell division; osteonecrosis; laser therapy; zoledronic acid-treated cells.

Accepted for publication 24 February 2014
Available online 19 March 2014

The aetiology of osteonecrosis has been related to the cytotoxic effects of bisphosphonates on bone cells,[1] a decrease in local vascularization and oxygen distribution, as well as the presence of local infection.[2]

Bisphosphonates are analogues of pyrophosphate that are prescribed for diseases associated with intense bone resorption, such as Paget's disease, multiple myeloma, osteoporosis, bone tumours, and metastasis.[3–5] Bisphosphonate-induced osteonecrosis has been characterized as a necrotic bone area in the oral cavity that persists for longer than 8 weeks without a history of head and neck radiotherapy.[3]

Previous studies have shown that bisphosphonates decrease the proliferation rate of endothelial cells, interfering with the tissue repair process.[6] Scheper et al.[7] demonstrated that zoledronic acid (ZA), a high-potency nitrogen-containing bisphosphonate, inhibits cell proliferation and induces apoptosis of fibroblasts.

0901-5027/0801030 + 05 $36.00/0

In addition, Ravosa et al.[8] reported a decrease in motility and synthesis of collagen type I by ZA-treated fibroblasts.

Regarding the controversial aspects of the treatment of osteonecrosis, topical and systemic antibiotic therapies, as well as surgical treatment, have been indicated widely.[9] Recently, low-level laser therapy (LLLT) has been used clinically as an adjuvant therapy for this pathological condition, mainly due to its positive effect on pain relief and tissue repair.[9–12]

Several researchers have demonstrated the biostimulatory effects of LLLT on different cell types, such as increased cell proliferation, migration, differentiation, and protein synthesis, as well as gene expression of collagen type I and growth factors.[13–17] Based on the positive effects of LLLT on bisphosphonate-induced osteonecrosis lesions and the toxic effects of these types of drugs on cells, the aim of the present study was to evaluate the proliferation and apoptosis rates of gingival fibroblasts exposed to ZA treatment and subjected to LLLT according to specific parameters.

Materials and methods

This research was developed in the university laboratory. All experiments were performed using a human gingival fibroblast continuous cell line (HGF). Cells were exposed to ZA and irradiated with a laser diode prototype according to selected parameters. The experimental and control groups are described in Table 1.

Cell culture and zoledronic acid treatment

Cells were seeded in the wells of 24-well plates (3×10^4 cells/cm^2) in culture medium (DMEM–Dulbecco's Modified Eagle's Medium; Gibco, Grand Island, NY, USA), supplemented with 10% foetal bovine serum (FBS; Gibco), and were maintained in an incubator at 37 °C and 5% CO_2 (Isotemp; Fisher Scientific, Pittsburgh, PA, USA).[18] After 48 h, the culture medium was replaced with serum-free DMEM, which was incubated in contact with the cells for 24 h. ZA at 5 μM (8.25 μl/ml) was then added to the serum-free DMEM and kept in contact with the cells for an additional 48 h.[19] The DMEM with ZA was then replaced with fresh DMEM, and the cells were subjected to irradiation by laser diode prototype. Cells not subjected to laser irradiation were used as control groups (G1 and G2). In these groups, the well plates containing the cells were placed in the laser diode prototype, which was not activated.

Table 1. Experimental groups.

Group	Zoledronic acid	Energy dose of LLLT (J/cm^2)
G1 (control group)	No	–
G2	Yes	–
G3	No	0.5
G4	Yes	0.5
G5	No	3.0
G6	Yes	3.0

LLLT, low-level laser therapy.

Low-level laser therapy (LLLT)

Irradiation was performed using a laser diode prototype (LaserTABLE, InGaAsP; 780 nm ± 3 nm, 25 mW).[16,17,19,20] This device is composed of 12 laser InGaAsP (indium–gallium–arsenide–phosphide) diodes that are positioned to irradiate each well in a standardized way and individually. Cells were irradiated three times every 24 h. The parameters selected for LLLT were based on the results of previous studies that have demonstrated increased cell metabolism and proliferation, as well as high migration capacity, after laser irradiation.[17] These parameters are shown in Table 2.

Table 2. LLLT irradiation parameters selected for the experiments.

Parameter	
Potency (W)	0.025
Wave length (nm)	780
Energy doses (J/cm^2)	0.5; 3.0
Irradiation area (cm^2)	2.0
Time (s)	40; 240

LLLT, low-level laser therapy.

Cell proliferation analysis (bromodioxyuridine incorporation)

The evaluation of cell proliferation was performed by the fluorescence method of bromodioxyuridine (BrdU) incorporation; BrdU is an analogue of thymidine. This compound is incorporated into DNA molecules during cell division, demonstrating the cells in DNA synthesis (proliferation). A fluorescence kit, Click-iT EdU Imaging Kit (Invitrogen, Carlsbad, CA, USA), was used for this evaluation, in accordance with the manufacturer's instructions.

Results were analyzed by fluorescence microscopy (Nikon Eclipse TS 100; Nikon Corporation, Tokyo, Japan). Fluorescent nuclei were considered positive. Image analyzer software (Image J 1.45S software; Wayne Rasband, National Institutes of Health, Bethesda, MD, USA) was used to determine the numbers of proliferating cells in four different image fields of each sample.

Analysis of cell apoptosis – TUNEL assay

Apoptotic cells were evaluated by TUNEL assay (terminal deoxynucleotidyl transferase dUTP nick end labelling), which identifies the DNA fragmentation that is characteristic of the apoptotic process.[20] This assay is based on the action of the enzyme terminal deoxynucleotidyl transferase, which adds fluorescent synthetic nucleotides to the DNA fragments, allowing the identification of DNA ruptures that are present in apoptotic cells rather than DNA condensation, observed for cell death by necrosis.

Permeabilization of the plasma cell membrane was performed to permit the influx of fluorescent nucleotides, since this membrane is intact during the apoptotic process.[20] After that, the TUNEL assay was performed with a fluorescence kit, C10245 Click-iT TUNEL (Alexa Fluor 488 Imaging Assay; Invitrogen). A positive group (treated with DNase) was included to improve the comparison. Samples were analyzed by fluorescence microscopy (Nikon Eclipse TS 100; Nikon Corporation). The positive cells were counted and analyzed with image software (Image J 1.45S), and were considered apoptotic cells.

Statistical analysis

The statistical analyses were performed using IBM SPSS version 20.0 (IBM Corp., Armonk, NY, USA). Data were evaluated for normal adherence, and as results did not show normal distribution, the non-parametric Mann–Whitney test was selected for the statistical analysis, using adjusted *P*-values, considering a 5% significance level.

Results

For ZA-treated cells, we observed a significant decrease in cell proliferation compared with the control group ($P < 0.05$).

Table 3. Proliferation rates (%) according to ZA treatment and LLLT.

Cell proliferation rate for each experimental group, median (IQR)*	Experimental groups (adjusted *P*-values of group comparisons)						
	Negative control group	Positive control group	ZA 5 μM	0.5 J/cm^2	ZA + 0.5 J/cm^2	3 J/cm^2	ZA + 3 J/cm^2
Negative control group (DMEM without FBS) 9.52 (0.00–19.04)	–	$P = 0.0001$	$P = 0.651$	$P = 0.003$	$P = 1.000$	$P = 0.0001$	$P = 0.651$
Positive control group (DMEM + 10% FBS) (G1) 104.76 (80.95–114.28)	–	–	$P = 0.007$	$P = 1.000$	$P = 0.001$	$P = 0.005$	$P = 0.0001$
ZA 5 μM (G2) 47.62 (23.80–57.14)	–	–	–	$P = 1.000$	$P = 1.000$	$P = 0.310$	$P = 1.000$
0.5 J/cm^2 (G3) 57.14 (57.14–71.43)	–	–	–	–	$P = 0.761$	$P = 1.000$	$P = 0.005$
ZA + 0.5 J/cm^2 (G4) 38.09 (23.80–52.38)	–	–	–	–	–	$P = 0.077$	$P = 1.000$
3 J/cm^2 (G5) 76.19 (61.90–76.19)	–	–	–	–	–	–	$P = 0.001$
ZA + 3 J/cm^2 (G6) 40.48 (38.09–53.57)	–	–	–	–	–	–	–

ZA, zoledronic acid; LLLT, low-level laser therapy; IQR, interquartile range; DMEM, Dulbecco's modified Eagle's medium; FBS, foetal bovine serum.

* $n = 8$; Mann–Whitney, $P > 0.05$.

The ZA-treated gingival fibroblasts that were subjected to LLLT presented proliferation rates similar to those of ZA-treated cells, at both energy doses tested ($P > 0.05$).

When the cultured cells were subjected solely to LLLT, cell proliferation was increased at both energy doses ($P < 0.05$). The highest cell proliferation rate was observed at 3 J/cm^2 (Table 3).

Concerning cell apoptosis, both energy doses used in this study resulted in similar apoptosis rates when compared to the control group (G1), in which the cells received no treatment, and between them ($P > 0.05$). The lowest apoptosis rate was observed for the cells irradiated at 3 J/cm^2 (Table 4 and Fig. 1).

Significantly increased apoptosis occurred for ZA-treated cells compared with the control group ($P < 0.05$). However, no difference was detected when ZA-treated cells were subjected to laser irradiation ($P > 0.05$).

Discussion

Low-level laser irradiation has been used as an adjuvant therapy for bisphosphonate-induced osteonecrosis, mainly due to its positive effects against pain, its capacity to reduce oedema formation, and a notable stimulation of tissue healing.[9–12]

The present study demonstrated that ZA significantly decreased the proliferation of cultured gingival fibroblasts and increased cell apoptosis. Similar data have been reported in previous studies,[8,19,21] in which the authors have stated that the decreased proliferation of epithelial cells and fibroblasts may interfere with the repair of oral mucosal tissue. In addition, in the present study it was shown that ZA increased fibroblast apoptosis rates, as has been reported previously.[6,7,22]

Table 4. Apoptosis rates of cultured gingival fibroblasts after ZA treatment and LLLT.

Cell apoptosis rate for each experimental group, median (IQR)*	Experimental groups (adjusted *P*-values of group comparisons)						
	Positive control group	Negative control group	ZA 5 μM	0.5 J/cm^2	ZA + 0.5 J/cm^2	3 J/cm^2	ZA + 3 J/cm^2
Positive control group (DNase) 102.5 (90.5–106.9)	–	$P = 0.0001$	$P = 1.000$	$P = 0.001$	$P = 0.615$	$P = 0.274$	$P = 0.0001$
Negative control group (G1) 2.1 (1.6–2.7)	–	–	$P = 0.0001$	$P = 1.000$	$P = 0.0001$	$P = 1.000$	$P = 0.0001$
ZA 5 μM (G2) 27.7 (20.9–33.4)	–	–	–	$P = 0.015$	$P = 1.000$	$P = 0.005$	$P = 1.000$
0.5 J/cm^2 (G3) 2.2 (1.2–2.3)	–	–	–	–	$P = 0.0001$	$P = 1.000$	$P = 0.159$
ZA + 0.5 J/cm^2 (G4) 22.7 (16.0–29.5)	–	–	–	–	–	$P = 0.055$	$P = 1.000$
3 J/cm^2 (G5) 1.6 (1.07–2.3)	–	–	–	–	–	–	$P = 0.061$
ZA + 3 J/cm^2 (G6) 21.9 (19.4–24.7)	–	–	–	–	–	–	–

ZA, zoledronic acid; LLLT, low-level laser therapy; IQR, interquartile range.

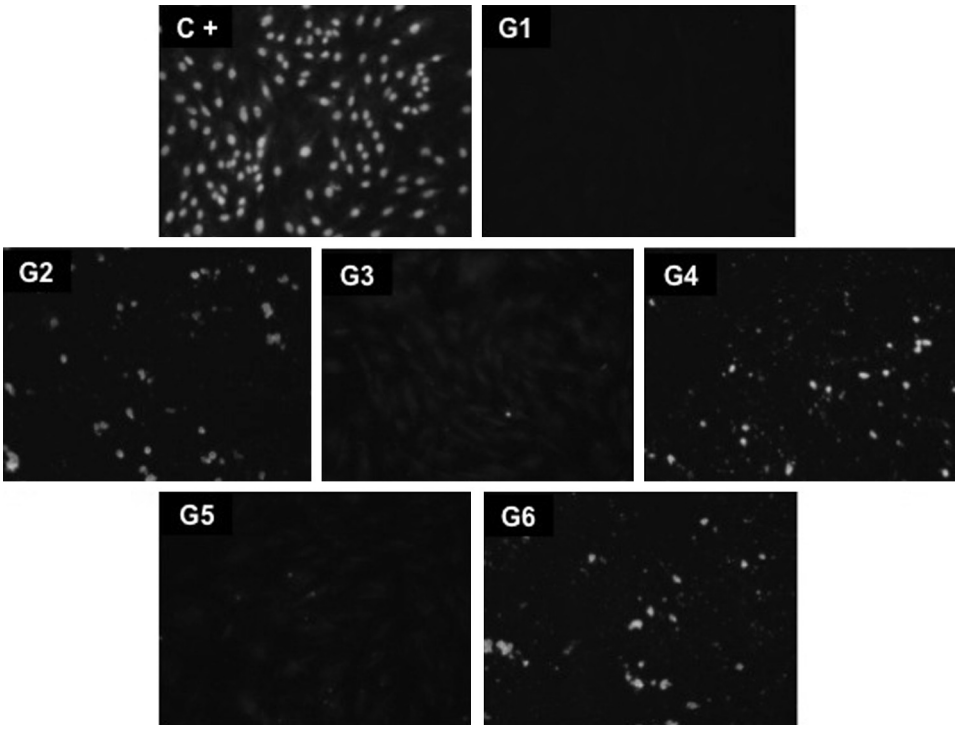

Fig. 1. Fluorescence microscopy photomicrographs showing apoptosis evaluation by TUNEL assay. Positive cells were considered as apoptotic cells–DNA fragmentation and incorporation of fluorescent nucleotides. Magnification, ×4.

ZA acts on the farnesyl diphosphate synthase signalling pathway, decreasing geranylgeraniol production, which is necessary in the location of intracellular proteins that play important roles in different cell functions.[4,23] Recent studies have demonstrated that the decrease in geranylgeraniol production by ZA-treated cells significantly reduces cell proliferation and migration, as well as inducing cell apoptosis.[23,24] Conversely, increased cell proliferation rates have been observed for LLLT-treated cells at both energy doses selected for use in this study (0.5 and 3 J/cm^2), confirming that this type of therapy, at specific parameter levels, may biomodulate cell functions.[13–18,25,26] Most of the effects of LLLT have been associated with the activation of mitochondrial cytochrome c oxidase, which leads to increased adenosine triphosphate (ATP) production and the activation of several cell-signalling pathways.[27,28] In the present study, it may be speculated that similar laser biostimulation occurred in those irradiated fibroblasts that presented significantly increased proliferation (Table 3).

When ZA-treated cells were subjected to LLLT, no increased cell proliferation was detected, suggesting that the concentration of ZA used in the present study was capable of causing immediate and intense cell damage. Therefore, one may speculate that the irreversible cell damage caused by ZA on the cultured fibroblasts may interfere negatively with tissue repair processes in vivo, as described in previous studies.[1,29] It appears that the intense toxic effect caused by ZA induced rapid fibroblast apoptosis, such that subsequent laser irradiation of ZA-treated cells at specific parameter levels had no positive effects, since the apoptotic process is considered an irreversible pathway.[30]

In this study, we demonstrated that LLLT can biostimulate cultured gingival fibroblasts, leading to increased cell proliferation. Analysis of these data may explain, at least in part, the excellent clinical results of this therapy.[9–12] Additionally, LLLT may be effective in biomodulating the oral mucosal cells adjacent to the necrotic area, thus improving the local tissue-healing process. However, further in vitro and in vivo studies are needed to elucidate the effects of bisphosphonates on oral mucosal cells and the association of these drugs with LLLT, which will certainly favour its use in the treatment of osteonecrosis.

According to the methodology used in the present study and based on analysis of the data obtained, it can be concluded that LLLT at selected parameter levels is capable of increasing gingival fibroblast proliferation, which is directly related to tissue healing potential. However, this therapy was not efficient in recovering the activity of this type of cell previously damaged by zoledronic acid.

Funding

The authors acknowledge the Fundação de Amparo à Pesquisa do Estado de São Paulo-FAPESP (grants 2009/54722-1 and BP.IC: 2010/08933-8) and the Conselho Nacional de Desenvolvimento Científico e Tecnológico-CNPq (grant 301029/2010-1) for financial support.

Competing interests

The authors declare no conflict of interest.

Ethical approval

Ethical approval for fibroblast isolation was obtained from the Piraciaba Dental School Ethics Committee (UNICAMP: 64/99).

Patient consent

Not required.

References

1. Reid IR. Osteonecrosis of the jaw – who gets it and why? *Bone* 2009;**44**:4–10. http://dx.doi.org/10.1016/j.bone.2008.09.012.

2. Woo S, Hellstein JW, Kalmar JR. Systematic review: bisphosphonates and osteonecrosis of the jaws. *Ann Intern Med* 2006;**144**:753–61. http://dx.doi.org/10.7326/0003-4819-144-10-200605160-00009.
3. Reid IR, Bolland MJ. Is bisphosphonate-associated osteonecrosis of the jaw caused by soft tissue toxicity? *Bone* 2007;**41**:318–20. http://dx.doi.org/10.1016/j.bone.2007.04.196.
4. Diel IJ, Fogelman I, Al-Nawas B, Hoffmeister B, Migliorati C, Gligorov J, et al. Pathophysiology, risk factors and management of bisphosphonate-associated osteonecrosis of the jaw: is there a diverse relationship of amino and non-amino bisphosphonates. *Crit Rev Oncol Hematol* 2007;**64**:198–207.
5. Migliorati CA, Casiglia J, Epstein J, Jacobsen PL, Siegel MA, Woo S. Managing the care of patients with bisphosphonate-associated osteonecrosis. *J Am Dent Assoc* 2005;**136**:1658–68.
6. Fournier P, Boissier S, Filleur S, Guglielmi J, Cabon F, Colombel M, et al. Bisphosphonates inhibit angiogenesis in vitro and testosterone-stimulated vascular regrowth in the ventral prostate in castrated rats. *Cancer Res* 2002;**62**:6538–44.
7. Scheper MA, Chaisuparat R, Cullen KJ, Meiller TF. A novel soft-tissue in vitro model for bisphosphonate-associated osteonecrosis. *Fibrinogenesis Tissue Repair* 2010;**3**:6.
8. Ravosa MJ, Ning J, Liu Y, Stack MS. Bisphosphonate effects on the behaviour of oral epithelial cells and oral fibroblasts. *Arch Oral Biol* 2011;**56**:491–8. http://dx.doi.org/10.1016/j.archoralbio.2010.11.003.
9. Vescovi P, Merigo E, Manfredi M, Meleti M, Fornaini C, Bonanini M, et al. Nd:YAG laser biostimulation in the treatment of bisphosphonate-associated osteonecrosis of the jaw: clinical experience in 28 cases. *Photomed Laser Surg* 2008;**26**:37–46. http://dx.doi.org/10.1016/j.joms.2007.11.025.
10. Angiero F, Sannino C, Borloni R, Crippa R, Benedicenti S, Romanos GE. Osteonecrosis of the jaws caused by bisphosphonates: evaluation of a new therapeutic approach using the Er:YAG laser. *Lasers Med Sci* 2009;**24**:849–56. http://dx.doi.org/10.1007/s10103-009-0654-7.
11. Scoletta M, Arduino PG, Reggio L, Dalmasso P, Mozatti M. Effect of low-level laser irradiation on bisphosphonate-induced osteonecrosis of the jaws: preliminary results of a prospective study. *Photomed Laser Surg* 2009;**28**:179–84. http://dx.doi.org/10.1089/pho.2009.2501.
12. Stübinger S, Dissmann J, Pinho NC, Saldamli B, Seitz O, Sader R. A preliminary report about treatment of bisphosphonate related osteonecrosis of the jaw with Er:YAG laser ablation. *Lasers Surg Med* 2009;**41**:26–30. http://dx.doi.org/10.1002/lsm.20730.
13. Marques MM, Pereira AN, Fujihara NA, Nogueira FN, Eduardo CP. Effect of low-power laser irradiation on protein synthesis and ultrastructure of human gingival fibroblasts. *Lasers Surg Med* 2004;**34**:260–5. http://dx.doi.org/10.1002/lsm.20008.
14. Moore P, Ridgway TD, Higbee RG, Howard EW, Lucroy MD. Effect of wavelengths on low-intensity laser irradiation-stimulated cell proliferation in vitro. *Lasers Surg Med* 2005;**36**:8–12. http://dx.doi.org/10.1002/lsm.20117.
15. Hawkins DH, Abrahamse H. The role of laser fluence in cell viability, proliferation, and membrane integrity of wounded human skin fibroblasts following helium–neon laser irradiation. *Lasers Surg Med* 2006;**38**:74–83. http://dx.doi.org/10.1002/lsm.20271.
16. Basso FG, Oliveira CF, Kurachi C, Hebling J, Costa CA. Biostimulatory effect of low-level laser therapy on keratinocytes in vitro. *Lasers Med Sci* 2012;**28**:367–74.
17. Basso FG, Pansani TN, Turrioni APS, Bagnato VS, Hebling J, Souza Costa CA. In vitro wound healing improvement by low-level laser therapy application in cultured gingival fibroblasts. *Int J Dent* 2012;**2012**:719452. http://dx.doi.org/10.1155/2012/719452.
18. Oliveira CF, Basso FG, Lins EC, Kurachi C, Hebling J, Bagnato VS, et al. In vitro effect of low-level laser on odontoblast-like cells. *Laser Phys Lett* 2011;**8**:155–63. http://dx.doi.org/10.1002/lapl.201010101.
19. Scheper MA, Badros A, Chaisuparat R, Cullen KJ, Meiller TF. Effect of zoledronic acid on oral fibroblasts and epithelial cells: a potential mechanism of bisphosphonate-associated osteonecrosis. *Br J Haematol* 2009;**144**:667–76. http://dx.doi.org/10.1111/j. 1365-2141.2008.07504.x.
20. Saraste A, Pulkki K. Morphologic and biochemical hallmarks of apoptosis. *Cardiovasc Res* 2000;**45**:528–37. http://dx.doi.org/10.1016/S0008-6363(99)00384-3.
21. Walter C, Klein MO, Pabst A, Al-Nawas B, Düschner H, Ziebart T. Influence of bisphosphonates on endothelial cells, fibroblasts, and osteogenic cells. *Clin Oral Invest* 2010;**14**:35–41. http://dx.doi.org/10.1007/s00784-009-0266-4.
22. Allam E, Allen MR, Chu T, Ghoneima A, Windsor LJ. In vivo effects of zoledronic acid on oral mucosal epithelial cells. *Oral Dis* 2011;**17**:291–7. http://dx.doi.org/10.1111/j. 1601-0825.2010.01739.x.
23. Ziebart T, Koch F, Klein MO, Guth J, Adler J, Pabst A, et al. Geranylgeraniol – a new potential therapeutic approach to bisphosphonate associated osteonecrosis of the jaw. *Oral Oncol* 2011;**47**:195–201. http://dx.doi.org/10.1016/j.oraloncology.2010.12.003.
24. Basi DL, Lee SW, Helfman S, Mariash A, Lunos SA. Accumulation of VEGFR2 in zoledronic acid-treated endothelial cells. *Mol Med Rep* 2010;**3**:399–403. http://dx.doi.org/10.3892/mmr_00000271.
25. Oliveira CF, Basso FG, Lins EC, Kurachi C, Hebling J, Bagnato VS, et al. Increased viability of odontoblast-like cells subjected to low-level laser irradiation. *Laser Phys* 2010;**20**:1659–66. http://dx.doi.org/10.1134/S1054660X10130153.
26. Damante CA, De Micheli G, Miyagi SPH, Feist IS, Marques MM. Effect of laser phototherapy on the release of fibroblast growth factors by human gingival fibroblasts. *Lasers Med Sci* 2009;**24**:885–91. http://dx.doi.org/10.1007/s10103-008-0582-y.
27. Karu TI. Photobiology of low-power laser effects. *Health Phys* 1989;**56**:691–704.
28. Karu TI. Mitochondrial signaling in mammalian cells activated by red and near-IR radiation. *Photochem Photobiol* 2008;**84**:1091–9. http://dx.doi.org/10.1111/j. 1751-1097.2008.00394.x.
29. Agis H, Blei J, Watzek G, Gruber R. Is zoledronate toxic to human periodontal fibroblasts? *J Dent Res* 2009;**89**:40–5. http://dx.doi.org/10.1177/0022034509354298.
30. Elmore S. Apoptosis: a review of programmed cell death. *Toxicol Pathol* 2007;**35**:495–516. http://dx.doi.org/10.1080/01926230701320337.

Address:
Fernanda Gonçalves Basso
Departamento de Fisiologia e Patologia
Faculdade de Odontologia de Araraquara
Universidade Estadual Paulista
Rua Humaitá
1680
Centro
Caixa Postal 331 CEP 14801-903 Araraquara
SP
Brazil
Tel: +55 16 3301 6478;
Fax: +55 16 3301 6488
E-mail: fergbasso@gmail.com

Support Care Cancer (2014) 22:2741–2748
DOI 10.1007/s00520-014-2267-3

ORIGINAL ARTICLE

Low-level laser therapy for osteonecrotic lesions: effects on osteoblasts treated with zoledronic acid

Fernanda Gonçalves. Basso · Ana Paula Silveira. Turrioni · Diana Gabiela Soares · Vanderlei Salvador Bagnato · Josimeri Hebling · Carlos Alberto de Souza Costa

Received: 19 November 2013 / Accepted: 22 April 2014 / Published online: 7 May 2014

Abstract
Purpose Clinical studies have shown that low-level laser therapy (LLLT) can improve local tissue healing of bisphosphonate-induced osteonecrosis of the jaw. However, the effects of laser irradiation on bisphosphonate-treated osteoblasts have not been completely elucidated.
Methods Human osteoblasts were cultured in plain culture medium (DMEM). After 48 h, plain DMEM was replaced by DMEM with no fetal bovine serum, for a 24-h incubation followed by addition of zoledronic acid (5 μM) for additional 48 h. Cells were subjected to LLLT (InGaAsP; 780±3 nm; 0.025 W) at 0.5, 1.5, 3, 5, and 7 J/cm^2, three times every 24 h. Cell viability, total protein production, alkaline phosphatase activity (ALP), mineral nodule formation, gene expression of collagen type I and ALP, and cell morphology were evaluated.
Results LLLT at 0.5 J/cm^2 increased cell viability of cultured osteoblasts. ALP activity and gene expression, in addition to mineral nodule formation and Col-I gene expression, were not increased by LLLT. LLLT applied to ZA-treated cells increased Col-I expression at 0.5, 1.5, and 3 J/cm^2 but did not improve any other cell activity assessed.
Conclusion LLLT showed limited effects on bisphosphonate-treated osteoblasts.

Keywords Bisphosphonates · Osteonecrosis · Osteoblasts · Low-level laser therapy · Cell culture

F. G. Basso · A. P. S. Turrioni · D. G. Soares · J. Hebling · C. A. de Souza Costa
Araraquara School of Dentistry, UNESP—Univ. Estadual Paulista, Araraquara, SP 14801-903, Brazil

V. S. Bagnato
Physics Institute, USP—Universidade de São Paulo, São Carlos, SP 13566-590, Brazil

C. A. de Souza Costa (✉)
Departamento de Fisiologia e Patologia, Faculdade de Odontologia de Araraquara, Universidade Estadual Paulista, Rua Humaitá, 1680. Centro, Caixa Postal: 331, 14801-903 Araraquara, SP, Brazil
e-mail: casouzac@foar.unesp.br

Introduction

Bisphosphonate-related osteonecrosis has been considered to have an adverse effect on bisphosphonate treatment [1, 2]. This condition is described in approximately 1 % of patients, but its incidence is directly related to the type of bisphosphonate, treatment period, and administration of the drug [1, 2]. In addition, oral health conditions, such as the presence of inflammatory conditions and trauma, have also been related to the development and maintenance of osteonecrosis [1–3].

Elucidation of the etiopathogenesis and treatment strategies for osteonecrosis has become critical, since its incidence has increased, associated with the fact that, in most cases, osteonecrosis can be very painful and frequently affects patients' quality of life [1–5].

Increased incidence of bisphosphonate-related osteonecrosis of the jaw has led to studies of the etiopathogenesis protocols [1, 2] and treatment [3] for this adverse effect of bisphosphonate treatment. It is known that the occurrence of osteonecrosis is associated, at least in part, with the type of bisphosphonate used, its administration, frequency, and duration of treatment. Additionally, this pathological condition may be associated with local factors, such as the presence of biofilm, inflammatory process, and direct cytotoxicity of bisphosphonates to oral mucosa cells [2, 4, 5].

Previous studies have shown that bisphosphonates have toxic effects on osteoblast, fibroblast, epithelial, and endothelial cells [5–7]. In addition, many researchers have

demonstrated that bisphosphonates can delay oral healing process as well as decrease bone formation and neovascularization [8, 9].

Standard strategies for the treatment of osteonecrosis of the jaw include local and systemic antibiotic administration and surgical intervention [1, 3]. Recent clinical reports have demonstrated that treatment of osteonecrotic lesions with low-level laser therapy (LLLT) in association with antimicrobial or surgical treatment improves tissue healing and reduces localized pain [10–13].

Positive effects of LLLT on different cell types have been demonstrated in several in vitro and in vivo studies [14, 15]. However, only scarce data have been provided concerning the effects of laser irradiation on oral tissues, especially on bone cells exposed in osteonecrotic jaw lesions.

Elucidation of the effects of LLLT on zoledronic acid-treated cells may validate or improve the safe use of this non-invasive therapy for osteonecrosis of the jaw for the treatment of patients receiving bisphosphonates and presenting osteonecrosis lesions. Therefore, the aim of this study was to evaluate the effects of LLLT on specific parameters of cultured osteoblasts, whether previously exposed to a specific type of bisphosphonate–zoledronic acid.

Materials and methods

Cell culture

An immortalized human osteoblastic cell line was selected for study (Saos-2–HTB-85). Cells were seeded in wells of 24-well plates in complete culture medium (DMEM-Gibco, Grand Island, NY, USA) supplemented with 10 % fetal bovine serum (FBS-Gibco) and maintained in a 5 % CO_2atm at 37 °C.

Zoledronic acid treatment

After 48-h incubation, the plain culture medium in contact with cells was replaced by serum-free DMEM. Following an additional 24-h incubation, ZA at 5 μM was added to the serum-free DMEM, which was maintained in contact with osteoblasts for 48 h.

ZA was used in this study because it is a highly potent bisphosphonate that has been frequently associated with osteonecrosis of the jaws. The ZA concentration used was based on a previous study in which the authors showed that 5 μM is the highest concentration of ZA found in the saliva and bone tissue of patients under ZA treatment [6].

LLLT

LLLT was performed with a laser diode prototype widely used in previous studies (LASERTable, InGaAsP; 780±3 nm; 0.025 W), since it provides complete, uniform, and standardized irradiation of the bottoms of the wells to which the seeded cells are attached [16–18]. Before each experiment, delivery energy was measured at the bottoms of the 24-well plates, to confirm LLLT parameters. The cells were irradiated every 24 h for specific times according to the energy doses of 0.5 J/cm^2 (40 s), 1.5 J/cm^2 (120 s), 3 J/cm^2 (240 s), 5 J/cm^2 (400 s), and 7 J/cm^2 (560 s). Cells were irradiated at a standardized distance of 2 cm, and the area of irradiation was also standardized at 2 cm^2.

The LLLT parameters used in this in vitro study were selected according to previous investigations in which the authors irradiated cultured osteoblasts, demonstrating increased cell viability and function [19–21].

Cell viability—MTT assay

Twenty-four hours after the last irradiation, the osteoblasts' viability was assessed by MTT assay (n=8), which is a well-described and standardized test that provides cell mitochondrial activity. The protocol was performed as previously described [16].

Total protein production

The total protein production by osteoblasts (n=8), whether exposed to ZA and whether subjected to different levels of LLLT, was analyzed by an end-point colorimetric test as described previously [16].

Alkaline phosphatase activity (ALP)

ALP activity is considered a phenotypic marker of osteoblasts, and alterations to this activity can affect osteoblastic mineralization functions. This assay is based on thymolphthaline hydrolysis by ALP and was performed as previously described (n=8) [22].

Mineralization nodule formation—alizarin red stain

Mineralization nodule formation was assessed by alizarin red stain, which also demonstrates the phenotypic capacity of osteoblasts to form a mineralized matrix [18].

For mineral nodule formation, cells were maintained in an osteogenic culture medium composed of DMEM (Gibco) containing 10 % FBS (Gibco), ß-glycerophosphate (Sigma-Aldrich, St. Louis, MO, USA), and ascorbic acid (Sigma-Aldrich) (n=8) [22].

Table 1 Viability of osteoblasts, whether exposed to ZA and then subjected to LLLT at different energy doses

ZA	Energy doses (J/cm^2)					
	0	0.5	1.5	3	5	7
+	34 (31–60) B, a	39 (33–52) B, a	36 (34–51) B, a	36 (34–55) B, a	31 (29–57) B, a	33 (30–58) B, a
−	101 (98–104) A, bc	113 (107–115) A, a	107 (106–113) A, ab	106 (102–109) A, bc	102 (95–107) A, bc	104 (101–106) A, bc

Values indicate median (25th to 75th percentiles), n=8

A, a Same upper-case letters in columns and lower-case letters in rows indicate no statistically significant difference (Mann–Whitney, p>0.05)

Briefly, after ZA treatment and LLLT application, cells were fixed in 70 % cold ethanol for 1 h. Immediately after the samples were rinsed with deionized water, mineral nodules were detected by alizarin red (40 nm; pH 4.2) incubation under shaking for 20 min at room temperature. For quantitative analysis, mineral nodules were dissolved in 10 % cetylpyridinium chloride (Sigma-Aldrich) for 15 min under shaking. Finally, mineral nodule formation was assessed by absorbance at 692 nm (Thermo Plate, Nanshan District, Shenzhen, China).

Gene expression—real-time PCR

Real-time PCR was used to evaluate the gene expression of Col-I and ALP as previously described (n=4) [23]. These genes participate in matrix synthesis and mineralization.

Briefly, messenger RNA (mRNA) isolation was obtained by the Trizol (Invitrogen, Carlsbad, CA, USA) method, followed by complementary DNA (cDNA) synthesis, with a high-capacity cDNA kit (Invitrogen).

For PCR analysis, specific primers and probe sets were designed. PCR reactions were prepared with standardized SYBR® Green reagents (Applied Biosystems, Foster City, CA, USA) for ALP analysis or Taqman reagents (Applied Biosystems) for Col-I and RPL13 analysis. These reactions were performed in the Step One Plus Real Time System (Applied Biosystems). Data were analyzed by Step One Plus Software (Applied Biosystems) with relative quantitation of each mRNA, considering constitutive gene (RPL13).

Scanning electronic microscopy (SEM)

Osteoblast morphology, whether exposed to ZA and whether subjected to LLLT, was evaluated by SEM. Cells were seeded on 13-mm sterile glass discs previously placed on the bottoms of wells of 24-well plates. After the osteoblasts were treated as described in Table 1, the cells were fixed with 2.5 % glutaraldehyde (Sigma-Aldrich), post-fixed with 1 % osmium tetroxide, and dehydrated in increasing ethanol concentrations (30, 50, 95, and 100 %). Finally, the cells were subjected to chemical drying with 1,1,1,3,3,3 hexamethyldisilazane (HMDS, Sigma-Aldrich).

The glass discs with cells on them were mounted in metallic stubs and stored in a desiccator for 7 days. The samples were then gold-sputtered, and cell morphology was assessed by SEM (Inspect Scanning Electron Microscope-S50, FEI, Hillsboro, OR, USA).

Statistical analysis

Cell viability, total protein production, mineral nodule formation, and qPCR data were analyzed by Kruskal–Wallis tests

Table 2 Total protein production by osteoblasts irradiated with LLLT and treated with ZA

ZA	Energy doses (J/cm^2)					
	0	0.5	1.5	3	5	7
+	61.34 (58.83-66.53) B, a	65.56 (57.48–75.02) B, a	54.58 (49.26–64.40) B, ab	54.53 (48.22–60.30) B, ab	48.87 (41.33–53.47) B, ab	39.86 (31.99–49.02) B, a
−	100.22 (98.19–101.27) A, a	109.02 (103.81–110.07) A, a	103.81 (99.53–104.37) A, a	100.23 (97.63–103.41) A, a	98.04 (89.97–101.88) A, a	101.06 (84.81–105.56) A, a

Values indicate median (25th to 75th percentiles), n=8

A, a Same upper-case letters in columns and lower-case letters in rows indicate no statistically significant difference (Mann–Whitney, p>0.05)

Table 3 Alkaline phosphatase activity by osteoblasts after ZA treatment followed by LLLT

ZA	Energy doses (J/cm^2)					
	0	0.5	1.5	3	5	7
+	35.56 (34.64–37.52) B, a	33.96 (30.21–36.13) B, a	26.43 (21.82–31.45) B, ab	20.57 (17.10–22.47) B, b	27.95 (21.71–30.02) B, ab	23.13 (17.74–24.65) B, b
−	100.15 (93.96–106.53) A, ab	103.56 (101.88–106.70) A, a	99.87 (90.13–106.19) A, ab	89.57 (85.00–92.66) A, b	98.06 (83.46–101.34) A, ab	95.71 (91.88–103.99) A, ab

Values indicate median (25th to 75th percentiles), n=8

A, a Same upper-case letters in columns and lower-case letters in rows indicate no statistically significant difference (Mann–Whitney, p>0.05)

complemented by Mann–Whitney tests, for groups. Statistical significance was set at 5 %. All experimental protocols were performed on three different occasions.

Results

In general, ZA caused an intense decrease in osteoblasts and viability, and, on the other hand, LLLT at 0.5 J/cm^2 increased viability of these cultured cells. However, osteoblasts exposed to ZA and subjected to laser irradiation presented no improvement in viability (Table 1).

In terms of total protein production, no difference was observed among all groups in which the cells were subjected to LLLT, whether or not they were exposed to ZA (Table 2). As determined for cell viability, osteoblasts treated only with ZA showed a significant decrease in total protein production.

The ALP activity of osteoblasts, whether or not they were treated with ZA, was not influenced by laser irradiation. The LLLT at energy doses of 3 and 7 J/cm^2 reduced ALP activity only slightly. In contrast, the same laser energy doses significantly decreased this enzyme activity in osteoblasts previously exposed to ZA (Table 3).

None of the laser energy doses evaluated in this study biostimulated mineral nodule formation by osteoblasts. When the cells were previously treated with ZA, the capacity for mineral nodule formation by cultured osteoblasts was significantly reduced (Table 4).

Gene expression of Col-I by osteoblasts subjected to all laser energy doses tested was similar to that of osteoblasts in the control group. However, for ZA-treated cells subjected to LLLT at 0.5, 1.5, and 3 J/cm^2, a significant increase in Col-l expression was observed (Table 5).

Increased ALP gene expression was observed only when the osteoblasts were subjected to LLLT at 1.5 J/cm^2. However, laser irradiation did not modulate the ALP gene expression in those cells previously treated with ZA (Table 6). Osteoblasts subjected only to ZA treatment showed significant decreases in Col-I and ALP expression.

The SEM evaluation of osteoblasts treated with ZA showed the occurrence of intense morphological cell alterations characterized by cytoplasm shrinkage as well as disaggregation and disruption of this cellular structure. Similar osteoblast alterations were also observed when the ZA-treated cells were subjected to LLLT (Figs. 1 and 2).

Increased numbers of cells attached to the glass substrate were seen when the osteoblasts were solely laser-irradiated at an energy dose of 5 J/cm^2. Cells subjected to all LLLT tested in this study exhibited normal morphology, as observed in the control group (Figs. 1 and 2).

Table 4 Mineral nodule formation by osteoblasts after ZA and LLLT treatment

ZA	Energy doses (J/cm^2)					
	0	0.5	1.5	3	5	7
+	6.26 (5.82–6.82) B, a	8.34 (7.99–8.81) B, a	6.35 (5.83–6.93) B, a	5.88 (5.29–6.58) B, a	7.88 (7.70–8.64) B, a	6.76 (6.40–7.17) B, a
−	96.41 (95.59–101.29) A, ab	99.98 (97.18–102.34) A, a	96.69 (95.24–96.94) A, ab	88.74 (85.48–93.98) A, b	88.26 (84.77–93.06) A, b	97.07 (96.47–97.35) A, ab

Values indicate median (25th to 75th percentiles), n=8

A, a Same upper-case letters in columns and lower-case letters in rows indicate no statistically significant difference (Mann–Whitney, p>0.05)

Table 5 Gene expression of Col-I by osteoblasts after ZA and LLLT treatment

ZA	Energy doses (J/cm^2)					
	0	0.5	1.5	3	5	7
+	0.593 (0.547–0.636) B, b	1.918 (1.494–1.993) A, a	1.863 (1.648–2.015) A, a	1.958 (1.927–1.979) A, a	0.857 (0.682–1.043) A, ab	0.932 (0.832–1.039) B, ab
−	1.000 (0.983–1.016) A, ab	2.293 (1.559–3.044) A, a	1.952 (1.893–1.992) A, ab	2.039 (1.471–2.890) A, ab	0.809 (0.688–0.932) A, b	1.212 (1.156–1.293) A, ab

Values indicate median (25th to 75th percentiles), n=4

A, a Same upper-case letters in columns and lower-case letters in rows indicate no statistically significant difference (Mann–Whitney, p>0.05)

Discussion

Several studies have evaluated the effects of ZA on osteoblasts, since this drug has been related to the etiopathogenesis of osteonecrosis as well as to delayed bone healing and remodeling in patients under ZA treatment [22]. In the present study, a highly cytotoxic effect was observed in osteoblasts treated with ZA, characterized by decreased viability, total protein production, mineral nodule formation, ALP activity and morphology, and gene expression of Col-I and ALP.

Several studies have introduced LLLT as an adjuvant therapy for bisphosphonate-induced osteonecrosis associated with antimicrobial or surgical treatment and have shown that this therapy can accelerate healing and lesion remission [10–13]. Low-power laser-irradiated osteoblasts enhance proliferation and protein synthesis, mainly those related to matrix formation and maturation, such as Col-I [20, 25, 26].

It was shown in the present study that specific parameters of LLLT can biostimulate osteoblasts in culture, increasing their viability. However, no effects of laser irradiation were observed on mineral nodule formation, ALP activity, and expression of genes related to matrix production and mineralization. The absence of positive effects of LLLT on ZA-treated cells may be related to the selected parameters of irradiation, since previous studies have demonstrated that different wavelengths, power outputs, or energy doses can promote diverse cellular responses [24]. As reported by other authors, higher energy doses can increase the metabolism of cultured osteoblasts [26, 27].

The data obtained in the present study may also be related to the fact that cultured osteoblasts were not previously subjected to cellular stress, such as nutritional restriction, which has been reported by many workers as a predictive factor for greater biostimulation [25, 27]. The cellular stress protocol was not used in the present study because the osteoblasts had already been subjected to the toxic effects of ZA, which seemed to be sufficiently high to inhibit the biomodulation of the cultured cells.

Regarding cell morphology, no alterations were observed in cultured human osteoblasts subjected to LLLT at all selected parameters, as previously demonstrated for other cell types [16]. SEM evaluation, which is an important tool for the morphologic evaluation of cells, can determine the cytotoxic effects of several treatments [28, 29] such as observed for ZA [18, 23]. Despite the fact that LLLT did not biostimulate the cultured osteoblasts, cell morphology was maintained during the study, thus determining the cells' resistance threshold.

The positive effects of LLLT on areas of osteonecrosis could be related to cellular biostimulation, as recently described by our group (eu laser phys) However, so far, only one study has been carried out to assess the effects of LLLT on ZA-treated osteoblasts [30] The authors demonstrated that LLLT applied to cultured human osteoblasts (SaOS-2) subjected to ZA treatment for 24 and 48 h showed increased ALP

Table 6 Gene expression of ALP by osteoblasts after ZA and LLLT treatment

ZA	Energy doses (J/cm^2)					
	0	0.5	1.5	3	5	7
+	0.344 (0.295–0.404) B, a	0.548 (0.442–0.624) B, a	0.334 (0.293–0.339) B, a	0.555 (0.521–0.605) B, a	0.486 (0.353–0.653) B, a	0.428 (0.347–0.488) B, a
−	1.045 (0.905–1.097) A, ab	1.975 (1.497–2.167) A, ab	2.167 (2.136–2.360) A, a	1.797 (1.382–2.188) A, ab	0.871 (0.830–0.910) A, b	1.211 (1.154–1.308) A, ab

Values indicate median (25th to 75th percentiles), n=4

A, a Same upper-case letters in columns and lower-case letters in rows indicate no statistically significant difference (Mann–Whitney, p>0.05)

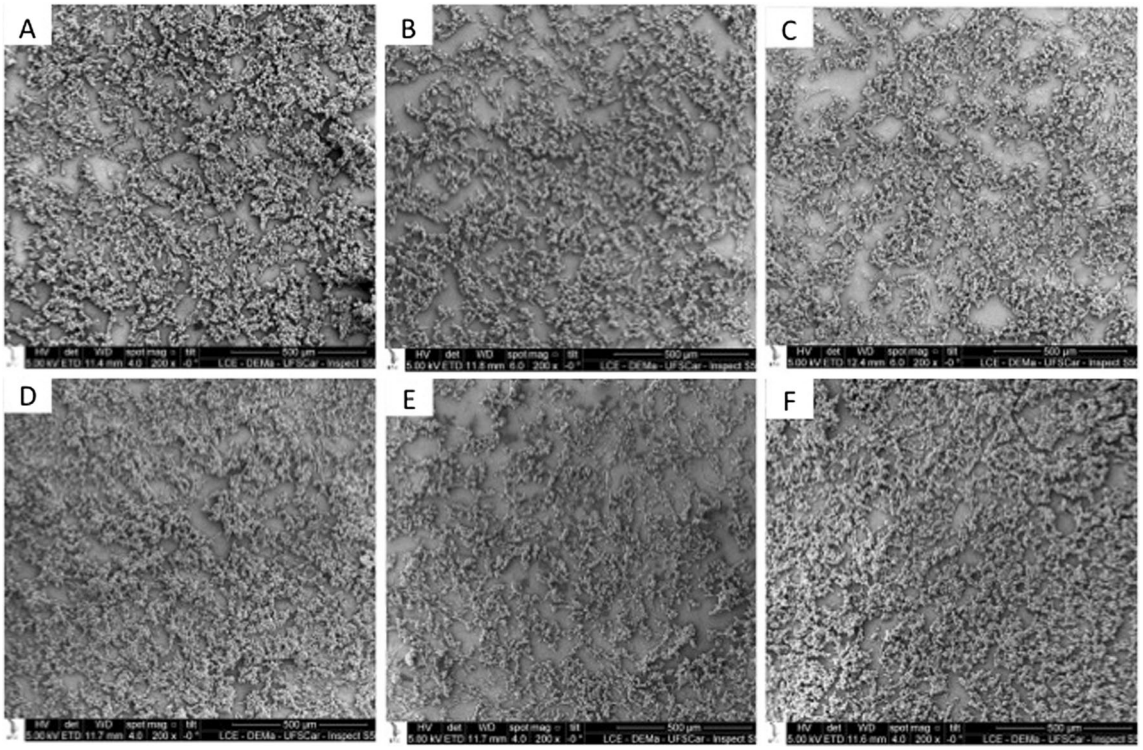

Fig. 1 Morphology of cultured human osteoblasts (Saos-2) subjected to LLLT at different energy doses (**a** Control group. **b** 0.5 J/cm^2. **c** 1.5 J/cm^2. **d** 3 J/cm^2. **e** 5 J/cm^2. **f** 7 J/cm^2). No significant difference was observed between LLLT-treated cells and the control group. All images show adherent and confluent cells. SEM, original magnification ×200

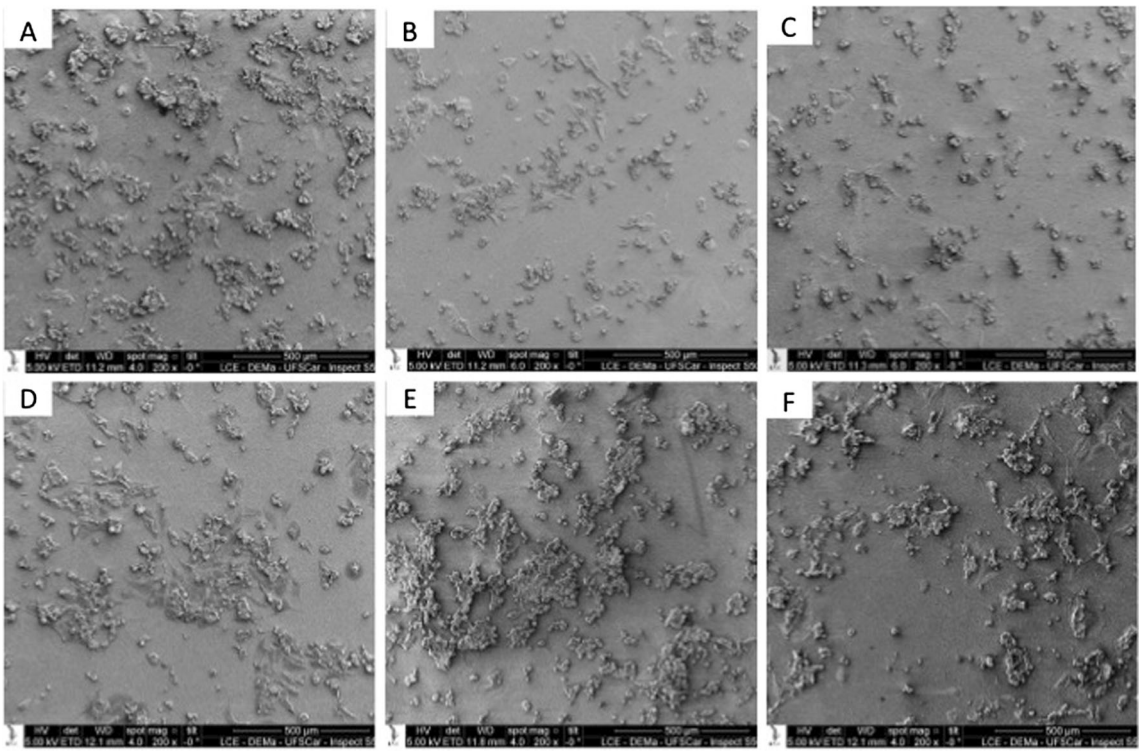

Fig. 2 Morphology of cultured human osteoblasts (Saos-2) subjected to ZA treatment and LLLT at different energy doses (**a** ZA. **b** ZA+0.5 J/cm^2. **c** ZA+1.5 J/cm^2. **d** ZA+3 J/cm^2. **e** ZA+5 J/cm^2. **f** ZA+7 J/cm^2). For all ZA-treated groups, a significant decrease in adherent cell numbers was observed. For group E, where LLLT was applied, an increase in adherent cells can be observed, compared with the ZA-treated group (**a**). SEM, original magnification ×200

activity and numbers of viable osteoblasts [30] Despite the similarity of methodology used by the authors compared with that used in the present study, the data obtained in both investigations cannot be compared, because the LLLT specifications were not reported,[30] and because, as already mentioned, current studies have demonstrated that different laser parameters cause various cell responses [15]. Therefore, in addition to several available studies about the effects of LLLT on different cell types, the lack of standardization of laser irradiation protocols for in vitro and in vivo investigations does not allow for adequate comparison among all data obtained.

Considering previous results [18, 30] and based on analysis of the data obtained in the present study, one may suggest that LLLT at specific parameters can promote biostimulation of cultured cells whether or not they are treated with ZA. However, further studies are needed to elucidate the effects of LLLT on ZA-treated cells and to improve and standardize the use of this kind of therapy as an adjuvant for the treatment of osteonecrosis.

Acknowledgments The authors acknowledge the Fundação de Amparo à Pesquisa do Estado de São Paulo-FAPESP (grants: 2013/05879-0 and BP.PD: 2012/17947-8) and the Conselho Nacional de Desenvolvimento Científico e Tecnológico-CNPq (grant: 305204/2010-6) for financial support.

Conflict of interest The authors declare no conflict of interest.

References

1. Migliorati CA, Woo S, Hewson I, Barasch A, Elting L, Spjikervet FKL, Brennan MT (2009) A systematic review of bisphosphonate osteonecrosis (BON) in cancer. Support Care Cancer 18:1099–1106. doi:10.2174/157488709788185978
2. Landesberg R, Woo V, Cremers S, Cozin M, Marolt D, Vunjak-Novakovic G, Kousteni S, Raghavan S (2011) Potential pathophysiological mechanism in osteonecrosis of the jaw. Ann N Y Acad Sci 1218:62–79. doi:10.1111/j.1749-6632.2010.05835.x
3. Migliorati CA, Casiglia J, Epstein J, Jacobsen PL, Siegel MA, Woo S (2005) Managing the care of patients with bisphosphonate-associated osteonecrosis. J Am Dent Assoc 136:1658–1668
4. Otto S, Pautke C, Opelz C, Westphal I, Drosse I, Schwager J, Bauss F, Ehrenfeld M, Scheker M (2010) Osteonecrosis of the jaw: effect of bisphosphonate type, local concentration, and acidic milieu on the pathomechanism. J Oral Maxillofac Surg 68:2837–2845
5. Ravosa MJ, Ning J, Liu Y, Stack MS (2011) Bisphosphonate effects on the behaviour of oral epithelial cells and oral fibroblasts. Arch Oral Biol 56:491–498. doi:10.1016/j.joms.2010.07.017
6. Scheper MA, Badros A, Salama AR, Warburton G, Cullen KJ, Weikel DS, Meiller TF (2009) A novel bioassay model to determine clinically significant bisphosphonate levels. Support Care Cancer 17:1553–1557. doi:10.1007/s00520-009-0710-7
7. Walter C, Klein MO, Pabst A, Al-Nawas B, Düschner H, Ziebart T (2010) Influence of bisphosphonates on endothelial cells, fibroblasts, and osteogenic cells. Clin Oral Investig 14:35–41. doi:10.1007/s00784-009-0266-4
8. Landesberg R, Cozin M, Cremers S, Woo V, Kousteni S, Sinha S, Garret-Sinha L, Raghavan S (2008) Inhibition of oral mucosal cell wound healing by bisphosphonates. J Oral Maxillofac Surg 66:839–847. doi:10.1016/j.joms.2008.01.026
9. Allen MR (2011) The effects of bisphosphonates on jaw bone remodeling, tissue properties, and extraction healing. Odontology 99:8–17. doi:10.1007/s10266-010-0153-0
10. Scoletta M, Arduino PG, Reggio L, Dalmasso P, Mozatti M (2010) Effect of low-level laser irradiation on bisphosphonate-induced osteonecrosis of the jaws: preliminary results of a prospective study. Photomed Laser Surg 28:179–184. doi:10.1089/pho.2009.2501
11. Romeo U, Galanakis A, Marias C, Del Vecchio A, Tenore G, Palaia G, Vescove I, Polimeni A (2011) Observation of pain control in patients with bisphosphonate-induced osteonecrosis using low level laser therapy: preliminary results. Photomed Laser Surg 29:447–452. doi:10.1089/pho.2010.2835
12. Vescovi P, Manfredi M, Merigo E, Guidotti R, Meleti M, Pedrazzi G, Fornaini C, Bonanini M, Ferri T, Nammour S (2012) Early surgical laser-assisted management of bisphosphonate-related osteonecrosis of the jaws (BRONJ): a retrospective analysis of 101 treated sites with long-term follow-up. Photomed Laser Surg 30:5–13. doi:10.1089/pho.2010.2955
13. Vescovi P, Merigo E, Meleti M, Manfredi M, Fornaini C, Nammour S (2012) Surgical approach and laser applications in BRONJ osteoporotic and cancer patients. J Osteoporos. doi:10.1155/2012/585434
14. Peplow PV, Chung T, Baxter GD (2010) Laser photobiomodulation of proliferation cells in culture: a review of human and animal studies. Photomed Laser Surg 28:S30–S40. doi:10.1089/pho.2010.2771
15. AlGhamdi KM, Kumar A, Moussa NA (2012) Low-level laser therapy: a useful technique for enhancing the proliferation of various cultured cells. Lasers Med Sci 27:237–249. doi:10.1007/s10103-011-0885-2
16. Basso FG, Oliveira CF, Kurachi C, Hebling J, Costa CA (2013) Biostimulatory effect of low-level laser therapy on keratinocytes in vitro. Lasers Med Sci 28:267–274. doi:10.1007/s10103-012-1057-8
17. Lins EC, Oliveira CF, Guimarães OCC, Costa CAS, Kurachi C, Bagnato VS (2013) A novel 785-nm laser diode-based system for standardization of cell culture irradiation. Photomed Laser Surg. doi:10.1089/pho.2012.3310
18. Basso FG, Pansani TN, Turrioni APS, Kurachi C, Bagnato VS, Hebling J, de Souza Costa CA (2013) Biostimulatory effects of low-level laser therapy on epithelial cells and gingival fibroblasts treated with zoledronic acid. Laser Phys 23 (Epub ahead of print). doi: 10.1088/1054-660X/23/5/055601
19. Noqueira GT, Mesquita-Ferrari RA, Souza NHC, Artilheiro PP, Albertini R, Bussadori SK, Fernandes KPS (2012) Effect of low-level laser therapy on proliferation, differentiation, and adhesion of steroid-treated osteoblasts. Lasers Med Sci 27:1189–1193. doi:10.1007/s10103-011-1035-6
20. Schwartz-Filho HO, Reimer AC, Marcantonio C, Marcantonio E Jr, Marcantonio RA (2011) Effects of low-level laser therapy (685nm) at different doses in osteogenic cell cultures. Lasers Med Sci 26:539–543. doi:10.1007/s10103-011-0902-5
21. Oliveira DAAP, Oliveira RF, Zangaro RA, Soares CP (2008) Evaluation of low-level laser therapy of osteoblastic cells. Photomed Laser Surg 26:401–404. doi:10.1089/pho.2007.2101
22. Idris A, Rojas J, Greig IR, van't Hof RJ, Ralston SH (2008) Aminobisphosphonates cause osteoblast apoptosis and inhibit bone nodule formation in vitro. Calcif Tissue Int 82:191–201. doi:10.1007/s00223-008-9104-y
23. Basso FG, Turrioni APS, Hebling J, de Souza Costa CA (2013) Effects of zoledronic acid on odontoblast-like cells. Arch Oral Biol 58:467–473. doi:10.1016/j.archoralbio.2012.09.016
24. Im G, Qureshi SA, Kenney J, Rubash HE, Shanbhag AS (2004) Osteoblast proliferation and maturation by bisphosphonates. Biomaterials 25:4105–4115. doi:10.1016/j.biomaterials.2003.11.024

25. Fujihara NA, Hiraki KRN, Marques MM (2006) Irradiation at 780 nm increases proliferation rate of osteoblasts independently of dexamethasone presence. Lasers Surg Med 38:332–336. doi:10.1002/lsm.20298
26. Haxsen V, Schikora D, Sommer U, Remppis A, Greten J, Kasperk C (2008) Relevance of laser irradiance threshold in the induction of alkaline phosphatase in human osteoblast cultures. Lasers Med Sci 23:381–384. doi:10.1007/s10103-007-0511-5
27. Tagliani MM, Oliveira CF, Lins EC, Kurachi C, Hebling J, Bagnato VS, de Souza Costa CA (2010) Nutritional stress enhances cell viability of odontoblastlike cells subjected to low level laser irradiation. Laser Phys Lett 7:247–251. doi:10.1002/lapl.200910137
28. Trindade FZ, Ribeiro APD, Sacono NT, Oliveira CF, Lessa FCR, Hebling J, Costa CAS (2009) Trans-enamel and trans-dentinal cytotoxic effects of 35% H_2O_2 bleaching gel on cultured odontoblast cell lines after consecutive applications. Int Endod J 42:516–524. doi:10.1111/j.1365-2591.2009.01544.x
29. Soares DGS, Ribeiro APD, Sacono NT, Coldebella CR, Hebling J, de Souza Costa CA (2011) Transenamel and transdentinal cytotoxicity of carbamide peroxide bleaching gels on odontoblast-like MDPC-23 cells. Int Endod J 44:116–125. doi:10.1111/j.1365-2591.2010.01810.x
30. Bayram H, Kenar H, Tasar F, Hasirci V (2013) Effect of low level laser therapy and zoledronate on the viability and ALP activity of Saos-2 cells. Int J Oral Maxillofac Surg 42:140–146. doi:10.1016/j.ijom.2012.03.026

CLIMACTERIC 2014;17:285–293

Phototherapy during treadmill training improves quadriceps performance in postmenopausal women

F. R. Paolillo[*], *A. V. Corazza*[†], *A. R. Paolillo*[‡], *A. Borghi-Silva*[**], *R. Arena*[††], *C. Kurachi*[*] *and V. S. Bagnato*[*]

[*]Optics Group from Physics Institute of São Carlos, University of São Paulo, Brazil; [†]Department of Morphology, Faculty of Dentistry of Piracicaba, State University of Campinas, Brazil; [‡]Bioengineer Program, University of São Paulo, Brazil; [**]Cardiopulmonary Physiotherapy Laboratory, Department of Physical Therapy, Federal University of São Carlos, Brazil; [††]Department of Physical Therapy, College of Applied Health Sciences, University of Illinois Chicago, Chicago, IL, USA

Key words: PHOTOTHERAPY, INFRARED, PHYSICAL TRAINING, MUSCLE PERFORMANCE, POSTMENOPAUSE

ABSTRACT

Objective To evaluate the effects of infrared-light-emitting diode (LED) during treadmill training on functional performance.

Methods Thirty postmenopausal women aged 50–60 years were randomly assigned to one of three groups and successfully completed the full study. The three groups were: (1) the LED group, which performed treadmill training associated with phototherapy ($n = 10$); (2) the exercise group, which carried out treadmill training only ($n = 10$); and (3) the sedentary group, which neither performed physical training nor underwent phototherapy ($n = 10$). Training was performed over a period of 6 months, twice a week for 45 min per session at 85–90% of maximal heart rate, which was obtained during progressive exercise testing. The irradiation parameters were 100 mW, 39 mW/cm^2 and 108 J/cm^2 for 45 min. Quadriceps performance was measured during isokinetic exercise testing at 60°/s and 300°/s.

Results Peak torque did not differ amongst the groups. However, the results showed significantly higher values of power and total work for the LED group ($\Delta = 21 \pm 6$ W and $\Delta = 634 \pm 156$ J, $p < 0.05$) when compared to both the exercise group ($\Delta = 13 \pm 10$ W and $\Delta = 410 \pm 270$ J) and the sedentary group ($\Delta = 10 \pm 9$ W and $\Delta = 357 \pm 327$ J). Fatigue was also significantly lower in the LED group ($\Delta = -7 \pm 4\%$, $p < 0.05$) compared to both the exercise group ($\Delta = 3 \pm 8\%$) and the sedentary group ($\Delta = -2 \pm 6\%$).

Conclusions Infrared-LED during treadmill training may improve quadriceps power and reduce peripheral fatigue in postmenopausal women.

INTRODUCTION

The decline in peak exercise performance occurs with advancing age. There is reduction of fast powerful movements that may contribute to a loss of the type II motor units. In addition, a reduction in maximal oxygen consumption (VO_{2max}), lactate threshold and energetic cost are associated with aging. Endurance 'masters' athletes strive to maintain or even improve upon the performance they achieved at younger ages, but some level of decline in athletic performance is inevitable[1]. Low estrogen levels during menopause can result in skeletal muscle atrophy and weakness, lower aerobic capacity and a progressive increase in fat mass. These factors may lead to early fatigue and decreased physical performance[2]. However, it is obvious that moderate- to high-intensity physical activity is a goal by which the physiologic and functional losses associated with aging may be altered. According to Tanaka and Seals[1], 'masters' endurance athletes are capable of remarkable athletic and physiological functional performance, thereby representing a uniquely positive example of 'exceptional aging'.

Correspondence: Dr F. R. Paolillo, University of São Paulo, Av. Trabalhador Sãocarlense, 400–Centro, CEP 13560-970, São Carlos, SP, Brazil; E-mail: fer.nanda.rp@hotmail.com

ORIGINAL ARTICLE

DOI: 10.3109/13697137.2013.828196

Received 10-04-2013
Revised 14-07-2013
Accepted 19-07-2013

In addition, new methods to increase physical performance and promote health can be applied in aging people. Adjunctive technologies, used in parallel with traditional exercise training, have been shown to elicit additional improvement in muscle function in postmenopausal women, such as neuromuscular electrical stimulation associated with exercise (climbing up and down the stairs)[3], unloaded static and dynamic exercises on a vibration platform (whole-body-vibration)[4], and phototherapy (850 nm light-emitting diodes, LEDs) during a treadmill training[5].

Some studies also suggest that the acute and chronic increases in muscle performance might be potentiated by using adjunctive technology in younger people participating in exercise training. Phototherapy (660/850 nm LEDs) applied before exercises in males was able to promote an acute attenuation in knee-extensor torque fatigue during a high-intensity concentric protocol[6]. In another similar study, 810 nm laser therapy applied before exercise attenuated the decrease in muscle strength and reduced the increase in lactate dehydrogenase and creatine kinase serum levels[7]. Phototherapy (808 nm laser) applied after strength training can increase knee-extensor peak torque in young males[8] and, when applied after a cycle ergometer training program, resulted in the reduction of quadriceps fatigue in young females[9]. The authors theorized that phototherapy enhanced mitochondrial function and increased aerobic adenosine triphosphate (ATP) synthesis, thereby reducing both blood lactate accumulation and biochemical markers of muscle damage.

Previous studies from our group have found that phototherapy significantly improved aerobic exercise performance in postmenopausal women participating in a high-intensity training program[10]. However, strength parameters during a 6-month longitudinal study, to our knowledge, have not been investigated. Thus, the aim of this study was to evaluate the synergistic effect of infrared radiation, emitted from LEDs, and treadmill training on quadriceps strength and fatigue in postmenopausal women. Our hypothesis was that muscle performance in postmenopausal women would be enhanced through the use of infrared-LED illumination during treadmill training.

METHODS

All procedures were approved by the National Ethics Committee of the Ministry of Health in Brasilia, Brazil (approval no. 688/2009) and by the Ethics Committee of Federal University of São Carlos in São Carlos, Brazil (approval no. 262/2009). All subjects provided written informed consent and agreed to participate in the study. The study was registered with NIH Clinical Trials (NCT01610232).

Participants

A prospective randomized trial was undertaken. A computer program was used for the randomization. The schematic flow chart describing the participants in this study can be seen in Figure 1. Postmenopausal women from São Carlos City, São Paulo State in Brazil were invited to participate in the study. The inclusion criteria were postmenopausal Caucasian women, aged between 50 and 60 years, non-users of hormone

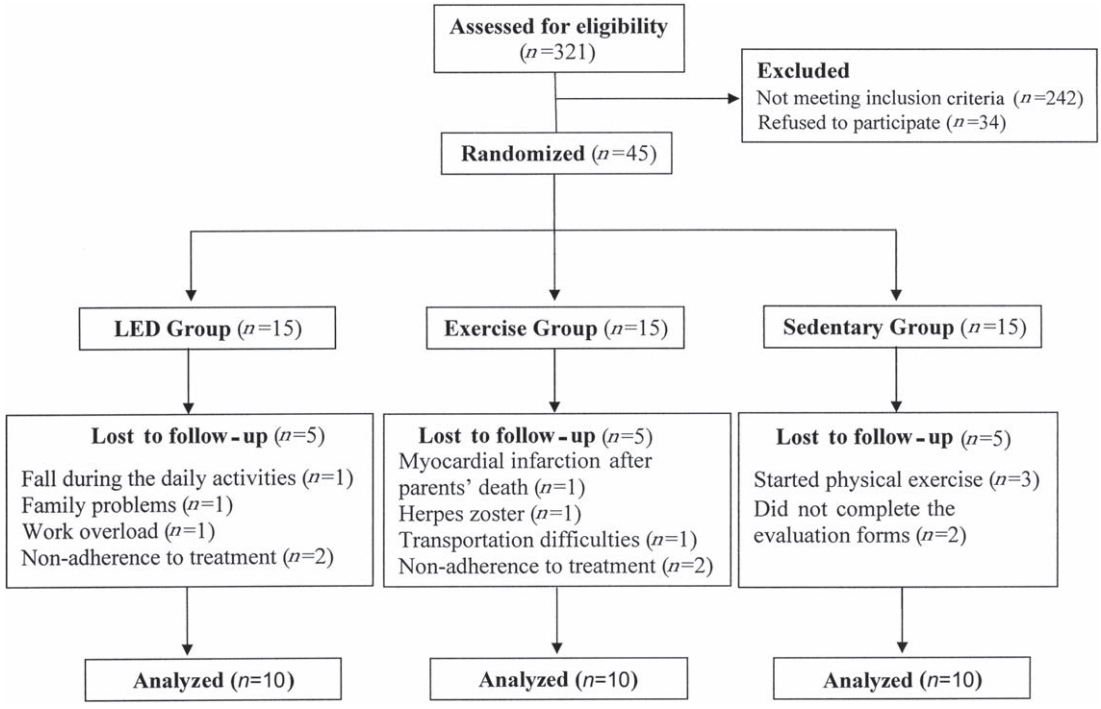

Figure 1 Schematic flow concerning the participants in the study

replacement therapy (HRT) and untrained. Postmenopausal status was defined by an absence of menstruation for more than 1 year. The exclusion criteria were: signs and symptoms of any neurological, metabolic, inflammatory, pulmonary, oncological or cardiac disease or endocrinopathy, musculotendinous or articular injuries and cigarette smoking. We excluded diseases, disorders or injuries which would have limited the ability to exercise, such as osteoarthritis. The anamnesis and clinical evaluation permitted the exclusion of 24% for a history of exercise training ($n = 57$); 21% for lower limb pain/disorders/injuries ($n = 52$); 18% for use of HRT ($n = 44$); 15% for being non-Caucasian ($n = 36$); 12% for cardiovascular disease ($n = 28$); 5% for smoking habits ($n = 12$); 3% for cancer ($n = 8$); and 2% for psychiatric symptoms ($n = 5$). Thirty postmenopausal Caucasian women with a mean age of 55 ± 2 years, mean menopause duration of 8 ± 5 years, and mean estradiol level of 17 ± 9 pg/ml were randomly divided into three groups: (1) the LED group which performed treadmill training associated with phototherapy, (2) the exercise group which carried out treadmill training only, and (3) the sedentary group which did not perform treadmill training or phototherapy. The demographic characteristics of this sample can be seen in Table 1.

Phototherapy and training

For the phototherapy performed during treadmill training, LED arrays were specially designed by the Optics Group from the Physics Institute of São Carlos, University of São Paulo to be used at the sides of the treadmill, illuminating the subject's thighs. The quadriceps muscles were illuminated because of their role during the stance and swing phases of gait cycle. Infrared radiation (850 nm) is not visible and was selected because this spectral range shows better skin penetration compared to the (visible) red light. The average power and power density on the women's skin was 100 mW and 39 mW/cm^2, respectively. The treatment time was 45 min bilaterally on both thighs during treadmill training. These parameters led to an approximate fluence of 108 J/cm^2. The volunteers wore safety glasses during infrared-LED illumination[5,10,11]. Figure 2 illustrates treadmill training with infrared-LED illumination; the women wore swimwear to ensure infrared absorption through the bare skin. However, the women in the exercise group wore sports clothing as they were not illuminated.

Treadmill training with and without phototherapy was performed twice a week, for 6 months; each session lasted 45 min at high intensity[12] (85–90% of maximal heart rate, HR_{max}, obtained during a progressive exercise testing as previously described[10]). Briefly, the women underwent a progressive aerobic exercise test on a treadmill (using the modified Bruce protocol). The test was terminated when the women demonstrated signs and/or limiting of maximal effort, such as fatigue of the lower limbs, general physical fatigue, dizziness, nausea, cyanosis, arrhythmias, excessive sweating, angina, or when the patient reached age-predicted HR_{max}.

Heart rate measurements were obtained by 12-lead electrocardiogram (ECG; HeartWare, Belo Horizonte, Minas Gerais, Brazil). The predicted HR_{max} for women was calculated by the formula: 210 minus age. For treadmill exercise, this formula provides a reasonable prediction of the HR_{max} response[13]. The maximal time of tolerance, the last stage of

Table 1 Statistical results of the demographic characteristics and the progressive exercise testing. Data are given as mean ± standard deviation. No significant differences were found between the groups (one-way ANOVA, $p \geq 0.05$)

	LED group	*Exercise group*	*Sedentary group*
Demographic data			
Age (years)	56 ± 2	55 ± 2	55 ± 2
Duration of menopause (years)	8 ± 6	9 ± 6	7 ± 6
Progressive exercise testing (baseline)			
Heart rate at rest (bpm)	73 ± 9	73 ± 10	71 ± 8
Modified Bruce (last stage)	2.5 ± 0.5	2.5 ± 0.5	2.5 ± 0.5
Maximal time of tolerance (min)	14 ± 2	13 ± 2	12 ± 2
Estimated VO_{2max} (ml.kg.min)	33 ± 8	29 ± 5	27 ± 7
Predicted heart rate (bpm)	154 ± 2	155 ± 3	154 ± 2
Maximal heart rate (bpm)	165 ± 9	156 ± 14	157 ± 15
Heart rate recovery (bpm)	95 ± 7	92 ± 12	96 ± 14

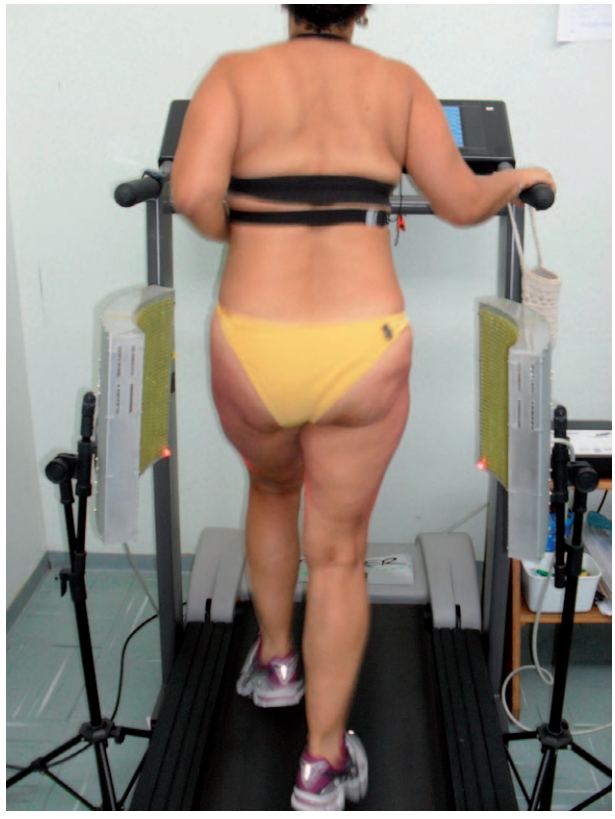

Figure 2 Infrared-LED illumination during treadmill training

modified Bruce and the estimated maximal oxygen consumption (VO_{2max}) were determined from the progressive exercise test[10]. Baseline values obtained for these variables are listed in Table 1. Baseline data for progressive exercise testing showed that the predicted HR_{max} was achieved and the estimated VO_{2max} indicated a sedentary state[14] for all groups, as observed in Table 1.

A cardiofrequencimeter monitor (Polar A3; Polar Electro, Woodbury, NY, USA) was used to monitor heart rate during training. The training heart rate and exercise velocity are illustrated in Figure 3. The training intensity of the exercise program was gradually increased until it reached a target of 85–90% of the HR_{max} obtained from the progressive exercise test. The training program was individualized for each subject, under the direction of a physical education teacher and a physiotherapist. All women wore heart rate monitors and they were instructed to maintain the heart rate prescribed for training. The feedback was the same for both exercise groups. The treadmill speed was titrated upward until the individualized training heart rate was obtained.

Training sessions and evaluations were carried out in a laboratory at an air temperature between 22°C and 24°C and a relative humidity between 50% and 60%, at the same time of day.

Anthropometric characteristics and body composition

Anthropometric data were used to determine body mass index (BMI, body weight (kg) divided by height $(m)^2$). Percent body fat, fat mass and lean mass were determined via bipolar electrical bioimpedance of the upper limbs (Omron BF306; Omron, Kyoto, Japan)[15].

Isokinetic testing

Peak torque (absolute and relative values, normalized by body mass), power, work, fatigue and the number of contractions of the dominant quadriceps were measured using an isokinetic dynamometer (Biodex Multi Joint System III; Biodex Medical Systems, New York, USA)[16,17]. Prior to the test, the load cell was properly calibrated using a standard weight and dynamometer lever arm horizontally positioned and stabilized in relation to the ground, according to the manufacturer's recommendations.

The positioning and stabilization of the subjects were standardized by maintaining the same measures of the Biodex accessories (e.g. chair and lever) during the pre- and post-test[5]. The subjects were seated in a comfortable, upright position (90° at the hip) on the Biodex accessory chair, with the knee at a 90° knee-flexion angle. In order to minimize extraneous body movements during the contractions and therefore avoid the contribution of muscles other than the knee extensors, straps were applied across the chest, pelvis and at mid-thigh level. The dynamometer lever arm was attached 2–3 cm above the lateral malleolus using a strap. The knee joint axis was adjusted to the Biodex ensuring an alignment between the center of rotation of the dynamometer resistance adapter and the axis of rotation of the knee at the lateral femoral epicondyle. The subjects were asked to relax their legs so that the passive determination of the effects of gravity on the limb and lever arm could be measured.

Each subject was required to fold her arms across her chest. The warm-up period and the familiarization exercises consisted of performing submaximal isometric contractions. All subjects were instructed to push the lever up and pull it down as hard and as fast as possible during knee extension. While the participants were performing the protocols, verbal encouragement and visual feedback were given. Details for the two protocols employed in the current study are as follows:

(1) Protocol for the analysis of maximum isokinetic strength: the subjects performed five maximal efforts to determine maximal peak torque (N·m) at an angular velocity of 60°/s; and
(2) Protocol for the analysis of isokinetic endurance: the subjects performed knee extension maneuvers for 1 min at an angular velocity of 300°/s to determine power (W), work (J), fatigue index (%) and the number of quadriceps muscle contractions. Muscle fatigue was determined using the following formula[6,16]: Percent decrease = 100 − [(work last third/work first third) × 100]. The data were analyzed in absolute and relative terms, through normalization (%) by body mass.

Statistical analysis

Continuous data were expressed as mean and standard deviations. The Shapiro–Wilk test was used to analyze data normality and the homogeneity of variances using Levene's test. One-way analysis of variance (ANOVA) was used to evaluate the differences in the demographic data and progressive exercise testing amongst the groups. Two-way ANOVA with repeated measures were used to compare changes before and after the treatment in the anthropometric characteristics, body composition, isokinetic parameters, training heart rate and exercise velocity. The independent factors were group (with three levels: LED group, exercise group and sedentary group) and time (with two levels: baseline and after 6 months), which was also considered as a repeated measurement (intragroup differences). The change between baseline and at 6 months (post-treatment - pretreatment) was used to compare groups using a one-way ANOVA (intergroup differences). When significant differences were found, Bonferroni adjustments were applied. The Statistica for Windows Release 7 software (Statsoft Inc., Tulsa, OK, USA) was used for the statistical analysis and the significance level was set at 5% ($p < 0.05$).

Table 2 Statistical results of the anthropometric characteristics and body composition (secondary variables) pre- and post-therapy. Data are given as mean ± standard deviation

	LED group		*Exercise group*		*Sedentary group*	
	Pre	*Post*	*Pre*	*Post*	*Pre*	*Post*
Anthropometric characteristics						
Body mass (kg)	71 ± 11	71 ± 12	67 ± 11	67 ± 10	80 ± 17	83 ± 22
Body height (cm)	153 ± 7	153 ± 6	158 ± 6	157 ± 7	155 ± 5	154 ± 6
Body mass index (kg/m^2)	30 ± 5	30 ± 4	27 ± 4	27 ± 5	33 ± 7	35 ± 8*
Body composition						
Body fat (%)	39 ± 7	37 ± 5	37 ± 4	36 ± 6	42 ± 5	43 ± 4
Fat mass (kg)	28 ± 8	27 ± 7	25 ± 6	24 ± 6	34 ± 11	36 ± 9
Lean mass (kg)	43 ± 5	43 ± 6	42 ± 6	42 ± 6	46 ± 6	47 ± 7

*, Significant difference for pre- vs. post-treatment (repeated measures ANOVA with Bonferroni adjustments) $p < 0.05$

RESULTS

Anthropometric characteristics and body composition

Data for anthropometric characteristics and body composition (secondary variables) for all three groups are listed in Table 2. Most of the characteristics amongst groups were similar ($p \geq 0.05$), with the exception of BMI, which was significantly higher in the sedentary group following the intervention ($p = 0.04$).

Isokinetic testing

The results of isokinetic testing at angular velocities of 60°/s and 300°/s are listed in Table 2. Peak torque did not differ significantly for any of the groups ($p \geq 0.05$, Table 3). Significant differences for the absolute values of average power and total work were found for all groups following completion of the 6-month protocol ($p < 0.05$). However, normalized values of average power and total work did not show significant differences for the sedentary group ($p \geq 0.05$). The absolute and normalized values of the fatigue index significantly decreased only in the LED group ($p = 0.003$). Moreover, the number of contractions significantly increased only in the LED group ($p = 0.01$). However, the fatigue index and number of contractions did not show any significant differences for both the exercise and sedentary groups ($p \geq 0.05$). In addition, a significant difference was found between the groups in the change between baseline and 6 months. Specifically, the LED group showed a higher change between baseline and 6 months for the average power (compared to the exercise group ($p = 0.04$) and compared to the sedentary group ($p = 0.03$), see Figure 4a), total work (compared to the exercise group ($p = 0.03$) and compared to the sedentary group ($p = 0.03$), see Figure 4b) and fatigue index (compared to the exercise

Table 3 Statistical results of the isokinetic testing pre- and post-therapy. Data are given as mean ± standard deviation

	LED group		*Exercise group*		*Sedentary group*	
	Pre	*Post*	*Pre*	*Post*	*Pre*	*Post*
Isokinetic testing: 60°/s						
Peak torque (N·m)	107 ± 19	111 ± 14	101 ± 23	105 ± 18	108 ± 13	109 ± 19
Peak torque/body mass (%)	157 ± 39	162 ± 31	156 ± 37	162 ± 34	139 ± 26	134 ± 27
Isokinetic testing: 300°/s						
Average power (W)	55 ± 9	76 ± 10**	62 ± 13	75 ± 12**	64 ± 14	74 ± 18**
Average power/body mass (%)	79 ± 20	110 ± 19**	94 ± 22	117 ± 26**	81 ± 14	91 ± 17
Total work (J)	1529 ± 336	2162 ± 319**	1646 ± 385	2055 ± 325**	1796 ± 404	2158 ± 579**
Total work/body mass (%)	2238 ± 684	3143 ± 632**	2517 ± 618	3198 ± 692**	2277 ± 409	2623 ± 198
Fatigue (%)	63 ± 6	57 ± 3*	51 ± 8	54 ± 6	59 ± 9	58 ± 5
Fatigue/body mass (%)	93 ± 19	83 ± 18*	79 ± 18	85 ± 24	79 ± 22	73 ± 20
Number of contractions	59 ± 5	64 ± 5*	59 ± 7	60 ± 5	64 ± 5	63 ± 6

Significant difference for pre- vs. post-treatment (repeated measures ANOVA with Bonferroni adjustments, *, $p < 0.05$; **, $p < 0.01$

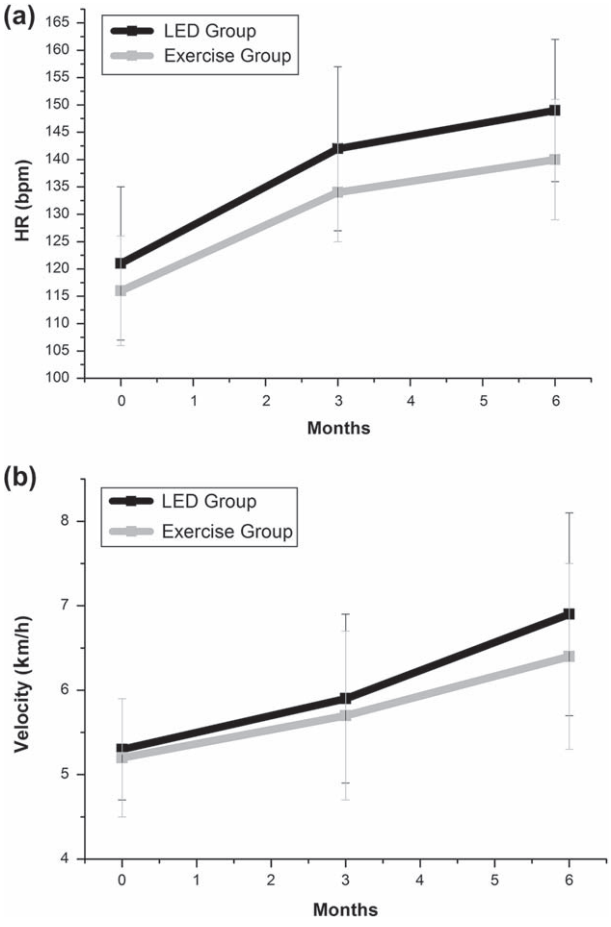

Figure 3 Heart rate (HR) training (a) and treadmill velocity (b). The training intensity of the exercise program was gradually increased until it reached a target of 85–90% of HR_{max} obtained from the progressive exercise test. There were no significant changes in the baseline and after 6 months (repeated measures ANOVA, $p \geq 0.05$). In addition, no significant difference was found between the groups (one-way ANOVA, $p \geq 0.05$)

group ($p = 0.006$) and compared to the sedentary group ($p = 0.04$), see Figure 4c).

DISCUSSION

This study emphasizes our previous findings concerning an improvement in muscle performance in postmenopausal women when combining infrared radiation with an aerobic exercise training program[5]. However, compared to the previous study, the clinical protocol in the current analysis was modified (the power, time of treatment and dose of infrared radiation as well as the period of the physical training were increased) and the improvements were enhanced. The infrared-LED illumination during treadmill training improved quadriceps strength and reduced peripheral fatigue in postmenopausal women. These results were apparent

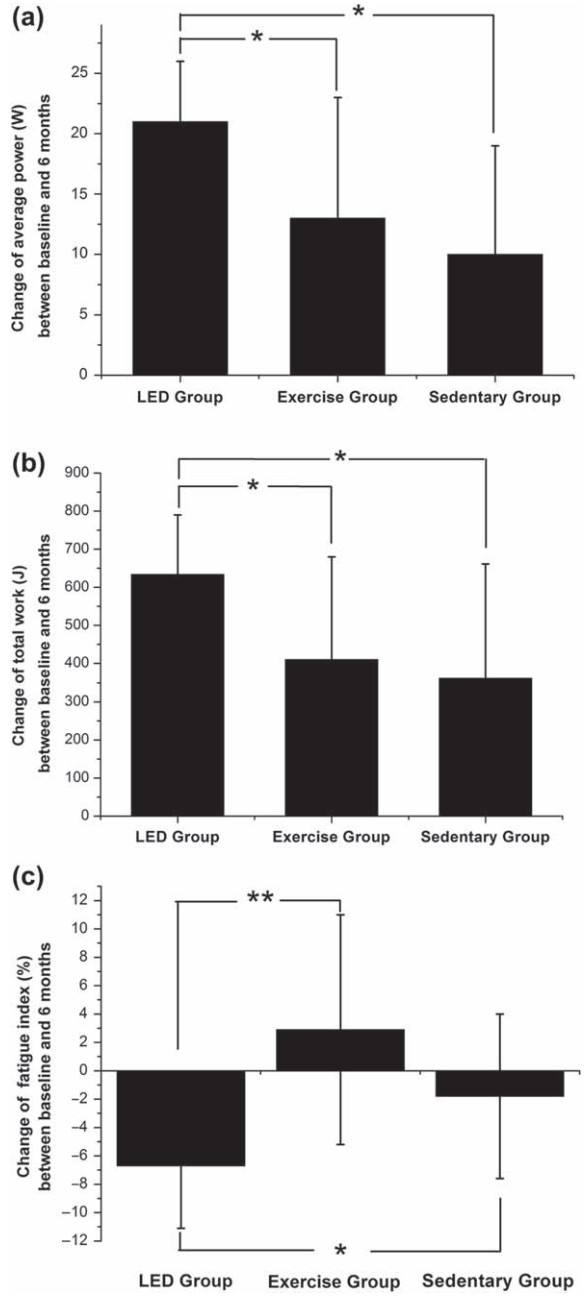

Figure 4 The gain of the quadriceps performance obtained by the groups. Results obtained for the average power (a) and the total work (b) are significantly higher for the LED group (21 ± 6 W and 634 ± 156 J) compared to the exercise group (13 ± 10 W and 410 ± 270 J) and the sedentary group (10 ± 9 W and 357 ± 327 J) in the change between baseline and 6 months. Results obtained for the fatigue index (c) are significantly lower for the LED group ($-7 \pm 4\%$) compared to the exercise group ($3 \pm 8\%$) and the sedentary group ($-2 \pm 6\%$) in the change between baseline and 6 months. The changes in the average power, the total work and fatigue index between baseline and 6 months show significant inter-group differences. *, Significant difference (one-way ANOVA, $p < 0.05$); **, significant difference (one-way ANOVA, $p < 0.01$)

during the 300°/s isokinetic assessment protocol, but not at the 60°/s protocol.

There were no significant changes in knee-extensor peak torque for all groups, when the isokinetic protocol at 60°/s was performed. Similar results were found in the study that investigated the immediate effects of infrared energy-emitting products (socks, T-shirts, bandages) activated before the exercise tests[18]. However, peak torque at 60°/s is an indicator of maximal muscle strength capabilities and requires the implementation of a strength training program to enhance this type of muscular performance[19]. The current investigation utilized an aerobic training program in conjunction with infrared-LED illumination. Thus, it is not entirely surprising that quadriceps performance was only improved during the isokinetic evaluation at 300°/s. The combination of infrared-LED illumination and strength training may elicit different outcomes.

The improvement of muscle performance in the LED group in the current study can also be explained by thermal effects[20]. The cutaneous temperature at rest (33.5 ± 0.5°C) increased by 1.08 ± 0.11°C during exercise with infrared-LED illumination. However, when exercise was performed without LEDs, there was a decrease in temperature of 0.86 ± 0.15°C[11].

In a study by Heinonen and colleagues[21], externally delivered local heating increased muscle blood flow in the lower legs due to vasodilation and warm blood shunted from the body's core to skin followed by a vasoconstriction response and heat release. Moreover, local heating enhanced nitric oxide release, ATP synthesis and tissue oxygen consumption[21].

We therefore believe that the higher circulation induced by local thermal effects can improve oxygen supply as well as transport and utilizes metabolic substrates (such as lactic acid), mainly when phototherapy is combined with the skeletal muscle pump during physical exercise, reducing muscle fatigue and increasing maximal exercise tolerance[10,20].

Similar results to those observed in the present study were obtained in animal studies as well. The effects of phototherapy, using lamp (780–1400 nm)[22] and laser (655 nm)[23], on the fatigue induced by a neuromuscular electrical stimulation showed an increased resistance to fatigue associated with a higher peak force and muscular work in rats. Moreover, when infrared-LED (850 nm) was applied after high-intensity resistance training in ovariectomized rats, there was an observed modulation of tumor necrosis factor (TNF-α) and interleukin-6, as well as enhanced anabolic activity by stimulating the production of insulin growth factor-1 (IGF-1), thereby increasing muscle volume. This is an important finding given the fact that muscle atrophy and reduced muscle function during aging are influenced by elevated levels of inflammatory cytokines, such as TNF-α, which may inhibit IGF-1 signaling with proliferative exhaustion of satellite cells[24].

Phototherapy with strength training appears to modulate some important skeletal muscle functions in young males as well[25]. Microarrays showed increased gene expression of mitochondrial biogenesis (peroxisome proliferative activated receptor-co-activator 1), protein synthesis (mammalian TOR) and tissue angiogenesis (angiogenic protein vascular endothelial growth factor) as well as reduced gene expression of protein degradation (muscle ring finger) and inflammation (interleukin-1β). These results suggest improved muscle repair and better muscle performance when phototherapy is applied[25].

High-intensity exercise training programs in postmenopausal women have shown beneficial effects on aerobic fitness, muscle function and bone structure[26–28], as also observed in the present study. However, the fatigue experienced by the exercise group was higher compared to that experienced by the LED group and was, surprisingly, also higher compared to that of the sedentary group. We found that twice-weekly, high-intensity physical training without infrared-LED was not sufficient to reduce fatigue. According to the recommendations of the American College of Cardiology/American Heart Association, older adults should perform moderate-intensity aerobic physical activity for a minimum of 30 min, most if not all days per week or vigorous-intensity aerobic activity for a minimum of 20 min, 3 days per week[12]. Thus, the amount of exercise training administered in the current study could have been greater. The metabolic stress induced by the physical exercise favors the actions of phototherapy, given that its effects are enhanced when the redox state of a cell is changed[29]. For this reason, we chose not to include a group receiving only infrared-LED during rest, given that it appears a training stimulus is needed to facilitate the positive effects of phototherapy.

Although electromyography and muscle biopsy were not performed in the current study, differences in percentage and/or recruitment of type I and II muscle fibers may have occurred between the groups. Infrared-LED may have improved muscle bioenergetics[8], mainly oxidative, with a higher percentage and/or recruitment of type I fibers that possess a higher resistance to fatigue. Moreover, although scores of pain were not evaluated, the women in the exercise group reported pain in the lower limbs and in the region of the lumbar spine during the treadmill training and isokinetic testing. At the same time, the women in the LED group reported that they were not feeling any pain. Phototherapy stimulates both anti-inflammatory[30] and analgesic[31] effects which can lessen pain in muscles and articulations, so that physical exercises can be performed with less hindrance, leading to an enhanced training effect. These subjective observations may also explain differences in fatigue amongst the groups. However, future studies should be performed to investigate potential mechanisms that may explain these observations as the effects of infrared radiation and physical exercise on pain, metabolic/inflammatory markers, characteristics of muscle fibers and fatigue, mainly because aging is associated with an inflammatory process and loss of motor units, resulting in atrophy and fiber type shifts, and thus resulting in increased fatigue and delayed onset muscle soreness.

The positive effects on quadriceps function observed in the sedentary group may have been influenced by an increased BMI, given that higher muscle mass/strength in the lower extremities can be precipitated by additional weight-bearing demands[32,33]. It became evident that, once the independent effects of body mass were controlled (i.e. normalized data), improvements in muscle performance in the sedentary group were no longer apparent.

This study has several limitations that warrant consideration. One of the limitations is the method for assessment of body composition; we only used bipolar electrical bioimpedance, which has an inherent degree of measurement error. Future studies should explore the results of body composition using other techniques that may provide better accuracy, such as whole body composition determined by dual-energy X-ray absorptiometry (DXA). However, DXA also shows limitations, such as the fact that calculations may not be accurate for separating bone and soft tissue or for separating soft tissue into fat and lean tissue at higher body masses[32,34]. Other limitations are the possible placebo effect and lack of blinding: the participants can probably assume that a new treatment will be better than a standard treatment and this may influence the results. However, blinding becomes less important in reducing observer bias, as the outcomes become less subjective, since objective (hard) outcomes leave little opportunity for bias, as gold-standard measurements[35]. In this context, the isokinetic dynamometer is considered a gold standard for measuring muscle performance, because the angular velocity is always controlled during articular movement and the force–velocity relationship does not affect muscle torque, work production or the muscle fatigue index[9,36]. Finally, the intensity applied in both training groups was based on the HR_{max} obtained during progressive exercise testing. Future studies should focus on intensity prescription based on the percentage of measured VO_{2max} or anaerobic threshold, because its accuracy could be better than the percentage of HR_{max} obtained.

Phototherapy is currently a common practice for physical therapy and dermatology, and the results of the current study create potentially new clinical application for phototherapy. Specifically, the current study demonstrates that phototherapy is a potentially promising complement to exercise training which may further enhance performance. Moreover, infrared radiation (e.g. 850 nm) appears to have no side-effects for the parameters employed. Therefore, marketed devices which emit infrared radiation, such as laser and LED, may be used before or after physical exercise with the intent of further increasing muscle performance in the clinical and athletic arenas.

CONCLUSION

Postmenopausal women who underwent an aerobic training program on treadmill with or without phototherapy showed an improvement in power and work of the quadriceps. However, infrared LED irradiation combined with treadmill training led to a higher increase in both quadriceps power and work. In addition, the number of contractions increased and fatiguability was only reduced in the LED group.

ACKNOWLEDGEMENTS

We would like to thank the Fundação de Amparo à Pesquisa do Estado de São Paulo, Conselho Nacional de Desenvolvimento Científico e Tecnológico and Coordenação de Aperfeiçoamento de Pessoal de Nível Superior for financial support. We also acknowledge the valuable technical assistance graciously provided by Ms. Juliana Cristina Milan (physical therapist), Ms. Isabela Verzola Aniceto (medical doctor) and Professor Nivaldo Antonio Parizotto, PhD (physical therapist).

Conflict of interest The authors report no conflicts of interest. The authors alone are responsible for the content and writing of the paper.

Source of funding The Fundação de Amparo à Pesquisa do Estado de São Paulo – Grant no. 98/14270-8, 2008/57858-9 and 2009/01842-0; Conselho Nacional de Desenvolvimento Científico e Tecnológico – Grant no. 573587/2008-6; and Coordenação de Aperfeiçoamento de Pessoal de Nível Superior.

References

1. Tanaka H, Seals DR. Endurance exercise performance in Masters athletes: age-associated changes and underlying physiological mechanisms. *J Physiol* 2008;586:55–63
2. Gorodeski GI. Update on cardiovascular disease in postmenopausal women. *Best Pract Res Clin Obstet Gynaecol* 2002; 16:329–55
3. Paillard T, Lafont C, Pérès C, *et al*. Is electrical stimulation with voluntary muscle contraction exercise of physiologic interest in aging women? *Ann Readapt Med Phys* 2005;48: 20–8
4. Machado A, García-López D, González-Gallego J, *et al*. Whole-body vibration training increases muscle strength and mass in older women: a randomized-controlled trial. *Scand J Med Sci Sports* 2010;20:200–7
5. Paolillo FR, Milan JC, Aniceto IV, *et al*. Effects of infrared-LED illumination applied during high-intensity treadmill training in postmenopausal women. *Photomed Laser Surg* 2011;29:639–45
6. Baroni BM, Leal Junior EC, Geremia JM, *et al*. Effect of light-emitting diodes therapy (LEDT) on knee extensor muscle fatigue. *Photomed Laser Surg* 2010;28:653–8

7. Baroni BM, Leal Junior ECP, De Marchi T, Lopes AL, Salvador M, Vaz MA. Low level laser therapy before eccentric exercise reduces muscle damage markers in humans. *Eur J Appl Physiol* 2010;110:789–96
8. Ferraresi C, Oliveira TB, Zafalon LO, *et al*. Effects of low level laser therapy (808 nm) on physical strength training in humans. *Lasers Med Sci* 2011;26:349–58
9. Vieira WHB, Ferraresi C, Perez SEA, *et al*. Effects of low-level laser therapy (808 Nm) on isokinetic muscle performance of young women submitted to endurance training: a randomized controlled clinical trial. *Lasers Med Sci* 2012;27:497–504
10. Paolillo FR, Corazza AV, Borghi-Silva A, *et al*. Infrared-LED applied during high-intensity treadmill training improved maximal exercise tolerance in postmenopausal women: a 6-month longitudinal study. *Lasers Med Sci* 2013;28:415–22
11. Paolillo FR, Borghi-Silva A, Parizotto NA, *et al*. New treatment of cellulite with infrared-LED illumination applied during high-intensity treadmill training. *J Cosmet Laser Ther* 2011;13: 166–71
12. Kemmler W, Bebenek M, von Stengel S, *et al*. Effect of block-periodized exercise training on bone and coronary heart disease risk factors in early post-menopausal women: a randomized controlled study. *Scand J Med Sci Sports* 2013; 23:121–9
13. Fletcher GF, Balady GJ, Amsterdam EA, *et al*. Exercise Standards for Testing and Training: A Statement for Healthcare Professionals from the American Heart Association. *Circulation* 2011;104: 1694–740.
14. Astrand PO. Maximal oxygen consumption in athletes. *J Appl Physiol* 1967;23:353
15. Fujibayashi M, Hamada T, Matsumoto T, *et al*. Thermoregulatory sympathetic nervous system activity and diet-induced waist-circumference reduction in obese Japanese women. *Am J Hum Biol* 2009;21:828–35
16. Pincivero DM, Gandaio CB, Ito Y. Gender-specific knee extensor torque, flexor torque, and muscle fatigue responses during maximal effort contractions. *Eur J Appl Physiol* 2003;89:134–41
17. Borghi-Silva A, Mendes RG, Toledo AC, *et al*. Adjuncts to physical training of patients with severe COPD: oxygen or noninvasive ventilation? *Respir Care* 2010;55:885–94
18. Kim J, Otzel D, Kim W, *et al*. Near infrared light and expectance effects on maximal isokinetic strength performance: a randomized, double-blind, placebo-controlled study. *J Strength Cond Res* 2006;20:378–82
19. Haèkkinen K, Kraemer WJ, Newton RU, *et al*. Changes in electromyographic activity, muscle fiber and force production characteristics during heavy resistance/power strength training in middle-aged and older men and women. *Acta Physiol Scand* 2001;171:51–62
20. Paolillo FR, Lins EC, Corazza AV, Kurachi C, Bagnato VS. Thermography applied during exercises with or without infrared light-emitting diode irradiation: individual and comparative analysis. *Photomed Laser Surg* 2013;31:349–55
21. Heinonen I, Brothers RM, Kemppainen J, Knuuti J, Kalliokoski KK, Crandall CG. Local heating, but not indirect whole body heating, increases human skeletal muscle blood flow. *J Appl Physiol* 2011;111:818–24
22. Abou-Hala AZ, Barbosa DG, Marcos RL, Pacheco-Soares C, Silva NA. Effects of the infrared lamp illumination during the process of muscle fatigue in rats. *Braz Arch Biol Technol* 2007; 50:403–7
23. Lopes-Martins RAB, Marcos RL, Leonardo OS, *et al*. Effect of low-level laser (Ga-Al-As 655 nm) on skeletal muscle fatigue induced by electrical stimulation in rats. *J Appl Physiol* 2006; 101:283–8
24. Corazza AV, Paolillo FR, Groppo FC, *et al*. Phototherapy and resistance training prevent sarcopenia in ovariectomized rats. *Lasers Med Sci* 2013 Jan 10. Epub ahead of print
25. Ferraresi C, Panepucci R, Reiff R, *et al*. Molecular effects of low-level laser therapy (808nm) on human muscle performance. *Phys Ther Sport* 2012;13[abstract]:e5
26. Chien MY, Wu YT, Hsu AT, *et al*. Efficacy of a 24-week aerobic exercise program for osteopenic postmenopausal women. *Calcif Tissue Int* 2000;67:443–8
27. Sheffield-Moore M, Yeckel CW, Volpi E, *et al*. Postexercise protein metabolism in older and younger men following moderate-intensity aerobic exercise. *Am J Physiol Endocrinol Metab* 2004;287:E513–22
28. Teomana N, Özcan A, Acar B. The effect of exercise on physical fitness and quality of life in postmenopausal women. *Maturitas* 2004;47:71–7
29. Sussai DA, Carvalho PTC, Ourado PM, *et al*. Low-level laser therapy attenuates creatine kinase levels and apoptosis during forced swimming in rats. *Lasers Med Sci* 2010;25: 115–20
30. Pallotta RC, Bjordal JM, Frigo L, *et al*. Infrared (810-nm) low-level laser therapy on rat experimental knee inflammation. *Lasers Med Sci* 2012;27:71–8
31. Djavid GE, Mehrdad R, Ghasemi M, Hasan-Zadeh H, Sotoodeh-Manesh A, Pouryaghoub G. In chronic low back pain, low level laser therapy combined with exercise is more beneficial than exercise alone in the long term: a randomised trial. *Aust J Physiother* 2007;53,155–60
32. Paolillo FR, Milan JC, Bueno P de G, *et al*. Effects of excess body mass on strength and fatigability of quadriceps in postmenopausal women. *Menopause* 2012;19:556–61
33. Wang MY, Flanagan SP, Song JE, *et al*. Relationships among body weight, joint moments generated during functional activities and hip bone mass in older adults. *Clin Biomech* 2006;21: 717–25
34. Aloia JF, Vaswani A, Ma R, *et al*. Comparative study of body composition by dual-energy x-ray absorptiometry. *J Nucl Med* 1995;36:1392–7
35. Schulz KF, Grimes DA. Blinding in randomized trials: hiding who got what. *Lancet* 2002;359:696–700
36. Drouin JM, Valovich-McLeod TC, Shultz SJ, *et al*. Reliability and validity of the Biodex system 3 pro isokinetic dynamometer velocity, torque and position measurements. *Eur J Appl Physiol* 2004;91:22–9

Design of high power LED-based UVA emission system and a photosensitive substance for clinical application in corneal radiation

Alessandro D. Mota*[1], André M. Cestari[1], André O. de Oliveira[1,2], Anselmo G. Oliveira[3], Cristina H. B. Terruggi[3], Giuliano Rossi[1], Jarbas C. Castro[2], João P. B. Ligabô[1], Tiago A. Ortega[1], Tiago Rosa[1]
[1]Opto Eletrônica S/A, 1071 Joaquim A. R. de Souza, São Carlos, SP, Brazil 13560-330;
[2]Instituto de Física de São Carlos, Universidade de São Paulo, 400 Trabalhador São Carlense, São Carlos, SP, Brazil 13560-970 ;
[3]Faculdade de Ciências Famacêuticas, Universidade Estadual Paulista, km1 Rodovia Araraquara – Jaú, Araraquara, SP, Brazil 14801-902

ABSTRACT

This work presents an innovative cross-linking procedure to keratoconus treatment, a corneal disease. It includes the development of an ultraviolet controlled emission portable device based on LED source and a new formulation of a photosensitive drug called riboflavin. This new formulation improves drug administration by its transepithelial property. The UV reaction with riboflavin in corneal tissue leads to a modification of corneal collagen fibers, turning them more rigid and denser, and consequently restraining the advance of the disease. We present the control procedures to maintain UV output power stable up to 45mw/cm^2, the optical architecture that leads to a homogeneous UV spot and the new formulation of Riboflavin.

Keywords: Ultraviolet LED, Cross-linking, Keratoconus, Riboflavin, Transepithelial, PID control system for LEDs, Close loop system for LED, UV based Optical system.

1. INTRODUCTION

Corneal collagen cross-linking (CXL) has introduced a promising alternative to Keratoconus treatment[1]. The keratoconus is an ectatic, non-inflammatory, progressive disease that causes corneal tissue structure weakening, leading to a conical shaped cornea, therefore loss of visual acuity (progressive myopic visual impairment and irregular astigmatism). Statistically, the incidence of this disease is between 20 and 230 per 100.000[2]. In recent years, cross-linking has been considered an alternative method to keratoconus stagnation, and can avoid cornea transplantation or introduction of contact lenses. Wollensak et al. have established the conventional treatment protocol, which is divided in two stages: Riboflavin administration and UV light exposure. This technique consists in administration of photosensitive substance called Riboflavin (solution of vitamin B2) to enhance the UV absorption in the cornea. The application of riboflavin drops is done every two minutes for 30 minutes (pre-soak time). The epithelium, membrane that covers the cornea, is removed in order to allow penetration of Riboflavin into the cornea in a region called stroma. After this, cornea is subjected to a low power density of UV, 3 mW/cm^2 for 30 minutes, resulting in a total dose of 5.4 J/cm^2. Interaction between riboflavin and UV light induces the formation of more bonds among adjacent collagen molecules, which modifies corneal structure by making it more rigid and denser. Therefore, the result is a less susceptible cornea to shape modification, avoiding the keratoconus advance.

Recently, the procedure to reduce the time of treatment by increasing the power density on corneal tissue, called accelerated procedure, has been investigated by doctors. Chew[3] presented that the same clinical results can be achieved by reducing the total time of UV exposure by increasing the power density to match with well-known energy dose of 5.4 J/cm^2. He got reports of doctors who are practicing the accelerated procedure with their patients, and they are confident that this technique is worthy and efficient. Ronald R. Krueger[4] has shown that short time treatment can provide same corneal strengthening as lower powers over longer time periods, or there is no statistically significant biomechanical difference in both cases. John Mashal[5], conducted an experiment of UV exposure to measure the effects on human endothelium cells, the deeper membrane in corneal tissue, which has to be preserved. He showed that viability of the cells did not show significant difference between low or high irradiance and was not cytotoxic to human endothelium

Fourteenth International Conference on Solid State Lighting and LED-based Illumination Systems
edited by Matthew H. Kane, Jianzhong Jiao, Nikolaus Dietz, Jian-Jang Huang, Proc. of SPIE Vol. 9571, 95710X · © 2015 SPIE · CCC code: 0277-786X/15/$18 · doi: 10.1117/12.2187265

cells. Additionally, Sliney[6] made a study of safety in accelerated cross-linking procedure offered by Avedro[7] relating corneal absorption dose of UV with depth of corneal tissue. In accelerated procedure, the pre-soak time duration, time that corneal is under Riboflavin presence before UV exposure, is shorter than conventional procedure, resulting in quite same dose of UV absorption in region nearby endothelium. It leads to conclusion that accelerated procedure is as safe as the conventional procedure.

The equipment presented in this work was developed to attend the standard and accelerated well-known established protocols applied in CXL Keratoconus treatment. It is a portable type A ultraviolet emission device with peak wavelength at 365 nm and output power density up to 45 mW/cm^2. This power let the procedure duration shorter, and can be theoretically performed in 2 minutes. It is composed of a UV illumination source attached to a special set of lenses and mirrors to project the light on the patient's cornea. Such light projection has uniform power distribution and homogeneous light density in the illuminated area. In addition, a red light source is coupled into the system to indicate to the doctor the focus of the optical system. An electronic system will be responsible to control light emission and is composed of a microcontroller circuit connected to a power control loop with feedback and a current driver. The critical point of this system is to maintain a constant light output for treatment and achieve a high level of optical efficiency capable to provide 45 mW / cm^2 at the output. This system results in constant output power and in uniform power distribution, with less than 10% of variation in both cases.

Additionally, Anselmo Oliveira presents new studies intending to eliminate the necessity to remove the corneal epithelium to permit Riboflavin penetration in cornea. He proposes the development of a solution that consists in the incorporation of the hydrophilic riboflavin in a system with nanometric dimensions, as the nanoemulsion, which combines the properties of bioadhesion and permeability increasing, to allow the riboflavin permeates through the epidermis of the cornea and fixes in stroma. Although he presents good results, the pre-soak time duration was too long for treatment purpose. A new formulation of the nanostrctured riboflavin was created and is presented in this work, and the main goal is to make possible the reduction of penetration time duration in CLX treatment procedure.

Finally, this work is divided as follows: section 1 is the introduction; the UV LED system device and the nanoemulsion of riboflavin are in section 2; the results obtained with the created control system and the formulation of new riboflavin are in section 3; conclusions are in section 4.

2. METHODOLOGY

2.1 Accelerated Cross-linking

The technique proposed by this work is already being applied by international companies such as Avedro[7] and doctors as Ronald R. Krueger[4]. Accelerated cross-linking consists in reducing the time of ultraviolet radiation application by increasing the power dose and keeping the same total treatment energy (5.4 J/cm²). The UV emission device developed in this work has output power enough to reduce the application time up to 2 minutes by setting output power to 45 mW/cm^2. The procedure consists in three steps. First, scrapes or flaps are made on corneal epithelium to permit riboflavin (photosensitive solution of vitamin B12) to penetrate in internal corneal tissue called stroma. Figure 1 shows the membranes involved on treatment. After some days the epithelium is naturally recomposed. Second, drops of riboflavin are dispensed on corneal surface every 5 minutes during a period of 10 to 30 minutes (time dependent of UV power). This time is called pre-soak time, which is suggested by recent researches to be of 10 minutes using a power of 30 mW/cm² [8-10]. Third, the cornea is exposed to ultraviolet light (4 minutes irradiation with 30 mW/cm^2, 365 nm UVA). Additionally, there are no treatment tests with a higher dose, but it is supposed that doctors will come up with new studies using shorter time application, as the new machine developed in this work is able to offer higher power. Furthermore, the procedure will use a new formulation of riboflavin that is based in nanoemulsion platform (riboflavin-5-phosphate), which does not demand removal of the corneal epithelium during pre-soak time. This application is called transepithelial. The advantages of using the accelerated cross-linking in junction with the transepithelial riboflavin are as follow: fast procedure, most patients can be treated; low risk of infection because of epithelium is not removed; painless procedure; quick recover of the patient; the procedure can be performed out of operating room because there is no surgical intervention (low treatment cost).

Figure 2 presents the simulation of UV procedure. Figure 2–A shows the corneal flaccid shape and weak bonds in collagen fibers of the cornea; Figure 2-B shows the pre-soak procedure, in which drops of riboflavin are dispensed on corneal tissue; Figure 2-C shows the UV light emission on corneal surface, which is responsible to create more bonds in collagen fibers and make corneal tissue more rigid; Figure 2-D shows the result of treatment, more bonds were created in cornea tissue, it is more rigid and denser, thus is less susceptible of shape changes (it avoids the advance of keratoconus).

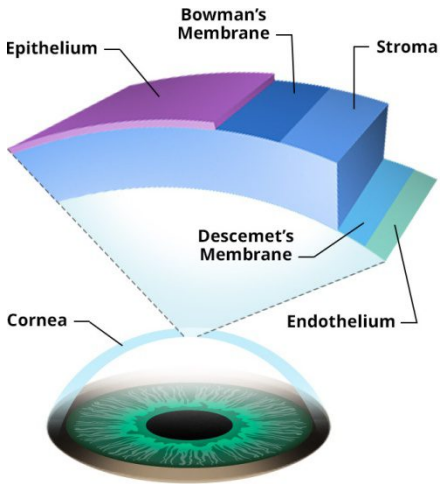

Figure 1. Corneal tissue structure[11].

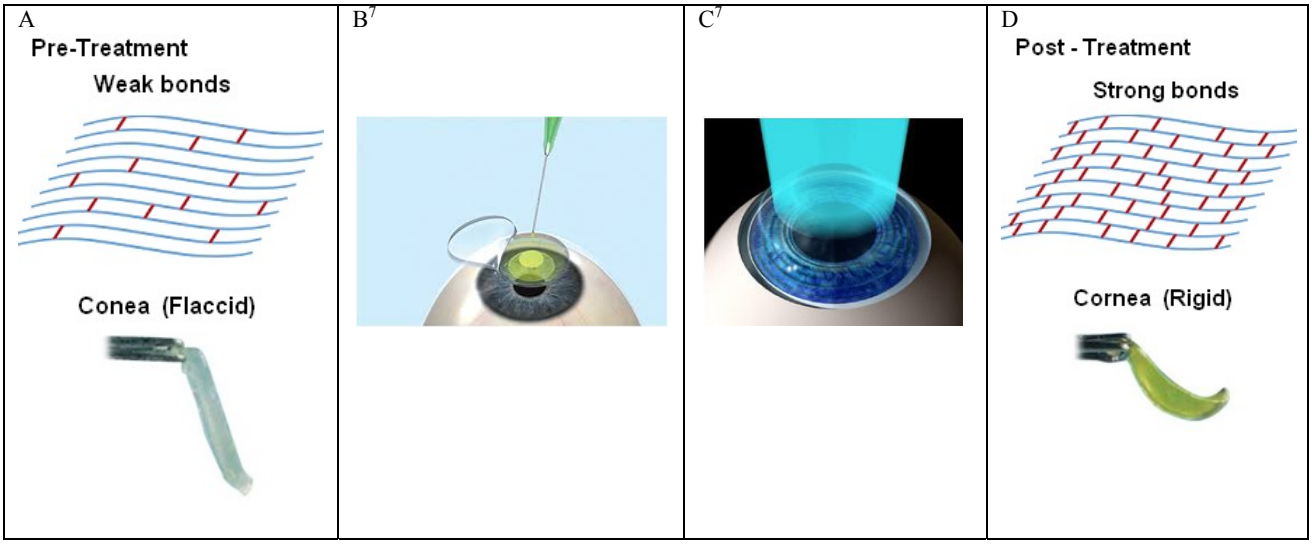

Figure 2. Illustration of cross-linking procedure. A – Cornea state before UV radiation, presents weak bonds in collagen fibers, flaccid shape; B – Epithelium removal and drops of riboflavin disposal; C – Application of UV homogenous radiation; D – Cornea state after treatment, presents stronger bonds in collagen fibers and a rigid shape.

2.2 Optics System

As formerly discussed, treatment requires a homogenized beam to be delivered in order to avoid hot spots which may lead to localized sub-threshold irradiation, causing some areas to become more flaccid then others, which may lead to development of a localized Keratoconus. An UV illumination system was designed based on LED as showed in Figure 3. Light from an UV LED with peak wavelength at 365 nm is focused first at surface 1, where a diaphragm is placed to

limit rays that go through it. This diaphragm controls beam size delivered at focal plane, illuminating patient's eye with top-hat beam of 6, 8 and 10 millimeters of diameter. As the user changes the aperture of the iris, power delivered by the LED is electronically balanced to maintain a constant power density at focal plane. Figure 4 shows the simulated power distribution on focal plane for beam size of 10 mm.

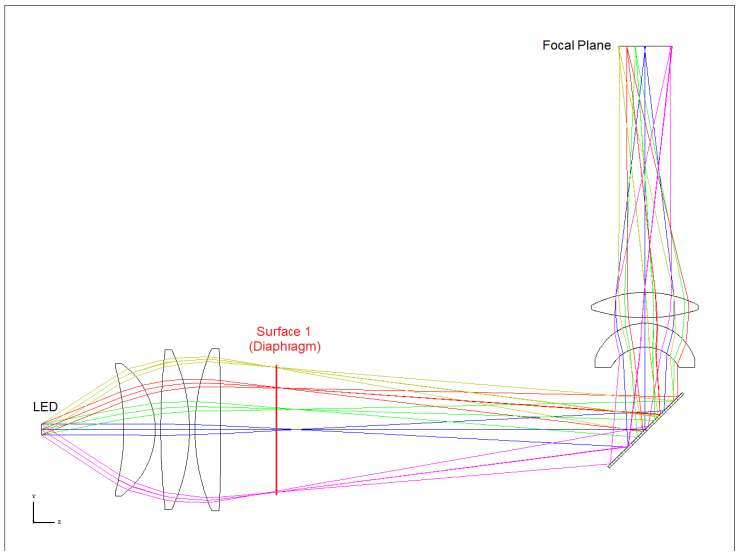

Figure 3. 3D Layout of optical design (obtained from ZEMAX®).

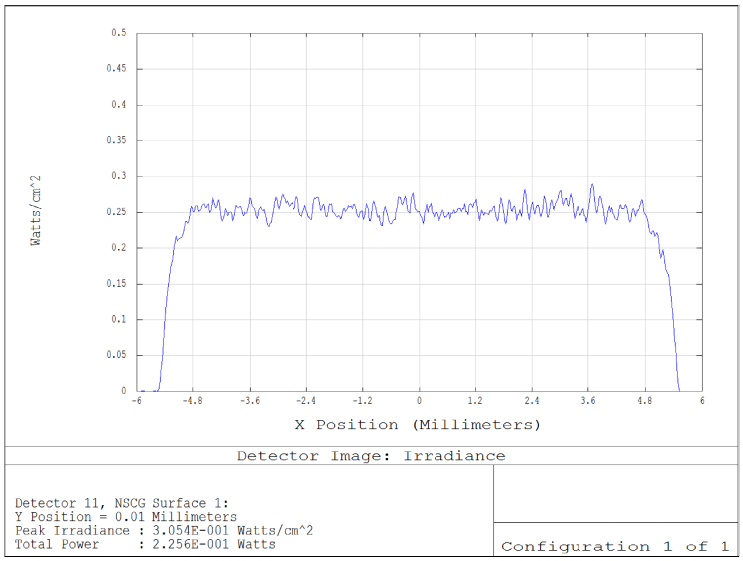

Figure 4. Focal plane simulation (obtained from ZEMAX®).

2.3 LED power Control system

Figure 5 shows the block diagram of the entire electronic control system. The opto-electronic equipment consists of one UV LED source (365 nm), one optical system projection that carries the UV light to patient's cornea with homogeneous power distribution and a microcontrolled electronic system for output power and time duration control. The controller is a system which aims to generate a desired output signal from a reference signal at the input. It is defined as a causal dynamic system, since the output depends not only on entry into the present moment, but also on the entry at the previous instant. There are two types of controllers: open and closed loop system. In the open loop system, the controller is basically an actuator using the reference for the desired response. The output does not affect the input reference. On

the other hand, the closed loop system uses sensors for measuring and adjusting the current output by changing the reference value to obtain the desired output. The sample of output signal is called feedback[12]. The controller used in this work is a closed loop system called PI (Proportional - integrative). The proportional gain allows signal stability for high frequency responses. This ensures that in fast response, a short rise time (milliseconds), the system remains stable. The integrative term guarantees that the average error (steady-state error) is close to zero, or the difference between the reference signal and the desired output tends to zero[13]. The presented control system has two PIs, PI1 in software, and PI2 in hardware, and they are connected in a cascade configuration. The current sensor (precision resistor), LED current driver, which is based on Mosfet current source[14], and PI2 are part of the current control loop. It guarantees that the LED current is auto-adjusted proportionally to the difference of current reference signal in the control loop input and the instantaneous current read by precision resistor. The photodiode and microcontroller with PI1 are part of power control loop. PI1 keeps output power constant by changing the current reference in PI2 input proportionally to any variation of output power read from photodiode. It avoids output power fluctuations due to non-linearity effects in LED or any loss of irradiance efficiency during its lifetime. The result of this topology is a linear and proportional relation between the power references from the microcontroller to the output power of the optical system. The PI1 digital controller obeys the sequence of equations (1), (2), (3), and (4), which are programmed in an eight bits microcontroller. It is divided in calculating the error between set power and the read power in (1), calculating the proportional portion of the controller in (2), calculating the integrative portion in (3) and summing the two responses to obtain the current reference, RefPot, to load the PI in hardware in (4). The performance of the controller is calibrated by *Kp* and *Ki* constants to operate in a stable state (no oscillations), without overshoot, minimum steady error, and fast responses (short rise time)[12]. The graphic on Figure 5 illustrate these signal quality parameters (Y(t) is normalized to output steady-state power). It is important to note that it was not necessary to use the derivative term of PID, as this term is responsible to enlarge the frequency response of the controller, and LED does not demand large frequency bandwidth.

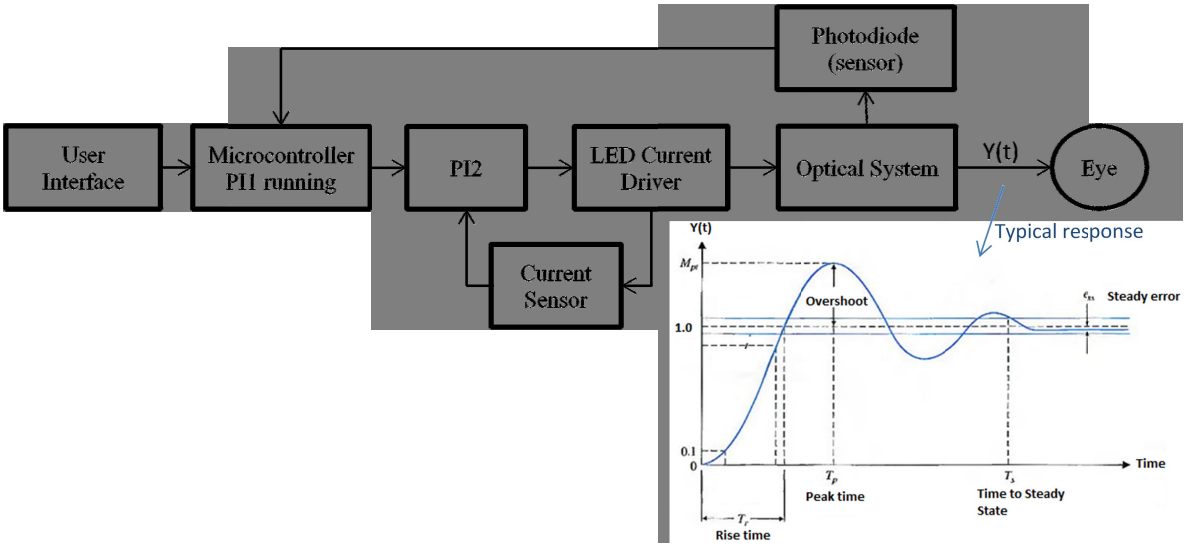

Figure 5. Block Diagram of Control Loop System.

$$Err = Pot - Pot_{365} \quad (1)$$

$$Prop = Err * Kp \quad (2)$$

$$Int_1 = Err * Ki + Int_0 \quad (3)$$

$$Ref_{Pot} = Prop + Int_1 \quad (4)$$

For equations (1) to (3), *Err* is the difference between output power set and read, *Pot* is the output power set, Pot_{365} is the LED output power read, *Prop* is the proportional term of controller PI, *Kp* is the proportional constant of PI, Int_1 is

current integrative term of PI, *Ki* is integrative constant of PI, Int_0 is the integrative term of the last interaction, and Ref_{Pot} is the resulting current reference[15].

2.4 Riboflavin-Nanostructured

The standard protocol of CXL proposed by Wollensak et al.[1] recommends removing the corneal epithelium before treatment to allow the penetration of riboflavin into the stroma. Experimental and clinical research has shown that the intact epithelium does not block the effects of ultraviolet light (UVA)[16], but reduces the effectiveness of treatment by altering adequate diffusion of riboflavin into the stroma[17]. However, epithelium removal causes risks and can increase the frequency of infections in the cornea, opacity, scars and infiltration[18-20]. Moreover, it can cause pain, photophobia and delayed visual rehabilitation. In a previous project, Anselmo et al. evaluated the stromal penetration of riboflavin phosphate in nanoemulsion biocompatible formulation, using intact rabbit corneas. Although the absorption of nanoemulsion riboflavin phosphate was similar to the standard technique of cross-linking with epithelium removal, the time of penetration was too large, around 120 minutes[21].

Among technological possibilities, pharmaceutical formulations based on nanotechnology platform constitute an innovative way to facilitate penetration of riboflavin through the corneal epithelium. The standard riboflavin solution (10 mg riboflavin-5-phosphate / 10 ml 20% dextran T-500) has hydrophilic characteristics which do not allow adequate diffusion through the corneal epithelium. Considering the physico-chemical properties of riboflavin base and riboflavin phosphate, they do not have the ability to permeate into the stroma. Due to lipophilic characteristic of corneal epithelium, riboflavin base interacts with the corneal epithelium and do not properly permeates into the stroma. Moreover, due to the riboflavin phosphate characteristic of hydrophilicity and anionic character, it is repelled from the surface of the cornea and riboflavin do not sufficiently permeate into the stroma. Thus, a technologically feasible delivery system involves incorporation of the hydrophilic riboflavin in a system with nanometric dimensions, as the nanoemulsion, which combines the properties of bioadhesion and permeability increasing, so as to allow the riboflavin to permeate through the corneal epidermis (lipophilic) and secure the stroma (hydrophilic). Thus, the bioadhesive property of the vehicle will allow the hydrophilic riboflavin have an intense contact with the surface of the cornea and increase the permeability of riboflavin. It will allow the passage through corneal tissue, with retention in the stroma, as the corneal endothelium also has lipophilic character. The main goal with this new formulation is to achieve proper concentration of riboflavin in stroma by not demanding hours of pre-soak time.

3. RESULTS

3.1 Control system

The embedded electronic was developed and assembled with all the principles shown earlier (Figure 5) in the UV LED console in order to evaluate the performance of the optics and control system. The embedded control software was developed in the same way as shown in equation 1 to 4. To evaluate the control system process, the LED control system was turned on and output power and LED current wave forms were collected by an oscilloscope. It is possible to analyze the behavior of the LED current and light output power during the transitory and steady-state regime and verify if the control system response time is capable to produce rise time of milliseconds and no oscillations. If the rise-time of the pulse is too long when compared to the pulse duration, the delivery energy will be reduced to values that will not produce the desired therapeutic effects. Due to cross-linking procedure establishment pulse duration of 30 minutes, or accelerated going to 10 minutes, rise time response in milliseconds is fast enough to do not compromise total energy density of treatment.

Figure 6 shows three different power responses of the LED control system. Chanel 1 of oscilloscope is the LED current read by precision resistor sensor, and channel 2 is the LED power output read by photodiode. The current relation in the sensor circuit is 23 V / 1 A, and the power relation in photodiode circuit is 0.133 V / 1 mW. *Graph A* is the power response to a set point value of 5 mW, g*raph B* is the power response to a set point value of 15 mW, and *Graph C* is the power response to a set point value of 36 mW. The responses are stable, no overshoot (current obeyed a smooth crescent ramp in the initial process), there is short rise time, and less than 10% of steady-state error. This parameter is important because the LED device is a medical equipment, and is supposed to attend IEC 60601-1 and IEC 60602-2-22 standards, which limit LED power output variations up to 20%.

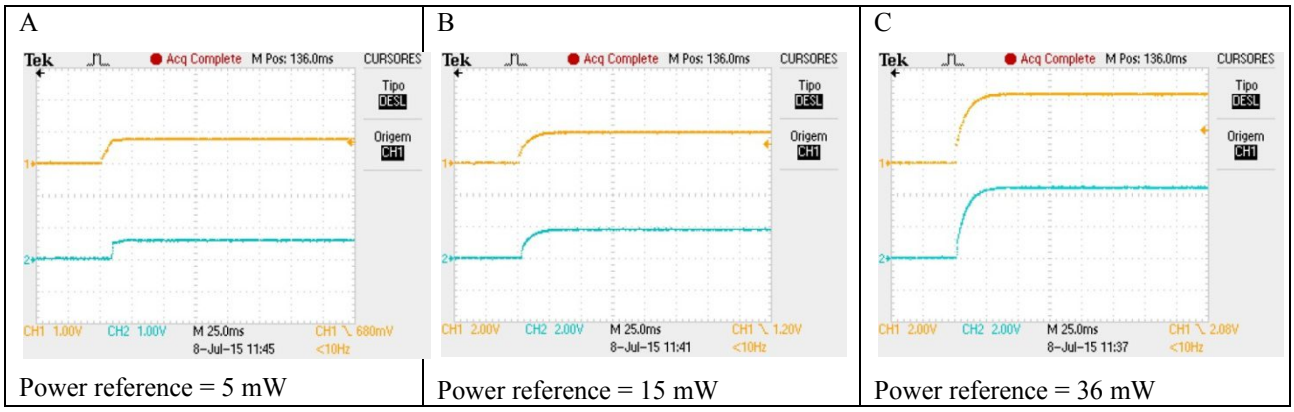

Figure 6. Laboratory power and current behavior of LED. Stored in oscilloscope Tektroniks TDS2024B.

Table 1 presents the final LED control system calibration performance, listing main parameters in different output power setting. The measures cover the output power range of the UV LED device. It is clear the linearity of set power to the output power, even though the LED current to power output is non-linear. It proves the effect of the power control loop system. Figure 7 shows the output power by LED current. Maximum power was set to 36 mW because it corresponds to 45 mW/cm^2 with a beam diameter of 10 mm. One interesting point is that the maximum power was achieved by running the LED with 190 mA. It is lower than the recommended work current of 500 mA on datasheet[22]. Then, if new researches demand more power, this device is ready to provide.

Table 1. Output power performance of UV LED control system. Power was measured by the power meter Coherent FiledMaxII TO and power head model PS19Q.

Power Set (mW)	Power Read (mW)	Steady-State error (%)	Rise-time (ms)	LED Current (mA)
1.00	1.00	0	10	26,96
5.00	4.90	2.04	15	34.78
15.00	15.60	3.85	25	86.96
25.00	26.60	5.30	28	130.45
36.00	38.00	5.26	30	187.84

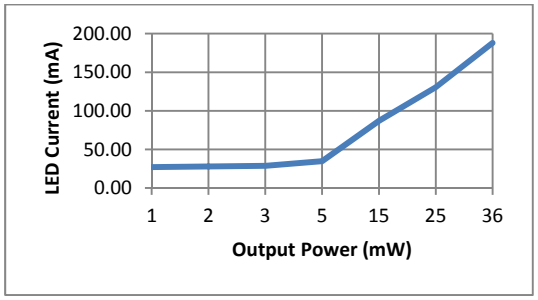

Figure 7. LED current versus Cross-linking device output power.

3.2 Optical system

The LED radiant flux at maximum output power of cross-linking device, for 187.84 mA, is 169 mW (0.9 mW/mA), data from LED datasheet[22]. It enables to measure the system efficiency (output flux/input flux) taking in account the power losses in the optical system, LED divergence and Joule effect in LED semiconductor. If the system delivers 36 mW @ 187.84 mA, and LED is emitting 169 mW, the efficiency is 21%, which is not an issue, as the LED works in a light current regime to obtain the desired output power.

Beam shape at focus plane is the most important characteristic imposed by the optical system. It has to present a homogeneous power distribution at the illuminated area to create an equal cross-linking effect at the entire corneal tissue. Figure 8, Figure 9 and Figure 10 present power distribution at focus plane got by beam analyzer Beamage Focus1 of GentecEO. They show that beam area has less than ±10% of power variations at average line of beam power. This work considered the standard applied in lasers (IEC 60601-2-22) for approval beam homogeneity, because it is also applied to high power LED medical devices. Variation less than ±20% of average power is acceptable to lasers devices. There are some not continuous points at image because of dead pixels on CCD sensor.

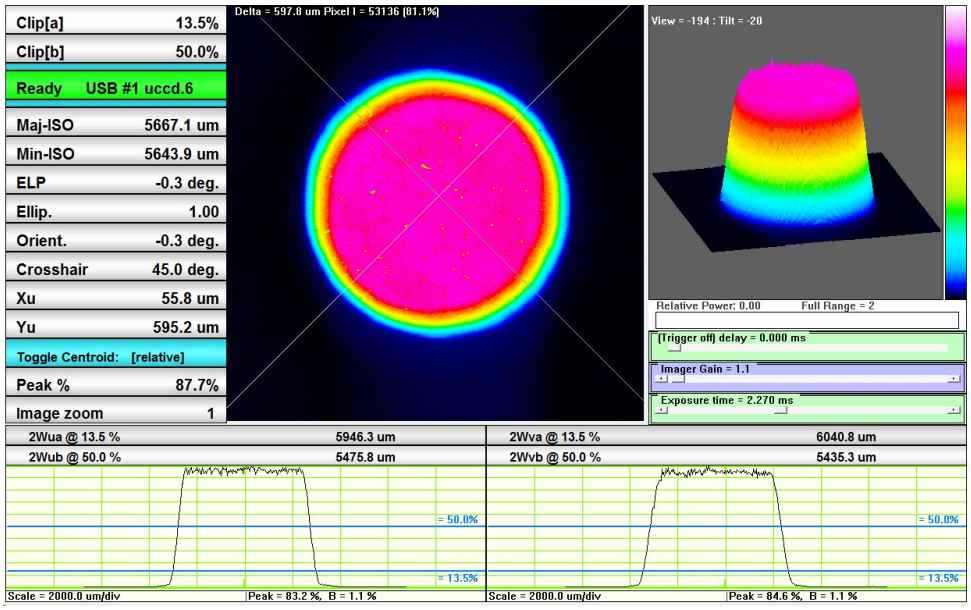

Figure 8. UV beam shape at focal plane, spot of 6 mm.

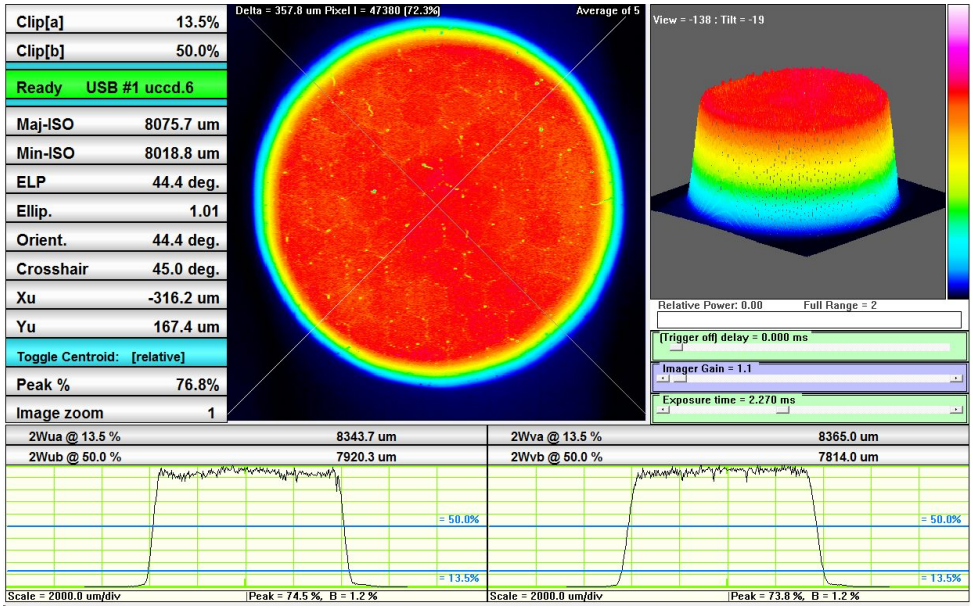

Figure 9. UV beam shape at focal plane, spot of 8mm.

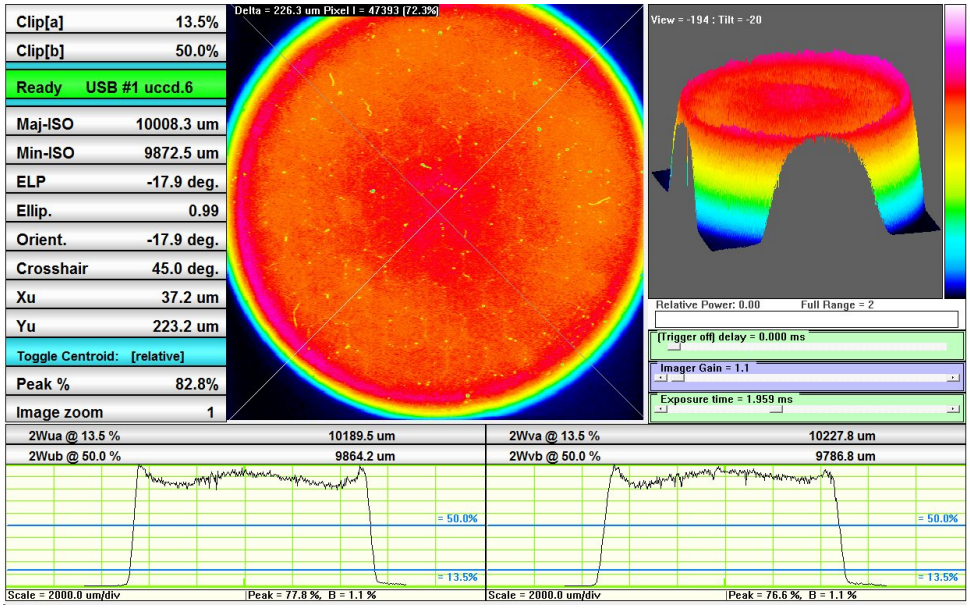

Figure 10. UV beam shape at focal plane, spot of 10 mm.

3.3 Cross-linking device

Figure 11 shows a picture of the Cross-linking console assembly. The optical system is placed inside a 3D plastic prototype, all optics are mounted inside machined aluminium mounts, electronic circuit and display are connected out of the console prototype. All tests were done using this assembly, which will pass through engineering process to turn into a final product to be manufactured soon by Opto Eletronica SA. Figure 12 shows the optical system of UV light and the red color crosshair aiming beam to guide doctor in aiming the beam on patient's cornea. Figure 13 shows the design of the device that will be produced and its commercial name is Opto XLink.

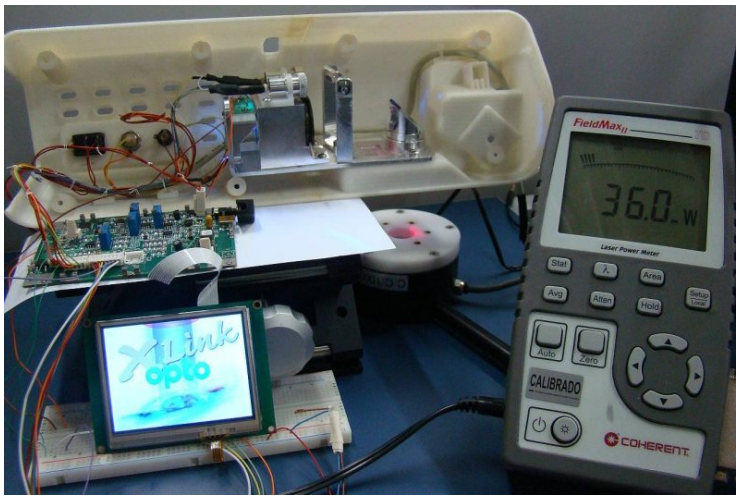

Figure 11. Cross-linking device assembly.

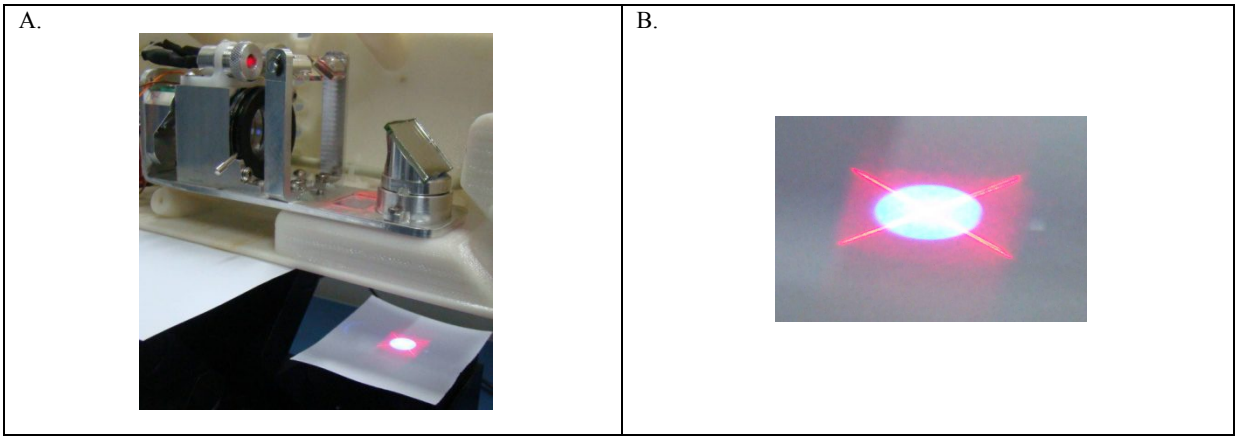

Figure 12. A - Prototype of the UV optical system. B – Details of the focal plane of aiming beam and UV light.

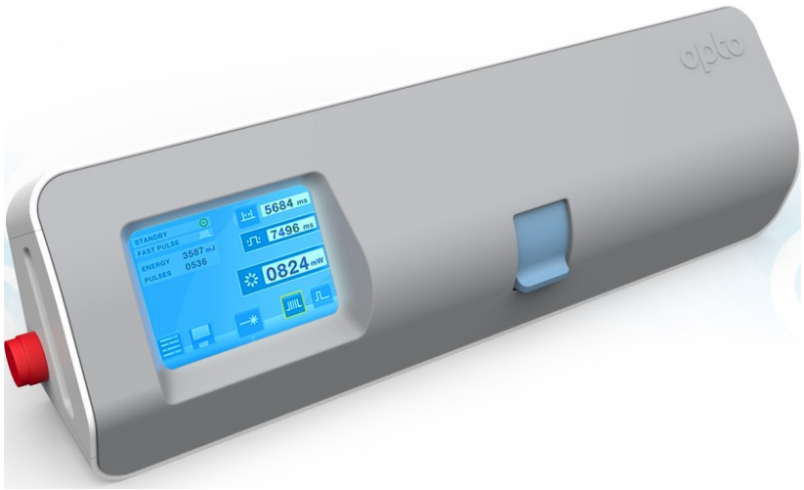

Figure 13. Opto XLink prototype design.

3.4 Riboflavin

The base formulation contains riboflavin phosphate 1%, soy phosphatidylcholine, nonionic surfactant, cationic surfactant, block copolymer and saline (Table 2). For the systems preparation, the samples were irradiated with ultrasound, in sonication tubes for 12 minutes in a batch regime with an irradiation time of 1 minute and 30 seconds, using amplitude 8. The determination of the hydrodynamic diameter and zeta potential were performed using the Zetasizer (Malvern Instruments) equipment[23]. Apparent viscosity measurements were performed with a rheometer[24].

Regardless of the ratio of lipid, the nanoemulsion showed rheological profile material and thixotropic non-Newtonian, but the viscosity decreases with shear rate. However, the relaxation of the shear rate leads to a viscosity recovery time dependent, which provides a superior viscosity profile at shear return to the initial situation. It was also found that increasing the proportion of the lipid in nanoemulsion resulted viscosity values higher than the lowest concentration (Figure 14), although it has not caused changes in the rheological. The maximum values for the zeta potential were about 32.5 and 36.5 mV (Table 3), and constant concentration of the block copolymer shows excellent stability of the colloidal dispersion. However, these values decrease to about 19 mV by increasing copolymer concentration, and it demonstrates that the PLU adhered on the surface of oil phase droplets, leaving their polyethylene chains exposed on the surface, causing an impediment to the approach of scattered ions in the medium and decreasing the reading surface potential (Table 3).

Table 2. Formulation of nanoemulsion of riboflavin phosphate

Constituent	Proportion
Soy phosphatidylcholine (SPC)	12%
Medium chain triglyceride (MCT)	5-10%
Block copolymer (PLU)	0,4-0,8%
Riboflavin phosphete (RP)	0.5%
Water for injection q.s.p.	100

Table 3. Results of zeta potential and hydrodynamic radius of nanoemulsion riboflavin phosphate

Samples (%)	Zeta potential (mV)	Hydrodynamic radius (nm)
CMT 5 + PLU 0,4	36.40	41.50
CMT 10 + PLU 0,4	32.56	41.90
CMT 5 + PLU 0,8	19.30	35.76
CMT 10 + PLU 0,8	18.80	35.81

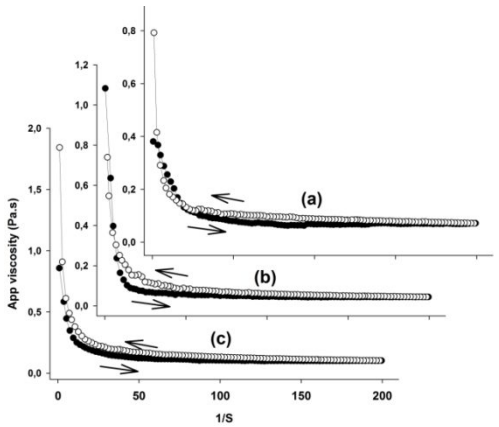

Figure 14. Rheological properties of nanoemulsion riboflavin phosphate. (a) Empty nanoemulsion. (b) nanoemulsion with 5% of CMT. (c) nanoemulsion with 10% of CMT.

4. CONCLUSION

The present work showed the implementation of a controlled UVA LED based optical system device and the formulation of a new riboflavin. Equipment and drug are designed to treat especially Keratoconus disease on corneal tissue, the first lens of human eye, by a process called cross-linking. The equipment aimed at accelerating the treatment time by increasing the power density and keeping the well-known energy dose of 5.4 J/cm^2 by reducing exposure time. Additionally, riboflavin is incorporated in a system with nanometric dimensions, nanoemulsion, which combines the properties of bioadhesion and permeability increasing, so as to allow the riboflavin permeate through the corneal epidermis and to be kept in the stroma. This procedure tends to be faster, it has less infection risk, it is a painless procedure and offers a quick recovery to the patient.

The optical system developed proved to be very efficient in delivering a homogeneous power distribution on focus plane. The variations observed are less then ±10% of average flux power, which complies with laser and high power LED standard IEC 60601-2-22. Therefore, the entire treating corneal area will receive the same radiation, resulting in equally collagen fibers bonds enlargement, which arise in a better treatment.

The power control system showed to be very efficient in controlling the LED output power. It has achieved the output power specification of 45 mW/cm^2 at a current below LED limit. The architecture of hardware and software controllers

in cascade resulted in increased output power velocity readings, pulse operation in steady-state regime, without overshoot and fast responses. When the UV light output reaches stability, the steady-state error is less than 10%. This rise-time value of 30 milliseconds, in worst case, denotes an insignificant loss of energy during entire treatment that takes minutes, and is perfectly acceptable by laser standard.

The device prototype had excellent performance to guarantee the mechanical distances between the lens involved and stability during the use. Additionally it has a portable and light design, which makes the transportation and set up easy to end user.

The riboflavin-nanostructured was developed and the first quality parameters were measured like zeta potential and rheological parameters. The results showed that the nanoemultion will have good bioadhesion to corneal surface and that it is ready to start the studies in rabbit's corneas. These studies will be carried out in partnership with Unifesp (Universidade Federal de São Paulo), which will receive one XLink prototype and samples of riboflavin to advance with riboflavin development.

ACKNOWLEDGMENT

The authors thank Opto Eletrônica S.A. and the Brazilian research and project financing FAPESP, for the financial support for this project.

REFERENCES

[1] Wollensak, G., Spoerl, E. and Seiler, T., "Riboflavin/ultraviolet-a-induced collagen crosslinking for the treatment of keratoconus," American Journal of Ophthalmology 135(5), 620-627 (2003).
[2] Schirmbeck, T., Paula, J. S., Taranta Martin, L. F., Crósio Filho, H., and Romão, E., "Eficácia e baixo custo no tratamento do ceratocone com o uso de lentes de contato rígidas gás-permeáveis," Arq Bras Oftalmol 68 (2), 219-222(2005).
[3] Chew, J., "Strengthen cornea in 11 minutes," The Straits Times, May 03, 2012.
[4] Krueger, Ronald R., Spoerl, E. and Herekar, S., "Rapid vs standard collagen CXL with equivalent energy dosing," Proc. 3rd International Congress of Corneal Collagen Cross-Linking, (2007).
[5] Jaycock, P.D., Lobo, L., Ibrahim, J., Tyrer, J. and Marshall, J., "Interferometric technique to measure biomechanical changes in the cornea induced by refractive surgery," Cataract & Refract Surgery 31(1), 175-184(2005).
[6] Sliney, D.H., and Wolbarsht, M.L., "Safety with LASERS and other optical sources", Plenum Publishing Corp, New York, (1980).
[7] Avedro Inc, "Implications of New Absorption, Diffusion and Scattering Coefficients for Corneal Cross-linking with Riboflavin", Clinical update & Reserch news 1, 1(2012).
[8] Kanellopoulos A.J., "Long term results of a prospective randomized bilateral eye comparison trial of higher fluence, shorter duration ultraviolet A radiation, and riboflavin collagen cross linking for progressive keratoconus," Clinical Ophthalmology 6, 97–101(2012).
[9] Touboul D., Efron N., Smadja D., Praud D., Malet F. and Colin J., "Corneal confocal microscopy following conventional, transepithelial, and accelerated corneal collagen cross-linking procedures for keratoconus," Refractive Surgery 28(11), 769–776(2012).
[10] Gatzioufas Z., Richoz O., Brugnoli E. and Hafezi F., "Safety profile of high-fluence corneal collagen cross-linking for progressive keratoconus: preliminary results from a prospective cohort study", Refractive Surgery 29(12), 846-848(2013).
[11] Trattler, W., "Corneal crosslinking for Keratoconus and LASIK complications," All about vision, May 2015,<http://www.allaboutvision.com/conditions/corneal-crosslinking.htm> (10 July 2015).
[12] Dorf R.C., [Modern Control Systems], 9th Ed. Prentice-Hall, 174-370 (2001).
[13] ELLIS, G., [Control System Design Guide], 3rd Ed. Elsevier, (2004).
[14] Sedra A. S. and Smith, K. C., [Microeletrônica], 5th Ed. Pearson Prentice-Hall, 141-579(2007).
[15] Mota, A. D. and Paiva, M. S. V., "Design of micro-second pulsed laser mode for ophthalmological CW Self-Raman laser," Proc. Spie Photonics West. Vol. 7912, 79121Y1 (2011).
[16] Bottos, K.M., Schor P., Dreyfuss J.L., Nader H.B. and Chamon W., "Effect of corneal epithelium on ultraviolet-A and riboflavin absorption," Arq Bras Oftalmologia 749, 348-351(2009).

[17] Bottos, K.M., Dreyfuss J.L., Regatieri C.V. et al, "Immunofluorescence confocal microscopy of porcine corneas following collagen cross-linking treatment with riboflavin and ultraviolet A," Refractive Surgery 24, 715-719 (2008).
[18] Kymionis, G.D., Bouzoukis, D.I., Diakonis, V.F., Portaliou, D.M., Pallikaris, A.I. and Yoo, S.H., "Diffuse lamellar keratitis after corneal crosslinking in a patient with post-laser in situ keratomileusis corneal ectasia," Cataract Refractive Surgery 33, 2135-2137 (2007).
[19] Kymionis, G.D., Portaliou, D.M., Bouzoukis, D.I., et al., "Herpetic keratitis with iritis after corneal crosslinking with riboflavin and ultraviolet A for keratoconus," Cataract & Refractive Surgery 33(11), 1982-1984(2007).
[20] Zamora, K.V. and Males, J.J., "Polymicrobial keratitis after a collagen cross-linking procedure with postoperative use of a contact lens: a case report," Cornea 28(4), 474-476(2009).
[21] Bottos, K.M., Oliveira, A.G., Bersametti, P.A., Nogueira, R.F., Lima-Filho, A.A., Schor, P. and Chamon, W., "Corneal absorption of a new riboflavin-nanostructured system for transepithelial collagen cross-linking," Ophthalmology, (2012).
[22] Nichia Corporation, "Specifications for UV LED", 07 July 2015, <http://www.nichia.co.jp/specification/products/led/NCSU033B-E.pdf>.
[23] Malvern, "Zeta potential", 07 July 2015, <http://www.malvern.com/en/products/measurement-type/zeta-potential/>.
[24] Malvern, "Kinexus Range", 07 July 2015, <http://www.malvern.com/en/products/product-range/kinexus-range/> .

IOP Publishing | Astro Ltd Laser Physics
Laser Phys. **25** (2015) 025601 (6pp) doi:10.1088/1054-660X/25/2/025601

Degree of conversion of different composite resins photo-activated with light-emitting diode and argon ion laser

A M Messias[1], M R Galvão[1], J M C Boaventura[1], D P Jacomassi[2], M I B Bernardi[3], V S Bagnato[2], A N S Rastelli[1,2] and M F Andrade[1]

[1] University Estadual Paulista—UNESP, Araraquara, School of Dentistry, Department of Restorative Dentistry, Araraquara, SP, Brazil
[2] University of São Paulo, São Carlos Physics Institute, Optical Group, Biophotonics Lab., São Carlos, SP, Brazil
[3] University of São Paulo, São Carlos Physics Institute, Crystal Growth and Ceramic Materials Group, São Carlos, SP, Brazil

E-mail: alrastelli@foar.unesp.br

Received 24 April 2014, revised 16 November 2014
Accepted for publication 16 November 2014
Published 24 December 2014

Abstract

This study evaluated the degree of conversion (DC%) of one experimental and different brands of composite resins light-cured by two light sources (one LED and one argon laser). The percentage of unreacted C = C was determined from the ratio of absorbance intensities of aliphatic C = C (peak at 1637 cm^{-1}) against internal standards before and after curing: aromatic C–C (peak at 1610 cm^{-1}) except for P90, where %C = C bonds was given for C–O–C (883 cm^{-1}) and C–C (1257 cm^{-1}). ANOVA and Tukey's test revealed no statistically significant difference among Z350 (67.17), Z250 (69.52) and experimental (66.61 ± 2.03) with LED, just among them and Evolu-X (75.51) and P90 (32.05) that showed higher and lower DC%, respectively. For the argon laser, there were no differences among Z250 (70.67), Z350 (69.60), experimental (65.66) and Evolu-X (73, 37), however a significant difference was observed for P90 (36.80), which showed lowest DC%. The light sources showed similar DC%, however the main difference was observed regarding the composite resins. The lowest DC% was observed for the argon laser. P90 showed the lowest DC% for both light-curing sources.

Keywords: composite resins, argon ion laser, LED, photopolymerization

(Some figures may appear in colour only in the online journal)

1. Introduction

Frequently, light-cured composite resins are prepared by the mixing of organic resin matrix with inorganic fillers. Different types of fillers such as silicon dioxide (silica, SiO_2), zirconium dioxide (zirconia, ZrO_2) and aluminum trioxide (alumina, Al_2O_3) of micron or submicron particle size are usually used [1]. The organic matrix is often composed of methacrylate resins, such as 2, 2-bis[4-(3-methacryloxy-2-hydroxypropoxy) phenyl] propane (Bis-GMA) and triethylene glycol dimethacrylate (TEGDMA). Bis-GMA is the primary organic compound in nearly every commercial restorative composite resin [2, 3]. Bis-GMA has become a vital monomer for dental restorative composites, due to its superior mechanical strength, less shrinkage, high modulus and reduced toxicity because of its lower volatility and diffusivity into the tissue. Because of the very high viscosity of Bis-GMA, TEGDMA is added to the composition in order to reduce its viscosity and to enhance filler loading and as a result, physical and mechanical properties [4, 5].

Composite resins have been classified in different ways, depending on their composition, to make it easier for dentists to identify and to use them for therapeutic purposes. A usual and very popular classification is based on filler particle size.

The composite resins are divided into macro filler composites (particles from 0.1 to 100 μm), micro filler composites (0.04 μm particles) and hybrid composites (fillers of different sizes) [6]. However, more recently, to create an universal composite resin used for both anterior and posterior teeth, a new kind of composite resin based on nanotechnology with filler particle size ranging between 5–75 nm was introduced in the market.

Nanotechnology is known as the production and manipulation of materials and structures with sizes ranging from approximately 0.1 to 100 nm. Much interest has been shown in research with composite resins. With the reduced size and distribution of particles, much more can be incorporated with a consequent reduction of polymerization shrinkage and increase in mechanical properties such as tensile strength, compression and fracture and an adequate clinical performance. These properties appear to be similar to those of hybrid composites and microhybrids and significantly higher than the microfilled composite [7–12].

Apart from the material's characteristics, light-curing units (LCUs) significantly influence the degree of polymerization of light-activated composite resins [13–17].

In this sense, LCUs are one part of the daily practice of restorative dentistry. Quartz–tungsten–halogen (QTH), plasma-arc (PAC), argon ion laser and light-emitting diodes (LED) are currently commercially available and may also influence the final physical properties of composite resins [18, 19]. Today, the most common LCU used to start the polymerization process is based on blue LEDs and has the advantage of a narrower spectral range than the QTH light and a better match of light emitted with the absorption spectrum of the photoinitiator camphorquinone [20, 21]. Additionally, LED units do not need filters, which are required with halogen units for wavelength selection. Thus, LED units represent an improvement over halogen lamps [22–25]. According to Aravamudhan *et al* [26] and Calixto *et al* [27], in general, there were no differences between the halogen and LED LCUs with the same parameters.

As an alternative but expensive and complex technology, argon ion lasers, have been used [28–30]. The main advantage of this LCU is the high-power density of the emitted radiation, which reduces the polymerization time. Additionally, the argon ion laser has a narrow wavelength band that is optimally correlated to the absorption peak for initiating the polymerization of composite resins with camphorquinone in their composition, coherency, collimation, low beam divergence and fiber delivery capability. They have been considered a suitable light source for the polymerization of composite resins, which effectively can provide a greater degree of conversion (DC) of monomers, reduce curing time and enhance physical properties of cured composites [31, 32].

The most important features associated with the effectiveness of light-curing seem to be the power density i.e. mW cm^{-2} of the light emitted, the spectral output of the light source and the curing mode. In this way, different LCUs have been evaluated regarding their effectiveness on light-curing composite resins, but there is still some controversy in the literature [15].

The degree of conversion is one important tool to verify the polymerization efficacy and measure the percentage conversion of carbon–carbon double bonds monomeric carbonic to carbonic simple polymer [33, 34]. This process results from the replacement of power connections of Van-der-Waals, pre-existing by covalent bonds [35]. According to Araújo *et al* [36], different techniques can be used to assess the degree of conversion of composite resins, such as FT-IR (Fourier transform infrared spectroscopy), micro-Raman and hardness.

The literature is still unclear about the influence of the nature of the LCU used to cure different composite resins. Then, the aim of this study was to evaluate the degree of conversion (DC%) of one experimental and different brands of composite resins light-cured by one light-emitting diode (LED) and one argon ion laser light-curing source.

2. Materials and methods

2.1. Composite resins

Four brands of composite resins, Filtek™ Z250, Filtek™ Z350 and Filtek™ P90 (3 M Espe, Dental Products, St Paul, MN, USA) and Evolu-X® (Dentsply DeTrey, Konstanz, Germany) at color A_2 (table 1) and one experimental nanofilled composite resin were used in this study. The main composition can be seen in table 1.

2.2. Light-curing units (LCUs)

One blue LED (LED D-2000® DMC, São Carlos, SP, Brazil, serial number: 002041) at 430–490 nm and one argon ion laser (Coherent, Innova 200–20 serial number 3240, USA) at 488 nm were used with a power density of 1100 mW cm^{-2}. First, the power output was measured using a Fieldmaster powermeter (Fieldmaster Power to Put, Coherent-model no. FM, set no. WX65, part no. 33–0506, USA) and then, the power density (mW cm^{-2}) was calculated.

2.3. Sample preparation

The samples ($n = 50$) were made in a metallic mould with central orifice (4 mm in diameter and 2 mm in thickness) according to ISO 4049 [34]. The metallic mould was positioned in a 10 mm thickness glass plate. The composite resin was packed in a single increment and the top and base surfaces were covered by a mylar strip. A 1 mm thickness glass sheet was positioned on the top surface and then a 1 kg weight was used to pack the composite resin. The photoactivation was performed by positioning the light tip on the top surface of the composite resin samples. The samples were irradiated for 40 s. Before making the samples with the experimental composite resin, their components were weighed on a precision balance (model BG Ltd Gehaka 440). The organic matrix was prepared by mixing bisphenol A glycol dimethacrylate (Bis-GMA) and triethylene glycol dimethacrylate (TEGDMA) that were obtained from Sigma-Aldrich Chemie GmbH, 82018 Taufkirchen, Germany)

Table 1. The main compositions of the composite resins used in this study (manufacturers' data).

Material (batch number)	Material type	Matrix	Filler size	Filler volume	Manufacture
Filtek™ Z250 (L.:N148344BR)	Microhybrid composite	Bis-GMA Bis-EMA UDMA	Zirconia/silica (medium size of 0.6 μm)	60% vol	3M Espe, St. Paul, MN, USA
Filtek™ Z350 (L.:N141344)	Nanofilled composite	Bis-GMA Bis-EMA UDMA TEGDMA PEG-DMA	Agglomerated/non-aggregated of 20 nm silica nanofiller and a loosely bound agglomerate silica nanocluster consisting of agglomerates of primary silica nanoparticles of 5 to 20 nm size fillers.The cluster size range is 0.6 to 1.4.	63% vol	3M Espe, St. Paul, MN, USA
Evolu-X® (L.:198846B)	Nanohybrid composite	Bis-GMA modificado TEGMA	Glass silanized barium aluminum boron silicate, barium glass silanized fluoraluminium boron silicate and silica nanoparticles.	58% vol	Dentsply. Petrópolis, RJ, Brasil
Filtek™ P90 (L.:N128528)	Microhybrid composite	Silorane	Nanoparticles of silica/silano with size range is 0.1 to 2 μm	55% vol	3 M Espe, St. Paul, MN, USA
Experimental composite resin	Nanofilled composite	Bis-GMA TEGDMA	Crystalline nanoparticles of zirconia with size range of 60 nm.	30% vol	–

and the inorganic fillers were based on crystalline zirconia nanoparticles (Zr_2O_3) at a ratio of 70/30%, respectively. The initiator system used in this study was the visible light-initiating system of camphorquinone (CQ) (0.5 wt%) and N, N′-dimethyl amino-ethyl methacrylate (DMAEMA, 0.5 wt%) (6×10^{-6} mol g^{-1}) Sigma-Aldrich Chemie GmbH, 82018 Taufkirchen, Germany).

After photo-activation, the samples were stored in a dry mean at 37 °C (±1 °C) for 24 h.

2.4. Degree of conversion measurements (%DC)

After 24 h, the composite resin was pulverized into fine powder. The pulverized composite resin was maintained in a dark room until the moment of the FT-IR analyses. Five milligrams of the ground powder was thoroughly mixed with one hundred milligrams of KBr powder salt. This mixture was placed into a pelleting device and then pressed in a press with a load of 10 tons for 1 min to obtain a pellet.

To measure the degree of conversion, the pellet was then placed into a holder attachment into the spectrophotometer Nexus-470 FT-IR (Thermo Nicolet, Vernon Hills, Illinois, USA) The Fourier transform infrared spectroscopy (FTIR) spectra for both uncured and cured samples were analyzed using an accessory of the diffuse reflectance. The measurements were recorded in the absorbance operating under the following conditions: 32 scans, a 4 cm^{-1} resolution and a 300 to 4000 cm^{-1} wavelength. The percentage of unreacted carbon–carbon double bonds (%C = C) was determined from the ratio of the absorbance intensities of aliphatic C = C (peak at 1637 cm^{-1}) against an internal standard before and after the photoactivation of the specimen: aromatic C–C (peak at 1610 cm^{-1}). This experiment was carried out in triplicate. The degree of conversion was determined by subtracting the % C = C from 100%, according to the formula:

$$\mathrm{DC}\,(\%) = 1 - \frac{(1637\,\mathrm{cm^{-1}} / 1610\,\mathrm{cm^{-1}})_{\mathrm{cured}}}{(1637\,\mathrm{cm^{-1}} / 1610\,\mathrm{cm^{-1}})_{\mathrm{uncured}}}.$$

For the resin-based silorane, the percentage of unreacted carbon–carbon double bonds (%C = C) was determined from the ratio of absorbance intensities of connections between C–O–C in 883 cm^{-1} compared with an internal standard peak at 1257 cm^{-1} [37]. The corresponding degree of conversion was calculated by the formula:

$$\mathrm{DC}\,(\%) = 1 - \frac{(883\,\mathrm{cm^{-1}} / 1257\,\mathrm{cm^{-1}})_{\mathrm{cured}}}{(883\,\mathrm{cm^{-1}} / 1257\mathrm{cm^{-1}})_{\mathrm{uncured}}}.$$

2.5. Statistical analysis

As data presented normal distribution and homogeneity, they were submitted to a factorial ANOVA and Tukey's Test at a significance level of 5% ($p < 0.05$) considering the light-curing sources and composite resins used.

The Shapiro–Wilks test was used to test the data for normality. The homogeneity of variance was tested by the Levene test.

3. Results

Regarding the factors evaluated in this study (composite resins and light-curing sources), composite resins showed a statistically significant effect ($p < 0.001$) on the degree of conversion. The two light-curing sources used did not show a statistically significant effect on the degree of conversion ($p = 0.227$).

Table 2 shows the mean values and standard deviations for the degree of conversion (DC%).

Regardless of light-curing sources (LCUs) evaluated in this study, there was a significant reduction for degree of

Table 2. Mean values and standard deviations (sd) for degree of conversion, according to composite resins and the light-curing units used.

	LED D-2000®	Argon laser	
Composite resin	Mean (sd)	Mean (sd)	
Filtek™ P90	32.05 (2.94)	36.80 (6.46)	a
Filtek™ Z250	69.52 (2.27)	70.67 (4.07)	bc
Filtek™ Z350	67.17 (2.24)	69.60 (3.55)	b
Evolu-X®	75.71 (3.22)	73.37 (4.78)	c
Experimental	66.61 (2.03)	65.66 (2.10)	b

* Means followed by different lowercase letters indicate statistical significant difference ($p < 0.05$).

conversion mean values mainly for Filtek™ P90. For this composite resin the lowest mean values were observed, while for Evolu-X® the highest mean values were observed. These results are displayed in figure 1.

4. Discussion

In the dental profession, there has been an increase in the use of light-cured restorative materials and hence a corresponding increase in research into the light-curing sources used to promote adequate polymerization of composite resins [38]. This *in vitro* study was conducted in order to compare the effectiveness of one LED and argon ion laser on the polymerization of composite resins with different filler loading and size by means of degree of conversion.

The two major components of dental composites are the polymer matrix and the filler particles. Changes in composition and chemistry of the constituent monomers and filler can change their physical properties [39].

Degree of conversion, defined as the percentage of aliphatic C = C bonds converted dimethacrylate monomer present in their polymeric matrices is critical for the optimization of physical and mechanical properties [40], clinical performance, longevity and biocompatibility in order not to cause cytotoxic effects in pulp tissue, an effect attributed to the unconverted monomers that are released uncured matrix [18, 41, 42].

Ideally, the degree of conversion during the polymerization reaction, should achieve a high percentage, which would imply a full conversion of monomers into polymers [19]. However, due to residual unsaturation at the end of the reaction, the conversion has a final average of between 43 and 75% [18, 42–45].

Factors such as the filler particle size and refraction index, restorative material thickness, nature of polymeric matrix and the radiant exposure generated by the light polymerization mode, can influence the DC of dental composites [46].

In this sense, according to the results presented in table 2 and figure 1 there was no statistical difference in the DC (%) values between the two light-curing sources and composite resins considered, except to Filtek™ Z250. For the composite resins based on methacrylate (Filtek™ Z250, Filtek™ Z350, Evolu-X® and experimental) the DC% mean values ranged from 65.66% to 75.71%. Just Filtek™ P90 did not show an adequate degree of conversion according to other studies previously published in the literature [18, 42–45]. Filtek™ P90 showed the low DC% mean values for both, LED and argon ion laser LCUs used.

For an experimental nanoparticulated dental composite based on dioxide zirconia it was possible to show the arithmetic mean of the degree of conversion when photo-activation with LED of 66.61 (± 2.03) and with argon ion laser of 65.66 (± 2.10), which was not statistically significant and for nanoparticulated resin Filtek™ Z350 also used in this study. This fact can be explained by the organic composition of such resins as well as the size, volume and type of particle, which according to Knezevic *et al* [47], interferes with the depth of cure and scattering of incident light.

The generation of radical species for methacrylate curing is produced using a two component system consisting of camphoroquinone, which is the actual photoinitiator and a tertiary amine, responsible for the hydrogen transfer reaction [48]. This system decomposes immediately due to exposure of light with a wavelength between 410 and 500 nm, generating the radical species to start the polymerization process [49]. The development of a photo-activated silorane-based composite occurs with a three component initiating system comprised of camphorquinone, iodonium salt and an electron donor. In this reaction path, the electron donor acts in a redox process and decomposes the iodonium salt into an acidic cation, which starts the ring opening polymerization process (1). It is beneficial to use non-coordinative counter-anions A—such as SbF_6 or $B[(C_6F_5)_4]$—to enhance the reactivity. The 3-component system provides the optimal balance between high polymerization reactivity and light stability [48]. In the present study, all composite resins presented camphorquinone as photoinitiator in their composition, except Filtek™ P90 which does not present camphorquinone. It is possible that the low degree of conversion mean values obtained for Filtek™ P90 can be explained by the differences on radical species generated systems used during the polymerization process as previously related.

The resin-based silorane (Filtek™ P90) showed a lower degree of conversion, getting around 32.05 (± 2.94%) when photo-activated with an LED and 36.80 (± 6.46%) when photo-activated with an argon laser. The differences between them were not statistically significant. These results are in agreement with Kusgoz *et al* [50].

Another factor to consider is described by Weinmann *et al* [48]. When resin-based methacrylate is compared to resin-based silorane, the polymerization process begins with an acid cation, which opens the oxirane ring and generates a new carbocation. Subsequently, the current spread of crosslinking, the polymerization continues. However, during this process, the acidic Si-OH groups on the particles' released inorganic quartz can potentially result in an undesired initiation of cationic polymerization process. This unwanted process could increase the total amount of unreacted monomer oxirane, causing a lower degree of conversion, which can explain the results found in this study. The lower degree of conversion for this process described above also implies lower mechanical properties of the material analyzed, as shown in the results of Lien *et al* [51] who observed these characteristics in Filtek™ P90 composite resin.

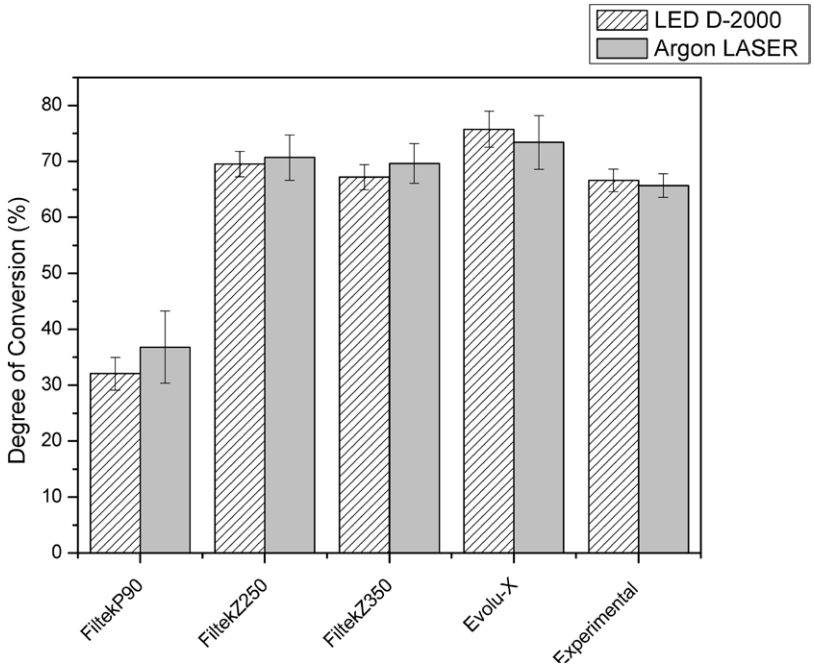

Figure 1. Degree of conversion for the different composite resins photo-activated by different light-curing units (LED and argon laser).

Another paper published by Xiong *et al* [52] showed that the degree of conversion for Filtek^{TM} P90 composite resin was the lowest among the other resins based on Bis-GMA and can be explained by the reaction described above.

Regarding the LCUs used in this study, the LED light-curing unit showed similar results for metahacrylate composite resins used in this study. When the argon ion laser was used, the differences among methacrylate based composite resins were just observed to Filtek^{TM} Z250.

Some factors related to LCUs can affect the polymerization of composite resins and then the degree of conversion. The total energy delivered by LCUs remarkably influences the degree of polymerization of composite resins. However, in this study, the LCUs were used with the same final power density.

The argon ion laser has been described as a promising source for light-curing, as its wavelength is expected to be highly absorbed by the initiator present in the composition of the most of composite resins [15].

Some authors have reported that the argon ion laser can promote a greater depth and degree of polymerization inducing enhancement of the physical properties of composite resins after polymerization [15, 53–59]. However, the absorption peak of camphoroquinone is at approximately 470 nm and the argon ion laser works at a wavelength of 488 nm and this distance between them can make the laser activation inefficient [60–62]. This fact can explain the results obtained in our study, where the blue LED showed similar degree of conversion for all composite resins used, except for Filtek^{TM} Z250.

Regarding the use of LEDs for composite resin curing, the technology appears to be interesting, because the internal components are very small and consequently, allow the equipment to be carried to and from the clinical office and mainly because it produces a low increase in temperature during its use [63, 64].

Under clinical conditions, it may be necessary to increase the exposure time in silorane-based composites, or use LCUs with greater irradiance than that of the LED and argon ion laser used in the present study (1100 mW cm^{-2}) to obtain the best results. The irradiance must be sufficient to form free radicals and form polymers in both silorane and methacrylate-based composites. In summary, silorane based composites are not as well polymerized as methacrylate-based composites.

5. Conclusion

Although this study was performed *in vitro* and thus has some limitations, the following conclusions can be drawn.

(1) The different light-curing sources promoted similar DC% values in methacrylate-based resins, however there was a great difference between them and silorane-based composites.
(2) The different composite resins showed different DC% mean values and this fact can be explained by the differences in chemical composition.

Acknowledgment

This study was supported by FAPESP–Process number: 2010/08998-2 and FUNDUNESP–Process number: 00832/11.

References

[1] Chen M, Chen C, Hsu S, Sun S H and Su W 2006 *Dent. Mater.* **22** 138–45
[2] Bowen R L 1962 *US Patent* 3066112

[3] Bowen R L 1962 *J. Dent. Res.* **58** 1493–503
[4] Sankarapandian M and Shobha H 1997 *J. Mater. Sci. Mater. Med.* **8** 465–8
[5] Khosroshahi M E, Atai M and Nourbakhsh M S 2008 *Lasers Med. Sci.* **23** 399–406
[6] Lutz F and Phillips R W 1983 *J. Prosthet. Dent.* **50** 480–8
[7] Beun S, Glorieux T, Devaux J, Vreven J and Leloup G 2007 *J. Dent. Mater.* **23** 51–9
[8] Kroschwitz J and Howe-Grant M (ed) 1991 *Kirk–Othmer Encyclopedia of Chemical Technology* 4th ed (New York: Wiley)
[9] Moszner N and Klapdohr S 2004 *Int. J. Nanotechnol.* **1** 130–56
[10] Moszner N and Salz U 2001 *Prog. Polym. Sci.* **26** 535–76
[11] Mitra S D, Wu D and Holmer B N 2003 *J. Am. Dent. Assoc.* **134** 1382–90
[12] Terry D A 2004 *Pract. Proc. Aest. Dent.* **16** 417–22
[13] Rahiotis C, Kakaboura A, Loukidis M and Vougiouklakis G 2004 *Eur. J. Oral Sci.* **112** 89–94
[14] Knobloch L A, Kerby R E, Clelland N and Lee J 2004 *Oper. Dent.* **29** 642–9
[15] Powell G L and Blankenau R J 2000 *Dent. Clin. North Am.* **44** 923–30
[16] Vandewalle K S, Roberts H W, Tiba A and Charlton D G 2005 *Oper. Dent.* **30** 257–64
[17] Peris A R, Mitsui F H O, Amaral C M, Ambrosano G M B and Pimenta L A F 2005 *Oper. Dent.* **30** 649–54
[18] Costa S X S, Martins L M, Franscisconi P A S, Bagnato V S, Saad J R C, Rastelli A N S and Andrade M F 2009 *Laser Phys.* **19** 2210–8
[19] Rastelli A N S, Jacomassi D P and Bagnato V S 2008 *Laser Phys.* **18** 1570–5
[20] Leonard D L, Charlton D G, Roberts H W and Cohen M E 2002 *J. Esthet. Restor. Dent.* **14** 286–95
[21] Nomura Y, Teshima W, Tanaka N, Yoshida Y, Nahara Y and Okazaki M 2002 *J. Biomed. Mater. Res.* **63** 209–13
[22] Mills R W, Uhl A, Blackwell G B and Jandt K D 2002 *Biomaterials* **23** 2955–63
[23] Uhl A, Mills R W, Rzanny A E and Jandt K D 2005 *Dent. Mater.* **21** 278–86
[24] Vandewalle K S, Roberts H W, Andrus J L and Dunn W J 2005 *J. Esthet. Restor. Dent.* **17** 244–54
[25] Leonard D L 2007 *J. Esthet. Restor. Dent.* **19** 56–62
[26] Aravamudhan K, Floyd C J, Rakowski D, Flaim G, Dickens S H, Eichmiller F C and Fan P L 2006 *J. Am. Dent. Assoc.* **137** 213–23
[27] Calixto L R, Lima D M, Queiroz R S, Rastelli A N S, Bagnato V S and Andrade M F 2008 *Laser Phys.* **18** 1365–9
[28] Vargas M A, Cobb D S and Rundle T 1998 *Oper. Dent.* **23** 87–93
[29] Blankenau R J, Kelsey W P, Powell G L, Shearer G O, Barkmeier W W and Cavel T 1991 *Am. J. Dent.* **4** 40–2
[30] Cobb D S, Vargas M A and Rundle T 1996 *Am. J. Dent.* **9** 199–2
[31] Fleming M and Mailet W 1999 *Clin. Pract.* **65** 447–50
[32] Conrado L, Munin E and Zangaro R 2004 *Lasers Med. Sci.* **19** 95–9
[33] Ruyter I E and Svedsen S A 1979 *Acta Odontol. Scand.* **36** 75–82
[34] Lovell L G, Elliott J E, Stansburry J W and Bowman C N 2001 *Dent. Mater.***17** 504–11
[35] Saade E G, Bandeca M C, Rastelli A N S, Bagnato V S and Porto-Neto S T 2009 *Laser Phys.* **19** 1276–81
[36] Araújo C S A, Schein M T, Znchi C H, Rodrigues S A Jr and Demarco F F 2008 *J. Contemp. Dent. Pract.* **9** 43–50
[37] Ilie N and Hickel R 2006 *Dent. Mater.* **25** 445–54
[38] Rode K M, Freitas P M, Lloret P R, Powell L G and Turbino M L 2009 *Laser Med. Sci.* **24** 87–92
[39] Mirsasaani S S, Atai M M and Hasani-Sadrabadi M M 2011 *Lasers Med. Sci.* **26** 553–61
[40] Ferracane J L 1985 *Dent. Mater.* **1** 11–4
[41] Cook W D 1992 *Polymer* **33** 600–9
[42] Emami N and Soderholm K J 2005 *J. Mater. Sci. Mater. Med.* **16** 47–52
[43] Ferracane J L and Greener E H 1986 *J. Biomed. Mater. Res.* **20** 121–31
[44] Halvorson R H, Erckson R L and Davidson C L 2003 *Dent. Mater.* **19** 327–33
[45] Moraes L G, Rocha R S, Menegazzo L M, Araujo E B, Yukimito K and Moraes J C 2008 *J. Appl. Oral Sci.* **16** 145–9
[46] Silva E M, Poskus L T, Guimarães J G A, Barcellos A A L and Fellows C E 2008 *J. Mater. Sci. Mater. Med.* **19** 1027–32
[47] Knezević A, Tarle Z, Meniga A, Sutalo J, Pichler G and Ristić M 2001 *J. Oral Rehabil.* **28** 586–91
[48] Weinmann W, Thalacher C and Guggenberger R 2005 *Dent. Mater.* **21** 68–8
[49] Cook W D 1982 *J. Dent. Res.* **61** 1436–8
[50] Kusgoz A, Ülker M, Yesilyurt C, Yoldas O H, Ozil M and Tanriver M 2011 *J. Esthet. Restor. Dent.* **23** 324–35
[51] Lien W and Vandewalle K S 2010 *Dent. Mater.* **26** 337–44
[52] Xiong J, Sun X, Li Y and Chen J 2011 *J. Appl. Polym. Sci.* **122** 1882–8
[53] Blankenau R J, Kelsey W P, Powell G L, Shearer G O, Barkmeier W W and Cavel W T 1991 *Am. J. Dent.* **4** 40–2
[54] Peutzfeldt A, Sahafi A and Asmussen E 2000 *Dent. Mater.* **16** 330–6
[55] Frentzen M and Koort H J 1990 *Int. Dent. J.* **40** 323–31
[56] Docktor M H 1994 *J. Esthet. Dent.* **6** 77–82
[57] Cobb D S, Vargas M A and Rundle T 1996 *Am. J. Dent.* **9** 199–202
[58] Vargas M A, Cobb D S and Schmit J L 1998 *Oper. Dent.* **23** 87–93
[59] Verheyen P J 2001 *J. Oral Laser Appl.* **1** 49–54
[60] Rode K M, Kawano Y and Turbino M L 2007 *Oper. Dent.* **32** 571–8
[61] Burgess J O, Walker R S, Porche C J and Rappold A J 2002 *Compendium* **23** 889–906
[62] Hammesfahr P D, O'Connor M T and Wang X 2002 *Comp. Contin. Educ. Dent.* **23** 18–24
[63] Cunha L G, Sinhoreti M A C, Consani S and Correr-Sobrinho L 2003 *Oper. Dent.* **28** 155–59
[64] Dunn W J and Bush A C 2002 *J. Am. Dent. Assoc.* **133** 335–41

Lasers Med Sci (2015) 30:1281–1287
DOI 10.1007/s10103-015-1728-3

ORIGINAL ARTICLE

Light-emitting diode therapy (LEDT) before matches prevents increase in creatine kinase with a light dose response in volleyball players

Cleber Ferraresi · Ricardo Vinicius dos Santos · Guilherme Marques · Marcelo Zangrande · Roberley Leonaldo · Michael R. Hamblin · Vanderlei Salvador Bagnato · Nivaldo Antonio Parizotto

Received: 29 October 2014 / Accepted: 18 February 2015 / Published online: 27 February 2015

Abstract Low-level laser (light) therapy (LLLT) has been applied over skeletal muscles before intense exercise (muscular pre-conditioning) in order to reduce fatigue and muscle damage (measured by creatine kinase, CK) in clinical trials. However, previous exercise protocols do not exactly simulate the real muscle demand required in sports. For this reason, the aim of this randomized and double-blind placebo-controlled trial was to investigate whether light-emitting diode therapy (LEDT) applied over the quadriceps femoris muscles, hamstrings, and triceps surae of volleyball players before official matches could prevent muscle damage (CK) with a dose response, establishing a therapeutic window. A professional male volleyball team (12 athletes) was enrolled in this study, and LEDT was applied before 4 matches during a national championship. LEDT used an array of 200 light-emitting diodes (LEDs) arranged in 25 clusters of 4 infrared LEDs (850±20 nm; 130 mW) and 25 clusters of 4 red LEDs (630±10 nm; 80 mW). Athletes were randomized to receive one of four different total doses over each muscle group in a double-blind protocol: 105 J (20 s), 210 J (40 s), 315 J (60 s), and placebo (no light for 30 s). CK in blood was assessed 1 h before and 24 h after each match. LEDT at 210 J avoided significant increases in CK (+10 %; P=0.993) as well as 315 J (+31 %, P=0.407). Placebo (0 J) allowed a significant increase in CK (+53 %; P=0.012) as well as LEDT at 105 J (+59 %; P=0.001). LEDT prevented significant increases of CK in blood in athletes when applied before official matches with a light dose response of 210–315 J, suggesting athletes might consider applying LEDT before competition.

Keywords Photobiomodulation · LLLT · CK · Muscle damage · Exercise recovery · Muscle performance

C. Ferraresi (✉) · N. A. Parizotto
Laboratory of Electrothermophototherapy, Department of Physical Therapy, Federal University of Sao Carlos, Rodovia Washington Luís, km 235, 13565-905 Sao Carlos, SP, Brazil
e-mail: cleber.ferraresi@gmail.com

C. Ferraresi · V. S. Bagnato · N. A. Parizotto
Post-Graduation Program in Biotechnology, Federal University of Sao Carlos, Sao Carlos, SP, Brazil

C. Ferraresi · V. S. Bagnato
Optics Group, Physics Institute of Sao Carlos, University of São Paulo, Sao Carlos, SP, Brazil

R. V. dos Santos · G. Marques · M. Zangrande · R. Leonaldo
Sao Bernardo Volleyball Team, Sao Bernardo do Campo, SP, Brazil

M. R. Hamblin
Wellman Center for Photomedicine, Massachusetts General Hospital, Boston, MA, USA

M. R. Hamblin
Department of Dermatology, Harvard Medical School, Boston, MA, USA

M. R. Hamblin
Harvard-MIT Division of Health Science and Technology, Cambridge, MA, USA

Introduction

The benefits of low-level laser (light) therapy (LLLT) to treat pain [1, 2], tendinopathies [3] and to promote tissue healing [2, 4] have been investigated for several years. The mechanism of the light-tissue interaction is thought to involve cytochrome c oxidase (Cox) as the main chromophore in the cells

able to absorb specific wavelengths of light [5–9]. Cox is a mitochondrial enzyme with a very important function in the electron transport chain and consequently promotes cell respiration and energy production in the form of adenosine triphosphate (ATP). For these reasons, LLLT has been widely used for several types of medical treatment, especially those indications that require stimulation of cells and improved healing.

Recently, LLLT has been used to increase muscle performance [10, 11]. When applied after exercise, LLLT promoted reduction of fatigue [12] and increased the workload in maximum effort tests [13] after training programs. When applied before the exercise (muscular pre-conditioning), LLLT increased the number of repetitions and was able to promote "muscle protection" against exercise-induced muscle damage [10, 11] measured by a lower increase of creatine kinase (CK) levels in the blood. In this context, it is valuable to highlight that CK is an important enzyme of the energy metabolism located inside muscle cells, but its increase in the bloodstream after a bout of exercise is an indicative of rupture of muscle cell membrane and consequently muscle damage [14].

In order to investigate the effects of LLLT on "muscle protection" against exercise-induced muscle damage, different protocols of exercise or neuromuscular electrical stimulation have been used to induce muscle fatigue and damage in experimental models [15–20] and in clinical trials [21–28]. These studies have evaluated different wavelengths and different light sources such as diode lasers and light-emitting diodes (LEDs) [29]. Three recent studies [10, 11, 30] reported fascinating results and point to the effectiveness of muscular pre-conditioning using diode lasers and LEDs to prevent muscle fatigue and muscle damage (CK) when applied before (5 min) a bout of exercise.

Having in mind all previous results for muscular pre-conditioning [10, 11, 30], the present study aimed to investigate the effectiveness of the LLLT by LED therapy (LEDT) in the prevention of muscle damage (CK) in professional volleyball players during a national championship. This randomized double-blind placebo-controlled study used an array of LEDs to irradiate equally all target muscle groups [13] with different doses of light in order to establish also a therapeutic window or dose response [31] for LEDT, thus translating these studies to clinical practice. Moreover, the LED array emitted red and infrared light at the same time based on studies that reported better absorption of the light by Cox using bandwidths in the red and near-infrared spectral regions [5–9]. The possible time response of 5 min widely reported in muscular pre-conditioning [10, 11, 30] was modified to 40–60 min, since previous studies already reported a range of 3–45 min for LLLT to increase ATP synthesis in cells [32, 33], and also made it possible to perform muscular pre-conditioning for all athletes before each official volleyball match.

Materials and methods

Study design and ethics statement

The present study was a randomized, double-blind, and placebo-controlled trial involving a professional team of volleyball players in the "Superliga" (national championship) in Brazil during four official matches. Each match was carried out in different stadiums, in accordance with the championship schedule. All researchers traveled with the coaching staff and volleyball players during the study. This study was conducted in compliance with the Declaration of Helsinki (1964) and its later amendments, and also approved by the Research Ethics Committee for Human Studies of the Federal University of Sao Carlos (number protocol approved 217/2012).

Volunteers

Twelve professional volleyball players (the whole team) were enrolled in the study. They had an average age of 25.5± 5.3 years old, body weight of 90.6±7.3 kg, and height of 200±8.7 cm. After their agreement, all players signed the informed consent statement.

Inclusion criteria and exclusion criteria

Inclusion criterion used was healthy professional volleyball players. Exclusion criterion used was volleyball players having musculoskeletal injuries prior to the study or injured during the course of the study.

Groups and randomization procedures

All athletes were randomly allocated into four different groups for muscular pre-conditioning in accordance with the assigned light dose (Joules, J) of the light-emitting diode therapy (LEDT):

- Dose 1—20 s of real LEDT (105 J total) over quadriceps femoris muscles, hamstrings, and triceps surae
- Dose 2—40 s of real LEDT (210 J total) over quadriceps femoris muscles, hamstrings, and triceps surae
- Dose 3—60 s of real LEDT (315 J total) over quadriceps femoris muscles, hamstrings, and triceps surae
- Dose 4—30 s of placebo LEDT (0 J total) over quadriceps femoris muscles, hamstrings, and triceps surae

Each athlete randomly received one of the light doses before each one of the four official matches of the championship. The randomization procedure was conducted at Randomization.com (http://www.randomization.com) using balanced permutations into one block with four different therapies: dose 1 to dose 4. The randomization procedure was carried out by evaluator #1 that operated

the LED device. This researcher was instructed not to inform athletes, researchers, and coaching staff which dose was applied to each athlete at each match.

During the course of the study, two athletes suffered musculoskeletal injuries and then were excluded. One athlete belonged to dose 4 (30 s of irradiation—placebo) and the second athlete belonged to dose 2 (20 s of irradiation). However, these exclusions did not affect the number of subjects per group once all statistical analyses were performed using data of all the six principal active players (not reserve players) in each match.

Experimental protocol

Light-emitting diode therapy

LEDT used a flexible array of 34×18 cm (612 cm^2) similar to the one used in a previous study developed by our research group [34]. However, this prototype device has 200 LEDs arranged in 25 clusters of four infrared LEDs (850±20 nm; 130 mW) and 25 clusters of four red LEDs (630±10 nm; 80 mW) displayed at five lines of ten clusters. Each line has one infrared cluster interspersed by one red cluster, totaling five infrared clusters plus five red clusters per line. Irradiation lasted 20, 40, 60, or 30 s (placebo) over each muscle group (quadriceps femoris, hamstrings, triceps surae) of each athlete's leg with fixed parameters as described in Table 1. Real LEDT or placebo was applied between 40 and 60 min before the start of each official match, in accordance with randomization procedures. LEDT placebo had no energy (0 J) and no power (0 mW) applied over these muscle groups. Optical power was measured with an optical energy meter PM100D Thorlabs® fitted with a sensor S130C (area of 0.70 cm^2). All athletes were blinded for these therapies as well as the coaching staff and evaluator #2 until the end of the study. There was no perceptible sensation of heat to the skin from real LEDT.

Blood samples for creatine kinase activity

Blood samples for creatine kinase activity measurement were collected by puncturing the athlete's ear lobe using sterile lancets 1 h before and 24 h after each official match. The puncture site was cleaned with alcohol and dried, and the first drop of blood was discarded. The blood collected (30 μL) was immediately analyzed with Reflotron Plus® biochemical analyzer (Roche, Germany) [14] following the manufacturer's guidelines. This analysis was conducted by evaluator #2, and all results were blinded for evaluator #1, athletes, and coaching staff until the end of the study.

Matches

The time of each match was monitored by evaluator #3 (coaching staff) as well as which were the six active players in each match (not reserve players).

Table 1 Parameters of light-emitting diode therapy (LEDT)

Number of LEDs	200 (100 infrared-IR and 100 red-RED)
Wavelength	850±20 nm (IR) and 630±10 nm (RED)
Number of clusters	25 (IR) and 25 (RED)
Frequency	Continuous output
Optical output (each cluster of 4 LEDs)	130 mW (IR) and 80 mW (RED)
Total optical output	5250 mW (25×130 mW plus 25×80 mW)
LED spot size (cm^2)	0.2
Power density (each cluster)	185.74 mW/cm^2 (IR) e 114.28 mW/cm^2 (RED)
Treatment time over each muscle group (s)	20, 40, or 60
Energy per cluster at 20 s	2.6 J (IR) and 1.6 J (RED)
Energy per cluster at 40 s	5.2 J (IR) and 3.2 J (RED)
Energy per cluster at 60 s	7.8 J (IR) and 4.8 J (RED)
Energy density per cluster at 20 s	3.71 J/cm^2 (IR) and 2.28 J/cm^2 (RED)
Energy density per cluster at 40 s	7.42 J/cm^2 (IR) and 4.56 J/cm^2 (RED)
Energy density per cluster at 60 s	11.13 J/cm^2 (IR) and 6.84 J/cm^2 (RED)
Total energy delivered per muscle group at 20 s	105 J [2.6 J×25=65 J (IR) plus 1.6×25=40 J (RED)]
Total energy delivered per muscle group at 40 s	210 J [5.2 J×25=130 J (IR) plus 3.2×25=80 J (RED)]
Total energy delivered per muscle group at 60 s	315 J [7.8 J×25=195 J (IR) plus 4.8×25=120 J (RED)]
Total energy delivered on body (J)	630
Total energy delivered on body (J)	1260
Total energy delivered on body (J)	1890
Application mode	Device held coupled in skin contact

Statistical analysis

Although this study enrolled a whole team (12 athletes), and all athletes received one of the light doses before each match, the statistical analysis was applied to the six principal active players (not reserve players) in each match. Thus, each group (light dose) had 6 subjects, and the study had a total sample size of 24 subjects. Shapiro-Wilk's *W* test verified the normality of the data distribution. Creatine kinase activity among all groups was compared using two-way analysis of variance (ANOVA) with repeated measures and Tukey honest significant difference (HSD) post hoc test. Significance was set at $P<0.05$.

Results

Matches

The average time of the matches was 133.75±8.99 min.

Creatine kinase activity

All results of CK activity were presented as mean ± standard deviation (SD). LEDT dose 1 (20 s, 105 J) allowed a significant mean increase in CK (from 328.0±188.9 to 499.6± 232.0 U/L; +59 %; $P=0.001$). Dose 4 (30 s—placebo, 0 J) also allowed a significant increase in CK (from 270.3±112.4 to 406.1±150.5 U/L; +53 %; $P=0.012$). However, LEDT dose 2 (40 s, 210 J) avoided a significant increase in CK (from 338.8±130.3 to 364.1±127.5 U/L; +10 %; $P=0.993$). Dose 3 (60 s, 315 J) also prevented a significant increase in CK (from 245.1±126.9 to 318.0±153.5 U/L; +31 %; $P=0.407$). These results were measured in all six principal active players of each match and presented in Fig. 1.

Discussion

This study investigated the dose response of light-emitting diode therapy to prevent significant increases in creatine kinase activity in volleyball players during official matches, establishing a "therapeutic window" (dose response of different doses of light). We applied LEDT on lower limb muscles aiming to cover the major muscle groups involved in jumping and landing movements that are required during volleyball matches. Moreover, the array of LEDs used in this study covered the entire target muscle groups as has been previously recommended by our research group [13]. To our knowledge, this is the first study that applied LEDT on muscles of professional athletes before official matches to prevent muscle damage.

The effects of low-level laser (light) therapy on muscle tissue when applied before or after intense exercise are mainly related to the prevention of exercise-induced damage, promotion of faster muscle recovery, and also producing increases in performance [10, 30, 11]. The use of LLLT to prevent muscle damage has been widely investigated in experimental models [15–20] and in clinical trials [21–28]. Experimental studies have used animal models to induce muscle damage, and clinical trials have used protocols of exercise in isokinetic dynamometers, fitness machines, or free weight lifting to induce muscle damage. However, all these studies could not exactly simulate the real muscular demand in athletes during official matches of any sport, motivating our research group to investigate the effectiveness of LEDT in volleyball players using a regimen of muscular pre-conditioning to prevent increases in CK.

Previous studies already reported benefits of the LLLT using diode lasers and LEDs to prevent increases in CK activity [10, 30, 11]. To our knowledge, the first study that used LLLT to prevent muscle damage was carried out by Lopes-Martins et al. [15] in an experimental animal model. These authors investigated the effects of different doses of light (0.5; 1.0 and 2.5 J/cm^2) in muscular pre-conditioning to prevent muscle fatigue and muscle damage (CK) induced by neuromuscular electrical stimulation. These authors reported a LLLT dose response to decrease CK activity in muscle tissue. Another experimental study trained rats on an inclined treadmill and measured inhibition of inflammation, reduction of CK activity, and lowering of oxidative stress (malondialdehyde, MDA). They also found increases in

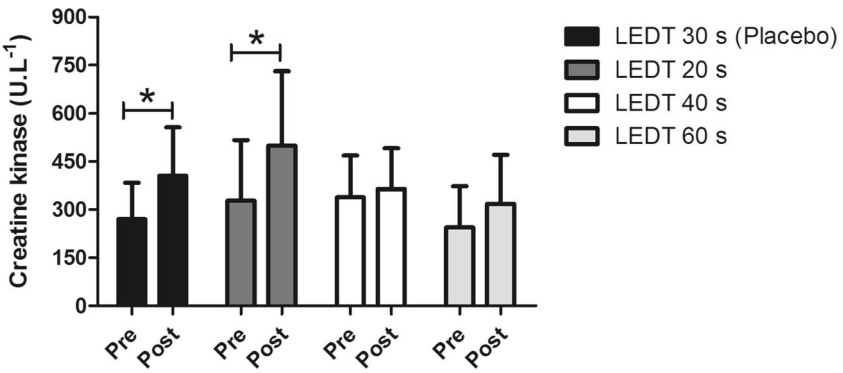

Fig. 1 Mean and standard deviation (SD) for creatine kinase activity (CK) in blood pre and post each official match between groups. *LEDT* light-emitting diode therapy; *asterisk* represents statistical significance ($P<0.05$) in two-way analysis of variance (ANOVA) with repeated measures and Tukey HSD post hoc test

defense against oxidative stress (increased activity of superoxide dismutase, SOD) 24 and 48 h after exercise [16]. These studies were important to demonstrate the benefits of LLLT on exercise-induced muscle damage, inflammation, and oxidative stress.

More studies using experimental models were conducted to investigate the effects of LLLT on CK activity [18, 17, 19, 20]. Using a similar model of neuromuscular electrical stimulation previously reported [15], other studies also found LLLT dose responses of muscular pre-conditioning by decreased CK activity [18, 19], including assessment of different wavelengths [20]. Another study observed a reduction in CK activity when LLLT was applied after exercises in a model of swimming with workload [17]. Recently, LLLT using LEDs (LEDT) has demonstrated similar benefits to decrease CK activity when applied after exercise [35] or during rest intervals between bouts of physical activity [36]. All these studies assessed CK activity after 24 h or during a time range of 24–48 h after the exercise.

These aforementioned experimental studies created the scientific basis for the use of the LLLT, including LEDT, in prospective clinical trials that aimed to prevent exercise-induced muscle damage by assessing CK activity. Recently, this effect of "muscle protection" by LLLT has been observed in humans using different exercises protocols for the upper and lower limbs [10, 11, 30]. These studies reported lower increases in CK activity measured in blood when LLLT was applied before intense exercises. Light doses (Joules, J) used in previous studies were between 1 and 6 J delivered per diode laser, totaling 4 J [21] or 60 J [22] delivered to the biceps brachii; 30 and 40 J [23] or 180 J [24] delivered to the quadriceps femoris muscles. When the light source was LED, these studies used a cluster of 69 LEDs and applied 0.3 or 0.9 J per LED, totaling 41.7 J per site of irradiation and a total dose of 41.7 J delivered on biceps brachii [25]; 83.4 J [26] or 125.1 J [27] or 208.5 J [28] delivered to quadriceps femoris muscles.

Our results are in accordance with the total dose used in previous studies that used LEDs (LEDT) or combined LEDs and super-pulsed lasers to prevent increases in CK activity in the quadriceps femoris muscles with total doses from 60 to 300 J [29]. Our effective total doses of LEDT were 210 J [130 J (IR) plus 80 J (RED)—40 s of irradiation] and 315 J [195 J (IR) plus 120 J (RED)—60 s of irradiation] as reported similarly by a previous study [29]. LEDT placebo and the total dose of 105 J [(65 J (IR) plus 40 J (RED)—20 s of irradiation] allowed a significant increase of CK activity, indicating potential muscle damage and failure of the LEDT to promote "muscle protection." In addition, we chose to use dual wavelengths (red and near-infrared at the same time) based on specific absorption bands of cytochrome c oxidase (Cox) [5–9] that is the main chromophore in the cells. Moreover, our results were observed using muscular pre-conditioning applied 40–60 min before the start of each official match. This consideration is important because the waiting time can allow the muscles more time to respond to the light and could change the accepted paradigm that muscular pre-conditioning using LLLT for the prevention of exercise-induced muscle damage should be applied 5 min before the exercise.

The optimum doses of light delivered from each cluster of four LEDs were between 5.2 and 7.8 J for infrared and between 3.2 and 4.8 J for red. These energy doses are similar to doses emitted by diode lasers in a previous study [24], reinforcing the idea that light is light [37] and there is not a large difference between these light sources to prevent exercise-induced muscle damage (CK) if the total dose applied per muscle group is adequate. However, it is important to remark that it is possible that the light dose used to prevent muscle damage with LEDT in a pre-conditioning regimen may not be the same dose necessary if the light therapy is applied after the exercise [38]. It is accepted that cells under biochemical or mechanical stress have better responses to light [39] than cells in homeostasis.

The number of jumps and landings or of any other movement performed by each athlete during each match was not equal and could not be standardized among the six principal active players. This could be understood as a limitation, but the course of each match was unpredictable and could not be standardized.

Finally, the present study was not designed to elucidate the mechanisms of action of LEDT when used in muscular pre-conditioning to prevent exercise-induced muscle damage. However, previous studies reported better defenses against oxidative stress [16] if LLLT is applied over muscles after intense exercises as well as before exercise as reported in a previous clinical trial [40]. As mentioned above, the main chromophore, or red/NIR light-sensitive protein, present in biological tissues is Cox [5]. After absorbance of light, mitochondrial metabolism is modulated, promoting increases in ATP synthesis as one of the secondary responses [5]. We suggest that "muscle protection" against exercise-induced damage by LLLT is also a secondary response, but the connection between the light absorption and this effect is not fully understood. As a suggestion for future studies, we believe that LLLT could possibly modulate the proteins of membrane channels in muscle cells and/or in proteins involved in the transduction of the mechanical stress generated during muscle contraction involving the extracellular matrix and cytoskeleton. These modulations could improve the biochemical environment and the mechanical response of the muscle cells to exercise by stabilizing the muscle cell membrane.

It should be noted that there is no current position taken by the World Anti-Doping Agency (WADA) or the International Olympic Committee (IOC) regarding the use of LLLT for the enhancement of muscle performance. However, if the use of LLLT before athletic competition becomes widespread, we

expect discussions will have to take place in the appropriate circles on whether its use constitutes an unfair advantage.

Conclusion

Use of red and near-infrared LEDT for muscular preconditioning was effective in the prevention of muscle damage (CK) in professional volleyball players during official matches. There was a therapeutic window (dose response) for this effect with a better dose of 210–315 J applied over the entire target muscles than with 0 J (placebo) or 105 J. Our results will stimulate more researchers and teams of high-performance sports to use LEDT for the prevention of muscle damage in professional athletes.

Acknowledgments Cleber Ferraresi would like to thank FAPESP for his PhD scholarships (numbers 2010/07194-7 and 2012/05919-0). MR Hamblin was supported by US NIH grant R01AI050875.

Ethical statement This study was conducted in compliance with the Declaration of Helsinki (1964) and its later amendments and also approved by the Research Ethics Committee for Human Studies of the Federal University of Sao Carlos (number protocol approved 217/2012).

Conflict of interest The authors declare no conflict of interest.

References

1. Chow RT, Johnson MI, Lopes-Martins RA, Bjordal JM (2009) Efficacy of low-level laser therapy in the management of neck pain: a systematic review and meta-analysis of randomised placebo or active-treatment controlled trials. Lancet 374(9705):1897–1908, doi: S0140-6736(09)61522-1
2. Enwemeka CS, Parker JC, Dowdy DS, Harkness EE, Sanford LE, Woodruff LD (2004) The efficacy of low-power lasers in tissue repair and pain control: a meta-analysis study. Photomed Laser Surg 22(4): 323–329. doi:10.1089/1549541041797841
3. Tumilty S, Munn J, McDonough S, Hurley DA, Basford JR, Baxter GD (2010) Low level laser treatment of tendinopathy: a systematic review with meta-analysis. Photomed Laser Surg 28(1):3–16. doi:10.1089/pho.2008.2470
4. Gupta A, Avci P, Sadasivam M, Chandran R, Parizotto N, Vecchio D, de Melo WC, Dai T, Chiang LY, Hamblin MR (2012) Shining light on nanotechnology to help repair and regeneration. Biotechnol Adv. doi:10.1016/j.biotechadv.2012.08.003
5. Karu T (1999) Primary and secondary mechanisms of action of visible to near-IR radiation on cells. J Photochem Photobiol B 49(1):1–17, doi: S1011-1344(98)00219-X
6. Karu TI, Pyatibrat LV, Afanasyeva NI (2004) A novel mitochondrial signaling pathway activated by visible-to-near infrared radiation. Photochem Photobiol 80(2):366–372. doi:10.1562/2004-03-25-RA-123
7. Karu TI, Kolyakov SF (2005) Exact action spectra for cellular responses relevant to phototherapy. Photomed Laser Surg 23(4):355–361. doi:10.1089/pho.2005.23.355
8. Karu TI, Pyatibrat LV, Kolyakov SF, Afanasyeva NI (2008) Absorption measurements of cell monolayers relevant to mechanisms of laser phototherapy: reduction or oxidation of cytochrome c oxidase under laser radiation at 632.8 nm. Photomed Laser Surg 26(6):593–599. doi:10.1089/pho.2008.2246
9. Karu TI (2010) Multiple roles of cytochrome c oxidase in mammalian cells under action of red and IR-A radiation. IUBMB Life 62(8): 607–610. doi:10.1002/iub.359
10. Ferraresi C, Hamblin MR, Parizotto NA (2012) Low-level laser (light) therapy (LLLT) on muscle tissue: performance, fatigue and repair benefited by the power of light. Photonics Lasers Med 1(4): 267–286. doi:10.1515/plm-2012-0032
11. Leal-Junior EC, Vanin AA, Miranda EF, de Carvalho PD, Dal Corso S, Bjordal JM (2013) Effect of phototherapy (low-level laser therapy and light-emitting diode therapy) on exercise performance and markers of exercise recovery: a systematic review with meta-analysis. Lasers Med Sci. doi:10.1007/s10103-013-1465-4
12. Vieira WH, Ferraresi C, Perez SE, Baldissera V, Parizotto NA (2012) Effects of low-level laser therapy (808 nm) on isokinetic muscle performance of young women submitted to endurance training: a randomized controlled clinical trial. Lasers Med Sci 27(2):497–504. doi:10.1007/s10103-011-0984-0
13. Ferraresi C, de Brito OT, de Oliveira ZL, de Menezes Reiff RB, Baldissera V, de Andrade Perez SE, Matheucci Junior E, Parizotto NA (2011) Effects of low level laser therapy (808 nm) on physical strength training in humans. Lasers Med Sci 26(3):349–358. doi:10.1007/s10103-010-0855-0
14. Hornery DJ, Farrow D, Mujika I, Young W (2007) An integrated physiological and performance profile of professional tennis. Br J Sports Med 41(8):531–536. doi:10.1136/bjsm.2006.031351, discussion 536
15. Lopes-Martins RA, Marcos RL, Leonardo PS, Prianti AC Jr, Muscara MN, Aimbire F, Frigo L, Iversen VV, Bjordal JM (2006) Effect of low-level laser (Ga-Al-As 655 nm) on skeletal muscle fatigue induced by electrical stimulation in rats. J Appl Physiol 101(1): 283–288. doi:10.1152/japplphysiol.01318.2005
16. Liu XG, Zhou YJ, Liu TC, Yuan JQ (2009) Effects of low-level laser irradiation on rat skeletal muscle injury after eccentric exercise. Photomed Laser Surg 27(6):863–869. doi:10.1089/pho.2008.2443
17. Sussai DA, Carvalho Pde T, Dourado DM, Belchior AC, dos Reis FA, Pereira DM (2010) Low-level laser therapy attenuates creatine kinase levels and apoptosis during forced swimming in rats. Lasers Med Sci 25(1):115–120. doi:10.1007/s10103-009-0697-9
18. Leal Junior EC, Lopes-Martins RA, de Almeida P, Ramos L, Iversen VV, Bjordal JM (2010) Effect of low-level laser therapy (GaAs 904 nm) in skeletal muscle fatigue and biochemical markers of muscle damage in rats. Eur J Appl Physiol 108(6):1083–1088. doi:10.1007/s00421-009-1321-1
19. de Almeida P, Lopes-Martins RA, Tomazoni SS, Silva JA Jr, de Carvalho PT, Bjordal JM, Leal Junior EC (2011) Low-level laser therapy improves skeletal muscle performance, decreases skeletal muscle damage and modulates mRNA expression of COX-1 and COX-2 in a dose-dependent manner. Photochem Photobiol 87(5): 1159–1163. doi:10.1111/j.1751-1097.2011.00968.x
20. Santos LA, Marcos RL, Tomazoni SS, Vanin AA, Antonialli FC, Grandinetti Vdos S, Albuquerque-Pontes GM, de Paiva PR, Lopes-Martins RA, de Carvalho PT, Bjordal JM, Leal-Junior EC (2014) Effects of pre-irradiation of low-level laser therapy with different doses and wavelengths in skeletal muscle performance, fatigue, and skeletal muscle damage induced by tetanic contractions in rats. Lasers Med Sci 29(5):1617–1626. doi:10.1007/s10103-014-1560-1
21. Felismino AS, Costa EC, Aoki MS, Ferraresi C, de Araujo Moura Lemos TM, de Brito Vieira WH (2014) Effect of low-level laser therapy (808 nm) on markers of muscle damage: a randomized double-blind placebo-controlled trial. Lasers Med Sci 29(3):933–938. doi:10.1007/s10103-013-1430-2
22. Leal Junior EC, Lopes-Martins RA, Frigo L, De Marchi T, Rossi RP, de Godoi V, Tomazoni SS, Silva DP, Basso M, Filho PL, de Valls CF, Iversen VV, Bjordal JM (2010) Effects of low-level laser therapy

(LLLT) in the development of exercise-induced skeletal muscle fatigue and changes in biochemical markers related to postexercise recovery. J Orthop Sports Phys Ther 40(8):524–532. doi:10.2519/jospt.2010.3294
23. Leal Junior EC, Lopes-Martins RA, Baroni BM, De Marchi T, Taufer D, Manfro DS, Rech M, Danna V, Grosselli D, Generosi RA, Marcos RL, Ramos L, Bjordal JM (2009) Effect of 830 nm low-level laser therapy applied before high-intensity exercises on skeletal muscle recovery in athletes. Lasers Med Sci 24(6):857–863. doi:10.1007/s10103-008-0633-4
24. Baroni BM, Leal Junior EC, De Marchi T, Lopes AL, Salvador M, Vaz MA (2010) Low level laser therapy before eccentric exercise reduces muscle damage markers in humans. Eur J Appl Physiol 110(4):789–796. doi:10.1007/s00421-010-1562-z
25. Leal Junior EC, Lopes-Martins RA, Rossi RP, De Marchi T, Baroni BM, de Godoi V, Marcos RL, Ramos L, Bjordal JM (2009) Effect of cluster multi-diode light emitting diode therapy (LEDT) on exercise-induced skeletal muscle fatigue and skeletal muscle recovery in humans. Lasers Surg Med 41(8):572–577. doi:10.1002/lsm.20810
26. Leal Junior EC, Lopes-Martins RA, Baroni BM, De Marchi T, Rossi RP, Grosselli D, Generosi RA, de Godoi V, Basso M, Mancalossi JL, Bjordal JM (2009) Comparison between single-diode low-level laser therapy (LLLT) and LED multi-diode (cluster) therapy (LEDT) applications before high-intensity exercise. Photomed Laser Surg 27(4):617–623. doi:10.1089/pho.2008.2350
27. Baroni BM, Leal Junior EC, Geremia JM, Diefenthaeler F, Vaz MA (2010) Effect of light-emitting diodes therapy (LEDT) on knee extensor muscle fatigue. Photomed Laser Surg 28(5):653–658. doi:10.1089/pho.2009.2688
28. Leal Junior EC, de Godoi V, Mancalossi JL, Rossi RP, De Marchi T, Parente M, Grosselli D, Generosi RA, Basso M, Frigo L, Tomazoni SS, Bjordal JM, Lopes-Martins RA (2011) Comparison between cold water immersion therapy (CWIT) and light emitting diode therapy (LEDT) in short-term skeletal muscle recovery after high-intensity exercise in athletes—preliminary results. Lasers Med Sci 26(4):493–501. doi:10.1007/s10103-010-0866-x
29. Antonialli FC, De Marchi T, Tomazoni SS, Vanin AA, Dos Santos Grandinetti V, de Paiva PR, Pinto HD, Miranda EF, de Tarso Camillo de Carvalho P, Leal-Junior EC (2014) Phototherapy in skeletal muscle performance and recovery after exercise: effect of combination of super-pulsed laser and light-emitting diodes. Lasers Med Sci. doi:10.1007/s10103-014-1611-7
30. Borsa PA, Larkin KA, True JM (2013) Does phototherapy enhance skeletal muscle contractile function and postexercise recovery? A systematic review. J Athl Train 48(1):57–67. doi:10.4085/1062-6050-48.1.12
31. Huang YY, Chen AC, Carroll JD, Hamblin MR (2009) Biphasic dose response in low level light therapy. Dose–Response 7(4):358–383. doi:10.2203/dose-response.09-027.Hamblin
32. Passarella S, Casamassima E, Molinari S, Pastore D, Quagliariello E, Catalano IM, Cingolani A (1984) Increase of proton electrochemical potential and ATP synthesis in rat liver mitochondria irradiated in vitro by helium-neon laser. FEBS Lett 175(1):95–99
33. Karu T, Pyatibrat L, Kalendo G (1995) Irradiation with He-Ne laser increases ATP level in cells cultivated in vitro. J Photochem Photobiol B 27(3):219–223
34. Ferraresi C, Beltrame T, Fabrizzi F, Nascimento ES, Karsten M, Francisco CO, Borghi-Silva A, Catai AM, Cardoso DR, Ferreira AG, Hamblin MR, Bagnato VS, Parizotto NA (2015) Muscular pre-conditioning using light-emitting diode therapy (LEDT) for high-intensity exercise: a randomized double-blind placebo-controlled trial with a single elite runner. Physiother Theory Pract:1–8. doi: 10.3109/09593985.2014.1003118
35. Camargo MZ, Siqueira CP, Preti MC, Nakamura FY, de Lima FM, Dias IF, Toginho Filho Dde O, Ramos Sde P (2012) Effects of light emitting diode (LED) therapy and cold water immersion therapy on exercise-induced muscle damage in rats. Lasers Med Sci 27(5):1051–1058. doi:10.1007/s10103-011-1039-2
36. da Costa Santos VB, de Paula RS, Milanez VF, Correa JC, de Andrade Alves RI, Dias IF, Nakamura FY (2014) LED therapy or cryotherapy between exercise intervals in Wistar rats: anti-inflammatory and ergogenic effects. Lasers Med Sci 29(2):599–605. doi:10.1007/s10103-013-1371-9
37. Enwemeka CS (2005) Light is light. Photomed Laser Surg 23(2):159–160. doi:10.1089/pho.2005.23.159
38. Dos Reis FA, da Silva BA, Laraia EM, de Melo RM, Silva PH, Leal-Junior EC, de Carvalho PT (2014) Effects of pre- or post-exercise low-level laser therapy (830 nm) on skeletal muscle fatigue and biochemical markers of recovery in humans: double-blind placebo-controlled trial. Photomed Laser Surg 32(2):106–112. doi:10.1089/pho.2013.3617
39. Karu T (2013) Is it time to consider photobiomodulation as a drug equivalent? Photomed Laser Surg 31(5):189–191. doi:10.1089/pho.2013.3510
40. De Marchi T, Leal Junior EC, Bortoli C, Tomazoni SS, Lopes-Martins RA, Salvador M (2012) Low-level laser therapy (LLLT) in human progressive-intensity running: effects on exercise performance, skeletal muscle status, and oxidative stress. Lasers Med Sci 27(1):231–236. doi:10.1007/s10103-011-0955-5

Photochemistry and Photobiology, 2015, 91: 411–416

Low-level Laser (Light) Therapy Increases Mitochondrial Membrane Potential and ATP Synthesis in C2C12 Myotubes with a Peak Response at 3–6 h

Cleber Ferraresi[1,2,3,4], Beatriz Kaippert[4,5], Pinar Avci[4,6], Ying-Ying Huang[4,6], Marcelo V. P. de Sousa[4,7], Vanderlei S. Bagnato[2,3], Nivaldo A. Parizotto[1,2] and Michael R. Hamblin[*4,6,8]

[1]Laboratory of Electrothermophototherapy, Department of Physical Therapy, Federal University of Sao Carlos, Sao Carlos, SP, Brazil
[2]Post-Graduation Program in Biotechnology, Federal University of Sao Carlos, Sao Carlos, SP, Brazil
[3]Optics Group, Physics Institute of Sao Carlos, University of São Paulo, Sao Carlos, SP, Brazil
[4]Wellman Center for Photomedicine, Massachusetts General Hospital, Boston, MA
[5]Federal University of Rio de Janeiro, Rio de Janeiro, RJ, Brazil
[6]Department of Dermatology, Harvard Medical School, Boston, MA
[7]Laboratory of Radiation Dosimetry and Medical Physics, Institute of Physics, Sao Paulo University, Sao Carlos, SP, Brazil
[8]Harvard-MIT Division of Health Science and Technology, Cambridge, MA

Received 2 September 2014, accepted 25 November 2014, DOI: 10.1111/php.12397

ABSTRACT

Low-level laser (light) therapy has been used before exercise to increase muscle performance in both experimental animals and in humans. However, uncertainty exists concerning the optimum time to apply the light before exercise. The mechanism of action is thought to be stimulation of mitochondrial respiration in muscles, and to increase adenosine triphosphate (ATP) needed to perform exercise. The goal of this study was to investigate the time course of the increases in mitochondrial membrane potential (MMP) and ATP in myotubes formed from C2C12 mouse muscle cells and exposed to light-emitting diode therapy (LEDT). LEDT employed a cluster of LEDs with 20 red (630 ± 10 nm, 25 mW) and 20 near-infrared (850 ± 10 nm, 50 mW) delivering 28 mW cm^2 for 90 s (2.5 J cm^2) with analysis at 5 min, 3 h, 6 h and 24 h post-LEDT. LEDT-6 h had the highest MMP, followed by LEDT-3 h, LEDT-24 h, LEDT-5 min and Control with significant differences. The same order (6 h > 3 h > 24 h > 5 min > Control) was found for ATP with significant differences. A good correlation was found (r = 0.89) between MMP and ATP. These data suggest an optimum time window of 3–6 h for LEDT stimulate muscle cells.

INTRODUCTION

Mitochondria are the organelles responsible for energy production in cells and for this reason have a very important role in cellular function and maintenance of homeostasis. This organelle has an intriguing and well-designed architecture to generate adenosine triphosphate (ATP) that is the basic energy supply for all cellular activity (1,2).

Mitochondria contain a respiratory electron transport chain (ETC.) able to transfer electrons through complexes I, II, III and IV by carrying out various redox reactions in conjunction with pumping hydrogen ions (H^+) from the mitochondrial matrix to the intermembrane space. These processes generate water as the metabolic end-product, as oxygen is the final acceptor of electrons from the ETC., that is coupled with synthesis of ATP when H^+ ions return back into mitochondrial matrix through complex V (ATP synthase), thus completing the ETC. Changes in the flow of electrons through the ETC. and consequently in H^+ pumping produce significant modulations in the total proton motive force and ATP synthesis. These changes can be measured by mitochondrial membrane potential (MMP) and content of ATP (1).

Since the earliest evidence that low-level laser (light) therapy (LLLT) can increase ATP synthesis (3,4), several mechanisms of action have been proposed to explain LLLT effects on mitochondria. One of the first studies reported increased MMP and ATP synthesis measured at an interval of 3 min after LLLT (3). Years later, other authors extended the measurement of this "extra" ATP-induced by LLLT in HeLa (human cervical cancer) cells (4). With intervals of 5 to 45 min, these authors found no change in ATP synthesis during the first 15 min after LLLT, but after 20–25 min ATP levels increased sharply and then came back to control levels at 45 min (4).

More recent studies have reported LLLT effects on mitochondria in different types of cells (5–9). In neural cells LLLT seems to also increase MMP, protect against oxidative stress (5) and increase ATP synthesis in intact cells (without stressor agents) (6). In mitochondria from fibroblast cells without stressor agents, LLLT also increased ATP synthesis and mitochondrial complex IV activity in a dose-dependent manner (7). In myotubes from C2C12 cells, LLLT could modulate the production of reactive oxygen species (ROS) and mitochondrial function in a dose-dependent manner in intact cells or in cells stressed by electrical stimulation (9).

Increases in mitochondrial metabolism and ATP synthesis have been proposed by several authors as a hypothesis to explain

*Corresponding author email: hamblin@helix.mgh.harvard.edu (Michael R. Hamblin)

LLLT effects on muscle performance when used for muscular preconditioning or muscle recovery postexercise (10–12). However, there is a lack in the literature to identify immediate and long-term effects of LLLT on mitochondrial metabolism and ATP synthesis in skeletal muscle cells that in turn could confirm these hypotheses.

This study aimed to identify the time-response for LLLT by light-emitting diode therapy (LEDT) in modulation of MMP and ATP content in myotubes from C2C12 intact cells (mouse muscle cells) only under the stress of the culture. Moreover, the second objective was to correlate MMP with ATP content within a time range of 5 min to 24 h after LLLT. Our goal was to find the best time-response for LLLT which could be useful in future experimental and clinical studies investigating muscular preconditioning, muscle recovery postexercise or any other photobiomodulation in muscle tissue.

MATERIALS AND METHODS

Cell culture. C2C12 cells were kindly provided by the Cardiovascular Division of the Beth Israel Deaconess Medical Center, Harvard Medical School, USA. Cells were grown in culture medium (DMEM, Dulbecco's Modified Eagle's Medium - Sigma-Aldrich) with fetal bovine serum (20% FBS - Sigma-Aldrich) and 1% antibiotic (penicillin and streptomycin) in humidified incubator at 37°C and 5% CO_2.

C2C12 cells were cultured and a total of 1.71×10^5 cells approximately were counted in a Neubauer chamber. Next, these cells were distributed equally into 30 wells (approximately 5.7×10^3 cells per well) into two different plates:

1 15 wells in black plate (Costar® 96-Well Black Clear-Bottom Plates) for analysis of MMP.
2 15 wells in white plate (Costar® 96-Well White Clear-Bottom Plates) for analysis of ATP synthesis.

Moreover, both plates were subdivided into five columns with three wells per column (triplicate):

1 LEDT-Control: no LEDT applied to the cells.
2 LEDT-5 min: LEDT applied to the cells and assessments of ATP and MMP after 5 min.
3 LEDT-3 h: LEDT applied to the cells and assessments of ATP and MMP after 3 h.
4 LEDT-6 h: LEDT applied to the cells and assessments of ATP and MMP after 6 h.
5 LEDT-24 h: LEDT applied to the cells and assessments of ATP and MMP after 24 h.

After plating C2C12 cells were cultured for 9 days in culture medium (DMEM) containing 2% heat-inactivated horse serum (Sigma-Aldrich) in a humidified incubator at 37°C and 5% CO_2 to induce cell differentiation into myotubes, as described in a previous study (9). At the 10th day, LEDT-24 h group received LEDT. At 11th day all remaining groups received LEDT and were assessed for ATP and MMP at specific times in accordance with each group.

Light-emitting diode therapy (LEDT). A cluster of 40 LEDs (20 red – 630 ± 10 nm; 20 infrared – 850 ± 20 nm) with a diameter of 76 mm was used in this study. The cluster was positioned at a distance of 156 mm from the top of each plate and irradiation lasted 90 s with fixed parameters as described in Table 1. Each group of wells received LEDT individually, and all others wells of each plate (groups) were covered with aluminum foil to avoid light irradiation (Fig. 1). LEDT parameters were measured and calibrated using an optical energy meter PM100D Thorlabs® and sensor S142C (area of 1.13 cm^2). In addition, we chose use red and near-infrared light therapy at the same time to promote a double band of absorption by cytochrome c oxidase (Cox) based on specific bands of absorption reported previously (2,13–16). The room temperature was controlled (22–23°C) during LEDT irradiation, which did not increase temperature on the top of plates more than 0.5°C. This increase of 0.5°C was dissipated to room within 2 min after LEDT.

Mitochondrial membrane potential (TMRM) assay. This analysis was performed using cells placed into black plate. MMP was assessed using tetramethyl rhodamine methyl ester (TMRM – Invitrogen/Molecular Probes) at a final concentration of 25 nM. Nuclei of myotubes from C2C12 cells were labeled using Hoechst (Sigma-Aldrich) at a concentration of 1 mg mL^{-1}. Each well was incubated for 30 min, 37°C and 5% CO_2 with 100 μL of solution containing TMRM and Hoechst. Next, this solution was carefully removed from each well and added 100 μL of buffer solution containing HBSS (Hank's Balanced Salt Solution – Life Technologies Corporation) and 15 mM HEPES (4-(2-hydroxyethyl)-1-piperazineethanesulfonic acid – Life Technologies Corporation). The myotubes were imaged in a confocal microscope (Olympus America Inc. Center Valley, PA) using an excitation at 559 nm and emission at 610 nm. Three random fields per well were imaged with a magnification of 40× water immersion lens. Images were exported and TMRM fluorescence incorporation into mitochondrial matrix was measured using software Image J (NIH, Bethesda, MD).

Adenosine triphosphate (ATP) assay. This analysis was performed using cells placed into white plate. First, the medium was carefully removed from each well followed by addition of 50 μL per well of CellTiter Glo Luminescent Cell Viability Assay reagent (Promega). After 10 min of incubation at room temperature (25°C), luminescence signals were measured in a SpectraMax M5 Multi-Mode Microplate Reader (Molecular Devices, Sunnyvale, CA) with integration time of 5 s to increase low signals (17). A standard curve was prepared using ATP standard (Sigma) according to manufacturer's guideline and then ATP concentration was calculated in nanomol (nmol) per well.

Pearson product-moment correlation coefficient (Pearson's r). The correlation between TMRM and ATP content in myotubes from C2C12 cells was calculated using Pearson's r. The *r* values were interpreted as recommended previously (18): 0.00–0.19 = none to slight; 0.20–0.39 = low; 0.40–0.69 = modest; 0.70–0.89 = high; and 0.90–1.00 = very high.

Sample size calculation. The sample size was calculated based on that necessary to obtain significant differences among all groups with ATP

Table 1. All parameters of light-emitting diode therapy (LEDT). Control did not receive LEDT.

Number of LEDs (cluster): 40 (20 infrared-IR and 20 red-RED)
Wavelength: 850 ± 20 nm (IR) and 630 ± 10 nm (RED)
LED spot size: 0.2 cm^2
Pulse frequency: continuous
Optical output of each LED: 50 mW (IR) and 25 mW (RED)
Optical output (cluster): 1000 mW (IR) and 500 mW (RED)
LED cluster size: 45 cm^2
Power density (at the top of plate): 28 mW cm^2
Treatment time: 90 s
Cluster energy density applied on the top plate: 2.5 J cm^2
Application mode: without contact
Distance from plate or power meter: 156 mm

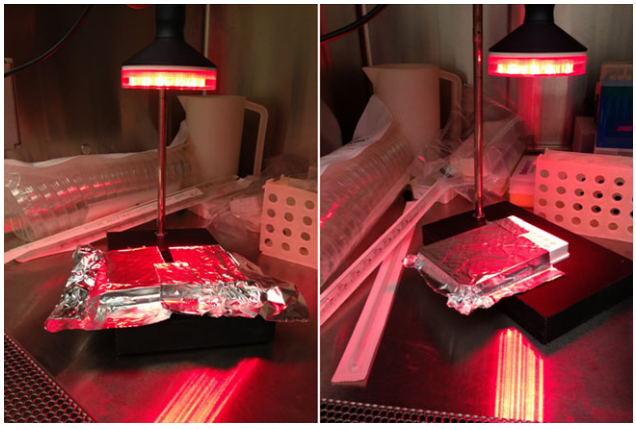

Figure 1. Myotubes from C2C12 cells. Experimental setup for irradiation of the white and black plates containing myotubes from C2C12 cells using light-emitting diode therapy (LEDT) without contact.

content. The statistical power of 80% and the effect size (greater than 0.75) were found to be satisfactory.

Statistical analysis. Shapiro–Wilk's W test verified the normality of the data distribution. ATP and TMRM were compared among all groups using one-way analysis of variance (ANOVA) with Tukey HSD post hoc test. Pearson product-moment correlation coefficient (Pearson's r) was conducted between TMRM and ATP. Significance was set at $P < 0.05$.

RESULTS

Mitochondrial membrane potential (TMRM)

LEDT-6 h group increased MMP (10.77 AU, SEM 0.88) compared to: Control (3.79 AU, SEM 0.46): $P < 0.001$; LEDT-5 min (4.11 AU, SEM 0.52): $P < 0.001$; LEDT-24 h (4.91 AU, SEM 0.47): $P = 0.001$. LEDT-3 h (7.87 AU, SEM 0.59) increased MMP compared to Control ($P = 0.019$) and LEDT-5 min ($P = 0.031$). These results are graphically presented in Fig. 2. All nonsignificant results were Control *versus* LEDT-5 min ($P = 0.997$) and *versus* LEDT-24 h ($P = 0.816$); LEDT-5 min *versus* LEDT-24 h ($P = 0.935$); LEDT-3 h *versus* LEDT-6 h ($P = 0.113$) and *versus* LEDT-24 h ($P = 0.103$).

ATP assay

LEDT-6 h increased ATP contents (4.53 nmol per well, SEM 0.19) compared to: Control (1.28 nmol per well, SEM 0.05): $P < 0.001$; LEDT-5 min (2.01 nmol per well, SEM 0.16): $P < 0.001$; LEDT-24 h (2.77 nmol per well, SEM 0.16): $P = 0.007$. LEDT-3 h increased ATP contents (3.73 nmol per well, SEM 0.17) compared to Control ($P < 0.001$) and LEDT-5 min ($P = 0.008$). LEDT-24 h increased ATP contents compared to Control ($P = 0.020$). These results are graphically presented in Fig. 3A. All nonsignificant results were Control *versus* LEDT-5 min ($P = 0.385$); LEDT-3 h *versus* LEDT-6 h ($P = 0.299$) and *versus* LEDT-24 h ($P = 0.169$); LEDT-24 h *versus* LEDT-5 min ($P = 0.338$).

Sample size

The statistical power and the effect size regarding ATP content in all groups were calculated to ensure the minimal power of 80% and large effect size (>0.75). We used the mean ATP content of each group and the highest value of standard deviation among all groups, which was observed in LEDT-6 h. Our results demonstrate a difference between groups with a statistical power of 99%, effect size of 3.42 (very large effect) and total sample size of 10, i.e. 2 wells per group (five groups). These calculations demonstrate that our sample size was small, but adequate (3 wells per group).

Pearson product-moment correlation coefficient (Pearson's r)

TMRM incorporation into mitochondrial matrix of myotubes from C2C12 cells showed a high correlation ($r = 0.89$) with ATP content ($P < 0.001$). This result is presented in Fig. 3B.

DISCUSSION

This study identified a well-defined time-response for the LEDT-mediated increase in MMP and ATP synthesis in myotubes from C2C12 cells under the stress of the cell culture. The light dose used was based on previous study that already reported benefits of LLLT on mitochondria of myotubes (9). In addition, we found a strong correlation between MMP and ATP content measured

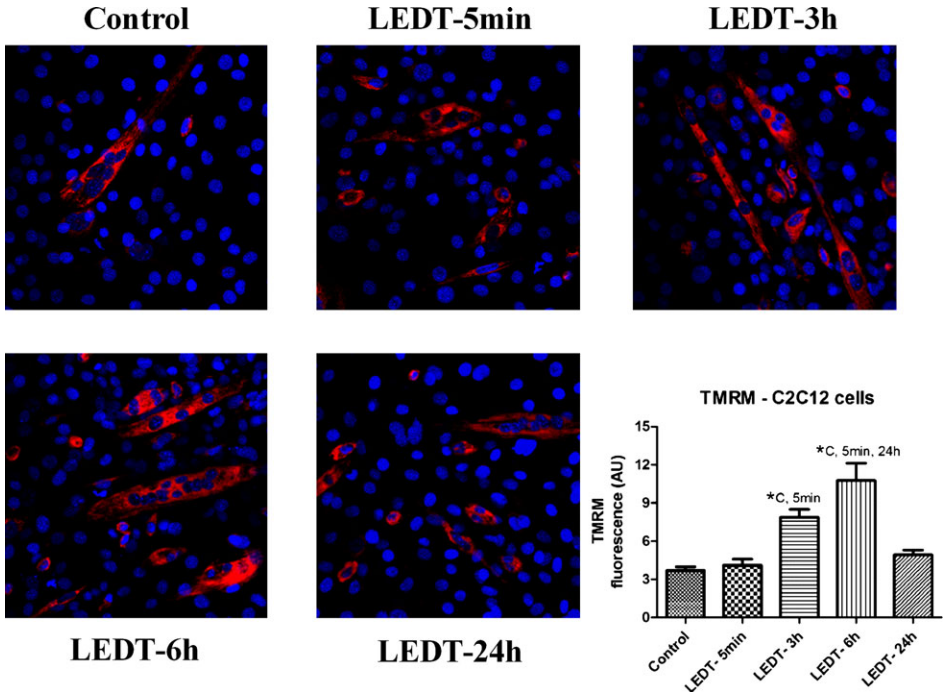

Figure 2. TMRM. Analysis of mitochondrial membrane potential using tetramethyl rhodamine methyl ester (TMRM) stained in red. Images with a magnification of 40×. Abbreviations: LEDT= light-emitting diode therapy; AU = arbitrary units; C = control group; 5 min = LEDT-5 min group; 24 h = LEDT-24 h group; * = statistical significance ($P < 0.05$) using one-way analysis of variance (ANOVA).

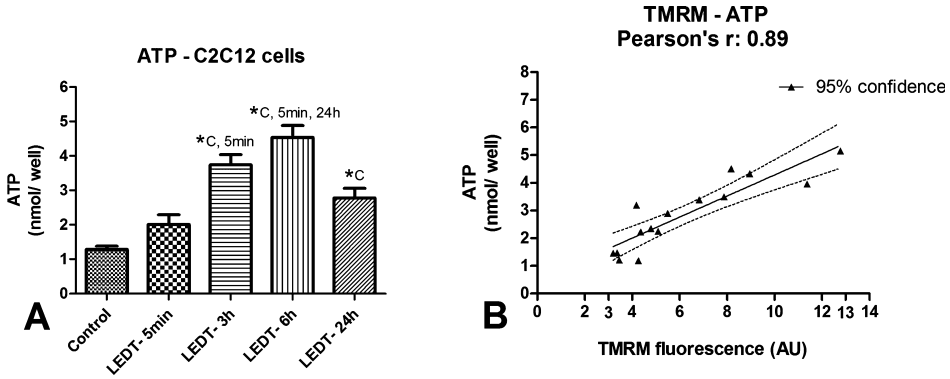

Figure 3. ATP and Pearson's *r*. (A) Analysis of adenosine triphosphate (ATP) content between groups. (B) Pearson product-moment correlation coefficient (Pearson's *r*) between ATP and mitochondrial membrane potential using TMRM. Abbreviations: LEDT = light-emitting diode therapy; TMRM = tetramethyl rhodamine methyl ester; nmol = nanomol; AU = arbitrary units; C = control group; 5 min = LEDT-5 min group; 24 h = LEDT-24 h group; * = statistical significance ($P < 0.05$) using one-way analysis of variance (ANOVA).

during a wide range from 5 min (immediate effect) to 24 h (prolonged effect). To our knowledge this is the first study investigating the time-response for light therapy modulation of mitochondrial metabolism in conjunction with ATP synthesis in muscle cells.

C2C12 is a cell line originally isolated from dystrophic muscles of C3H mice by Yaffe and Saxel (19). In culture it rapidly differentiates into contractile myotubes (muscle fibers) especially when treated with horse serum instead of fetal bovine serum. These myotubes contain multinucleated cells that express proteins characteristic of skeletal muscle such as myosin heavy chain and creatine kinase (20).

One of first effects of LLLT reported in literature was a modulation on MMP and ATP synthesis in mitochondria isolated from rat liver (3) and in HeLa cells (4). Our results are in accordance with these previous studies, showing an increased MMP and ATP synthesis in myotubes from C2C12 cells. However, light therapy seems to produce a different time-response of MMP and ATP synthesis among different cell types. While HeLa cells showed a peak of ATP synthesis around 20 min after light therapy (4), mitochondria from liver showed an immediate increase in MMP and ATP synthesis (3). In this study, we found that muscle cells need a longer time in the range of 3 h to 6 h to show the maximum effect of light therapy and convert it into a significant increase in MMP and ATP synthesis, comprising an increase around 200% to 350% over the control values. In addition, we found that 24 h after irradiation, myotubes could still produce significantly more ATP compared to LEDT-Control while LEDT-5 min showed no significant difference.

Cytochrome c oxidase (Cox) has been reported to be the main chromophore in cells exposed to red and near-infrared light (2,15,16,21). However, although Cox activity is important in the immediate effects of photon absorption, the measurement of its activity may be insufficient to confirm whether light therapy can induce "extra" ATP synthesis. For this reason, the measurement of MMP in conjunction with ATP synthesis can provide information on how fast changes occur in the electron transport chain (ETC.), and H^+ pumping from the mitochondrial matrix to the intermembrane space, as well as how much H^+ ions are returning to the mitochondrial matrix (1). In this perspective, our results are consistent with Xu *et al.* (9) who reported no immediate effects of light therapy on MMP. Moreover, although Xu *et al.*

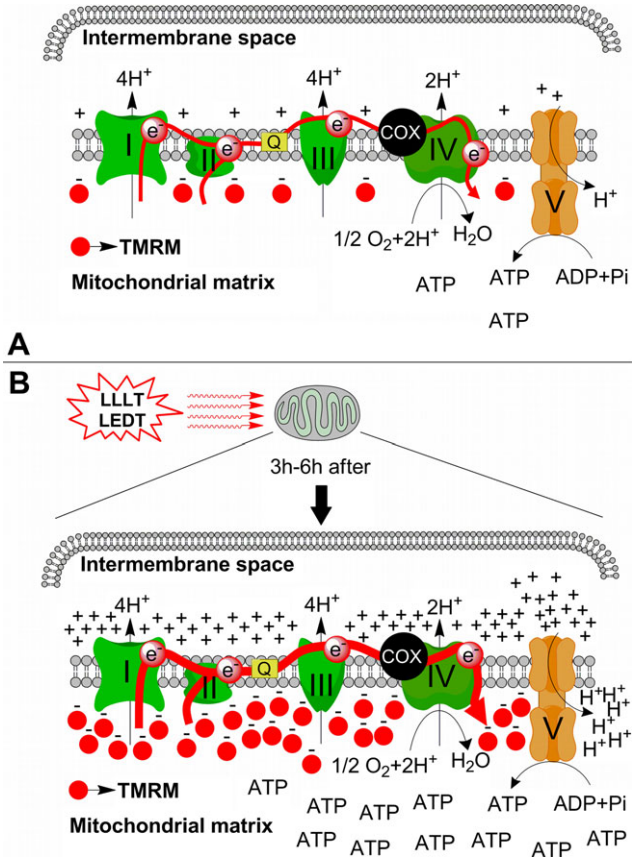

Figure 4. Mechanism of action of LEDT on mitochondria. (A) Mitochondria of myotubes from C2C12 cells without low-level laser therapy (LLLT) or light-emitting diode therapy (LEDT). There is a normal flux of electrons (red arrow) through all complexes of electron transport chain, normal pumping of H^+, normal synthesis of ATP and modest take up of TMRM by the mitochondrial matrix. (B) Mitochondria of myotubes from C2C12 cells 3–6 h after LEDT. There is an increased flux of electrons (ticker red arrow), increased pumping of H^+, increased synthesis of ATP and increased take up of TMRM by the mitochondrial matrix. Abbreviations: I, II, III, IV and V = complexes of the mitochondrial electron transport chain; H^+ = proton of hydrogen; - = electron of hydrogen; O_2 = oxygen; H_2O = metabolic water; Q = quinone; Cox = cytochrome c oxidase; ATP = adenosine triphosphate;TMRM = tetramethyl rhodamine methyl ester.

(9) did not assess ATP content, our results showed no significant responses for ATP increment immediately after light therapy compared to control group.

Our results for MMP in conjunction with ATP content had a high correlation (Pearson's $r = 0.89$) during the time range of 5 min to 24 h, suggesting a linear and positive dependence of ATP synthesis on the value of MMP (ETC. and H^+ pumping) in muscle cells, suggesting a new and more efficient time-response or time window for LEDT stimulate muscle cells (see Fig. 4A, B). These results are very important for muscle recovery postexercise (10,11) because they suggest a prolonged effect of light therapy on ATP synthesis necessary to repair muscle damage. In addition, muscular preconditioning using light therapy for improvement of performance before a bout of exercise (12) could possibly be optimized by application at the appropriate time. However, more studies *in vivo* and clinical trials are needed to confirm our hypotheses.

Muscular preconditioning using LLLT or LEDT have been reported as therapeutic approaches to improve muscle performance in both experimental models (22–24) and in clinical trials (12). However, although this improvement reported in the literature has been significant, some studies have not found positive results (25). Furthermore, differences between groups treated with light therapy or placebo seem to be not so large. These differences reported in experimental models varied between 80% and 150% of the values found for control groups for fatigue test induced by electrical stimulation (22–24). In clinical trials these differences varied between 5% and 57% increases in number of repetitions and maximal voluntary contraction (12). Possibly these relatively modest increases could be due to allowing insufficient time necessary for the muscle cells to convert light therapy into biological responses as identified in our study for MMP and ATP synthesis. Consequently, protocols for muscular preconditioning that have been done up to now (12,22–24), i.e. generally applying light 5 min before the exercise, may not possibly achieve the best result. On the basis of our results, we suggest to wait 3–6 h after light therapy irradiation to obtain the best increase in muscle performance in muscular preconditioning regimen, as MMP and ATP availability are important for muscle performance (26,27). Once more time, we would like to remark the needed of more studies *in vivo* and clinical trials to confirm our hypotheses. At this point, it is valuable to reference two previous studies that had a similar initiative (28,29). Hayworth *et al.* (28) found increments in Cox activity 24 h after apply LEDT over rats muscles; Albuquerque-Pontes *et al.* (29) found a time window, wavelength-dependence and dose response for Cox activity increase also after LLLT in rats muscles. Both studies used animals without any kind of stress, such as this study used cells only under the stress of the cell culture. We believe that these previous studies combined with our results are extremely valuable for the discovery and understanding of mechanisms of action of LLLT on muscle tissue, and may offer guidance on the future use of LLLT in clinical practice.

Our study was designed to test one dose of light during a time-response to show that there is time-dependency for LLLT to produce secondary responses in muscle cells. For this reason, this study used a constant dose (fluence) of light as reported in a previous study (9) as well as a constant power density. As there is a possible biphasic dose response (30,31), use of different parameters such as fluence, wavelengths or irradiance could produce different responses. In addition, red and near-infrared light therapy was delivered at the same time to take advantage of the double bands in Cox to absorb the light (2,13–16).

CONCLUSION

This is the first study reporting the benefits of mixed red and near-infrared light therapy on MMP in conjunction with ATP synthesis in myotubes from C2C12 cells (muscle cells from mice). Moreover, a well-defined time-response was found for the increase in ATP synthesis mediated by MMP increased by light therapy in myotubes.

Our data suggest that 3–6 h could be the best time-response for light therapy to improve muscle metabolism. In addition, our results lead us to think there may be possible cumulative effects if light therapy is applied at intervals less than 24 h that may have clinical relevance when LLLT is used for muscle postexercise recovery. Finally, we believe that use of light therapy for muscular preconditioning could be optimized in future studies whether the time-response for increases in ATP and MMP found in this study are taken account.

Acknowledgements—We thank Professor Zoltan Pierre Arany and his instructor Glenn C. Rowe for the C2C12 cells and Andrea Brissette for assistance with multiple roles including purchase of reagents. Cleber Ferraresi thank FAPESP for his PhD scholarships (numbers 2010/07194-7 and 2012/05919-0). MR Hamblin was supported by US NIH grant R01AI050875.

REFERENCES

1. Perry, S. W., J. P. Norman, J. Barbieri, E. B. Brown and H. A. Gelbard (2011) Mitochondrial membrane potential probes and the proton gradient: A practical usage guide. *Biotechniques* **50**, 98–115.
2. Karu, T. (1999) Primary and secondary mechanisms of action of visible to near-IR radiation on cells. *J. Photochem. Photobiol., B* **49**, 1–17.
3. Passarella, S., E. Casamassima, S. Molinari, D. Pastore, E. Quagliariello, I. M. Catalano and A. Cingolani (1984) Increase of proton electrochemical potential and ATP synthesis in rat liver mitochondria irradiated in vitro by helium-neon laser. *FEBS Lett.* **175**, 95–99.
4. Karu, T., L. Pyatibrat and G. Kalendo (1995) Irradiation with He-Ne laser increases ATP level in cells cultivated in vitro. *J. Photochem. Photobiol., B* **27**, 219–223.
5. Giuliani, A., L. Lorenzini, M. Gallamini, A. Massella, L. Giardino and L. Calza (2009) Low infra red laser light irradiation on cultured neural cells: Effects on mitochondria and cell viability after oxidative stress. *BMC Complement. Altern. Med.* **9**, 8.
6. Oron, U., S. Ilic, L. De Taboada and J. Streeter (2007) Ga-As (808 nm) laser irradiation enhances ATP production in human neuronal cells in culture. *Photomed. Laser Surg.* **25**, 180–182.
7. Houreld, N. N., R. T. Masha and H. Abrahamse (2012) Low-intensity laser irradiation at 660 nm stimulates cytochrome c oxidase in stressed fibroblast cells. *Lasers Surg. Med.* **44**, 429–434.
8. Masha, R. T., N. N. Houreld and H. Abrahamse (2013) Low-intensity laser irradiation at 660 nm stimulates transcription of genes involved in the electron transport chain. *Photomed. Laser Surg.* **31**, 47–53.
9. Xu, X., X. Zhao, T. C. Liu and H. Pan (2008) Low-intensity laser irradiation improves the mitochondrial dysfunction of C2C12 induced by electrical stimulation. *Photomed. Laser Surg.* **26**, 197–202.
10. Ferraresi, C., M. R. Hamblin and N. A. Parizotto (2012) Low-level laser (light) therapy (LLLT) on muscle tissue: Performance, fatigue and repair benefited by the power of light. *Photonics Lasers Med.* **1**, 267–286.
11. Borsa, P. A., K. A. Larkin and J. M. True (2013) Does phototherapy enhance skeletal muscle contractile function and postexercise recovery? A systematic review. *J. Athl. Train.* **48**, 57–67.

12. Leal-Junior, E. C., A. A. Vanin, E. F. Miranda, P. D. de Carvalho, S. Dal Corso and J. M. Bjordal (2013) Effect of phototherapy (low-level laser therapy and light-emitting diode therapy) on exercise performance and markers of exercise recovery: A systematic review with meta-analysis. *Lasers Med. Sci.* [Epub ahead of print].
13. Karu, T. I., L. V. Pyatibrat and N. I. Afanasyeva (2004) A novel mitochondrial signaling pathway activated by visible-to-near infrared radiation. *Photochem. Photobiol.* **80**, 366–372.
14. Karu, T. I. and S. F. Kolyakov (2005) Exact action spectra for cellular responses relevant to phototherapy. *Photomed. Laser Surg.* **23**, 355–361.
15. Karu, T. I., L. V. Pyatibrat, S. F. Kolyakov and N. I. Afanasyeva (2008) Absorption measurements of cell monolayers relevant to mechanisms of laser phototherapy: Reduction or oxidation of cytochrome c oxidase under laser radiation at 632.8 nm. *Photomed. Laser Surg.* **26**, 593–599.
16. Karu, T. I. (2010) Multiple roles of cytochrome c oxidase in mammalian cells under action of red and IR-A radiation. *IUBMB Life* **62**, 607–610.
17. Khan, H. A. (2003) Bioluminometric assay of ATP in mouse brain: Determinant factors for enhanced test sensitivity. *J. Biosci.* **28**, 379–382.
18. Weber, J. and D. Lamb (1970) *Statistics and Research in Physical Education*. C. V. Mosby Co., Saint Louis.
19. Yaffe, D. and O. Saxel (1977) Serial passaging and differentiation of myogenic cells isolated from dystrophic mouse muscle. *Nature* **270**, 725–727.
20. Tannu, N. S., V. K. Rao, R. M. Chaudhary, F. Giorgianni, A. E. Saeed, Y. Gao and R. Raghow (2004) Comparative proteomes of the proliferating C(2)C(12) myoblasts and fully differentiated myotubes reveal the complexity of the skeletal muscle differentiation program. *Mol. Cell Proteomics* **3**, 1065–1082.
21. Karu, T. I. (2008) Mitochondrial signaling in mammalian cells activated by red and near-IR radiation. *Photochem. Photobiol.* **84**, 1091–1099.
22. Lopes-Martins, R. A., R. L. Marcos, P. S. Leonardo, A. C. Jr Prianti, M. N. Muscara, F. Aimbire, L. Frigo, V. V. Iversen and J. M. Bjordal (2006) Effect of low-level laser (Ga-Al-As 655 nm) on skeletal muscle fatigue induced by electrical stimulation in rats. *J. Appl. Physiol. (1985)*, **101**, 283–288.
23. Leal Junior, E. C., R. A. Lopes-Martins, P. de Almeida, L. Ramos, V. V. Iversen and J. M. Bjordal (2010) Effect of low-level laser therapy (GaAs 904 nm) in skeletal muscle fatigue and biochemical markers of muscle damage in rats. *Eur. J. Appl. Physiol.* **108**, 1083–1088.
24. Santos, L. A., R. L. Marcos, S. S. Tomazoni, A. A. Vanin, F. C. Antonialli, V. D. Grandinetti, G. M. Albuquerque-Pontes, P. R. de Paiva, R. A. Lopes-Martins, P. D. de Carvalho, J. M. Bjordal and E. C. Leal-Junior (2014) Effects of pre-irradiation of low-level laser therapy with different doses and wavelengths in skeletal muscle performance, fatigue, and skeletal muscle damage induced by tetanic contractions in rats. *Lasers Med. Sci.* [Epub ahead of print].
25. Higashi, R. H., R. L. Toma, H. T. Tucci, C. R. Pedroni, P. D. Ferreira, G. Baldini, M. C. Aveiro, A. Borghi-Silva, A. S. de Oliveira and A. C. Renno (2013) Effects of low-level laser therapy on biceps braquialis muscle fatigue in young women. *Photomed. Laser Surg.* **31**, 586–594.
26. Allen, D. G., G. D. Lamb and H. Westerblad (2008) Skeletal muscle fatigue: Cellular mechanisms. *Physiol. Rev.* **88**, 287–332.
27. Ferraresi, C., T. de Brito Oliveira, L. de Oliveira Zafalon, R. B. de Menezes Reiff, V. Baldissera, S. E. de Andrade Perez, E. Matheucci Junior and N. A. Parizotto (2011) Effects of low level laser therapy (808 nm) on physical strength training in humans. *Lasers Med. Sci.* **26**, 349–358.
28. Hayworth, C. R., J. C. Rojas, E. Padilla, G. M. Holmes, E. C. Sheridan and F. Gonzalez-Lima (2010) In vivo low-level light therapy increases cytochrome oxidase in skeletal muscle. *Photochem. Photobiol.* **86**, 673–680.
29. Albuquerque-Pontes, G. M., R. D. Vieira, S. S. Tomazoni, C. O. Caires, V. Nemeth, A. A. Vanin, L. A. Santos, H. D. Pinto, R. L. Marcos, J. M. Bjordal, P. D. de Carvalho and E. C. Leal-Junior (2014) Effect of pre-irradiation with different doses, wavelengths, and application intervals of low-level laser therapy on cytochrome c oxidase activity in intact skeletal muscle of rats. *Lasers Med. Sci.* [Epub ahead of print].
30. Huang, Y. Y., A. C. Chen, J. D. Carroll and M. R. Hamblin (2009) Biphasic dose response in low level light therapy. *Dose Response* **7**, 358–383.
31. Huang, Y. Y., S. K. Sharma, J. Carroll and M. R. Hamblin (2011) Biphasic dose response in low level light therapy - an update. *Dose Response* **9**, 602–618.

Lasers Med Sci (2015) 30:1553–1563
DOI 10.1007/s10103-015-1759-9

ORIGINAL ARTICLE

Low-level laser therapy (LLLT) associated with aerobic plus resistance training to improve inflammatory biomarkers in obese adults

Raquel Munhoz da Silveira Campos[1] · Ana Raimunda Dâmaso[1] · Deborah Cristina Landi Masquio[1] · Antonio Eduardo Aquino Jr.[2,3] · Marcela Sene-Fiorese[2] · Fernanda Oliveira Duarte[4] · Lian Tock[5] · Nivaldo Antonio Parizotto[3,4] · Vanderlei Salvador Bagnato[2,3]

Received: 19 August 2014 / Accepted: 23 April 2015 / Published online: 10 May 2015

Abstract Recently, investigations suggest the benefits of low-level laser (light) therapy (LLLT) in noninvasive treatment of cellulite, improvement of body countering, and control of lipid profile. However, the underlying key mechanism for such potential effects associated to aerobic plus resistance training to reduce body fat and inflammatory process, related to obesity in women still unclear. The purpose of the present investigation was to evaluate the effects of combined therapy of LLLT and aerobic plus resistance training in inflammatory profile and body composition of obese women. For this study, it involved 40 obese women with age of 20–40 years. Inclusion criteria were primary obesity and body mass index (BMI) greater than 30 kg/m^2 and less than 40 kg/m^2. The voluntaries were allocated in two different groups: phototherapy group and SHAM group. The interventions consisted on physical exercise training and application of phototherapy (808 nm), immediately after the physical exercise, with special designed device. Proinflammatory/anti-inflammatory adipokines were measured. It was showed that LLLT associated to physical exercise is more effective than physical exercise alone to increase adiponectin concentration, an anti-inflammatory adipokine. Also, it showed reduced values of neck circumference (cm), insulin concentration (μU/ml), and interleukin-6 (pg/ml) in LLLT group. In conclusion, phototherapy can be an important tool in the obesity, mostly considering its potential effects associated to exercise training in attenuating inflammation in women, being these results applicable in the clinical practices to control related risk associated to obesity.

Keywords Phototherapy · Obesity · Adiponectin · Interlukin-6

✉ Raquel Munhoz da Silveira Campos
raquelmunhoz@hotmail.com

✉ Ana Raimunda Dâmaso
ana.damaso@unifesp.br

[1] Paulista Medicine School–Universidade Federal de São Paulo, Rua Marselhesa, 650–Vila Clementino, São Paulo, SP 04020-050, Brazil

[2] São Carlos Institute of Physics, University of São Paulo (USP), PO Box 369, São Carlos 13560-970, Brazil

[3] Post Graduated Program of Biotechnology, Federal University of São Carlos (UFSCar), São Carlos, SP 13565-905, Brazil

[4] Department of Physiotherapy, Therapeutic Resouses Laboratory, Federal University of São Carlos (UFSCar), São Carlos, SP 13565-905, Brazil

[5] Weight Science, São Paulo, SP, Brazil

Introduction

Nowadays, strong evidence has been found that LLLT is an important tool in widely clinical applications, including esthetic treatments, chronic kidney disease, cancer, and different branches of regenerative medicine and dentistry [1]. Supporting this, it was recently demonstrated in experimental conditions that LLLT promoted improvement in some metabolic syndrome parameters in rats [2], although its effects in human obesity are unknown in the literature.

Metabolic syndrome is a constellation of metabolic alterations leading to cardiovascular diseases. In this way, obesity, mostly considering central and visceral fat and insulin resistance, has been strongly associated with the development of metabolic syndrome and cardiovascular diseases [3, 4]. In addition, the prevalence of metabolic syndrome in obese people ranges between 30 and 70 % [5, 6] in adolescents and adults, respectively, showing the necessity for new techniques to optimize the treatment of metabolic comorbidities. Moreover, the related inflammatory process involved in obesity promotes an increase in the proinflammatory adipokines and a reduction in the anti-inflammatory adipokines which are associated with several metabolic disorders such as type 2 diabetes, obesity, and cardiovascular disease [7, 8].

The key inflammatory mediators in obesity are adiponectin, interleukin-6 (IL-6), and TNF-alpha. Adiponectin is a 244-amino acid-long protein that is secreted from adipocytes and has anti-inflammatory and insulin-sensitizing properties [9]. However, reduced levels of this adipokine are linked to increased carotid intima-media thickness (cIMT), visceral adiposity, insulin resistance, diabetes, dyslipidemia, hypertension, hyperleptinemia, cardiovascular disease, metabolic syndrome, and systemic inflammation [10].

On the other hand, the members of proinflammatory cytokines, IL-6 and TNF-alpha, are known to be elevated in obesity and its comorbidities [11, 12] and have been accepted as clinical markers. Additionally, in metabolic syndrome patients, it is known that both are strong inhibitors of adiponectin. Nonetheless, weight loss therapies including physical exercise promote an improvement in the inflammatory biomarkers, showing that an increase in the adiponectin concentration and a reduction in the interleukin-6 and TNF-alpha occur [13, 14].

Interestingly, an initial proof-of-concept was previously shown suggesting that LLLT can be used in some inflammatory diseases to provide a noninvasive and clinical therapeutic strategy due to photochemical effects that change cellular functions in irradiated cells; thus, the therapeutic effect is not thermal [15, 16].

It is well settled in the literature that physical exercise favors the control of obesity and related inflammatory processes, since this kind of strategy leads to a reduction in body weight, visceral fat, and insulin resistance through an increase in the lipolysis [17, 18]. However, the association of LLLT with aerobic plus resistance training in obese women is scarce in the literature. Therefore, in the present study, it was hypothesized that in obese women, changes in proinflammatory markers should be compensated by altered anti-inflammatory markers after treatment with LLLT combined with aerobic plus resistance training.

Material and methods

Population

For this study, it involved 40 obese women with age of 20–40 years. Inclusion criteria were primary obesity and body mass index (BMI) greater than 30 kg/m^2 and less than 40 kg/m^2. Noninclusion criteria were the use of cortisone, antiepileptic drugs, history of renal disease, alcohol intake, smoking, and secondary obesity due to endocrine disorders.

The main reasons for dropout (n=4) in our study were financial and family problems, followed by job opportunities. The study was conducted with the principles of the Declaration of Helsinki and was approved by the ethics committee on research at the Universidade Federal de São Carlos-UFSCar with the number (237.050), Clinical Trial: 231.286. All procedures were clear to the volunteers, and it obtained consent for research. All evaluations were performed at two different times (baseline and at the end of therapy: after 4 months of interdisciplinary intervention).

The voluntaries were allocated in two different groups: phototherapy group and SHAM group. The interventions consisted in to participate of physical exercise intervention, and immediately after physical exercises, the voluntaries received, individually, the application of phototherapy. The SHAM group participated the same interventions of phototherapy group, although, during the application of phototherapy, this group did not receive the incidence of laser light. It is important to note that the voluntaries do not know which group they belonged (Fig. 1).

Anthropometric measurements

Weight and height were measured for all patients who wore minimum clothing. After obtaining, the data was calculated using the BMI by dividing the weight by height squared (kg/m^2). Fat mass (% and kg) and lean mass (% and kg) were obtained through the Bioelectrical Impedance InBody®.

Serum analysis

Blood samples were collected at the outpatient clinic at approximately 8:00 A.M. after an overnight fast (12 h). Insulin resistance was assessed using the homeostasis model assessment-insulin resistance (HOMA-IR) calculated by the fasting blood glucose (FBG) and the immunoreactive insulin (I): [FBG (in milligrams per deciliter)×I (in milliunits per liter)]/405. The cutoff value determined for Brazilian population is HOMA-IR>2.71 for classifying the subjects with insulin resistance [19]. The normal range for insulin is 2.60–24.90 μU/ml [20]. The adipokines adiponectin (ng/l) and interleukin-6 (pg/ml) concentrations were measured using a commercially available multiplex assay (EMD Millipore;

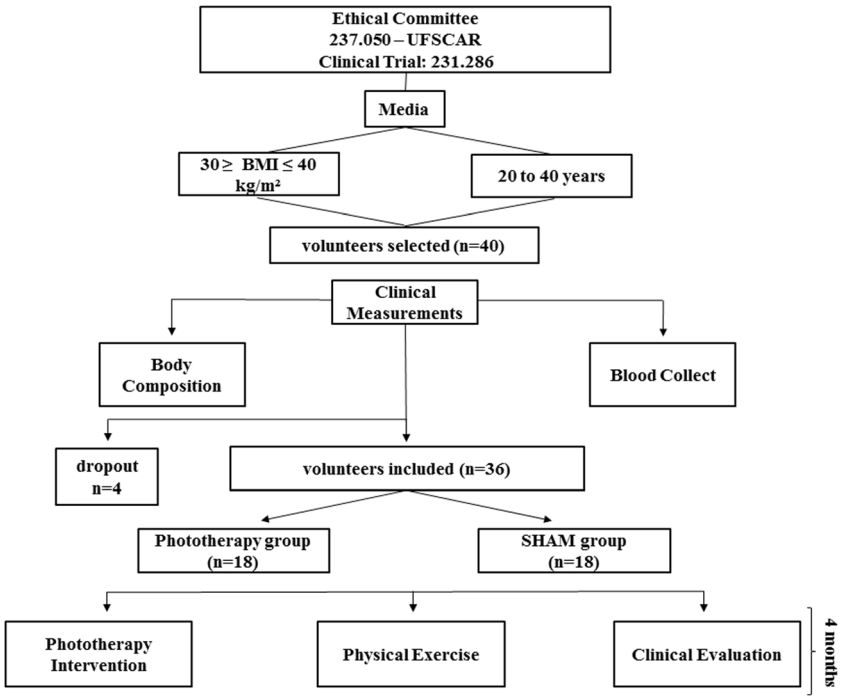

Fig. 1 Diagram of methodology study

HMHMAG-34 K). Manufacture-supplied controls were included to measure assay variation, and all samples were analyzed on the same day to minimize day-to-day variation. A minimum of 100 beads were collected for each analyzed using a Luminex MagPix System (Austin, Texas), which was calibrated and verified prior to sample analysis. Unknown sample values were calculated offline using Milliplex Analyst Software (EMD Millipore) [21].

Descriptive methodology of weight loss therapy

All voluntaries visited the team of health professionals (endocrinologist, nutritionist, and physical educator) three times during the intervention period: (1) baseline (before the participation in the physical exercise and LLLT interventions); (2) after 2 months of participation in the interventions; and (3) after therapy (in the end of 4 months of interventions). They monitored and evaluated all clinical exams of voluntaries and treated health problems during intervention. The medical follow-up included the initial medical history, and a physical examination of blood pressure, cardiac frequency, and body composition were checked.

Physical exercise intervention

Aerobic plus resistance training

During the 4-month period, the voluntaries followed a combined exercise training therapy. The protocol was performed three times per week and included 30 min of aerobic training and 30 min of resistance training per session. At each training session, subjects were instructed to invert the order of the physical exercises, that is, in one session, the individual started the training session with resistance training, and in the subsequent session, the same individual started with aerobic training. The aerobic training consisted of running on a motor-driven treadmill (Movement®) at a 50–75 % of cardiac frequency maximum intensity established by Bruce test adapted. The resistance training was made recruiting the muscle groups: pectoralis major, quadriceps, back, hamstrings, calf, deltoid, biceps, triceps, abdomen, and extensor muscles by performing the following exercises: chest press, leg press, lat pulldown, hamstring curls, calf raises, military press, arm curls, bench press, sit ups, and lower back. The first 2 weeks were used for training adaptation and to learn the movements (3 sets of 15–20 maximal repetitions [MRs]). The protocol consisted of weekly changes of the load, divided into weeks of high loads (6–8 MR), weeks of moderate loads (10–12 MR), and weeks of light loads (15–20 MR). The volunteers performed 18 sets per session, divided into 3 sets of each exercise, followed by rest intervals between the series and exercises: 15–20 MR=45 s, 10–12 MR=1 min, and 6–8 MR=1.5 min of rest. The physical exercise intervention was based on the guidelines from the American College of Sports Medicine (ACSM) [22, 23].

Device description

The phototherapy equipment was developed by the Laboratory Technology Support-LAT, Center for Research in Optics

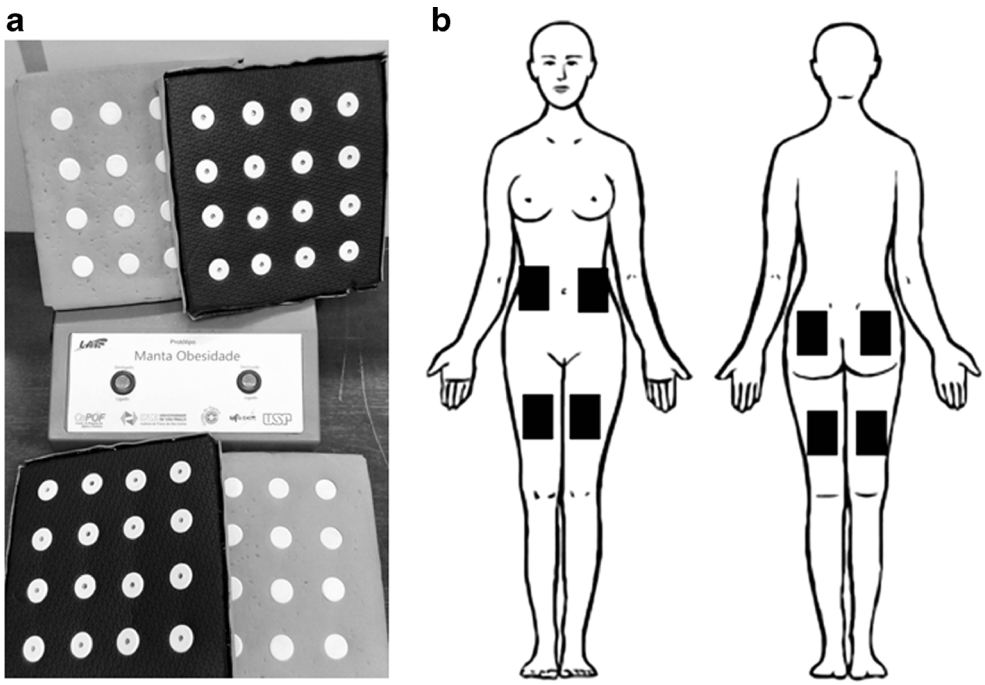

Fig. 2 **a** Illustrative of phototherapy design, **b** illustrative regions of phototherapy application

and Photonics Institute of Physics in São Carlos city at University of São Paulo-USP. The device is composed of four plates made of rubberized material measuring 20 by 20 cm each. Each two plates are connected to an electronic control box. The emitters of Ga-Al-As diode Lasers are distributed in the plate every 2.5 cm, totaling 16 emitters per plate and 64 emitters in total. The device is illustrated in Fig. 2a, and irradiation parameters are in Table 1 [24].

Phototherapy intervention

The application of phototherapy by continuous wave lasers (808 nm) occurs always at the final of training session. Thus, in each week, the patients received 3 sessions of phototherapy. The emitters were arranged perpendicularly to the skin and were allocated in the anterior region: abdominal and quadriceps simultaneously during 8 min. After this, change the position to irradiate the posterior region: gluteus and biceps femoral during 8 min, totalizing 16 min of its application (Fig. 2b).

According with the disposition of the emitters, the irradiance per emitter was 6.0 W/cm^2. The energy delivered per session, per point, was 96 J. The diameters of elliptical spot were 0.3692 cm for horizontal and 0.0582 cm for vertical. The value of spot area was 0.0169 cm^2. The emission and device parameters are described in Table 1 to become reproducible conditions.

Statistical analysis

Statistical analysis was performed using the program STATISTICA version 7.0 for Windows. The adopted significant value was $\alpha<5$ %. Data normality was verified with the Kolmogorov-Smirnov test. Parametric data were expressed as mean±SD, and nonparametric data were expressed as median, minimum, and maximum values. To analyze the effects of intervention and difference between the groups, it applied ANOVA for repeated measures (ANOVA two-way) followed by Tukey post hoc test. The delta values (Δ) were used for the statistical analysis obtained from the difference between the after therapy and baseline values for each variable: Δ variable=after therapy value−baseline value. Comparing the delta values between the groups was performed by *t* test independent by groups to parametric variables and Mann-Whitney test to nonparametric variables.

Results

In the beginning of interdisciplinary intervention, no statistical differences were observed between the groups for the variables: age (years), height (m), weight (kg), BMI (kg/m^2), fat mass (% and kg), lean mass (% and kg), neck circumference (cm), glucose (mg/dl), insulin (μU/ml), HOMA-IR, adiponectin (ng/l), IL-6 (pg/ml), adiponectin/IL-6 ratio, adiponectin/fat mass (kg and %) ratio, and lean mass/fat mass (kg and %) ratio. These data are important to show that the groups present in the investigation were paired at the beginning of the study and future alterations could result by the possible influence of the purpose interdisciplinary therapy in the study (Table 2).

Table 1 Device information, irradiation, and treatment parameters

Type	Ga-Al-As semiconductor diode laser
Wavelength	808 nm
Operating mode	Continuous wave
Number of emitters	16 (per plate)
Number of plate	4
Number of electronic control box	2
	Per emitter
Spot diameter (elliptical shape)	Horizontal 0.3692/vertical 0.0582 cm
Spot area	0.0169 cm^2
Output power	100 mW
Irradiance	6,0 W/cm^2
Radiant energy	96 J
Application technique	Plates over the following perpendicularly to the skin in the regions: anterior region: abdominal and quadriceps simultaneously during 8 min. Change the position to irradiate the posterior region: gluteus and biceps femoral during 8 min totalizing 16 min
Number of points irradiated	64 (per position)/ 128 (total)
Total radiant energy delivered	Per session (16 min) : 6,144 J/all sessions (48): 294,912 J
Number and frequency of treatment sessions	Three times per week after physical exercise, totalizing 48 sessions of treatment

These are the characteristics of equipment and wavelength used during the study. All applications were realized by the same person

Effects of weight loss therapy in the phototherapy group

After 4 months of interdisciplinary intervention associated with the phototherapy sessions, a reduction was observed in the phototherapy group in the body mass (kg), BMI (kg/m^2), fat mass (kg and %), neck circumference (cm), insulin (μU/ml), interleukin-6 (pg/ml) [from 1.11 (0.56–6.8) to 0.56 (0.28–3.62) $p=0.01$] and an increase in the lean mass (%), adiponectin concentration (ng/l) [from 7.01 (2.44–15.14) to 8.44 (5.42–17.14) $p=0.00$], adiponectin/interleukin-6 ratio, lean mass/fat mass (kg and %) ratio, and adiponectin/fat mass (kg and %) ratio. No statistical differences were observed for the variables lean mass (kg), glucose (mg/dl), and HOMA-IR (Table 2 and Fig. 3a, b).

Effects of weight loss therapy in the SHAM group

After 4 months of interdisciplinary intervention, a reduction was observed in the SHAM group in the body mass (kg), BMI (kg/m^2), fat mass (kg and %), neck circumference (cm), increase in the lean mass (% and kg), and lean mass/fat mass (kg and %) ratio. No statistical differences were observed for the variables glucose (mg/dl), insulin (uU/ml), HOMA-IR, adiponectin (ng/l) [from 6.20 (2.38–16.53) to 5.76 (3.14–9.22) $p=0,86$], IL-6 (pg/ml) [from 0.91 (0.28–2.79) to 0.56 (0.28–3.34) $p=0.13$], and adiponectin/fat mass (kg/%) ratio (Table 2 and Fig. 3a, b).

Effects of weight loss therapy between the groups

Comparing the delta values between the groups, it was observed that the phototherapy group showed a statistical reduction in the values of neck circumference (cm) [−2.08±1.49 to −0.88±1.08; $p=0.01$], insulin concentration (μU/ml) [−5.72±3.68 to −1.60±4.05; $p=0.00$], interleukin-6 (pg/ml) [−0.97 (−4.29–0.76) to −0.20 (−0.81–1.8); $p=0.00$] compared to SHAM group. Also, an increase in the adiponectin concentration (ng/ml) [1.08 (0.04–3.62) to −0.42 (−3.15–2.26); $p=0.03$] and adiponectin/fat mass (%) ratio [0.09±0.13 to 0.003±0.04; $p=0.05$] was shown compared with SHAM group (Table 3; Figs. 4 and 5a–d).

Discussion

The most important finding in the present investigation is that we were able to show an increase in adiponectin concentration associated with a reduction in IL-6 after 20 weeks of treatment with LLLT associated with aerobic plus resistance training (Fig. 3a, b). There is strong evidence that demonstrates that LLLT was effective as a supporting noninvasive tool in the treatment for the reduction of body measurements and cellulite and improvement of lipid profile [20, 21]. However, the underlying key mechanism of actions for such potential effects to reduce body fat and the inflammatory process related to obesity in women is still unclear.

As we know, adiponectin has a great anti-inflammatory effect, mediated by an increase in the insulin sensitivity and improvement of glucose metabolism, providing an antiatherogenic effect in humans [22, 25]. This is supported by the present investigation where a significant reduction in the insulin concentration was only shown in the phototherapy group, suggesting a possible improvement in insulin sensitivity. However, no changes were observed in the glucose concentration and HOMA-IR, probably because the volunteers showed glucose concentration and insulin levels according to reference values [26]. Nevertheless, this needs to be confirmed in a long-term therapy using LLLT.

Furthermore, there is a consensus that a state of hypoadiponectinemia was present in the metabolic syndrome and obesity population exacerbating the inflammatory process and increasing cardiovascular risk [22]. It has also been shown that hypoadiponectinemia was inversely correlated with

Table 2 Effects of aerobic plus resistance training associate with phototherapy in body composition and inflammatory biomarkers in obese adults

	Phototherapy group			SHAM group			
	Baseline	After therapy	p #	Baseline	After therapy	p #	p *
Age (years)	33.06±4.72	—	—	34.33±4.95	—	—	—
Height (m)	1.66±0.07	1.66±0.07	—	1.62±0.05	1.62±0.04	—	—
Body mass (kg)	96.60±11.36	91.86±13.20	**0.00**	90.73±11.25	86.74±11.05	**0.00**	0.80
BMI (kg/m^2)	34.35 (29.13–42.18)	31.67 (27.47–38.28)	**0.00**	34.19 (29.76–40.31)	33.03 (0–40.23)	**0.00**	0.99
Fat mass (%)	40.12±3.14	37.77±3.44	**0.00**	40.42±2.97	38.07±3.37	**0.00**	0.97
Fat mass (kg)	38.92±6.92	36.30±6.90	**0.00**	36.44±7.40	33.88±7.41	**0.00**	0.78
Lean mass (%)	59.88±3.14	63.70±6.90	**0.01**	59.57±2.97	66.11±7.42	**0.00**	0.87
Lean mass (kg)	57.52±5.42	56.44±5.31	0.08	54.03±4.44	53.35±4.29	**0.02**	0.56
Neck circumference (cm)	37.51±2.97	36.21±2.01	**0.00**	36.92±2.08	36.22±2.04	**0.04**	1.00
Glucose (mg/dl)	91.47±8.69	93.06±6.63	0.77	92.67±7.89	93.89±10.89	0.87	0.99
Insulin (μU/ml)	16.90±5.61	11.34±4.17	**0.01**	16.69±6.26	14.3±6.89	0.39	0.97
HOMA-IR	3.72±1.77	2.99±1.67	0.42	3.87±1.62	3.04±1.54	0.31	0.99
Adiponectin/IL-6 ratio	6.08±5.28	16.47±12.29	**0.01**	9.15±7.83	11.41±6.88	0.65	0.95
Adiponectin/fat mass (kg) ratio	0.19±0.09	0.31±0.15	**0.00**	0.19±0.10	0.16±0.05	0.99	0.16
Adiponectin/fat mass (%) ratio	0.19±0.08	0.27±0.13	**0.00**	0.16±0.08	0.14±0.04	0.99	0.92
Lean mass/fat mass (kg) ratio	1.5±0.19	1.61±0.24	**0.00**	1.52±0.21	1.65±0.23	**0.00**	0.98
lean mass/fat mass (%) ratio	1.5±0.19	1.71±0.31	**0.00**	1.48±0.18	1.76±0.34	**0.00**	0.95

HOMA-IR homeostasis model assessment-insulin resistance, *IL-6* interleukin-6

Statistical significance $p<0.05$

Statistical differences are related to comparison of baseline vs after therapy values in the same group

* Statistical differences are related to comparison of after therapy values between the groups

cIMT, an important subclinical surrogate of inflammation, confirming its key role in atherogenesis [27]. This is substantiated by our results which may support the evidence that LLLT is an important tool in the inflammatory process related to obesity since we were able to show a significant increase in adiponectin concentration in the LLLT group alone; it is important to note that in the SHAM group, this adipokine concentration was not changed.

In corroboration, Wu and colleagues [28] recently showed that human adipose-derived stem cells (hADSCs) expressed toll-like receptors (TLR) and that lipopolysaccharide (LPS) increased the production of proinflammatory interleukin-6

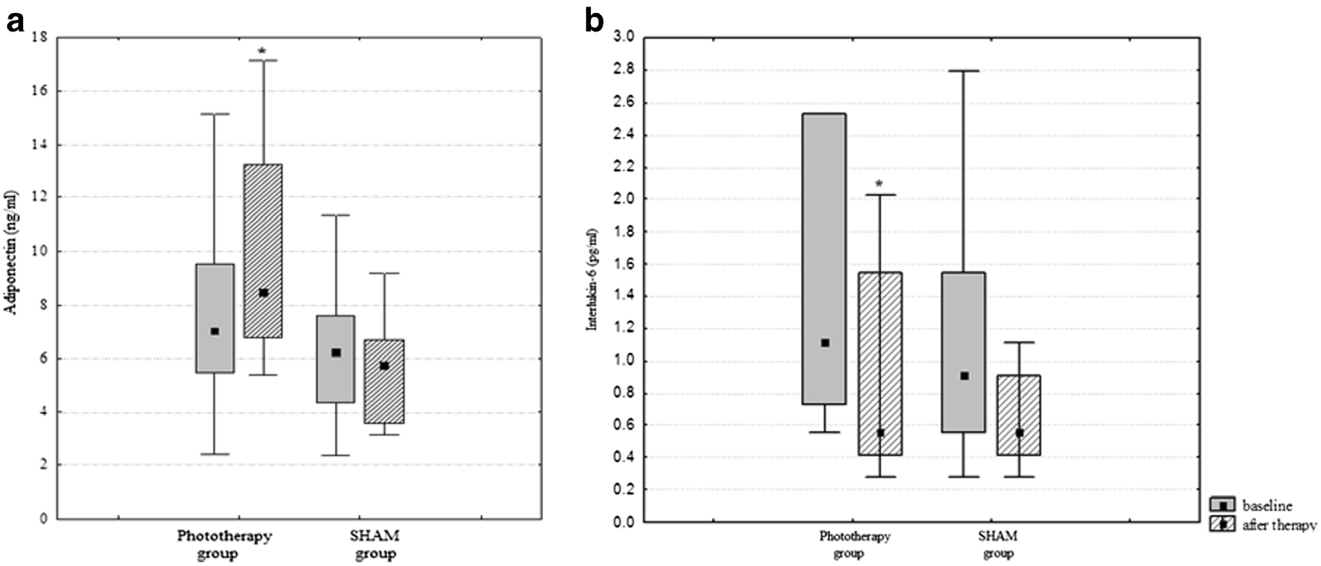

Fig. 3 Effects of interdisciplinary weight loss therapy in both groups. **a** Adiponectin, **b** Interleukin-6. *Statistical difference

Table 3 Comparison of magnitude effects of therapy between groups

	Phototherapy group	SHAM group	$p^{\#}$
Body mass (kg)	−4.60±3.083	−5.72±2.43	0.27
BMI (kg/m^2)	−1.9±1.02	−1.99±1.05	0.81
Fat mass (%)	−2.1±1.51	−2.26±1.22	0.73
Fat mass (kg)	−3.52±2.18	−3.94±1.97	0.57
Lean mass (%)	3.94±4.65	6.16±5.04	0.21
Lean mass (kg)	−0.92±1.75	−1.21±1.21	0.58
Glucose (mg/dl)	1.59±5.75	1.22±7.63	0.87
HOMA-IR	−0.73±2.43	−0.82±1.26	0.29
Adiponectin/IL-6 ratio	12.69±12.51	2.96±8.37	0.07
Adiponectin/fat mass (kg) ratio	0.04±0.10	0.004±0.04	0.22
Lean mass/fat mass (kg) ratio	0.13±0.11	0.14±0.10	0.67
Lean mass/fat mass (%) ratio	0.20±0.18	0.25±0.19	0.46

HOMA-IR homeostasis model assessment-insulin resistance, *IL-6* interleukin-6

Statistical significance $p<0.05$

Statistical differences are related to comparison between the groups

(IL-6). On the other hand, it was proposed that LLLT markedly inhibited LPS induction, corroborating the reduction in the expression of proinflammatory cytokines. In fact, LLLT promoted a reduction in IL-1β, IL-6, and TNF-α in experimental studies [29, 30]. Some mechanisms are proposed to explain the LLLT action; one is based on the production of transient pores in adipocytes which stimulates lipolysis. Furthermore, it has been suggested that LLLT activates a cascade of activities, which could cause the induction of adipocyte apoptosis leading to a release of lipids [31].

Interestingly, it has been shown that the application of phototherapy can promote biochemical adaptation of the mitochondria with changes in the redox state, leading to a conversion of electromagnetic to biochemical energy and consequently increasing the oxygen binding, production of ATP, respiration rate, and formation of giant mitochondria [32, 33]. Also, LLLT may activate enzymatic processes in cells to improve metabolism and lipid profile [16, 34]. Recent evidence in experimental investigations suggests that LLLT promotes skeletal muscle regeneration by reducing the duration of acute inflammation and accelerating tissue repair. This would happen through modulated cytokine expression during short-term muscle remodeling, inducing a decrease in TNF-α, TGF-β, and IL-1β without cytotoxic effects [29, 30].

Our results support these findings since the significant reduction in IL-6 was only observed in the phototherapy group compared with the SHAM group. These results confirm our hypothesis that LLLT can modulate a cascade of reactions to change body homeostasis leading to better association between proinflammatory/anti-inflammatory adipokines, improving health in obese women. LLLT also acts on the markers of oxidative stress, such as protein carbonyls and superoxide dismutase [35, 36], in addition to yielding clinical signs of improvement, delayed muscle fatigue, and improved physical performance [36–39]. Corroborating this, it is known that IL-6 is an important interleukin produced by myocytes to improve muscle repair, and its production is stimulated by resistance training [36]. In fact, it was recently suggested that LLLT in conjunction with aerobic training may provide a therapeutic approach to intensely reduce proinflammatory markers in an experimental study, including a reduction in IL-6 and TNF-alpha. However, LLLT without exercise was not able to improve physical performance in elderly animals [36].

Altogether, these results reinforce the potential effects of LLLT associated with combined training to promote some amelioration in the inflammatory process related to obesity in both animals and humans. Corroborating these findings,

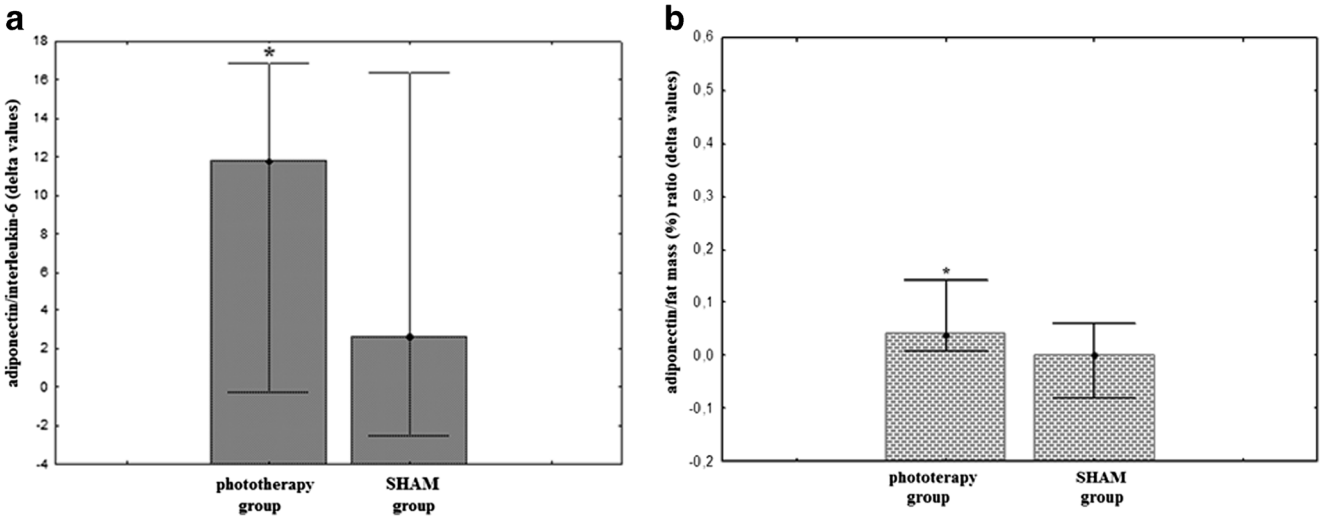

Fig. 4 Comparative effects of interdisciplinary weight loss therapy both groups. Adiponectin/fat mass (%) ratio. Delta value; *statistical difference

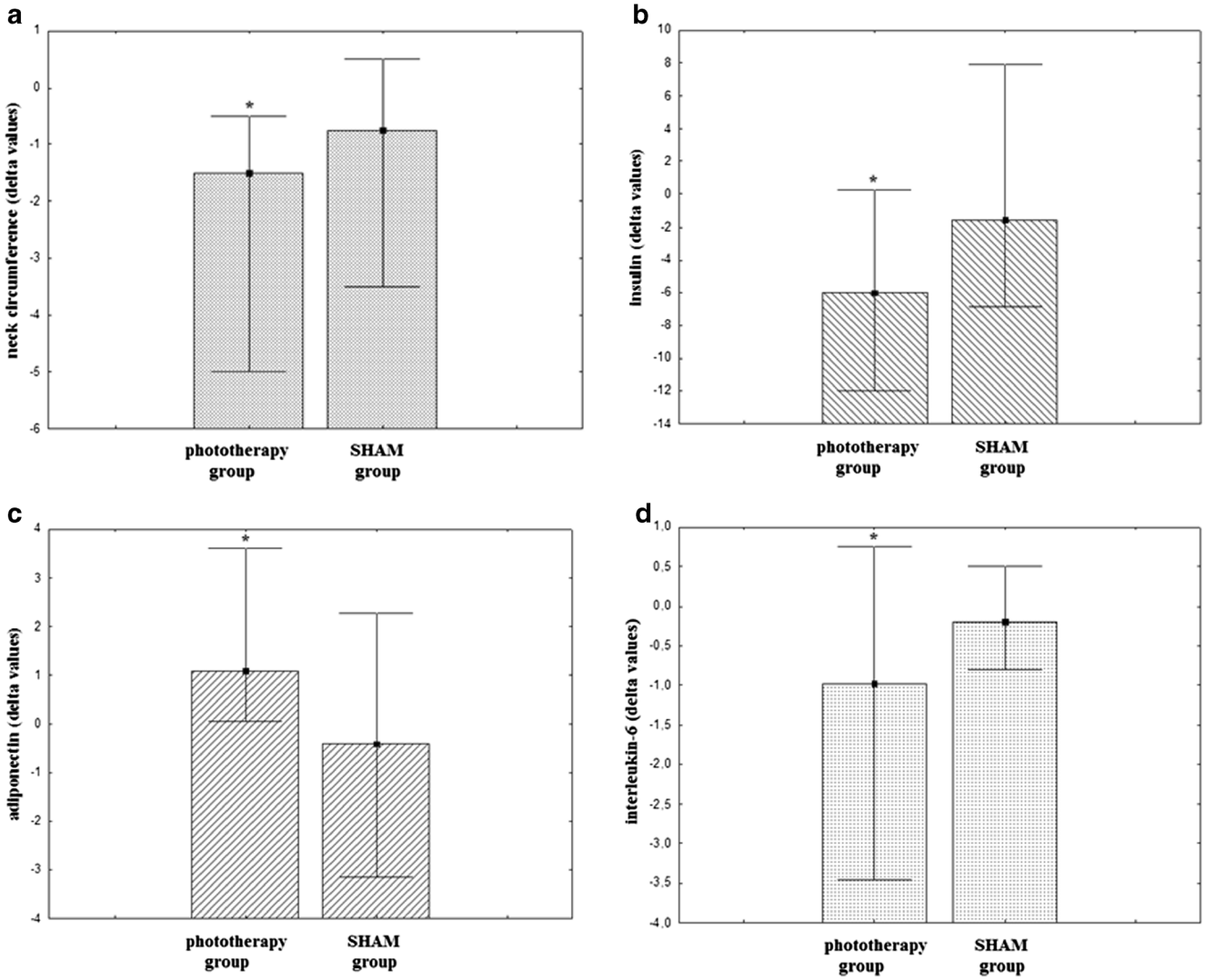

Fig. 5 Comparative effects of interdisciplinary weight loss therapy both groups. **a** Neck circumference, **b** insulin, **c** adiponectin, **d** interleukin-6. Delta values; *statistical difference

in the present study, we observed an increase in adiponectin concentration, a reduction in IL-6 and insulinemia, and a significant improvement in the adiponectin/interleukin-6 ratio, important markers of inflammatory state only in the phototherapy group.

Additionally, we were able to show an increase in the adiponectin/fat mass (kg and %) ratio in the phototherapy group. In fact, results published in the current year suggest that the use of LLLT may enhance cellular homeostasis, promoting an increase in the concentration of active mitochondria in irradiated cells through an upregulation of the genes involved in the mitochondrial complexes [40, 41]. In addition, physical exercise promotes biochemical and structural changes in the mitochondria [42]. Collectively, these results might suggest the hypothesis that phototherapy may help enhance the effects of physical exercise training proposed in the present investigation. The exact mechanisms of action following LLLT are not yet well understood; however, it has been proposed that the chronic application of LLLT can activate or inhibit enzymes. In this context, it was previously suggested that LLLT intensifies the transfer of electrons within cytochrome-c oxidase by making more electrons available. Thus, it may accelerate oxidative metabolism leading to an increase in ATP synthesis [43].

There has been a recent discovery of irisin which is predominantly secreted by muscle tissue acting as an endocrine organ in response to physical exercise. During physical exercise, peroxisome proliferator-activated receptor coactivator 1α (PGC1α) is activated, inducing the release of fibronectin domain-containing protein 5 (FNDC5) which is then cleaved to irisin. This hormone may improve the transdifferentiation of white adipocyte to beige and brown, in both white and brown adipose tissues, by enhancing the lipid mobilization and activating the uncoupling protein 1 (UCP1) in mitochondria, resulting in the synthesis of adenosine triphosphate (ATP) and the dissipation of energy in the form of heat. This

process could promote reductions in body weight and improvements in metabolic profile, suggesting that irisin could be a possible novel treatment for diabetes and obesity [44]. Therefore, it is possible to hypothesize that the combination of LLLT associated with combined exercise in the present study may accentuate the response in the control of fat mass correspondent to a reduction in the inflammatory state, since we were able to show an increase in the adiponectin/fat mass (% and kg) in the phototherapy group. However, this needs to be confirmed in future research with a focus on investigations into the possible influences of LLLT intervention in the transdifferentiation process of white adipocyte to beige and brown associated with exercise training.

Our findings present some limitations, including the absence of experiments with different kinds of laser irradiation. The effects of laser irradiation are highly dependent on characteristics such as wavelength, power density, and fluency [40, 45–47].

However, to our knowledge, the current study is the first investigation to show that LLLT improves the inflammatory process related to obesity in obese women, particularly by promoting a reduction in the proinflammatory IL-6 and an increase in the anti-inflammatory adiponectin, adiponectin/interleuckin-6, and adiponectin/fat mass ratio (kg and %). In addition, the LLLT showed higher changes in the control of neck circumference compared with the SHAM group. Interestingly, it was recently suggested that there is growing evidence that neck circumference is considered an interesting marker of inflammation and cardiovascular diseases [48, 49]. Nevertheless, it is important to note that in both analyzed groups, the BMI, body mass, and body fat presented similar changes, considering delta values after 20 weeks of LLLT associated with physical exercise training.

Finally, there are a limited number of clinical studies with the application of LLLT in obesity. However, a number of clinical applications have been found for the lasers in a variety of medical specialties [33]. Therefore, this needs to be confirmed in a large cohort study of the obesity population.

Conclusions

In the present investigation, we were able to show that the association of physical exercise training with low-level laser (light) therapy applied in obese women during a 4-month period promotes an improvement in the inflammatory framework and body composition. These are important results that suggest that phototherapy can be an important tool in the treatment of obesity, principally considering its potential effects associated with physical exercise training in attenuating inflammation in women, and as such, these results are applicable in the clinical practices to control the related risks associated with obesity.

Acknowledgments Support Foundation of São Paulo Research-FAPESP (2013/041364; 2013/19046-0; 002804928-41), National Council for Scientific and Technological Development–CNPq (150177/2014-3), and Coordination of Higher Education Personnel Training–CAPES.

Conflict of interest The authors have nothing to disclose.

References

1. Gasparyan VC (2000) Method of determination of aortic valve parameters for its reconstruction with autopericardium: an experimental study. J Thorac Cardiovasc Surg 119:386–387
2. Ucero AC, Sabban B, Benito-Martin A, Carrasco S, Joeken S, Ortiz A (2013) Laser therapy in metabolic syndrome-related kidney injury. Photochem Photobiol 89(4):953–960
3. Mitu F, Cobzaru R, Leon MM (2013) Influence of metabolic syndrome profile on cardiovascular risk. Rev Med Chir Soc Med Nat Iasi 117(2):308–314
4. Padwal RS (2013) Obesity, Diabetes, and the Metabolic Syndrome: The Global Scourge. Can J Cardiol 8. pii: S0828-282X(13)01635-8.
5. Correia F, Poínhos R, Freitas P, Pinhão S, Maia A, Carvalho D, Medina JL (2006) Prevalence of the metabolic syndrome: comparison between ATPIII and IDF criteria in a feminine population with severe obesity. Acta Med Port 19(4):289–293
6. Caranti DA, Lazzer S, Dâmaso AR, Agosti F, Zennaro R, de Mello MT, Tufik S, Sartorio A (2008) Prevalence and risk factors of metabolic syndrome in Brazilian and Italian obese adolescents: a comparison study. Int J Clin Pract 62(10):1526–1532
7. Phillips CM, Perry IJ (2013) Does inflammation determine metabolic health status in obese and nonobese adults? J Clin Endocrinol Metab 98(10):E1610–1619
8. Matos MF, Lourenço DM, Orikaza CM, Gouveia CP, Morelli VM (2013) Abdominal obesity and the risk of venous thromboembolism among women: a potential role of interleukin-6. Metab Syndr Relat Disord 11(1):29–34
9. Mirza S, Qu HQ, Li Q, Martinez PJ, Rentfro AR, McCormick JB, Fisher-Hoch SP (2011) Adiponectin/leptin ratio and metabolic syndrome in a Mexican American population. Clin Invest Med 34(5), E290
10. Masquio DC, de Piano A, Sanches PL, Corgosinho FC, Campos RM, Carnier J, da Silva PL, Caranti DA, Tock L, Oyama LM, Oller do Nascimento CM, de Mello MT, Tufik S, Dâmaso AR (2013) The effect of weight loss magnitude on pro-/anti-inflammatory adipokines and carotid intima-media thickness in obese adolescents engaged in interdisciplinary weight loss therapy. Clin Endocrinol (Oxf) 79(1):55–64
11. Lukic L, Lalic NM, Rajkovic N, Jotic A, Lalic K, Milicic T, Seferovic JP, Macesic M, Gajovic JS (2014) Hypertension in obese type 2 diabetes patients is associated with increases in insulin resistance and IL-6 cytokine levels: potential targets for an efficient preventive intervention. Int J Environ Res Public Health 11(4): 3586–3598
12. Corgosinho FC, de Piano A, Sanches PL, Campos RM, Silva PL, Carnier J, Oyama LM, Tock L, Tufik S, de Mello MT, Dâmaso AR (2012) The role of PAI-1 and adiponectin on the inflammatory state and energy balance in obese adolescents with metabolic syndrome. Inflammation 35(3):944–951
13. Su SC, Pei D, Hsieh CH, Hsiao FC, Wu CZ, Hung YJ (2011) Circulating pro-inflammatory cytokines and adiponectin in young men with type 2 diabetes. Acta Diabetol 48(2):113–119
14. Lira FS, Rosa JC, Dos Santos RV, Venancio DP, Carnier J, Sanches Pde L, do Nascimento CM, de Piano A, Tock L, Tufik S, de Mello

MT, Dâmaso AR, Oyama LM (2011) Visceral fat decreased by long-term interdisciplinary lifestyle therapy correlated positively with interleukin-6 and tumor necrosis factor-α and negatively with adiponectin levels in obese adolescents. Metabolism 60(3):359–365
15. Hrnjak M, Kuljic-Kapulica N, Budisin A, Giser A (1995) Stimulatory effect of low-power density He-Ne laser radiation on human fibroblasts in vitro. Vojnosanit Pregl 52:539–546
16. Aquino AE Jr, Sene-Fiorese M, Paolillo FR, Duarte FO, Oishi JC, Pena AA Jr, Duarte AC, Hamblin MR, Bagnato VS, Parizotto NA (2013) Low-level laser therapy (LLLT) combined with swimming training improved the lipid profile in rats fed with high-fat diet. Lasers Med Sci 28(5):1271–1280
17. Ryan AS, Ge S, Blumenthal JB, Serra MC, Prior SJ, Goldberg AP (2014) Aerobic Exercise and Weight Loss Reduce Vascular Markers of Inflammation and Improve Insulin Sensitivity in Obese Women. J Am Geriatr Soc 62(4):607–614
18. Dobrosielski DA, Barone Gibbs B, Chaudhari S, Ouyang P, Silber HA, Stewart KJ (2013) Effect of exercise on abdominal fat loss in men and women with and without type 2 diabetes. BMJ Open 3(11):e003897
19. Geloneze B, Repetto EM, Geloneze SR, Tambascia MA, Ermetice MN (2006) The threshold value for insulin resistance (HOMA-IR) in an admixtured population IR in the Brazilian Metabolic Syndrome Study. Diabetes Res Clin Pract 72(2):219–220
20. Shan W, Ning C, Luo X, Zhou Q, Gu C, Zhang Z, Chen X (2014) Hyperinsulinemia is associated with endometrial hyperplasia and disordered proliferative endometrium: a prospective cross-sectional study. Gynecol Oncol 32(3):606–610
21. Dossus L, Becker S, Achaintre D, Kaaks R, Rinaldi S (2009) Validity of multiplex-based assays for cytokine measurements in serum and plasma from "non-diseased" subjects: comparison with ELISA. J Immunol Methods 350:125–132
22. Donnelly JE, Blair SN, Jakicic JM, Manore MM, Rankin JW, Smith BK, American College of Sports Medicine (2009) American College of Sports Medicine Position Stand. Appropriate physical activity intervention strategies for weight loss and prevention of weight regain for adults. Med Sci Sports Exerc 41:459–471
23. Kraemer WJ, Ratamess NA, French DN (2002) Resistance training for health and performance. Curr Sports Med Rep 1:165–171
24. Jenkins PA, Carroll JD (2011) How to report low-level laser therapy (LLLT)/photomedicine dose and beam parameters in clinical and laboratory studies. Photomed Laser Surg 29(12):785–787
25. Matsuda M, Shimomura I (2014) Roles of adiponectin and oxidative stress in obesity-associated metabolic and cardiovascular diseases. Rev Endocr Metab Disord 15(1):1–10
26. Alberti KG, Zimmet P, Shaw J (2006) Metabolic syndrome: a new world-wide definition: a consensus statement from the International Diabetes Federation. Diabet Med 23(5):469–480
27. Rubio-Guerra AF, Cabrera-Miranda LJ, Vargas-Robles H, Maceda-Serrano A, Lozano-Nuevo JJ, Escalante-Acosta BA (2013) Correlation between levels of circulating adipokines and adiponectin/resistin index with carotid intima-media thickness in hypertensive type 2 diabetic patients. Cardiology 125(3):150–153
28. Wu JY, Chen CH, Wang CZ, Ho ML, Yeh ML, Wang YH (2013) Low-power laser irradiation suppresses inflammatory response of human adipose-derived stem cells by modulating intracellular cyclic AMP level and NF-κB activity. PLoS One 8(1), e54067
29. Mesquita-Ferrari RA, Martins MD, Silva JA Jr, da Silva TD, Piovesan RF, Pavesi VC, Bussadori SK, Fernandes KP (2011) Effects of low-level laser therapy on expression of TNF-α and TGF-β in skeletal muscle during the repair process. Lasers Med Sci 26(3):335–340
30. Lima AA, Spínola LG, Baccan G, Correia K, Oliva M, Vasconcelos JF, Soares MB, Reis SR, Medrado AP (2014) Evaluation of corticosterone and IL-1β, IL-6, IL-10 and TNF-α expression after 670-nm laser photobiomodulation in rats. Lasers Med Sci 29(2):709–715
31. Avci P, Nyame TT, Gupta GK, Sadasivam M, Hamblin MR (2013) Low-level laser therapy for fat layer reduction: a comprehensive review. Lasers Surg Med 45(6):349–357
32. Amat A, Rigau J, Waynant RW, Ilev IK, Tomas J, Anders JJ (2005) Modification of the intrinsic fluorescence and the biochemical behavior of ATP after irradiation with visible and near-infrared laser light. J Photochem Photobiol B 81:26–32
33. Bakeeva LE, Manteifel VM, Rodichev EB, Karu TI (1993) Formation of gigantic mitochondria in human blood lymphocytes under the effect of an He-Ne laser. Mol Biol (Mosk) 27:608–617
34. Ferraresi C, de Brito OT, de Oliveira ZL, de Menezes Reiff RB, Baldissera V, de Andrade Perez SE, Matheucci Junior E, Parizotto NA (2011) Effects of low level laser therapy (808 nm) on physical strength training in humans. Lasers Med Sci 26(3):349–358
35. Leal Junior EC, Lopes-Martins RA, Frigo L, De Marchi T, Rossi RP, de Godoi V, Tomazoni SS, Silva DP, Basso M, Filho PL, de Valls CF, Iversen VV, Bjordal JM (2010) Effects of low-level laser therapy (LLLT) in the development of exercise-induced skeletal muscle fatigue and changes in biochemical markers related to post-exercise recovery. J Orthop Sports Phys Ther 40(8):524–532
36. Amadio EM, Serra AJ, Guaraldo SA, Silva JA Jr, Antônio EL, Silva F, Portes LA, Tucci PJ, Leal-Junior EC, de Carvalho PT (2015) The action of pre-exercise low-level laser therapy (LLLT) on the expression of IL-6 and TNF-α proteins and on the functional fitness of elderly rats subjected to aerobic training. Lasers Med Sci Feb 3.
37. Leal Junior EC, Lopes-Martins RA, Dalan F, Ferrari M, Sbabo FM, Generosi RA, Baroni BM, Penna SC, Iversen VV, Bjordal JM (2008) Effect of 655-nm low-level laser therapy on exercise-induced skeletal muscle fatigue in humans. Photomed Laser Surg 26(5):419–424
38. Leal-Junior EC, Vanin AA, Miranda EF, de Carvalho PT, Dal Corso S, Bjordal JM (2015) Effect of phototherapy (low-level laser therapy and light-emitting diode therapy) on exercise performance and markers of exercise recovery: a systematic review with meta-analysis. Lasers Med Sci 30(2):925–939
39. Lopes-Martins RA, Marcos RL, Leonardo PS, Prianti AC Jr, Muscará MN, Aimbire F, Frigo L, Iversen VV, Bjordal JM (1985) Effect of low-level laser (Ga-Al-As 655 nm) on skeletal muscle fatigue induced by electrical stimulation in rats. J Appl Physiol 101(1):283–288
40. Houreld NN (2014) Shedding light on a new treatment for diabetic wound healing: a review on phototherapy. ScientificWorldJournal 6:398412
41. Masha RT, Houreld NN, Abrahamse H (2013) Low-intensity laser irradiation at 660 nm stimulates transcription of genes involved in the electron transport chain. Photomed Laser Surg 31(2):47–53
42. Irrcher I, Adhihetty PJ, Joseph AM, Ljubicic V, Hood DA (2003) Regulation of mitochondrial biogenesis in muscle by endurance exercise. Sports Med 33:783–793
43. Silveira PC, Silva LA, Fraga DB, Freitas TP, Streck EL, Pinho R (2009) Evaluation of mitochondrial respiratory chain activity in muscle healing by low-level laser therapy. J Photochem Photobiol B 95(2):89–92
44. Novelle MG, Contreras C, Romero-Picó A, López M, Diéguez C (2013) Irisin, two years later. Int J Endocrinol 2013:746281
45. Houreld N, Abrahamse H (2007) In vitro exposure of wounded diabetic fibroblast cells to a helium-neon laser at 5 and 16 J/cm2. Photomed Laser Surg 25(2):78–84
46. Houreld NN, Abrahamse H (2007) Effectiveness of helium-neon laser irradiation on viability and cytotoxicity of diabetic-wounded fibroblast cells. Photomed Laser Surg 25(6):474–481
47. Hawkins DH, Abrahamse H (2006) The role of laser fluence in cell viability, proliferation, and membrane integrity of wounded human

skin fibroblasts following helium-neon laser irradiation. Lasers Surg Med 38(1):74–83

48. Preis SR, Pencina MJ, D'Agostino RB Sr, Meigs JB, Vasan RS, Fox CS (2013) Neck circumference and the development of cardiovascular disease risk factors in the Framingham Heart Study. Diabetes Care 36(1), e3

49. Jamar G, Pisani LP, Oyama LM, Belote C, Masquio DC, Furuya VA, Carvalho-Ferreira JP, Andrade-Silva SG, Dâmaso AR, Caranti DA (2013) Is the neck circumference an emergent predictor for inflammatory status in obese adults? Int J Clin Pract 67(3):217–224

Lasers Med Sci (2015) 30:1259–1267
DOI 10.1007/s10103-015-1723-8

ORIGINAL ARTICLE

Time response of increases in ATP and muscle resistance to fatigue after low-level laser (light) therapy (LLLT) in mice

Cleber Ferraresi · Marcelo Victor Pires de Sousa · Ying-Ying Huang · Vanderlei Salvador Bagnato · Nivaldo Antonio Parizotto · Michael R. Hamblin

Received: 24 November 2014 / Accepted: 9 February 2015 / Published online: 21 February 2015

Abstract Recently, low-level laser (light) therapy has been used to increase muscle performance in intense exercises. However, there is a lack of understanding of the time response of muscles to light therapy. The first purpose of this study was to determine the time response for light-emitting diode therapy (LEDT)-mediated increase in adenosine triphosphate (ATP) in the soleus and gastrocnemius muscles in mice. Second purpose was to test whether LEDT can increase the resistance of muscles to fatigue during intense exercise. Fifty male Balb/c mice were randomly allocated into two equal groups: LEDT-ATP and LEDT-fatigue. Both groups were subdivided into five equal subgroups: LEDT-sham, LEDT-5 min, LEDT-3 h, LEDT-6 h, and LEDT-24 h. Each subgroup was analyzed for muscle ATP content or fatigue at specified time after LEDT. The fatigue test was performed by mice repeatedly climbing an inclined ladder bearing a load of 150 % of body weight until exhaustion. LEDT used a cluster of LEDs with 20 red (630± 10 nm, 25 mW) and 20 infrared (850±20 nm, 50 mW) delivering 80 mW/cm^2 for 90 s (7.2 J/cm^2) applied to legs, gluteus, and lower back muscles. LEDT-6 h was the subgroup with the highest ATP content in soleus and gastrocnemius compared to all subgroups ($P<0.001$). In addition, mice in LEDT-6 h group performed more repetitions in the fatigue test ($P<0.001$) compared to all subgroups: LEDT-sham and LEDT-5 min (~600 %), LEDT-3 h (~200 %), and LEDT-24 h (~300 %). A high correlation between the fatigue test repetitions and the ATP content in soleus ($r=0.84$) and gastrocnemius ($r=0.94$) muscles was observed. LEDT increased ATP content in muscles and fatigue resistance in mice with a peak at 6 h. Although the time response in mice and humans is not the same, athletes might consider applying LEDT at 6 h before competition.

Keywords Light-emitting diode therapy · Muscle ATP content · Photobiomodulation · Resistance to exercise fatigue · Time response

C. Ferraresi · N. A. Parizotto
Laboratory of Electrothermophototherapy, Department of Physical Therapy, Federal University of São Carlos, São Paulo, Brazil

C. Ferraresi · N. A. Parizotto
Post-Graduation Program in Biotechnology, Federal University of Sao Carlos, São Paulo, Brazil

C. Ferraresi · V. S. Bagnato
Physics Institute of Sao Carlos, University of Sao Paulo, Sao Carlos, Brazil

C. Ferraresi · M. V. P. de Sousa · Y.-Y. Huang · M. R. Hamblin (✉)
Wellman Center for Photomedicine, Massachusetts General Hospital, 40 Blossom Street, Boston, MA, USA
e-mail: mhamblin@partners.org

M. V. P. de Sousa
Laboratory of Radiation Dosimetry and Medical Physics, Institute of Physics, Sao Paulo University, São Paulo, SP, Brazil

Y.-Y. Huang · M. R. Hamblin
Department of Dermatology, Harvard Medical School, Boston, MA, USA

M. R. Hamblin
Harvard-MIT Division of Health Science and Technology, Cambridge, MA, USA

Introduction

Low-level laser (light) therapy (LLLT) uses visible or near-infrared light to produce photobiomodulation in biological tissues which can either stimulate or inhibit biological responses depending on dose. Since 1967, this therapy has been used for several applications in medicine to treat disorders such as inflammation, pain, or accelerate healing [1–3]. Light therapy can be delivered by laser diodes, light-emitting diodes

(LEDs), or other light sources with specific wavelengths ("colors") [1].

Several researchers have investigated the mechanism of how LLLT interacts with biological tissues to produce the photobiomodulation phenomenon [4–6]. One of first studies published reported the formation of "giant mitochondria" after the use of light therapy [7]. Several studies discovered molecules (called chromophores) inside cells that could absorb the light producing modulations in cell metabolism [4]. Among these molecules, cytochrome c oxidase (Cox) which is the complex IV of the mitochondrial electron transport chain has received special attention [4, 8–11].

Recently, Hayworth et al. [12] used an array of LED (660 nm) to increase Cox activity after 24 h after light therapy when applied to rat muscles without contact. These authors reported differences in Cox activity depending on the type of muscle fibers.

Increased Cox activity is supposed to be responsible for stimulating the synthesis of adenosine triphosphate (ATP) [4]. Karu [4] reported several years ago that light therapy effects on biological tissues can be classified as either primary (light-tissue interactions) or secondary mechanisms (photobiomodulation). One of the most frequently observed effects of photobiomodulation is the increased ATP synthesis in cultured cells [4, 13, 14].

Increased Cox activity resulting in more ATP synthesis has been the principle explanation in studies that have used LLLT to increase muscle performance before (muscular pre-conditioning) or after (muscle recovery) different types of exercise [15–17]. Combined with other metabolic products as lactate and accumulation of adenosine diphosphate (ADP), ATP synthesis is important for optimum muscle performance since reduced levels of ATP in muscles have been held responsible for lowered resistance of muscles to fatigue and decreased performance in many types of exercise [18].

The scientific literature reports several strategies and therapies to increase muscle performance in different sports. However, several drugs have been prohibited from being used for this purpose as they are considered "doping" [19]. With this perspective in mind, over the last decade, some researchers have used light therapy to promote muscular pre-conditioning and to increase performance in intense exercise [15–17]. These reports have found good effects with this regimen of light therapy in muscular pre-conditioning, preventing muscle damage, and increasing the number of repetitions in fatigue tests. However, the majority of these results have only reported a small improvement compared to control groups, mainly measuring the number of repetitions in fatigue tests [20–22]. There may be a lack of understanding of the time response of muscles to light therapy and uncertainty about the best time to apply the light for optimal fatigue-muscle resistance in exercise until exhaustion.

The present study aimed to investigate (a) if light-emitting diode therapy (LEDT) can increase muscle ATP synthesis in vivo, (b) the possible time response for ATP synthesis in gastrocnemius and soleus muscles in mice mediated by LEDT, (c) the possible time response after LEDT for increased muscle performance in fatigue test, and (d) correlations between ATP contents in soleus and gastrocnemius muscles with the fatigue test. This study suggests that LEDT may be a new strategy for improved muscle performance as well as indicates which time is better to use light therapy in muscular pre-conditioning.

Materials and methods

Animals

This study was performed with 8-week-old male Balb/c mice, weighing on average 20.38±1.10 g, housed at five mice per cage, and kept on a 12-h light 12-h dark cycle. All 50 animals were provided by Charles River Inc and were treated with water and fed ad libitum at Animal Facility of the Massachusetts General Hospital. All procedures were approved by the IACUC of the Massachusetts General Hospital and met the guidelines of the National Institutes of Health.

Experimental groups

Fifty mice were randomly allocated into two equal groups: LEDT-ATP and LEDT-fatigue. ATP contents in gastrocnemius and soleus muscles were evaluated in animals allocated into LEDT-ATP group. Fatigue-muscle resistance was analyzed in animals allocated into LEDT-fatigue group. Each one of these groups was subdivided into five equal subgroups (n=5) with random allocation of the mice (Fig. 1):

1. LEDT-ATP subgroups

   - LEDT-sham: animals were treated with LEDT placebo (LEDT device in placebo mode) over both legs, gluteus, and lower back muscles immediately before (5 min) surgery procedures and sacrifice.
   - LEDT-5 min: animals were treated with real LEDT over both legs, gluteus, and lower back muscles immediately before (5 min) surgery procedures and sacrifice.
   - LEDT-3 h: animals were treated with real LEDT over both legs, gluteus, and lower back muscles 3 h before surgery procedures and sacrifice.
   - LEDT-6 h: animals were treated with real LEDT over both legs, gluteus, and lower back muscles 6 h before surgery procedures and sacrifice.

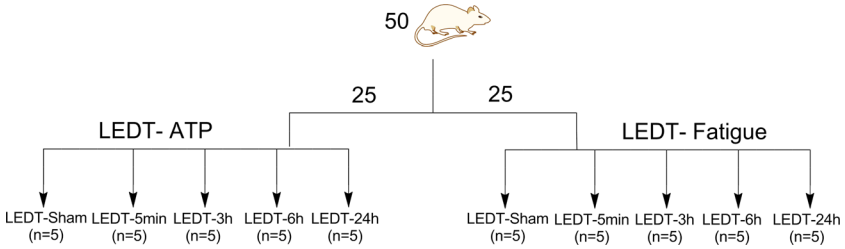

Fig. 1 Randomization and groups. Fifty male Balb/c mice were first allocated into two equal groups: LEDT-ATP and LEDT-fatigue. Next, both groups were subdivided into five equal groups: LEDT-sham, LEDT-5 min, LEDT-3 h, LEDT-6 h, and LEDT-24 h. *LEDT* light-emitting diode therapy, *ATP* adenosine triphosphate

- LEDT-24 h: animals were treated with real LEDT over both legs, gluteus, and lower back muscles 24 h before surgery procedures and sacrifice.

2. LEDT-fatigue subgroups

- LEDT-sham: animals were treated with LEDT placebo (LEDT device in placebo mode) over both legs, gluteus, and lower back muscles immediately before (5 min) fatigue test on inclined ladder.
- LEDT-5 min: animals were treated with real LEDT over both legs, gluteus, and lower back muscles immediately before (5 min) fatigue test on inclined ladder.
- LEDT-3 h: animals were treated with real LEDT over both legs, gluteus, and lower back muscles 3 h before fatigue test on inclined ladder.
- LEDT-6 h: animals were treated with real LEDT over both legs, gluteus, and lower back muscles 6 h before fatigue test on inclined ladder.
- LEDT-24 h: animals were treated with real LEDT over both legs, gluteus, and lower back muscles 24 h before fatigue test on inclined ladder.

Procedures

Familiarization with climbing ladder

An inclined ladder (80°) with 100×9 cm (length and width, respectively) with bars spaced at 0.5-cm intervals was used in this study as reported in a previous study [23]. However, the maximum distance available to climb was set at 70 cm in order to avoid possible contact between the load and the floor [24] (Fig. 2). The familiarization procedure was set as 4 sets of 10 climbs on ladder (repetitions) with rest times of 2 min between sets. No load was attached to the mouse tail during this procedure as reported in the previous study [24]. Animals allocated into LEDT-fatigue subgroups were familiarized to climb the ladder 2 days before the start of the fatigue test.

Light-emitting diode therapy

This study used a non-commercial cluster of 40 LEDs of 76 mm: 20 red LEDs (630±10 nm) and 20 infrared LEDs (850±20 nm). LEDT parameters presented in Table 1 are the same used in the previous study [24]. The optical power

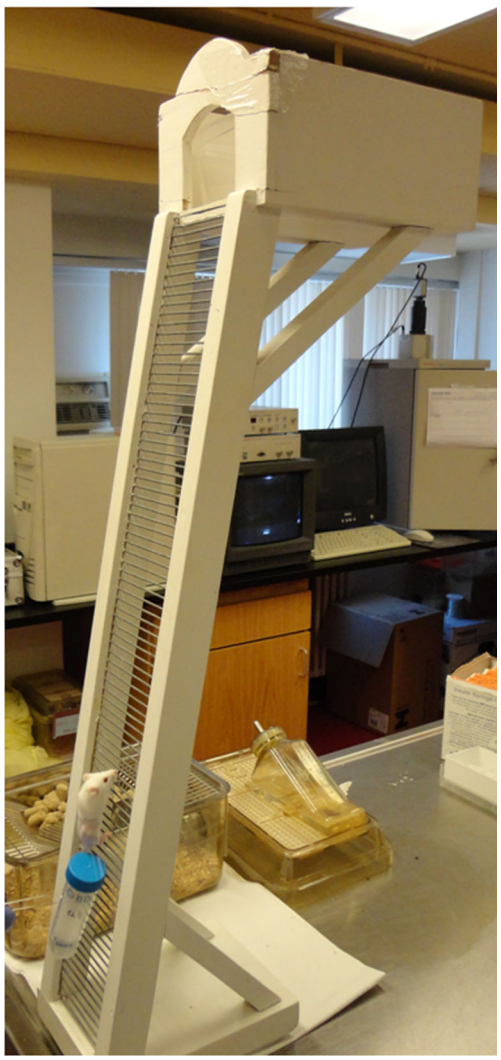

Fig. 2 Ladder. Inclined ladder (80°) with 100×9 cm (length and width, respectively) used for the fatigue test. Falcon tube filled with water and attached to mouse tail

Table 1 Optical parameters of light-emitting diode therapy (LEDT). LEDT-sham group received a placebo therapy (device switched off) with the same time of treatment

Number of LEDs (cluster): 40 (20 infrared-IR and 20 red-RED)
Wavelength: 850±20 nm (IR) and 630±10 nm (RED)
Pulse frequency: continuous
Optical output of each LED: 50 mW (IR) and 25 mW (RED)
Optical output (cluster): 1,000 mW (IR) and 500 mW (RED)
LED cluster size: 45 cm^2
Power density (at skin surface): 80 mW/cm^2
Treatment time: 90 s
Energy density applied (at skin surface): 7.2 J/cm^2
Application mode: without contact
Distance from mice or power meter: 45 mm

(power density) and energy density of LED cluster was measured with an optical and energy meter PM100D Thorlabs® and sensor S142C (area of 1.13 cm^2) at a distance of 45 mm as described previously [24]. Mice were shaved and fixed on a plastic plate using adhesive tapes without anesthesia. Afterwards in accordance with experimental subgroups, all animals were treated with LEDT over both legs, gluteus, and lower back muscles at a distance of 45 mm (without contact) [24] (Fig. 3). Irradiation lasted 90 s per session with fixed parameters as described in Table 1. LEDT placebo had no energy (0 J) and power (0 mW) applied over these muscles. The temperature on the mice skin was monitored before LEDT irradiation and after 5 min using a precise thermometer. There was no change observed on temperature.

Anesthesia, surgical, and sacrifice procedures

All mice of LEDT-ATP group were subjected to anesthesia, surgery, and sacrifice procedures at the specified time after LEDT for each subgroup. Animals of LEDT-fatigue subgroups after finishing fatigue test were anesthetized and sacrificed immediately.

Anesthesia Mice were anesthetized using ketamine and xylazine at a proportion of 80 mg/kg of ketamine and 12 mg/kg of xylazine.

Surgery After the anesthesia procedure, the gastrocnemius and soleus muscles were excised bilaterally, separated surgically, and immediately frozen in liquid nitrogen. Next, both muscles were stored at −80 °C until analysis of ATP performed exactly 7 days after the surgery.

Sacrifice Animals were sacrificed under anesthesia by cervical dislocation at same period of day (afternoon).

It is important to remark the order of the procedures conducted in this study. The first procedure was irradiating all mice of LEDT-ATP subgroups (except LEDT-Sham) with LEDT. During 7 days between sacrifice of these animals and ATP analysis, the fatigue test with mice of the LEDT-fatigue subgroups was performed.

Outcomes

Muscular ATP content

The gastrocnemius and soleus muscles from one leg of each animal were used for this analysis. Muscle samples were thawed in ice for 5 min and homogenized at a proportion of 3–4 mg of tissue to 500 μl of 10 % perchloric acid ($HClO_4$) following procedures previously published [24, 25]. Afterwards, an aliquot of 10 μl of the muscle homogenate plus 40 μl of CellTiter Glo Luminescent Cell Viability Assay kit (Promega), totaling 50 μl, was placed in a 96-well microplate (Costar™ 96-Well White Clear-Bottom Plates). Luminescence signals were measured in a SpectraMax M5 Multi-Mode Microplate Reader (Molecular Devices, Sunnyvale,

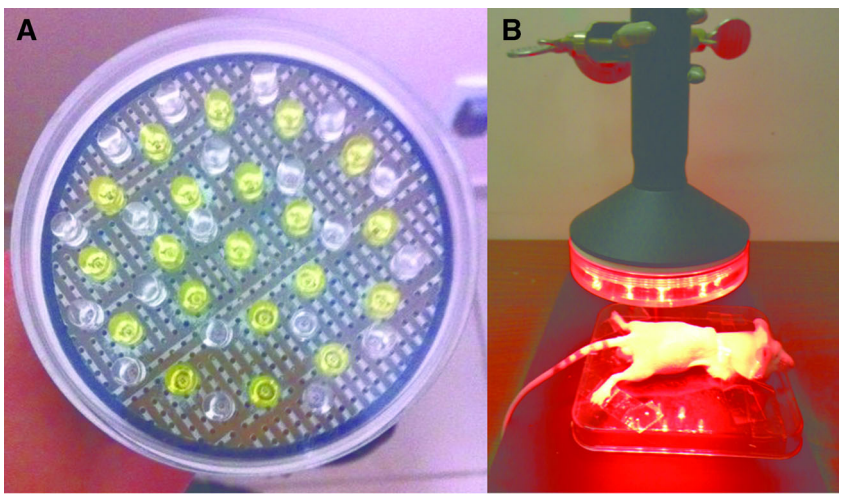

Fig. 3 LEDT. **a** Internal distribution of light-emitting diodes (LEDs) in the cluster. White LEDs emit red (630±10 nm) and yellow LEDs emit infrared (850±20 nm). **b** Positioning of the mice to receive LED therapy (LEDT) over legs, gluteus, and lower back muscles without contact

CA) with integration time of 5 s to increase low signals [25]. A standard curve was prepared using ATP standard (Sigma) according to manufacturer's guideline and then ATP concentration was calculated in nanomole (nmol) per milligram (mg) of protein. An aliquot of muscle homogenate was used to quantify the total protein by QuantiPro™ BCA Assay kit (Sigma-Aldrich) following manufacturer's guidelines.

Fatigue test

This test was performed 48 h after the familiarization procedure with a load corresponding to 150 % of the mice body weight. All animals allocated into LEDT-fatigue subgroups were weighed on a precise scale and then the target load was calculated. A Falcon tube (50 ml) was filled with specific milliliters of water until the total matched the target load in grams [24]. Next, this tube was attached to the mouse tail using adhesive tape (Fig. 2). Mice performed this test exactly 5 min, or 3 h, or 6 h, or 24 h after LEDT procedure in accordance with LEDT-fatigue subgroups. Slight pressures with tweezers were applied to the mouse tail if the animal stopped climbing. The test stopped when mice were not able to climb or lost their grip and slid on the ladder due to failure of concentric muscle contraction after. The number of climbs on the ladder (repetitions) of each mouse was quantified during this test. The room temperature was monitored and kept on 22–25 °C.

Pearson product-moment correlation coefficient (Pearson's r)

Correlations were calculated between ATP contents in soleus muscle and number of repetitions in the fatigue test, as well as ATP contents in gastrocnemius muscle and fatigue test. The *r* values were interpreted as recommended previously [26]: 0.00–0.19=none to slight, 0.20–0.39=low, 0.40–0.69=modest, 0.70–0.89=high, and 0.90–1.00=very high.

Sample size calculation

The sample size was calculated based on the necessary number of animals to obtain significant differences among the groups regarding ATP content in soleus and gastrocnemius and the number of repetitions in fatigue test. The statistical power of 80 % and the effect size (greater than 0.75), and alpha (α) of 5 % were found to be satisfactory.

Statistical analysis

Shapiro-Wilk's *W* test verified the normality of the data distribution. ATP contents in soleus and gastrocnemius muscles among all groups were compared using one-way analysis of variance (one-way ANOVA) with Tukey HSD post hoc test. Pearson product-moment correlation coefficient (Pearson's *r*) was conducted between fatigue test and ATP contents in soleus and gastrocnemius muscles. Significance was set at $P<0.05$.

Results

ATP content in soleus muscle

ATP content in soleus was modulated significantly by LEDT and presented a time response for this photobiomodulation. The group LEDT-6 h (85.80±16.41 nmol/mg protein) had the highest ATP content in soleus compared to LEDT-sham (27.48±2.28 nmol/mg protein; $P<0.001$), LEDT-5 min (36.62±12.36 nmol/mg protein; $P<0.001$), LEDT-3 h (57.92±7.40 nmol/mg protein; $P=0.011$), and LEDT-24 h (45.54±13.84 nmol/mg protein; $P<0.001$). The second group with more ATP content was LEDT-3 h when compared to LEDT-sham ($P=0.005$), but LEDT-3 h had no statistical difference compared to LEDT-5 min ($P=0.070$) and LEDT-24 h ($P=0.491$). LEDT-24 h had no difference in ATP content compared to LEDT-sham ($P=0.158$) and LEDT-5 min ($P=0.761$). Finally, LEDT-5 min had no difference in ATP content compared to LEDT-sham ($P=0.745$) (Fig. 4a).

ATP contents in gastrocnemius

Similarly to ATP content in soleus muscles, the group LEDT-6 h (142.30±11.13 nmol/mg protein) had also the highest ATP content in gastrocnemius muscle compared to LEDT-sham (18.71±4.27 nmol/mg protein; $P<0.001$), LEDT-5 min (23.30±3.14 nmol/mg protein; $P<0.001$), LEDT-3 h (87.67±15.66 nmol/mg protein; $P<0.001$), and LEDT-24 h (39.72±10.76 nmol/mg protein; $P<0.001$). LEDT-3 h was the second group with highest ATP content in gastrocnemius muscle compared to LEDT-sham ($P<0.001$), LEDT-5 min ($P<0.001$), and LEDT-24 h ($P<0.001$). In addition, LEDT-24 h had higher ATP content compared to LEDT-sham ($P=0.028$) but without statistical difference compared to LEDT-5 min ($P=0.117$). Finally, LEDT-5 min had no difference in ATP content compared to LEDT-sham ($P=0.950$) (Fig. 4b).

Fatigue test

LEDT-6 h was the best group among all LEDT-fatigue subgroups, performing 67.40 (±3.05) repetitions with significant differences compared to LEDT-sham (11.86±0.89 repetitions; $P<0.001$), LEDT-5 min (13.90±0.82 repetitions; $P<0.001$), LEDT-3 h (31.04±3.42 repetitions; $P<0.001$), and LEDT-24 h (23.60±3.02 repetitions; $P<0.001$). LEDT-3 h was the second best group, performing more repetitions compared to LEDT-sham ($P<0.001$), LEDT-5 min ($P<0.001$), and LEDT-

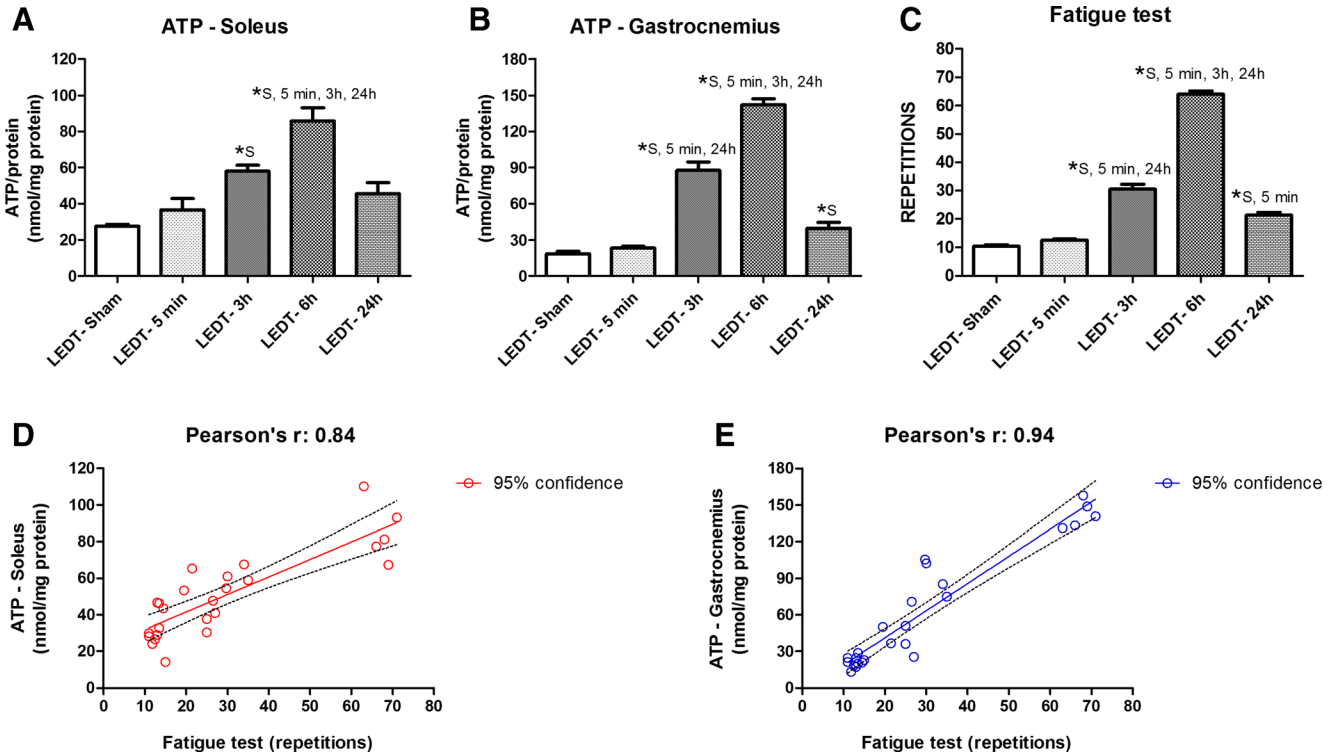

Fig. 4 ATP, fatigue test, and correlations (n=5 animals per subgroup). **a** ATP contents in soleus muscle for LEDT-ATP subgroups: LEDT-sham, LEDT-5 min, LEDT-3 h, LEDT-6 h, and LEDT-24 h. **b** ATP contents in gastrocnemius muscle for LEDT-ATP subgroups: LEDT-sham, LEDT-5 min, LEDT-3 h, LEDT-6 h, and LEDT-24 h. **c** Fatigue test for LEDT-fatigue subgroups: LEDT-sham, LEDT-5 min, LEDT-3 h, LEDT-6 h, and LEDT-24 h. **d** Pearson's r correlation between ATP contents in soleus muscle and fatigue test. **e** Pearson's r correlation between ATP contents in gastrocnemius and fatigue test. *LEDT* light-emitting diode therapy, *ATP* adenosine triphosphate, *S* LEDT-sham, *5 min* LEDT-5 min, *3 h* LEDT-3 h; *24 h* LEDT-24 h; *P<0.05 (statistical significance)

24 h (P=0.001). LEDT-24 h performed more repetitions compared to LEDT-sham (P<0.001) and LEDT-5 min (P<0.001). Finally, LEDT-5 min presented no statistical difference compared to LEDT-sham (P=0.700) (Fig. 4c).

Sample size

Statistical power and effect size regarding the ATP content in soleus and gastrocnemius muscles among all groups were calculated in order to ensure the minimal power of 80 %, alpha (α) of 5 %, and large effect size (greater than 0.75). We used the mean of ATP content of the each LEDT-ATP subgroup and the highest value of standard deviation among all these subgroups. For ATP content in soleus, our results demonstrate a difference between groups with a statistical power of 87 %, effect size of 1.23 (very large effect size), and total sample size of 15, i.e., three animals per group (five groups). For ATP content in gastrocnemius, our results demonstrate a difference between groups with a statistical power of 99 %, effect size of 2.99 (huge effect size) and total sample size of 10, i.e., two animals per group (five groups). For fatigue test, we used the same criteria for ATP content in muscles: minimal power of 80 %, alpha (α) of 5 %, and large effect size (upper to 0.75). Using the mean of repetitions of each LEDT-fatigue subgroup and the highest value of standard deviation among all these subgroups, our results demonstrate a difference between groups with a statistical power of 100 %, effect size of 5.88 (huge effect size), and total sample size of 10, i.e., two animals per group (five groups). All these calculations demonstrate that sample size, power, and effect size of this study were adequate for ATP content in soleus and gastrocnemius, and for fatigue test, supporting the conclusion regarding the time response of muscles to LEDT observed in this current study.

Pearson product-moment correlation coefficient (Pearson's r)

ATP contents in soleus and gastrocnemius muscles presented a high correlation (r=0.84) and very high correlation (r=0.94) with the number of repetitions performed in the fatigue test (P<0.001; P<0.001), respectively (Fig. 4d, e).

Discussion

Our study found strong positive effects of LEDT for increasing muscle ATP synthesis in vivo, as well as establishing the time response for this photobiomodulation phenomenon. We found also similar results for the LEDT-mediated increase in

fatigue-muscle resistance in the exercise test performed on an inclined ladder. In addition, contents of muscle ATP and fatigue-muscle resistance were highly correlated. To our knowledge, this is the first study reporting the time response for the effects of light therapy on muscle ATP synthesis and fatigue-muscle resistance in vivo.

Since cytochrome c oxidase (Cox) has been reported as the principle chromophore in cells [4, 8–11], changes in mitochondrial metabolism, oxidative stress, and increased ATP synthesis have been considered important mechanisms in LLLT [4]. Therefore, this study used light therapy to modulate ATP synthesis as has already been done previously in vitro [4, 13, 14] but explored what was the best time to apply the light before the exercise.

Previous studies have used light therapy for muscular preconditioning by delivering the light therapy over the target muscles 5 min before fatigue tests in vivo [27, 28] or in clinical trials [20–22]. These studies reported an increased number of repetitions and consequently a better fatigue-muscle resistance. Our results for fatigue-muscle resistance on the ladder for LEDT-3 h, LEDT-6 h, and LEDT-24 h groups confirmed these previous results, except for LEDT-5 min. The number of repetitions was greatly increased in LEDT-6 h (~600 %), LEDT-3 h (~300 %), and LEDT-24 h (~200 %) compared to LEDT-sham and LEDT-5 min, thus establishing a well-defined time response for LEDT to increase fatigue-muscle resistance. Although LEDT-5 min slightly increased the number of climbs on ladder (around 20 %) compared to LEDT-sham, this increase was really small and for this reason had no significance. A study with a larger number of animals would be necessary to provide the statistical power to prove this difference. Possibly, the use of a *t* test between LEDT-sham and LEDT-5 min groups could show a statistically significant difference, such as has been reported in previous studies involving LLLT and muscular pre-conditioning [20–22].

Hayworth et al. [12] reported modulations in Cox activity 24 h after the use of light therapy on the temporalis muscles in rats, but these modulations were dependent on the type of metabolism in muscle fibers that in turn suggested differences in energy synthesis (ATP). For this reason, our study assessed the effect of LEDT on ATP synthesis in muscles with either a predominance of aerobic metabolism (soleus) and mixed aerobic and glycolytic metabolism (gastrocnemius) [29]. Our results clearly show an increased ATP synthesis in both types of muscles after LEDT, both responses showing a well-defined time response. Previous studies already reported increased ATP synthesis in cells after light therapy [4, 13, 14]. In our study, we show that increases in ATP occur in muscle tissue occurring over a wide time range (5 min to 24 h) showing that secondary reactions [4] occur over time in vivo.

Increased ATP content in muscle tissue suggests more energy available for all metabolic processes, including muscle contraction [18, 24]. Corroborating this statement, our results for muscular ATP content and fatigue-muscle resistance were highly correlated, reinforcing the importance of a good energy supply to achieve the best performance in exercise [18]. In the context of energy metabolism, previous studies already reported possible effects of light therapy on resynthesis of creatine-phosphate (Cr-P) using ATP produced in mitochondria, as well as the consumption of lactate produced by anaerobic metabolism during fatigue or strength exercise [15, 30, 31]. Therefore, we believe that these mechanisms could provide better energy restore/supply during the fatiguing exercise.

Looking more deeply into our results, we observed that although the increased ATP content in soleus muscle showed how mitochondrial metabolism was stimulated by light therapy, the gastrocnemius muscle showed the best correlation (Pearson's $r=0.94$) with the fatigue test. The gastrocnemius muscle has a mixed metabolism (oxidative and glycolytic) [29] and perhaps light therapy could modulate both of these different metabolic pathways. In summary, our results suggest that both glycolytic and oxidative metabolisms were stimulated by light therapy, considering that mitochondria need acetyl coenzyme A (acetyl-CoA) coming from glycolysis and/or from β-oxidation to perform ATP synthesis.

The power density (irradiance) and dose (fluence) of the light therapy used in this current study were based on the possible biphasic dose response reported previously [5, 1]. However, we used red and near-infrared light (two wavelengths) delivered at the same time based on specific absorptions of the chromophores in the cells to absorb these lights [4, 8–11]. It is possible that taking advantage of the double absorption bands (red and near-infrared together) could optimize the effects of photobiomodulation to promote ATP synthesis and fatigue-muscle resistance. Moreover, light therapy was delivered without contact as reported previously [12, 24], covering all target muscles (gastrocnemius, soleus, gluteus, and lower back muscles) and made it possible to stimulate entire muscle groups simultaneously as reported previously [31]. Finally, as the light irradiation was performed without contact, possibly reflection of the light on the animal surface (mainly on the curved areas) would have occurred in our study. This phenomenon could promote loss of photons penetrating through the skin and reaching the muscles. However, light-tissue interaction is strongly dependent on the power of the light (Beer-Lambert law) and the chromophores that absorb this light [4, 8–11]. For these reasons, light irradiation with large LED array was without contact (instead of point by point using a small beam area) in order to cover entire area of all muscles at the same time.

Conclusion

This is the first study reporting a well-defined time response for improving both muscle ATP content and also resistance to

fatigue by mixed red and near-infrared light therapy applied over skeletal muscles.

Our data presented in this study could be used in future studies that aim to determine whether a similar time response of muscles after LEDT applies in humans with an adjusted light dose for humans. It may be possible to use light therapy to enhance performance in athletics and high-performance sports, as well as in a myriad of different medical or health science applications.

Acknowledgments We would like to thank Andrea L. Brissette for your assistance with multiple roles including purchase of reagents. Cleber Ferraresi would like to thank FAPESP for his PhD scholarships (numbers 2010/07194-7 and 2012/05919-0). Michael R. Hamblin was supported by US NIH grant R01AI050875.

References

1. Huang YY, Sharma SK, Carroll J, Hamblin MR (2011) Biphasic dose response in low level light therapy—an update. Dose Response 9(4): 602–618. doi:10.2203/dose-response.11-009.Hamblin
2. Chow RT, Johnson MI, Lopes-Martins RA, Bjordal JM (2009) Efficacy of low-level laser therapy in the management of neck pain: a systematic review and meta-analysis of randomised placebo or active-treatment controlled trials. Lancet 374(9705):1897–1908. doi:10.1016/S0140-6736(09)61522-1
3. Enwemeka CS, Parker JC, Dowdy DS, Harkness EE, Sanford LE, Woodruff LD (2004) The efficacy of low-power lasers in tissue repair and pain control: a meta-analysis study. Photomed Laser Surg 22(4): 323–329. doi:10.1089/1549541041797841
4. Karu T (1999) Primary and secondary mechanisms of action of visible to near-IR radiation on cells. J Photochem Photobiol B 49(1):1–17. doi:10.1016/S1011-1344(98)00219-X
5. Huang YY, Chen AC, Carroll JD, Hamblin MR (2009) Biphasic dose response in low level light therapy. Dose Response 7(4):358–383. doi:10.2203/dose-response.09-027.Hamblin
6. Vladimirov YA, Osipov AN, Klebanov GI (2004) Photobiological principles of therapeutic applications of laser radiation. Biochemistry (Mosc) 69(1):81–90
7. Bakeeva LE, Manteifel VM, Rodichev EB, Karu TI (1993) Formation of gigantic mitochondria in human blood lymphocytes under the effect of an He-Ne laser. Mol Biol (Mosk) 27(3):608–617
8. Karu TI, Pyatibrat LV, Afanasyeva NI (2004) A novel mitochondrial signaling pathway activated by visible-to-near infrared radiation. Photochem Photobiol 80(2):366–372. doi:10.1562/2004-03-25-RA-1232004-03-25-RA-123
9. Karu TI, Kolyakov SF (2005) Exact action spectra for cellular responses relevant to phototherapy. Photomed Laser Surg 23(4):355–361. doi:10.1089/pho.2005.23.355
10. Karu TI, Pyatibrat LV, Kolyakov SF, Afanasyeva NI (2008) Absorption measurements of cell monolayers relevant to mechanisms of laser phototherapy: reduction or oxidation of cytochrome c oxidase under laser radiation at 632.8 nm. Photomed Laser Surg 26(6):593–599. doi:10.1089/pho.2008.2246
11. Karu TI (2010) Multiple roles of cytochrome c oxidase in mammalian cells under action of red and IR-A radiation. IUBMB Life 62(8):607–610. doi:10.1002/iub.359
12. Hayworth CR, Rojas JC, Padilla E, Holmes GM, Sheridan EC, Gonzalez-Lima F (2010) In vivo low-level light therapy increases cytochrome oxidase in skeletal muscle. Photochem Photobiol 86(3):673–680. doi:10.1111/j.1751-1097.2010.00732.x
13. Karu T, Pyatibrat L, Kalendo G (1995) Irradiation with He-Ne laser increases ATP level in cells cultivated in vitro. J Photochem Photobiol B 27(3):219–223
14. Passarella S, Casamassima E, Molinari S, Pastore D, Quagliariello E, Catalano IM, Cingolani A (1984) Increase of proton electrochemical potential and ATP synthesis in rat liver mitochondria irradiated in vitro by helium-neon laser. FEBS Lett 175(1):95–99
15. Ferraresi C, Hamblin MR, Parizotto NA (2012) Low-level laser (light) therapy (LLLT) on muscle tissue: performance, fatigue and repair benefited by the power of light. Photonics Lasers Med 1(4): 267–286. doi:10.1515/plm-2012-0032
16. Borsa PA, Larkin KA, True JM (2013) Does phototherapy enhance skeletal muscle contractile function and postexercise recovery? A systematic review. J Athl Train 48(1):57–67. doi:10.4085/1062-6050-48.1.12
17. Leal-Junior EC, Vanin AA, Miranda EF, de Carvalho PD, Dal Corso S, Bjordal JM (2013) Effect of phototherapy (low-level laser therapy and light-emitting diode therapy) on exercise performance and markers of exercise recovery: a systematic review with meta-analysis. Lasers Med Sci. doi:10.1007/s10103-013-1465-4
18. Allen DG, Lamb GD, Westerblad H (2008) Skeletal muscle fatigue: cellular mechanisms. Physiol Rev 88(1):287–332. doi:10.1152/physrev.00015.2007
19. Hoffman JR, Kraemer WJ, Bhasin S, Storer T, Ratamess NA, Haff GG, Willoughby DS, Rogol AD (2009) Position stand on androgen and human growth hormone use. J Strength Cond Res 23(5 Suppl): S1–S59. doi:10.1519/JSC.0b013e31819df2e6
20. Leal Junior EC, Lopes-Martins RA, Dalan F, Ferrari M, Sbabo FM, Generosi RA, Baroni BM, Penna SC, Iversen VV, Bjordal JM (2008) Effect of 655-nm low-level laser therapy on exercise-induced skeletal muscle fatigue in humans. Photomed Laser Surg 26(5):419–424. doi:10.1089/pho.2007.2160
21. Leal Junior EC, Lopes-Martins RA, Vanin AA, Baroni BM, Grosselli D, De Marchi T, Iversen VV, Bjordal JM (2009) Effect of 830 nm low-level laser therapy in exercise-induced skeletal muscle fatigue in humans. Lasers Med Sci 24(3):425–431. doi:10.1007/s10103-008-0592-9
22. Leal Junior EC, Lopes-Martins RA, Frigo L, De Marchi T, Rossi RP, de Godoi V, Tomazoni SS, Silva DP, Basso M, Filho PL, de Valls Corsetti F, Iversen VV, Bjordal JM (2010) Effects of low-level laser therapy (LLLT) in the development of exercise-induced skeletal muscle fatigue and changes in biochemical markers related to postexercise recovery. J Orthop Sports Phys Ther 40(8):524–532. doi:10.2519/jospt.2010.3294
23. Lee S, Barton ER, Sweeney HL (1985) Farrar RP (2004) Viral expression of insulin-like growth factor-I enhances muscle hypertrophy in resistance-trained rats. J Appl Physiol 96(3):1097–1104. doi:10.1152/japplphysiol.00479.2003
24. Ferraresi C, Parizotto NA, Pires de Sousa MV, Kaippert B, Huang Y-Y, Koiso T, Bagnato VS, Hamblin MR (2014) Light-emitting diode therapy in exercise-trained mice increases muscle performance, cytochrome c oxidase activity, ATP and cell proliferation. J Biophoton 9999 (9999):n/a-n/a. doi:10.1002/jbio.201400087
25. Khan HA (2003) Bioluminometric assay of ATP in mouse brain: determinant factors for enhanced test sensitivity. J Biosci 28(4): 379–382
26. Weber J, Lamb D (1970) Statistics and research in physical education. C. V. Mosby Co., Saint Louis
27. de Almeida P, Lopes-Martins RA, Tomazoni SS, Silva JA Jr, de Carvalho PT, Bjordal JM, Leal Junior EC (2011) Low-level laser therapy improves skeletal muscle performance, decreases skeletal muscle damage and modulates mRNA expression of COX-1 and COX-2 in a dose-dependent manner. Photochem Photobiol 87(5):1159–1163. doi:10.1111/j.1751-1097.2011.00968.x

28. Leal Junior EC, Lopes-Martins RA, de Almeida P, Ramos L, Iversen VV, Bjordal JM (2010) Effect of low-level laser therapy (GaAs 904 nm) in skeletal muscle fatigue and biochemical markers of muscle damage in rats. Eur J Appl Physiol 108(6):1083–1088. doi:10.1007/s00421-009-1321-1
29. Schuenke MD, Kopchick JJ, Hikida RS, Kraemer WJ, Staron RS (2008) Effects of growth hormone overexpression vs. growth hormone receptor gene disruption on mouse hindlimb muscle fiber type composition. Growth Hormon IGF Res 18(6):479–486. doi:10.1016/j.ghir.2008.04.003
30. Vieira WH, Ferraresi C, Perez SE, Baldissera V, Parizotto NA (2012) Effects of low-level laser therapy (808 nm) on isokinetic muscle performance of young women submitted to endurance training: a randomized controlled clinical trial. Lasers Med Sci 27(2):497–504. doi:10.1007/s10103-011-0984-0
31. Ferraresi C, de Brito OT, de Oliveira ZL, de Menezes Reiff RB, Baldissera V, de Andrade Perez SE, Matheucci Junior E, Parizotto NA (2011) Effects of low level laser therapy (808 nm) on physical strength training in humans. Lasers Med Sci 26(3):349–358. doi:10.1007/s10103-010-0855-0

©Operative Dentistry, 2015, **40-1,** 102-111

Transdentinal Cell Photobiomodulation Using Different Wavelengths

APS Turrioni • FG Basso • JRL Alonso
CF de Oliveira • J Hebling • VS Bagnato
CA de Souza Costa

Clinical Relevance

Determining the optimal irradiation parameters of odontoblast-like cell stimulation using dentinal barrier as a function of the wavelength is the first step toward establishing the ideal window for biostimulation of pulp tissue previously injured by caries lesion progression and cavity preparation.

SUMMARY

Objective: The aim of this study was to investigate the effects of transdentinal irradiation with different light-emitting diode (LED) parameters on odontoblast-like cells (MDPC-23).

Methods and Materials: Human dentin discs (0.2 mm thick) were obtained, and cells were seeded on their pulp surfaces with complete culture medium (Dulbecco modified Eagle medium). Discs were irradiated from the occlusal surfaces with LED at different wavelengths (450, 630, and 840 nm) and energy densities (0, 4, and 25 J/cm^2). Cell viability (methyltetrazolium assay), alkaline phosphatase activity (ALP), total protein synthesis (TP), and cell morphology (scanning electron microscopy) were evaluated. Gene expression of collagen type I (Col-I) was analyzed by quantitative polymerase chain reaction (PCR). Data were

Ana Paula Silveira Turrioni, DDS, MS, Araraquara School of Dentistry, Univ. Estadual Paulista, UNESP, Department of Pediatric Dentistry and Orthodontics,Araraquara, São Paulo, Brazil

Fernanda Gonçalves Basso, DDS, MS, PhD, Araraquara School of Dentistry, Univ. Estadual Paulista, UNESP, Department of Pediatric Dentistry and Orthodontics, Araraquara, São Paulo, Brazil

Juliana Rosa Luiz Alonso, DDS, Araraquara School of Dentistry, Univ. Estadual Paulista, UNESP, Department of Pediatric Dentistry and Orthodontics, Araraquara, São Paulo, Brazil

Camila Fávero de Oliveira, DDS, MS, PhD, University of Ribeirão Preto, UNAERP, Department of Morphology, Ribeirão Preto, São Paulo, Brazil

Josimeri Hebling, DDS, MS, PhD, Araraquara School of Dentistry, Univ. Estadual Paulista, UNESP, Department of Orthodontics and Pediatric Dentistry, Araraquara, São Paulo, Brazil

Vanderlei S Bagnato, BSc, MS, PhD, University of São Paulo, USP, Physics Institute of São Carlos, São Carlos, São Paulo, Brazil

*Carlos Alberto de Souza Costa, DDS, MS, PhD, Araraquara School of Dentistry, Univ. Estadual Paulista, UNESP, Department of Physiology and Pathology, Araraquara, São Paulo, Brazil

*Corresponding author: Rua Humaitá, 1680, Centro, CEP: 14.801-903, Araraquara, São Paulo Brazil; e-mail: casouzac@foar.unesp.br

DOI: 10.2341/13-370-L

analyzed by the Mann-Whitney test with a 5% significance level.

Results: Higher cell viability (21.8%) occurred when the cells were irradiated with 630 nm LED at 25 J/cm^2. Concerning TP, no statistically significant difference was observed between irradiated and control groups. A significant increase in ALP activity was observed for all tested LED parameters, except for 450 nm at 4 J/cm^2. Quantitative PCR showed a higher expression of Col-I by the cells subjected to infrared LED irradiation at 4 J/cm^2. More attached cells were observed on dentin discs subjected to irradiation at 25 J/cm^2 than at 4 J/cm^2.

Conclusion: The infrared LED irradiation at an energy density of 4 J/cm^2 and red LED at an energy density of 25 J/cm^2 were the most effective parameters for transdentinal photobiomodulation of cultured odontoblast-like cells.

INTRODUCTION

Inflammatory pulp reaction is commonly observed subjacent to active decay. The intensity of tissue inflammation may increase during mechanical cavity preparation and following cavity restoration with dental materials with nonbiocompatible components. About and others[1] reported that the sum of damages experienced by the pulp tissue can result in pain and exacerbate local inflammatory reactions. Therefore, several products and techniques have been proposed to prevent or relieve pulp sensitivity and biostimulate the healing of this specific connective tissue. Phototherapy has appeared as a promising treatment for this purpose.[2]

Recent studies have demonstrated that light-emitting diode (LED) irradiation is capable of stimulating cells to synthesize collagen-rich matrix and proteins that play a role in its mineralization.[3-5] Additionally, several *in vitro* experiments with LED at different wavelengths have demonstrated a significant increase in the proliferation of fibroblasts, osteoblasts, muscle cells in rats, human epithelial cells, and mesenchymal stem cells.[4-7] Other positive effects caused by light, such as reduced dentin sensitivity, formation of mineralized tissue stimulus, improvement in rheumatoid arthritis, and mucositis healing, have also been reported.[8-12]

Despite these interesting scientific data, little is known about the transdentinal effects of LED irradiation on pulp cells. In current studies, it was demonstrated that the power density that reaches cells is much lower than the one applied to dentin, mainly because of light scattering.[13,14] For 0.2 mm, specifically, the mean of power loss in dentin discs is approximately 40.0%.[14] Some recent studies have shown that phototherapy promotes biomodulation when applied directly to cells with an odontoblast phenotype, increasing the synthesis and expression of dentin matrix proteins.[15] Therefore, it could be speculated that, in clinical situations, the transdentinal LED biomodulation of odontoblasts subjacent to the dental cavity may cause deposition of tertiary dentin, protecting the pulp tissue against further assaults from different sources.[16] It is known that transdentinal irradiation causes an effective decrease of energy density.[13,14] Although the energy density applied on the external surface is known, the energy density that actually reaches the cell layer is much lower due to light scattering. One purpose of this study was to determine that, even with this loss, LED irradiation is capable of causing biostimulatory effect on odontoblast-like cells.

Since there is no previous information about the possibility of transdentinal stimulation of odontoblasts by LED irradiation, the aim of this study was to evaluate whether specific LED parameters at different wavelengths are capable of diffusing through a 0.2-mm-thick dentin barrier to biostimulate cultured odontoblast-like MDPC-23 cells.

METHODS AND MATERIALS

LED Devices and Irradiation Parameters

Irradiation was performed with three devices (LEDTables) containing 24 diodes with wavelengths at 450, 630, or 840 nm. The InGaN diodes (indium, gallium, and nitride) were individually positioned in the LEDTables in such a way that each could homogeneously irradiate the cells attached to the bottom of a well in a 24-well plate. During cell irradiation, the LED device was applied in noncontact mode and perpendicular to the bottom of the well. The distance between the dentin disc and the LED device tip was 2.0 cm.

The energy densities of 4 and 25 J/cm^2 used in this investigation were selected based on previous studies in which the authors irradiated different cell types.[5,15,17] The irradiance emitted by the LEDs was 88 mW/cm^2, and the power loss caused by the plate and the dentin disc was considered, resulting in irradiation times of 1 minute and 20 seconds (4 J/cm^2) and 8 minutes and 40 seconds (25 J/cm^2). For all groups, cells were maintained in contact with

phosphate-buffered saline (PBS) for the irradiation procedure, as previously described.[18]

Temperature Monitoring

PBS temperature variations were evaluated by means of a multimeter (38XR; Metermam, Everett, WA, USA) and a calibrated thermistor (38XR, Metermam) placed at the bottom of the well. This preliminary analysis was performed because PBS heating may cause cell damage.

Obtaining Dentin Discs

This study was approved by the Research Ethics Committee (Protocol 26/09) of the Araraquara School of Dentistry, UNESP, University Estadual Paulista, Brazil. One hundred and eighty-two human dentin discs from sound human molars were obtained, selected by stereomicroscopy as previously described,[13,14] and reduced to 8-mm diameter. The dentin surfaces were rinsed with 0.5 M ethylenediaminetetraacetic acid (pH 7.2) according to a previous study.[19] The discs were then washed with sterile deionized water for 60 seconds and were subjected to measurement of transdentinal LED light transmission.

Measurement of Transdentinal LED Light Attenuation

This test was performed to determine the light attenuation through the disc structure and provide a homogeneous distribution of discs among groups, according to the power loss values of each one. The protocol of transdentinal power measurement was described in detail in a previous study.[13]

MDPC-23 Cell Culture

The MDPC-23 cells were cultivated in Dulbecco modified Eagle medium (Sigma-Aldrich, St. Louis, MO, USA) supplemented with 10% fetal bovine serum (Gibco, Grand Island, NY, USA), 100 IU/mL of penicillin, 100 μg/mL of streptomycin, and 2 mmol/L of glutamine (Gibco). The cells were maintained in a humidified incubator with 5% CO_2 and 95% air at 37°C (Isotemp, Fisher Scientific, Bellefonte, PA, USA).

Experimental Conditions

After distribution into the experimental and control groups, the dentin discs were packaged and sterilized by ethylene oxide[19] and, finally, adapted to metal devices designed for this study (Figure 1). The devices and silicon O-rings were autoclaved for 15 minutes at 120°C and 1 kgf of pressure. Each device containing the dentin disc allowed for LED irradiation of the occlusal surface of the disc (facing down), while the pulpal surface on which the cells were seeded remained in contact with the culture medium. The MDPC-23 cells were seeded (3×10^4 cells/disc) on the pulp surfaces of the discs and incubated for 48 hours at 37°C and 5% CO_2.

After this period, the culture medium was replaced by a new culture medium supplemented with 2% fetal bovine serum (FBS),[20,21] and the cells were incubated for an additional 24 hours. Immediately before irradiation, the culture medium was replaced by sterile buffered saline solution (PBS) at room temperature.[18] The 24-well plates were then placed on the LEDTables (Figure 1) for specific periods, according to the energy density. A single LED irradiation was performed to simulate a clinical situation in which a deep cavity is available for restoration. Cells were irradiated in a dark room; thus, the LED irradiation was the only light source that the cells were exposed to.

After irradiation, the PBS was aspirated, and 1 mL of fresh culture medium containing 10% FBS was added to each well. Following incubation for 72 hours, the cell viability (methyltetrazolium [MTT] assay), alkaline phosphatase (ALP) activity, total protein (TP) synthesis, and cell morphology (scanning electron microscopy [SEM]) were evaluated. The expression of collagen type I (Col-I) was analyzed by real-time polymerase chain reaction (RT-PCR). In the control group, the same cell manipulation procedures were performed, but the diodes were not activated.

Cell Viability (MTT assay)

Cell viability (n=8) was evaluated using the MTT assay (Sigma-Aldrich), which determines the activity of SDH enzyme produced by mitochondria in cells. The dentin discs were carefully removed from the devices and individually placed in wells of 24-well plates. The MTT assay was performed as described in previous studies.[15,21]

TP Production and ALP Activity

Eight samples were selected to evaluate TP production and ALP activity.

TP Production—The production of TP was measured for each experimental and control group according to the protocol described in a previous study by the Lowry method.[15]

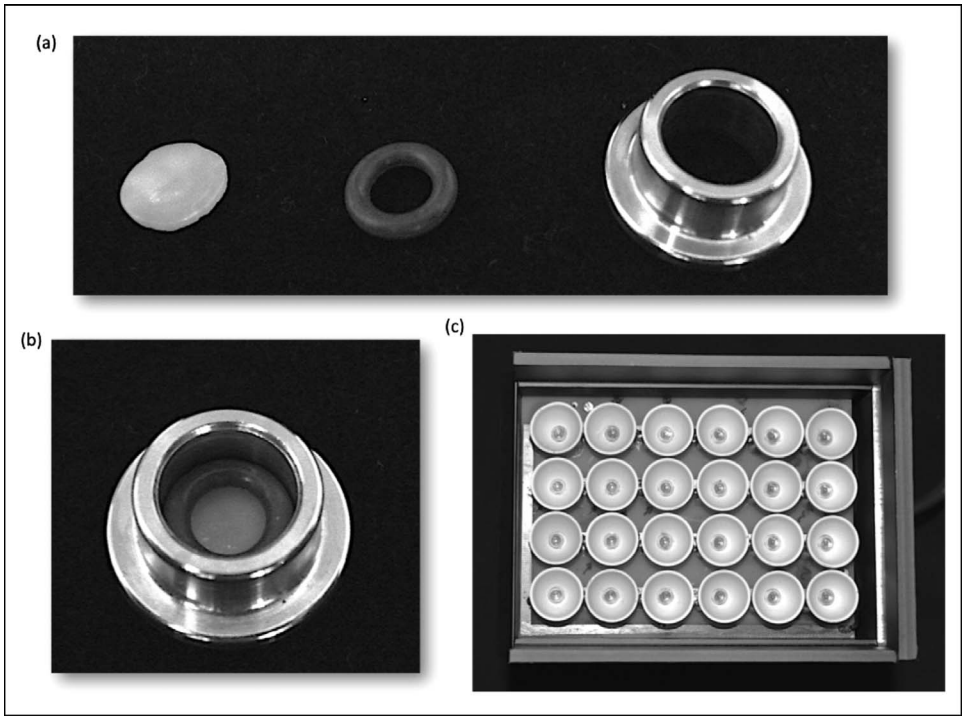

Figure 1. *Illustration of the dentin disc/device set and irradiation apparatus (LEDTable). (a): Dentin disc, silicon O-ring, and the irradiation apparatus, separately. (b): The dentin disc/device set. (c): Top view of LEDTable with 24 diodes and their collimators used to irradiate the dentin discs.*

ALP Activity—ALP activity was evaluated according to the protocol of the Alkaline Phosphatase Kit-colorimetric endpoint assay (Labtest Diagnóstico SA, Lagoa Santa, MG, Brazil). This assay utilizes thymolphthalein monophosphate, a substrate of phosphoric acid ester. ALP hydrolyzes the thymolphthalein monophosphate, releasing thymolphthalein. The enzymatic activity was measured as previously described.[15]

Analysis of Cell Morphology by SEM

For each experimental and control group, samples were prepared for cell morphology analysis by SEM (JEOL-JMS-T33A Scanning Microscope; JEOL USA Inc, Peabody, MA, USA). The laboratory protocol employed in this study is well established and has been widely used.[15,19]

Col-I Expression—RT-PCR

RNA extraction was performed by the Trizol method, which was detailed by Basso and others.[22] The cDNA was obtained by means of the High Capacity cDNA Reverse Transcriptions Kit (Applied Biosystems, Foster City, CA, USA) as previously described.

After cDNA synthesis, the effect of LED irradiation was assessed on the expression of Col-I with β-actin as the endogenous control. For each of these genes, specific primers were designed from the mRNA sequence (Table 1).

The reactions were prepared with standardized reagents for RT-PCR SYBR® Green PCR Master Mix (Applied Biosystems) in addition to sets of primers for each gene. Fluorescence readings were performed by Step One Plus (Applied Biosystems) in each amplification cycle and were subsequently analyzed by Step One Software 2.1 (Applied Biosystems). All reactions were subjected to the same analysis conditions and normalized by the signal from the passive reference dye ROX to correct for fluctuations in readings due to changes in volume and evaporation during the reaction. Individual results expressed in CT values were transferred to spreadsheets and grouped according to the experimental groups, normalized according to expression of the endogenous gene selected (β-actin). Then the

Table 1: *Primer Sequences and Applications for Mus musculus Used in This Work*

Primer Sequences	Gene
S: 5′-AGC CAT GTA CGT AGC CAT CC-3′	βAct
AS: 5′-CT CTC AGC TGT GGT GGT GAA-3′	
S: 5′-TGA GGT CCA GGA GGT CCA-3′	Col-I
AS: 5′-AAC TTT GCT TCC CAG ATG TCC-3′	

concentrations of target gene mRNA were evaluated statistically.

Statistical Analysis

The data set for each variable—cell viability, TP production, ALP activity, and Col-I expression—were evaluated concerning their distribution. In compliance with the requirements for the selection of parametric tests, nonparametric Kruskal-Wallis tests were complemented by the Mann-Whitney test, set at a predetermined significance of 5%.

RESULTS

Temperature Monitoring

The 630-nm wavelength (red LED) yielded no temperature increase during 10-minute irradiation, which was the maximum time used for cell irradiation. The 450-nm (blue LED) and 840-nm (infrared) wavelengths caused an increase of only 2°C after 8 minutes of irradiation. Thus, the temperature rise did not cause damage to cells; temperature increase of up to 3.4°C does not cause detrimental effects on MDPC-23 cells.[23]

Cell Viability (MTT Assay), TP, ALP, and Col-I Expression

The data for cell viability, ALP, TP, and collagen type-I expression, according to the energy densities and wavelengths used in this study, are shown in Figure 2. When the LED energy densities were compared for cell viability, it was observed that for the 450-nm wavelength (blue LED), there was no statistical difference between the irradiated groups and the control, which was considered with 100% cell viability ($p>0.05$). For the 630-nm wavelength (red LED), the energy density of 25 J/cm^2 increased the cell viability by 21.8% ($p<0.05$). For the 840-nm wavelength (infrared LED), energy densities of 4 and 25 J/cm^2 reduced the cell viability by 18.6% and 29.1%, respectively; all of them were statistically different from the control group ($p<0.05$). Concerning the LED wavelengths at the energy density of 4 J/cm^2, 450 nm (blue light) caused statistically higher cell viability compared to 840 nm ($p<0.05$). For energy density of 25 J/cm^2, the cells irradiated with red LED (630 nm) presented greater viability compared to the infrared LED (840 nm; $p<0.05$).

Concerning ALP, it was observed that the wavelengths used for all irradiated groups showed higher values of ALP activity when compared to the control group, except for the blue LED at 4 J/cm^2 ($p>0.05$). For the wavelength of 450 nm (blue LED), the group irradiated with 25 J/cm^2 provided statistically better results than the control group ($p<0.05$), with an increase of 113% in ALP activity. For the wavelength of 630 nm (red LED), groups irradiated with 4 and 25 J/cm^2 also showed statistically greater values when compared with the control group ($p<0.05$), with an increase of 46.7% and 81.7% in ALP activity, respectively. For 840 nm wavelength (infrared LED), groups irradiated with 4 and 25 J/cm^2 also had higher levels of ALP ($p<0.05$), and the increase in ALP activity compared to the control group was 220% and 121%, respectively. When the wavelengths were compared, it was observed that there was no difference among the groups for 25 J/cm^2 ($p>0.05$). However, when the irradiation was performed with 4 J/cm^2, increased ALP activity was observed for the wavelength of 840 nm ($p<0.05$).

For TP, regarding the energy densities used for this *in vitro* study, it was observed that there was no statistical difference between the irradiated and control groups for all wavelengths ($p>0.05$). But when the wavelengths were compared, there was a statistically significant difference between the 630-nm wavelength (red LED) and the 840-nm wavelength (infrared LED) only for 4 J/cm^2, and the wavelength representing the red region spectra showed the best results ($p<0.05$).

Finally, for Col-I expression, comparing the energy densities of 4 and 25 J/cm^2, it was possible to determine that the 450-nm irradiation resulted in a decrease of 64% and 56% in the Col-I expression, respectively. For the red LED, the group of 4 J/cm^2 was not statistically different from the control group ($p>0.05$). However, the energy density of 25 J/cm^2 showed a decrease of 40% in the expression of Col-I, and this difference was statistically significant when compared to the control group ($p<0.05$). For the infrared LED, an energy density of 4 J/cm^2 caused a 168% increase in the Col-I expression when compared with the control group ($p<0.05$). Moreover, the energy density of 25 J/cm^2 did not differ statistically from the control group ($p>0.05$). When the wavelengths were compared, it was observed that for 4 J/cm^2, there was a statistically significant difference among all evaluated wavelengths ($p<0.05$). However, the 840-nm wavelength (infrared) showed the best results for the expression of Col-I, followed by 630 nm (red) and 450 nm (blue). At 25 J/cm^2 energy density, the 840-nm wavelength showed significantly higher values compared to 450 and 630 nm ($p<0.05$).

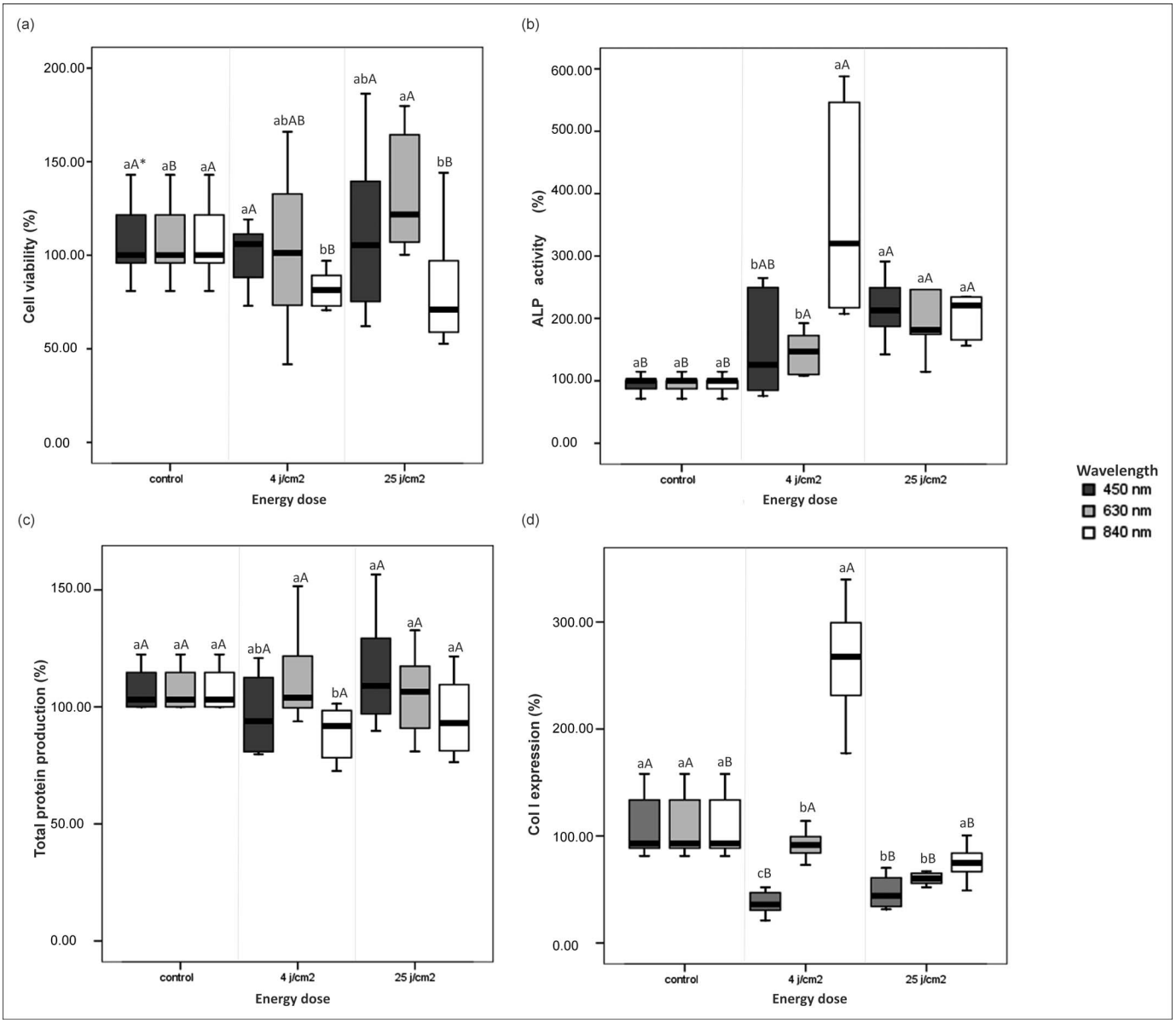

Figure 2. *Box plot indicating data for cell viability, total protein(TP), alkaline phosphatase (ALP) activity, and collagen type I (Col-I) expression. (a): Cell viability (%) detected by the methyltetrazolium (MTT) assay according to energy densities and wavelengths. (b): ALP activity (%) according to the energy densities and wavelength. (c): TP production (%) according to the energy densities and wavelength. (d): Col-I expression (%) according to the energy densities and wavelength (n=8). *Uppercase letters allow for comparison among energy densities, and lowercase letters allow for comparison among wavelengths. Same letters indicate no statistically significant difference (Mann-Whitney, p>0.05).*

Cell Morphology—SEM

Cells subjected to LED irradiation presented number and morphology similar to that of control group cells. More attached cells were observed on dentin discs subjected to irradiation at 25 J/cm^2 than at 4 J/cm^2 (Figure 3).

DISCUSSION

LED therapy has been used in different areas of human health, especially in dermatology[24-26] and neurology.[17] Additionally, this type of light has also been employed for muscle analgesia, anti-inflammatory effect,[7,27,28] and regeneration of injured tissues.[29,30] Specifically, in dentistry, LED has been evaluated as an alternative adjuvant therapy for treatment of mucositis,[11] dentin hypersensitivity,[10,31] and pulp cell stimulation.[32]

Tate and others[9] irradiated sound molars of rats with low-power laser and observed an intense formation of mineralized tissue within 30 days after

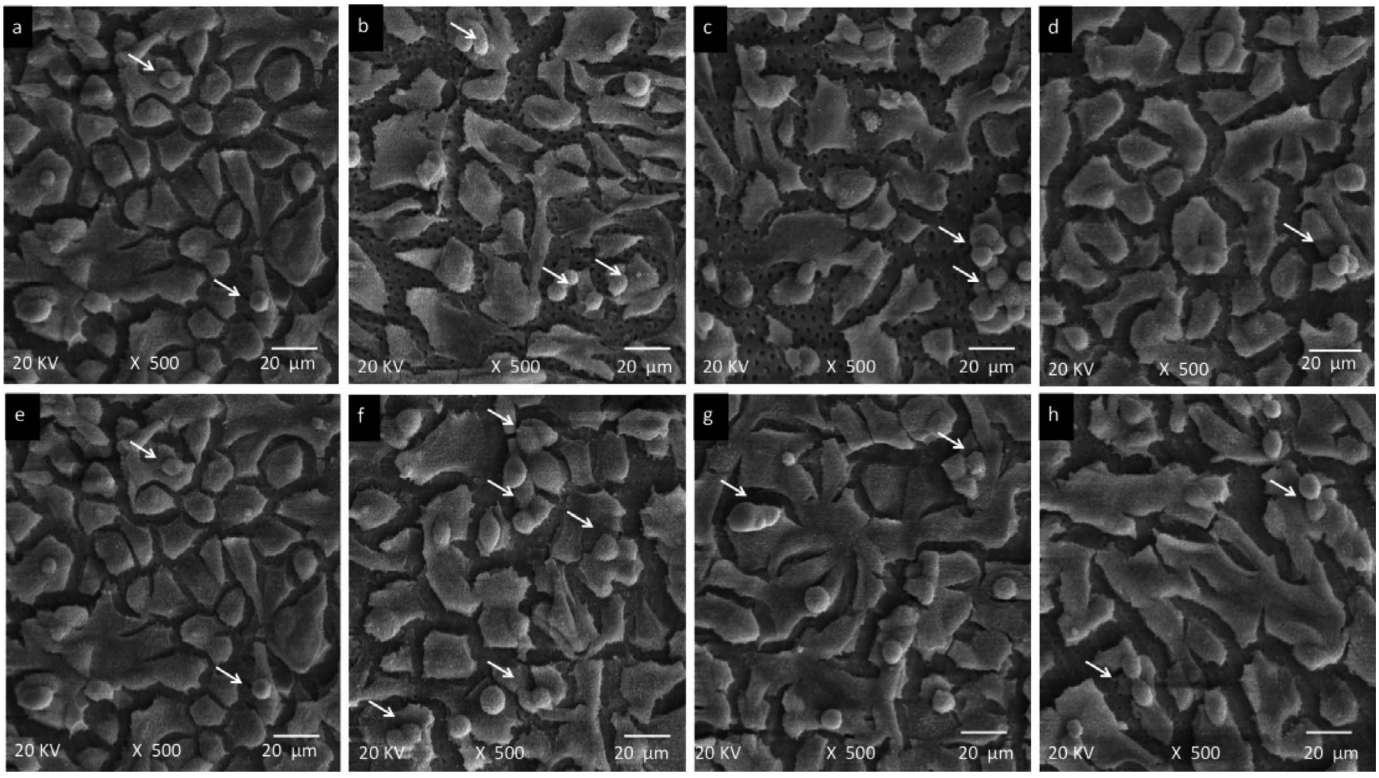

Figure 3. *Panel of SEM micrographs representative of cell morphology for each group. (a-d): Control group, 450 nm, 630 nm, and 840 nm LED, respectively, for 4 J/cm^2. (e-h): Control group, 450 nm, 630 nm, and 840 nm LED, respectively, for 25 J/cm^2. Arrows indicate mitosis. More attached cells were observed on dentin discs subjected to irradiation at 25 J/cm^2 than at 4 J/cm^2. Magnification 500×.*

procedure. However, the light irradiation of dentin-pulp complex able to promote biostimulation of human pulp cells previously subjected to an aggressive stimulus is not well known. To cause any effect on the pulp tissue, light must be transmitted through the hard dental tissues to reach the pulp cells with sufficient energy density to induce biostimulation. Despite the scarce basic research data concerning the optimal parameters of light application for different therapeutic activities, the clinical effects of light have already been assessed and even used as adjuvant therapy.[33] Therefore, this study evaluated the effect of transdentinal LED irradiation on odontoblast-like MDPC-23 cells seeded on dentin discs, using three different wavelengths, for which some positive cellular effects were described in the literature.[5,6,12,34]

In the present study, a significant increase in cell metabolism was observed in the group in which cells were subjected to irradiation with red LED at an energy density of 25 J/cm^2. In contrast, cells irradiated with infrared LED showed decreased metabolism after 72 hours of irradiation. Vinck and others[35] irradiated fibroblasts with red and infrared LED and observed increased cell metabolism 24 hours after irradiation and decreased cell metabolism 72 hours after irradiation. The authors suggested that this reduction in fibroblast metabolism at 72 hours postirradiation may be due to the occurrence of cell confluence after a long incubation, leading to contact-cell inhibition. This inhibitory phenomenon may also explain the negative effects obtained in the present study when the cells were irradiated with infrared wavelengths. The SEM analysis showed that, no matter the energy densities and wavelengths evaluated in this study, the morphology of MDPC-23 cells did not change. Thus, it may be suggested that the infrared LED, at energy densities of 4 and 25 J/cm^2, affected negatively the cell metabolism without causing detectable changes in cell morphology. Other studies have also evaluated the effect of light on cell metabolism, and generally the diverse responses found after irradiation were increased metabolism after 24[35,36] and 72 hours[31,37] and metabolism similar to the control group.[4,38] Importantly, the responses of irradiated cells were always dependent on the type of cell culture and irradiation parameters employed. Thus, cells that showed increased

metabolism 24 hours after the last irradiation were from a fibroblastic lineage, seeded at a density of 7×10^4 cells/cm^2, incubated for 24 hours, and subjected to three daily irradiations.[35,36] Particularly, this irradiation therapy used by Vinck and others)[36] does not match the protocol tested in the present study since the purpose of this study was to simulate a clinical situation in which a very deep dental cavity needs to be restored. Then, for economic, practical, and time reasons, the clinician has the possibility of irradiating the cavity floor one time only before filling the cavity. Also, since the cells internally lining the dentin tissue are odontoblasts, MDPC-23 cells were used in this study because they have the odontoblast phenotype and have been widely employed in various studies of light biomodulation.[15,21,31,38]

In addition to cell metabolism, ALP activity was evaluated. An increased expression of this enzyme by irradiated cells may indicate an interesting improvement in pulp tissue healing. However, previous studies showed that depending on the irradiation parameters used, different responses may occur in the ALP activity.[31,38] This cell behavior has been confirmed in the present study, where there was an increase in the activity of this protein for almost all irradiated groups. Thus, considering the positive results of ALP activity and correlating it with increased cell metabolism, particularly for the red LED at an energy density of 25 J/cm^2, it may be speculated that this parameter could be studied more deeply in future research both *in vitro* and *in vivo*. Moreover, other studies have shown an increase in ALP expression by mesenchymal cells irradiated with red LED.[4,5] Therefore, besides biomodulation of odontoblast-like cells, LED-specific parameters may also act positively on mesenchymal stem cells, which, in the case of injury by external factors, such as caries, heating, trauma, and so on, can effectively participate in the repair of the pulp-dentin complex.

Regarding Col-I expression, it was observed that irradiation with the infrared wavelength, at an energy density of 4 J/cm^2, increased the expression of this gene by 167% compared with that of the control group. Previous studies that evaluated the expression of Col-I by laser and LED phototherapy, in the red and infrared spectra, reported either similar behavior of irradiated groups compared with the control group[21] or increased expression of this gene after irradiation.[3,4] This result demonstrates that the use of this wavelength in transdentinal irradiation may be effective in forming nonmineralized matrix.

In general, the red light stood out from the other wavelengths, as did the blue light, which caused the lowest cell stimulation. These data can be explained, at least in part, by the occurrence of high scattering when lower wavelengths, like blue light, are applied to tissues, decreasing the energy density that reaches the local cells.[12,14] It is known that infrared light has the lowest scattering; however, it shows lower absorption by cells when compared with the red light.[12,39] Thus, it may be suggested that simultaneous effects of scattering and absorption by cultured pulp cells subjected to transdentinal LED irradiation occurred in the present investigation. It is known that wavelengths above 500 nm are better absorbed by cytochrome *c* oxidase, resulting in a greater synthesis of adenosine triphosphate by the cell with consequent increase of energy by oxidative phosphorylation.[40] On the other hand, flavins are small water-soluble molecules known to initiate free radical reactions when excited by light at wavelengths below 500 nm.[41] This information may explain, at least partially, the different cell responses found in the present study.

The results of this study underscore the importance of determining the optimal parameters for cellular biomodulation by LED phototherapy. For this study, wavelength and energy densities were factors that interfered with the cellular responses to transdentinal irradiation with LEDs, and all three wavelengths were able to cross the dentin barrier and cause some stimulus on pulp cells. Further *in vivo* studies are required to elucidate the effects of LED on the pulp-dentin complex as well as to determine whether LED irradiation may interact with different cells at the same time to trigger distinct pathways of biomodulation and tissue repair.

CONCLUSION

Based on the data obtained in this *in vitro* study, it can be concluded that infrared LED irradiation (840 nm) at an energy density of 4 J/cm^2 and red LED (630 nm) at an energy density of 25 J/cm^2 were the most effective parameters for transdentinal photobiomodulation of cultured odontoblast-like cells.

Acknowledgements

The authors acknowledge the Fundação de Amparo à Pesquisa do Estado de São Paulo, FAPESP (grants 2011/13895-0 and 2009/03615-0), and the Conselho Nacional de Desenvolvimen-

to Científico e Tecnológico, CNPq (grant 301291/2010-1), for financial support.

Conflict of Interest

The authors of this manuscript certify that they have no proprietary, financial, or other personal interest of any nature or kind in any product, service, and/or company that is presented in this article.

(Accepted 5 April 2014)

REFERENCES

1. About I, Camps J, Burger AS, Mitsiadis TA, Butler WT, & Franquin JC (2005) Polymerized bonding agents and the differentiation in vitro of human pulp cells into odontoblast-like cells *Dental Materials* **21(2)** 156-163.
2. Villa GEP, Catirse ABC, Lia RCC, & Lizarelli RFZ (2007) In vivo analysis of low-power laser effects irradiation at stimulation of reactive dentine *Laser Physics Letter* **4(9)** 690-695.
3. Barolet D, Roberge CJ, Auger FA, Boucher A, & Germain L (2009) Regulation of skin collagen metabolism in vitro using a pulsed 660 nm LED light source: Clinical correlation with a single-blinded study *Journal of Investigative Dermatology* **129(12)** 2751-2759.
4. Kim HK, Kim JH, Abbas AA, Kim DO, Park SJ, Chung JY, Song EK, & Yoon TR (2009) Red light of 647 nm enhances osteogenic differentiation in mesenchymal stem cells *Lasers in Medical Science* **24(2)** 214-222.
5. Li WT, Leu YC, & Wu JL (2010) Red-light light-emitting diode irradiation increases the proliferation and osteogenic differentiation of rat bone marrow mesenchymal stem cells *Photomedicine and Laser Surgery* **28(1)** 157-165.
6. Huang PJ, Huang YC, Su MF, Yang TY, Huang JR, & Jiang CP (2007) In vitro observations on the influence of copper peptide aids for the LED photoirradiation of fibroblast collagen synthesis *Photomedicine and Laser Surgery* **25(3)** 183-190.
7. Lim JH, Lee J, Choi J, Hong J, Jhun H, Han J, & Kim S (2009) The effects of light-emitting diode irradiation at 610 nm and 710 nm on murine T-cell subset populations *Photomedicine and Laser Surgery* **27(5)** 813-818.
8. Ferreira ANS, Silveira S, Genovese WJ, Cavalcante de Araújo V, Frigo L, de Mesquita RA, & Guedes E (2006) Effect of GaAIAs laser on reactional dentinogenesis induction in human teeth *Photomedicine and Laser Surgery* **24(3)** 358-365.
9. Tate Y, Yoshiba K, Yoshiba N, & Iwaku M (2006) Odontoblast responses to GaAIAs laser irradiation in rat molars: An experimental study using heat-shock protein-25 immunohistochemistry *European Journal of Oral Sciences* **114(1)** 50-57.
10. Lizarelli RFZ, Miguel FAC, Villa GEP, Filho EC, Pelino JEP, & Bagnato VS (2007) Clinical effects of low-intensity laser vs light-emitting diode therapy on dentin hypersensitivity *Journal of Oral Laser Applications* **7(2)** 1-8.
11. Sacono NT, Costa CA, Bagnato VS, & Abreu-e-Lima FC (2008) Light-emitting diode therapy in chemotherapy-induced mucositis *Lasers in Surgery and Medicine* **40(9)** 625-633.
12. Neupane J, Ghimire S, Shakya S, Chaudhary L, & Shrivastava VP (2010) Effect of light emitting diodes in the photodynamic therapy of rheumatoid arthritis *Photodiagnosis and Photodynamic Therapy* **7(1)** 44-49.
13. Turrioni AP, de Oliveira CF, Basso FG, Moriyama LT, Kurachi C, Hebling J, & de Souza Costa CA (2012) Correlation between light transmission and permeability of human dentin *Lasers in Medical Science* **27(1)** 191-196.
14. Turrioni AP, Alonso JRL, Basso FG, Moriyama LT, Hebling J, Bagnato VS, & de Souza Costa (2014) LED light attenuation through human dentin: A first step toward pulp photobiomodulation after cavity preparation *American Journal of Dentistry* **26(6)** 319-323.
15. Oliveira CF, Basso FG, Lins EC, Kurachi C, Hebling J, Bagnato VS, & de Souza Costa CA (2011) In vitro effect of low-level laser on odontoblast-like cells *Laser Physics Letter* **8(2)** 155-163.
16. Goldberg M, & Smith AJ (2004) Cells and extracellular matrices of dentin and pulp: A biological basis for repair and tissue engineering *Critical Reviews in Oral Biology and Medicine* **15(1)** 13-27.
17. Wong-Riley MT, Liang HL, Eells JT, Chance B, Henry MM, Buchmann E, Kane M, & Whelan HT (2005) Photobiomodulation directly benefits primary neurons functionally inactivated by toxins: Role of cytochrome C oxidase *Journal of Biological Chemistry* **280(6)** 4761-4771.
18. Alghamdi KM, Kumar A, & Moussa NA (2012) Low-level laser therapy: A useful technique for enhancing the proliferation of various cultured cells *Lasers in Medical Science* **27(1)** 237-249.
19. Lanza CRM, Costa CAS, Alecio AC, Furlan M, & Hebling J (2009) Transdentinal diffusion and cytotoxicity of self-etching adhesive systems *Cell Biology and Toxicology* **25(6)** 533-543.
20. Almeida-Lopes L, Rigau J, Zângaro RA, Guidugli-Neto J, & Jaeger MM (2001) Comparison of the low level laser therapy effects on cultured human gingival fibroblasts proliferation using different irradiance and same fluence *Lasers in Surgery and Medicine* **29(2)** 179-184.
21. Oliveira CF, Basso FG, Lins EC, Kurachi C, Hebling J, Bagnato VS, & de Souza Costa CA (2010) Increased viability of odobtoblast-like cells subjected to low-level laser irradiation *Laser Physics* **20(7)** 1659-1666.
22. Basso FG, Oliveira CF, Kurachi C, Hebling, J & Costa CA (2013) Biostimulatory effect of low-level laser therapy on keratinocytes in vitro *Lasers in Medical Science* **28(2)** 367-374.
23. Souza PPC, Hebling J, Scalon MG, Aranha AM, & Costa CA (2009) Effects of intrapulpal temperature change induced by visible light units on the metabolism of odontoblast-like cells *American Journal of Dentistry* **22(3)** 151-156.
24. Ablon G (2010) Combination 830-nm and 633-nm light-emitting diode phototherapy shows promise in the

treatment of recalcitrant psoriasis: preliminary findings *Photomedicine and Laser Surgery* **28(1)** 141-146.

25. Chang YS, Hwang JH, Kwon HN, Choi CW, Ko SY, Park WS, Shin SM, & Lee M (2005) In vitro and in vivo efficacy of new blue light emitting diode phototherapy compared to conventional halogen quartz phototherapy for neonatal jaundice *Journal of Korean Medical Science* **20(1)** 61-64.
26. DeLand MM, Weiss RA, McDaniel DH, & Geronemus RG (2007) Treatment of radiation-induced dermatitis with light-emitting diode (LED) photomodulation *Lasers in Surgery and Medicine* **39(2)** 164-168.
27. Leal EC Jr, Lopes-Martins RA, Rossi RP, De Marchi T, Baroni BM, de Godoi V, Marcos RL, Ramos L, & Bjordal JM (2009) Effect of cluster multi-diode light emitting diode therapy (LEDT) on exercise-induced skeletal muscle fatigue and skeletal muscle recovery in humans *Lasers in Surgery and Medicine* **41(8)** 572-577.
28. Vinck EM, Cagnie BJ, Coorevits P, Vanderstraeten G, & Cambier D (2006) Pain reduction by infrared light-emitting diode irradiation: A pilot study on experimentally induced delayed-onset muscle soreness in humans *Lasers in Medical Science* **21(1)** 11-18.
29. Dall Agnol MA, Nicolau RA, de Lima CJ, & Munin E (2009) Comparative analysis of coherent light action (laser) versus non-coherent light (light-emitting diode) for tissue repair in diabetic rats *Lasers in Medical Science* **24(6)** 909-916.
30. De Sousa APC, Santos JN, dos Reis JA, Ramos TA, de Souza J, Cangussú MCT, & Pinheiro ALB (2010) Effect of LED phototherapy of three distinct wavelengths on fibroblasts on wound healing: A histological study in a rodent model *Photomedicine and Laser Surgery* **28(4)** 547-552.
31. Oliveira CF, Basso FG, dos Reis RI, Parreiras-e-Silva LT, Lins EC, Kurachi C, Hebling J, Bagnato VS, & de Souza Costa CA (2013) In vitro transdentinal effect of low-level laser therapy *Laser Phys*ics **23(5)** 55604-55614.
32. Holder MJ, Milward MR, Palin WM, Hadis MA, & Cooper PR (2012) Effects of red light-emitting diode irradiation on dental pulp cells *Journal of Dental Research* **91(10)** 961-966.
33. Gao X, & Xing D (2009) Molecular mechanisms of cell proliferation induced by low power laser irradiation *Journal of Biomedical Science* **16(1)** 4-19.
34. Higuchi A, Watanabe T, Noguchi Y, Chang Y, Chen WY, & Matsuoka Y (2007) Visible light regulates neurite outgrowth of nerve cells *Cytotechnology* **54(3)** 181-188.
35. Vinck EM, Cagnie BJ, Cornelissen MJ, Declercq HA, & Cambier DC (2003) Increased fibroblast proliferation induced by light emitting diode and low power laser irradiation *Lasers in Medical Science* **18(2)** 95-99.
36. Vinck EM, Cagnie BJ, Cornelissen MJ, Declercq HA, & Cambier DC (2005) Green light emitting diode irradiation enhances fibroblast growth impaired by high glucose level *Photomedicine and Laser Surgery* **23(2)** 167-171.
37. Li WT, Chen HL, & Wang CT (2006) Effect of light emitting diode irradiation on proliferation of human bone marrow mesenchymal stem cells *Journal of Medical and Biological Engineering* **26(1)** 35-42.
38. Oliveira CF, Hebling J, Souza PPC, Sacono NT, Lessa FR, Lizarelli RFZ, & de Souza Costa CA (2008) Effect of low-level laser irradiation on odontoblast-like cells *Laser Physics* **5(9)** 680-685.
39. Karu TI, Pyatibrat LV, Kalendo GS, & Esenaliev RO (1996) Effects of monochromatic low-intensity light and laser irradiation on adhesion of He La cells in vitro *Lasers in Surgery and Medicine* **18(2)** 171-177.
40. Karu, TI, & Kolyakov SF (2005) Exact action spectra for cellular responses relevant to phototherapy *Photomedicine and Laser Surgery* **23(4)** 355-361.
41. Eichler M, Lavi R, Shainberg A, & Lubart R (2005) Flavins are source of visible-light-induced free radical formation in cells *Lasers in Surgery and Medicine* **37(4)** 314-319.

Lasers Med Sci (2012) 27:191–196
DOI 10.1007/s10103-011-0931-0

ORIGINAL ARTICLE

Correlation between light transmission and permeability of human dentin

Ana Paula Silveira Turrioni · Camila Fávero de Oliveira · Fernanda Gonçalves Basso · Lilian Tan Moriyama · Cristina Kurachi · Josimeri Hebling · Vanderlei S. Bagnato · Carlos Alberto de Souza Costa

Received: 25 November 2010 / Accepted: 18 April 2011 / Published online: 10 May 2011

Abstract The influence of dentin permeability on transdentinal LED light propagation should be evaluated since this kind of phototherapy may further be clinically used to stimulate the metabolism of pulp cells, improving the healing of damaged pulps. This study evaluated the influence of the dentin permeability on the transdentinal LED light (630 nm) transmission. Forty-five 0.5-mm-thick dentin disks were prepared from the coronal dentin of extracted sound human molars. An initial measurement of transdentinal LED light transmission was carried out by illuminating the discs in the occlusal-to-pulpal direction onto a light power sensor to determine light attenuation. The discs were treated with EDTA for smear layer removal, subjected to analysis of hydraulic conductance, and a new measurement of transdentinal LED light transmission was taken. Spearman's correlation coefficient was used for analysis of data and showed a weak correlation between dentin permeability and light attenuation (coefficient= 0.19). This result indicates that higher or lower dentin permeability does not reflect the transdentinal propagation of LED light. Significantly greater transdentinal propagation of light was observed after treatment of dentin surface with EDTA (Wilcoxon test, $p<0.05$). According to the experimental conditions of this in vitro study, it may be concluded that dentin permeability does not interfere in the transdentinal LED light transmission, and that smear layer removal facilitates this propagation.

Keywords Dentin permeability · LED · Transillumination · Light propagation

A. P. S. Turrioni · C. F. de Oliveira · J. Hebling
Department of Pediatric Dentistry and Orthodontics,
UNESP - Univ. Estadual Paulista,
Araraquara, SP 14801903, Brazil

F. G. Basso
Department of Oral Diagnosis,
UNICAMP - Universidade de Campinas,
Piracicaba, SP 13414-903, Brazil

L. T. Moriyama · C. Kurachi · V. S. Bagnato
USP - Universidade de São Paulo, Institute of Physics,
São Carlos, SP 13560-970, Brazil

C. A. de Souza Costa
Department of Physiology and Pathology,
UNESP - Univ. Estadual Paulista,
Araraquara, SP 14801903, Brazil

C. A. de Souza Costa (✉)
Departamento de Fisiologia and Patologia. Faculdade de Odontologia de Araraquara, Universidade Estadual Paulista,
Rua Humaitá, 1680. Centro,
Caixa Postal: 331 Cep: 14801903, Araraquara, SP, Brazil
e-mail: casouzac@foar.unesp.br

Introduction

Phototherapy using light emitting diodes (LEDs) has been used in several health fields, including the treatment of dermatitis, Alzheimer's disease, and muscle analgesia [1–3]. Light has also been applied combined with a photosensitizing agent in the photodynamic therapy for the treatment of neoplasias [4]. In dentistry, several studies have been directed to investigate the effects of LED light irradiation on oral mucositis [5, 6], dentin hypersensitivity [7], candidiasis [8], and decontamination of carious cavities [9]. A LED therapy protocol established by Sacono et al. [6] was effective in reducing the severity of mucositis induced by a chemotherapeutic agent associated with superficial scratching of the cheek pouch of hamsters. Lizarelli et al. [7] evaluated the clinical effect of LED and low-level laser therapy (LLLT) on

dentin hypersensitivity and observed that both treatments were effective in reducing pain.

Other positive effects of phototherapy have been reported, including acceleration of the wound healing process [10–12], enamel remineralization [13], cell proliferation and collagen synthesis [14], increase of cell metabolism [15], expression of growth factors and extracellular matrix components, as well as stimulation of ATP synthesis and reactive oxygen species (ROS) production [2, 3].

Vinck et al. [16] irradiated fibroblast cell cultures with an LED light source emitting several wavelengths (950 nm, 660 nm, and 570 nm) and found increased fibroblast proliferation. In the same study, comparison between LED light and laser light revealed that both illumination systems promoted an increase in fibroblast proliferation, confirming that LED light can be used as a substitute for the laser. Other in vitro studies have also found that light irradiation stimulates proliferation of different cell lines [14, 17–19].

An LED is a semiconductor device that emits non-coherent narrow-spectrum light when electrically biased in the forward direction. This effect is a form of electroluminescence. The color of the emitted light depends on the chemical composition of the semiconducting material used, and can be near-ultraviolet, visible, or infrared [20]. LEDs have become an effective alternative to laser systems for a number of reasons: their lower cost, availability in a variety of wavelengths, ranging from ultraviolet to near-infrared region of the spectrum, narrow emission band (about 5–10 nm), light fluence rate that can achieve hundreds of mW/cm^2, the arrays can be constructed in various sizes to accommodate large areas, and they do not emit any heat, which eliminates the danger of additional tissue damage [20]. According to the literature, lasers and LEDs with the same wavelength, intensity, and dose promote the same biological response [7].

It is known that dentin has a tubular structure and that the relative number (tubular density) and diameter increase from the outer to the inner layers of dentin and close to the pulp tissue [22]. This morphological variation leads to the occurrence of regional differences in dentin permeability. The analysis of dentin permeability is important for studies investigating the transdentinal diffusion of components of dental materials and their possible indirect cytotoxic effects on pulp cells. The greater the dentin permeability, the greater the contact of the dentin fluid with the material, which can cause solubilization of its components and release of toxic products that are capable of diffusing through the tubules and causing pulp cell damage [23].

The relationship between dentin permeability and transdentinal light transmission and its consequences to the biological events on the pulp cells have not yet been investigated. According to Zijp and Bosch [24], transdentinal light transmission is guided mainly by light scattering caused by the presence of dentin tubules, mineral crystals, and collagen fibrils. The dentin tubules are considered as the predominant cause of scattering in dentin. Studies investigating the optical properties of dentin [25, 26] have shown that the transdentinal laser light transmission is related to the shape and arrangement of dentin tubules. Hence, it is possible to suggest the existence of a direct relationship between dentin permeability and light transmission through dentin.

Based on this research data, recent studies investigating the transdentinal effect of light originated from different sources on cell cultures have evaluated dentin permeability (hydraulic conductance) in order to obtain a homogenous sample and a standardized experimental design. The dentin discs are subjected to analysis of hydraulic conductance and those with similar values are selected and distributed to the study groups [21]. However, it is not well understood how LED light propagates through dentin and whether the diameter and number of tubules play the main role in this transmission. Therefore, the aim of this study was to evaluate the relationship between dentin permeability and transdentinal LED light transmission.

Material and methods

Sound human third molars free of cracks, defects, or morphological alterations were obtained from the Human Tooth Bank of Araraquara School of Dentistry, UNESP - Univ. Estadual Paulista, Brazil, after approval of the research project by the local Research Ethics Committee (Protocol 26/09). The teeth were immersed in 70% ethanol for 5 days and scaled for removal of periodontal ligament remnants and other surface-adhered debris.

Dentin discs were cut transversally from the middle portion of each tooth crown in a precision cutting machine (Isomet 1000, Buehler Ltda., Lake Bluff, IL, USA) with a water-cooled diamond saw (11–4254, 4" × 0.012"/series 15LC, Diamond Wafering blade, Buehler Ltda.). The dentin surface was polished with wet 400- and 600-grit silicon carbide paper (T469-SF- Norton, Saint-Gobain Abrasivos Ltda., Jundiaí, SP, Brazil) until obtaining 0.5-mm-thick dentin discs, confirmed by checking the thickness with a digital caliper (Model 500-144B, Mitutoyo Sul América Ltda., São Paulo, SP, Brazil). For disinfection purposes, each disc was dipped in a well of 24-well plates (Costar Corp., Cambridge, MA, USA) containing 1 ml of 70% ethanol [23]. After 6 h, the discs were washed with three 5-min rinses with phosphate buffer saline (PBS, pH 7.4).

Experimental design

Forty-five 0.5-mm-thick discs were used. An initial measurement of transdentinal LED light transmission was done by

illuminating the discs in the occlusal-to-pulpal direction onto a light power sensor (Coherent LM-2 VIS High-Sensitivity Optical Sensor; USA) to determine the light attenuation that occurred through the disc structure. The pulpal side of the disc was in contact with the light power sensor, while the light beam of an LED light source (λ=630) was directed to the occlusal side of the disc at a fixed distance in such a way that the disc could be illuminated in a uniform manner. An acrylic cylinder was attached to the LED light guide tip to collimate the light and direct it to the disc-sensor set. The LED source was regulated to reach maximum power of 50 mW, which is the detection limit of the light power sensor used in this study. The percent light attenuation in each disc was calculated by the ratio between illumination with and without interposition of the dentin disc.

After measurement of the initial transdentinal LED light transmission, a 0.5 M ethylenediaminetetraacetic acid (EDTA) solution (pH 7.2) was applied on the surface of the discs (occlusal and pulpal) for 2 min for removal of the smear layer, and then the discs were thoroughly rinsed with sterile deionized water for 60 s. Then, each dentin disc was subjected to analysis of hydraulic conductance. Permeability is derived from the hydraulic conductance or ease of fluid flow through a surface with known area and under certain pressure within a certain time duration. Outhwaite et al. [27] developed a device to facilitate the study of dentin permeability, known as in vitro pulp chamber or filtration chamber, which has been widely used in several studies [23]. The hydraulic conductance was analyzed using a split filtration chamber with an upper and a lower compartment, between which the dentin disc is placed for examination. The system starts working when the 1.8-m-high water column valve (corresponding to a pressure of 180 cm H_2O or 17.65 kPa) is opened and releases the water that exerts a hydrostatic pressure. This reservoir or water column is directly connected to a micropipette through polyethylene capillaries with diameter of 18 gauges (Embramed, São Paulo, SP, Brazil). The pressure was converted to kPa (1 cm H_2O= 0.098 kPa). This micropipette is juxtaposed to a measurement scale in millimeters, which allows measuring the dislodgement of liquid in a fraction of time, according to the filtration rate of the dentin discs. The dislodgement of deionized water is visualized through the movement of a microbubble created by a syringe coupled to a capillary extension between the micropipette and the filtration chamber. This filtration chamber is the final part of the system that houses the dentin discs and is connected to the hydrostatic pressure column by the polyethylene capillaries.

After determination of the hydraulic conductance of each disc, a new measurement of transdentinal LED light transmission was performed as previously described. However, at this time, the discs were clean (without smear layer) and with known hydraulic conductance.

The transdentinal light attenuation (%) data, obtained before and after dentin treatment with EDTA, were compared using the Wilcoxon test. The correlation between transdentinal light attenuation and permeability of each dentin disc was analyzed by the Spearman's correlation coefficient. A significance level of 5% was set for all analyses.

Results

A statistically significant difference of transdentinal light attenuation was observed as a function of EDTA treatment for the hydraulic conductance test (Wilcoxon, $p<0.05$). Significantly greater (61%) transdentinal light attenuation was observed when the discs were not pretreated with EDTA (smear-covered discs) compared to those treated with the chelating agent (smear-free discs) (59%) (Fig. 1).

Moderate to weak correlation (coefficient=0.19) was observed between transdentinal light attenuation (%) and dentin permeability after treatment of the discs with EDTA (no smear layer). Figure 2 illustrates the dispersion data of transdentinal light attenuation as a function of dentin disc permeability.

Discussion

LED phototherapy has been shown to produce positive biological effects, such as an increase of cell proliferation and collagen synthesis [14], as well as expression of growth factors and different extracellular matrix components [2, 3].

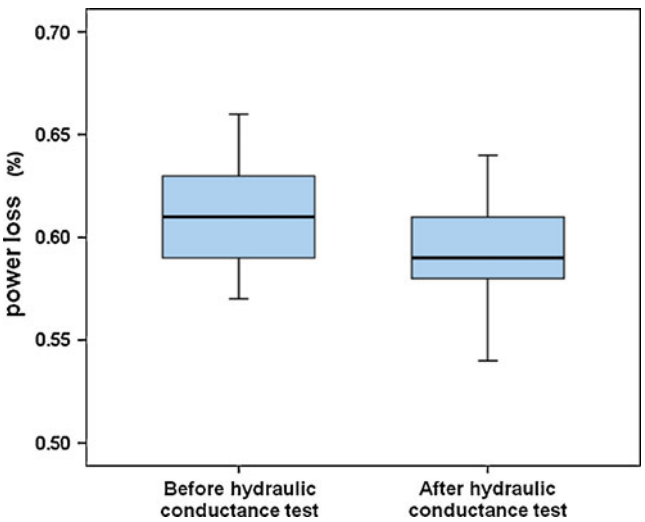

Fig. 1 Box-plot (minimum value [percentile 25–median–percentile 75] maximum value) of the attenuation (%) occurring during irradiation of dentin discs (n=45) before and after treatment with EDTA for the permeability test. Statistically significant difference (Wilcoxon, $p<0.05$) was observed between the two conditions

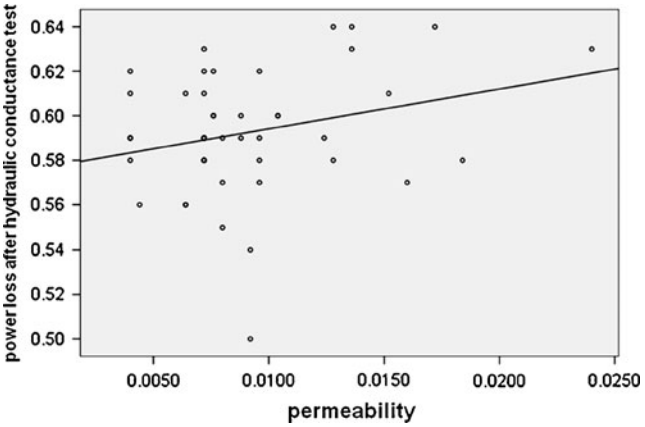

Fig. 2 Correlation between transdentinal light attenuation (%) and dentin permeability (kPa) after treatment of the discs with EDTA for the hydraulic conductance

However, although the mechanisms that guide the beneficial effects of LED light have been investigated in vitro, little is known about LED light transmission through the hard tissues of the body (e.g., bone, cartilage, enamel, dentin). Until now, several studies have referred only to the effects of light applied directly to different cell lines [14, 16–19]. It is important to obtain data about the effects of transdentinal illumination on the behavior of typical pulp cells because the light has to propagate through the dentin barrier to interact with the pulp cells during clinical application of phototherapy to reduce dental pain and/or accelerate tissue healing. Therefore, the present study investigated the relationship between dentin permeability and transdentinal LED light transmission using 0.5-mm-thick dentin discs. This experimental condition aimed at mimicking a specific clinical situation in which deep cavities are prepared in human teeth. Then, it is possible to investigate if the number and diameter of dentin tubules could interfere in the transdentinal transmission of LED light.

The hydraulic conductance test has been widely used in studies carried out to evaluate the cytotoxicity of dental materials, since the experimental and control groups should not present statistically significant differences in dentin permeability [23]. Based on the diffusion mechanism of these materials and/or their components through the dentin tubules, the use of the hydraulic conductance test has also been recommended to evaluate transdentinal light transmission across dentin [21]. The results presented in Fig. 2 show that light transmission through the dentin structure did not vary significantly, regardless of greater or lower dentin permeability. These findings suggest that the individual analysis of hydraulic conductance may not be the most adequate method to obtain a homogenous distribution of specimens to experimental groups in studies investigating the effect of light applied through dentin discs on cell cultures. The measurement of transdentinal light transmission to determine light attenuation seems to be a more accurate method in these cases.

Some studies have evaluated the optical characteristics of dentin and enamel light diffusion through these tissues. Vaarkamp et al. [25] irradiated dentin blocks with laser light at different angles to determine the transmission of light at the different faces. The authors concluded that the dentin tubules are structural dentin components that interfere directly on light scattering on this tissue. Light transmission through dentin was more intense when illumination was applied parallel to the dentin tubule direction. On the other hand, illumination perpendicular to the dentin tubule axis resulted in greater loss of intensity, conferring to dentin an anisotropic characteristic [28]. These data demonstrate that transdentinal transmission of laser light occurs, at least in part, through the dentin tubules. However, Vaarkamp et al. [25] evaluated laser transmission through dentin using an optical fiber with small spot size in contact with enamel surface to promote transillumination.

Studies on light transmission in turbid media (highly scattering media) have shown that light intensity at a certain depth depends on the diameter of the incident beam and increases as larger is the beam diameter [29]. As LED sources usually present a wide illumination area, it is likely that they have a different dosimetry from that used for lasers. In another study [26], horizontal and vertical sections of different regions of molar teeth were prepared and light transmission through the sections was examined varying the irradiation angle. Although the authors did not specify the type of light applied to the dental structures, the ability of light to propagate through dentin tubules with high refractive index was demonstrated. However, the authors [26] claim that, although possible, light transport along the tubule centers does not play an important role, and that light propagation in a dentin section is apparently based on the total internal reflection through the peritubular dentin. The optical properties of a tooth as a whole are determined by its architectonics, i.e., the tubules specifically distributed over the dentin. These structural features should be taken into account in optical studies and, in particular, in developing an optical model of the whole tooth.

Both Vaarkamp et al. [25] and Zolortev et al. [26] analyzed light transmission and its possible relationship with dentin tubules using various irradiation directions on different dentin regions. In the present study, two factors are important to justify the weak correlation between dentin permeability and light attenuation. The first is that the dentin discs were cut from the same region of the tooth (center of the tooth crown). The second and main factor refers to the LED light itself, which was applied in the same direction (along the dentin tubules) in all discs. The results obtained in the present study suggest that the LED

irradiation protocol employed, according to which neither the irradiation angle nor the dentin region varied from one specimen to another, did not interfere significantly on the transdentinal light transmission. Regional differences in the number and diameter of tubules could interfere in light transmission, but there is no published study reporting on a significant influence of these factors on LED light scattering through dentin structure. Therefore, it may be speculated that the number and diameter of dentin tubules may contribute to LED scattering, but not in a significant manner.

Although a direct correlation between dentin permeability and transdentinal light attenuation could not be established in this study when the discs were illuminated with a LED source, cleaning of the dentin surface with EDTA before the permeability test was important because tubule openings facilitate light transmission. The dentin discs were cut from tooth crowns in a precision cutting machine and then ground wet with abrasive paper, which produced a smear layer on their surfaces. As the smear layer is composed by organic and inorganic debris originated from the cutting procedure and water, it can reduce dentin permeability by 86% [30]. The maintenance of the smear layer in the present study could hinder light transmission through the dentin, leading to inaccurate results. It should be emphasized that the smear layer was formed on both sides of the disc (pulpal and occlusal) in the present study, probably obliterating the tubule entrances almost completely. In spite of this, 61% light attenuation was obtained, which indicates that the LED light beam was able to propagate through the dentin even when the tubules were obliterated. This result confirms the findings of Kienle et al. [29], who also consider the occurrence of light transmission through the intertubular dentin, which is mainly composed of collagen fibrils and hydroxyapatite crystals. After treatment of the discs with EDTA to clean dentin surface, the light attenuation decreased by only 2% (from 61 to 59%) compared to the smear-covered discs. This finding indicates that under the tested conditions and LED parameters, the dentin tubules per se did not play a key role in the transdentinal light transmission.

In this in vitro study, 0.5-mm-thick dentin discs were used to simulate a clinical condition of irradiating the floor of a deep cavity, and the thickness of the discs could eliminate the anisotropic characteristic of dentin. Our results cannot be directly compared to those of previously cited authors [25, 26], who irradiated dentin blocks obtained from the proximal region of the teeth or thicker dentin discs, in which the dentin tissue presented tubules with varied curvatures. Further research should investigate the transmission of LED light with different parameters through dentin discs of varied thicknesses obtained from different regions of the teeth.

There is no study in the literature comparing laser and LED propagation through dentin. However, the biological effect of these light sources has been evaluated individually in previous studies [11, 16, 33, 34]. Regarding possible differences around coherent light (laser) versus non-coherent light (LED), it has been shown that the coherence of light is not a determinant factor to the clinical effects of low-level lasers. Moreover, the primary difference between laser and LED is that the laser's coherent beam produces "speckles" of relatively high power density, which may cause local heating of inhomogeneous tissues [31, 32]. Another difference is that the coherent optical radiation produced by the laser is intrinsically monochromatic and the laser is expected to be more chromophore-specific than the light emitted by non-coherent sources, such as LED. On the other hand, the non-coherent light can simultaneously stimulate different chromophores and therefore unchain several biochemical reactions [11]. It has also been reported that the photochemical effects in the organism occur independently of light coherence, as the coherence is lost in the most superficial skin layer, before the light is absorbed by the chromophores of the subjacent cells [11]. There is evidence that both coherent and non-coherent lights can stimulate in vitro cell proliferation, transition from the inflammatory to the proliferative phase, and the activity of the superoxide dismutase enzyme, decreasing the oxidative stress [33, 34]. There has also been evidence that coherent and the non-coherent lights produce similar effects in biological tissues. This fact has been demonstrated in several studies [11, 16, 33, 34] in which both types of light produced positive effects.

Based on the results obtained in this study, it is possible to conclude that for further studies evaluating the effect of transdentinal LED light transmission on pulp cells, the most indicated laboratorial protocol for a homogeneous distribution of dentin discs into experimental and control groups is the one that determines the light attenuation after light application through each dentin disc. This methodology should be preceded by cleaning of the discs in order to open the dentin tubules and facilitate light transmission. It is expected that the results of this investigation can be used to establish an adequate methodology to evaluate the transdentinal action of different LED parameters and wavelengths on cell cultures. All data presented in this in vitro study will also be useful to guide future research on this field and widen the possibilities of studying, in a more detailed manner, the mechanisms involved in the LED effects on reducing and/or preventing dentin hypersensitivity, as well as LED light participation on the pulp healing process.

Acknowledgments The authors acknowledge the Fundação de Amparo à Pesquisa do Estado de São Paulo – FAPESP (grant nos. 2010/50798-0 and BP.MS: 2009/03615-0) and the Conselho Nacional de Desenvolvimento Científico e Tecnológico – CNPq (grant nº 301291/2010-1 for the financial support.

References

1. DeLand MM, Weiss RA, McDaniel DH, Geronemus RG (2007) Treatment of radiation-induced dermatitis with light-emitting diode (LED) photomodulation. Lasers Surg Med 39:164–168
2. Lim W, Lee S, Kim I, Chung M, Kim M, Lim H, Park J, Kim O, Choi H (2007) The anti-inflammatory mechanism of 635-nm light-emitting-diode irradiation compared with existing COX inhibitors. Lasers Surg Med 39:614–621
3. Liang HL, Whelan HT, Eells JT, Wong-Riley MT (2008) Near-infrared light via light-emitting diode treatment is therapeutic against rotenone- and 1-methyl-4-phenylpyridinium ion-induced neurotoxicity. Neuroscience 153:963–974
4. Machado AH, Pacheco Soares C, da Silva NS, Moraes KC (2009) Cellular and molecular studies of the initial process of the photodynamic therapy in HEp-2 cells using LED light source and two different photosensitizers. Cell Biol Int 33:785–795
5. Corti L, Chiarion-Sileni V, Aversa S, Ponzoni A, D'Arcais R, Pagnutti S, Fiore D, Sotti G (2006) Treatment of chemotherapy-induced oral mucositis with light-emitting diode. Photomed Laser Surg 24:207–213
6. Sacono NT, Costa CA, Bagnato VS, Abreu-e-Lima FC (2008) Light-emitting diode therapy in chemotherapy-induced mucositis. Lasers Surg Med 40:625–633
7. Lizarelli RFZ, Miguel FAC, Villa GEP, Filho EC, Pelino JEP, Bagnato VS (2007) Clinical effects of low-intensity laser vs light-emitting diode therapy on dentin hypersensitivity. J Oral Laser Appli 7:1–8
8. Mima EG, Pavarina AC, Dovigo LN, Vergani CE, Costa CA, Kurachi C, Bagnato VS (2010) Susceptibility of *Candida albicans* to photodynamic therapy in a murine model of oral candidosis. Oral Surg Oral Med Oral Pathol Oral Radiol Endod 109:392–401
9. Giusti JSM, Santos-Pinto L, Pizzolitto AC, Kurachi C, Bagnato VS (2006) Effectiveness of Photogem® activated by LED on the decontamination of artificial carious bovine dentin. Laser Phys 16:859–864
10. Bastos JLN, Lizarelli RFZ, Parizotto NA (2009) Comparative study of laser and LED systems of low intensity applied to tendon healing. Laser Phys 19:1925–31
11. Dall Agnol MA, Nicolau RA, de Lima CJ, Munin E (2009) Comparative analysis of coherent light action (laser) versus non-coherent light (light-emitting diode) for tissue repair in diabetic rats. Lasers Med Sci 24:909–916
12. de Sousa AP, Santos JN, Dos Reis JA, Ramos TA, de Souza J, Cangussú MC, Pinheiro AL (2010) Effect of LED phototherapy of three distinct wavelengths on fibroblasts on wound healing: a histological study in a rodent model. Photomed Laser Surg 28:547–552
13. Kato IT, Zezell DM, Mendes FM, Wetter NU (2010) Alterations in enamel remineralization in vitro induced by blue light. Laser Phys 20:1469–1474
14. Huang PJ, Huang YC, Su MF, Yang TY, Huang JR, Jiang CP (2007) In vitro observations on the influence of copper peptide aids for the LED photoirradiation of fibroblast collagen synthesis. Photomed Laser Surg 25:183–90
15. Oliveira CF, Basso FG, Lins EC, Kurachi C, Hebling J, Bagnato VS, de Souza Costa CA (2010) Increased viability of odontoblast-like cells subjected to low-level laser irradiation. Laser Phys 19:1–6
16. Vinck EM, Cagnie BJ, Cornelissen MJ, Declercq HA, Cambier DC (2003) Increased fibroblast proliferation induced by light emitting diode and low power laser irradiation. Lasers Med Sci 18:95–99
17. Whelan HT, Smits RL Jr, Buchman EV, Whelan NT, Turner SG, Margolis DA, Cevenini V, Stinson H, Ignatius R, Martin T, Cwiklinski J, Philippi AF, Graf WR, Hodgson B, Gould L, Kane M, Chen G, Caviness J (2001) Effects of NASA light-emitting diode irradiation on wound healing. J Clin Laser Med Surg 19:305–314
18. Weiss RA, McDaniel DH, Geronemus RG, Weiss MA, Beasley KL, Munavalli GM, Bellew SG (2005) Clinical experience with light-emitting diode (LED) photomodulation. Dermatol Surg 31:1199–11205
19. Kim HK, Kim JH, Abbas AA, Kim DO, Park SJ, Chung JY, Song EK, Yoon TR (2009) Red light of 647 nm enhances osteogenic differentiation in mesenchymal stem cells. Lasers Med Sci 24:214–22
20. Desmet KD, Paz DA, Corry JJ, Eells JT, Wong-Riley MTT, Henry MM, Buchmann EV, Connelly MP, Dovi JV, Liang HL, Henshel DS, Yeager RL, Millsap DS, Lim J, Gould LJ, Das R, Jett M, Hodgson BD, Margolis D, Whelan HT (2006) Clinical and experimental applications of NIR-LED photobiomodulation. Photomed Laser Surg 24:121–128
21. de Souza PP, Hebling J, Scalon MG, Aranha AM, Costa CA (2009) Effects of intrapulpal temperature change induced by visible light units on the metabolism of odontoblast-like cells. Am J Dent 22:151–156
22. Fogel HM, Marshall FJ, Pashley DH (1988) Effects of distance from the pulp and thickness on the hydraulic conductance of human radicular dentin. J Dent Res 67:1381–1385
23. Lanza CR, de Souza Costa CA, Furlan M, Alécio A, Hebling J (2009) Transdentinal diffusion and cytotoxicity of self-etching adhesive systems. Cell Biol Toxicol 25:533–543
24. Lessa FC, Nogueira I, Huck C, Hebling J, Costa CA (2010) Transdentinal cytotoxic effects of different concentrations of chlorhexidine gel applied on acid-conditioned dentin substrate. J Biomed Mater Res B Appl Biomater 92:40–47
25. Zijp JR, ten Bosch JJ (1993) Theoretical model for the scattering of light by dentin and comparison with measurements. Appl Opt 32:411–415
26. Vaarkamp J, ten Bosch JJ, Verdonschot EH (1995) Propagation of Light through human dental enamel and dentine. Caries Res 29:8–13
27. Zolotarev VM, Grisimov VN (2001) Architectonics and optical properties of dentin and dental enamel. Opt Spectrosc 90:753–759
28. Outhwaite WC, Mickenzie DM, Pashley DH (1974) A versatile split-chamber device for studying dentin permeability. J Dent Res 53:1503
29. Kienle A, Michels R, Hibst R (2006) Magnification–a new look at a long-known optical property of dentin. J Dent Res 85:955–959
30. Marijnissen JPA, Star WM (1987) Quantitative light dosimetry in vitro and in vivo. Lasers Med Sci 2:235–242
31. Perdigão J (2010) Dentin bonding-variables related to the clinical situation and the substrate treatment. Dent Mater 26:24–37
32. Peplow PV, Chung TY, Baxter GD (2010) Laser photobiomodulation of wound healing: a review of experimental studies in mouse and rat animal models. Photomed Laser Surg 28(3):291–325
33. Kelencz CA, Muñoz IS, Amorim CF, Nicolau RA (2010) Effect of low-power gallium-aluminum-arsenium noncoherent light (640 nm) on muscle activity: a clinical study. Photomed Laser Surg 28(5):647–52
34. Klebanov GI, Shuraeva NY, Chichuk TV, Osipov AN, Vladimirov YA (2006) Comparison of the effects of laser and light-emitting diodes on lipid peroxidation in rat wound exudate. Biofizika 51:332–339

Development of the micro-scanning optical system of yellow laser applied to the ophthalmologic area

Tiago A. Ortega[a,b], Alessandro D. Mota*[a], Glauco Z. Costal[a], Yuri C. Fontes[a], Giuliano Rossi[a]
Fatima M. M. Yasuoka[a,b], Mario A. Stefani[a], Jarbas C. de Castro N.[a,b]
[a]Opto Eletrônica S/A, 1071 Joaquim A. R. de Souza, São Carlos, SP, Brazil 13560-330;
[b]Instituto de Física de São Carlos, Universidade de São Paulo, 400 Trabalhador São Carlense, São Carlos, SP, Brazil 13560-970;

ABSTRACT

In this work, the development of a laser scanning system for ophthalmology with micrometric positioning precision is presented. It is a semi-automatic scanning system for retina photocoagulation and laser trabeculoplasty. The equipment is a solid state laser fully integrated to the slit lamp. An optical system is responsible for producing different laser spot sizes on the image plane and a pair of galvanometer mirrors generates the scanning patterns.

Keywords: self-Raman laser, solid state laser, laser scanning, photocoagulation, laser trabeculoplasty, retinal treatment

1. INTRODUCTION

Several ophthalmological surgeries are performed with visible and near infrared lasers systems. In the most protocols, the success is strongly related to the uniformity of the energy density over treatment area. The equipment developed in this work enables one to treat ocular diseases with a micro-positioned laser scanning system. The electro-optic scanning control enables the production of patterns – treatment masks – suitable to a vast set of the surgical protocols.

1.1 Retinal photocoagulation

Retinal diseases such as retinal detachment, diabetic retinopathy, retinal tears, retinal hemorrhage, vein occlusion, macular edema, etc, are often treated with laser-based ophthalmic equipment called photocoagulators. The standard method for delivering laser radiation to the patient's retina is via Slit Lamp Adapter (SLA). The SLA is an optical system which projects a single laser spot of hundreds of microns in diameter on the patient's eye. The spot position is mechanically adjusted by the physician's hand. Nevertheless, a regular retinal photocoagulation consists of several hundred of pulses[1] and a pan-retinal photocoagulation procedure usually consists of approximately 1500 to 2000 spots of laser per eye. Such procedure takes hours to be performed and is often divided in two or more sessions. Figure 1 shows a typical retina after photocoagulation procedure.

1.2 Laser Trabeculoplasty

Laser Trabeculoplasty (LT) is defined as the laser treatment to the trabecular meshwork (TM) to enhance outflow of aqueous humor from the eye[2]. It is a safe and effective technique for lowering intraocular pressure (IOP) in primary open angle glaucoma, pigmentary glaucoma, and pseudoexfoliation glaucoma. LT is generally performed treating a 180º portion of the TM with 50 parts equally spaced, that is, 50μm diameter lasers spots. In some patients, the treatment is repeated on the remaining 180º portion of the eye.

1.3 Treatment masks

The elevated number of spots associated to the manual positioning of each individual spot on the patient's eye are factors that consume extremely the time in ophthalmological laser surgeries. Furthermore, precise spacing between adjacent

Laser Beam Shaping XIII, edited by Andrew Forbes, Todd E. Lizotte, Proc. of SPIE Vol. 8490, 84900M

spots is required in most procedures. A system producing high quality laser spot patterns with micrometric precision is hence ideal for application in retinal photocoagulation and glaucoma therapies.

These patterns are composed by several laser spots forming typical figures called treatment masks. Useful masks for retinal photocoagulation are depicted in Figure 2.

An optical system can produce treatment masks with the aid of high speed galvanometer scanning mirrors. A refined electronic control is mandatory to guarantee laser positioning and power stability.

*alessandro@opto.com.br ; phone 55 16 2106-7078 ; fax 55 16 2106-7001; www.opto.com.br

Figure 1. Retinal photocoagulation.

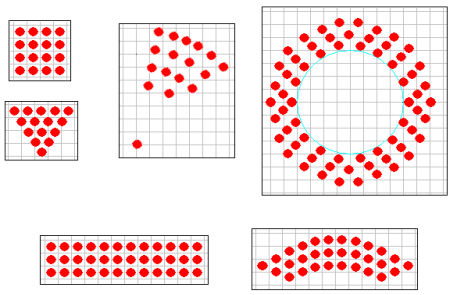

Figure 2. Representation of the treatment masks.

2. EXPERIMENTAL ARRANGEMENT

2.1 Overview

A micro-scanning optical system was projected as in Figure 3. A fiber coupled in Diode Pumped Solid State Laser (DPSSL) is the optical system input. Fiber radiation output is first collimated and passes through a pair of galvanometer scanning mirrors, responsible for producing the treatment masks. Collimated light is then directed to a variable magnification system, which is an afocal optical system responsible for the different spot sizes in the focal plane. The

magnified laser beam is folded by a beam splitter. Finally, the objective focuses laser radiation on the focal plane. It is important to note that the physician uses contact lenses to translate the focal plane to the retina or TM. The objective is shared with the slit lamp (the ophthalmic instrument to visualize ocular main structures) simplified in Figure 3 by an eyepiece and objective.

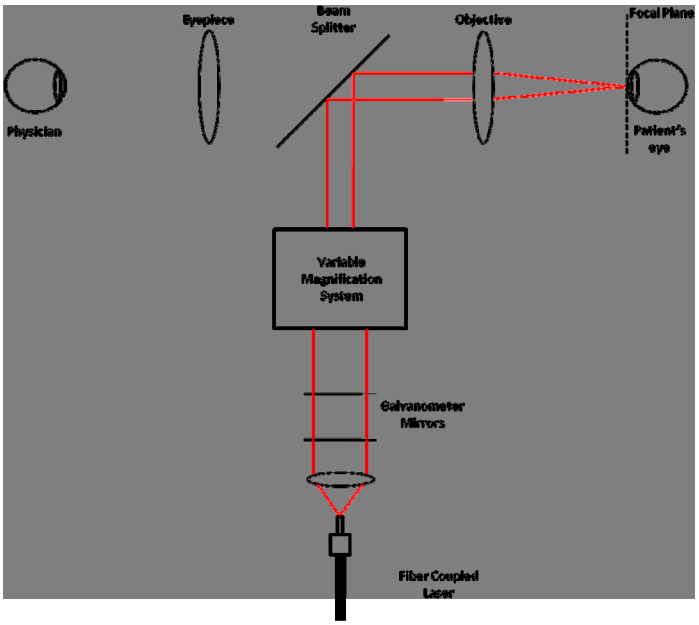

Figure 3. Micro-scanning optical system overview.

2.2 Laser cavity

A diode pumped, self-Raman intracavity doubled solid state laser operating in 586,5nm is utilized in this system[3]. Laser cavity specifications are summarized in Table 1. Figure 4 depicts the yellow laser cavity.

Table 1. Yellow laser cavity specifications.

Parameter	Specification
Wavelenghth	586,5nm
Output power	2W
Optical fiber core diameter	50μm
Aim beam wavelength	635±20nm
Aim beam power	<1mW

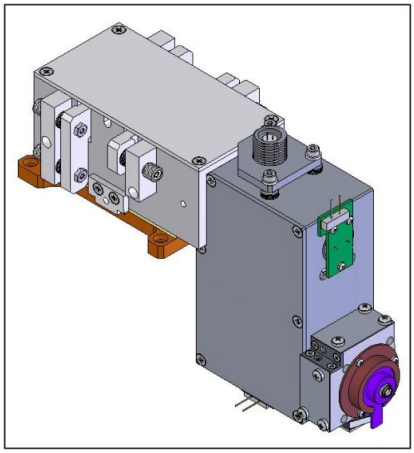

Figure 4. Yellow laser cavity solid model.

Laser cavities operating in different wavelengths may also be used in this system provided that it is coupled to the same optical fiber.

2.3 Optical system

The projected optical system is composed by three subsystems highlighted in Figure 5. Optical system layout for one possible configuration is depicted in Figure 6:

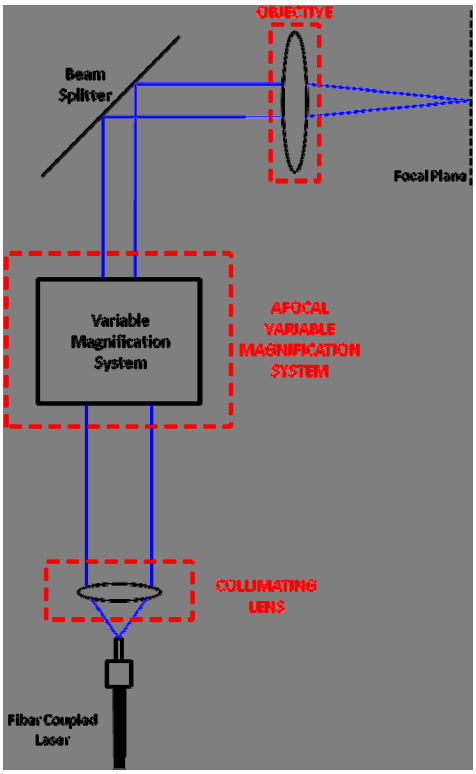

Figure 5. Optical subsystems.

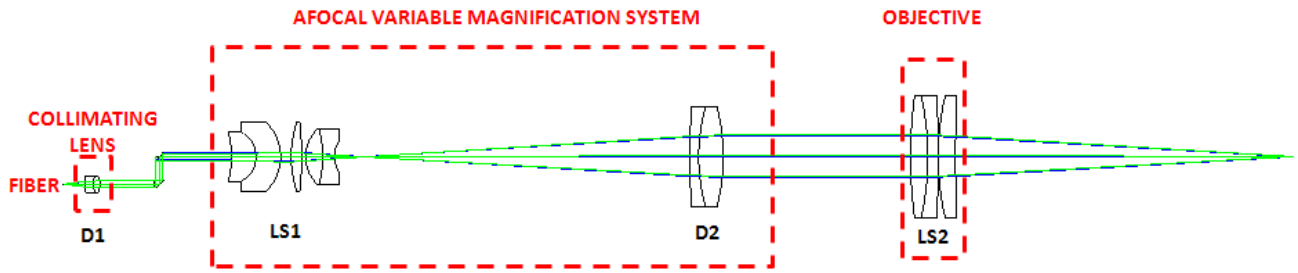

Figure 6. Optical system layout for 2X magnification.

Doublet D1 is responsible for collimating the output of a 50µm core optical fiber. The collimated radiation enters an afocal variable magnification system, composed by a lens system LS1 and doublet D2. Different magnifications are achieved exchanging LS1. Magnified radiation is then directed to the objective and focused on the focal plane. Table 2 shows the permitted magnifications and the resulting spot size diameter on image plane.

Table 2. Optical system magnification and resulting spot size diameter.

Magnifications	Spot size diameter (µm)
1X	50
2X	100
3X	200
4X	300
5X	400

The five different spot sizes produced by the optical system are validated in ophthalmic clinical protocols.

2.4 Electronic control

Electronic control main functions are laser cavity control and automatic laser spot micro-positioning. A block diagram of the electronics is represented in Figure 7. The 32bit microcontroller executes mathematic routines for galvanometer mirrors positioning and software PID control loop[4]. Moreover, it constantly monitors several electric parameters for safety maintenance, performs display am memory communication, etc.

Hardware analog signal interface is converted by analogic-digital(AD) or digital-analog (DA) converters. User interface is performed by the touchscreen display, encoders and pedal.

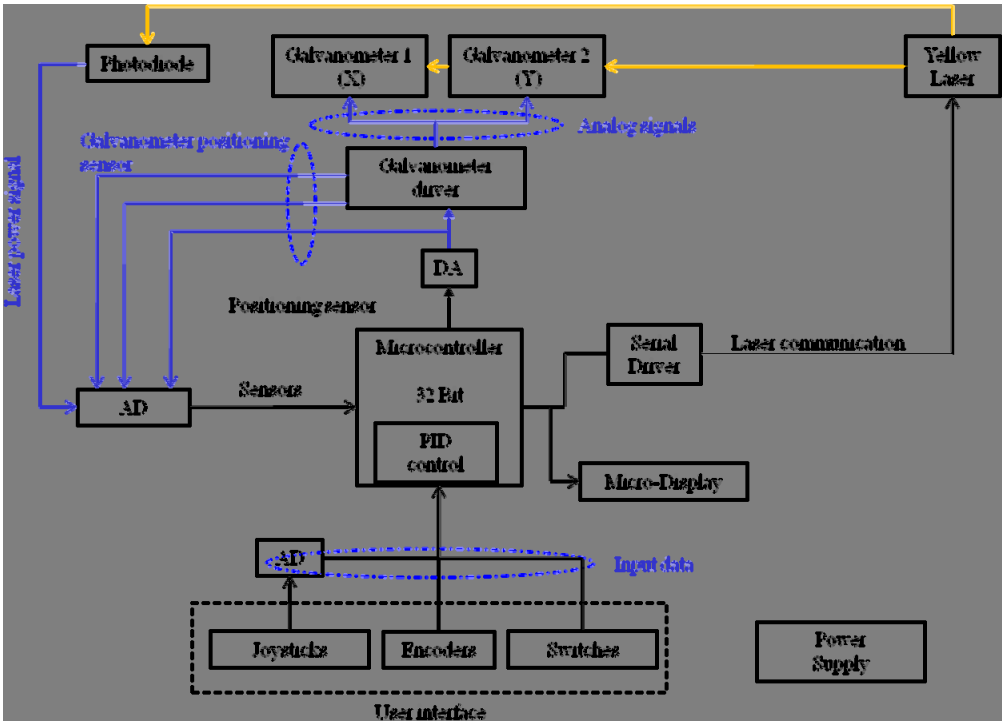

Figure 7. Electronic control block diagram.

The galvanometer scanning mirrors automatically translates laser spot on image plane according to the selected pattern. Mirror position is constantly read, and during the galvo movement laser is always turned off. It is only switched on when mirrors are on the exact position of each spot composing the pattern.

Galvanometer mirrors scanning covers a 7x7mm^2 area with 1.7µm precision. Scanning speed is on the order of 20mm/ms.

3. RESULTS

A photograph of the system is shown in Figure 8. As can be seen, the opto-mechanical and electronic system are fully integrated to the laser cavity and slit lamp. Software main screen is shown in Figure 9 with selectable treatment masks highlighted on the bottom.

Figure 8. Micro-scanning optical system setup.

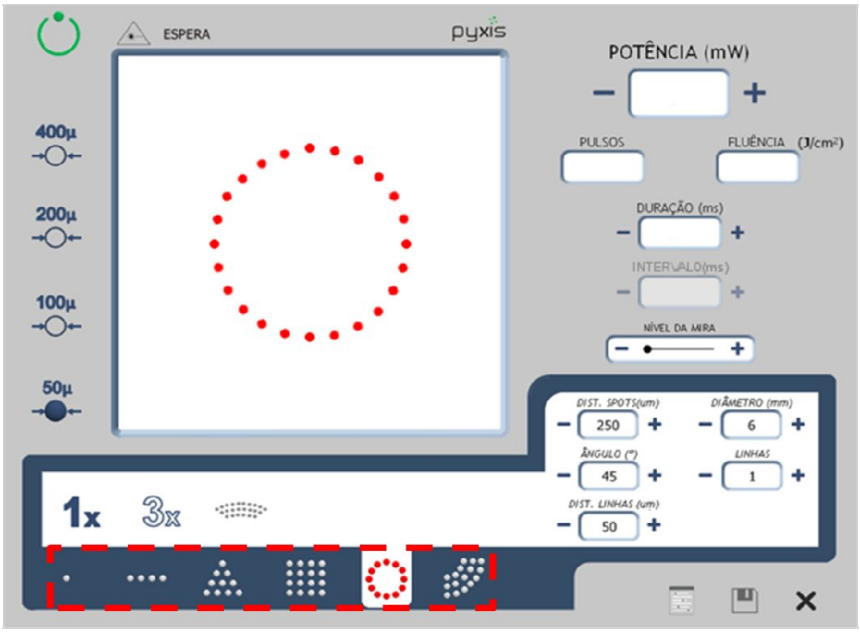

Figure 9. Software main screen.

Laser spot sizes were measured with a beam profiler (Gentec EO Beamage Focus) as shown in Figure 10. Table 3 exhibits the nominal and measured spot sizes.

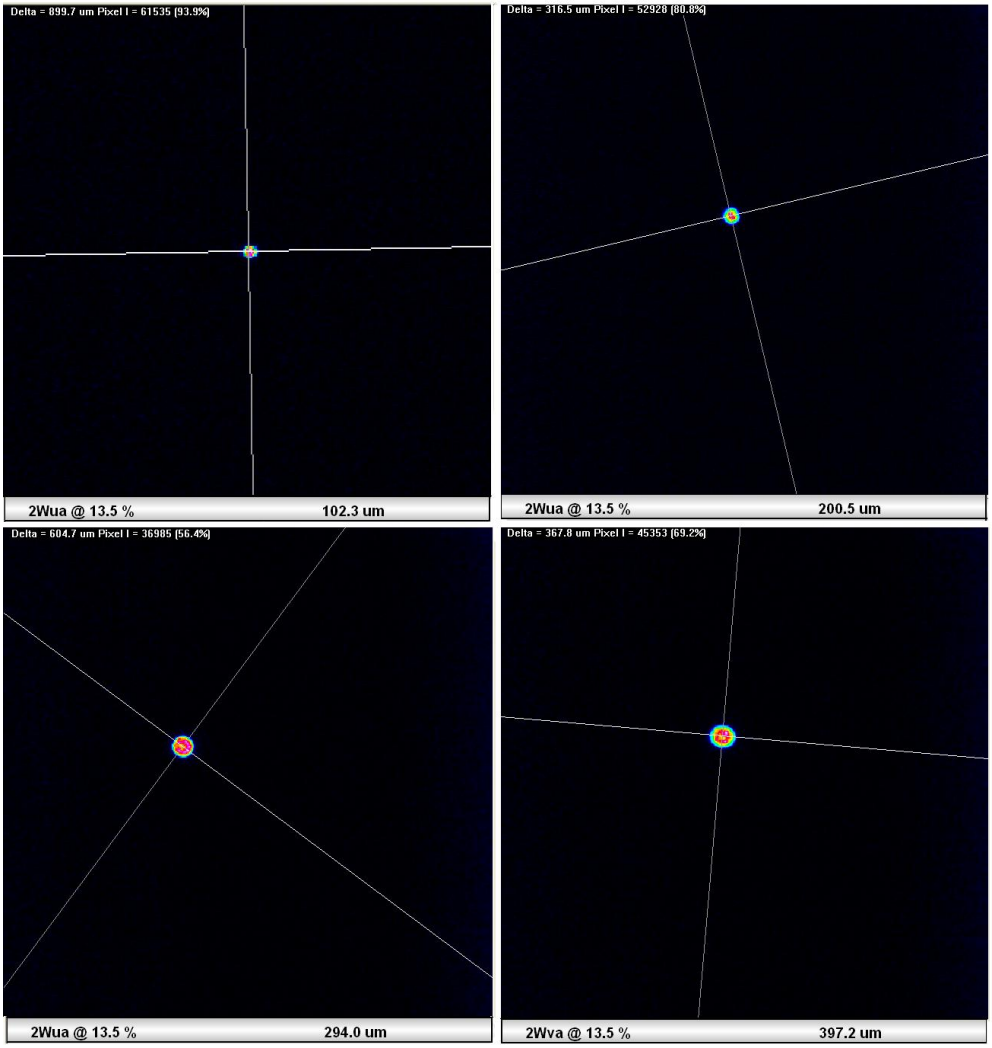

Figure 10. Spot size measurement.

Table 3. Nominal and measured spot size diameter.

Nominal spot size diameter (µm)	**Measured spot size diameter (µm)**	**Error (%)**
100	102.3	2.30
200	200.5	0.25
300	294.0	2.00
400	397.2	0.70

The beam profiler pixels are 10.5x10.5µm and minimum recommended measurable spot is 105µm. For this reason the 50µm spot was not measured. It also explains the greater error on the 100µm spot measurement.

Treatment mask were produced by the system with the aim beam for the 200μm as depicted in Figure 11. Laser was shot at 1000mW and 10ms pulse duration on each spot. The corresponding marks are shown in Figure 12. Laser cavity was adjusted to 2000mW and 1574mW was measured after the objective with a laser power meter.

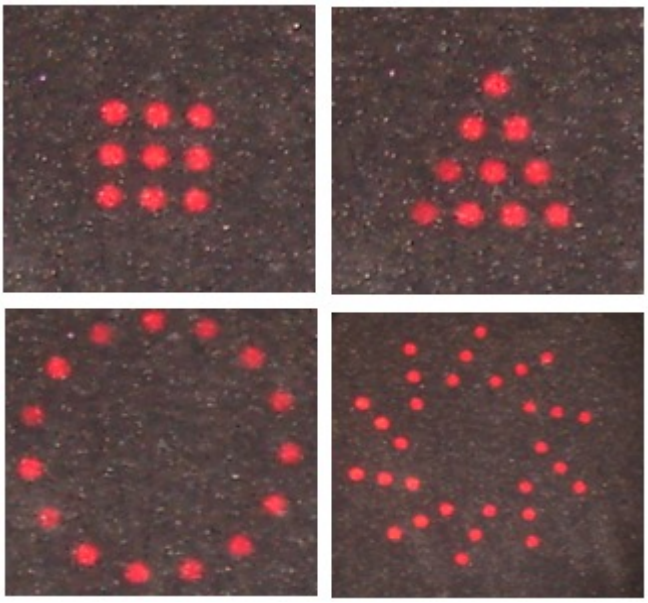

Figure 11. Treatment masks

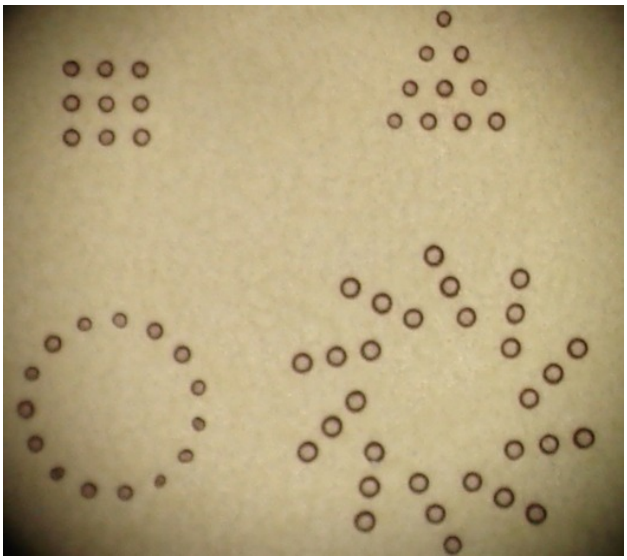

Figure 12. Laser marks

A cover for the system was designed. A photograph of the completed equipment is shown in Figure 13.

Figure13. Opto Eletrônica's Pyxis iPattern Laser

4. CONCLUSION

In conclusion we have successfully produced a micro-scanning optical system for fiber coupled lasers. The optical system produced the nominal spot sizes within a 2.30% and 0.25% error in worst and best cases, respectively. Treatment maks were produced and visualized by the aim beam laser. Treatment laser activation enabled the production of laser marks in accordance to the desired patterns. More than 1500mW laser power was measured in the focal plane. There is some potential to engineer the optics and thin film coatings to improve fiber to focal plane power efficiency.

Nevertheless we have clearly demonstrated a scanning optical system that meets our specifications for ophthalmic equipment. In April 2011, the Opto Eletrônica company exhibited to the Brazilian market the Pyxis iPattern Laser, the first laser based on scanning system for ophthalmological produced in Latin America.

5. ACKNOWLEDGEMENT

The authors thank to Opto Eletrônica company and mainly to FAPESP for the financial support for this project.

REFERENCES

1. Karlin, D., B., [Lasers in Ophthalmologic Surgery], Blackwell, USA, 22-25 (1995)
2. Yanoff, M., Duker,J. S., [Ophthalmology], Mosby, 1227 (2004)
3. T. A. Ortega, "Very compact and high-power CW self-Raman laser for ophthalmological applications",SPIE Photonics West, 2010. Proc. SPIE Vol. 7578 757822-1. San Francisco, USA.
4. Sedra A. S.; Smith, K. C. **Microeletrônica**. 5. Ed. Pearson Prentice-Hall. 2007

Influence of effective number of pulses on the morphological structure of teeth and bovine femur after femtosecond laser ablation

Gustavo Nicolodelli, Rosane de Fátima Zanirato Lizarelli, and Vanderlei Salvador Bagnato
University of São Paulo, Physics Institute of São Carlos, São Carlos, Instituto de Física de São Carlos, USP/Grupo de Óptica, Av. Trabalhador Sancarlense, 400; Caixa Postal: 369 São Carlos, CEP: 13560-970, SP, Brazil

Abstract. Femtosecond lasers have been widely used in laser surgery as an instrument for contact-free tissue removal of hard dental, restorative materials, and osseous tissues, complementing conventional drilling or cutting tools. In order to obtain a laser system that provides an ablation efficiency comparable to mechanical instruments, the laser pulse rate must be maximal without causing thermal damage. The aim of this study was to compare the different morphological characteristics of the hard tissue after exposure to lasers operating in the femtosecond pulse regime. Two different kinds of samples were irradiated: dentin from human extracted teeth and bovine femur samples. Different procedures were applied, while paying special care to preserving the structures. The incubation factor S was calculated to be 0.788 ± 0.004 for the bovine femur bone. These results indicate that the incubation effect is still substantial during the femtosecond laser ablation of hard tissues. The plasma-induced ablation has reduced side effects, i.e., we observe less thermal and mechanical damage when using a superficial femtosecond laser irradiation close to the threshold conditions. In the femtosecond regime, the morphology characteristics of the cavity were strongly influenced by the change of the effective number of pulses. [DOI: 10.1117/1.JBO.17.4.048001]

Keywords: ablation; femtosecond lasers; dentin; bones.

Paper 11423 received Aug. 3, 2011; revised manuscript received Jan. 18, 2012; accepted for publication Jan. 30, 2012; published online Mar. 19, 2012; corrected Mar. 27, 2012.

1 Introduction

Femtosecond lasers have been used widely in laser surgery for contact-free tissue removal. Targets as hard dental,[1,2] restorative materials,[3,4] and bone tissues[5,6] have been studied with lasers in order to complement conventional drilling or cutting tools.

Use of ultrafast laser pulses to modify, sculpture, and remove various materials has recently made a breakthrough.[7] Different lasers have been evaluated for the removal and preparation of hard dental tissues and bones, and some of these are already in clinical use.[8–10] Among the possible applications of femtosecond laser systems, their ability to cut bone in surgical applications without vibration and thermal damage presents numerous advantages over the use of other mechanical instruments. As the mechanical vibration can reduce surgical precision,[6] and the rotational trajectories on the tissue can lead to collateral damage,[5,11] and, in fact, as the most important feature of conservative surgery is high precision, this is something an ultrafast laser can offer. Still, it is heavily debated whether the laser can replace mechanical instruments for many other applications working with hard tissues.[12] One of the biggest limitations is the slow rate of material removal, and then, in many cases, the usually unacceptable collateral damage, which is caused by overheating.

In order to obtain a laser system that has an ablation efficiency comparable to mechanical instruments, the laser pulse rate must be maximal without causing thermal damage. If the repetition rate is very high, the incoming pulses may interact with the plasma, which is highly absorbing, and lead to heat generation in the sample. Additionally, the presence of plume ejected from the target may also hinder incoming pulses from reaching the target and thereby reduce the ablation efficiency. Thus the optimal laser system should have a repetition rate fast enough to maximize tissue removal, while allowing enough time for the plasma and plume to dissipate.[6]

High power densities (intensity or irradiance) could promote induced ablation by plasma, resulting in more precise and well-defined cavity edges. Certainly, ultrashort pulses have been identified as an alternative, and several indications to use femtosecond pulse ablation are under investigation.[2–5] The advantages of femtosecond microsurgery lasers, including the high structural precision and a small thermally affected area may be more effectively obtained during a microdrilling close to the ablation threshold conditions, i.e., using a minimal fluence necessary for material ablation.[13] The laser ablation in the femtosecond regime also has advantages regarding chemical attacks, such as the removal of calcium ion, trainers, which play an important role to keep the cariogenic resistance within those oral cavity tissues.[14]

Femtosecond lasers can be used to reduce thermal influence due to a lower heat present when compared to lasers with long pulses. A lower heat is present because, when using femtosecond lasers, the fluence needed for achieving micropores is magnitudes smaller than when using ns lasers for the same repetition rate and wavelength. The noncreation of microcracks for short

Address all correspondence to: Gustavo Nicolodelli, USP, Physics Institute of São Carlos, São Carlos, Instituto de Física de São Carlos, USP/Grupo de Óptica, Av. Trabalhador Sancarlense, 400; Caixa Postal: 369 São Carlos, CEP: 13560-970, SP, Brasil. Tel: 55 16 3373-9810; Fax: 55 16 3373-9811; E-mail: nicolodelli@ursa.ifsc.usp.br

0091-3286/2012/$25.00 © 2012 SPIE

pulses is of great importance in dentistry because microcracks would weaken the tissue and increase external permeability, therefore resulting in new tooth decay.[13]

A comparative study of the different morphological characteristics of the hard tissue after exposure to the lasers operating in the femtosecond pulse regime was done. The study aims at removing the superficial tissues and making sure to preserve the structure of the sample at the same time. The preservation of the remaining tissue may be important for various surgical applications including implants. The threshold condition for femtosecond laser pulses to ablate bovine femur was also determined in this paper.

2 Materials and Methods

A Ti: Sapphire femtosecond (Libra-S, Coherent, Palo Alto, CA, USA) laser was used in this study emitting pulses of approximately 70 fs, the emission being centered at a wavelength of 801 nm and operating at a pulse repetition rate of 10 to 1000 Hz or in the single shot mode. The pulse duration of 70 fs was measured using a second-order autocorrelator (Coherent, SSA™).

In this study, two different kinds of samples were irradiated: dentin from human extracted teeth and bovine femur cortical pieces. These pieces were polished to obtain a smooth and level surface.

We used fresh bovine femur and six human teeth (third molar) newly extracted following an orthodontic indication. The bovine bone was cut into six pieces of 10 mm × 5 mm × 2 mm. The teeth were cut into two parts, excluding the root part and keeping the crown part. All tissues were included in a polyester resin so that the surface of all could be positioned strictly perpendicular to the laser beam. The samples were polished in a politriz machine, using sandpaper water increasing the grain (up to 600 grit). The teeth were polished until the dentin was exposed.

The samples were positioned on a sample stage with $x - y - z$ axis. Using highly reflective coated dielectric mirrors, the beam was passed through a 200-mm focal length lens before reaching the target sample.

The samples were irradiated using different energy levels per pulse (EPP) <1 mJ and different operation modes, with the single shot mode or with a repetition rate between 10 and 1000 Hz. Irradiation times were controlled by a mechanical shutter. The laser system was operated without an additional cooling system.

After each irradiation, the samples were prepared following a defined routine and then transferred to the scanning electron microscope (SEM) to evaluate the morphological variations of the irradiated hard materials and to measure the diameters of the ablation craters.

3 Results and Discussion

Hard tissues were used to determine conditions of the ablation threshold,[13] using both simple and multiple pulses for different laser fluences. In order to determine precisely the threshold of the modified structure, the laser beam diameter on the surface of the target and the energy of the laser pulse must be known. For a Gaussian laser beam, the spatial variation of the fluence of the laser can be represented by:[14]

$$F(r) = F_0 \exp\left(\frac{-2r^2}{w_0^2}\right) \quad F_0 = \frac{2E_p}{\pi w_0^2}, \tag{1}$$

where r is the distance from the beam center, w_0 is the beam waist, i.e., the radius of the laser spot on the target surface at $1/e^2$ of the peak fluence F_0, and E_p is the incident laser pulse energy. When the threshold of the laser fluence is denoted by Fth, the radius (r_a) or diameter ($D = 2r_a$) of the cavity ablation can be written in terms of peak fluence as in Ref. 15:

$$D^2 = 2w_0^2 \ln\left(\frac{F_0}{F_{\text{th}}}\right). \tag{2}$$

To apply Eq. (2) to determine the radius of the spot radius w_0, precise measurements of the diameter are necessary, especially when we consider the typical asymmetry of cavities. For these measurements, the shape of the cavities was almost circular, as seen in the SEM image, although the actual cavities are not perfectly circular.

Figure 1 shows the results of the measurements of the diameter of the cavity squared, as a function of the laser fluence peak on a semi-logarithmic scale, for the bovine femur. This chart allows calculating the radius of the laser beam, based on a graph obtained

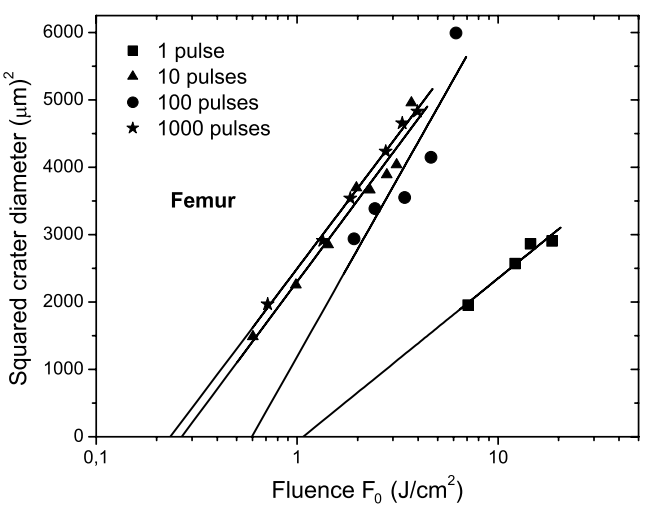

Fig. 1 Graphs of the diameter squared cavities versus fluence, when the bone was irradiated with the femtosecond laser with: $N = 1000$ pulses, $N = 100$, $N = 10$, and $N = 1$ pulses per second.

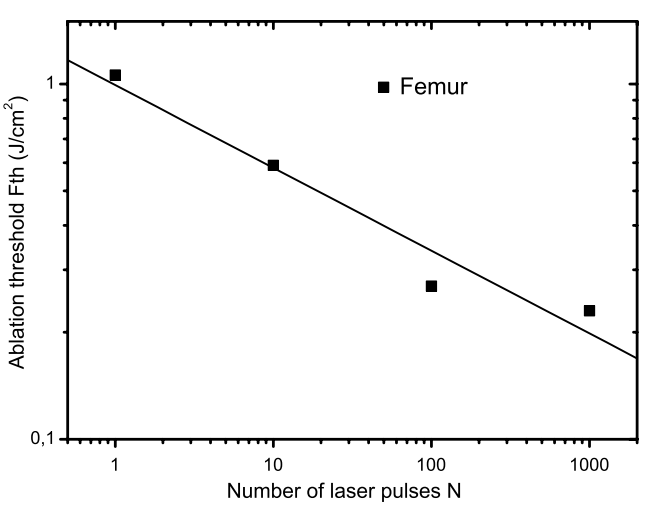

Fig. 2 Threshold graph, fluence versus number of pulses for bone tissue.

by fitting the experimental data. The radius of the laser spot was estimated to be 45 ± 1 μm and 44 ± 1.6 μm for samples irradiated with 1000 to 100 pulses, respectively. For the effective number of pulses $N = 10$ pulses and single pulse, the spot radius was estimated to be 51 ± 5.9 μm and 35 ± 2.6 μm, respectively. As it is difficult to judge the diameter for a few short pulses, due to their structures being much less pronounced and highly influenced by statistical processes, therefore the laser spot size changes for the different measurements with different effective number of pulses.

From the lines in Fig. 1, the fluence ablation threshold (Fth) was determined by locating the value of fluence where the fitted line crosses the x-axis for 1, 10, 100, and 1000 pulses; the threshold values obtained were 1.06, 0.59, 0.27, and 0.23 J/cm^2, respectively. This method to determine the ablation threshold is usually used for other materials, e.g. ceramic dielectrics[16,17] and hard dental tissue.[7] There are also other geometric methods used to determine the damage threshold due to ablation.[18] One of these methods consists in the formation of a superficial damage profile for a sample motion across the laser focus. A simple measurement of the maximal cross-sectional dimension of the damage profile, which depends only on the power of the laser beam, is used to compute the local intensity threshold. Girard et al. determined the ablation threshold for bone tissues to be 0.69 J/cm^2 through direct analysis of the SEM images.[5] The value found by Girard et al. was higher than the one we found in this study (0.23 J/cm^2), although both studies were performed working with a repetition rate of 1 kHz, but Girard et al. were using a pulse width of 200 fs. Since a longer pulse duration has been used, the ablation threshold is increased because the maximum intensity is reduced for similar fluences, and less electrons are generated from multiphoton processes.[5,19]

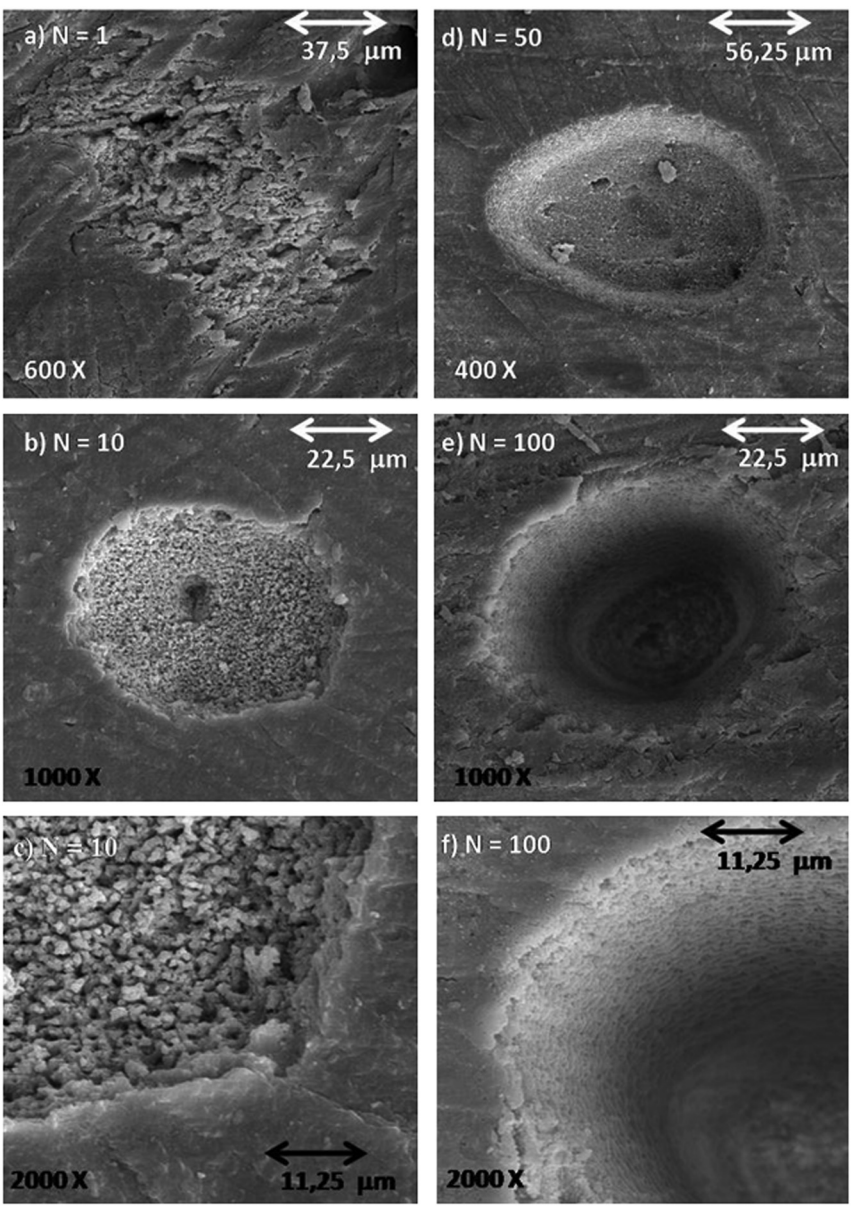

Fig. 3 SEM microimages of bovine femur irradiated with a femtosecond laser in the focused mode: (a) pulse energy Epp = 0.41 mJ, pulse number $N = 1$; (b) Epp = 0.1 mJ, $N = 10$ and detailed in (c); (d) Epp = 0.085 mJ, $N = 50$; (e) Epp = 0.06 mJ, $N = 100$ and detailed in (f). Morphological variations of the femur bone were obtained.

One of the effects of incubation for bovine femur investigated was to study the reduction of the fluence ablation threshold when we increased the number of pulses.[16] Ablation was observed in these tissues and shown in Fig. 2, where the threshold decreases continuously when the number N of pulses is increased from 1 to 10, 100 or 1000. This reduced threshold during accumulative ablation (Fth, N) can be represented by:[14,16,17]

$$F_{th,N=}F_{th,1}N^{S-1}, \tag{3}$$

where the exponent S characterizes the material's response to cumulative ablation, based on the following conditions: (1) for $S < 1$, where the incubation effect exists; (2) for $S = 1$, where the fluence at the threshold conditions is independent of the number of pulses; and (3) for $S > 1$, where the material becomes stronger during cumulative ablation,[16] i.e., the ablation efficiency decreases.

From Eq. (3), the incubation factor was calculated to be $S = 0.788 \pm 0.004$ for the bovine femur. This result shows that the effect of incubation is also substantial during ablation of the bone using the femtosecond laser. Incubation effects can become significant and may change the structure of the tissue during the process. These effects can result in a lowered ablation threshold for subsequent pulses, thereby changing the overall ablation dynamics. Depending on the geometry of the ablation region and of the laser system operation (for example, repetition rate and exposure time), multipulse exposure may also cause beam distortion and shadowing effects as well as light scattering due to residual debris.

In Fig. 3 we show SEM microimages of the bone tissue irradiated with a femtosecond laser, with a varying effective number of pulses of the laser.

From Fig. 3 we see that it was sufficient to use only one femtosecond pulse [Fig. 3(a)] with a fluence of 1 J/cm^2 in order to modify the surface of the tissue. Using an effective number of pulses $N = 10$ pulses, we obtained morphological variations of the tissue [see Fig. 3(b)], and details are also shown in Fig. 3(c). From these images we noticed that cavitation occurs, where the edges of the cavity are relatively well-defined boundaries with small exfoliations, when compared to $N = 1$. After a more thorough analysis, we see that an exposure of bone trabeculae [see Fig. 3(c)] takes place, and no evidence of heat damage, i.e., carbonization is visible. This is an important feature, because if we get an only superficial [see Fig. 3(c)] ablation, we can increase the capacity of the cell adhesion to facilitate integration of the bone; for example, in the case of bone implants. When we apply 50 pulses (1 s, 50 Hz) to the tissue, [see Fig. 3(d)] we see that, despite the beam profile not being perfectly round, the cavity does not show signs of charring or redeposition of material on its surface or its inner walls. The same occurs for $N = 100$ pulses (1 s, 100 Hz) [Figs. 3(e) and 3(f)], without effect of a thermal (carbonization) or mechanical damage, with well-defined borders, and the internal walls were preserved [see Fig. 3(f)].

As we used the laser as a surgical tool, we know that it has been suggested to work with higher repetition rates in order to obtain a higher pulse ablation rate. In Fig. 4 we present SEM microimages of the femur bovine tissue irradiated with a femtosecond laser in the focused mode using $N = 1000$ pulses (1 s, 1 kHz).

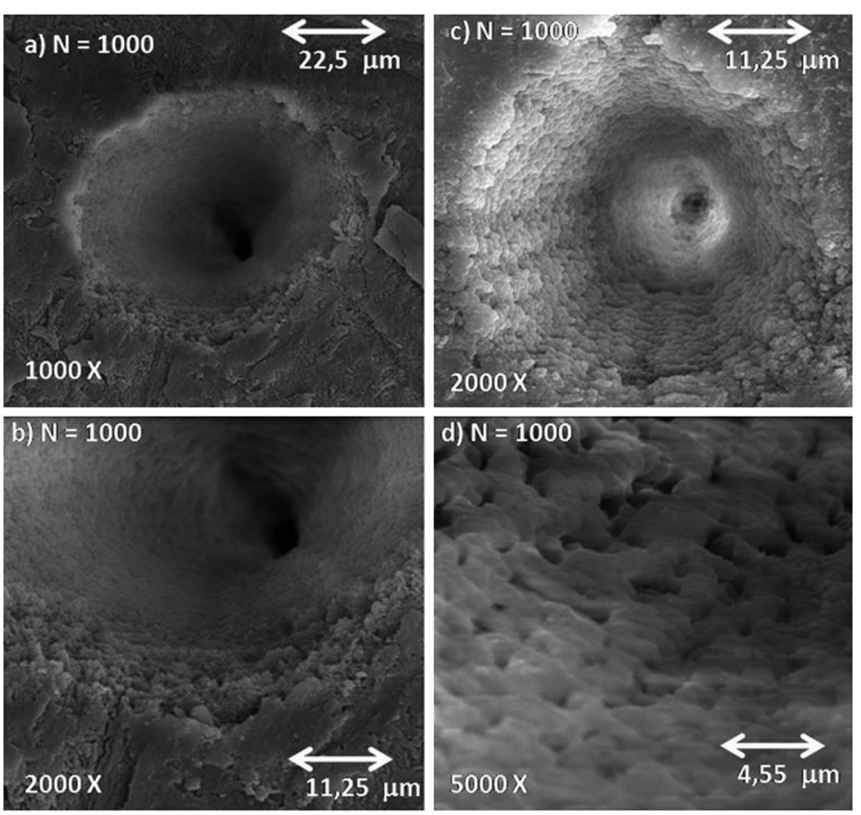

Fig. 4 SEM microimages of bovine femur irradiated with a femtosecond laser in the focused mode: (a) Epp = 0.178 mJ, $N = 1000$, and detailed in (b); (c) Epp = 0.120 mJ, $N = 1000$ and detailed in (d). Morphological preservation of the femur bone was obtained.

For an energy pulse of 0.178 mJ and a pulse number of 1000 pulses [see Fig. 4(b)], we found that the cavity still shows well-defined borders and no redeposition of material as had occurred when applying the other effective number of pulses (see Fig. 3). From Figs. 3 and 4, it is obvious that the ablated volume grew when the effective number of pulses was increased, but this information was not quantified here. Moreover, despite the higher effective number of pulses ($N = 1000$), no heat affected zones emerged and no mechanical damage, e.g. cracks, were seen. The effective number of pulses was increased, for example, from 100 to 1000 pulses, but the ablated morphological cavity did not change much because the time between the pulses continued to be quite long. The mechanisms responsible for the laser ablation were the same. The same can be observed in Fig. 4(c) and in more details in Fig. 4(d): when we vary the fluence of the laser, the internal walls of the cavity show small regions with signs of melting, which in turn may help insulating the tissue. This phenomenon is interesting because, in order to get a precise ablation based on a nonlinear absorption (plasma-mediated ablation), low pulse energies must be used to minimize the mechanical shearing effects.[20] When multiple pulses are delivered to one single position, the degree of thermal damage can be influenced by heat accumulation. The effective number of pulses per second should be low enough to avoid the progressive accumulation of residual heat within the tissue. An alternative strategy to avoid the accumulation of heat in a hard tissue involves a scanning laser beam in order to extend the time intervals between the subsequent expositions of each location of the ablated area.[6] For bone-processing, other systems are also under evaluation, e.g. excimer lasers, which feature a high UV absorption of electronic transitions of almost all molecules. These excimer lasers have shown a very accurate cutting, but generated zones of thermal damage of approximately 50 μm.[21,22] CO_2 lasers (wavelength 10.8 μm),

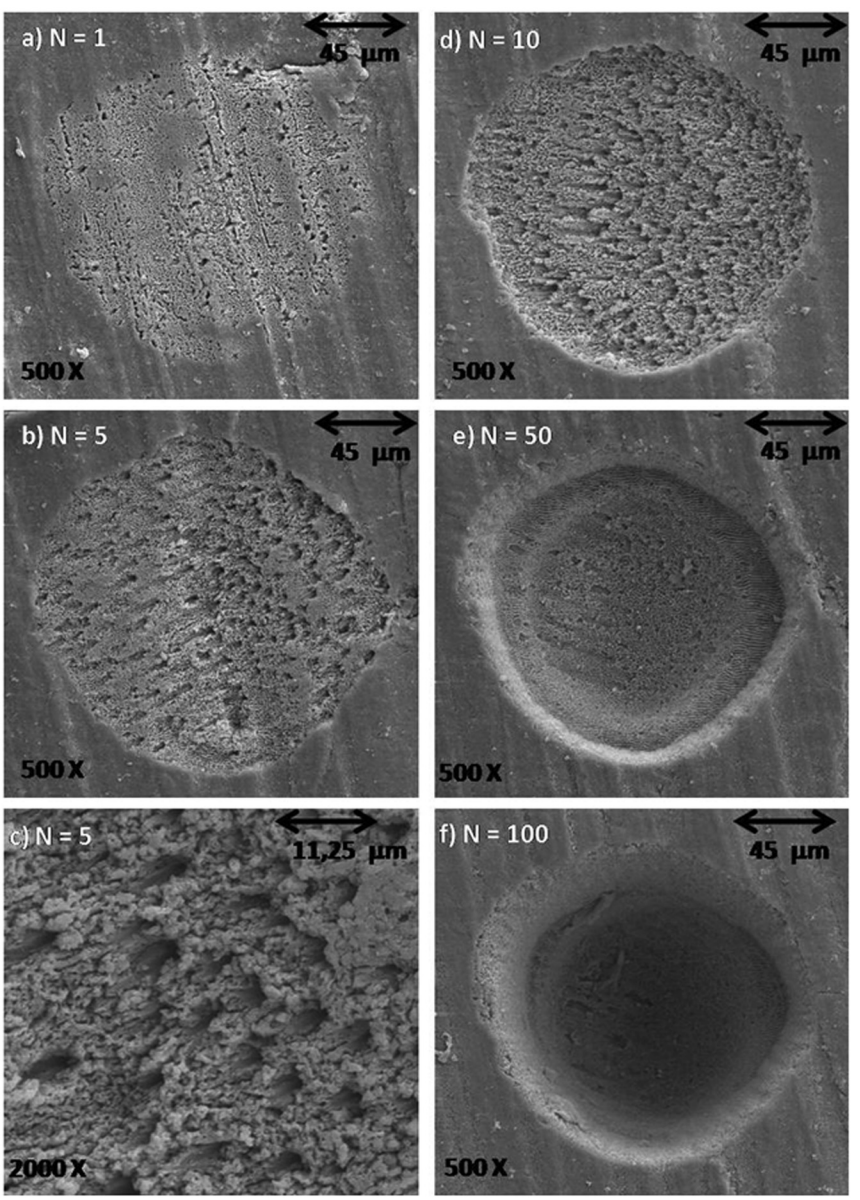

Fig. 5 Microimages obtained by SEM of human dentin irradiated with a femtosecond laser in the focused mode: (a) Epp = 0.6 mJ, $N = 1$; (b) Epp = 0.6 mJ, $N = 5$) and (c) in detail; (d) Epp = 0.6 mJ, $N = 10$; (e) Epp = 0.6 mJ, $N = 50$; (f) Epp = 0.6 mJ, $N = 100$. Morphological variations of the human dentin were obtained.

aiming at the mineral component of the tissue successfully removed the tissue but may generate carbonization.[23,24] A Er:YAG laser (wavelength 2.94 μm) with a strong water absorption became popular in the past years for applications in orthopaedical, maxilofacial, and dental surgeries and for possible use in periodontal surgery.[23,25,26] Carbonizations were also observed using Nd:YAG lasers,[12,26,27] unlike what happened in our study using a femtosecond laser.

In Fig. 5 we present micrographs obtained by SEM of human dentin irradiated with a femtosecond laser system, with the laser operating with different effective number of pulses.

In Fig. 5 we see that using only one femtosecond pulse [see Fig. 5(a)] with a high pulse energy (0.6 mJ) was sufficient to modify the surface of the tissue. After applying five pulses in a range of 1 s per pulse, we evaluate the morphological variations of the tissue [see Fig. 5(b)] and in more detail in Fig. 5(c). From these images we can see that a tissue cavitation occurs, where the edges of the cavity show well-defined boundaries. After a more thorough analysis, we see that the tubules are preserved, an evidence of nonthermal damage on the ablated surface. However, in some regions the tubules were not exposed because there must have been a redeposition of material, due to insufficient energy to eject the material. The phenomena of exposition of these tubules are interesting, as it can be applied in dentistry, e.g. it could help increase the penetrability of adhesive systems used in restoration. For $N = 10$ pulses (1 s, 10 Hz), the tubules are also exposed and preserve a healthy tissue (see Fig. 5). When we apply 50 pulses to the tissue, the cavity does not show signs of charring or redeposition of material on its surface or its inner walls. The same occurs for $N = 100$ pulses (1 s, 100 Hz) [see Fig. 5(f)] without any presence of thermal (carbonization) or mechanical damage, with well-defined borders and while preserving the internal walls. Similar results were found by Korte et al.[13] during laser ablation of dental tissue in the femtosecond regime. For lasers operating in a nanosecond (ns) pulse regime, dental tissue-ablation is less efficient and can be accompanied by collateral damage in the tissue, i.e., mechanical stress and fractures.[26] For laser ablation in picoseconds (ps), the destruction of the surrounding material is minimized due to the formation of plasma during the ablation process.[12] However, for both schemes (ns and ps) we still found evidence of thermal adjacent tissue damage.[12,25]

4 Conclusion

Characteristics of laser ablation on biological hard tissues, morphology, selective, and controlled ablation, all of these were addressed in this paper. We determined the conditions of the ablation threshold of bone tissues for different regimes of laser operation. A morphological comparison between the different regimes of operation has been investigated, and special care was taken to preserve the structures. The incubation factor S was calculated to be 0.788 for bovine femur bone; these results indicate that the incubation effect is also substantial during the femtosecond laser ablation of hard tissues. The induced-plasma ablation has reduced side effects, e.g. less thermal and mechanical damage, using a superficial femtosecond laser irradiation near threshold conditions. In the femtosecond regime, the morphological characteristics of the cavity were strongly influenced by a change of the effective number of pulses. But even for the highest effective number of pulses and high fluence, we do not see the secondary effect of thermal and mechanical damage in the cavities of hard tissues. Furthermore, in cases of surface treatment, a femtosecond laser proved to be an appropriate tool to process ultraconservative tissues, being efficient removing tissues and not promoting collateral damage, capable of irreversibly modifying the original structure of the tissue. This system of laser ablation in the ultrashort pulse regime proved to be effective and promising for surgical procedures to remove, cut, and modify surfaces of human dentin hard tissues and femur bones.

Acknowledgments

This research effort is financially supported by the Fundação de Amparo à Pesquisa do Estado de São Paulo (Fapesp) and National Counsel of Technological and Scientific Development (CNPq).

References

1. M. H. Niemz et al., "Tooth ablation using a CPA-free thin disk femtosecond laser system," *Appl. Phys. B* **79**(3), 269–271 (2004).
2. R. F. Z. Lizarelli et al., "Selective ablation of dental enamel and dentin using femtosecond laser pulses," *Laser Phys. Lett.* **5**(1), 63–69 (2008).
3. A. Z. Freitas et al., "Determination of ablation threshold for composite resins and amalgam irradiated with femtosecond laser pulses," *Laser Phys. Lett.* **7**(3), 236–241 (2010).
4. G. Nicolodelli, C. Kurachi, and V. S. Bagnato, "Femtosecond laser ablation profile near an interface: analysis based on the correlation with superficial properties of individual materials," *Appl. Surf. Sci.* **257**(7), 419–422 (2011).
5. B. Girard et al., "Effects of femtosecond laser irradiation on osseous tissues," *Lasers Surg. Med.* **39**(3), 273–285 (2007).
6. Y. Liu and M. Niemz, "Ablation of femoral bone with femtosecond laser pulses—a feasibility study," *Lasers Med. Sci.* **22**(3), 171–174 (2007).
7. D. Bäuerle, *Laser Processing and Chemistry*, 4th ed., Springer-Verlag, Heidelberg, Berlin (2011).
8. R. Esenaliev et al., "Mechanism of dye-enhanced pulsed laser ablation of hard tissues: implications for dentistry," *IEEE J. Sel. Top. Quant. Electron.* **2**(4), 836–846 (1996).
9. L. Goldman et al., "Impact of the laser on dental caries," *Nature* **203**, 417 (1964).
10. I. M. White et al., "Surface temperature and thermal penetration depth of Nd:YAG laser applied to enamel and dentin," *Proc. SPIE* **1643**, 423–436 (1992).
11. J. Kruger, W. Kautek, and H. Newesely, "Femtosecond-pulse laser ablation of dental hydroxyapatite and single-crystalline fluoroapatite," *Appl. Phys. A* **69**(7), S403–S407 (1999).
12. R. F. Z. Lizarelli et al., "Characterization of enamel and dentin response to Nd:Y AG picosecond laser ablation," *J. Clin. Laser Med. Surg.* **17**(3), 127–131 (1999).
13. F. Korte et al., "Towards nanostructuring with femtosecond laser pulse," *Appl. Phys. A* **77**(2), 229–335 (2003).
14. J. Bonse et al., "Ultrashort-pulse laser ablation of indium phosphide in air," *Appl. Phys. A* **72**(1), 89–94 (2001).
15. J. M. Liu, "Simple technique for measurements of pulsed Gaussian-beam spot sizes," *Opt. Lett.* **7**(5), 196–198 (1982).
16. H. Kim, Ik-Bu Sohn, and S. Jeong, "Ablation characteristics of aluminum oxide and nitride ceramics during femtosecond laser micromachining," *Appl. Surf. Sci.* **255**(24), 9717–9720 (2009).
17. S. Martin et al., "Spot-size dependence of the ablation threshold in dielectrics for femtosecond laser pulses," *Appl. Phys. A* **77**(7), 883–884 (2003).
18. R. E. Samad and N. D. Vieira Jr., "Geometrical method for determining the surface damage threshold for femtosecond laser pulses," *Laser Phys.* **16**(2), 336–339 (2006).
19. B. H. Christensen and P. Balling, "Modeling ultrashort-pulse laser ablation of dielectric materials," *Phys. Rev. B* **79**(15), 155424–10 (2009).

20. A. Vogel et al., "Intraocular Nd:YAG laser surgery: light-tissue interaction, damage range, and the reduction of collateral effects," *IEEE J. Quant. Electron.* **26**(12), 2240–2260 (1990).
21. Y. Nakamura et al., "Morphological changes of rat mandibular bone with ArF excimer laser *in vivo*," *J. Clin. Lasers Med. Surg.* **17**(4), 145–149 (1999).
22. M. L. Walter et al., "Photoablation of bone by excimer laser radiation," *Lasers Surg. Med.* **25**(2), 153–158 (1999).
23. N. M. Fried and D. Fried, "Comparison of Er:YAG and 9.6-μm TE CO_2 lasers for ablation of skull tissue," *Lasers Surg. Med.* **28**(4), 335–343 (2001).
24. M. Frentzen et al., "Osteotomy with 80-μs CO_2 laser pulses—histological results," *Lasers Med. Sci.* **18**(2), 119–124 (2003).
25. M. Abu-Serriah et al., "Removal of partially erupted third molars using an erbium (Er):YAG laser: a randomised controlled clinical trial," *Br. J. Oral Maxillofac. Surg.* **42**(3), 203–208 (2004).
26. B. H. Kivanç, Ö. İ. A. Ulusoy, and G. Görgül, "Effects of Er:YAG laser and Nd:YAG laser treatment on the root canal dentin of human teeth: a SEM study," *Lasers Med. Sci.* **23**(3), 247–252 (2008).
27. R. F. Z. Lizarelli et al., "A comparative study of nanosecond and picosecond laser ablation in enamel: morphological aspects," *J. Clin. Laser Med. Surg.* **18**(3), 151–157 (2000).

Optical characterization of one dental composite resin using bovine enamel as reinforcing filler

[1]*Tribioli J. T., [1]Jacomassi D., [1,2]Rastelli A. N. S., [1]Pratavieira S., [1]Bagnato V.S., [1]Kurachi C.

[1]University of São Paulo – USP, Physics Institute of São Carlos, Optical Group, CEP:13566-590 São Carlos, SP, Brazil
[2] University Estadual Paulista - UNESP, Araraquara School of Dentistry, Department of Restorative Dentistry, CEP: 14801-903 Araraquara, SP, Brazil

ABSTRACT

The use of composite resins for restorative procedure in anterior and posterior cavities is highly common in Dentistry due to its mechanical and aesthetic properties that are compatible with the remaining dental structure. Thus, the aim of this study was to evaluate the optical characterization of one dental composite resin using bovine enamel as reinforcing filler. The same organic matrix of the commercially available resins was used for this experimental resin. The reinforcing filler was obtained after the gridding of bovine enamel fragments and a superficial treatment was performed to allow the adhesion of the filler particles with the organic matrix. Different optical images as fluorescence and reflectance were performed to compare the experimental composite with the human teeth. The present experimental resin shows similar optical properties compared with human teeth.

Keyword list: Composite resin; fluorescence; optical phenomena.

INTRODUCTION

One of the greatest advanced in esthetic dentistry has been the development of composite resins. Similar to other composite materials, a dental composite typically consists of a resin-based oligomer matrix, such as a bisphenol A-glycidyl methacrylate (BISGMA) or urethane dimethacrylate (UDMA), and inorganic fillers such as silicon dioxide (SiO_2). The first study began with the introduction of monomers systems, as BISGMA developed by Bowen in 1962[1]. Since then, several changes have been made. Changes related with their composition, i.e., resin matrix are mainly based on the development of new monomers,[2-4] while other studies on the filler content focus on loading, particle size and shape, silanation and on the development of new particles[5-6] and in the activation system for the polymerization reaction improve their physical, chemical and mechanical properties, seeking to increase the longevity of restorations[4].

Corresponding author: jeisontribioli@gmail.com

Lasers in Dentistry XVIII, edited by Peter Rechmann, Daniel Fried,
Proc. of SPIE Vol. 8208, 82080R · © 2012 SPIE · CCC code: 1605-7422/12/$18
doi: 10.1117/12.909195

The addition of the silanized quartz particles decreased dramatically BISGMA polymerization shrinkage, thermal expansion and water adsorption, while it increases the elastic modulus and surface hardness[1]. However, the development of commercial resins is performed primarily on the organic matrix, and poor interest in strengthening particles, with the exception of particle size was done[7]. In addition the physicochemical properties needs are similar to dental structure. Currently there is a need of restorative materials present optical similarities to dental tissues in order to improve aesthetic item. The components used to improve the optical properties such as opalescence and fluorescence are rare earths such as europium, cerium, ytterbium components that make the end product extremely expensive [8,9].

Ideal esthetic restorative materials should have similar properties of light reflection and fluorescence as those of natural teeth. Therefore, the search for particles that can be used as dental optical characteristics and act as reinforcing filler is an option.

The most widely used commercial composite resins have good optical properties and reflectance and opalescence, however generally have lower fluorescence intensity when compared to the dental structure, which the aesthetic point discourages the use of such resins mainly for anterior restorations[10].

Thus the objective of this study was to verify the reflectance and fluorescence of one experimental composite resin using bovine enamel as reinforcing filler when illuminated with different wavelengths of light: violet, blue, green, red, and white.

MATERIAL AND METHODS

Composite Resin

The charged particles were obtained from bovine enamel incisors extracted from 250 bovine teeth in good conditions. The separation of the enamel and dentin was done mechanically. Then, the enamel fragments were crushed in home-built ball mill for two different times 12 and 24 hours of grinding.

For the addition of bovine enamel particles in the organic matrix was necessary to treat a surface area for better adhesion particle matrix. The treatment process used in this specific area superficial was based on study by Jong-Hyuk Lee and et. al.[11].

The composition of the resin matrix was based on well-established formula in the literature [12,13]. The components used can be found in commercial dental composites. After treatment, the particles of bovine enamel were mixed with of the composite resin monomers.

The experimental composite resins were prepared with 60, 70 and 85% by filler weight, where 80% percentage corresponds to the distribution of particles loads with micrometers average diameter size and the other 20% load with nanometers diameter. The variation of the ratio filler/matrix was required for various compositions and their optical properties were tested. For comparison with the experimental composite resins, optical tests were also performed using two commercial composite resins Filtek Z250™ and Filtek Supreme XT™ for enamel (3M Espe, St. Paul, MN, USA) at color A2. These non-fluorescent resins were chosen because they are frequently used in Dentistry.

Samples Preparation for Images

For the fluorescence test were randomly selected five maxillary canines healthy and freshly extracted for periodontal reasons obtained from the tooth bank of Araraquara School of Dentistry, UNESP, SP, Brazil (approval by the Ethics Committee of University Center of Araraquara – UNIARA, SP, Brazil, Protocol number 1164/10). Prior to fluorescence measurements, the teeth were cleaned with pumice and water and then were stored in distilled water. Cavity preparations were performed in the cervical third of labial surface of the upper canines. The cavities were prepared with the gingival cavosurface margins located 1 mm below the cementoenamel junction and 2 millimeter deep. To carry out the preparations was used carbide burs number #245 (KG Sorensen, Barueri, SP, Brazil) undertaken using an air-water spray. Burs were replaced after 4 cavity preparations to ensure high cutting efficiency. The measurements standardization of the preparations was measured using calipers. For light-cure composite resin was used a blue LED with wavelength centered at 470 nm spectral region within the range of greater absorption of camphorquinone from Sigma Aldrich [14,15]. The light intensity used was 1000 mW/cm² during 60 seconds, parameters conventionally employed to cure commercial composite resins.

Prior to restorative procedures, the cavity was cleaned with chlorhexidine digluconate solution at 0.2% in order to remove debris and impurities from handling and preparation of cavities. Subsequently, restorative procedures were carried out as follows:

1) Application of acid gel, for 15 seconds, 15 s on enamel and 10s dentin;
2) Dry the cavity with abundant water for 30 seconds;
3) Carefully drying of the cavity with paper towels so there is no dentin dehydration which could impair adhesion
4) Application of conventional two steps adhesive system Adper™ Single Bond 2 (3M Espe, St. Paul, MN, USA). According to the manufacturer's protocol which recommends the following application technique: apply the first layer with microbrush, wait 20 seconds, mild air jet, apply the second layer, wait 20 seconds; light-cure during 10 seconds;
5) The composite resins were inserted in three oblique increments, as follows: the first layer was inserted in the incisal third and photo-activated for 60 seconds, the second layer in the cervical third of the cavity and photo-activated for 60 seconds and final layer restoring the cavity, taking care to leave slight excess restorative material.

Image System

System illumination is based on two LED arrays, one for narrow visible range reflectance and another for UV-induced fluorescence. For narrowband reflectance images, LEDs emitting at Red (640±15nm), Green (530±25nm), Blue (460±20nm), White light (450-750nm) (Luxeon III Emiter, Philips, USA) and UV (Ultraviolet Edixeon, Edison Opto Corporation, USA) (400±30nm) were used. To acquire the fluorescence images, the UV LED was combined with a long-pass emission filter at 475nm (Schott GG475, Schott USA). A special optics provides an uniform illumination in the focal plane. The image acquisition was performed using a high resolution color CCD camera (PixelFly qe, The Cooke

Corporation, Germany) with a simple objective lens. To acquire the images the teeth were placed on the focal plane of the lighting system[16].

Image Processing

After the acquisition of six types of images, the images were converted to grayscale. The intensity of the region with the composite resins and the dental structure was obtained through the average intensity of pixels. With these values it was possible to calculate the contrast ratio of the tooth restoration with respect to the different types of lighting. All images processing and analysis were performed with Image J 1.45 (Publisher NIH).

RESULTS AND DISCUSSION

The Figure 1 presents the images obtained from the experimental composites prepared with 60% (R60), 70% (R70) and 85% of bovine enamel, and the two commercial composite resins Filtek™ Supreme XT (XT), and Filtek™ Z250 (Z250).

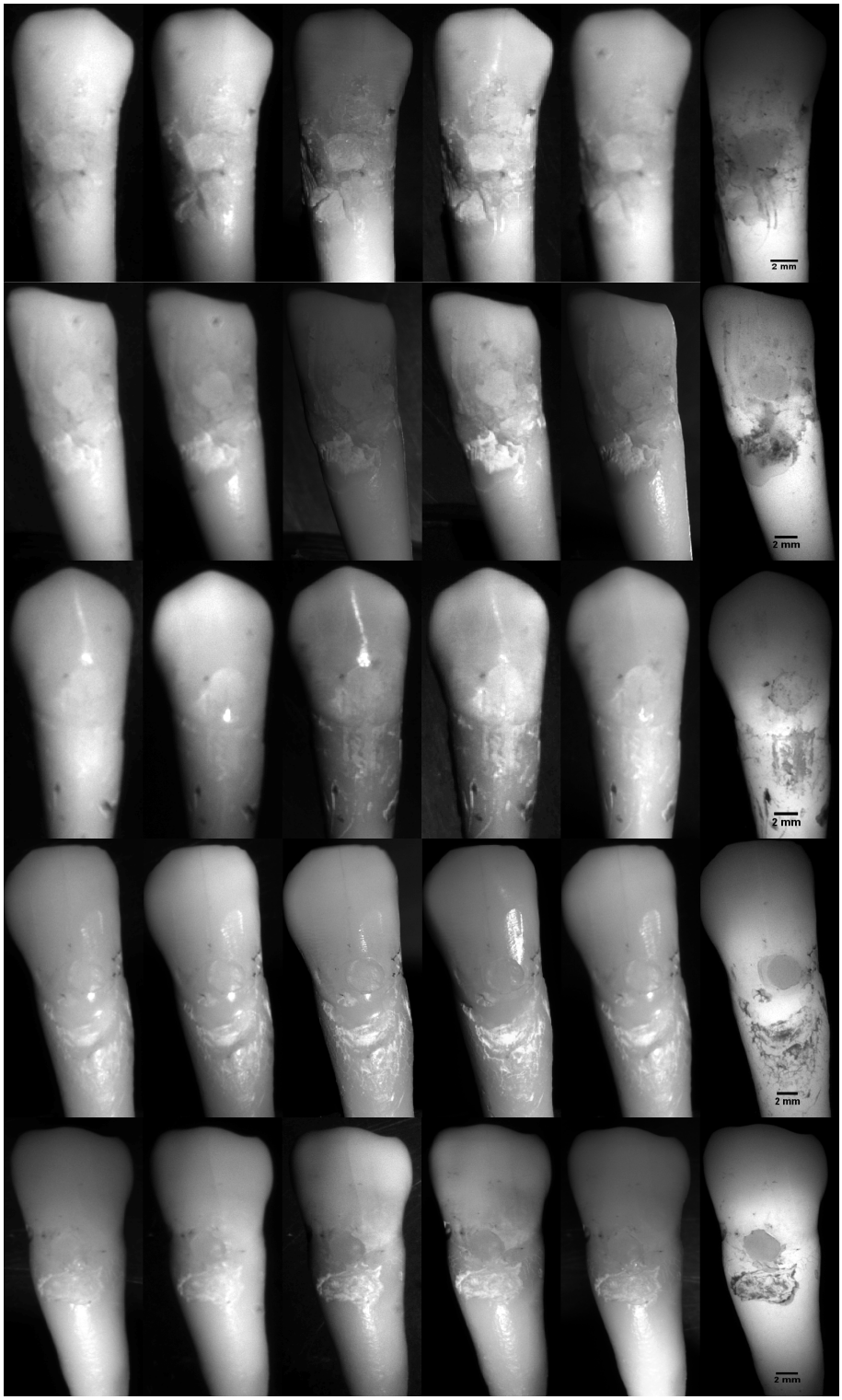

Figure 1. From top to bottom the experimental and commercial composite resins R60, R70, R85, XT, and Z250. And from left to right the images of reflectance in Red, Green, Blue, UV, White light, and Fluorescence images.

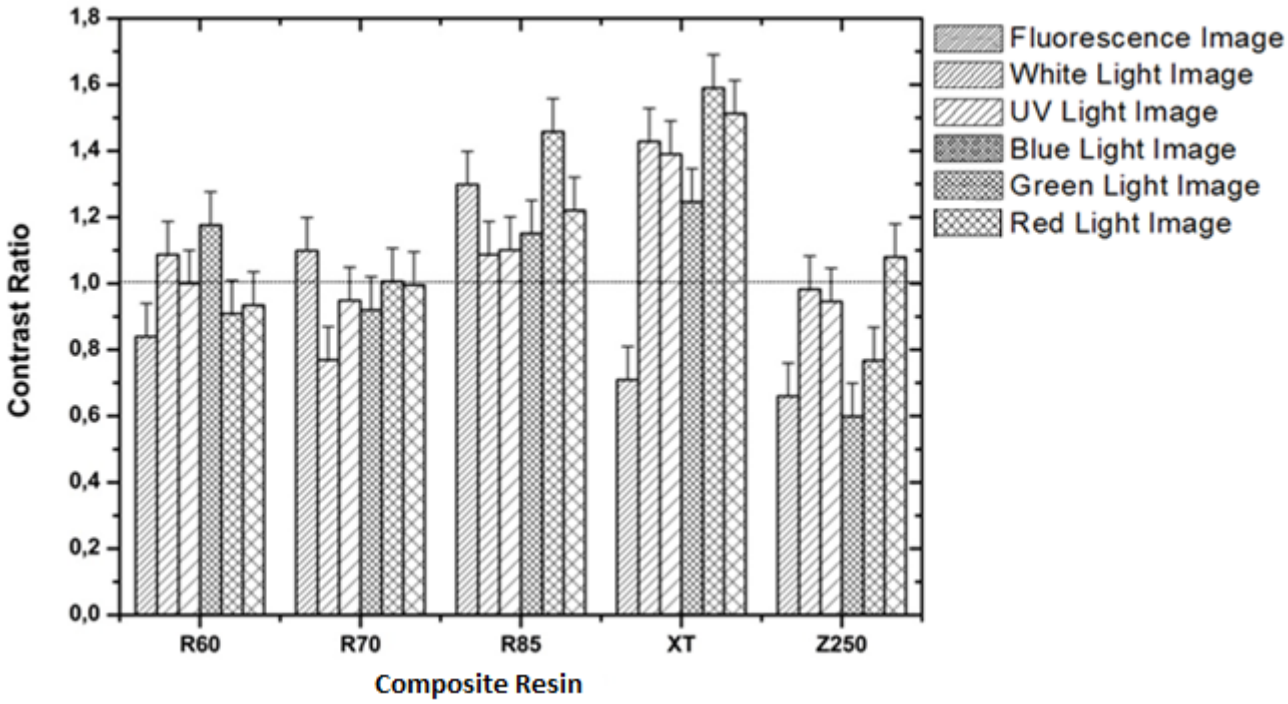

Figure 2. Contrast Ratio as function of different composite resins, commercial and experimental.

The Figure 2 showed the contrast ratio for each composite resin, experimental and commercials. A fluorescent ratio contrast was lower than one indicated for composite resin, then composite resins exhibited lower fluorescence than dental structure. The experimental composite resins, especially R70, showed optical characteristics similar to the dental structure. An ideal composite resin should exhibit one (dotted line) contrast ratio for all different images. Fluorescence of commercial composites were low, however the others showed contrast ratio more similar to the tooth.

The error bars was due to intensity variation of the tooth. This type of comparison has some problems. There were related with imperfections and irregularities on the tooth structure, which cause small changes in the fluorescence and reflectance intensity of the samples. A more efficient analysis could be done with a large sample of teeth. Nevertheless, today obtaining human teeth is extremely difficult.

An ideal composite resin does not exhibit contrast to the tooth, i.e., could not be perceptible under any lighting.

The use of this technique presented in this study by the clinicians before performing a restorative procedure mainly in anterior teeth can allow a more imperceptible restoration. The traditional chose of composite resins is only by check the color of the composite resins and the tooth. The comparison under different lights conditions to choose the composite resins will allow a more customized treatment.

CONCLUSION

The experimental composite resins used in this study showed reflectance properties similar to commercial. Nevertheless, the fluorescence of proposed experimental resin was greater than commercial resin used in this study. The fluorescence images showed that the experimental composite resins had fluorescence more similar to tooth structure.

ACKNOWLEDGMENTS

The authors gratefully acknowledge support from FAPESP (CEPOF – CEPID Program and Scholarships) and CNPq (INOF – INCT Program).

REFERENCES

[1] Bowen, R.L. Properties of a Silica-Reinforced Polymer for Dental Restorations. Journal of the American Dental Association, v. 66, n.1, p. 57-&, 1963.

[2] Beun, S.; Glorieux, T.; Devaux, J.; Vreven, J.; Leloup, G. Characterization of nanofilled compared to universal and microfilled composites. Dental Materials, v. 23, n.1, p. 51-9, 2007.

[3] Curtis, A.R.; Palin, W.M.; Fleming, G.J.; Shortall, A.C.; Marquis, P.M. The mechanical properties of nanofilled resin-based composites: the impact of dry and wet cyclic pre-loading on bi-axial flexure strength. Dental Materials, v. 25, n.2, p. 188-97, 2009.

[4] 1 Jandt, K.D.; Sigusch, B.W. Future perspectives of resin-based dental materials. Dental Materials, v. 25, n.8, p. 1001-1006, 2009.

[5] Peutzfelt, A. Resin composite in dentistry; the monomer systems. European Journal Oral Science, v. 105, n.2, p. 97-116, 1997.

[6] Krishnan, V. K.; Yamuna, V. Effect of initiator concentration, exposure time and particle size of the filler upon the mechanical properties of a lightcuring radiopaque dental composite. Journal of Oral Rehabilitation, v. 25, p.747-751, 1998.

[7] Ferracane, J.L. Resin composite-state of the art. Dental Materials, 2010.In press.

[8] Wozniak, W.T.; Moore, B.K. Luminescence spectra of dental porcelains. Journal of Dental Research, v. 57, n.11-12, p. 971-4, 1978.

[9] Ecker, G.A.; Moser, J.B.; Wozniak, W.T.; Brinsden, G.I. Effect of repeated firing on fluorescence of porcelain-fused-to-metal porcelains.The Journal of prosthetic dentistry, v. 54, n.2, p. 207-14, 1985.

[10] Dos Reis, R.S.A.; Casemiro, L.A.; Carlino, G.V.; Lins, E.C.C.C.; Kurachi, C.; Bagnato, V.S.; pires-de-Souza, F.D.P.; Panzeri, H. Evaluation of fluorescence of dental composites using contrast ratios to adjacent tooth structure: A pilot study. Journal of Esthetic and Restorative Dentistry, v. 19, n.4, p. 199-206, 2007.

[11] Lee, J.H.; Um, C.M.; Lee, I.B. Rheological properties of resin composites according to variations in monomer and filler composition. Dental Materials, v. 22, n.6, p. 515-526, 2006.

[12] Asmussen, E.; Peutzfeldt, A. Influence of UEDMA, BisGMA and TEGDMA on selected mechanical properties of experimental resin composites. Dental Materials, v. 14, n.1, p. 51-56, 1998.

[13] Moszner, N.; Fischer, U.K.; Angermann, J.; Rheinberyer, V. A partially aromatic urethane dimethacrylate as a new substitute for Bis-GMA in restorative composites. Dental Materials, v. 24, n.5, p. 694-699, 2008.

[14] Bandeca, M.C.; El-Mowafy, O.; Saade, E.G.; Rastelli, A.N.S.; Bagnato, V.S.; Porto-Neto, S.T. Changes on degree of conversion of dual-cure luting light-cured with blue LED. Laser Physics, v. 19, n.5, p. 1050-1055, 2009.

[15] Jacomassi, D.P. Estudo da fotoativação de resina composta variando o comprimento de onda com laser de argônio, por meio dos testes de microdureza, variação térmica, grau de conversão e ablação. 2007. 87 f. Dissertação (Mestrado em Ciência e Engenharia de Materiais) - Escola de Engenharia\ Instituto de Química de São Carlos\ Instituto de Física de São Carlos, Universidade de São Paulo, São Carlos, 2007.

[16] Pratavieira S, Santos P. L. A., Bagnato V. S. and Kurachi C., "Development of a widefield reflectance and fluorescence imaging device for the detection of skin and oral cancer", Proc. SPIE 7380, 73805G (2009); doi:10.1117/12.822984

The Filler Content of the Dental Composite Resins and Their Influence on Different Properties

ALESSANDRA N.S. RASTELLI,[1,2*] DENIS P. JACOMASSI,[2] ANA PAULA S. FALONI,[1] THALLITA P. QUEIROZ,[1] SEILA S. ROJAS,[3] MARIA INÊS B. BERNARDI,[3] VANDERLEI S. BAGNATO,[2] AND ANTÔNIO C. HERNANDES[3]

[1]*Araraquara Center University–UNIARA, School of Dentistry, Department of Health Sciences, Implantology Post Graduation Course, Avenida Maria Antonia Camargo de Oliveira, Vila Suconasa, 14807-120 Araraquara, São Paulo, Brazil*

[2]*University of São Paulo–USP, Physics Institute of São Carlos, Optical Group, Biophotonics Lab., São Carlos, São Paulo, Brazil*

[3]*University of São Paulo - USP, Physics Institute of São Carlos, Grupo Crescimento de Cristais e Materiais Cerâmicos, São Carlos, SP, Brazil.*

KEY WORDS composite resins; nanofillers; polymerization; hardness; filler morphology; LED

ABSTRACT The purpose of this study was to compare the inorganic content and morphology of one nanofilled and one nanohybrid composite with one universal microhybrid composite. The Vickers hardness, degree of conversion and scanning electron microscope of the materials light-cured using LED unit were also investigated. One nanofilled (Filtek™ Supreme XT), one nanohybrid (TPH®$_3$) and one universal microhybrid (Filtek™ Z-250) composite resins at color A_2 were used in this study. The samples were made in a metallic mould (4 mm in diameter and 2 mm in thickness). Their filler weight content was measured by thermogravimetric analysis (TG). The morphology of the filler particles was determined using scanning electron microscope equipped with a field emission gun (SEM-FEG). Vickers hardness and degree of conversion using FT-IR spectroscopy were measured. Filtek™ Z-250 (microhybrid) composite resin shows higher degree of conversion and hardness than those of Filtek™ Supreme XT (nanofilled) and TPH®$_3$ (nanohybrid) composites, respectively. The TPH$_3$® (nanohybrid) composite exhibits by far the lowest mechanical property. Nanofilled composite resins show mechanical properties at least as good as those of universal hybrids and could thus be used for the same clinical indications as well as for anterior restorations due to their high aesthetic properties. *Microsc. Res. Tech. 75:758–765, 2012.*

INTRODUCTION

Light activated composite resins are now the widely used materials in Restorative Dentistry. In this sense, many efforts to improve their clinical performance have been undertaken (Ruddell et al., 2002).

Researches on the resin matrix are mainly based on the development of new monomers (Atai et al., 2004; Chung et al., 2002; Lu et al., 2005; Taylor et al., 1998), whereas other studies on the filler content focus on loading, particle size and shape, silanation and on the development of new particles (Ikejima et al., 2003; Xu et al., 2002).

Filler size is only one of several parameters affecting the overall properties of composite resins (Masourasa et al., 2008). However, the properties of dental composite resins depend on many factors: the chemical, physical and mechanical properties of the monomer, polymer matrix, the coupling agent used, and the concentration, type, size and distribution of the particles. Besides, the photo-activation process including the nature of the photo-initiator and the activator, their concentration, the power density of light-curing unit and exposure times (Ikejima et al., 2003; Ruddell et al., 2002).

In the last few years one of the most important advances in this field is the application of nanotechnology to dental composite resins. Nanotechnology is known as the production and manipulation of materials and structures in the range of about 0.1–100 nm by various physical or chemical methods (Kirk et al., 1991). While the size of the filler particles lies around 0.04–20 μm in hybrid composites and 0.7–3.6 μm in microhybrid composites (Venhoven et al., 1996), recently, new fillers with size ranging from around 5–100 nm have been developed and applied in Dentistry (Moszner and Klapdohr, 2004). These particles could thus be considered for preparation of the nanofilled dental composites.

In Dentistry, posterior class I or II restorations require composites that show high mechanical properties whereas anterior restorations need composites that have superior aesthetics. The composite resin that meets all the requirements of both posterior and anterior restorations has not emerged yet (Beun et al., 2007).

Therefore, nanotechnology is of great interest in composite resin research, due to the reduced dimension of the particles and to a wide size distribution. Furthermore, an increased filler load can be achieved with the consequence of reducing the polymerization shrinkage (Mitra et al., 2003) and increasing the mechanical properties such as hardness, tensile strength, compressive strength and resistance to fracture (Moszner and Klapdohr, 2004; Wagner and Vaia, 2004). These seem to be equivalent or even sometimes higher than those of universal composites and significantly higher than those of microfilled composites (Mitra et al., 2003;

*Correspondence to: Alessandra Nara de Souza Rastelli, Araraquara Center University – UNIARA, School of Dentistry, Avenida Maria Antonia Camargo de Oliveira, No. 170 (Via Expressa), Vila Suconasa, 14807-120 Araraquara, São Paulo, Brazil. E-mail: alerastelli@yahoo.com.br

Received 23 June 2011; accepted in revised form 27 October 2011

DOI 10.1002/jemt.21122

Published online 30 December 2011 in Wiley Online Library (wileyonlinelibrary.com).

TABLE 1. Dental composite resins used in this study

Composite resin	Resinous matrix	Filler type loading (vol%)	Batch number
Filtek™ Z-250	Bis-GMA, UDMA, Bis- EMA	Zirconia/Silica (60%) 0.19–3.3 μm	1370
Filtek™ Supreme XT	Bis-GMA, UDMA, TEG-DMA, Bis-EMA	Zirconia/Silica (59.5%) 0.6–1.4 μm, nanoaglomerated nano silica filler (20 nm)	3910
TPH_3®	Bis-GMA, Bis-EMA, Dimetracrylate	Bariumaluminoborosilicate glass, Bariumaluminofluorosilicate 49.7% and highly dispersed silicon dioxide, 24.6% fluoroaluminoborosilicate glass with 1 μm and nanofiller silica with 0.04 μm	647011

Moszner and Klapdohr, 2004; Terry, 2004). On the other hand, the small size of the filler particles improve the optical properties of composite resins because their diameter is a fraction of the wavelength of visible light (0.4–0.8 μm), resulting in the human's eye inability to detect the particles (Mitra et al., 2003). In addition, the wear rate is diminished and the gloss retention is better (Terry, 2004). Consequently, manufacturers now recommend the use of nanocomposites for both anterior and posterior restorations.

Therefore, dental composites resins containing nanosized fillers reflect the growing interest of the dental community in nanostructured restorative materials. Thus, the purposes of the present study were to determine the influence of inorganic filler fraction and to measure the mechanical property, the degree of conversion of one commercially available nanofilled composite compared to one universal or microhybrid and one nanohybrid composites. The inorganic fraction was characterized by scanning electron microscope equipped with a field emission gun (SEM-FEG) and by thermogravimetric analysis (TGA). The mechanical property measured was Vickers hardness. The degree of conversion was evaluated by FT-IR spectrophotometry.

MATERIALS AND METHODS

Materials

The dental composite resins used in this study were: Filtek™ Z-250 (3M Espe, Dental Products St. Paul, MN), Filtek Supreme™ XT (3M Espe, Dental Products St. Paul, MN) and TPH_3® (Dentsply De Trey GmbH, Konstanz, Germany) at color A_2. The Table 1 summarizes the dental composite resins and the batch number.

Light-Curing Unit (LCU)

The samples were photo-activated for 40s (seconds) of irradiation time by using one LED LCU (LEC 1000/ MMOptics, São Carlos, SP, Brazil). The LED LCU was used in standard mode (continuous, constant power density) and power density value of 400 mW/cm^2. The power output emitted by the light tip (tip diameter = 8 mm) was measured before each light activation using a power meter Fieldmaster (Coherent Commercial Products Division - model number FM, set no. WX65, part number 33-0506 made in USA) and the power densities values were calculated by the formula:

$$I = \frac{P}{A} \quad (1)$$

where P = power in mW (milliwatts); A = area of the light tip in cm^2 (centimeter square).

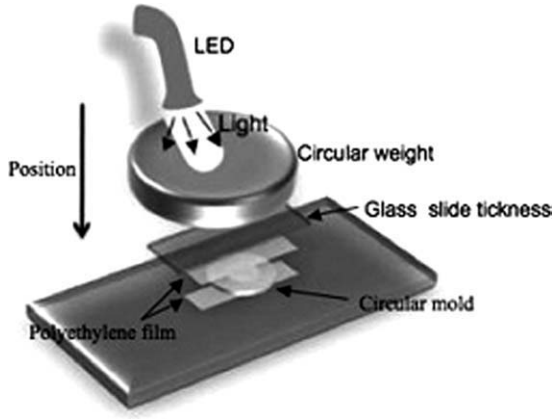

Fig. 1. Experimental setup for samples preparation.

Samples Preparation

For Vickers hardness and degree of conversion the samples were made in a metallic mould (4 mm diameter and 2 mm thickness), according to ISO 4049 (ISO 2000).

The metallic mould was positioned in a glass plate of 10 mm thickness. The composite resin was packed in bulk and the top and bottom surfaces were covered with a polyethylene film. A glass sheet (1 mm thickness) and a weight (1 kg) were positioned to pack the composite resin. The top surface of the samples was placed in contact with the light curing tip and photo-activated for 40 s (seconds) of irradiation time. The Figure 1 shows the experimental setup for samples preparation. Five samples were prepared in each experimental Group. After 24-h dry storage at 37°C (±1°C), the hardness and degree of conversion measurements were conducted.

Percentage and Morphology of Inorganic Fraction

Weight Percentage of Fillers. The weight percentage of fillers was determined using thermogravimetric analysis, which consists of the elimination of the organic component of the composite by heating it at constant temperature (Sabbagh et al., 2004). Thermogravimetric analyses (TGA) were performed with a TG 209 (Netzsch), operating in N_2 under a gas flow of 20 mL/ min with alumina pan containing ~20 mg of the samples. It evaluated weight changes as a function of time and temperature during a thermal program ranging from 30 to 900°C at the rate of 10°C/min in normal atmosphere followed by air cooling to room temperature. The runs were single ones and carried out in dynamic conditions at the constant heating rate of 10°C/min. Calibration of the device was performed according to stand-

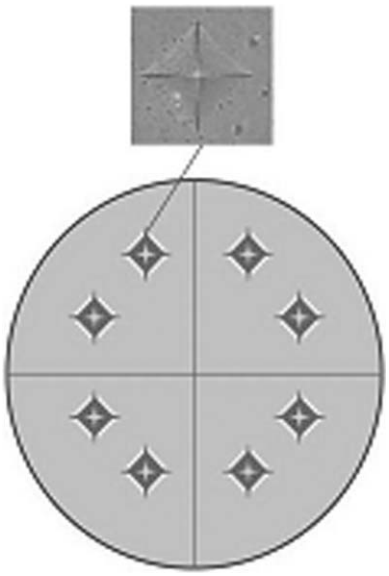

Fig. 2. Esquematic distribution of the indentations on the top and bottom surfaces of the samples.

ard procedure available on TA Instruments online help. The TG mass and baseline calibration was conducted with and without α-alumina standards positioned on the sensors. The temperature calibration was performed using a high purity zinc sample.

The calculated ratio between the final weight of the sample and its nominal weight is assigned to the inorganic fraction. The wt% of the filler fraction in the materials was considered to be the difference in weight before (W_0) and immediately after ashing (W_1), according to the following equation:

$$\text{Filler wt}(\%) = \frac{(W_1)}{(W_0)} \times 100 \qquad (2)$$

Morphology of Inorganic Fraction. The fillers morphology was determined using SEM-FEG. Unpolymerized monomers were removed by a washing technique: 0.5 g of each composite resin was dissolved in 5 mL of acetone and centrifuged for 5 min at 700 × *g*. This process was repeated three times using acetone and three others with chloroform for a further washing and to ensure a complete elimination of the unpolymerized resin. The remaining fillers including prepolymerized fillers were suspended in acetone, smeared on a silicon substrate (2.5 cm × 2.5 cm) and dried at 35°C (±1°C) during 15 min in over. Fillers were observed by ZEISS (DSM-940A) scanning electron microscope equipped with a field emission gun (SEM-FEG), at 10,000 KX magnification.

Vickers Hardness Test

After the photo-activation, the samples were stored in dry mean at 37°C (±1°C) for 24 h. The Vickers hardness test was performed on the top and bottom surfaces of the composite resin samples, using a Leica VMHT Mot (Germany) testing machine. The Vickers hardness measurements were obtained using a 50 gf load applied with a 30-s dwell time. Eight indentations were made on both the top and bottom surfaces of the samples Fig. 2). The results were expressed first in μm (micrometers), and after were transformed into Vickers hardness (VHN) values directly for the hardness testing machine.

Determination of the Degree of Conversion (% DC)

The number of double carbon bonds which are converted in single bonds provides the degree of conversion (%DC) of composite resins.

After 24 h of the photo-activation, the composite resin was pulverized into fine powder and maintained in a dark room until the moment of the FT-IR analyzes. Ten milligrams of the ground powder was thoroughly mixed with one hundred milligrams of KBr powder salt. This mixture was placed into a pelleting device and then pressed in a press with a load of 10 tons during 1 min to obtain a pellet.

Fourier transform infra-red spectroscopy (FT-IR) measurements of both uncured and cured samples were carried out by using a Nexus™ 470 FT-IR E.S.P (Thermo Nicolet, serial number: AEP0301044). The experiments were done in absorbance mode under the following conditions: 32 scans, 4 cm^{-1} resolution, 300–4000 cm^{-1} wavelength.

The percentage of unreacted carbon-carbon double bonds (% C=C) was determined from the ratio of absorbance intensities of aliphatic C=C (peak at 1638 cm^{-1}) against internal standard before and after curing of the specimen: aromatic C—C (peak at 1608 cm^{-1}). This experiment was carried out in triplicate. The degree of conversion was determined by subtracting the % C=C from 100%, according to the formula:

$$\frac{(1638\ \text{cm}^{-1}/1608\ \text{cm}^{-1})\text{cured}}{(1638\ \text{cm}^{-1}/1608\ \text{cm}^{-1})\ \text{uncured}} \times 100 \qquad (3)$$

Statistical Analysis

Statistical analysis for Vickers hardness and degree of conversion (%) measurements was made using ANOVA and post hoc Tukey's test at $P < 0.05$ level. This was performed separately for each measurement, Vickers hardness and degree of conversion (%).

RESULTS

Percentage and Morphology of Inorganic Fraction

The thermogravimetric measurements of the samples are shown in Figure 3. The residual mass was 76.0% for the Filtek™ Supreme XT, 73.0% for the TPH_3® and 82.0% for the universal microhybrid composite, Filtek™ Z-250.

The average particle sizes and the morphology of inorganic fraction were determined from the SEM-FEG images presented in Figure 4. Filtek™ Supreme XT showed spherical particles (~20–25 nm). Irregular shaped particles and a glassy phase were found in Filtek™ Z-250 (~70–90 nm). For TPH_3® irregular shaped

particles (~100–1 μm) were also observed, however, the glassy phase and grain boundary were not possible to be identified.

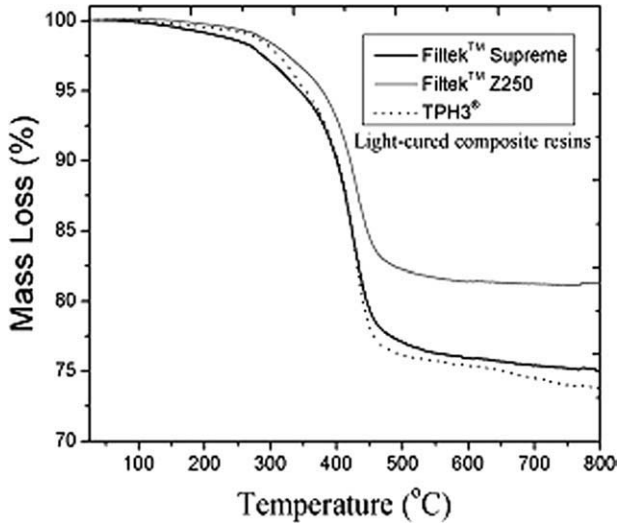

Fig. 3. Residual mass of the composite resins determined by thermogravimetric analysis.

Vickers Hardness Measurements

The results for Vickers hardness measurements ranged from 53.7 (TPH_3®) to 72.5 (Filtek™ Z-250) and 46.3 (TPH_3®) to 71.0 (Filtek™ Z-250) for the top and bottom surfaces, respectively. For Filtek™ Supreme XT the Vickers hardness mean values ranged from 72.12 to 56.8 for the top and bottom surfaces, respectively. Mean values and standard deviations are shown in Figure 5. Hardness mean values were significantly higher at the top surface for both composites. Yet, the hardness at the top surface of the nanofill composite was similar to the hardness of the bottom surface of the microhybrid composite.

The Vickers hardness mean values and the *B*/*T* hardness ratio are shown in Table 2. The ANOVA and Tukey's test showed statistically significant differences ($P < 0.05$) between top and bottom hardness, and between *B*/*T* ratios, for Vickers hardness test.

The Figure 6 shows the *B*/*T* ratios obtained for Vickers hardness test. The area between 80 and 90% represents the literature acceptable *B*/*T* ratio range (Caldas et al., 2003; Torno et al., 2008).

Degree of Conversion Measurements (%)

The degrees of conversion of all dental composite resins tested are shown in Figure 7. One-way ANOVA and Tukey's test showed that different dental composite

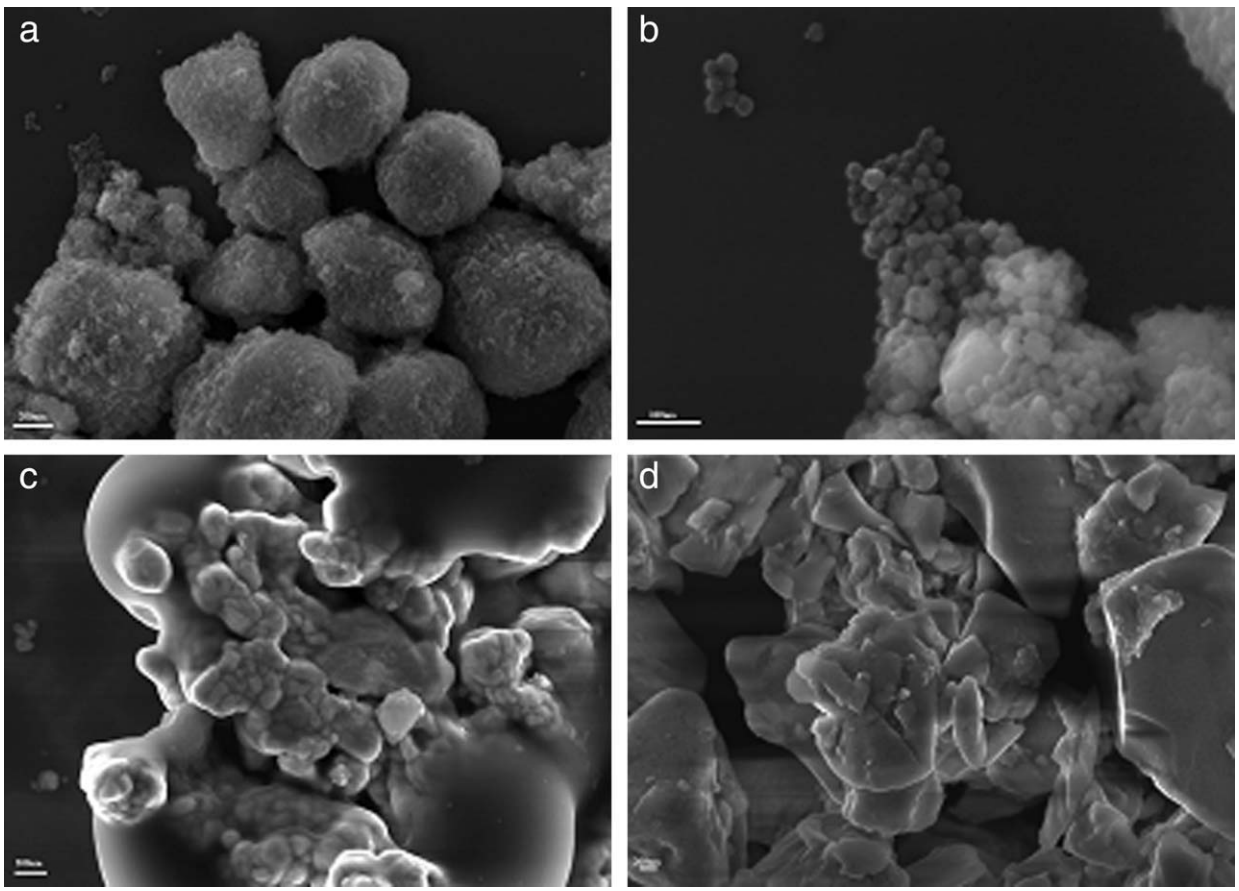

Fig. 4. Fillers by scanning-electron microscopy at 100,00 KX, and inset 300,00 KX magnifications.

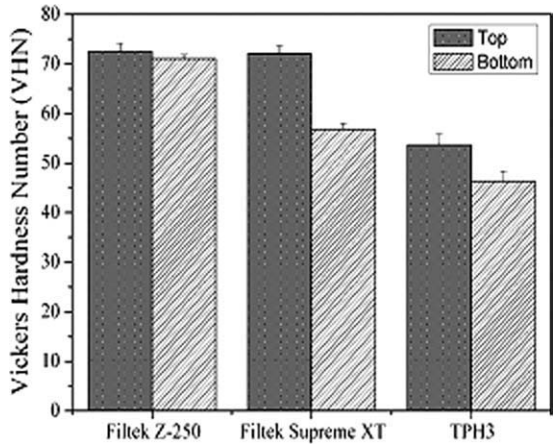

Fig. 5. Vickers hardness mean values and standard deviation of the composite resins tested.

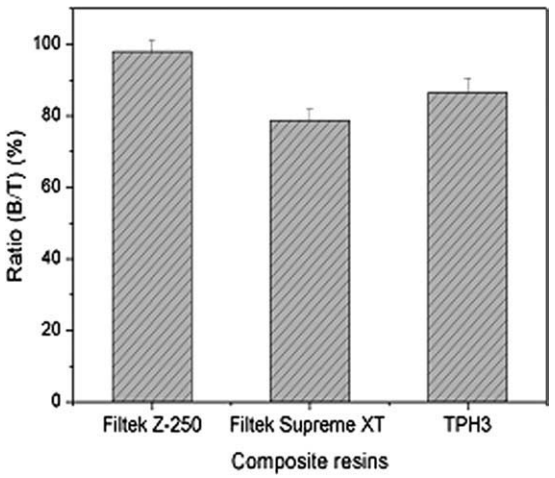

Fig. 6. *B/T* ratios (%) for Vickers hardness test. The area between 80 and 90% represents the convention for an acceptable *B/T* ratio.

TABLE 2. Vickers Hardness means values for the top and bottom surfaces and corresponding B/T ratio for the different dental composite resins (standard deviation between parentheses)

	Vickers Hardness number (VHN)		
Composite resins	Top	Bottom	*B/T* ratio
Filtek™ Z-250	72.6 (1.7)	71.0 (0.9)	97.9 (3.2)
Filtek™ Supreme XT	72.1 (1.7)	56.8 (1.3)	78.7 (3.2)
TPH_3®	53.7 (2.1)	46.3 (1.9)	86.5 (3.9)

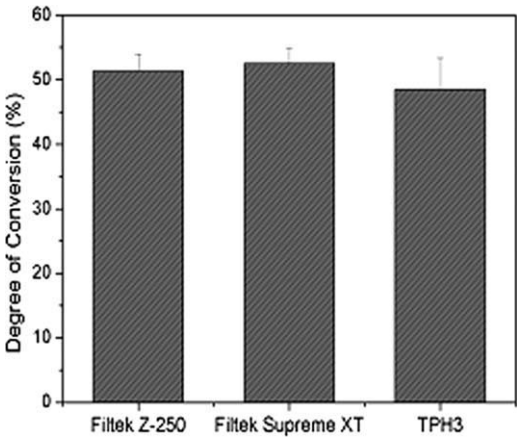

Fig. 7. Degree of conversion obtained for the different composite resins used after 40 s of irradiation.

resins had significant effects on DC% ($P < 0.05$). The DC of the microhybrid composite was similar to nanofill composite.

DISCUSSION

Filler Load

The use of thermogravimetric analysis have been a good method to evaluate the filler load in weight of dental composite resins, as showed by Sabbagh et al. (2004). The structural and thermal properties of three different dental composite resins, Filtek™ Z-250, Filtek™ Supreme XT and TPH_3® were investigated in a previous study (Bernardi et al., 2008). As glass transition (T_g), degradation, and the thermal stability showed that the Filtek™ Z-250 composite resin presented the major residual mass and a major *T*g value (58°C) that suggest a better influence of the fillers and an increased cross-linking as related to the other dental composite resins evaluated. The same composite resin (Filtek™ Z-250) presents a well interconnected more homogeneous morphology and, suggesting with this one better degree of conversion correlated with the glass phase transition temperature.

The nanofilled and universal composite resins exhibit almost the same range of percentages of fillers and the nanohybrid composite resin (TPH_3®), which filler load is significantly lower than the highest value obtained with the universal microhybrid (Filtek™ Z-250).

Filler Shape

Most filler particles are of irregular shape. Spherical particles are found in Filtek™ Supreme XT. It has been shown that spherical shape presented many advantages such as to allow an increased filler load in composites (Beun et al., 2007; Kim et al., 2002; Sabbagh et al., 2004; Suzuki et al., 1995). The SEM analysis also revealed that the nanofiller particles in Filtek™ Supreme XT are arranged in clusters that approximate the size of the individual filler particles of the microhybrid composite Filtek™ Z-250. Irregular particles are found in Filtek™ Z-250 and TPH_3®.

Vickers Hardness Measurements

Vickers hardness evaluation is a widely used test to examine composite resin polymerization (Bouschlicher et al., 2004; Jain and Pershing, 2003). The hardness of different composite resins may be related to its wear resistance and ability to maintain their stability in the oral environment (Yoldas et al., 2004).

The Vickers hardness can be affected by many factors. It is well known that factors, such as resin type, filler levels, resin shade, irradiation times, power density and spectrum of the light-curing unit used, influ-

ence final hardness of dental composite resins (Moore et al., 2008).

In this study, when hardness was evaluated, different results were obtained. The Filtek™ Z-250 composite resin shows the higher Vickers hardness mean values, directly followed by Filtek™ Supreme XT. The TPH$_3$® nanohybrid composite resin showed lower mean values, significantly lower than those measured for the universal microhybrid and nanofilled composite resins (Fig. 5). These results can be related to the fillers fraction, size and shape of the different dental composite resins tested. For both irregularly (Filtek™ Z-250) and spherically (Filtek™ Supreme XT) shaped filler particle materials (70–90 nm and 20–25 nm, respectively) rendered higher Vickers hardness mean values than the composite resin containing the largest fillers only (TPH$_3$® 100 nm – 1μm). The two composite resins that have the highest filler load (Filtek™ Z-250 and Filtek™ Supreme XT) show the highest mechanical property: the universal microhybrid one and the nanofilled one has higher hardness mean values for both top and bottom surfaces. These results suggest that the glassy phase present in the Filtek™ Z-250 sample could improve the packing of the fillers in the polymer matrix.

The hardness mean values for bottom surface were lower than the top. This is expected once the light reaching the bottom surface is decreased with depth, as well as the curing efficiency (Torno et al., 2008). Some studies showed that when light passes through the bulk of a restorative material, its intensity is greatly reduced, thus decreasing the polymerization potential (Bayne et al., 1994; Conti et al., 2005). Composite resins has the property of dispersing the light of the curing unit, thus when the light passes through the bulk of the composite, its intensity is reduced due to light scattering by filler particles and the resin matrix (Bayne et al., 1994; Conti et al., 2005). Braga and Ferracane have shown that with the increasing of the fillers diameter, the scattering of the light can be increase (Braga and Ferracane, 2002). Absorption and scatter within the material are the major factors associated with light attenuation (Yearn, 1985), other than reflection from the restoration surface (Watts and Cash, 1994), for this is dependent on the formulation of the material, particularly the filler size, type and content (Campbell et al., 1986; Ruyter and Øysæd, 1982), and the shape of the material (Cook and Standish, 1983; Ferracane et al., 1986; Harrington and Wilson, 1993). There are marked variations in formulation between products so that similar variation in the rate of light attenuation may reasonably be expected. Previous studies have clearly shown significant variations in depth of cure between products (DeWald and Ferracane, 1987; Kawaguchi et al., 1994; Watts et al., 1984), which has primarily been attributed to scattering of the activating radiation, thus indirectly demonstrating differences in light attenuation between materials. However, despite these clear differences, a 2 mm incremental thickness at a minimum irradiance of 400 mW/cm^2 has been recommended (Caughman et al., 1995), apparently for all filled-composite resins.

In the present study, the TPH$_3$® composite resin showed the lower hardness mean values (Fig. 5). This fact can be related to the fillers diameter, where the scattering of the light have been suggested will be increased. The others two composites that have the lowest fillers diameter (Filtek™ Z-250 and Supreme™ XT) and consequently, showed the highest Vickers hardness mean values.

Additionally, the high fillers fraction of the Filtek™ Z-250 presented a polymerization more homogeneous than the other composite resins tested. This fact can be explained by the ratio bottom/top surfaces obtained (Table 2 and Fig. 6). To define depth of cure based on top and bottom hardness measurements, it is common to calculate the ratio of bottom/top hardness and give an arbitrary minimum value for this ratio to consider the bottom surface as adequately cured. Values of 0.80 and 0.85 have often been used (Kim et al., 2002; Rueggeberg et al., 1993). Previous studies have used bottom/top Vickers hardness ratios to obtain a percentage depth of cure, and if that value exceeded 80%, specimens were considered to be adequately cured (Kim et al., 2002; Rueggeberg et al., 1993). Using this criterion, Filtek™ Z-250 and TPH$_3$® exhibited a *B/T* ratio higher than 80%. Filtek™ Z-250 and Filtek™Supreme XT showed the highest bottom hardness followed by the TPH$_3$®. However, the calculation of the depth of cure based only in this *B/T* ratio could lead to erroneous interpretations. A test sample could be poorly polymerized and, if the hardness of the bottom surface was similar to the top, its ratio might be higher than 80%. If only this ratio is taken into consideration, the TPH$_3$® (Top: 53.7 and Bottom: 46.3) that resulted in a 0.86 *B/T* ratio, could show adequate polymerization. These results show this dental composite resin have the adequate curing efficiency, which is not shown by their hardness values (Table 2 and Fig. 5). Consequently, the *B/T* ratio convention of 80–90% appears to be not appropriate to evaluate curing efficiency of composites, unless it is defined a lower limit for top or bottom composite resin hardness.

Degree of Conversion Measurements (DC%)

The DC is another relevant property as it influences the mechanical properties as well as the long-term resistance to degradation of the composites (Rodrigues et al., 2008). When light-cured composite resins are irradiated, the radicals generated attack the double bonds of the monomers, creating cross-linked three-dimensional network polymers (Leszczynska et al., 2007).

A certain degree of conversion (DC %) in dental composite resins must be achieved for the material to develop 'adequate' physical and mechanical properties so as to withstand masticatory forces and also attain adequate biocompatibility (i.e. with respect to leachable substances). In addition, the unreacted monomer may generate radical species responsible for some pathological states (Conti et al., 2005). These substances have the potential to irritate soft tissues and pulp, stimulate the growth of bacteria and promote allergic reactions (Sideridou and Achilias, 2005). For photoactivated, resin-based composite, conversions ranging from 43 to 73% have been reported using FT-IR measurements. The values obtained for degree of conversion of composites fall within the range of conversion values reported for most composite resins. In this study, the mean values ranged from 47 to 53%.

Many factors can influence the DC (%) of composite resins, specially, resin matrix composition. However, differences in filler geometry, size and fractions may also influence the DC (%) values. In this study, Filtek™ Supreme XT composite resin shows the higher degree of conversion, directly followed by the Filtek™ Z-250. The TPH_3® nanohybrid composite resin showed lower values, significantly lower than those measured for the universal microhybrid and nanofilled materials. The higher degree of conversion seen in Filtek™ Supreme XT and Filtek™ Z-250 composite resins can be explained by the presence of UDMA. The UDMA-based resins have been shown to be more reactive than bisGMA-based resins (Stansbury et al., 2001). The higher conversion level may also have been related to partial substitution of the relatively stiff and hydrogen-bonded bisGMA molecules with the longer and more flexible bisEMA molecules. For Filtek™ Z-250, the lower aliphatic:aromatic ratio is another reason (Emami and Soderholm, 2003).

In this study, since both Filtek™ Z-250 and Filtek™ Supreme XT composite resins have the same polymeric matrix, then the difference could be explained by the filler particle size. These results are in agreement with Halvorson et al. (2003) study, which found that conversion progressively decreased with increasing the filler loading because the mobility of resin-monomers was restricted due to existence fillers. This lead to decreased molecular and radical mobility and resulted lower monomer conversion.

CONCLUSIONS

The characterization of composite resins used in the present study revealed that for microhybrid and nanofilled composites different sizes of filler particles might result in different microstructures and filler contents. Among the factors evaluated, the filler content seems to be the most important factor in the determination of the properties of composites.

ACKNOWLEDGMENTS

The authors thank the Brazilian agencies FAPESP (Process number: 04/15816-7) and CNPq for financial support.

REFERENCES

Atai M, Nekoomanesh M, Hashemi SA, Amani S. 2004. Physical and mechanical properties of an experimental dental composite based on a new monomer. Dent Mater 20:663–668.

Bayne S, Heymann H, Swift E. 1994. Update on dental composites restorations. J Am Dent Assoc 25:687–701.

Bernardi MIB, Rojas SS, Andreeta MRB, Rastelli ANS, Hernandes AC, Bagnato VS. 2008. Thermal analysis and structural investigation of different dental composites resins. J Therm Anal Calorim 94:791–796.

Beun S, Glorieux T, Devaux J, Vreven J, Leloup G. 2007. Characterization of nanofilled compared to universal and microfilled composites. Dent Mater 23:51–59.

Bouschlicher MR, Rueggeberg FA, Wilson BM. 2004. Correlation of bottom to top surface microhardness and conversion ratios for a variety of resin composite compositions. Oper Dent 29:698–704.

Braga RR, Ferracane JL. 2002. Contraction stress related to degree of conversion and reaction kinetics. J Dent Res 81:114–118.

Caldas DBM, Almeida JB, Correr-Sobrinho L, Sinhoreti MAC, Consani S. 2003. Influence of curing tip distance on resin composite Knoop hardness number, using three different light curing units. Oper Dent 28:315–320.

Campbell PM, Johnston WM, O'Brien WJ. 1986. Light scattering and gloss of an experimental quartz-filled composite. J Dent Res 65:892–894.

Caughman WF, Rueggeberg FA, Curtis JW. 1995. Clinical guidelines for photocuring restorative resins. J Am Dent Assoc 126:1280–1286.

Chung C-M, Kim J-G, Kim M-S, Kim K-M, Kim K-N. 2002. Development of a new photocurable composite resin with reduced curing shrinkage. Dent Mater 18:174–178.

Conti C, Giorgini E, Landi L, Putignano A, Tosi G. 2005. Spectroscopic and mechanical properties of dental resin composites cured with different light sources. J Mol Struct 744–747:641–646.

Cook WD, Standish PM. 1983. Polymerization kinetics of resin based restorative materials. J Biomed Mater Res 17:275–282.

DeWald JP, Ferracane JL. 1987. A comparison of four modes of evaluating depth of cure of light-activated composites. J Dent Res 66:727–730.

Emami N, Soderholm K-JM. 2003. How light irradiance and curing time affect monomer conversion in light-cured resin composites. Eur J Oral Sci 111:536–542.

Ferracane JL, Aday P, Matsumoto H, Marker VA. 1986. Relationship between shade and depth of cure for light-activated dental resin composite. Dent Mater 2:80–84.

Halvorson RH, Erickson RL, Davidson CL. 2003. The effect of filler and silane content on conversion of resin-based composite. Dent Mater 19:327–333.

Harrington E, Wilson HJ. 1993. Depth of cure of radiation-activated materials—Effect of mould material and cavity size. J Dent 21:305–311.

Ikejima I, Nomoto R, McCabe JF. 2003. Shear punch strength and flexural strength of model composites with varying filler volume fraction, particle size and silanation. Dent Mater 19:206–211.

International Organization for Standardization. ISO 4049. 2000. Dentistry—polymer–based filling, restorative and luting materials,3rd ed. Geneva: ISO.

Jain P, Pershing A. 2003. Depth of cure and microleakage with high-intensity and ramped resin-based composite curing lights. J Am Dent Assoc 134:1215–1223.

Kawaguchi M, Fukushima T, Miyazaki K. 1994. The relationship between cure depth and transmission coefficient of visible light-activated resin composite. J Dent Res 73:516–521.

Kim K-H, Ong JL, Okuno O. 2002. The effect of filler loading and morphology on the mechanical properties of contemporary composites. J Prosthet Dent 87:642–649.

Kirk RE, Othmer DF, Kroschwitz J, Howe-Grant M. 1991. Encyclopedia of chemical technology,4th ed. New York: Wiley. p.397.

Leszczynska A, Njuguna J, Pielichowshi K, Banerjee JR. 2007. Polymer/montmorillonite nanocomposites with improved thermal properties: Part I. Factors influencing thermal stability and mechanisms of thermal stability improvement. Thermochim Acta 453:75–96.

Lu H, Stansbury JW, Nie J, Berchtold KA, Bowman CN. 2005. Development of highly reactive mono-(meth) acrylates as reactive diluents for dimethacrylate-based dental resin systems. Biomaterials 26:1329–1336.

Masourasa K, Silikas N, Watts DC. 2008. Correlation of filler content and elastic properties of resin-composites. Dent Mater 24:932–939.

Mitra SB, WU D, Holmes BN. 2003. An application of nanotechnology in advanced dental materials. J Am Dent Assoc 2003; 134:1382–1390.

Moore BK, Platt JA, Borges G, Chu T-MG, Katsilieri I. 2008. Depth of cure of dental resin composites: ISO 4049 depth and microhardness of types of materials and shades. Oper Dent 33–34:408–412.

Moszner N, Klapdohr S. 2004. Nanotechnology for dental composites. Int J Nanotechnol 1:130–156.

Rodrigues SA Jr, Scherrer SS, Ferracane JL, Della Bona A. 2008. Microstructural characterization and fracture behavior of a microhybrid and a nanofill composite. Dent Mater 24:1281–1288.

Ruddell DE, Maloney MM, Thompson JY. 2002. Effect of novel filler particles on the mechanical and wear properties of dental composites. Dent Mater 18:72–80.

Rueggeberg FA, Caughman WF, Curtis JW, Davis HC. 1993. Factors affecting cure at depths within light-activated resin composites. Am J Dent 6:91–95.

Ruyter IE, Øysæd H. 1982. Conversion in different depths of ultraviolet and visible light activated composite materials. Acta Odontol Scand 40:179–192.

Sabbagh J, Ryelandt L, Bacherius L, Biebuyck J-J, Vreven J, Lambrechts P, Leloup G. 2004. Characterization of the inorganic fraction of resin composites. J Oral Rehab 31:1090–1101.

Sideridou ID, Achilias DS. 2005. Elution study of unreacted Bis-GMA, TEGDMA, UDMA, and Bis-EMA from light-cured dental resins and resin composites using HPLC. J Biomed Mater Res Part B: Appl Biomater 74:617–626.

Stansbury JW, Dickens SH. 2001. Network formation and compositional drift during photo-initiated copolymerization of dimethacrylate monomers. Polymer 42:6363–6369.
Suzuki S, Leinfelder KF, Kawai K, Tsuchitani Y. 1995. Effect of particle variation on wear rates of posterior composites. Am J Dent 8:173–178.
Taylor DF, Kalachandra S, Sankarapandian M, McGrath JE. 1998. Relationship between filler and matrix resin characteristics and the properties of uncured composite pastes. Biomater 19:197–204.
Terry DA. 2004. Direct applications of a nanocomposites resin system. Part 1. The evolution of contemporary composite materials. Pract Proc Aesthet Dent 16:417–422.
Torno V, Soares P, Martin JMH., Mazur RF, Souza EM, Vieira S. 2008. Effects of irradiance, wavelength, and thermal emission of different light curing units on the knoop and Vickers hardness of a composite resin. J Biomed Mater Res Part B: Appl Biomater 85B:166–171.
Venhoven BAM, de Gee AJ, Werner A, Davidson CL. 1996. Influence of filler parameters on the mechanical coherence of dental restorative resin composites. Biomater 17:735–740.
Wagner HD, Vaia RA. 2004. Nanocomposites: Issues at the interface. Mater Today 7:38–42.
Watts DC, Amer O, Combe E. 1984. Characteristics of visible-light-activated composite systems. Br Dent J 156:209–215.
Watts DC, Cash AJ. 1994. Analysis of optical transmission by 400–500nm visible light into aesthetic dental materials. J Dent 22:112–117.
Xu HH, Quinn JB, Smith DT, Antonucci JM, Schumacher GE, Eichmiller FC. 2002. Dental resin composites containing silica-fused whiskers—effects of whisker-to-silica ratio on fracture toughness and indentation properties. Biomater 23:735–742.
Yearn JA. 1985. Factors affecting cure of visible light activated composites. Int Dent J 35:218–225.
Yoldas O, Akova T, Uysal H. 2004. Influence of different indentation load and dwell time on Knoop microhardness tests for composite materials. Polym Test 23:343–346.

Hindawi Publishing Corporation
International Journal of Dentistry
Volume 2012, Article ID 719452, 6 pages
doi:10.1155/2012/719452

Research Article

In Vitro Wound Healing Improvement by Low-Level Laser Therapy Application in Cultured Gingival Fibroblasts

Fernanda G. Basso,[1] Taisa N. Pansani,[2] Ana Paula S. Turrioni,[2] Vanderlei S. Bagnato,[3] Josimeri Hebling,[2] and Carlos A. de Souza Costa[2,4]

[1] *Faculdade de Odontologia de Piracicaba, Universidade Estadual de Campinas (UNICAMP), 13414-903 Piracicaba, SP, Brazil*
[2] *Faculdade de Odontologia de Araraquara, Universidade de Estadual Paulista (UNESP), 14801-903 Araraquara, SP, Brazil*
[3] *Instituto de Física de São Carlos, Universidade de São Paulo (USP), 13560-970 São Carlos, SP, Brazil*
[4] *Departamento de Fisiologia e Patologia, Faculdade de Odontologia de Araraquara, Universidade Estadual Paulista, Rua Humaitá, 1680, Centro, Caixa Postal: 331, 14801903 Araraquara, SP, Brazil*

Correspondence should be addressed to Carlos A. de Souza Costa, casouzac@foar.unesp.br

Received 4 April 2012; Revised 25 May 2012; Accepted 25 May 2012

Academic Editor: S. Nammour

The aim of this study was to determine adequate energy doses using specific parameters of LLLT to produce biostimulatory effects on human gingival fibroblast culture. Cells (3×10^4 cells/cm^2) were seeded on 24-well acrylic plates using plain DMEM supplemented with 10% fetal bovine serum. After 48-hour incubation with 5% CO_2 at 37°C, cells were irradiated with a InGaAsP diode laser prototype (LASERTable; 780 ± 3 nm; 40 mW) with energy doses of 0.5, 1.5, 3, 5, and 7 J/cm^2. Cells were irradiated every 24 h totalizing 3 applications. Twenty-four hours after the last irradiation, cell metabolism was evaluated by the MTT assay and the two most effective doses (0.5 and 3 J/cm^2) were selected to evaluate the cell number (trypan blue assay) and the cell migration capacity (wound healing assay; transwell migration assay). Data were analyzed by the Kruskal-Wallis and Mann-Whitney nonparametric tests with statistical significance of 5%. Irradiation of the fibroblasts with 0.5 and 3 J/cm^2 resulted in significant increase in cell metabolism compared with the nonrradiated group ($P < 0.05$). Both energy doses promoted significant increase in the cell number as well as in cell migration ($P < 0.05$). These results demonstrate that, under the tested conditions, LLLT promoted biostimulation of fibroblasts in vitro.

1. Introduction

Tissue healing involves an intense activity of diverse cell types, such as epithelial and endothelial cells, as well as fibroblasts which play a key role in this process [1]. Fibroblasts secrete multiple growth factors during wound reepitelialization and participate actively in the formation of granulation tissue and the synthesis of a complex extracellular matrix after reepitelialization [1]. All these processes directly involve the proliferation and migration capacity to these cells [1]. The use of low-level laser therapy (LLLT) has been proposed to promote biostimulation of fibroblasts and accelerate the healing process [2].

Previous studies have evaluated the effect of LLLT on the proliferation and migration of human gingival fibroblasts as well as other cellular effects and responses, such as protein production and growth factor expression [2–6]. Nevertheless, there is a shortage of studies investigating irradiation parameters capable of promoting biostimulatory effects on fibroblasts in order to establish an ideal irradiation protocol for these cells [7]. Therefore, the aim of this study was to determine the most adequate energy doses using specific parameters of LLLT to produce biostimulatory effects on human gingival fibroblast cultures in an in vitro wound healing model.

2. Material and Methods

2.1. Gingival Fibroblast Cell Culture. All experiments were performed using human gingival fibroblast cell culture (continuous cell line; Ethics Committee 64/99-Piracicaba

Dental School, UNICAMP, Brazil). The fibroblast cells were cultured in Dulbecco's Modified Eagle's Medium (DMEM; Sigma-Aldrich, St. Louis, MO, USA) supplemented with 10% fetal bovine serum (FBS; Gibco, Grand Island, NY, USA), with 100 IU/mL penicillin, 100 μg/mL streptomycin, and 2 mmol/L glutamine (Gibco, Grand Island, NY, USA) in an humidified incubator with 5% CO_2 and 95% air at 37°C (Isotemp; Fisher Scientific, Pittsburgh, PA, USA) [8]. The cells were subcultured every 2 days in the incubator under the conditions described above until an adequate number of cells were obtained for the study. The cells (3×10^4 cells/cm^2) were then seeded on sterile 24-well acrylic plates using plain DMEM supplemented with 10% FBS for 48 h.

2.2. LLLT on Fibroblast Culture. The LLLT device used in this study was a near infrared indium gallium arsenide phosphide (InGaAsP) diode laser prototype (LASERTable; 780 ± 3 nm wavelength, 0.04 W maximum power output), which was specifically designed to provide a uniform irradiation of each well (2 cm^2) in which cultured cells are seeded [8, 9]. The power loss through the acrylic plate was calculated using a potentiometer (Coherent LM-2 VIS High-Sensitivity Optical Sensor, USA), which was placed inside the culture plate. After this measure, the power loss of the plate was determined as 5%. After that, the power of all diodes was checked and standardized. Therefore, a final power of 0.025 W reached the cultured cells. This standardization was performed as previously described in the literature [8, 9]. For the evaluation of cell metabolism, the radiation originated from the LASERTable was delivered on the base of each 24-well plate with energy doses of 0.5, 1.5, 3, 5, and 7 J/cm^2, and irradiation times of 40, 120, 240, 400, and 560 s, respectively. The laser light reached the cells on the bottom of each well with a final power of 0.025 W because of the loss of optical power in each well due to the interposition of the acrylic plate. The cells were irradiated every 24 h totalizing 3 applications during 3 consecutive days. The cells assigned to control groups received the same treatment as that of the experimental groups. The 24-well plates containing the control cells were maintained at the LASERTable for the same irradiation times used in the respective irradiated groups, though without activating the laser source (sham irradiation) [8, 9]. Twenty-four hours after the last irradiation (active or sham), the metabolic activity of the cells was evaluated using the MTT assay (described below). Based on cell metabolism results, the two most effective irradiation doses were selected to evaluate the cell number (trypan blue assay), cell migration capacity by using the wound healing assay (qualitative analysis) and the transwell migration assay (quantitative analysis), as described below.

2.3. Analysis of Cell Metabolism (MTT Assay). Cell metabolism was evaluated using the methyltetrazolium (MTT) assay [8–10]. This method determines the activity of succinic dehydrogenase (SDH) enzyme, which is a measure of cellular (mitochondrial) respiration and can be considered as the metabolic rate of cells.

Each well with the fibroblasts received 900 μL of DMEM plus 100 μL of MTT solution (5 mg/mL sterile PBS). The cells were incubated at 37°C for 4 h. Thereafter, the culture medium (DMEM; Sigma Chemical Co., St. Louis, MO, USA) with the MTT solution were aspirated and replaced by 700 μL of acidified isopropanol solution (0.04 N HCl) in each well to dissolve the violet formazan crystals resulting from the cleavage of the MTT salt ring by the SDH enzyme present in the mitochondria of viable cells, producing a homogenous bluish solution. Three 100 μL aliquots of each well were transferred to a 96-well plate (Costar Corp., Cambridge, MA, USA). Cell metabolism was evaluated by spectrophotometry as being proportional to the absorbance measured at 570 nm wavelength with an ELISA plate reader (Thermo Plate, Nanshan District, Shenzhen, China) [8, 9]. The values obtained from the three aliquots were averaged to provide a single value. The absorbance was expressed in numerical values, which were subjected to statistical analysis to determine the effect of LLLT on the mitochondrial activity of the cells.

2.4. Viable Cell Counting (Trypan Blue Assay). Trypan blue assay was used to evaluate the number of cells in the culture after LLLT application. This test provides a direct assessment of the total number of viable cells in the samples as the trypan blue dye can penetrate only porous, permeable membranes of lethally damaged (dead) cells, which is clearly detectable under optical microscopy [11]. The LLLT protocol was undertaken as previously described using energy doses of 0.5 and 3 J/cm^2. Cell counting was performed in the experimental and control groups 24 h after the last irradiation (active or sham). The DMEM in contact with the cells was aspirated and replaced by 0.12% trypsin (Invitrogen, Carlsbad, CA, USA), which remained in contact with the cells for 10 min to promote their detachment from the acrylic substrate. Then, 50 μL aliquots of this cell suspension were added to 50 μL of 0.04% trypan blue dye (Sigma Aldrich Corp., St. Louis, MO, USA), and the resulting solution was maintained at room temperature for 2 min so that the trypan blue dye could pass through the cytoplasmic membrane of the nonviable cells, changing their color into blue. Ten microliters of the solution were taken to a hemocytometer and examined with an inverted light microscope (Nikon Eclipse TS 100, Nikon Corporation, Tokyo, Japan) to determine the number of total cells and nonviable cells. The number of viable cells was calculated by deducting the number of nonviable cells from the number of total cells [8]. The number of cells obtained in the counting corresponded to $n \times 10^4$ cells per milliliter of suspension.

2.5. Cell Migration

2.5.1. Wound Healing Assay. The wound healing assay was used because it is a classic method of evaluation in vitro tissue healing assays [12, 13]. After 48 h of cell culture, a sterile 5 mL pipette tip was used to make a straight scratch on the monolayer of cells attached to the acrylic substrate, simulating a wound. Formation of the in vitro wound

was confirmed under an inverted microscope (TS 100, Nikon, Tokyo, Japan). The LLLT protocol was undertaken as previously described using energy doses of 0.5 and 3 J/cm^2. Twenty-four hours after the last irradiation, the cells were fixed in 1.5% glutaraldehyde for 1 h, stained with 0.1% violet crystal for 15 min, and washed twice with distilled water. Wound repopulation was assessed with a light microscope (Olympus BX51, Miami, FL, USA) equipped with a digital camera (Olympus C5060, Miami, FL, USA).

2.5.2. Transwell Migration Assay. The capacity of human gingival fibroblasts to migrate through a cell permeable membrane was assessed using 6.5 mm-diameter transwell chambers (Corning Costar, Cambridge, MA, USA) with polycarbonate membrane inserts (8 μm pore size) [14]. The chambers were placed in 24-well plates containing 1 mL of plain DMEM per well. The cells were seeded onto the upper compartment of the chamber (1.5×10^4 cells/cm^2) and incubated at 37°C for 48 h. After this period, the LLLT protocol was undertaken as previously described using energy doses of 0.5 and 3 J/cm^2. Twenty-four hours after the last irradiation (active or sham), the cells that had migrated through the membrane to the lower compartment of the chamber were fixed in 1.5% glutaraldehyde for 1 h, incubated with 0.1% violet crystal dye for 15 min, and washed twice with distilled water. After the last wash, the stained cells were viewed under a light microscope (Olympus BX51, Miami, FL, USA) equipped with a digital camera (Olympus C5060, Miami, FL, USA) and photomicrographs from three randomly chosen fields were taken at ×10 magnification for counting the number of migrated cells using the image-analysis J 1.45S software (Wayne Rasband, National Institutes of Health, Bethesda, MD, USA). Two samples of each group were evaluated and the experiment was performed in triplicate.

2.6. Analysis of Migrated Cells by Scanning Electron Microscopy (SEM). Part of the specimens used in the transwell migration assay was also used for the analysis of the cells by SEM. Twenty-four hours after the last irradiation (active or sham), the culture medium was aspirated and the transwell inserts were fixed in 1 mL of 2.5% glutaraldehyde in PBS for 2 h. Then, the glutaraldehyde solution was aspirated and the cells adhered to the transwell inserts were washed with PBS and distilled water two consecutive times (5 min each) and then dehydrated in a series of increasing ethanol concentrations (30, 50 and 70%, one time for 30 min each; 95 and 100%, two times for 60 min each) and covered 3 times with 200 μL of 1,1,1,3,3,3-hexamethyldisilazane (HMDS; Sigma Aldrich Corp., St. Louis, USA) [8]. The transwell inserts were stored in a desiccator for 24 h, sputter-coated with gold, and the morphology of the surface-adhered cells was examined with a scanning electron microscope (JMS-T33A scanning microscope, JEOL, Tokyo, Japan).

2.7. Statistical Analysis. Data from MTT, Trypan blue and Transwell assay had a nonnormal distribution (Kolmogorov-Smirnov, $P < 0.05$) and were analyzed by the Kruskal-Wallis and Mann-Whitney nonparametric tests. A significance level of 5% was set for all analyses.

Table 1: Succinate dehydrogenase enzyme (SDH) production by human gingival fibroblasts detected by the MTT assay according to the energy dose used in the low-level laser therapy.

Energy dose (J/cm^2)	MTT (%)
0 (control)	100 (96–104) C*
0.5	111 (110–113) B
1.5	94 (92–97) D
3	117 (113–119) A
5	95 (81–108) CD
7	92 (91–96) D

Values expressed as medians of SDH production (P25–P75) ($n = 12$). *Same letters indicate no statistically significant difference (Mann-Whitney, $P > 0.05$).

Table 2: Number of viable cells (%) detected by the trypan blue assay, according to the energy doses used in the low-level laser therapy.

Energy dose (J/cm^2)	Number of viable cells (%)
0 (control)	100 (95–104) B*
0.5	133 (112–175) A
3	168 (149–181) A

Values expressed as medians of SDH production (P25–P75) ($n = 8$). *Same letters indicate no statistically significant difference (Mann-Whitney, $P > 0.05$).

3. Results

3.1. Analysis of Cell Metabolism (MTT Assay). Data from SDH production by human gingival fibroblast cultures (MTT assay) after LLLT, according to the energy dose are presented in Table 1.

Regarding the energy dose of 5 J/cm^2 no statistically significant difference between the irradiated group and the nonirradiated control group was observed ($P > 0.05$). Conversely, irradiation of the fibroblast cultures with doses of 0.5 J/cm^2 and 3 J/cm^2 resulted in 11% and 17% increases in cell metabolism, respectively, differing significantly from the control group ($P < 0.05$). The cells irradiated with 1.5 J/cm^2 and 7 J/cm^2 presented the lowest metabolic rate compared with the nonirradiated control group (6% and 8% decrease, resp., $P < 0.05$).

3.2. Viable Cell Counting (Trypan Blue Assay). The number of viable cells (%) after LLLT application, according to the energy dose, is presented in Table 2.

Comparison among the energy doses revealed that irradiation of the human gingival fibroblast cultures with 0.5 J/cm^2 and 3 J/cm^2 increased the number of viable cells by 31% and 66%, respectively, differing significantly from the control ($P < 0.05$), but without statistically significant difference between each other ($P > 0.05$).

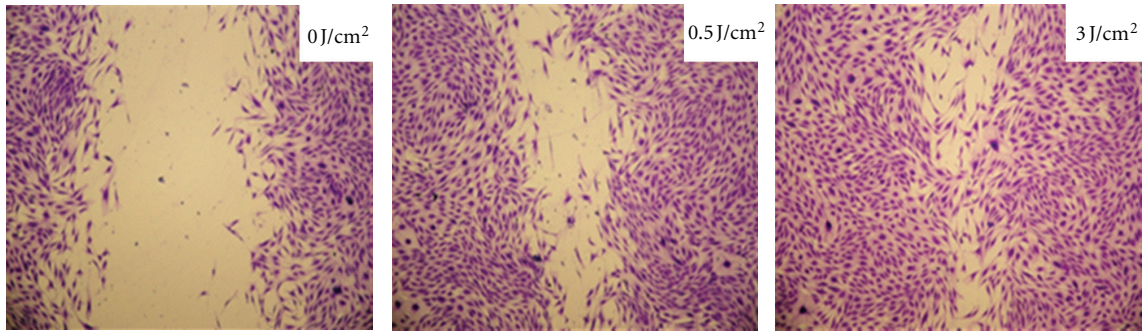

Figure 1: Photomicrographs showing human gingival fibroblast cultures seeded in 24-well plates after LLLT. The control group exhibits a large cell-free area on acrylic surface. The group irradiated with 0.5 J/cm^2 exhibits cell proliferation and migration, with consequent reduction of the "in vitro wound" size. The group irradiated with 3.0 J/cm^2 presented more intense cell proliferation and migration, resulting in almost complete closure of the "in vitro wound."

Table 3: Cell migration (%) by the transwell assay, according to the energy dose used in the low-level laser therapy.

Energy dose (J/cm^2)	Cell migration (%)
0 (control)	100 (91–107) B*
0.5	118 (109–123) A
3	120 (116–122) A

Values expressed as medians of SDH production (P25–P75) ($n = 6$). *Same letters indicate no statistically significant difference (Mann-Whitney, $P > 0.05$).

3.3. Fibroblast Migration

3.3.1. Wound Healing Assay. The analysis of the monolayer of human gingival fibroblasts after irradiation of the "in vitro wound" showed more intense cell migration, with consequent better coverage of the substrate (wound repopulation) (Figure 1).

3.3.2. Transwell Assay. Data from the transwell assay after LLLT, according to the energy dose are, presented in Table 3.

Comparison among the energy doses revealed that irradiation of the human gingival fibroblast cultures with 0.5 J/cm^2 and 3 J/cm^2 increased cell migration by 16% and 18%, respectively, differing significantly from the control ($P < 0.05$), but without statistically significant difference between each other ($P > 0.05$).

3.4. Analysis of Migrated Cells by Scanning Electron Microscopy (SEM). The SEM analysis of the transwell inserts, which complemented the viable cell counting by the trypan blue assay, revealed that the fibroblasts were capable of migrating through the transwell membrane. The cells obtained from human gengiva did not change their morphology after been submitted to LLLT (Figure 2).

4. Discussion

Different LLLT modalities have been used for diverse treatments in the health fields. In Dentistry, LLLT has been widely investigated and indicated for accelerating the healing process, especially in the treatment of ulcerative oral mucosa lesions [15, 16].

Several in vitro studies have evaluated the effect of LLLT on healing [7, 17]. Nevertheless, current research involving irradiation of cell cultures has not yet established the irradiation patterns specific for the different cell lines. Establishing the ideal irradiation parameters and techniques is mandatory for the development of sequential studies that can determine the potential biostimulatory effect of LLLT on oral mucosa cells, such as keratinocytes and fibroblasts, which are directly involved in the local healing process.

In the present study, the metabolic activity of human gingival fibroblast cultures after LLLT with different energy doses was evaluated to determine the adequate doses to produce biostimulatory effects on these cells in vitro. The results for SDH production showed that the 0.5 and 3 J/cm^2 doses increased cell metabolism. Therefore, these two most effective irradiation doses were selected to evaluate the number of viable cells as well as the cell migration capacity. The increase of SDH production after irradiation of gingival fibroblasts has also been observed by Damante et al. [18], using a similar laser prototype to the one used in the present study. In the same way as in the present study, the SDH production results also served as guide for subsequent experiments that evaluated the expression of growth factors by cultured fibroblasts.

In the present study, a significant increase in the number of viable cells that presented normal morphological characteristics (SEM analysis) was observed after LLLT using doses of 0.5 and 3 J/cm^2. These results confirm those of previous laboratory investigations in which LLLT with the same wavelength as that of the present study (780 nm) increased the proliferation of gingival fibroblasts [19, 20]. Kreisler et al. [2] also reported increase of fibroblast cell culture in vitro after direct and consecutive low level laser irradiations. The mechanism by which LLLT can promote biostimulation and induce proliferation of different cell types remains a controversial subject [20, 21]. Some authors [21, 22] claim that this mechanism is derived from light absorption by the enzyme cytochrome c oxidase in the cells, which participates in the cascade of oxidative respiration.

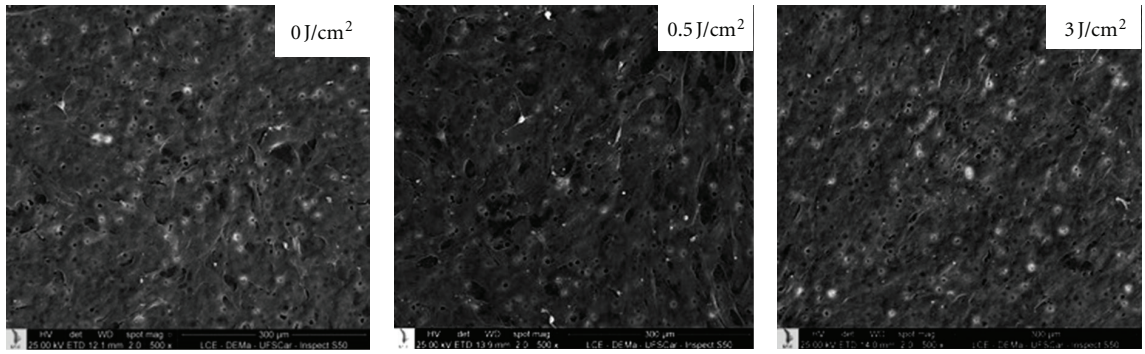

Figure 2: SEM micrograph showing cells with normal morphology that migrated through the transwell membrane. SEM ×500.

Eells et al. [23] demonstrated the increase in the production of this enzyme after different LLLT application of cell cultures. It has also been suggested that the mechanism of cell proliferation induced by LLLT might be derived from the activation of singling pathways, such as the MAPK and PI3K/Akt pathways, which control both cell proliferation and regulation of gene expression [21, 24].

Fibroblast cell migration and proliferation are essential events for tissue healing and are directly related with its success [1, 3]. In the present study, the effect of LLLT on the capacity of gingival fibroblast migration, using two energy doses capable of increasing cell metabolism (0.5 and 3 J/cm^2), was evaluated qualitatively, by the wound healing assay, and quantitatively, by the transwell migration assay. Both methodologies demonstrated that LLLT was able to increase the migration capacity of fibroblasts and the quantitative analysis of the results revealed no significant difference between the energy doses. These results are in accordance with those of previous investigations [7, 17], but studies using the transwell migration method to evaluate the LLLT on cell cultures are still scarce. This methodology is relevant because it measures the number of cells that can pass through the transwell membrane inserts, demonstrating their migration capacity after stimulation by LLLT.

Diverse mechanisms are involved in cell migration during tissue healing, including expression and secretion of growth factors [1]. Previous studies demonstrated that LLLT may cause positive effects on cells by increasing growth factor expression, which could be a form of action of specific laser parameters on cell migration [2, 25]. A recent study of our research group demonstrated that LLLT had a biostimulatory effect on epithelial cells in vitro by increasing their metabolic activity, number of viable cells and expression of growth factors [8]. In the present paper, the biostimulation of human gingival fibroblast cultures by LLLT with consequent increase in the number of viable cells and cell migration capacity demonstrates the efficacy of specific laser parameters and irradiation technique on the healing process. In addition, the obtained results are supportive to those of previous in vivo studies in which acceleration of the healing process was observed after LLLT [15, 16, 26], but the limitations of an in vitro experiment should be considered.

In conclusion, the findings of the present study demonstrated that the preset laser parameters in combination with the sequential irradiation technique caused biostimulation, proliferation, and migration of human gingival fibroblast cultures. These encouraging laboratory outcomes should guide forthcoming studies involving tissue irradiation with laser and its effects on in vivo tissue healing.

Acknowledgments

The authors acknowledge the Fundação de Amparo à Pesquisa do Estado de São Paulo-FAPESP (Grants: 2009/54722-1 and BP.DR: 2009/52326-1) and the Conselho Nacional de Desenvolvimento Científico e Tecnológico—CNPq (Grant: 301029/2010-1) for the financial support.

References

[1] L. Häkkinen, V. J. Uitto, and H. Larjava, "Cell biology of gingival wound healing," *Periodontology 2000*, vol. 24, no. 1, pp. 127–152, 2000.

[2] M. Kreisler, A. B. Christoffers, H. Al-Haj, B. Willershausen, and B. D'Hoedt, "Low level 809-nm diode laser-induced in vitro stimulation of the proliferation of human gingival fibroblasts," *Lasers in Surgery and Medicine*, vol. 30, no. 5, pp. 365–369, 2002.

[3] W. Posten, D. A. Wrone, J. S. Dover, K. A. Arndt, S. Silapunt, and M. Alam, "Low-level laser therapy for wound healing: mechanism and efficacy," *Dermatologic Surgery*, vol. 31, no. 3, pp. 334–340, 2005.

[4] I. Saygun, S. Karacay, M. Serdar, A. U. Ural, M. Sencimen, and B. Kurtis, "Effects of laser irradiation on the release of basic fibroblast growth factor (bFGF), insulin like growth factor-1 (IGF-1), and receptor of IGF-1 (IGFBP3) from gingival fibroblasts," *Lasers in Medical Science*, vol. 23, no. 2, pp. 211–215, 2008.

[5] M. D. Skopin and S. C. Molitor, "Effects of near-infrared laser exposure in a cellular model of wound healing," *Photodermatology Photoimmunology and Photomedicine*, vol. 25, no. 2, pp. 75–80, 2009.

[6] S. S. Hakki and S. B. Bozkurt, "Effects of different setting of diode laser on the mRNA expression of growth factors and type I collagen of human gingival fibroblasts," *Lasers in Medical Science*, vol. 27, no. 2, pp. 325–331, 2012.

[7] P. V. Peplow, T. Y. Chung, and G. D. Baxter, "Laser photobiomodulation of proliferation of cells in culture: a review of human and animal studies," *Photomedicine and Laser Surgery*, vol. 28, supplement 1, pp. S3–S40, 2010.

[8] F. G. Basso, C. F. Oliveira, C. Kurachi, J. Hebling, and C. A. Costa, "Biostimulatory effect of low-level laser therapy on keratinocytes in vitro," *Lasers in Medical Science*. In press.

[9] C. F. Oliveira, F. G. Basso, E. C. Lins et al., "In vitro effect of low-level laser on odontoblast-like cells," *Laser Physics Letters*, vol. 8, no. 2, pp. 155–163, 2011.

[10] T. Mosmann, "Rapid colorimetric assay for cellular growth and survival: application to proliferation and cytotoxicity assays," *Journal of Immunological Methods*, vol. 65, no. 1-2, pp. 55–63, 1983.

[11] C. Wiegand and U. Hipler, "Methods for the measurement of cell and tissue compatibility including tissue regeneration process," *GMS Krankenhaushygiene Interdisziplinär*, vol. 3, no. 1, pp. 1863–5245, 2008.

[12] A. M. Hoang, T. W. Oates, and D. L. Cochran, "In vitro wound healing responses to enamel matrix derivative," *Journal of Periodontology*, vol. 71, no. 8, pp. 1270–1277, 2000.

[13] C. C. Liang, A. Y. Park, and J. L. Guan, "In vitro scratch assay: a convenient and inexpensive method for analysis of cell migration in vitro," *Nature Protocols*, vol. 2, no. 2, pp. 329–333, 2007.

[14] M. Cáceres, A. Romero, M. Copaja, G. Díaz-Araya, J. Martínez, and P. C. Smith, "Simvastatin alters fibroblastic cell responses involved in tissue repair," *Journal of Periodontal Research*, vol. 46, no. 4, pp. 456–463, 2011.

[15] A. Chor, A. M. de Azevedo, A. Maiolino, and M. Nucci, "Successful treatment of oral lesions of chronic lichenoid graft-vs.-host disease by the addition of low-level laser therapy to systemic immunosuppression," *European Journal of Haematology*, vol. 72, no. 3, pp. 222–224, 2004.

[16] M. M. F. Abramoff, N. N. F. Lopes, L. A. Lopes et al., "Low-level laser therapy in the prevention and treatment of chemotherapy-induced oral mucositis in young patients," *Photomedicine and Laser Surgery*, vol. 26, no. 4, pp. 393–400, 2008.

[17] L. D. Woodruff, J. M. Bounkeo, W. M. Brannon et al., "The efficacy of laser therapy in wound repair: a meta-analysis of the literature," *Photomedicine and Laser Surgery*, vol. 22, no. 3, pp. 241–247, 2004.

[18] C. A. Damante, G. De Micheli, S. P. H. Miyagi, I. S. Feist, and M. M. Marques, "Effect of laser phototherapy on the release of fibroblast growth factors by human gingival fibroblasts," *Lasers in Medical Science*, vol. 24, no. 6, pp. 885–891, 2009.

[19] L. Almeida-Lopes, J. Rigau, R. A. Zângaro, J. Guidugli-Neto, and M. M. M. Jaeger, "Comparison of the low level laser therapy effects on cultured human gingival fibroblasts proliferation using different irradiance and same fluence," *Lasers in Surgery and Medicine*, vol. 29, no. 2, pp. 179–184, 2001.

[20] K. M. AlGhamdi, A. Kumar, and N. A. Moussa, "Low-level laser therapy: a useful technique for enhancing the proliferation of various cultured cells," *Lasers in Medical Science*, vol. 27, no. 1, pp. 237–249, 2011.

[21] X. Gao and D. Xing, "Molecular mechanisms of cell proliferation induced by low power laser irradiation," *Journal of Biomedical Science*, vol. 16, article 4, 2009.

[22] T. I. Karu, L. V. Pyatibrat, S. F. Kolyakov, and N. I. Afanasyeva, "Absorption measurements of a cell monolayer relevant to phototherapy: reduction of cytochrome c oxidase under near IR radiation," *Journal of Photochemistry and Photobiology B*, vol. 81, no. 2, pp. 98–106, 2005.

[23] J. T. Eells, M. M. Henry, P. Summerfelt et al., "Therapeutic photobiomodulation for methanol-induced retinal toxicity," *Proceedings of the National Academy of Sciences of the United States of America*, vol. 100, no. 6, pp. 3439–3444, 2003.

[24] L. Zhang, D. Xing, X. Gao, and S. Wu, "Low-power laser irradiation promotes cell proliferation by activating PI3K/Akt pathway," *Journal of Cellular Physiology*, vol. 219, no. 3, pp. 553–562, 2009.

[25] L. H. Azevedo, F. De Paula Eduardo, M. S. Moreira, C. De Paula Eduardo, and M. M. Marques, "Influence of different power densities of LILT on cultured human fibroblast growth: a pilot study," *Lasers in Medical Science*, vol. 21, no. 2, pp. 86–89, 2006.

[26] K. M. Lagan, B. A. Clements, S. McDonough, and G. A. Baxter, "Low intensity laser therapy (830 nm) in the management of minor postsurgical wounds: a controlled clinical study," *Lasers in Surgery and Medicine*, vol. 28, no. 1, pp. 27–32, 2001.

Laser Phys. **23** (2013) 066003 (6pp) doi:10.1088/1054-660X/23/6/066003

In vivo photothermal tumour ablation using gold nanorods

L F de Freitas[1], L C Zanelatto[2], M S Mantovani[2], P B G Silva[2], R Ceccini[3], C Grecco[4], L T Moriyama[4], C Kurachi[4], V C A Martins[5] and A M G Plepis[1,5]

[1] Programa de Pós Graduação Interunidades Bioengenharia—FMRP/EESC/IQSC, Universidade de São Paulo, Brazil
[2] Laboratório de Genética Toxicológica, Universidade Estadual de Londrina, Brazil
[3] Departamento de Patologia, Universidade Estadual de Londrina, Brazil
[4] Instituto de Física de São Carlos, Universidade de São Paulo, Brazil
[5] Instituto de Química de São Carlos, Universidade de São Paulo, Brazil

E-mail: lucasfreitas@usp.br

Received 4 October 2012, in final form 6 December 2012
Accepted for publication 15 March 2013
Published 30 April 2013
Online at stacks.iop.org/LP/23/066003

Abstract
Less invasive and more effective cancer treatments have been the aim of research in recent decades, e.g. photothermal tumour ablation using gold nanorods. In this study we investigate the cell death pathways activated, and confirm the possibility of CTAB-coated nanoparticle use *in vivo*. Nanorods were synthesized by the seeding method; some of them were centrifuged and washed to eliminate soluble CTAB. The MTT cytotoxicity test was performed to evaluate cytotoxicity, and the particles' viability after their synthesis was assessed. Once it had been observed that centrifuged and washed nanorods are harmless, and that nanoparticles must be used within 48 h after their synthesis, *in vivo* hyperthermic treatment was performed. After irradiation, a tumour biopsy was subjected to a chemiluminescence assay to evaluate membrane lipoperoxidation, and to a TRAP assay to evaluate total antioxidant capacity. There was a 47 °C rise in temperature observed at the tumour site. Animals irradiated with a laser (with or without nanorods) showed similar membrane lipoperoxidation, more intense than in control animals. The antioxidant capacity of experimental animal tumours was elevated. Our results indicate that necrosis is possibly the cell death pathway activated in this case, and that nanorod treatment is worthwhile.

1. Introduction

Cancer, a very common disorder, is characterized by an abnormal cell growth rate and a high metabolic demand; despite all advances obtained in this research field, current treatments are often degrading, expensive and do not guarantee complete elimination of tumours. This fact instigates the search for more effective and less invasive therapeutic interventions.

In recent decades, a significant effort has been made to develop treatments based on light and its interaction with cells (Atif *et al* 2011). The desired effect of the interaction between electromagnetic waves and tissues is, most of the time, hyperthermia, which can be accessed directly or with adjuvant devices (Bartczak *et al* 2011, Zhao *et al* 2011, Dombrovsky *et al* 2012), such as metals and their plasmonic surfaces (Pustovalov 2011).

It has been observed that hyperthermia promotes changes in membrane conformation and permeability, but little is known about the relation between these alterations and the cell death rates observed after the treatment. Besides, cytoskeleton alterations are also seen after hyperthermic stimulus, causing cell deformities and cell cycle deregulations. There is also aggregation of denatured nuclear proteins on nuclear matrix, which leads to impaired cellular functions, i.e. DNA and RNA synthesis and repair (Hildebrandt *et al* 2002).

In vitro studies are most frequently performed, and have shown that just a few seconds of laser irradiation in the near infrared are enough to compromise the plasma membrane integrity of tumour cells (Burke *et al* 2012), with almost no damage to non-malignant cells (Lapotko *et al* 2006b, 2006a).

Finally, hyperthermia is capable of initiating cell death, whether by apoptosis (programmed cell death) or by necrosis, but the exact mechanism of cell death triggering is not completely known. Research indicates a rise in p53 protein activity in hyperthermically treated cells. This protein constitutes one of the most important initiators of the apoptosis cascade, and is synthesized in great amounts due to apoptotic stimuli (Hildebrandt *et al* 2002). Membrane blebbing, very common after hyperthermic interventions, can initiate apoptosis, but the signalling pathway still remains unclear (Lapotko *et al* 2006b, 2006a).

The cell death rates can be enhanced if adjuvant devices are used in hyperthermic therapy. Among all adjuvant devices that can be used, metallic nanoparticles, mainly silver and gold ones, are very promising due to low toxicity, conformational flexibility and plasmonic resonance with the visible and near infrared regions of the light spectrum. This last property allows heat generation through electromagnetic irradiation (Du *et al* 2011).

A new conformation of metallic nanoparticles has attracted the attention of researchers: gold nanorods (Wei *et al* 2004). They are easily synthesized from pre-formed gold nanospheres, and present a greater area of interaction with near infrared light per unit volume compared to other particle shapes. They are usually coated with cetyltrimethylammonium bromide (CTAB), a very toxic compound (Huff *et al* 2007a, 2007b). To prevent generalized toxicity, it is common to modify the coating of gold nanoparticles to more biotolerated molecules, such as polyethylene glycol and chitosan (Huff *et al* 2007a, 2007b, Hansen *et al* 2008). There are a few data in the literature, however, indicating that surface-coating CTAB is not toxic like CTAB free in solution (Alkilany *et al* 2012).

Based on all this, we propose the investigation of CTAB-coated gold nanorods in hyperthermic treatment of tumours in an animal model, regarding its possibility of use and its efficacy as well as its mechanism of action.

2. Methods

2.1. Experimental animals

24 male Swiss mice, with 30–40 g body weight, were inoculated with Ehrlich tumour cells and divided into four experimental groups. The control group was composed of six tumour-bearing animals which were administered with sterile saline solution instead of nanorods, and were not irradiated with a near infrared laser. Group N consisted of six animals which were administered nanorods, but were not irradiated with a near infrared laser; group L was composed of six animals which did not receive nanorods, but were irradiated with a near infrared laser; finally, group H was composed of six animals that received gold nanorods and were treated hyperthermically with a near infrared laser. Another two mice were used to maintain the tumour cells.

2.2. Gold nanorod synthesis

2.2.1. Seed synthesis. 5 ml of a 0.2 mol l^{-1} CTAB solution were mixed with 5 ml of a 5×10^{-4} mol l^{-1} auric chloride solution. After a gentle stirring, 600 μl of a 0.01 mol l^{-1} sodium borohydride was added, and the solution was stirred for 2 min. The solution was then left to stand for 6 h at 25 °C in the dark. It was stocked in dark flasks until being used in nanorod synthesis (Murphy and Jana 2002).

2.2.2. Nanorod synthesis. 200 μl of a 0.004 mol l^{-1} silver nitrate was mixed with 5 ml of a 0.2 mol l^{-1} CTAB solution and 5 ml of 0.001 mol l^{-1} auric chloride. The solution was gently stirred, and 70 μl of 0.0788 mol l^{-1} ascorbic acid added to reduce gold, leaving the solution colourless. Finally, 12 μl of seed suspension were added, and the solution was left to stand for 15 min at 27 °C in the dark. The solution goes from colourless to wine coloured within this time. The average size of the obtained nanorods was 4.92 $\pm$ 0.82 nm in diameter and 52.64 $\pm$ 4.91 nm in length, as observed in scanning electron microscopy measurements. This method was first described by Murphy and Jana (2002).

2.2.3. Seed influence on nanorod synthesis. In order to evaluate the influence of the seeds on nanorods, they were used after 24, 48, 72 and 96 h of their synthesis. The absorption spectra of nanorods and seeds were analysed in a spectrophotometer, from 200 to 1000 nm.

2.3. MTT cytotoxicity assay

The MTT (3-(4,5-dimethylthiazol-2-yl)-2,5-diphenyltetrazolium bromide) cytotoxicity assay (Mosmann 1983) was performed to evaluate the toxicity of nanorods coated with CTAB. Four different cell lines were used: HTC (derived from rat hepatoma), HT-29 (from human colon cancer), HepG2 (from human hepatoma) and 786-O cells (from human renal cancer). All cell lines were grown in culture flasks containing DMEM culture media (Gibco) with 10% bovine foetal serum (Gibco), and maintained in 5% CO_2 atmosphere. In these conditions, the cell cycle is completed in about 24 h.

In this experiment, centrifuged (CTAB-free) and not centrifuged (with CTAB in the media) solutions of nanorods were tested. Concentrations from 2×10^{-7} to 2×10^{-3} μl of nanorod solution per μl of DMEM media were used for non-centrifuged solution, and from 0.01 to 0.2 μl μl^{-1} of DMEM media for CTAB-free solution. 0.125 mg ml^{-1} doxorubicin was used as a cytotoxicity control.

2.4. Ehrlich tumour inoculation

A solution containing 2.0×10^6 tumour cells was inoculated subcutaneously in the left inguinal region of mice (Kuroda *et al* 1976). When the tumour diameter was about 10 mm, hyperthermic treatment was performed.

2.5. Hyperthermic treatment

When the tumours were 10 mm sized, 100 μl of centrifuged nanorod solution, at a 0.5 optical density, were administered through the tail vein. Group L animals received 100 μl of sterile saline solution. 72 h later, mice were anaesthetized with 10 mg xylazine and 100 mg ketamine per kg of body weight. The tumour region of L and H group mice was irradiated with a near infrared (808 nm, 2 W cm^{-2}) laser for 5 min (O'Neal *et al* 2004). The temperatures of the tumour and of the peritumoral regions were measured. After the treatment, the tumour was collected and stored in liquid nitrogen until the biochemical tests were performed.

2.6. Oxidative stress and antioxidant parameter verification

2.6.1. Tert-butyl hydroxide-initiated chemiluminescence assay. Tert-butyl hydroperoxide reacts with membrane lipids previously oxidized by nitrogen or oxygen reactive species, and this reaction's product is an unstable compound, which liberates photons in order to stabilize itself. Those photons can be detected with a luminometer. For this assay, tumours collected from mice were homogenized in phosphate buffer, at a 10% dilution. This suspension was centrifuged at 3000 rpm for 10 min, and 1 ml of the supernatant was mixed with tert-butyl hydroperoxide. The results are expressed in relative units of luminescence (Flecha *et al* 1990).

2.6.2. Total antioxidant capacity assessment. Total antioxidant capacity of tumour cells was assessed by the TRAP assay (Wayner *et al* 1985), which is based on the defensive action of antioxidants to an oxidative challenge. The oxidant compound, in this case, is 2,2′ azo-bis (2-amidinopropane) (ABAP), a peroxyl radical generator. The generation of peroxyl radicals emits light that can also be detected in a luminometer. For this assay, the same cell solution as prepared for the chemiluminescence assay was used. The results are expressed as equivalent μM of Trolox per mg of proteins.

2.6.3. Statistical analysis. Chemiluminescence curves were tested by two-way ANOVA, with Bonferroni post-test, and the differences were considered significant when the p value was less than 0.05.

For other results, one-way ANOVA was used, and the significance conditions were the same.

3. Results

3.1. Seed influence on nanorod synthesis

After 48 h of the seed synthesis, the absorption peak necessary for hyperthermic treatment tends to be blue-shifted, until it fuses with the smaller absorption peak. Before 48 h, there is no difference from the resonance peaks (figure 1). The most blue-shifted absorption spectra observed for the nanoparticles is similar to the spectra of larger nanospheres (Murphy and Jana 2002).

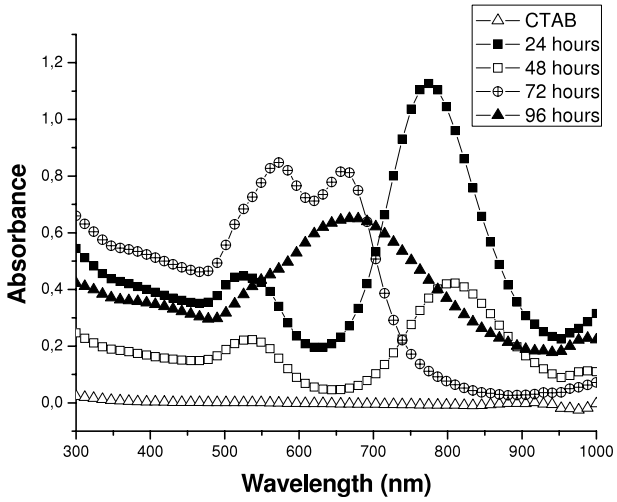

Figure 1. Absorption spectra of nanorods synthesized after 24, 48, 72 and 96 h of seed assembly.

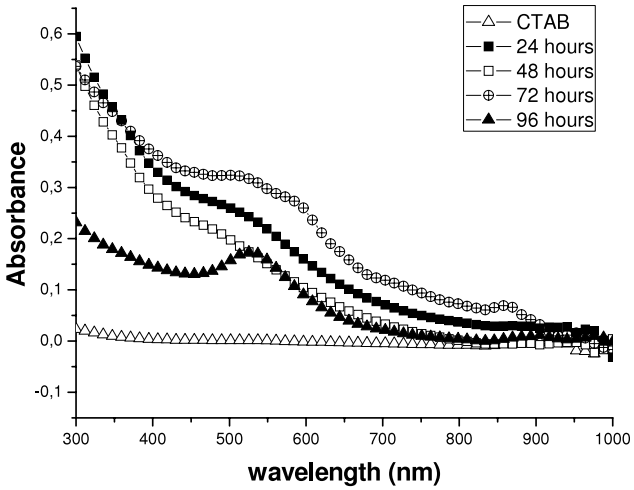

Figure 2. Absorption spectra of the seeds 24, 48, 72 and 96 h after their synthesis.

The absorption spectra of seeds tend to generate a peak at 512 nm after 48 h (figure 2), indicating that seeds and nanorods have their aspect ratio and size dependent on the seeds' age.

3.2. MTT cytotoxicity assay

The cytotoxicity assay revealed that, when cells were incubated in a medium containing 2×10^{-4} μl of non-centrifuged nanorod solution, this great dilution was enough to kill 40–80% of cells, and a 100% death rate was observed in all cell lines in 0.002 μl per μl of DMEM medium (figure 3). On the other hand, CTAB-free solution presented cytotoxicity a thousand times lower, and this toxic effect was considered significant at a 0.1 μl μl^{-1} concentration (50 times more concentrated than the most toxic concentration of the other solution) (figure 4). This concentration is higher than that used for *in vivo* treatments.

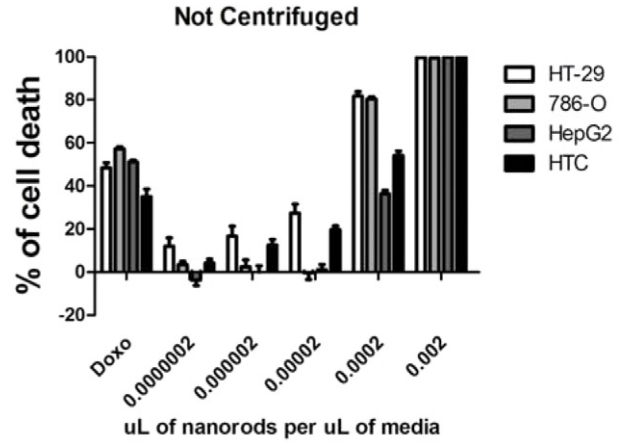

Figure 3. Percentage of cell death after inoculation with non-centrifuged nanorod solution.

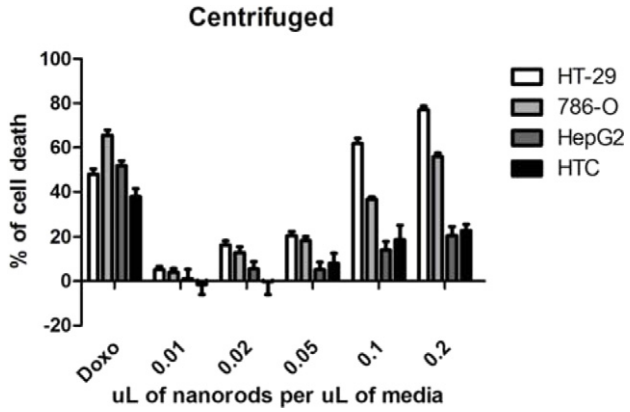

Figure 4. Percentage of cell death observed after inoculation of CTAB-free nanorod solution.

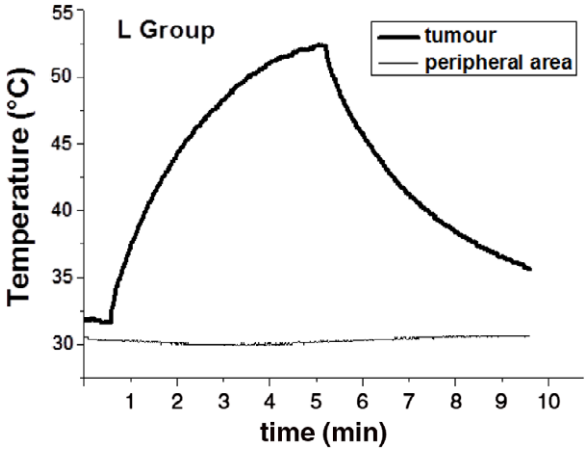

Figure 5. Temperature rise in the tumours of L group animals during laser irradiation.

3.3. Hyperthermic treatment

During hyperthermic treatment, the temperature on the tumour basis rose to 52 °C (an approximately 20° rise) in L group animals, while there was no rise in temperature in the peripheral region (figure 5). There was a 47 °C rise in tumour temperature in H group animals, 36° more intense than in the peripheral region of the tumour (figure 6).

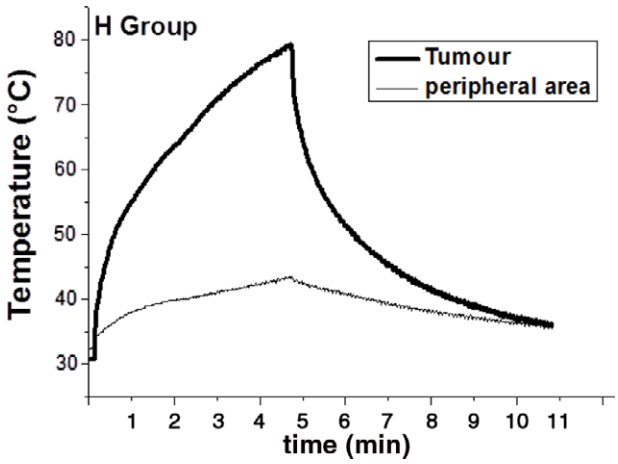

Figure 6. Temperature rising in the tumours of H group animals during laser irradiation.

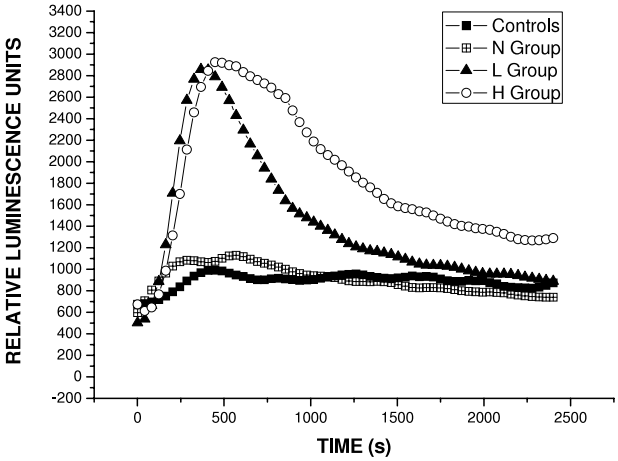

Figure 7. Membrane lipoperoxidation assessed by chemiluminescence assay.

3.4. Tert-butyl hydroperoxide-initiated chemiluminescence assay

The tumours of L and H groups showed intense membrane lipoperoxidation, as can be seen by the short initiation period (time taken to initiate the rising of a luminescence peak) and the high amplitude of the peaks observed, indicating a strong oxidative stress. Both curves are statistically different from controls and N group, but are not different between themselves ($p < 0.05$), as figure 7 shows.

3.5. Total antioxidant capacity assessment

Control, L and N groups did not present a statistical difference, but group H showed increased antioxidant capacity, most likely due to a response to an increased oxidative stress generated by hyperthermic therapy (figure 8).

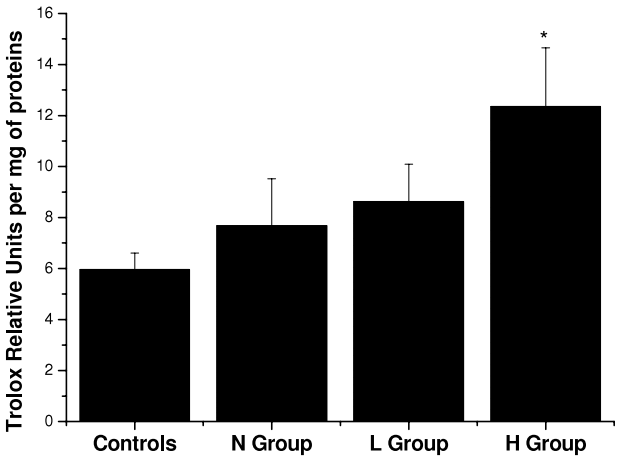

Figure 8. Total antioxidant capacity of the experimental groups.

4. Discussion

Regarding the lack of reliable and efficient treatments, cancer is one of the most common targets of research. Advances have been obtained with therapeutic methods based on electromagnetic fields, light (AlSalhi *et al* 2011, Tian *et al* 2012) and even antimatter (Fahimian *et al* 2009). Photothermal therapy, which damages tumour cells directly or with the help of adjuvant devices, such as metallic nanoparticles, is one of the most promising therapeutic interventions.

Gold nanorods, easily synthesized by the seeding method, present a great area for interaction with light, and consequently intense surface plasmonic resonance, and can have their absorption peaks shifted according to their aspect ratio.

It was possible to observe that the time passed since seed synthesis directly influences the aspect ratio of the nanorods, especially after 48 h. The seeds tend to increase their radius, which can be deduced by the growth of a peak around 512 nm, while the nanorods tend to become more and more spherical, proved by the fact that the two resonance peaks tend to fuse themselves. The resultant spectrum is typical of a nanoshell (Lapotko *et al* 2006b, 2006a).

CTAB used in nanorod synthesis is very cytotoxic, and is often taken off the nanorod surface and solution, and changed for another biopolymer (Huff *et al* 2007a, 2007b, Hansen *et al* 2008). However, some studies indicate that surface-adhered CTAB is not cytotoxic (Alkilany *et al* 2012), a fact that was confirmed by the obtained results. A low cytotoxicity was observed for the nanorods without free CTAB in the solution, a fact that is extremely important for biomedical applications. It was shown that there is no need to change the coating of nanorods if the CTAB free in the solution is eliminated after centrifugation–washing cycles. This way, hyperthermic treatment can become less expensive and much simpler.

The results also indicate that just the near infrared irradiation with a 2 W cm^{-2} laser is enough to initiate cell death, once there was a 20 °C rise in temperature. These results are in accordance with some data on the literature (Nadejda and JinZhong 2009, von Maltzahn *et al* 2009). When H group animals were irradiated, there was a 47 °C rise in the temperature of the tumour, making it almost impossible for a cell to survive. There was no difference in membrane oxidative damage levels between irradiated groups, indicating that the laser can be the main damaging agent. The intracellular antioxidants were increased in group H, indicating that nanorods play an important role in intracellular damage (Huff *et al* 2007a, 2007b).

Our findings indicate that the biomedical application of CTAB-coated gold nanorods is possible when the free CTAB is removed, and when the seeds used in the nanorod synthesis have the proper size. There is a combined action between the laser, directly on the membranes, and the heat generated by the interaction of the nanorods with light, and this combined action leads to the success of the therapy. The molecular action mechanism of hyperthermic therapy and its long-term effects *in vivo* should be investigated next in order to verify the applicability of gold nanorod hyperthermia to human tumours.

5. Conclusion

These results contribute to the comprehension of factors that influence nanorod synthesis, i.e. the time after the seed assembly. Besides this, the results indicate that necrosis is the cell death pathway initiated after hyperthermic treatment in the conditions applied in this study, and make clear that intracellular damage occurs mainly due to nanorod surface plasmon resonance and heat generation, while membrane damage occurs because of the action of the laser itself.

More experiments should be performed in order to investigate the molecular mechanism of hyperthermic treatment, as well as to assess the efficacy of hyperthermia after the irradiation.

References

Alkilany A M, Thompson L B, Boulos S P, Sisco P N and Murphy C J 2012 Gold nanorods: their potential for photothermal therapeutics and drug delivery, tempered by the complexity of their biological interactions *Adv. Drug Deliv. Rev.* **64** 190–9

AlSalhi M S, Atif M, AlObiadi A A and Aldwayyan A S 2011 Photodynamic damage study of HeLa cell line using ALA *Laser Phys.* **21–24** 733–9

Atif M, Firdous S, Mahmood R, Fakhar-e-Alam M, Zaidi S S Z, Suleman R, Ikram M and Nawaz M 2011 Cytotoxic and photocytotoxic effect of photofrin® on human laryngeal carcinoma (Hep2c) cell line *Laser Phys.* **21** 1235–42

Bartczak D, Muskens O L, Millar T M, Sanchez-Elsner T and Kanaras A G 2011 Laser-induced damage and recovery of plasmonically targeted human endothelial cells *Nano Lett.* **11** 1358–63

Burke A R, Singh R N, Carroll D L, Wood J C S, D'Agostino R B Jr, Ajayan P M, Torti F M and Torti S V 2012 The resistance of breast cancer stem cells to conventional hyperthermia and their sensitivity to nanoparticle-mediated photothermal therapy *Biomaterials* **33** 2961–70

Dombrovsky L A, Timchenko V and Jackson M 2012 Indirect heating strategy for laser induced hyperthermia: an advanced thermal model *Int. J. Heat Mass Transfer* **55** 4688–700

Du G-X, Saito S and Takahashi M 2011 Magnetic field effect on the localized plasmon resonance in patterned noble metal nanostructures *IEEE Trans. Magn.* **47** 3167–9

Fahimian B P, DeMarco J J, Keyes R, Bassler N, Iwamoto K S, Zankl M and Holzscheiter M H 2009 Antiproton radiotherapy: peripheral dose from secondary neutrons *Hyperfine Interact.* **194** 313–8

Flecha B G, Llesuy S and Boveris A 1990 Hidroperoxide-initiated chemiluminescence: an assay for oxidative stress in biopsies of heart, liver and muscle *Free Radical Biol. Med.* **10** 93–100

Hansen M N, Chang L-S and Wei A 2008 Resorcirene-encapsulated gold nanorods: solvatochromatism and magnetic nanoshell formation *Supramol. Chem.* **20** 35–40

Hildebrandt B, Wust P, Ahlers O, Dieing A, Sreenivasa G, Kerner T, Feliz R and Riess H 2002 The cellular and molecular basis of hyperthermia *Crit. Rev. Oncol./Hematol.* **43** 33–56

Huff T B, Hansen M N, Zhao Y, Cheng J-S and Wei A 2007a Controlling the cellular uptake of gold nanorods *Langmuir* **23** 1596–9

Huff T B, Tong L, Zhao Y, Hansen M N, Cheng J-X and Wei A 2007b Hyperthermic effects of gold nanorods on tumour cells *Nanomedicine* **2** 125–32

Kuroda K, Akao M, Kanisawa M and Miyaki K 1976 Inhibitory effect of *Capsella bursa-pastoris* extract on growth of Ehrlich solid tumour in mice *Cancer Res.* **36** 1900–3

Lapotko D, Lukianova E, Potapnev M, Aleinikova O and Oraevsky A 2006a Method of laser activated nano-thermolysis for elimination of tumour cells *Cancer Lett.* **239** 36–45

Lapotko D O, Lukianova E and Oraevsky A A 2006b Selective laser nano-thermolysis of human leukemia cells with microbubbles generated around clusters of gold nanoparticles *Laser Surg. Med.* **38** 631–42

Mosmann T 1983 Rapid colorimetric assay for cellular growth and survival: application to proliferation cytotoxic assays *J. Immunol. Methods* **65** 55–63

Murphy C J and Jana N R 2002 Controlling the aspect ratio of inorganic nanorods and nanowires *Adv. Mater.* **14** 80–2

Nadejda R and JinZhong Z 2009 Photothermal ablation therapy for cancer based on metal nanostructures *Sci. China* B **52** 1559–75

O'Neal D P, Hirsch L R, Halas N J, Payne J D and West J L 2004 Photo-thermal tumour ablation in mice using near infrared-absorbing nanoparticles *Cancer Lett.* **209** 171–6

Pustovalov V K 2011 Modeling of the process of laser–nanoparticle interaction taking into account temperature dependences of parameters *Laser Phys.* **21** 906–12

Tian Y Y, Hu X Y, Leung W N, Yuan H Q, Zhang L Y, Cui F A and Tian X 2012 Investigation of photodynamic effect caused by MPPa-PDT on breast cancer *Laser Phys. Lett.* **9** 754–8

von Maltzahn G, Park J-H, Agrawal A, Bandaru N K, Das S K, Sailor M J and Bhatia S N 2009 Computationally guided photothermal tumour therapy using long-circulating gold nanorods antennas *Cancer Res.* **69** OF1–9

Wayner D D M, Burton G W, Ingold K U and Locke S 1985 Quantitative measurement of the total, peroxyl radical-trapping antioxidant capacity of human blood plasma by controlled peroxidation. The important contribution made by plasma proteins *FEBS Lett.* **187** 33–7

Wei Z, Mieszawska A J and Zamborini F P 2004 Synthesis and manipulation of high aspect ratio gold nanorods grown directly on surfaces *Langmuir* **20** 4322–6

Zhao Q L *et al* 2011 Heat treatment of human esophageal tissues: effect on esophageal cancer detection using oxygenated haemoglobin diffuse reflectance ratio *Laser Phys.* **21** 559–65

Photomedicine and Laser Surgery
Volume 31, Number 10, 2013

Pp. 466–473
DOI: 10.1089/pho.2012.3310

Original Research

A Novel 785-nm Laser Diode-Based System for Standardization of Cell Culture Irradiation

Emery C. Lins, PhD,[1] Camila F. Oliveira, DDS, PhD,[2] Orlando C.C. Guimarães, Eng,[3] Carlos A. de Souza Costa, DDS, PhD,[4] Cristina Kurachi, DDS, PhD,[3] and Vanderlei S. Bagnato, PhD[3]

Abstract

Objective: The purpose of this study was to develop a novel device that concatenates alignment of infrared lasers and parallel procedure of irradiation. The purpose of this is to seek standardization of *in vitro* cell irradiation, which allows analysis and credible comparisons between outcomes of different experiments. ***Background data:*** Experimental data obtained from infrared laser therapies have been strongly dependent upon the irradiation setup. Although further optical alignment is difficult to achieve, in contact irradiation it usually occurs. Moreover, these methods eventually use laser in a serial procedure, extending the time to irradiate experimental samples. ***Methods:*** A LASERTable (LT) device was designed to provide similar infrared laser irradiation in 12 wells of a 24 well test plate. It irradiated each well by expanding the laser beam until it covers the well bottom, as occurs with unexpanded irradiation. To evaluate the effectiveness of this device, the spatial distribution of radiation was measured, and the heating of plain culture medium was monitored during the LT operation. The irradiation of LT (up to $25\,J/cm^2$ – $20\,mW/cm^2$; 1.250 sec) was assessed on odontoblast-like cells adhered to the bottom of wells containing 1 mL of plain culture medium. Cell morphology and metabolism were also evaluated. ***Results:*** Irradiation with LT presented a Gaussian-like profile when the culture medium was not heated >1°C. It was also observed that the LT made it 10 times faster to perform the experiment than did serial laser irradiation. In addition, the data of this study revealed that the odontoblast-like cells exposed to low-level laser therapy (LLLT) using the LT presented higher metabolism and normal morphology. ***Conclusions:*** The experimental LASERTable assessed in this study provided parameters for standardization of infrared cell irradiation, minimizing the time spent to irradiate all samples. Therefore, this device is a helpful tool that can be effectively used to evaluate experimental LLLT protocols.

Introduction

It is known that low-level laser therapy(LLLT) can modulate various biological processes.[1] LLLT using far-red to near-infrared (NIR) spectra has been found to modulate different biological processes in cell cultures such as: increasing ATP synthesis,[2] producing analgesic effects,[3] accelerating tissue healing,[4,5] and triggering acid nucleic production, increasing cell proliferation and metabolism.[5–7] Some specific types of laser can also stimulate fibroblasts to synthesize and deposit collagen matrix.[8–10]

A number of *in vitro* investigations using a wide range of cell cultures have provided different data concerning cell proliferation[11,12] and differentiation,[13] DNA and bone protein synthesis,[1,14–16] and bone tissue formation without genotoxic or cytotoxic damage.[17] Unfortunately, these studies have particular irradiation setups and different methodologies, so that the results obtained cannot be compared with or extrapolated to others. In some of these studies, cells were seeded in 96 well plates and irradiated through the bottom using wavelengths of 810 or 830 nm.[12,18–20] In others, the cells were seeded in Petri dishes and the probe was positioned at a distance of 9 cm[1] or 13 cm[21] from the cell cultures. Cells seeded in wells of 24 well plates were also irradiated at a distance of 0.5 mm[22] or 550 mm.[15] There is a significant difference in experimental methodologies when only one light source (serial procedure) has been used to irradiate a 96 well and a 24 well test plate or a Petri dish, especially when comparing the delay between irradiating the first and last sample of plate, or a limitation of the maximum power

[1]Centro de Engenharia, Modelagem e Ciências Sociais Aplicadas, Universidade Federal do ABC, Santo André, SP, Brasil.
[2]Instituto Butantan. São Paulo, SP, Brasil.
[3]Instituto de Física de São Carlos, Universidade de São Paulo, São Carlos, SP, Brasil.
[4]Faculdade de Odontologia de Araraquara, Universidade Estadual Paulista "Júlio de Mesquita Filho," Araraquara, SP, Brasil.

density reached in experimental protocol, because of the need to irradiate the entire area of the well bottom. In addition, different culture media and solutions have been used to irradiate cell cultures.[18–21,23] One should be aware that the laser system used,[24] its pulse width,[25,26] or even the use of a single-diode LLT or multi-diode light-emitting diode therapy (LEDT)[27] may promote different interactions with a biological environment, which should not be compared.[12]

Therefore, the purpose of this study was to develop a device capable of irradiating samples of cell cultures in a standard manner and with a parallel procedure of irradiation. This homemade device, termed LASERTable (LT), simultaneously and in a similar way, irradiates 12 wells of a 24 well plate, taking into account the area of the bottom of each well. The LT still preserves laser as its source, as its monochromaticity and spectral resolution are effective in the modulation of biological processes.

This article describes both assembly of the LT and its profile of lighting on each well of a plate, with the aim of highlighting that cell irradiation is more valuable than an experimental setup for the standardization of LLLT experiments. Ideally, all LLLT experiments should submit the cells of samples in the same experimental group to an equal optical power density. When facing the real situation, it is no trivial matter to reach this homogeneity in irradiation. It depends upon the manufacturing design of each individual light source, and the use of additional optical elements the in experiment, such as lenses; and the optical alignment of visible or infrared beams performed by the researcher. Therefore, detailing of irradiation should consider the spatial profile of irradiation inside each well of a test plate, the total irradiated area, spectral peak and band width of the light source, and the time of irradiation throughout the experiment.

Materials and Methods

LASERTable (LT) system

In a brief overview, LT is composed of laser diodes, an electrical source, a drive board with 12 electrical circuits, three plano-convex cylindrical lenses, metal heat sinks, and a mechanical assembly for optical alignment and support of the test plate. A schematic view of LT presenting the main components is shown in Fig. 1.

Twelve units of the laser diode DL-7140-201S (SANYO Electric Co., Ltd., Japan) were used in the LT. In the typical mode of operation, these units emit 70 mW of NIR radiation at 785 nm in the continuous wave mode. The lasers were aligned in groups of four in-line diodes as in Fig. 1a; three such groups were mounted in order to irradiate 12 wells. This strategy favored both the lens design and optical alignment of the LT. Usually, laser diode beams present a particular angular divergence between the parallel and perpendicular axes, which modulates the emission in an ellipse-shaped profile. The diode datasheet updates us about the 17 degrees of divergence for the perpendicular axis, and the 8 degrees for the parallel axis in the typical mode of operation. Therefore, three cylindrical acrylic lenses (24 mm width, 82 mm length, 12 mm radius) were manufactured and aligned with the groups of in-line diodes, taking the more divergent axis of the lasers parallel to the curved surface of the lens. Therefore, only the larger divergence of the laser beam was the corrected by lens; the smaller divergence of the beam was explored to irradiate the entire bottom area of a well by adjusting the distance between the laser and the well plate.

The electrical supply of the lasers was provided by a 160 W power source MPS-303 (MINIPA Ltda., São Paulo, Brazil) and 12 circuits configured as the source of electric current. Each diode was wired to one current source in order to control its electrical current individually. Regulations were performed setting each diode in its typical mode of operation (100 mA, 2V). Finally, an acrylic box was designed and manufactured for coupling the LT components, and for aligning the diodes and lenses with the test plate. The final LT design is shown in Fig. 1b.

Heat sinks of the laser diodes

As the higher operating temperatures lead to early failure of laser diodes, particular attention should be paid to fabrication of the heat sinks and coupling the lasers to them. This unfortunate situation was experienced during the LT development. Initially, LT was mounted using diodes DL-7141-035 (SANYO Electric Co., Ltd., Japan; 808 nm, 100 mW) and it was successfully used in some experiments.[19,20] Failure of these diodes occurred in an experiment with a long irradiation time (25 min, 30 J/cm^2) in which the laser temperature increased beyond its limit. After this, these elements were replaced by current laser diodes, and new heat sinks were manufactured.

Each new heat sink was composed of a cylindrical metal body (18 mm in diameter, 22 mm long) and a metal cover

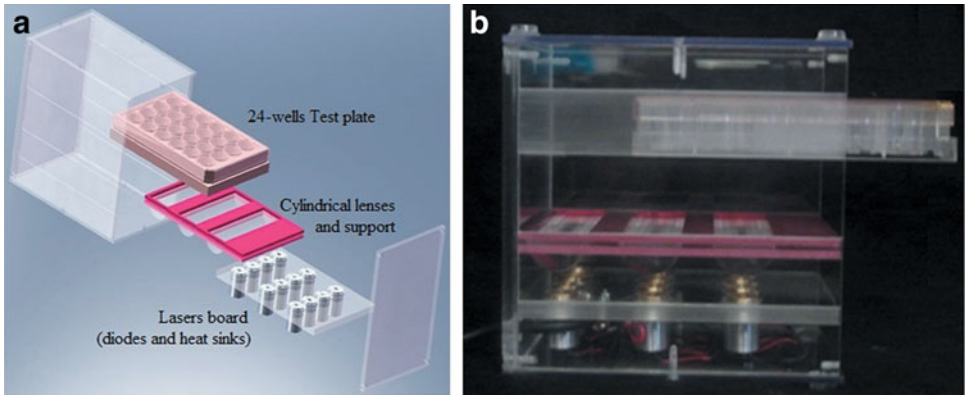

FIG. 1. **(a)** Schematic drawing of LASERTable emphasizing the components: 24 well cell culture test plate, three plano-convex cylindrical lenses and support, infrared diode lasers sealed on the heat sink, and the acrylic box. **(b)** LASERTable system without the electrical source.

(10 mm in diameter, 2 mm thick), both made of aluminum. A large opening (10 mm in diameter, 4 mm deep) was drilled into the body to accommodate the laser; small concentric openings (5 mm diameter) were also drilled throughout the entire piece, in order to wire the diode pins to the current source. Threads were made in the wall of the large opening, and covered so that the diode was sandwiched between the body and the cover, which kept it in permanent contact with the heat sink. The contact surface between the laser and the body was covered with thermal grease in order to deliver the maximum amount of heat from the laser to the heat sink. The temperature of the diode package was monitored, revealing that LT could be used in long-term protocols. Finally, the sets of diode coupled to the heat sink were bonded to an acrylic plate, forming the laser board.

Bottom-up and top-down irradiation configuration

The LT was designed to irradiate a well plate individually in two configurations: top-down and bottom-up, switching between them by simply changing the position of the laser board. In the bottom-up configuration, each laser irradiated the entire area of one well (18 mm in diameter, 2.5 cm^2 in area).

In the top-down configuration, the laser board was turned upside down and placed 3 mm above the plate. Here there were no lenses between the lasers and well, so that an unexpanded irradiation was performed (5 mm in diameter, 0.2 cm^2 in area). The top-down configuration was used in a particular experiment with laser transillumination of dentin discs. Here, odontoblast-like cells were cultured on the obverse surface of the disc, and illumination was performed on the reverse surface, projecting light through the disc. The discs floated on cell culture medium with the obverse face immersed in liquid to allow the growth of cells. This experimental model tried to simulate transdentinal irradiation of odontoblast cells in dental pulp tissue, taking the dentin disc as the pulp chamber wall. The dentin disc acted as an optical barrier that scattered and absorbed light, so that the top-down configuration increased the light dose on the cells.[28]

Optical alignment and profile of laser irradiation

Optical alignment of the LT was reached by displacing the laser board from the test plate, and then calibrating the distance between the laser board and the lenses. The distance between the diodes and lenses was set at 25 mm, whereas that between the lenses and the plate was set at 44 mm. These values were used to design the acrylic box for the LT. However, this alignment was used only for the bottom-up configuration; in the top-down configuration the laser board was set at 3 mm above the test plate.

The emission of a single laser of the LT in the bottom-up configuration was measured, using an optical power meter FieldMaster-GS with a LM-2-VIS sensor (Coherent Inc., San Jose, CA) (8 mm in diameter, 50 mm^2 in area). An SMA fiberoptic connector (component of the sensor) was used to increase the spatial resolution of calibration by reducing the measurement area to 8.5 mm^2 (3.3 mm in diameter). A circular mark on the acrylic cover of the test plate was used as reference of a well. The sensor was fixed to a mechanical stage with millimeter displacement; then the laser emission was scanned along the diameter of the circular mark surface. Scans with a 3 mm displacement step were performed in triplicate, followed by calculation of mean and standard deviation. The total optical power on the circular mark was measured using the sensor (Coherent Inc., USA) (16 mm in diameter, 2 cm^2 in area). LM-10 has a detection area slightly smaller than the area of one well; therefore, almost all the radiation that flowed through a circular mark could be detected.

After this, a digital image of the LT operating in the dark was obtained, in order to observe the emission of all diodes simultaneously. This image was captured by placing a sheet of white paper (neutral light diffuser) on the acrylic cover. As the image was captured in a dark environment without using a flash light, the emission detected depended only upon the shutter of the digital camera.

Temperature tests

The temperature of the culture medium (Dulbecco's Modified Eagle Medium [DMEM]), either supplemented with fetal bovine serum (FBS), or not, was monitored during a bottom-up irradiation of 1200 sec (20 mW/cm^2, 24 J/cm^2), simulating different LLLT protocols. FBS was tested at three concentrations (2%, 5%, and 10%). A digital thermometer MT-600 (MINIPA Ltda., São Paulo, Brazil) was used with the sensor fixed to the bottom of a well. Initially, the temperature was monitored using an empty well; these data revealed the heating induced by radiation directly on a sensor; therefore, it was taken as a baseline. Then the well was filled with culture medium, which remained at rest for $\sim$3 min in the container, until it reached a constant temperature approximating the room temperature; after this, the temperature was measured again. The baseline value was subtracted from the new temperature value found, and the difference was the amount of culture medium heating that occurred during the protocol. This procedure was repeated in triplicate. Finally, the mean and standard deviation of temperature were calculated.

LLLT applied on odontoblast-like cells

The metabolism of odontoblast-like MDPC-23 cells under nutritional stress, subjected to direct LLL irradiation, was evaluated. The complete description of experimental method, results, and data analysis can be found in the work of Oliveira et al.[29] Actually, the focus is to emphasize the performance of the LT in this study, and present the experimental results obtained.

Cells were seeded (12,500 cells/well) in the wells of 24 well plates, and incubated for 24 h at 37°C. The DMEM was replaced by fresh DMEM supplemented with 2% or 5% (cell stress induced by nutritional deficit) or 10% FBS. The cells were irradiated (2, 4, 10, 15, and 25 J/cm^2) using the LT in the bottom-up configuration. One control group was established for each experimental condition. Seventy-two hours after the last irradiation, cells were assessed with regard to metabolism, morphology, and total protein expression.

Results

Light distribution and temperature tests

The normalized (percent) spatial distribution of optical power density provided by each laser of the LT is presented in Fig. 2. Lasers irradiate samples with a Gaussian-like

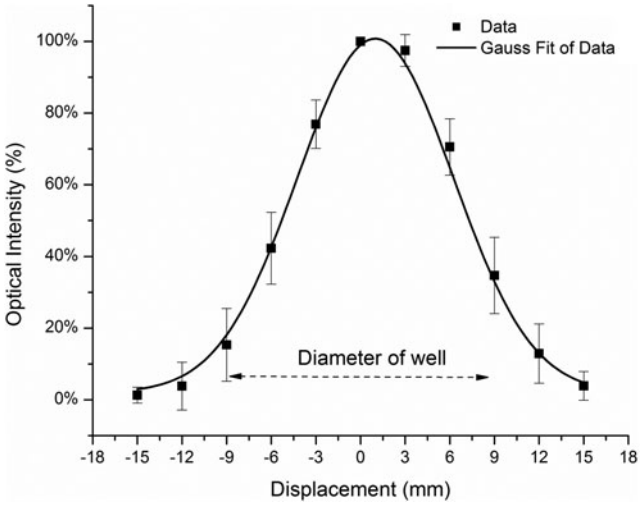

FIG. 2. LASERTable with bottom-up configuration provides a Gaussian-like profile of irradiation in wells. Circular marks on the acrylic cover of the test plate were used as a reference to measure optical power inside and outside the wells of the test plate. The curve shows that a significant amount of irradiation is concentrated inside the well.

profile, which is characteristic of laser diodes. This profile demonstrates that radiation is preferentially concentrated in the center of a well, determining the effectiveness of optical alignment; however, it also reveals that optical intensity at the periphery is 30% lower than in the center. The total optical power was measured, showing 48.3 ± 0.6 mW per well, which leads to a mean power density of $\sim 20\,\mathrm{mW/cm^2}$. These values are significantly different from those of the top-down configuration, which presents optical power of >68.5 mW and a mean power density of $>350\,\mathrm{mW/cm^2}$.

A qualitative profile of irradiation using all the diodes simultaneously is presented in Fig. 3. Figure 3a shows a digital image of emission revealing preferential illumination by all diodes illuminating inside the wells. Nevertheless, a small part of the radiation is scattered out of the well by the cylindrical lenses. Figure 3a also shows that the laser speckle originated on the paper surface. Figure 3b presents an image resulting from the processing applied to Fig. 3a, which increased the image contrast. It normalized the pixel intensities to a maximum in the image, and replaced the gray tones with false colors. This picture shows that the maximum irradiance is always in the center of a well, although there is little difference in the peak values among the wells.

The temperature of DMEM was verified by means of a simulated protocol with 1200 sec of irradiation ($24\,\mathrm{J/cm^2}$) (Fig. 4). In general, the DMEM is heated by no more than 1°C, which attests that this protocol can be used in *in vitro* cell irradiation experiments. The standard deviation in Figs. 4a and c is higher than in the others; however, these data are associated only with the performance of the digital thermometer during the experiment. It should be noted that the resolution of the digital thermometer is 0.5°C, which is close to the magnitude of heating reached by the culture medium.

Performance of the LT

Numbers of groups and specimens per group as well as time spent to irradiate one sample from a group are presented in Table 1, in which experimental samples submitted to five LT doses are represented by irradiation time (or energy density). For each dose, three different FBS concentrations were used, totaling 15 experimental groups with 40 specimens per group, totalizing 120 samples that were exposed to the same irradiation time. Table 1 also compares the time spent to irradiate all 120 samples, considering a hypothetic serial procedure with a single laser system and the parallel procedure performed with the LT device. Because of the properties of the LT and the number of specimens per group, the time spent in a serial procedure was 10 times longer than in a parallel procedure. These data revealed that the total time spent to irradiate all 600 specimens was 93 h and 20 min for the serial procedure and 9 h and 20 min for the parallel procedure.

Summarized results of the LLLT experiment

There was higher metabolism and total protein expression observed 72 h after the last laser irradiation at the doses of 15 and $25\,\mathrm{J/cm^2}$ (Mann–Whitney; $p < 0.05$).

In all irradiated and sham-irradiated groups, the lowest succinate dehydrogenase (SDH) enzyme production was observed when the DMEM was supplemented with 2%, whereas the 5% and 10% FBS concentrations did not differ from each other (Table 2, rows).

As regards the FBS concentrations and irradiation with 2, 4, and $10\,\mathrm{J/cm^2}$, a significantly lower total protein expression occurred than in the control group. However, cell irradiation with $25\,\mathrm{J/cm^2}$ resulted in significantly higher total protein expression than in the control group for all FBS concentrations evaluated. The energy doses of 2, 4, and $10\,\mathrm{J/cm^2}$ did not differ significantly from each other in any of the FBS

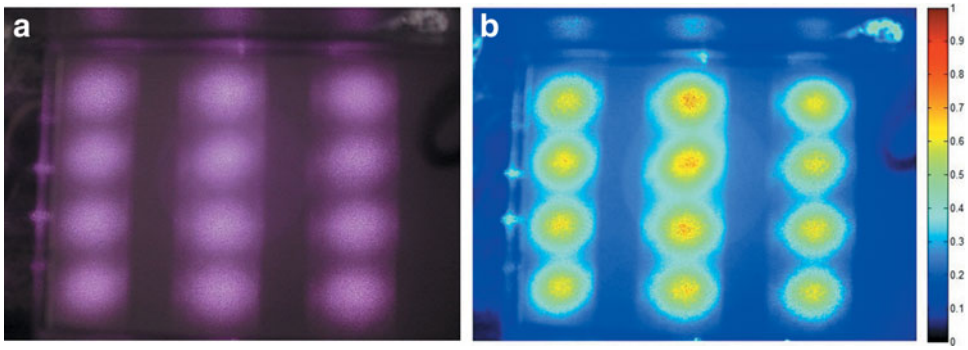

FIG. 3. **(a)** Digital image of the LASERTable (LT) operating in bottom-up configuration. This image reveals the profile of irradiation from all diodes simultaneously. **(b)** The result of an image processing applied on **(a)**, where the intensities of image were normalized and replaced by false colors.

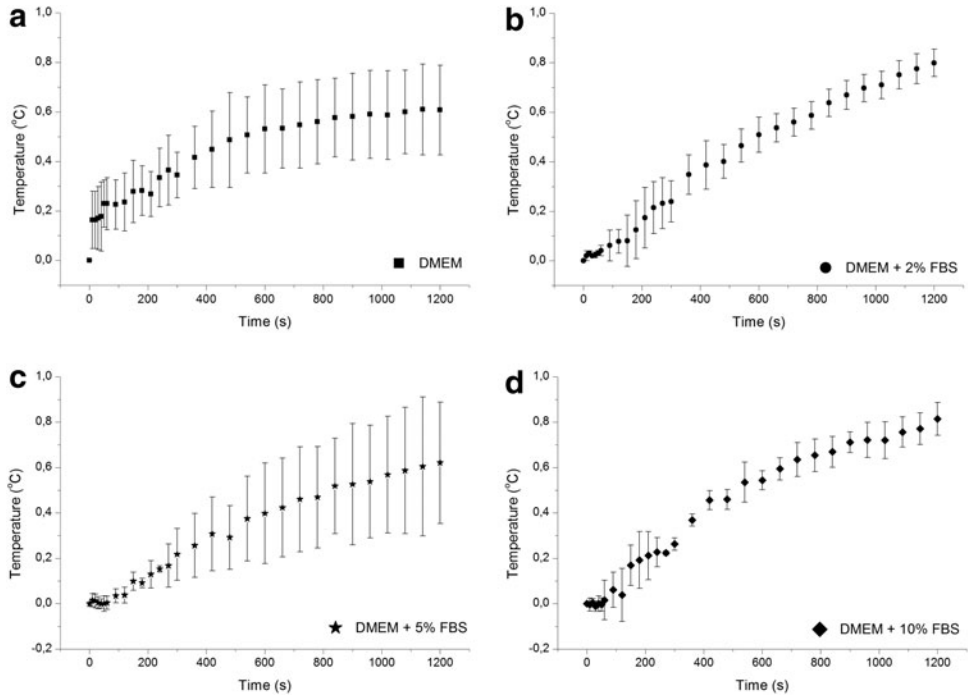

FIG. 4. Graphs of temperature into culture medium along a low-level laser therapy (LLLT) protocol. **(a)** Dulbecco's Modified Eagle Medium (DMEM) only. **(b)** DMEM +2% fetal bovine serum (FBS). **(c)** DMEM+5% FBS. **(d)** DMEM+10% FBS. The graphs reveal that the increase of culture medium temperature is no longer than 1°C.

concentrations. The laser dose of 25 J/cm^2 was superior in terms of the stimulus of total protein expression, in comparison with 15 J/cm^2 only when the DMEM was supplemented with 5 and 10% FBS. When the medium was supplemented with 2% FBS, these energy doses did not differ significantly from each other (Table 3, columns).

Unirradiated cells subjected to nutritional deficit exhibited a normal morphology such as was observed when the cells were cultured in DMEM supplemented with 10% FBS (Fig. 5). Similar morphological characteristics were also observed in irradiated MDPC-23 cells subjected to stress conditions.[29]

Discussion

Development of the LT was motivated by the vast amount of data available in the literature about cell biomodulation induced by light irradiation. In general, most of these data are complementary and enhance understanding of the effects of LLLT. On the other hand, sometimes there are contradictory conclusions among experiments that investigate the same cell response, and one reason for that lack of agreement is the absence of standardization of the research protocols used. Moore et al.[12] described that a wide range of protocols and experimental models are important factors that make it difficult to understand the modulatory effects of phototherapy on cultured cells.

The LT was designed to standardize irradiation parameters (wavelength, irradiance, and energy density), so that the results of LLLT experiments could be more reliable. As regards the light beam, it may be detached from the Gaussian-like profile of irradiation on each well of the cell culture test plate. This emission profile is characterized by concentrating more light in the center of the beam than at the periphery, and it is a particular characteristic LEDs and laser systems, even when coupled to a fiberoptic device. This light distribution certainly interferes with cell irradiation. This profile of illumination has even more influence on *in vitro* phototherapy experiments, in which the light source is displaced from the cell culture to irradiate all areas of the test plate with an expanded light beam (magnitude of tens of centimeters squared). Unexpanded light beams are more attractive for use in *in vivo* experiments when the light source probe is placed in contact with the target tissue and limits the area of irradiation to the magnitude of millimeters squared.

Table 1. Organization of the Experiment, Taking into Account the Energy Densities, Times of Irradiation, the Concentrations of Fetal Bovine Serum (FBS), and the Number of Irradiated Samples

Energy density, J/cm^2	*Irradiation time, sec*	*% FBS*			*Number of specimens*	*Irradiation time in serial procedure, sec*	*Irradiation time in parallel procedure, sec*
		2%	*5%*	*10%*			
2	100	G1	G2	G3	120	12,000	1200
4	200	G4	G5	G6	120	24,000	2400
10	500	G7	G8	G9	120	60,000	6000
15	750	G10	G11	G12	120	90,000	9000
25	1250	G13	G14	G15	120	150,000	15,000

This is also an analysis of time spent irradiating all the samples if a serial or a parallel procedure of irradiation is applied.

Table 2. Production of Succinic Dehydrogenase (SDH) Enzyme Detected by the MTT Assay in the Non-Irradiated (Control[a]) and Irradiated Groups at 72 h After the Last Active or Sham Irradiation, According to the Laser Dose (J/cm^2) and Fetal Bovine Serum Concentration (%FBS)

	% FBS		
Irradiation dose (J/cm^2)	*2%*	*5%*	*10%*
2	0.717 (0.629–0.797) a B	0.887 (0.816–0.992) a A	0.933 (0.833–0.989) a A
4	0.688 (0.601–0.748) ab B	0.882 (0.780–0.989) a A	0.878 (0.823–0.941) ab A
10	0.737 (0.661–0.778) a B	0.866 (0.781–0.908) a A	0.856 (0.807–0.902) ab A
15	0.712 (0.630–0.782) ab B	0.864 (0.837–0.963) a A	0.849 (0.801–0.909) ab A
25	0.663 (0.632–0.765) ab B	0.825 (0.724–0.914) a A	0.821 (0.768–0.926) b A
0[a] (control)	0.643 (0.528–0.749) b B	0.846 (0.731–0.997) a A	0.829 (0.727–0.936) b A

[a]Represents the sham irradiation (0 J/cm^2), that is, the control cells were maintained in the LASERTable for the same irradiation times used in the experimental groups, although without activating the laser source. As none of the sham irradiation times had statistically significant effects on SDH enzyme production, all controls were compiled in a single control group ($n = 80$).
[b]Values represent median (P25-P75), $n = 16$ (except for the control group, $n = 80$). Values followed by same lowercase letters in columns and uppercase letters in rows did not differ statistically (Mann–Whitney, $p > 0.05$).

Moreover, even in this specific situation, there are profiles of irradiation on tissue; however, their effects are minimized by expecting the macroscopic effects of phototherapy and irradiation on a set of points across the tissue surface.

As there is a Gaussian-like profile of irradiation, two points should be discussed: (1) distribution of cells inside the well, and (2) consequences of the lighting profile for phototherapy. After being seeded, the cells are distributed homogeneously over the entire area of the well. However, with time, there is a slight tendency of the cells to accumulate and proliferate at its periphery. It is intuitively clear that to increase the efficiency of LLLT experiments using cell culture, a uniform spatial distribution of light should reach the bottom of the wells to which the cells are attached. Therefore, a specific optical assembly should be designed for each diode, which makes the LT more expensive. An alternative to this would be to couple each diode to an integrating sphere. However, apart from the costly system and spatial limitation for adding 12 optical spheres, in this case multiple reflections inside a sphere would minimize the final intensity of the light beam.

Another relevant point of discussion is the light absorbed by the cells subjected to irradiation. It is evident that not all the luminous energy delivered to the well is absorbed by the cells, as there is a significant amount of light that passes through the layer of proliferated cells and dissipates into space. One possible interpretation of this fact is that there is a threshold of light absorption by cells, and that the excess light delivered to cells during irradiation is lost; in this case, the Gaussian-like profile of illumination could be less influential in the experiment than only the threshold of light absorption that was reached by cells in all areas of the well. Unfortunately, to date, there are no published results that demonstrate this hypothesis. However, studies have proven the importance of light power density in modulating the biochemical outcomes of phototherapy.[21,23,29]

Statistical analysis of the results has been the best tool to validate the changes in the metabolism of cells subjected to LLLT and the influence of the Gaussian-like lighting on results. When comparing data from Table 2 (MTT assay) and Table 3 (total protein expression), it should be noted that the mean of the control group eventually differs from the mean of the experimental group, revealing differences, as expected, between cells from the control and experimental groups; however, the variance of data in percent is similar, even in the control group, and this behavior was not expected. One

Table 3. Total Protein Expression Detected by the Lowry's Method Assay in the Non-Irradiated (Control[a]) and Irradiated Groups at 72 h After the Last Active or Sham Irradiation, According to the Laser Dose (J/cm^2) and Fetal Bovine Serum Concentration (%FBS)

	% FBS		
Irradiation dose (J/cm^2)	*2%*	*5%*	*10%*
2	0.700 (0.664–0.761) c B	0.833 (0.779–0.864) c A	0.853 (0.789–0.925) c A
4	0.730 (0.683–0.753) c B	0.802 (0.750–0.862) c A	0.841 (0.765–0.905) c A
10	0.729 (0.667–0.752) c B	0.789 (0.769–0.822) c A	0.799 (0.778–0.852) c A
15	0.842 (0.812–0.874) a B	0.936 (0.913–0.996) b A	0.983 (0.932–1.021) b A
25	0.860 (0.832–0.897) a B	0.952 (0.932–1.032) a A	0.991 (0.953–1.036) a A
0[a] (control)	0.809 (0.766–0.862) b B	0.915 (0.886–0.964) b C	0.953 (0.905–0.985) b A

[a]Represents the sham irradiation (0 J/cm^2), that is, the control cells were maintained in the LASERTable for the same irradiation times used in the experimental groups, though without activating the laser source. As none of the sham-irradiation times had statistically significant effects on total protein expression, all controls were compiled in a single control group ($n = 80$).
[b]Values represent median (P25-P75), $n = 16$ (except for the control group, $n = 80$). Values followed by same lowercase letters in columns and uppercase letters in rows did not differ statistically (Mann–Whitney, $p > 0.05$).

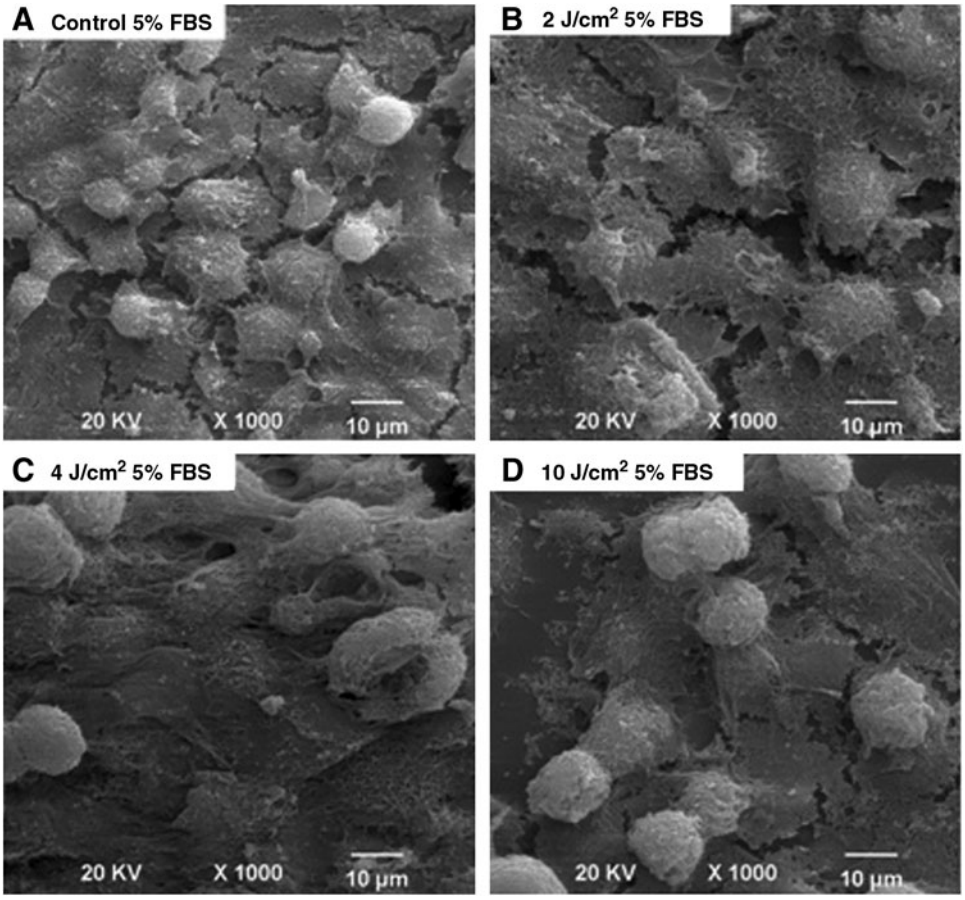

FIG. 5. Panel of scanning electron micrographs (SEM) representative of cell morphology in each group. **(A)** (Control) MDPC-23 cells with a wide cytoplasm and numerous several thin cytoplasmic processes originating from their membrane cover the glass substrate, characterizing an epithelioid nodule. **(B)** Cells with normal morphology can be observed on the cover glass. **(C)** Note the dense epithelioid nodule, with some cells undergoing mitosis. **(D)** Similarly to what was observed in the other groups, the glass substrate is covered by MDPC-23 cells with normal morphology. SEM, magnification original $\times 1000$.

possible reason for this magnitude of variance in the control group could have been the response of cells themselves to biochemical tests, especially those whose results depended upon the number of cells in the sample. In general, the process of cell proliferation in cell cultures induces samples with differences in the number of cells, even in the control group. Therefore, it is possible for the variation in the number of cells of a sample to be more significant in MTT and total protein expression experimental results, than in the Gaussian-like profile of illumination.

The LT allows standardization of LLLT experiments from several aspects, especially considering the absorption of visible and infrared radiation by the culture medium and test plate, as well as heating of the culture medium induced by absorption of radiation. Nevertheless, we believe that a significant variation in control and experimental data will be present in the results of *in vitro* cell culture LLLT whether or not light sources with a Gaussian-like profile of illumination are used.

Conclusions

This report presented a novel 785 nm laser-based system for parallel infrared irradiation of cell cultures. The LASER-Table device was designed to provide two configurations of irradiation in cell cultures stored in a 24 well plate. The bottom-up configuration delivers irradiation in the entire bottom the area of twelve wells of a 24 well plate, whereas the top-down configuration delivers unexpanded irradiation. The bottom-up configuration provides 20 mW/cm^2 power density per well, whereas the top-down configuration provides 350 mW/cm^2 power density per well.

The LT device achieved the objective of providing standardization for infrared cell irradiation, reducing the time spent to irradiate all the experimental samples by approximately 10-fold. LT used in an experimental protocol on odontoblast-like cells attested to the effectiveness of this device, as laser irradiation stimulated the metabolic activity.

Acknowledgments

The authors thank the Conselho Nacional de Desenvolvimento Científico e Tecnológico–CNPq (Grants: Instituto Nacional de Óptica e Fotônica) and the Fundação de Amparo à Pesquisa do Estado de São Paulo–FAPESP (Grants: 2007/50646-3, 2008/08424-6, and 2008/54785-0) for providing financial support.

Author Disclosure Statement

No competing financial interests exist.

References

1. Khadra, M., Lyngstadaas, S.P., Haanaes, H.R., and Mustafa, K. (2005). Determining optimal dose of laser therapy for attachment and proliferation of human oral fibroblasts cultured on titanium implant material. J. Biomed. Mater. Res. 73A, 55–62.

2. Lubart, R., Eichler, M., Lavi, R., Friedman, H., and Shainberg, A. (2005). Low-energy laser irradiation promotes cellular redox activity. Photomed. Laser Surg. 23, 3–9.
3. Chow, R., Armati, P., Laakso, E-L., Bjordal, J.M., and Baxter, G.D. (2011). Inhibitory effects of laser irradiation on peripheral mammalian nerves and relevance to analgesic effects: a systematic review. Photomed. Laser Surg. 29, 365–381.
4. Kim, Y-D., Kim, S-S., Hwang, D-S., et al. (2007). Effect of low level laser treatment after installation of dental titanium implant-immunohistochemical study of vascular endothelial growth factor: an experimental study in rats. Laser Phys. Lett. 4, 681–685.
5. Koutná, M., Janisch, R., and Veselská, R. (2003). Effects of low-power irradiation on cell proliferation. Scr. Med. (BRNO) 76, 163–172.
6. Karu, T., Pyatibrat, L.V., Kalendo, G.S., and Esenaliev, R.O. (1996). Effects of monochromatic low-intensity light and laser irradiation on adhesion of HeLa cells in vitro. Lasers Surg. Med. 18, 171–177.
7. Kikuchi, H., Sawada, T., and Yanagisawa, T. (1996). Effects of a functional agar surface on in vitro dentinogenesis induced in proteolytically isolated agar-coated dental papillae in rat mandibular incisors. Arch. Oral Biol. 41, 871–883.
8. Nara, Y., Tsukamoto, Y., Fukutani, S., Yamaguchi, N., Mori, M., and Morioka, T. (1992). Stimulative effect of He-Ne laser irradiation on cultured fibroblasts derived from human dental pulp. Lasers Life Sci. 4, 249–256.
9. Reddy, G.K., Stehno–Bittel, L., and Enwemeka, C.S. (1998). Laser photostimulation of collagen production in healing rabbit Achilles tendons. Lasers Surg. Med. 22, 281–287.
10. Romanos, G.E., Pelekanos, S., and Strub, J.R. (1995). Effects of Nd:YAG laser on wound healing processes: clinical and immuno-histochemical findings in rat skin. Lasers Surg. Med. 16, 368–379.
11. Grossman, N., Schneid, N., Reuveni, H., Halevy, S., and Lubart, R. (1998). 780-nm low power diode laser irradiation stimulates proliferation of keratinocyte cultures: involvement of reactive oxygen species. Lasers Surg. Med. 22, 212–218.
12. Moore, P., Ridgway, T.D., Higbee, R.G., Howard, E.W., and Lucroy, M.D. (2005). Effect of wavelength on low-intensity laser irradiation-stimulated cell proliferation in vitro. Lasers Surg. Med. 36, 8–12.
13. Aihara, N., Yamaguchi, M., and Kasai, K. (2006). Low-energy irradiation stimulates formation of osteoclast-like cells via RANK express in vitro. Lasers Med. Sci. 21, 24–33.
14. Yamada, K. (1991). Biological effects of low power laser irradiation on clonal osteoblastic cells (MTC3T3-E1). Nihon Seikeigeka Gakkai Zasshi. 65, 787–799.
15. Hamajima, S., Hiratsuka, K., Kiyama–Kishikawa, M., et al. (2003). Effect of low-level irradiation on osteoglycin gene expression in osteoblasts. Lasers Med. Sci. 18, 78–82.
16. Stein, A., Benayahu, D., Maltz, D., and Oron, U. (2005). Low-level laser irradiation promotes proliferation and differentiation of human osteoblasts in vitro. Photomed. Laser Surg. 23, 161–166.
17. Kujawa, J., Zavodnik, I.B., Lapshina, A., Labieniec, M., and Bryszewska, M. (2004). Cell survival, DNA, and protein damage in b14 cells under low-intensity near-infrared (810-nm) laser irradiation. Photomed. Laser Surg. 22, 504–508.
18. Vinck, E.M., Cagnie, B.J., Cornelissen, M.J., Declercq, H.A., and Cambier D.C. (2003). Increased fibroblast proliferation induced by light emitting diode and low power laser irradiation. Lasers Med. Sci. 18, 95–99.
19. Oliveira, C.F., Basso, F.G., Lins, E.C., et al. (2010). Increased viability of odontoblast-like cells subjected to low-level laser irradiation. Laser Phys. 20, 1659–1666.
20. Tagliani, M.M., Oliveira, C.F., Lins, E.M.M., et al. (2010). Nutritional stress enhances cell viability of odontoblast-like cells subjected to low level laser irradiation. Laser Phys. Lett. 7, 247–251.
21. Oliveira, C.F., Hebling, J., Souza, P.P.C., et al. (2008). Effect of low-level laser irradiation on odontoblast-like cells. Laser Phys. Lett. 5, 1–6.
22. Kreisler, M., Daubländer, M., Willershausen–Zönnchen, B., and d'Hoedt, B. (2001). Effect of diode laser irradiation on the survival rate of gingival fibroblast cell cultures. Lasers Surg. Med. 28, 445–450.
23. Oliveira, D.A.A., Oliveira, R.F., Zangaro, R.A., and Soares, C.P. (2008). Evaluation of low-level laser therapy of osteoblastic cells. Photomed. Laser Surg. 26, 401–404.
24. Lizareli, R.F.Z., Kurachi, C., Misoguti, L., and Bagnato, V.S. (2000). A comparative study of nanosecond and picosecond laser ablation in enamel. J. Clin. Laser Med. Surg. 18, 151–157.
25. Carrinho, P.M., Renno, A.C.M., Koeke, P., Salate, A.C.B., Parizotto, N.A., and Vidal, B.C. (2006). Comparative study using 685-nm and 830-nm lasers in the tissue repair of tenotomized tendons in the mouse. Photomed. Laser Surg. 24, 754–758.
26. Morkunas, V., Ruksenas, O., Vengris, M., Gabryte, E., Danieliene, E., and Danielius, R. (2011). DNA damage in bone marrow cells induced by ultraviolet femtosecond laser irradiation. Photomed. Laser Surg. 29, 239–244.
27. Leal Junior, E.C.P., Lopes–Martins, R.A.B., Baroni, B.M., et al. (2009). Comparison between single-diode low-level laser therapy (LLLT) and LED multi-diode (cluster) therapy (LEDT) applications before high-intensity exercise. Photomed. Laser Surg. 27, 617–623.
28. Oliveira, C.F., Basso, F.G., dos Reis, R.I., et al. (2013). In vitro transdentinal effect of low-level laser therapy. Laser Phys. 23, 055604.
29. Oliveira, C.F., Basso, F.G., Lins, E.C., et al. (2011). In vitro effect of low-level laser on odontoblast-like cells. Laser Phys. Lett. 8, 155–163.

Address correspondence to:
Emery C. Lins
Centro de Engenharia
Modelagem e Ciências Sociais Aplicadas
Universidade Federal do ABC
Rua Santa Adélia, 166
Santo André, SP
Brasil 09.210-170

E-mail: emery.lins@ufabc.edu.br.

Lasers Med Sci (2013) 28:215–222
DOI 10.1007/s10103-012-1118-z

ORIGINAL ARTICLE

Influence of the hydration state on the ultrashort laser ablation of dental hard tissues

Francisco de Assis M. G. Rego Filho · Maristela Dutra-Corrêa · Gustavo Nicolodelli · Vanderlei S. Bagnato · Maria Tereza de Araujo

Received: 16 February 2011 / Accepted: 1 May 2012 / Published online: 15 May 2012

Abstract Since about 40 years, laser-based surgical tools have been used in medicine and dentistry to improve clinical protocols. In dentistry, femtosecond lasers have been claimed to be a potential ablation tool. It would, however, be good to perform a more fundamental investigation to understand ablation interaction mechanisms and possible side effects, depending on different specific components of the target tissue. The goal of this study is to show the changes of ablation characteristics in the femtosecond regime at different levels of structural water within dental hard tissues. Thirty human teeth samples were split into three hydration groups and subdivided into dentin and enamel groups (n=5). The specimens were irradiated using a 70-fs Ti:sapphire laser (with a 1-kHz repetition rate and a 801-nm wavelength output). Ablation was performed using five different power levels and three exposure times. The results clearly show an inversely proportional dependence of the ablation threshold to the hydration level of the tissues. A known mathematical model was adapted in order to include the influence of the changes on the relative fractional composition of dental hard tissues. This analysis was consistent with the experimental results regarding the ablation threshold. High thermal and mechanical damages were observed as a high repetition rate had been applied. Macroscopic images and scanning electron microscopy images were used to preliminarily analyze both the thermal and mechanical damage thresholds, and their variations according to the hydration level present. By manipulating the hydration states, the modifications in the proportions of the molecules that build dental hard tissues clearly shift, and therefore, the characteristics of a plasma-induced ablation change.

Keywords Enamel · Dentin · Femtosecond ablation · Hydration state

F. A. M. G. Rego Filho (✉) · M. T. de Araujo
Instituto de Física, Universidade Federal de Alagoas,
Maceió, Alagoas 57072-970, Brazil
e-mail: francisco.rego@fis.ufal.br

M. Dutra-Corrêa
Mestrado em Odontologia, Universidade Paulista (UNIP),
São Paulo, São Paulo 04026-002, Brazil

G. Nicolodelli · V. S. Bagnato
Instituto de Física de São Carlos, Universidade de São Paulo,
São Carlos, São Paulo 13560-970, Brazil

Introduction

Today, lasers are important tools used in a large number of medical applications. In dentistry, lasers have been considered as a potential substitute for conventional rotary drills in order to reduce thermal and mechanical stress. Initial studies of laser effects on dental hard tissues were realized by Goldman et. al. [1] and Stern and Sognnaes [2]. These works presented disordered ablation accompanied by the formation of a plume of ejected material, as well as crystallographic changes on the remaining structures by thermal damage. Other authors reported fusion and resolidification of hard materials and obliteration of dentin tubules [3]. The structural changes reported may have positive clinical implications [4, 5], although a high temperature increase is not clinically acceptable [6].

Several authors have shown that use of CO_2, Er:YAG and Er,Cr:YSSG lasers can cause high thermal and mechanical stress due to their output wavelengths (9.6, 2.9, and 2.79 μm, respectively) if the pulse delivery method is stationary and exposure time is prolonged. As the linear absorption of light by tissue components occurs in these spectral regions, heat is produced, and this causes structural

water to instantly vaporize forming pressure bubbles within tissue layers, which subsequently give rise to microexplosions [7–9]. In these cases, there is usually an intrinsic thermal loading and consequently a temperature rise, which can, however, be reduced if done in combination with water coolants [10, 11]. However, the water cooling may not be completely efficient when applying high repetition rate lasers. The application of high repetition rates reduces the interpulse time that the molecules need to dissipate the absorbed heat, which in turn further increases the thermal loading. The use of the abovementioned laser sources is possible because, clinically, their application to dental surfaces is usually nonstationary, sweeping over a treatment area, which reduces the effective interaction time. The pulsed Nd:YAG laser irradiation at 1,064 nm likewise produces ablation, but the intrinsic thermal loading also causes crystallographic changes on the ablated surface, thus creating a surface with enhanced acid resistance. This fact indicated a potential application of this laser in dentistry for caries prevention [12].

Another important parameter in describing ablation side effects is the pulse duration. Long laser pulses (10^{-12} s$<\tau<$ 10^{-3} s) are known to produce more severe thermal and mechanical damage during ablation because of their long interaction times. In the 1990s, ultrashort lasers ($\tau<10^{-12}$ s) began to be used as a tool for dental hard tissues ablation with reduced thermal or mechanical damages. These improved ablation properties are due to a plasma-induced ablation mechanism—a well known interaction that predominates in the femtosecond time regime. As the interaction time is in this time range, and therefore faster than most of the thermal excitation modes, the nature of this process is predominantly electronic [13–16]. Furthermore, as the plasma formation is a multiphoton process in this time regime, the wavelength is not a relevant parameter.

The majority of the results reported in literature on femtosecond ablation are based on single or few laser shot experiments. However, thermal damage may occur when a high number of pulses are delivered [17]. Thermal loading comparable to long pulsed laser ablation can occur when attempting to reach clinically viable tissue ablation rates of dental hard tissues by employing high repetition rates and long exposure times in a stationary application.

Earlier studies explored femtosecond laser ablation of dental hard tissues, by varying irradiation parameters (pulse delivery methods, water cooling, light dose, etc.) to evaluate main ablation properties (e.g., ablation threshold, thermomechanical damage extent, tissue morphology, etc.) of the material. At the same time, enamel and dentin are heterogeneous compounds. By changing the composition ratio of the constituents of enamel and dentin, ablation properties can be described more completely. Therefore, the target tissue composition has to be considered a relevant variable when exploring new aspects of femtosecond ablation mechanisms.

This study aims to evaluate the characteristics of femtosecond laser ablation of human dental hard tissues, previously subjected to controlled dehydration. The dehydration produces different levels of inherent hydration states (structural water composition). The changes observed in the ablation threshold will be shown to follow the Niemz theoretical model for plasma-induced ablation when the hydration condition is incorporated into the avalanche parameter.

Materials and methods

Sample preparation and storage

Thirty human teeth samples were used in this work, consisting of molars and premolars at stage 10 of Nolla (ANO), orthodontically indicated for extraction and obtained from a surgical department. The study was authorized by the Ethical Committee for Human Experimentation. The remaining periodontal tissue was removed, and a prophylaxis was performed using a brush with pumice powder and water at low speed. Finally, the teeth were cut below the cementoenamel junction using a carborundum disk at a low speed under air/water cooling. The segment containing the crown was used as the target surface.

The samples were polished to obtain plane surfaces of the target tissues using water and different types of sandpaper with growing granulation number (100, 180, 240, 320, 400, and 600, the higher granulation number standing for smoother polish). Half of the samples were polished until a plane surface of the enamel was obtained. The other half was polished until a favorable dentin plane surface was formed. For all specimens, the surfaces were located on the crown segment.

The samples (15 enamel and 15 dentin) were divided into three hydration groups: (1) hydrated, samples stored in distilled water until irradiation (control group); (2) dry, samples kept dry at room atmosphere for 24 h; and (3) ultradry, samples put in a 60 °C oven for 4 h. The groups were defined in this way in order to produce approximately equal hydration shifts (i.e., the percentage of structural water loss). This division resulted in $n=5$ specimens per group. Enamel and dentin layers were not separated. The weight of the specimens as a whole was measured to obtain a water loss percentage. The analysis of the ablation results are therefore based on a qualitative correlation, i.e., on the overall water loss percentage in the specimens with the local ablation effects. For all groups, the specimens were weighed using a precision balance (Marte®).

Femtosecond laser irradiation

All specimens were irradiated using a 70-fs, Q-Switched and Mode-Locked Libra® (Coherent, Palo Alto, CA,

USA) Ti:sapphire laser with three different exposure times (5, 10, and 15 s) and five different power levels, totalizing 15 different irradiation conditions per specimen. The irradiation spots were placed on the enamel or dentin surfaces following a 5×3 arrangement that resembled a table (five powers—columns; three irradiation times—lines). The separation between lines and columns were of 1 mm, approximately.

The laser was directed towards the previously polished surface of every specimen using a 20-cm-focus lens, which gave us a 16.8-μm spot diameter. The exposure time was determined by a mechanical shutter head controlled by a PC. The power levels were different for enamel and dentin. For enamel samples, power settings ranging from 200, 400, 600, 800 mW to 1 W were used. For dentin samples, we applied: 200, 400, 600, 670, and 730 mW. Different power levels for enamel and dentin were chosen based on a previous observation of strong thermal damage in dentin when powers above 600 mW had been applied. Following these conditions, we obtained 450 microcavities, being five for every irradiation condition, type of tissue (enamel or dentin), and hydration state. The samples were kept stationary during the irradiation with a set power and exposure time configuration, fixed on a micrometric *x*–*y* moving platform, which allowed the sample to be displaced precisely between distinct irradiation configurations.

Analysis method—diameter versus ablation threshold

All microcavities were analyzed under a microscope coupled with a charge-coupled device camera. A double white lamp is used for additional external illumination to improve the visibility of the specimens. Images of each microcavity border at the laser irradiation surface were obtained with a ×100 magnification.

The digital images were treated using Mat Lab® and an algorithm that returned a numeric output value for the microcavity edge diameter. To obtain such values, the edge diameters of a significant number of craters were measured under a microscope (which was coupled to a table driven by micrometric screws). The different distances measured were computed on the software based on the number of pixels within a horizontal line. Such lines were determined by two points, chosen by the user, representing the start and the end of the crater. The correlation between the number of pixels and the real distances measured on the first craters set the scale to obtain the diameter of the remaining craters. When comparing the error magnitude of the diameter measurements obtained using the microscope-table set versus using the software were found to be equivalent.

The main parameter targeted in the present work, the ablation threshold, was obtained indirectly through the measured microcavity diameter. This was achieved by relating the laser's Gaussian spatial distribution to the surface ablation profile, with the microcavity border defining the limit where ablation stops occurring. This gave us an estimate of the energy ablation threshold. From the previous description of the spatial beam profile, the threshold (I_{th}) is obtained by substituting the diameter of the microcavity (D) by two times the radius variable ($D=2r_{dist}$) in its Gaussian distribution [18]:

$$I_{th} = I_0 . \exp\left[-\frac{D^2}{2\omega_0^2}\right] \quad , \tag{1}$$

where I_0 and ω_0 stand for Gaussian peak intensity and the beam waist at the ablation surface, respectively. This technique allowed us to obtain the ablation threshold from surface characteristics, without the need of measuring the tissue volume removed.

Scanning electron microscopy

Scanning electron microscopy (SEM) imaging has been used to analyze the ablation results on the irradiated tissues having different hydration states. A specimen from each subgroup was chosen randomly and dehydrated in solutions of growing concentrations of alcohol. The specimens were sputter-coated with gold in a Balzers SDC-050 apparatus. The scanning electron microscope (LEO 440, 10 kV, 100 pA) was used to observe the microcavities produced by the 200 mW and 10-s irradiation condition. Electron micrographs were obtained at a magnification of ×1,800, ×5,000, and ×8,000.

Results

The hydration percentage values ($\%_{hyd}$) were calculated for human dentin and enamel specimens, based on weight measurements, and are shown in Table 1.

The hydration percentage values of dry and ultradry groups were obtained from the ratio between the weight of the samples after the group preparation and the weight in their previous hydrated state. The value 100 % was attributed to the hydrated samples group (control). This calculation can be summarized by the expression:

$$\%_{hyd} = W_{dehyd}/W_{hyd} \tag{2}$$

where $\%_{hyd}$ is the hydration percentage, and W_{hyd} and

Table 1 Average hydration percentage of the dry and ultradry specimens (sample number $n=5$), compared to the hydrated samples (control group): all percentages are taken after dehydration

Tissues	Hydrated (wt%)	Dry (wt%)	Ultradry (wt%)
Human enamel	100.00	98.85±0,06	97.58±0,20
Human dentin	100.00	98.58±0,24	96.65±0,08

W_{dehyd} are the respective weight of hydrated and dehydrated samples. The water losses are expected to be different for enamel and dentin [19].

The images of every microcavity edge of the irradiated specimens were captured. Figure 1a–d corresponds to the microcavity borders produced in human hydrated enamel for different powers and exposure times. We observe that, for the same power applied to the irradiated surface even at an increased irradiation time, the microcavity diameter does not change. This means that even when the resulting fluence has been tripled, there is no modification in the microcavity diameter.

Figure 2 shows that the dentin exposed surfaces reveal similar effects as the enamel samples when low power levels are applied, but strong thermal damage occurs for higher powers. Figure 2c and d shows thermal damage occurring after 670 mW irradiation power has been applied. Four distinct and quite distinguishable damage zones can be identified: Z1, microcavity; Z2, strong thermal damage/carbonization (black); Z3, lower thermal damage zone (dark gray); and Z4, unaffected region (light gray) [20]. A white rim can be seen in the images of the microcavity borders. This white rim is an artifact of the illumination set used to collect the images and cannot be interpreted as a damage zone. This four-zone configuration was present in every dentin specimen irradiated with powers above 600 mW. It differs from previous reports in literature, where a three-zone configuration has been observed when using a picosecond-pulsed laser [21].

From the obtained images in the present study, the thermal damage size was measured using the same method as previously for the measurement of the ablation diameter. The result was plotted as a function of the dehydration percentage ($\%_{dehyd}$) for a fixed configuration (Fig. 3). The dehydration percentage is calculated by $\%_{dehyd}=100-\%_{hyd}$. No predominant behavior can be obtained from the graph, as the number of hydration groups is small.

During the experiments, a growing number of microcracks were observed. These were produced during ablation for an increased dehydration, especially for dentin samples. The presence of microcracks is expected during the plasma-induced ablation with high applied fluence, as a consequence of shock-wave formation during the plasma expansion [22]. For this reason, such an increase has indeed been observed for higher power levels.

In Fig. 4, the microcavity edge diameter was converted into an ablation threshold, according to Eq. 1, and plotted as a function of the dehydration level for both human enamel and dentin. In Fig. 4, the ablation threshold clearly increases for higher dehydration levels, for both enamel and dentin. During the ablation promoted by ultrashort laser pulses (mainly plasma induced ablation), the threshold behavior states that the lesser water is present within dental hard tissues, the harder it is to remove it.

To analyze the dependence of the ablative, thermal and mechanical damage during ultrashort pulsed laser irradiation in greater detail, the SEM imaging can give useful information on tissue morphology. In Fig. 5a–d, microcavity walls of the ablated human dental hard tissues are shown. In Fig. 5a, an extremely precise border definition in hydrated human enamel can be seen, even for the multipulse interaction used in this work. However, Fig. 5b shows the enamel morphology for dry ablated human enamel, for the same power and exposure time (200 mW, 10 s). Based on the pictures, all observations made for hydrated enamel can be extended to dry enamel, except for the thermal damage done at low power levels. Looking closely at Fig. 5b, spherical-

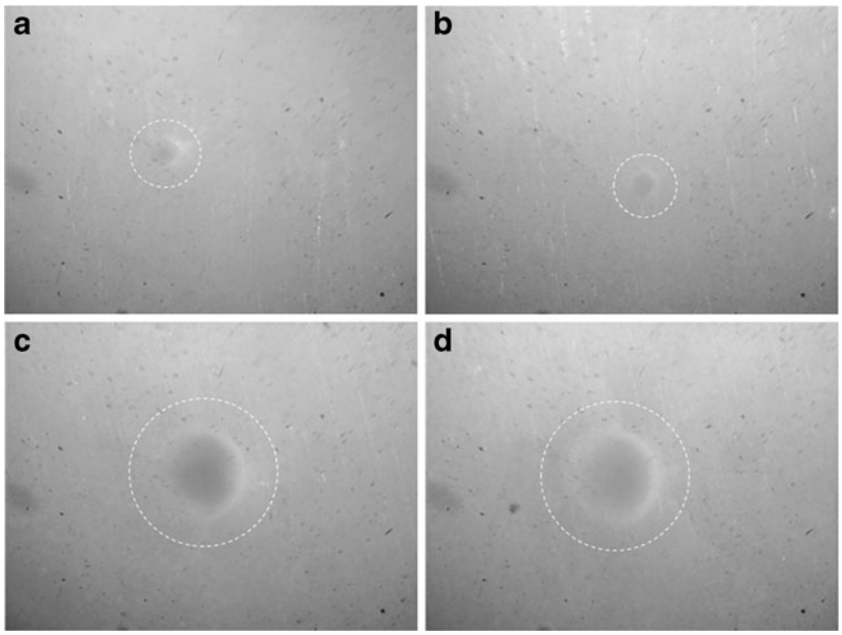

Fig. 1 Human hydrated enamel irradiated surfaces (×100): **a** 200 mW, 5 s; **b** 200 mW, 15 s, **c** 1 W, 5 s; and **d** 1 W, 15 s

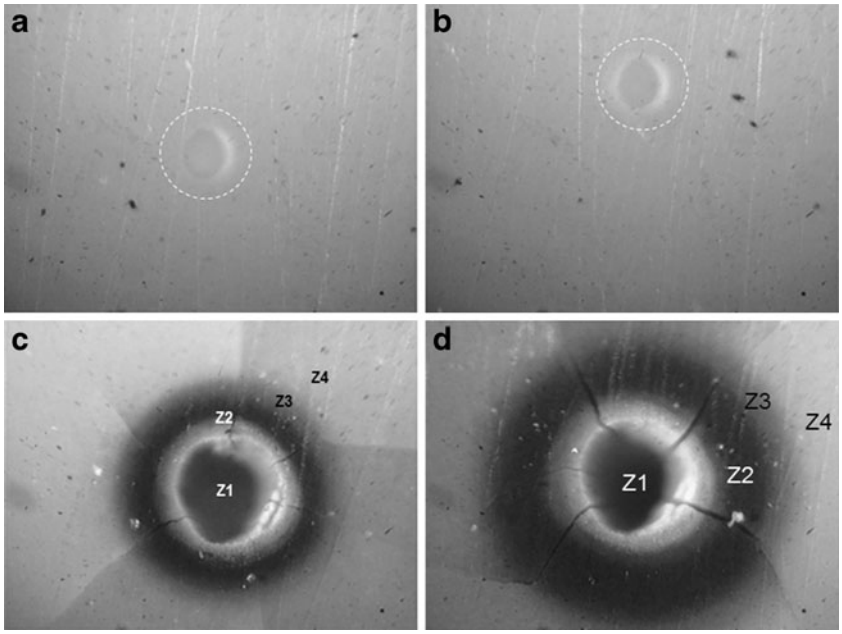

Fig. 2 Human hydrated dentin irradiated surfaces (×100): **a** 200 mW, 5 s; **b** 200 mW, 15 s, **c** 670 mW, 5 s; and **d** 670 mW, 15 s

shaped domains become evident. These domains are a sign of tissue melting and resolidification. In Fig. 5c and d (dentin specimens, hydrated and dry, respectively), similar aspects as those for the enamel specimens are visible, an additional evidence that the ejected material on the micro-cavity walls is responsible for obliterating the dentin tubules.

Mathematical and theoretical efforts have been made to describe the plasma-induced ablation. One of these models was presented by Niemz [23] and Lossel et al. [24], where plasma formation is described through the temporal behavior of the electron density function. This equation can be solved in the regime of optical breakdown happening during the pulse interaction interval, to obtain the fluency ablation threshold:

$$\eta F_{\mathrm{th}} = \frac{s}{2} + \sqrt{\left(\frac{s}{2}\right)^2 + \frac{\tau}{2\tau_{\mathrm{c}}}} + \frac{\tau}{\tau_{\mathrm{d}}} \quad , \tag{3}$$

where η stands for the ionization probability ($\beta=\eta I_0$) for a simplified square-shaped pulse model, F_{th} is the fluency threshold ($F_{\mathrm{th}}=\tau I_{\mathrm{th}}$), τ is the pulse width, τ_{c} is the characteristic mean time of inelastic collisions, and τ_{d} is the diffusion mean time constant.

The term s is called threshold parameter and stands for the ratio between the electron density at the instant of optical breakdown (N_τ) to the density at the beginning of the plasma

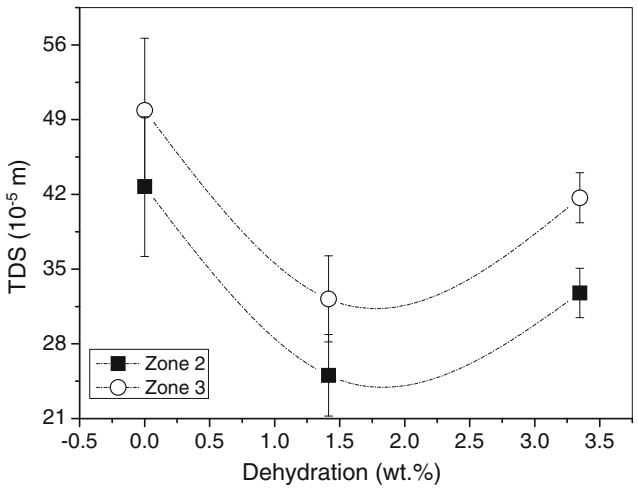

Fig. 3 Comparison of the average size of the thermal damage zone (Z2 versus Z3) as a function of dehydration for human dentin (730 mW, 10 s). Standard deviation are show as error bars ($n=5$)

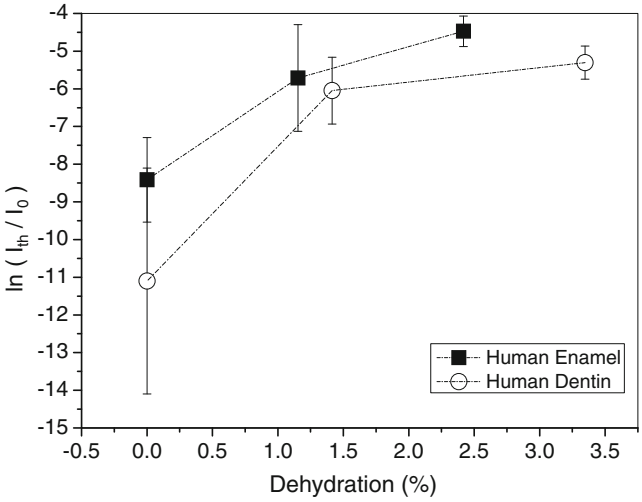

Fig. 4 Average ablation threshold versus dehydration growth of human dental hard tissues. Exposure time: 5 s. $F=1.13\times10^5$ J/cm^2 (200 mW). Standard deviation are show as error bars ($n=5$)

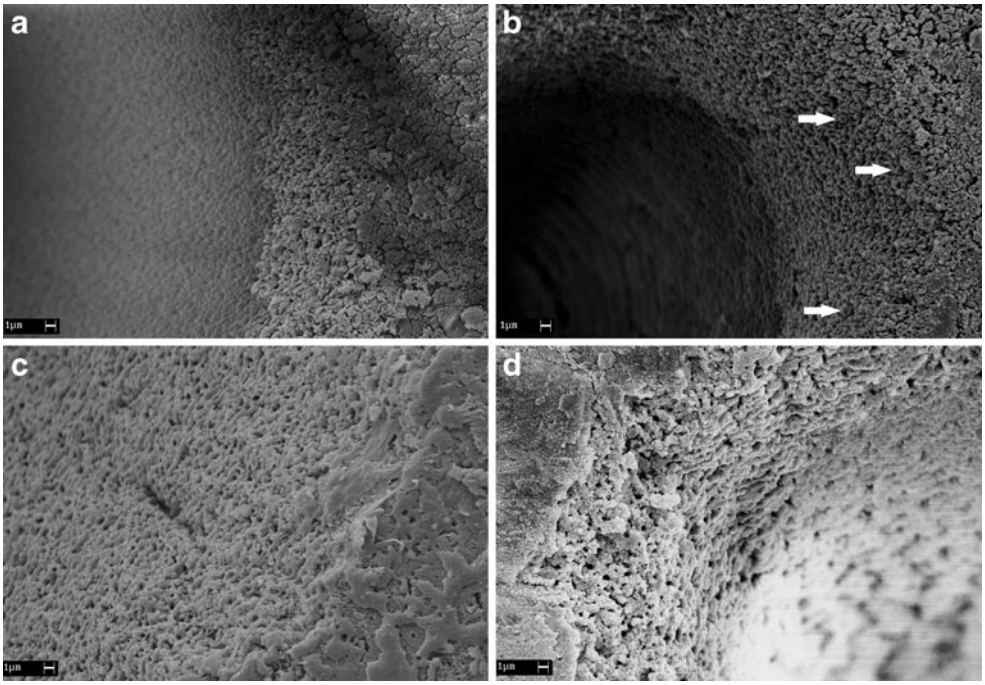

Fig. 5 SEM images of the microcavity walls of irradiated spots of: **a** hydrated enamel, **b** dry enamel, **c** hydrated dentin, and **d** ultradry dentin [200 mW, 10 s (×8,000 magnification)]. The *arrows* in **b** indicate the spherical-shaped domains, which is a sign of hard tissue fusion and resolidification

formation (N_0) [22]:

$$s = (\beta - \delta) - \ln\left(1 + \frac{\gamma N_\tau}{\beta - \delta}\right) \quad , \tag{4}$$

where δ is the electron diffusion parameter, and γ is the electron-tissue inelastic collision parameter. The parameter β is the avalanche parameter, describing the ionization process (source term).

In this work, we propose an adaptation on the description of the avalanche parameter appearing in this mathematical model. The ionization energy must be different for every type of molecule, as it depends on the energy level configuration for each molecule. The contribution to plasma formation must therefore differ for every tissue component. The electron avalanche parameter can be split into individual parameters for distinct molecular types:

$$\beta = \sum_i f_i \beta_i = I_0 \sum_i f_i \eta_i \quad , \tag{5}$$

$$\sum_i f_i = 1 \ . \tag{6}$$

The f_i term is the molecular fraction of the ith component species, normalized to unity. The ith ionization probability can be written as:

$$\eta_i \propto \exp\left(-\frac{E_i}{k_B T}\right) \quad , \tag{7}$$

where E_i is the ionization energy, k_B the Boltzmann constant, and T is the temperature.

Discussion

Literature describes two classes of water within the tooth structure, namely, structural and interstitial water. The structural water is understood as being the water adsorbed on the surfaces of the hard tissue microstructure (pores, tubules, and defects). The interstitial water is water-trapped within the hydroxyapatite crystals and prisms. As the temperature obtained during the preparation of the samples was fixed at 60 °C, the structural water is the only class of water that can be set free in our procedures. Interstitial water is thermally unstable only at temperatures between 200 and 400 °C and above [25–27]. An additional measurement was done to determine the maximum amount of water that could be removed following a more severe dehydration treatment (60 °C oven). The measurements were performed every 60 min, for 10 h. The maximum of 6 % of dehydration percentage for human teeth specimens was observed at the end of the experiment. After 10 h of measurement, the specimens reached a critical dehydration point, shattering into several pieces. Therefore, considering 6 % of the total amount of water that can be eliminated as a maximum from the specimens, we fixed half of this total amount (3 %) to be removed for the ultradry group.

In relation to the light microscopy images (Figs. 1 and 2), it is worth mentioning that the observed diameter, at the irradiated surface, is related to the first instants of plasma formation. At that point in time, the tripled fluence for a fixed power by only increasing the exposure time does not affect the microcavity diameter. Irradiation time may have an impact on the ablated volume, a parameter not taken into consideration in this study. Contrary to this, the ablated

surface diameter responds strongly to an increase in power (Fig. 1c, d), as this means a larger beam waist applied and, consequently, a wider superficial area of the plasma. No significant thermal or mechanical damage is observed for this group with this imaging technique.

For dentin specimens, the observed thermal damage is explained when high pulse repetition rates (a high number of delivered pulses) are applied. The interaction with ultrafast pulses enhances the multiphoton absorption, but does not prevent linear absorption from occurring. Therefore, high pulse repetition rates enable thermal energy to be accumulated between pulses. As the number of applied pulses in this work is very high (minimum of 5,000 pulses), the nonthermal damage pattern of few-shot experiments and low repetition rates, as reported by other authors, is not expected.

The observed increasing number of microcracks for higher dehydration is an evidence of the influence of water on the mechanical properties of dental hard tissues. This result can be interpreted as a decrease in the mechanical damage threshold for a condition of low structural water composition.

It must be highlighted that during plasma induced ablation, only plasma generation and expansion are governed by ultrashort interactions. Once the plasma is formed, the way in which thermal energy is transferred to the surrounding tissue does not necessarily follow the ultrashort dynamics. It seems that heat is transferred from the plasma to the surrounding tissue by simple heat flow dynamics as a secondary interaction mechanism. This hypothesis is reinforced as both zones respond equally to dehydration, probably as a result of the same thermal energy progression. It has also been stated that the energy portion below the ablation threshold contributes to the formation of thermal damage zones [17, 28].

It seems that the behavior of the ablation threshold observed (Fig. 4) may be linked to the hydrogen bonding, which is responsible for coupling the water to the hydroxyapatite through hydroxyl sites [29]. These strong intermolecular interactions are oriented opposite to the interactions, which compose the crystalline structure of hydroxyapatite (covalent bonding). As a result, the bound energy that forms the crystalline structure is decreased when water is present. Once it is removed, the material becomes more energetically bonded, requiring a larger amount of energy from the plasma to break the crystalline bonds, thus increasing the ablation threshold.

It is noticeable that, for all points on the graph (Fig. 4), the ablation threshold of enamel is always higher than for dentin. As it is known [30, 31], dentin has a higher percentage of water composition than enamel. Furthermore, the higher water percentage contained within the dentin structure makes the crystalline formation more diffuse and the hydroxyapatite crystals smaller, thus leading to a structure with a higher number of defects [32, 33].

Another possible hypothesis is that the dynamics of the plasma formation changes for distinct hydration conditions. Water, as well as other components of the hard dental tissues, can contribute to a generation of plasma. Each of the contributions can be accounted for separately. As plasma-induced ablation relies on the ionization of molecules, the plasma formation of a heterogeneous material is composed macroscopically by the set of all microscopic ionization processes. If the relative fraction of the component molecules is maintained constant, the ablation threshold will also be constant, and it can be assumed to be an intrinsic property of the material.

In this study, the relative fraction of water, hydroxyapatite, and the organic matrix has been changed. As a result, each set of molecules have their particular contribution to the plasma formation shifted, which, in turn, changes the ablation threshold as a whole. According to the theoretical modeling described in the previous section, the probability of a molecule to be ionized decreases for higher ionization energies. Therefore, the relative composition fraction for hydroxyapatite and organic components attains higher values during dehydration in order to keep the normalization valid. Hydroxyapatite and organic molecules have lower ionization energies and, therefore, higher ionization probabilities. When adding these assumptions to Eq. 5, the total electron avalanche parameter β must increase, causing the threshold parameter s to increase as given by Eq. 4. This in turn causes the ablation threshold to increase, as observed experimentally.

In addition, the SEM images show an amount of ejected material that did not have enough energy to leave the microcavity. We assume, however, that the hydroxyapatite prisms are preserved after the laser irradiation, keeping their original form, size, and spatial disposition underneath the ejected material layer. The molecule ejection is responsible for consuming most of the energy accumulated by the plasma.

The energy transferred from the plasma also leads to a temperature increase in the surrounding tissue up to the melting point. The spherical-shaped domains appearing in Fig. 5b are reported as signs of tissue fusion and resolidification [34]. As such domains appear more dramatically for the dry groups, this can be interpreted as a decreased thermal threshold with dehydration. Due to its high heat capacity, water is said to be responsible for absorbing locally the heat. Its absence causes heat to be transferred exclusively to the remaining structure, enhancing the melting process.

For dentin specimens, the obliteration of dentin tubules may have clinical implications, e.g., a pain reduction, as the obliteration blocks the transmission of the external environment conditions to the nerves inside the tubules.

Conclusions

In conclusion, dental hard tissues in different hydration states presented shifts in their ablation properties when

irradiated with femtosecond laser pulses. An increase in the ablation threshold was observed when the structural water composition of the tissue had been decreased. This fact was supported after having incorporated composition-dependent parameters into the plasma-induced ablation theory, describing how water participates in the plasma formation. We also found that the structural water of dental hard tissue can act as a tension controller, minimizing the local mechanical stress. Furthermore, using SEM imaging, a local increase in the thermal damage levels was observed for growing dehydration, but no significant increase in the size of the macroscopic thermal damage zones was observed. This phenomenon may occur due to the fact that the presence of structural water locally suppresses the heat absorption by other tissue components. This fact has its origin on the high specific and latent heats of water compared to these other components, as well as the heat loss during vapor formation.

Acknowledgments We would like to thank the Brazilian funding agencies CAPES, CNPq, FAPESP, and FAPEAL for the financial support of this work. The research of F.G. Rego-Filho and G. Nicolodelli are supported by graduate studentships from CAPES and CNPq.

References

1. Goldman L, Hornby P, Meyer R, Goldman B (1964) Impact of the laser on dental caries. Nature 203:417–417
2. Stern RH, Sognnaes RF (1964) Laser beam effect on dental hard tissues. J Dent Res 43:873–873
3. Hsu PJ, Chen JH, Chuang FH, Roan RT (2006) The combined occluding effects of fluoride-containing dentin desensitizer and Nd–Yag laser irradiation on human dentinal tubules: an in vitro study. Kaohsiung J Med Sci 22:24–29
4. Porto ICCM, Andrade AKM, Montes MAJR (2009) Diagnosis and treatment of dentinal hypersensitivity. J Oral Sci 51:323–332
5. Moriyama EH, Zângaro RA, Villaverde AB, Lobo PD, Munin E, Watanabe IS, Júnior DR, Pacheco MT (2004) Dentin evaluation after Nd:YAG laser irradiation using short and long pulses. J Clin Laser Med Surg 22:43–50
6. Zach L, Cohen G (1965) Pulp response to externally applied heat. Oral Surg Oral Med Oral Pathol 19:515–530
7. Hibst R, Keller U (1989) Experimental studies of the application of the Er:YAG laser on dental hard substances. Laser Surg Med 9:338–344
8. Walsh LJ, Perham S (1991) Enamel fusion using a carbon dioxide laser: a technique for sealing pits and fissures. Clin Prev Dent 13:16–20
9. Altundasar E, Özçelik B, Cehreli ZC, Matsumoto K (2006) Ultramorphological and histochemical changes after ER, CR:YSGG laser irradiation and two different irrigation regimes. J Endodontics 32:465–468
10. Mir M, Gutknecht N, Poprawe R, Vanweersch L, Lampert F (2009) Visualising the procedures in the influence of water on the ablation of dental hard tissue with erbium:yttrium-aluminium-garnet and erbium, chromium:yttrium–scandium–gallium–garnet laser pulses. Lasers Med Sci 24(3):365–374
11. Burkes EJ Jr, Hoke J, Gomes E, Wolbarsht M (1992) Wet versus dry enamel ablation by Er:YAG laser. J Prosthet Dent 67:847–851
12. Tsai C-L, Lin Y-T, Huang S-T, Chang H-W (2002) In vitro acid resistance of CO_2 and Nd:YAG laser-treated human tooth enamel. Caries Res 36:423–429
13. Perry MD, Stuart BC, Banks PS, Feit MD, Yvanovsky V, Rubenchik AM (1999) Ultrashort-pulse laser machining of dielectric materials. J Appl Phys 85:6803–6810
14. Neev J, Da Silva LB, Feit MD, Perry MD, Rubenchik AM, Stuart BC (1996) Ultrashort pulse lasers for hard tissue ablation. IEEE J Sel Top Quant Electron 2(4):790–800
15. Rode AV, Gamaly EG, Luther-Davis B, Taylor BT, Dawes J, Chan A, Lowe RM, Hannaford P (2002) Subpicosecond laser ablation of dental enamel. J Appl Phys 92(4):2153–2158
16. Dumitru G, Romano V, Weber HP, Sentis M, Marine W (2002) Femtosecond ablation of ultrahard materials. Appl Phys A 74 (6):729–739
17. Dong Y, Molian P (2003) Femtosecond pulsed laser ablation of 3C–SiC thin film on silicon. Appl Phys A 77:839–846
18. Liu JM (1982) Simple technique for measurements of pulsed Gaussian-beam spot sizes. Opt Lett 7(5):196–198
19. Dutra-Correa M, Rodrigues JR, Moriyama LT, Lizarelli RFZ, Bagnato VS (2005) Avaliação das Propriedades Térmicas. Químicas e Mecânicas Comparando Dente Bovino e Dente Humano. Braz Oral Res 19:184
20. Dutra-Correa M, Rodrigues JR, Nicolodelli G, Kurachi C, Bagnato VS (2010) Femtosecond LASER ablation of bovine and human hard dental tissues: comparative morphological and physicochemical analysis. J Bras Laser 2:25–32
21. Lizarelli RFZ, Kurachi C, Misoguti L, Bagnato VS (1999) Characterization of enamel and dentin response to Nd:YAG picosecond laser ablation. J Clin Laser Med Surg 17(3):127–131
22. Niemz MH (2003) In: Niemz MH (ed) Laser tissue interactions: fundamentals and applications. Springer, New York, p 328
23. Niemz MH (1995) Theshold dependance of laser-induced optical breakdown on pulse duration. Appl Phys Lett 66:1181–1183
24. Lossel FH, Niemz MH, Bille JF, Juhasz T (1996) Laser-induced optical breakdown on hard and soft tissues and its dependence on the pulse duration: experiment and model. IEEE J Quantum Electron 32(10):1717–1722
25. Holcomb DW, Young RA (1980) Thermal decomposition of human tooth enamel. Calcif Tissue Int 31:189–201
26. Little MF, Casciani FS (1966) The nature of water in sound human enamel: a preliminary study. Arch Oral Biol 11(6):565–571
27. LeGeros RZ, Bonel G, Legros R (1978) Types of H_2O in human enamel and in precipitated apatites. Calcif Tissue Int 26:111–118
28. Ladieu F, Martin Ph, Guizard S (2002) Measuring thermal effects in femtosecond laser-induced breakdown of dielectrics. Appl Phys Lett 81(6):957–959
29. Dry ME, Beebe RA (1960) Adsorption studies on bone mineral and synthetic hydroxyapatite. J Phys Chem B 64(9):1300–1304
30. Baratieri LN, Baratieri LN (2001) Odontologia Restauradora: fundamentos e possibilidades. Santos, São Paulo, p 740
31. Katchburian E, Arana-Chavez VE (1999) In: Katchburian E, Arana-Chavez VE (eds) Histologia e embriologia oral. Médica Panamericana, São Paulo, p 381
32. Bachmann L, Zezell DM (2005) Estrutura e Composição do Esmalte e da Dentina: tratamento térmico e irradiação Laser. Livraria da Física, São Paulo, p 298
33. Krüger J, Kautek W, Newesely H (1999) Femtosecond-pulse laser ablation of dental hydroxyapatite and single-crystalline fluoroapatite. Appl Phys A 69:403–407
34. Paghdiwala AF (1991) Does the laser work on hard dental tissue? J Am Dent Assoc 122:79–80

Compressive Strength of Dental Composite Resins Photo-Activated with Different Light Tips

ARTICLE *in* LASER PHYSICS · APRIL 2013

Impact Factor: 1.03 · DOI: 10.1088/1054-660X/23/4/045604

12 AUTHORS, INCLUDING:

Sergei Rabelo Caldas

Universidade Federal do Rio Grande do Norte

19 PUBLICATIONS **12** CITATIONS

SEE PROFILE

Saturnino Calabrez-Filho

São Paulo State University, UNIUBE

14 PUBLICATIONS **10** CITATIONS

SEE PROFILE

Edson Alves Campos

São Paulo State University

78 PUBLICATIONS **322** CITATIONS

SEE PROFILE

Marcelo Ferrarezi de Andrade

São Paulo State University

89 PUBLICATIONS **292** CITATIONS

SEE PROFILE

Laser Phys. **23** (2013) 045604 (5pp) doi:10.1088/1054-660X/23/4/045604

Compressive strength of dental composites photo-activated with different light tips

M R Galvão[1], S G F R Caldas[2], S Calabrez-Filho[3], E A Campos[1], V S Bagnato[4], A N S Rastelli[1,4,5] and M F Andrade[1]

[1] Department of Restorative Dentistry, Araraquara School of Dentistry, Univ. Estadual Paulista-UNESP Araraquara, SP, Brazil
[2] Department of Pediatric Dentistry, Araraquara School of Dentistry, Univ. Estadual Paulista-UNESP, Araraquara, SP, Brazil
[3] Department of Dental Materials and Restorative Dentistry, University of Uberaba, Uberaba, MG, Brazil
[4] São Carlos Physics Institute, Optical Group, Biophotonics Lab., University of São Paulo, São Carlos-SP, Brazil

E-mail: alrastelli@foar.unesp.br

Received 31 March 2012, in final form 9 October 2012
Accepted for publication 18 October 2012
Published 21 February 2013
Online at stacks.iop.org/LP/23/045604

Abstract
The aim of this study was to evaluate the compressive strength of microhybrid (Filtek^{TM} Z250) and nanofilled (Filtek^{TM} Supreme XT) composite resins photo-activated with two different light guide tips, fiber optic and polymer, coupled with one LED. The power density was 653 mW cm^{-2} when using the fiber optic light tip and 596 mW cm^{-2} with the polymer. After storage in distilled water at 37 ± 2 °C for seven days, the samples were subjected to mechanical testing of compressive strength in an EMIC universal mechanical testing machine with a load cell of 5 kN and speed of 0.5 mm min^{-1}. The statistical analysis was performed using ANOVA with a confidence interval of 95% and Tamhane's test. The results showed that the mean values of compressive strength were not influenced by the different light tips ($p > 0.05$). However, a statistical difference was observed ($p < 0.001$) between the microhybrid composite resin photo-activated with the fiber optic light tip and the nanofilled composite resin. Based on these results, it can be concluded that microhybrid composite resin photo-activated with the fiber optic light tip showed better results than nanofilled, regardless of the tip used, and the type of the light tip did not influence the compressive strength of either composite. Thus, the presented results suggest that both the fiber optic and polymer light guide tips provide adequate compressive strength to be used to make restorations. However, the fiber optic light tip associated with microhybrid composite resin may be an interesting option for restorations mainly in posterior teeth.

(Some figures may appear in colour only in the online journal)

1. Introduction

Dental composite was developed by Bowen in the 1960s. Since then, this material has suffered various transformations to improve its physical and mechanical properties, making it increasingly acceptable for dental restorations in the posterior teeth [1, 2].

The photo-activation systems previously used were based on ultraviolet light sources. These systems were replaced by quartz–halogen tungsten (QTH) as an improvement over ultraviolet lights because of their harmful effects on the

[5] Address for correspondence: Araraquara School of Dentistry, Department of Restorative Dentistry, Univ. Estadual Paulista-UNESP, Araraquara, SP, Brazil. Humaitá St. 1680, Araraquara, SP, 14.801-903, Brazil.

Table 1. Characteristics of composite resins used in the study (manufacturers' data).

Material	Manufacturer	Shade	Material type	Matrix	Filler size	Filler volume	Lot
Filtek ™ Supreme XT	3M Espe	A_2	Nanofilled composite	Bis-GMA TEGDMA UDMA and Bis-EMA	Agglomerated/non-aggregated of 20 nm silica nanofiller and a loosely bound agglomeratic silica nanocluster consisting of agglomerates of primary silica nanoparticles of 20 nm size fillers.	59.5%	8BK
Filtek ™ Z250	3M Espe	A_2	Microhybrid composite	Bis-GMA TEGDMA UDMA and Bis-EMA	Zirconia/silica (medium size of 0.6 μm)	60%	9KK

human eye and limitations of curing depth [3]. QTH lamps are composed of a quartz tungsten thread found in the bulb, enclosed by an inert gas filter, refrigerating system and optic fibers for light conduction. Besides the heat production, another inconvenience is that the lamp, reflector and filter can degrade over time due to high operating temperatures. This effect leads to decreased effectiveness of polymerization, promoting inadequate physical properties and increased risk of premature failure of restorations [4, 5].

Different light-curing units (LCUs) have been developed, with newer types of light-curing source using other curing methods such as lasers and xenon arcs. Laser and xenon arc curing units have the advantage of reduced curing times; however, these LCUs have a larger and more complicated construction, and are more costly than halogen. The use of lasers is currently more concerned with the suppression of dental hypersensitivity, soft tissue surgeries, intracanal disinfection, caries removal, and cavity preparation [6–11].

More recently, to overcome the problems inherent to halogen light, light emitting diodes (LEDs) have been used for curing resinous materials. LED units have some advantages over QTH lamps as they have lifetimes of over 10,000 h and no need for cooling systems or filters, and the thermal emission is significantly lower than that of halogen lamps with little wasted energy and minimum heat generation [4, 12–14].

Technologies have been developed that enable production of the appropriate amount of light for the efficient conversion of composite resins [15–18], resulting in improved physical and chemical properties, which can be analyzed and studied by several methods, such as hardness testing and analysis of the degree of conversion and compressive strength [19–23]. The compressive strength indicates the ability demonstrated by a material to withstand vertical stress. It is known that, during the act of chewing, the forces that are transmitted to the restorations can break them or promote tooth fracture [24–27].

Some factors can influence the polymerization of composite resins such as the different LCUs, power density, and wavelength and irradiation times. Another factor affecting the polymerization process is the light guide tip used for light transmission [28–30]. Nowadays, a wide variety of commercially available light guide tips claim to fit different operative procedures related to various clinical situations. Another problem that should be pointed out is that the light guide tips which are available for LED LCUs have a variety of diameters and are made from different materials. The light conductor system of such devices is based on a rigid tube that contains optical fibers with a vitreous inclusion, usually covered with amber glass, metal, fiber optic, or polymer. This coating is important to prevent the passage of light, especially on the lateral surface of the tip, and decrease the light scattering. Some studies have shown that the polymer tip scatters the guided light, thus reducing the power density at the end of the tip, which would have direct repercussions in the polymerization process of the composite [17, 31, 32].

Therefore, it is believed that the material covering the tips of the LCU can influence the values of final power density due to light scattering over its route. In this way, this study evaluated the influence of the light guide tips used in the photo-activation on the compressive strength of dental composite resins.

2. Material and methods

In this experiment two different composites were used: the universal microhybrid Filtek™ Z250 (3M ESPE Dental Products Division, St Paul, MN, USA), and the nanofilled Filtek™ Supreme XT (3M ESPE Dental Products Division, St Paul, MN, USA) (table 1).

A blue LED LCU (Ultrablue IS, DMC, São Carlos, SP, Brazil, serial number 002041) with two different light guide tips (fiber optic and polymer) was used in this study. The power output was measured using a Fieldmaster power meter (Fieldmaster Power to Put, Coherent model no FM, set no WX65, part no 33-0506, USA). The values of power density (mW cm^{-2}) were computed as the ratio of the output power and the area of the tip with the following formula:

$$I = P/A$$

where P is the power in milliwatts, A is the area of the light tip in squared centimeters and I is the power density. The LED LCU produced 653 mW cm^{-2} coupled with the metal light guide tip and 596 mW cm^{-2} with the polymeric tip. The characteristics of the light guide tips are shown in table 2.

Cylindrical specimens, 4 mm in diameter and 8 mm in height, were prepared by composite insertion into a stainless steel split mold. The specimens were photo-activated for

Table 2. Characteristics of the light guide tip used in the study.

LCU	Light guide tip	Diameter entry (mm)	Diameter exit (mm)	Geometry
Ultrablue IS	Fiber optic	11	8	Turbo
	Polymer	10	8	Turbo

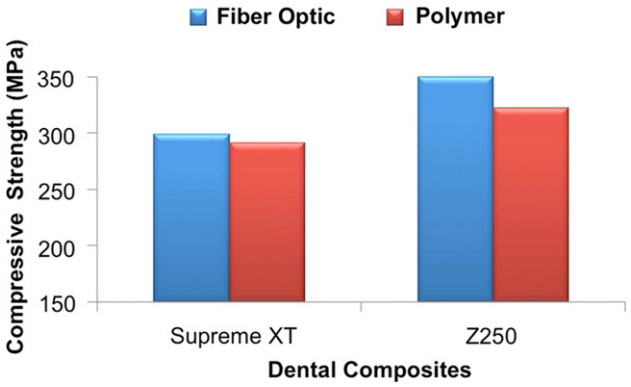

Figure 1. Mean values of compressive strength depending on the light guide tip and dental composites.

20 s ($n = 8$). The photo-activation was carried out at every increment of 2 mm. The specimens were removed from the split mold and were photo-activated for a further 20 s on the bottom and on the four lateral surfaces. The specimens were then stored in distilled water at $37 \pm 2\,^{\circ}\mathrm{C}$ for 7 days [33].

Following the storage period, the compressive strength test was performed employing an EMIC mechanical test machine (model DL2000, São José dos Pinhais, Brazil), with a load cell of 5 kN and programmed speed of 0.5 mm min^{-1}. Data recording and processing for compressive strength values in megapascals were performed by the computer program Tesc.

The data were statistically analyzed by analysis of variance (ANOVA) using a confidence interval of 95% and Tamhane's test.

3. Results

Figure 1 shows the mean values of compressive strength obtained with the different light guide tips and dental composites. The statistical test showed that the compressive strength was not influenced by the light guide tips ($p > 0.05$); however, some differences were observed for dental composites.

By observing the results of the nanofilled composite resin photo-activated with different tips, it was found that there were no statistically significant differences. The same can be observed for microhybrid composite resin, which was not influenced by the different tips.

Tamhane's test indicates that significant differences were found between the microhybrid composite resin photo-activated with the fiber optic light guide and the nanofilled composite resin photo-activated with both light guide tips. In absolute values, the nanofilled composite resins associated with the polymer tip showed the lowest values for compressive strength. However, they were statistically equivalent to the microhybrid composite resin photo-activated using the polymer light tip.

4. Discussion

The purpose of this study was to evaluate whether the type of material used in the light guide tip might have an influence on the resulting compressive strength of resin composites. For this purpose, two light guide tips (fiber optic and polymer) were used coupled to one LED LCU, and two composites (microhybrid and nanofilled).

Adequate polymerization is a crucial factor to obtain optimal physical properties and clinical performance of composite resins. Inadequate polymerization has been associated with poor physical properties, high solubility, low retention, adverse pulpal responses and low biocompatibility, which may affect the clinical performance of restorative procedures [13, 34].

To compare the ability of different light guide tips coupled to an LED to cure dental composite material, suitable tests had to be chosen. Although many methods for testing the physical properties of dental composites are known, most are orientated towards comparing the properties of the different materials rather than the LCUs [35–37]. Compressive strength tests have previously been used to compare different LCUs but specifically in the present study this test was employed to compare different light guide tips [38, 39].

Compressive strength has a particularly important role in the mastication process since most of the masticatory forces are of compressive nature. The maximum resistance to compression is calculated by the original cross-sectional area of the test specimen and the maximum force applied [4, 40].

A clinically relevant compressive strength value may be based on the compressive strength values of natural mineralized tissues. The compressive strength of enamel has been measured to be 384 MPa. The fracture strength of natural molars however is around 305 MPa while other teeth have generally lower fracture strengths. The latter value may offer a good mechanical standard to select the optimal strength of composite resins used in posterior teeth [20, 41].

In this study, photo-activation using a fiber optic light guide tip produced a compressive strength of 299.37 MPa for nanofilled resin and 350.48 MPa for microhybrid resin. However, when a polymer light guide tip was used the compressive strength was 291.96 MPa (nanofilled resin) and 322.31 MPa (microhybrid resin). Thus, according to these results, it seems that the microhybrid composite showed better compressive strength outcomes than nanofilled, mainly when the fiber optic tip was used.

Simply considering each material, no statistically significant differences in compressive strength were found between groups light cured with fiber optic or polymer light guide tips, although there was a tendency to higher compressive strength values for the fiber optic light guide tip. This can be explained by the dispersion of light in the route of the tip, which have direct impact on the final power density, and then on mechanical properties [28].

The power density from the LCU, also referred as light intensity, is the number of photons per second (watts, W) emitted by the light source per unit area (W cm^{-2}). It has been reported that a minimum power density of 300–400 mW cm^{-2} is required to adequately cure one increment of 1.5–2 mm of composite resin at the manufacturers' recommended curing time [42]. In a more effective LCU, more photons will be available for absorption by the photosensitizers. With more photons, more camphoroquinone molecules are raised to the excited state, react with the amine and form free radicals for polymerization [43–45]. This is in agreement with our study, because the power density using the fiber optic tip was 653 mW cm^{-2} and that using the polymer was 596 mW cm^{-2}, and as a final result the compressive strength of composite resins photo-activated with the fiber optic light tip was greater than that obtained with the polymer tip.

In the present study, the dental composites (microhybrid and nanofilled) provided an important role in polymerization. The microhybrid composite resin presented higher absolutes values of compressive strength than the nanofilled one (figure 1). The literature has shown that chemical composition can influence mechanical properties [46–49]. According to Yearn [50] and Swartz *et al* [51], factors related to composites include shade, translucency and filler particle size, load and distribution. Mitra *et al* [2] believe that the composite of nanoparticles has good light transmission and presents physical and mechanical properties equivalent to those of microhybrid resin.

The resin matrix composites are an important group of materials in restorative dentistry [52, 53]. Their development and formulation are based on the fact that the addition of inert fillers to acrylic and dimethacrylate resins can significantly improve certain properties. The effect of filler depends on the type, shape, size and amount used and on the existence of efficient coupling between filler and matrix resin [54–56]. Many properties (e.g. compressive strength) are improved as the filler content is increased.

Another interesting observation is that the variability of the compressive strength of composite resins photo-activated with the polymer tip was greater than with the fiber optic, as shown by the standard deviation (±SD). This can be considered an important characteristic of the tip, as it was shown to be less predictable than the fiber optic tip, which probably resulted in lower values of compressive strength.

5. Conclusions

The results obtained for this study indicate that the light guide tips did not influence the compressive strength of the dental composites. The microhybrid Filtek Z250 composite photo-activated with a fiber optic tip showed better results than the nanofilled composite resin, mainly when the fiber optic tip was used.

Based on the results of this study it may be suggested that the fiber optic tip associated with microhybrid composite resin may be an interesting option for restorations in the posterior teeth.

Acknowledgments

This study was supported by CAPES Brazil. The authors would like thank the Physics Institute of São Carlos, University of São Paulo, São Carlos, SP, Brazil, Department of Dental Materials and the Laboratory of Mechanics Faculty of Dentistry of Araraquara Universidade Estadual Paulista 'Júlio de Mesquita Filho'—UNESP, Araraquara School of Dentistry, University of São Paulo, SP, Brazil, for the use of the EMIC mechanical test machine.

References

[1] St-Georges A J, Swift E J, Thompson J Y and Heymann H O 2003 *Dent. Mater. J.* **19** 406
[2] Mitra S B, Wu D and Holmes B N 2003 *J. Am. Dent. Assoc.* **134** 1382
[3] Saade E G, Bandéca M C, Rastelli A N S, Bagnato V S and Porto-Neto S T 2009 *Laser Phys.* **19** 1276
[4] Silva C M and Dias K R H C 2009 *Braz. Dent. J.* **20** 54
[5] Rueggeberg F A 1999 *Compend. Cont. Educ. Dent.* **20** 4
[6] Jelínková H, Dostálová T, Nemec M, Koranda P, Miyagi M, Iwai K, Shi W-Y and Matsuura Y 2007 *Laser Phys. Lett.* **4** 835
[7] Malta D A M P, Kreidler M A M, Villa G E, Andrade M F, Fontana C R and Lizarelli R F Z 2007 *Laser Phys. Lett.* **4** 153
[8] Marraccini T M, Bachmann L, Wigdor H A, Walsh J T Jr, Turbino M L, Stabholtz A and Zezell D M 2006 *Laser Phys. Lett.* **3** 96
[9] Marraccini T M, Bachmann L, Wigdor H A, Walsh J T Jr, Stabholtz A and Zezell D M 2005 *Laser Phys. Lett.* **2** 551
[10] Clavijo V R G, Bandéca M C, Calixto L R, Nadalin M R, Saade E G, Oliveira-junior O B and Andrade M F 2009 *Laser Phys.* **19** 1920
[11] Rossato D M, Bandéca M C, Saade E G, Lizarelli R F Z, Bagnato V S and Saad J R C 2009 *Laser Phys.* **19** 2144
[12] Nomoto R 1997 *Dent. Mater. J.* **16** 60
[13] Rastelli A N S, Jacomassi D P and Bagnato V S 2008 *Laser Phys.* **18** 1570
[14] Rastelli A N S, Jacomassi D P and Bagnato V S 2008 *Laser Phys.* **18** 1003
[15] Rode K M, Kawano Y and Turbino M L 2007 *Oper. Dent.* **32** 571
[16] Hammesfahr P D, O'Connor M T and Wang X 2002 *Compend. Cont. Educ. Dent.* **23** 18
[17] Galvão M R, Costa S X S, Victorino K R, Ribeiro A A, Menezes F C H, Rastelli A N S, Bagnato V S and Andrade M F 2010 *Laser Phys.* **20** 1
[18] Calixto L R, Bandéca M C, Silva F B, Rastelli A N S, Porto-Neto S T and Andrade M F 2009 *Laser Phys.* **19** 1867
[19] Aravamudhan K, Floyd C J, Rakowski D, Flaim G, Dickens S H, Eichmiller F C and Fan P L 2006 *J. Am. Dent. Assoc.* **137** 213
[20] Jandt K D, Mills R W, Blackwell G B and Ashworth S H 2000 *Dent. Mater. J.* **16** 41

[21] Aguiar T C, Lima D M, Calixto L R, Saad J R C, Bandeca M C, Pinto S C S and Silva M A S 2011 *Polymers* **3** 998
[22] Rastelli A N S, Jacomassi D P and Bagnato V S 2008 *Laser Phys.* **18** 1074
[23] Bandéca M C, El-Mowafy O, Saade E G, Rastelli A N S, Bagnato V S and Porto-Neto S T 2009 *Laser Phys.* **19** 1050
[24] Maciel D, Dias A L, Moysés M R, Ribeiro J C R, Dias S C and Reis A C 2005 *Arch. Dent.* **41** 235
[25] Baharav H, Abraham D, Cardash H S and Helft M 1988 *J. Oral Rehabil.* **15** 167
[26] Oliveira F C, Denehy G E and Boyer D B 1987 *J. Am. Dent. Assoc.* **117** 57
[27] Roulet J F 1988 *J. Dent.* **16** 101
[28] Bhamra G S and Fleming G J 2008 *J. Dent.* **36** 643
[29] Kabbach W, Zezell D M, Bandéca M C, Pereira T M and Andrade M F 2010 *Laser Phys.* **20** 1833
[30] Kabbach W, Zezell D M, Bandéca M C and Andrade M F 2010 *Laser Phys.* **20** 1654
[31] Soares L E, Liporoni P C and Martin A A 2007 *Oper. Dent.* **32** 160
[32] Corciolani G, Vichi A, Davidson C L and Ferrari M 2008 *Oper. Dent.* **33** 325
[33] Brandao L, Adabo G L, Vaz L G and Saad J R 2005 *Braz. Oral Res.* **19** 272
[34] Queiroz R S, Bandéca M C, Calixto L R, Gaiao U, Cuin A and Porto-Neto S T 2010 *Laser Phys.* **20** 1647
[35] Bandéca M C, Kassem A S, El-Mowafy O, Nadalin M R, Queiroz R S, Clavijo V G R and Saad J R C 2010 *Mater. Res.* **13** 25
[36] Queiroz R S, Bandéca M C, Calixto L R, Saade E G, Nadalin M R, Andrade M F and Porto-Neto S T 2009 *Laser Phys.* **1** 1909
[37] Bandeca M C, Pinto S C S, Calixto L R, Saad J R C, Barros E L R D, El-Mowafy O and Porto-Neto S T 2012 *Mater. Res.* **15** 1
[38] Tanoue N, Matsumura H and Atsuta M 1998 *J. Oral Rehab.* **25** 358
[39] Cobb D S, Vargas M A and Rundle T 1996 *Am. J. Dent.* **9** 199
[40] Rueggeberg F A, Caughman W F and Curtis J W Jr 1994 *Oper. Dent.* **19** 26
[41] Willems G, Lambrechts P, Braem M and Vanherle G 1993 *Quint. Int.* **24** 641
[42] Price R B, Felix C A and Andreou P 2005 *Compend. Contin. Educ. Dent.* **25** 336
[43] Vandewalle K S, Ferracane J L, Hilton T J, Erickson R L and Sakaguchi R L 2004 *Dent. Mater. J.* **20** 96
[44] Silva P C G, Porto-Neto S T, Lizarelli R F Z and Bagnato V S 2008 *Laser Phys. Lett.* **5** 220
[45] Valentino T A, Calabrez-Filho S, Menezes F C H, Cavalcante L M A, Pimenta L F A, Andrade M F, Dantas A A R and Rastelli A N S 2011 *Laser Phys.* **21** 1
[46] Koupis N S, Vercruysse C W, Marks L A, Martens L C and Verbeeck R M 2004 *Dent. Mater. J.* **20** 908
[47] Obici A C, Sinhoreti M A, de Goes M F, Consani S and Sobrinho L C 2002 *Oper. Dent.* **27** 192
[48] Soh M S, Yap A U and Siow K S 2003 *Oper. Dent.* **28** 707
[49] Tolosa M C, Paulillo L A, Giannini M, Santos A J and Dias C T 2005 *Braz. Oral Res.* **19** 123
[50] Yearn J A 1985 *Int. Dent. J.* **35** 218
[51] Swartz M L, Phillips R W and Rhodes B 1983 *J. Am. Dent. Assoc.* **106** 634
[52] Bowen R L 1963 *J. Am. Dent. Assoc.* **66** 57
[53] Bowen R L 1964 *J. Am. Dent. Assoc.* **69** 481
[54] Costa S X S, Galvão M R, Jacomassi D P, Bernardi M I B, Hernandez A C, Rastelli A N S and Andrade M F 2011 *J. Thermodyn. Anal. Calorim.* **103** 219
[55] Schulze K A, Zaman A A and Soderholm K J 2003 *J. Dent.* **31** 373
[56] Sabatini C, Campillo M, Hoelz S, Davis E L and Munoz C A 2012 *Oper. Dent.* **37** 41

Evaluation of degree of conversion and hardness of dental composites photo-activated with different light guide tips

Marília Regalado Galvão[1,2]
Sergei Godeiro Fernandes Rabelo Caldas[1]
Vanderlei Salvador Bagnato[3]
Alessandra Nara de Souza Rastelli[1,3]
Marcelo Ferrarezi de Andrade[1]

ABSTRACT

Objective: The aim of this study was to evaluate the degree of conversion and hardness of different composite resins, photo-activated for 40 s with two different light guide tips, fiber optic and polymer.

Methods: Five specimens were made for each group evaluated. The percentage of unreacted carbon double bonds (% C=C) was determined from the ratio of absorbance intensities of aliphatic C=C (peak at 1637 cm-1) against internal standard before and after curing of the specimen: aromatic C-C (peak at 1610 cm-1). The Vickers hardness measurements were performed in a universal testing machine. A 50 gf load was used and the indenter with a dwell time of 30 seconds. The degree of conversion and hardness mean values were analyzed separately by ANOVA and Tukey's test, with a significance level set at 5%.

Results: The mean values of degree of conversion for the polymer and fiber optic light guide tip were statistically different (P<.001). The hardness mean values were statistically different among the light guide tips (P<.001), but also there was difference between top and bottom surfaces (P<.001).

Conclusions: The results showed that the resins photo-activated with the fiber optic light guide tip promoted higher values for degree of conversion and hardness. (Eur J Dent 2013;7:86-93)

Key words: Composite resins; hardness; polymerization

[1] Department of Restorative Dentistry, Araraquara School of Dentistry, Univ. Estadual Paulista-UNESP, Araraquara, SP, BRAZIL
[2] Department of Dentistry, Rio Grande do Norte Federal University-UFRN, Natal, RN, BRAZIL
[3] São Carlos Physics Institute, Optical Group, Biophotonics Lab., University of São Paulo, São Carlos, SP, BRAZIL

Corresponding author: Dr. Marília Regalado Galvão
Department of Restorative Dentistry, Araraquara School of Dentistry, Univ. Estadual Paulista-UNESP. Rua Humaitá, 1740 – ZipCode 14801-385, Araraquara – SP – BRAZIL
Tel: +55 16 33367222
Fax: +55 16 33016395
Email: mariliaregalado@hotmail.com

INTRODUCTION

Light-cured composite resins are widely used in dental restorations, as they are mercury-free and esthetically pleasing to the patient.[1]

The introduction of the visible light system for the photo-activation of composite resins had its beginning in 1970 with the use of ultraviolet light. However, due to the adverse effects caused by this light system, it was substituted quickly by the halogen light system.[2]

Previously, the halogen lamp was the most common light source used for composite photo-

activation. However, heat generation is the major disadvantage of these LCUs (Light Curing Unit).[3-7] Moreover, the bulb, reflector and filter can degrade over time due to high operating temperatures caused by a large quantity of heat, which is produced during cycles.[3]

In recent years, light-emitting diodes (LEDs) have been used to create compact, cordless LCUs.[8] They have a working lifetime of over 10,000 h, can have wavelength peaks of around 470 nm, it is not necessary to use filters and can be portable. In addition, the thermal emission of the LED LCUs is significantly lower than of halogen lamp LCUs. Studies using dental resins irradiated with blue light LEDs have been reported to have a higher degree of polymerization, a more stable three-dimensional structure, and a significantly greater curing depth than those cured with conventional QTH (Quartz tungsten-halogen) lights.[1,2,9,10]

The quality of the polymerization has been one of the most studied since the development of composite resins polymerized by light. Thus, there is the need for light sources that promote an appropriate conversion of monomers in polymers, so that the restoration has appropriate physical, chemical and mechanical properties.[10-16]

The study of some properties can be made by the degree of conversion and hardness tests. Degree of conversion (DC) is an important parameter in determining the final physical, mechanical and biological properties of photo-activated composite resins.[17] The DC is determined by the proportion of the remaining concentration of the aliphatic C=C double bonds in a cured sample relative to the total number of C=C bonds in the uncured material. Fourier Transform Infra-red Spectroscopy (FT-IR) is one of the most widely used techniques for measurement of DC in dental composites.[13,18]

Several factors can influence the DC such as light source used, power density, wavelength, irradiation time, light-tip size, photo-activation method, distribution, quantity of inorganic fillers, the type and quantity of the photoinitiator, and color also strongly affect the DC of the composite resins.[13]

Vickers hardness measurement is one of the most important to compare restorative materials, and is defined as the resistance to indenter penetration or standing on the surface. It is a mechanical property that should always be taken into account, especially when they are faced with large areas of masticatory effort.[19-21]

Technologies have been developed that enable production of the appropriate amount of light required for the efficient conversion of composite resins. Now, light-curing units have used different kinds of conductive systems based on a rigid probe that it contains the fiber optic involved by a glass material covered for glass amber or metal.[2,22-25]

The type of material of the light guide tips can hinder the light passage in its itinerary, increasing her dispersion. A wide variety of commercial light guide tips with variation of the material that covers them, diameters, and shape, with the objective of facilitating the access to the different areas or cavities have been developed.[3,4,9,24] These differences on light guide tips can provide changes in the power density values and then compromising the polymerization of the composite resins.[3]

It has been hypothesized that the material that covers the light guide tips of the light-curing units promote the light dispersion in the itinerary of the light. In this way, the aim this study was evaluated the influence of the light guide tips used in the photo-activation of dental composites by means of degree of conversion and Vickers hardness.

MATERIAL AND METHODS

One blue LED LCU (Ultrablue IS, DMC, São Carlos, SP, Brazil, serial number: 002041) with two different light guide tips, fiber optic and polymeric was used in this study. Prior to the curing procedures, the power output of the LCU was measured with a calibrated power meter (Fieldmaster Power Meter, Coherent-model n° FM, set n° WX65, part n° 33-0506, USA) and the diameter of the light guide tip was measured with a digital caliper (Mitutoyo, Tokyo, Japan). Power density (mW/cm^2) was computed as the ratio of the power output and the area of the tip with the following formula: I = P/A, where P is the power in (mW/cm^2, milliwatts per centimeter square) and A is the area of the light tip in centimeters square.

The LED LCU coupled with the fiber optic light guide tip presented 653 mW/cm^2 and with the polymeric 596 mW/cm^2. The characteristics of the light guide tips are shown in Table 1.

Experiments were performed with two restorative systems: Filtek™ Z 250 (3M Espe Dental Products Division, St. Paul, MN 55144-1000, USA),

a universal microhybrid and Filtek™ Supreme XT (3M Espe Dental Products Division, St. Paul, MN 55144-1000, USA), a nanofilled.

The specimens were made using a metallic mould with a central orifice (4 mm in diameter and 2 mm in thickness) according to ISO 4049.[26] The metallic mould was positioned on a 10 mm thick glass plate. The composite resin was packed in a single increment and the top and base surfaces were covered by a mylar strip. A glass sheet 1 mm thickness was positioned and a mass of 1 kg was used to pack the composite resin. Photo-activation was performed by positioning the light guide tip on the top surface of the composite resin specimens. The specimens were irradiated during 40 s. After photo-activation, the specimens were removed from the mould and stored in a dry mean, in dark containers, at 37° C (±1°C) for 24 hours.

Degree of Conversion Measurements (DC%)

For this technique, five specimens were made for each investigated Group (n=20) and 24 h after photo-activation, the specimens were pulverized into a fine powder. The pulverized composite resin was maintained in a dark room until the moment of the FT-IR analysis. Five milligrams (5 mg) of the ground powder were thoroughly mixed with 100 mg of the KBr powder salt. This mixture was placed into a pelleting device, and then pressed in a press with a load of 10 tons over 1 min to obtain a pellet.

To measure the degree of conversion, the pellet was then placed into a holder attachment into the spectrophotometer Nexus-470 FT-IR (Thermo Nicolet, Vernon Hills, Illinois, USA). The Fourier transform infrared spectroscopy (FT-IR) spectra for both uncured and cured specimens were analyzed using an accessory of the diffuse reflectance. The measurements were recorded in the absorbance operating under the following conditions: 32 scans, a 4 cm^{-1} resolution, and a 300 to 4000 cm^{-1} wavelength. The percentage of unreacted carbon–carbon double bonds (% C=C) was determined from the ratio of the absorbance intensities of aliphatic C=C (peak at 1637 cm^{-1}) against an internal standard before and after the curing of the specimen: aromatic C–C (peak at 1610 cm^{-1}). This experiment was carried out in triplicate. The degree of conversion was determined by subtracting the % C=C from 100%, according to the formula:

The percentage of unreacted carbon-carbon double bonds (% C=C) was determined from the ratio of absorbance intensities of aliphatic C=C (peak at 1637 cm^{-1}) against internal reference aromatic C=C (peak at 1610 cm^{-1}) before and after curing of the specimens.

Vickers Hardness Measurements

For this technique, five specimens for each investigated Group were made (n=20) and then the Vickers hardness was measured on the top and the bottom surfaces of the specimens. The Vickers hardness test was performed in a hardness testing machine, MMT-3 Hardness Tester (Buehler Lake Bluff, Ilinois USA), equipped with Vickers diamond (VHN), which has a pyramidal diamond microindentor of 136° where the two diagonals are measured using a load of 50 gf (gram force) during 30 s. Each surface of the specimen was divided into 4 equal quadrants. On each surface, the top (turned to the light source) and bottom (opposite to the light source) surfaces, one indentation took place for each quadrant. Eight indentations were taken from each specimen (4 to the top and 4 to the bottom). The hardness mean values were calculated for each surface.

The data for degree of conversion and hardness were statistically analyzed by Analysis of Variance (ANOVA) using a confidence interval of 95% and Tukey's test.

RESULTS

Degree of Conversion

The Table 2 shows the degree of conversion (DC%) mean values obtained from different dental composites and different light guide tips. The degree of conversion values varied from 67.99% (±1.00) to 55.63% (±2.27) for nanofilled resin photo-activated by fiber optic and polymer light guide tips, respectively. For microhybrid resin, the de-

Table 1. Characteristics of the light guide tip used in the study.

Light-Curing Unit	Light Guide Tip	Diameter entry	Diameter exit	Geometry
Ultrablue IS	Fiber Optic	11mm	8mm	Turbo
	Polymer	10mm	8mm	Turbo

gree of conversion values varied from 68.37% (±1.02) to 55.71% (±2.54) when fiber optic and polymer light guide tips were used, respectively.

ANOVA showed that the degree of conversion was influenced by light guide tips (P<.001), however differences were not observed for different dental composites. According to the results presented, the fiber optic light guide tip presented higher values for DC% regardless the type of dental composite used.

After 24 hours, using the irradiation time recommended by the manufacturers (20 seconds), DC% of microhybrid resin and nanofilled resin, were not statistically different (P=0.988) when the different light guide tips were used (P=1). Therefore, the results suggested that the light guide tips used had a significant (P<.001) impact on the DC%, whereas the type of resin did not influence DC%.

Hardness

The Tables 3 and 4 shows the VHN mean values (Kgf/mm^2) for the top and bottom surfaces for each Group measured. The ANOVA showed that the hardness values was influenced by light guide tips (P<.001) and was also observed for dental composites (P<.001).

The hardness mean values for the top surface varied from 67.72 (±0.68) to 51.58 (±1.39) for nanofilled resin photo-activated by fiber optic and polymer light guide tips, respectively. For microhybrid resin, the hardness mean values for the top surface varied from 72.01 (±0.71) to 61.72 (±1.34) when fiber optic and polymer light guide tips were used.

As can be seen in Table 5, there was statistical significant differences between top and bottom surfaces (P<.001). The top surface showed the higher mean values than the bottom surface.

The hardness mean values of the specimens photo-activated with fiber optic light guide tip showed highest mean values when compared with the mean values for polymer light guide tip. The differences were statistically significant (P<.001).

Table 2. Mean, Standard Deviation (±SD) and P value for degree of conversion.

Light Guide Tip	Dental Composite	Mean	SD	*	P value
Fiber Optic	Nanofilled Resin	67,99	1,00	a	0,988
	Microhybrid resin	68,37	1,02	a	
Polymer	Nanofilled Resin	55,63	2,27	b	1
	Microhybrid resin	55,71	2,54	b	

* Different letters denote significant difference (P<.001).

Table 3. Hardness mean values, Standard Deviation (±SD) and and P value for the top surfaces of the dental composite resin photo-activated with different light guides tips.

Light Guide Tip	Dental Composite	Mean	SD	*	P value
Fiber Optic	Microhybrid resin	72,01	0,71	a	<.001
	Nanofilled resin	67,72	0,68	b	
Polymer	Microhybrid Resin	61,72	1,34	c	
	Nanofilled resin	51,58	1,39	d	

* Different letters denote significant difference (P<.001).

Table 4. Hardness mean values, Standard Deviation (±SD) and P value for the bottom surfaces of the dental composite resin photo-activated with different light guides tips.

Light Guide Tip	Dental Composite	Mean	SD	*	P value
Fiber Optic	Microhybrid Resin	61,77	0,40	a	<.001
	Nanofilled resin	52,04	1,59	c	
Polymer	Microhybrid Resin	56,03	1,81	b	
	Nanofilled resin	42,51	1,12	d	

* Different letters denote significant difference (P<.001).

Table 5. Hardness mean values for the top and bottom surfaces and corresponding B/T ratio of the dental composite resin photo-activated with different light guides tips.

Light Guide Tip	Dental Composite	Top Surface	Bottom Surface	B/T%
Fiber Optic	Nanofilled Resin	67,72	52,04	82,75
	Microhybrid resin	72,01	61,77	85,75
Polymer	Nanofilled Resin	51,58	42,51	82,41
	Microhybrid resin	61,72	56,03	84,3

DISCUSSION

A lower degree of conversion could affect the longevity of the composite restoration, because an incomplete conversion may result in unreacted monomers, which might dissolve in a wet environment. In addition, reactive sites (double bonds) are susceptible to hydrolization or oxidation and, thereby, lead to a degradation of the material.[27,28]

Then, the degree of conversion is an important tool to determine the final physical, mechanical, and biological properties of composite resins, since it has been showed that composite properties tend to improve as the degree of conversion attained during photo-polymerization is increased.[15] In addition, increased cure may result in a lower amount of uncured, potentially leachable monomer, leading to a more biocompatible restoration.[29] Moreover, uncured functional groups can act as plasticizers, reducing the mechanical properties.[30]

The minimum DC% for a clinically satisfactory restoration has not been precisely established. Nevertheless, a negative correlation of in vivo abrasive wear depth with DC has been found for values in the range of 55-65%. This suggests that, at least for occlusal restorative layers, DC values below 55% may be contraindicated.[3] According to some authors the dimethacrylate monomers used in restorative materials exhibit considerable residual unsaturation in the final material, with a degree of conversion (%) ranging from 55 to 75% under conventional irradiation conditions.[21-33]

In this our experiment, the DC mean values ranged from 67.99 to 68.37 % for fiber optic and 55.63 to 55.71% for polymer light tip, and according to these results presented on Table 3 there was statistical difference in DC (%) mean values between the light guide tips. These findings showing that the two light guide tips were able to light-cure microhybrid as nanofilled composite resins with 2 mm thickness. However, the degree of conversion of composites photo-activated with the fiber optic light guide tip was statistically higher than those observed with polymer light guide tip. This fact can be explained by the material of the tip. Polymer materials provide the dispersion of the light in its itinerary decreasing power density.[3]

In a previous study, Soares et al[3] reported that the type of light guide tip material did not present a statistical significant difference on the final DC (%) of dental composite. However, this result can be explained by the low power density delivered by the light-curing units, which was around 130/140 mW/cm^2. As shown by Galvão et al[24] it was not observed statistical significant difference for degree of conversion of dental composites photo-activated with the different light guide tips. However, this result may be explained by the low quality of the fiber optic light guide tip used.

Factors such as light source, irradiation times, power density, correct wavelength of the light source, light-tip size, distribution, light guide tip and material's composition can influence the degree of conversion (%) and, then, the final characteristics of the dental composite resin.[13] All these factors strongly influence the degree of conversion (%), which is a number of ethylene double carbon bonds that are converted into single bonds of the composite resin obtaining optimal chemical-physical and clinical performance. Therefore, it plays an important role in determining the ultimate success of the restoration.[34-36]

Hardness evaluation is a widely used test to examine composite curing and, as a consequence, the efficiency of the light source.[37] It is applied especially to restorative materials that are used where high bite forces and stresses can exacerbate inherent material defects, resulting in inadequate fracture resistance of the materials.[38,39]

According to some authors,[40] there is still no consensus for the Vickers hardness be considered optimal. Some authors believe that for composite resins, a hardness values can exceeding 50 (VHN) to be considered ideal.[41] In this investigation, nanofilled and microhybrid dental composite resins photo-activated with the fiber optic light tip showed hardness mean values at the top surface above 50 VHN. At the bottom surface, only one Group did not reach 50 VHN when polymer tip was used.

Johnston et al[42] believe that the curing efficiency could be measured by the ratio between bottom and top surface hardness (B/T), which should be 90%, however according to some authors,[43,44] the bottom surface of the specimens can be at least 80% of the hardness of top surface, which is consistent with our findings which showed a ratio of 82.41% and 85.75% between top and bottom surfaces of the specimens cured with fiber optic and polymer light tips, respectively, as shown in Table 5.

As shown in Table 3 and 4 statistical significant differences among the light guide tips (P<.001) and dental composites (P<.001) were observed. Statistical differences were also found when comparing top and bottom surfaces, for both the light guide tips and for the dental composites. On the top surface, the power density is usually sufficient for adequate polymerization, however, on the bottom surface the light of the light-curing unit frequently disperses, and then the polymerization can be compromised. As a result, when the light passes through the bulk of the composite, its power density is greatly reduced due to the scattering of light by filler particles and the resin matrix.[5,27,45] The results obtained in this study, showed statistical significant differences among the dental composites, demonstrating that the type of resin used can also influence the results of hardness obtained. In this study a microhybrid dental composite showed higher hardness mean values than the nanofilled for both, top and the bottom surfaces.

According to Wu et al[46] the composite resins based on nanotechnology describe research or products where critical component dimensions are in the range of 0.1 to 100 nanomers (nanometric scale), through several physical and chemical methods. In 2003, the first composite resin with these characteristics was introduced in Dentistry. The goal was to use nanotechnology to create a composite that offers the polish retention of a microfill with the strength of a hybrid composite.[47,48] However, in our study it was observed that the nanofilled composite presented hardness values lower than those microhybrid, for the top and bottom surfaces especially photo-activated with the polymer light guide tip of.

This can be primarily explained by the difference in the composition of the resin matrix, filler size, filler volume, and filler type of the materials. Although the organic phase of composite resins evaluated in this study are similar, there are differences in the inorganic phase (size, shape, and volume filler content). The filler volume% of the microhybrid composite and nanofilled composite are also similar around of 60%, however the microhybrid filler size has an average medium size of 0.6µm and nanofilled nanoparticles of 20nm size fillers.[17,49] This statement may explain the results found in this study.

In this study, it was observed that there were difference in the degree of conversion and hardness of composite resins photo-activated with fiber optic and polymer light tips, showing that the materials of the light guide tips used may have direct impact on the power density, which would have great influence on the physical, chemical and mechanical and properties of composite resins.

CONCLUSIONS

The results obtained in this study indicated that the light guide tips used in the photo-activation (fiber optic and polymer) promoted differences in the degree and conversion, regardless of the type of dental composite. The fiber optic light guide tip provided higher degree of conversion. However, hardness was influenced by light guide tip, but also by the type of dental composite. The microhybrid dental composite photo-activated by fiber optic light guide tip provided the highest values for hardness, either top and bottom surfaces.

REFERENCES

1. Felix CA, Price RB. The effect of distance from light source on light intensity from curing lights. *J Adhes Dent* 2003;5:283-291.
2. Calixto LR, Lima DM, Queiroz RS, Rastelli ANS, Bagnato VS, Andrade MF. Curing depth of composite resin light cured by LED and halogen light-curing units. *Las Phys* 2008;18:1365-1369.
3. Soares LE, Liporoni PC, Martin AA. The effect of soft-start polymerization by second generation LEDs on the degree of conversion of resin composite. *Oper Dent* 2007;32:160-165.
4. Nitta K. Effect of light guide tip diameter of LED-light curing unit on polymerization of light-cured composites. *Dent Mater* 2005;2:217-223.
5. Yoon TH, Lee YK, Lim BS, Kim CW. Degree of polymerization of resin composites by different light sources. *J Oral Rehabil* 2002;29:1165-1173.
6. Fujibayashi K, Ishimaru K, Takahashi N, Kohno A. Newly developed curing unit using blue light-emitting diodes. *Dent Japan* 1998;34:49-53.
7. Tarle Z, Meniga A, Knezevic A, Sutalo J, Ristic M, Pichler G. Composite conversion and temperature rise using a conventional, plasma arc, and an experimental blue LED curing unit. *J Oral Rehabil* 2002;29:662-667.

8. Price RBT, Fahey J, Felix CM. Knoop Microhardness Mapping Used to Compare the Efficacy of LED, QTH and PAC Curing Lights. *Oper Dent* 2010;35:58-68.
9. Corciolani G, Vichi A, Davidson CL, Ferrari M. The influence of tip geometry and distance on light-curing efficacy. *Oper Dent* 2008;33:325-331.
10. Stahl F, Ashworth SH, Jandt KD, Mills RW. Light-emitting diode (LED) polymerization of dental composites: flexural properties and polymerization potential. *Biomater* 2002;1:379-1385.
11. Roberts HW, Vandewalle KS, Berzins DW, Charlton DG. Accuracy of LED and halogen radiometers using different light sources. *J Esthet Restor Dent* 2006;18:214-222.
12. Jandt KD, Mills RW, Blackwell GB, Ashworth SH. Depth of cure and compressive strength of dental composites cured with blue light emitting diodes (LEDs). *Dent Mater* 2001;6:41-47.
13. Rastelli ANS, Jacomassi DP, Bagnato VS. Degree of conversion and temperature increase of a composite resin light-cured with argon laser and blue LED. *Las Phys* 2008;18:1570-1575.
14. Rode KM, Kawano Y, Turbino ML. Evaluation of curing light distance on resin composite microhardness and polymerization. *Oper Dent* 2007;32:571-578.
15. Lovell LG, Lu H, Elliott JE, Stansbury JW, Bowman CN. The effect of cure rate on the mechanical properties of dental resins. *Dent Mater* 2001;17:504-511.
16. Ak AT, Alpoz AR, Bayraktar O, Ertugrul F. Monomer Release from Resin Based Dental Materials Cured With LED and Halogen Lights. *Eur J Dent* 2010;4:34-40.
17. Costa SXS, Galvão MR, Jacomass DP, Bernardi MIB, Hernandes AC, Rastelli ANS, Andrade MF. Continuous and gradual photo-activation methods: influence on degree of conversion and crosslink density of composite resins. *J Ther Anal Calorim* 2011; 103:219-227.
18. Moraes LG, Rocha RS, Menegazzo LM, De Araujo EB, Yukimito K, Moraes JC. Infrared spectroscopy: a tool for determination of the degree of conversion in dental composites. *J Appl Oral Sci* 2008;16:145-149.
19. Vandewalle KS, Ferracane JL, Hilton TJ, Erickson RL, Sakaguchi RL. Effect of energy density on properties and marginal integrity of posterior resin composite restorations. *Dent Mater* 2004;20:96-106.
20. Alpöz AR, Ertuğrul F, Coguluc D, Akc AT, Tanoğlud M, Kayae E. Effects of Light Curing Method and Exposure Time on Mechanical Properties of Resin Based Dental Materials. *Eur J Dent* 2008;2:37-42
21. Kurachi C, Tuboy AM, Magalhaes DV, Bagnato VS. Hardness evaluation of a dental composite polymerized with experimental LED-based devices. *Dent Mater* 2001;17:309-315.
22. Rode K.M, Kawano Y, Turbino ML. Evaluation of Curing Light Distance on Resin Composite Microhardness and Polymerization. *Oper Dent* 2007;32:571-578.
23. Hammesfahr PD, O'Connor MT, Wang X. Compend. Light-curing technology: past, present, and future. *Compend Contin Educ Dent* 2002;23:18-24.
24. Galvão MR, Costa SXS, Victorino KR, Ribeiro AA, Menezes FCH, Rastelli ANS, Bagnato VS, Andrade MF. Influence of light guide tip used in the photo-activation on degree of conversion and hardness of one nanofilled dental composite. *Las Phys* 2010;20:1-6.
25. Burgess JO, Walker RS, Porche CJ, Rappold AJ. Light curing--an update. *Compend Contin Educ Dent* 2002;23:889-892.
26. International Standard Organization-British Standard. Dentistry-Polymer-based filling, restorative and luting materials BS EN International Standard Organization 4049:2000. Dentistry-Polymer-based filling, restorative and luting materials. 2000, Geneva, Switzerland.
27. Yap AU, Wong NY, Siow KS. Composite cure and shrinkage associated with high intensity curing light. *Oper Dent* 2003;28:357-364.
28. Øysæd H, Ruyter IE, Sjøvik, Kleven IJ. Release of formaldehyde from dental composites. *J Dent Res* 1988;67:1289–1294.
29. Yap AU, Soh MS, Han TT, Siow KS. Influence of curing lights and modes on cross-link density of dental composites. *Oper Dent* 2004;29:410-415.
30. Asmussen E, Peutzfeldt A. Influence of pulse-delay curing on softening of polymer structures. *J Dent Res* 2001;80:1570-1573.
31. Ferracane JL, Greener EH. The effect of resin formulation on the degree of conversion and mechanical properties of dental restorative resins. *J Biomed Mater Res* 1986;20:121-131.
32. Ruyter IE, Oysaed I. Conversion in different depths of ultraviolet and visible light activated composite materials. *Acta Odont Scand* 1982;40:179-192.
33. Silikas N, Eliades G, Watts DC. Light intensity effects on resin-composite degree of conversion and shrinkage strain. *Dent Mater* 2001;6:292-296.
34. Ferracane JL. Correlation between hardness and degree of conversion during setting reaction of unfilled dental restorative resins. *Dent Mater* 1985;1:11-14.
35. Witzel MF, Calheiros FC, Goncalves F, Kawano Y, Braga RR. Influence of photoactivation method on conversion, mechanical properties, degradation in ethanol and contraction stress of resin-based materials. *J Dent* 2005;33:773-779.

36. Cekic-Nagas Isil, Egilmez F, Ergun G. The Effect of Irradiation Distance on Microhardness of Resin Composites Cured with Different Light Curing Units. *Eur J Dent* 2010;4:440-446.
37. Mousavinasab SM, Meyers I. Comparison of Depth of Cure, Hardness and Heat Generation of LED and High Intensity QTH Light Sources. *Eur J Dent* 2011;5:299-304.
38. Sobrinho LC, Goes MF, Consani S, Sinhoreti MA, Knowles JC. Correlation between light intensity and exposure time on the hardness of composite resin. *J Mater Scien: Mater Medec* 2000;11:361-364.
39. Mills RW, Uhl A, Blackwell GB, Klaus D. Jandt. High power light emitting diode (LED) arrays versus halogen light polymerization of oral biomaterials: Barcol hardness, compressive strength and radiometric properties. *Biomater* 2002;23:2955-2963.
40. Craig RG, Powers JM. Restorative Dental Materials. St. Louis: Ed. Mosby, 2002.
41. Sharkey S, Ray N, Burke F, Ziada H, Hannigan A. Surface hardness of light-activated resin composites cured by two different visible-light sources: an in vitro study. *Quintessence Int* 2001;32:401-405.
42. Johnston WM, Leung RL, Fan PL. A mathematical model for post-irradiation hardening of photoactivated composite resins. *Dent Mater* 1985;1:191-194.
43. Polydorou O, Manolakis A, Hellwig E, Hahn P. Evaluation of the curing depth of two translucent composite materials using a halogen and two LED curing units. *Clin Oral Invest* 2008;12:45-51.
44. Watts DC, Amer O, Combe EC. Characteristics of visible-light-activated composite systems. *Br Dent J* 1984;156:209-215.
45. Sobrinho LC, De Lima AA, Consani S, Sinhoreti MA, Knowles JC. Influence of curing tip distance on composite Knoop hardness values. *Braz Dent J* 2000;11:11-17.
46. Wu D, Holmes BN, Mitra SB, Kolb BU, Thompson W, Johnson NJ. Wear resistance and mechanical properties of novel dental nanocomposites. *J Dent Res* 2002;81:p A-37.
47. Debastiani FS, Lopes GC. Direct posterior composite resins restoration. *Intern Journal Braz Dent* 2005;1:31-39.
48. Mitra SB, Wu D, Holmes BN. An application of nanotechnology in advanced dental materials. *J Am Dent Assoc* 2003;134:1382-1390.
49. Bala O, Ölmez A, Kalayci S. Effect of LED and halogen light curing on polymerization of resin-based composites. *J Oral Rehabil* 2005;32:134–140.

Lasers Med Sci (2013) 28:367–374
DOI 10.1007/s10103-012-1057-8

ORIGINAL ARTICLE

Biostimulatory effect of low-level laser therapy on keratinocytes in vitro

Fernanda G. Basso · Camila F. Oliveira · Cristina Kurachi · Josimeri Hebling · Carlos A. de Souza Costa

Received: 5 September 2011 / Accepted: 18 January 2012 / Published online: 8 February 2012

Abstract Epithelial cells play an important role in reparative events. Therefore, therapies that can stimulate the proliferation and metabolism of these cells could accelerate the healing process. To evaluate the effects of low-level laser therapy (LLLT), human keratinocytes were irradiated with an InGaAsP diode laser prototype (LASERTable; 780±3 nm; 40 mW) using 0.5, 1.5, 3, 5, and 7 J/cm^2 energy doses. Irradiations were done every 24 h totaling three applications. Evaluation of cell metabolism (MTT assay) showed that LLLT with all energy doses promoted an increase of cell metabolism, being more effective for 0.5, 1.5, and 3 J/cm^2. The highest cell counts (Trypan blue assay) were observed with 0.5, 3, and 5 J/cm^2. No statistically significant difference for total protein (TP) production was observed and cell morphology analysis by scanning electron microscopy revealed that LLLT did not promote morphological alterations on the keratinocytes. Real-time polymerase chain reaction (qPCR) revealed that LLLT also promoted an increase of type I collagen (Col-I) and vascular endothelial growth factor (VEGF) gene expression, especially for 1.5 J/cm^2, but no change on fibroblast growth factor-2 (FGF-2) expression was observed. LLLT at energy doses ranging from 0.5 to 3 J/cm^2 promoted the most significant biostimulatory effects on cultured keratinocytes.

Keywords Epithelial cells · Low-level laser therapy · Gene expression

F. G. Basso
Piracicaba School of Dentistry,
UNICAMP – University of Campinas,
Piracicaba, SP 13414-903, Brazil

C. F. Oliveira · J. Hebling · C. A. d. S. Costa
Araraquara School of Dentistry, UNESP – Univ. Estadual Paulista,
Araraquara, SP 14801-903, Brazil

C. Kurachi
Physics Institute of São Carlos, USP – University of São Paulo,
São Carlos, SP 13560-970, Brazil

C. A. d. S. Costa (✉)
Departamento de Fisiologia and Patologia, Faculdade de Odontologia de Araraquara, Universidade Estadual Paulista,
Rua Humaitá, 1680. Centro, Caixa Postal: 331 Cep,
14801903 Araraquara, SP, Brazil
e-mail: casouzac@foar.unesp.br

Introduction

Low-level laser therapy (LLLT) has been used in the treatment of several oral diseases with the main goal of stimulating tissue healing capacity, such as in cases of oral mucositis, oral graft-versus-host disease (GVHD), and, more recently, bisphosphonate-induced osteonecrosis [1–4]. This effect seems to be attributed to an increase in cell proliferation and metabolism and as well in the expression of several genes, e.g., the vascular endothelial growth factor (VEGF), which are intimately involved in healing processes [2, 5–9].

The biomodulatory effects of LLLT have been demonstrated in vitro in studies using different cell types such as fibroblasts, keratinocytes, osteoblasts, and odontoblasts [5–9]. However, the cell mechanisms of LLLT have not yet been fully elucidated and neither has the interaction of laser irradiation with different cell types present in the target tissue [5–13]. In vivo studies have also shown that LLLT has positive effects like reduction of painful symptoms, attenuation of inflammatory process, and acceleration of tissue healing in several oral conditions [1–4].

Previous studies have demonstrated that the application of LLLT on fibroblast and epithelial cell cultures promoted an increase in cell proliferation with a significant stimulus of type I collagen (Col-1) gene expression [6, 14–18]. Likewise, the

application of LLLT on osteoblast culture has been shown to increase the proliferation of these cells and the expression of genes involved in calcification, such as osteoglycin [18–22].

The reparative process is complex and involves different tissues. Epithelial cells play an important role in reparative events as they are responsible for recovering the injured areas and stimulating subjacent tissues, such as connective and endothelial tissues, by the expression of growth factors [23–25]. In addition, the epithelium is the first tissue to be irradiated during the treatment of oral lesions with LLLT. Therefore, therapies that can biostimulate and increase the proliferation of epithelial cells could have a beneficial effect on the healing of injured tissues. The aim of this study was to investigate the effect of LLLT on keratinocytes by evaluating their proliferation, respiratory metabolism, protein production, and morphology after irradiation with a diode laser.

Material and methods

Keratinocytes culture

All experiments were performed using human keratinocyte (HaCaT – CLS 300493) culture. The cells were cultured in Dulbecco's modified Eagle's medium (DMEM; Sigma-Aldrich, St. Louis, MO, USA) supplemented with 10% fetal bovine serum (FBS; Gibco, Grand Island, NY, USA), with 100 IU/ml penicillin, 100 μg/ml streptomycin and 2 mmol/l glutamine (Gibco) in an humidified incubator with 5% CO_2 and 95% air at 37°C (Isotemp; Fisher Scientific, Pittsburgh, PA, USA). The cells were sub-cultured every 2 days in the incubator under the conditions described above until an adequate number of cells were obtained for the study. Then the cells (3×10^4 cells/cm^2) were seeded on sterile 24-well acrylic plates using plain DMEM supplemented with 10% FBS for 48 h.

LLLT on keratinocyte culture

The LLLT device used in this study was a near-infrared indium gallium arsenide phosphide (InGaAsP) diode laser prototype (LASERTable; 780±3 nm wavelength, 0.1 W maximum power output; developed by the Optics Group of the Optics and Photonics Research Center at the Physics Institute of São Carlos, University of São Paulo, Brazil), which was specifically designed to provide a uniform irradiation of each well (2 cm^2) in which cultured cells are seeded [11–13]. The radiation originated from the LASERTable was delivered on the base of each 24-well plate at laser doses of 0.5, 1.5, 3, 5, and 7 J/cm^2, and irradiation times of 40, 120, 240, 400, and 560 s, respectively. The laser light reached the cells on the bottom of each well with a final power of 0.04 W because of the loss of optical power in each well due to the interposition of the acrylic plate. The optical power reaching the bottom of the culture wells was calculated using a potentiometer (Coherent LM-2 VIS High-Sensitivity Optical Sensor; USA), which was placed inside the culture plate, and the power of all diodes was checked and standardized, such as performed in previous investigations [12, 13].

The epithelial cells were irradiated every 24 h totaling three applications during three consecutive days. Twenty-four hours after the last irradiation, the effects of LLLT on the cell culture were investigated by evaluating cell metabolism (MTT assay), total protein production, cell proliferation (Trypan blue assay), and cell morphology (scanning electron microscopy). In addition, fibroblast growth factor-2 (FGF-2), VEGF and Col-1 gene expression was analyzed by real-time PCR.

The cells assigned to the control groups received the same treatment as that of the experimental groups. The 24-well plates containing the control cells were maintained at the LASERTable for the same irradiation times used in the respective irradiated groups, though without activating the laser source (sham irradiation).

Analysis of cell metabolism (MTT assay)

Cell metabolism was evaluated using the methyl tetrazolium (MTT) assay [26]. This method determines the activity of succinic dehydrogenase (SDH) enzyme, which is a measure of cellular (mitochondrial) respiration, and can be considered as the metabolic rate of cells.

Each well with the keratinocytes received 900 μl of DMEM plus 100 μl of MTT solution (5 mg/ml sterile PBS). The cells were incubated at 37°C for 4 h. Thereafter, the culture medium (DMEM; Sigma Chemical Co., St. Louis, MO, USA) with the MTT solution was aspirated and replaced by 700 μl of acidified isopropanol solution (0.04 N HCl) in each well to dissolve the violet formazan crystals resulting from the cleavage of the MTT salt ring by the SDH enzyme present in the mitochondria of viable cells, producing a homogenous bluish solution. Three 100-μl aliquots of each well were transferred to a 96-well plate (Costar Corp., Cambridge, MA, USA). Cell metabolism was evaluated by spectrophotometry as being proportional to the absorbance measured at 570-nm wavelength with an ELISA plate reader (Thermo Plate, Nanshan District, Shenzhen, China). The values obtained from the three aliquots were averaged to provide a single value. The absorbance was expressed in numerical values, which were subjected to statistical analysis to determine the effect of LLLT on the mitochondrial activity of the cells.

Total protein production

Total protein production was evaluated according to the Read & Northcote [27] protocol. The culture medium was aspirated and the cells were washed three times with 1 ml of PBS at 37°C. An amount of 1 ml of 0.1% sodium laurel

sulfate (Sigma-Aldrich) was added to each well and maintained for 40 min at room temperature to produce cell lysis. The samples were homogenized and 1 ml from each well was transferred to properly labeled Falcon tubes (Corning Incorporated, Corning, NY, USA). One milliliter of distilled water was added to the blank tube. Next, 1 ml of Lowry reagent solution (Sigma-Aldrich) was added to all tubes, which were agitated for 10 s in a tube agitator (Phoenix AP 56, Araraquara, SP, Brazil). After 20 min at room temperature, 500 μl of Folin-Ciocalteau's phenol reagent solution (Sigma-Aldrich) were added to each tube followed by 10-s agitation. Thirty minutes later, three 100-μl aliquots of each tube were transferred to a 96-well plate and the absorbance of the test and blank tubes was measured at 655-nm wavelength with the ELISA plate reader (Thermo Plate, Nanshan District, Shenzhen, China). Total protein production was calculated from a standard curve created using known protein concentrations.

Cell counting (Trypan blue assay)

Trypan blue assay was used to evaluate the number of cells in the culture after LLLT. This test was selected because it provides a direct and simple assessment of the total number of viable cells in the samples as the Trypan blue dye does not pass through the membranes of intact cells and can penetrate only porous, permeable membranes of lethally damaged (dead) cells, which is clearly detectable under optical microscopy [28].

Cell counting was evaluated in all experimental and control groups 24 h after the last irradiation. According to the protocol, the DMEM in contact with the cells was aspirated and replaced by 0.12% trypsin (Invitrogen, Carlsbad, CA, USA), which remained in contact with the cells for 10 min to promote their desegregation from the substrate. Then, 50-μl aliquots of this cell suspension were added to 50 μl of 0.04% Trypan blue dye (Sigma-Aldrich), and the resulting solution was maintained at room temperature for 2 min so that the Trypan blue dye could pass through the cytoplasmic membrane of the non-viable cells, changing their color into blue. Ten microliters of the solution was taken to a hemocytometer and examined with an inverted light microscope (Nikon Eclipse TS 100, Nikon Corporation, Tokyo, Japan) to determine the number of total cells and non-viable cells. The number of viable cells was calculated by deducting the number of non-viable cells from the number of total cells. The number of cells obtained in the counting corresponded to $n \times 10^4$ cells per milliliter of suspension.

Analysis of cell morphology by scanning electron microscopy (SEM)

Twenty-four hours after the last irradiation, sterile 12-mm-diameter cover glasses (Fisher Scientific, Pittsburgh, PA, USA) were placed on the bottom of the wells immediately before seeding the cells. The culture medium was aspirated and the viable cells that remained adhered to the glass substrate were fixed in 1 ml of 2.5% glutaraldehyde in PBS for 1 h. Then, the glutaraldehyde was removed and the cells were washed with PBS and post-fixed with 1% osmium tetroxide for 1 h at room temperature. The cells that adhered to the glass substrate were washed with PBS and distilled water two consecutive times (5 min each) and then dehydrated in a series of increasing ethanol concentrations (30, 50, and 70%, one time for 30 min each; 95 and 100%, two times for 60 min each) and covered three times with 200 μl of 1,1,1,3,3,3-hexamethyldisilazane (HMDS; Sigma-Aldrich). The cover glasses were then mounted on metallic stubs, stored in a desiccator for 24 h, sputter-coated with gold, and the morphology of the surface-adhered cells was examined with a scanning electron microscope (JMS-T33A scanning microscope, JEOL, Tokyo, Japan). For this morphological analysis, a positive control group was included using a 0.029% hydrogen peroxide solution, which was maintained for 48 h in contact to the cultured HaCaT cells.

Analysis of VEGF, Col-1, and FGF-2 expression

RNA extraction and cDNA synthesis

The effect of LLLT on VEGF, Col-1, and FGF-2 expression was evaluated 24 h after the last irradiation by two-step real-time polymerase chain reaction (qPCR), which is a sensitive and fast method to evaluate gene expression. In contrast to conventional PCR, this technique needs less standardization, less samples, and do not request any contaminant reagents. Another advantage of this method is the fact that the amplification can be observed at any cycle, and there is no need of post-processing of samples.

For this test, 1 ml of TRIzol (Invitrogen, Carlsbad, CA, USA) was added to the cells to inhibit the action of RNAases and was incubated for 5 min at room temperature. Next, 0.2 ml of chloroform was added for each 1.0 ml of TRIzol (Sigma-Aldrich) to promote the release of the cytoplasmic proteins. The tubes were agitated manually for 15 s, left undisturbed at room temperature for 2–3 min, and centrifuged at 1,200 rcf (microcentrifuge, Eppendorf model 5415R, Hamburg, Germany) for 15 min at 4°C. After centrifugation, the samples presented three phases: a precipitated phase, corresponding to the organic portion (phenol, chloroform, DNA), an intermediate phase (proteins) and a more aqueous supernatant phase, corresponding to RNA (RNA and buffer).

An aliquot of the aqueous phase was transferred to a new tube, in which 0.5 ml of isopropanol (Sigma-Aldrich) was added for each 1.0 ml of TRIzol to promote precipitation of RNA from the aqueous solution. The samples were

Table 1 Sequences of primers and probes used for analysis of gene expression of the irradiated cells

Gene	Sequences
VEGF	*Forward – 5′ GCACCCATGGCAGAAGG 3′*
	Reverse – 5′ CTCGATTGGATGGCAGTAGCT 3′
	Probe – 5′ ACGAAGTGGTGAAGTTCATGGATGTCTATCA 3′
Col-1	*Forward -5′ CAGCCGCTTCACCTACAGC 3′*
	Reverse – 5′ TTTTGTATTCAATCACTGTCTTGCC 3′
	Probe - 5′ CCGGTGTGACTCGTGCAGCCATC 3′
FGF-2	*Forward – 5′ ACCCCGACGGCCGA 3′*
	Reverse – 5′ TCTTCTGCTTGAAGTTGTAGCTTGA 3′
	Probe -5′ TCCGGGAGAAGAGCGACCCTCAC 3′
RPL13	*Forward – 5′ CCGCTCTGGACCGTCTCAA 3′*
	Reverse – 5′ CCTGGTACTTCCAGCCAACCT 3′
	Probe -5′ TGACGGCATCCCACCGCCCT 3′

maintained at room temperature for 10 min and then centrifuged at 12,000 rcf for 10 min at 4°C. After this stage, formation of a precipitated fraction (pellet) was observed at the bottom of the tube. The supernatant fraction was discarded and 1.0 ml of 75% ethanol (Sigma-Aldrich) was added for each 1.0 ml of TRIzol and the samples were agitated and centrifuged at 7,500 rcf for 5 min at 4°C. The supernatant fraction was discarded and the RNA was subjected to a drying procedure for 30 min. The RNA was then resuspended in 10 μl of ultrapure water (Invitrogen, Carlsbad, CA, USA) and the resulting solution was incubated at 55°C for 10 min. Part of the obtained RNA (1.0 ml) was diluted in ultrapure water at 1:49 for quantification of RNA in an Eppendorf biophotometer (model Eppendorf RS – 232 C, Hamburg, Germany).

cDNA was synthesized from each RNA sample for qPCR using the High Capacity cDNA Reverse Transcription Kit (Applied Biosystems, Foster City, CA, USA), according to the following protocol. In a microcentrifuge tube were added 10×RT Buffer, 10X RT Random Primers, 25X dNTP Mix, reverse transcriptase and 0.5 μg of the RNA of each sample. The amplification cycling conditions used were 25° C (10 min), 37° (120 min), 85°C (5 s), and 4°C thereafter.

qPCR

After synthesis of cDNA, the expression of the genes that encode for VEGF, Col-1, and FGF-2 was evaluated by qPCR. For each gene, specific primers were synthesized from the mRNA sequence (Table 1).

The reactions were prepared with standard reagents for real-time PCR, TaqMan Universal PCR Master Mix (Applied Biosystems) together with the primer/probe sets specific for each gene (Table 1). The fluorescence readings were performed using the Step One Plus System (Applied Biosystems) at each amplification cycle, and were analyzed subsequently using the Step One Software 2.1 (Applied Biosystems). All reactions were subjected to the same analytical conditions and were normalized by the ROX™ passive reference dye to correct fluctuations on reading resulting from variations of volume and evaporation during the reaction. The result, expressed in CT values, refers to the number of PCR cycles necessary for the fluorescent signal to reach the detection threshold. The individual results expressed in CT values were recorded in worksheets, grouped according to the irradiated groups, and normalized according to the expression of the selected endogenous

Table 2 Production of SDH enzyme, total protein, and number of HaCaT cells ($\times 10^4$) after LLLT with different energy doses (J/cm^2)

Energy dose (J/cm^2)	Cell metabolism (n=12)		Total protein (n=9)		N cells x 10^4 (n=8)	
0.5	1.50 (0.11)*	ab	8.18 (6.84–9.32)**	ab	113 (111–119)**	a
1.5	1.54 (0.06)	a	6.89 (6.60–7.06)	b	95 (88–99)	b
3	1.49 (0.18)	ab	9.56 (7.56–10.29)	a	109 (106–113)	a
5	1.38 (0.08)	bc	7.85 (7.78–8.06)	a	115 (103–125)	a
7	1.44 (0.10)	abc	8.82 (7.30–9.27)	a	67 (62–77)	c
0	1.34 (0.10)	c	7.85 (7.14–9.44)	a	38 (29–53)	d

*Values for cell metabolism are means (standard deviation); **Values for total protein production and cell proliferation are medians (percentile 25–percentile 75). Values followed by the same letters in columns do not differ significantly (Tukey's and Mann–Whitney test, $p>0.05$).

reference gene (RPL13). The RNAm concentrations of each target gene were then analyzed statistically.

Statistical analysis

The cell metabolism data had a normal distribution and were analyzed statistically by one-way ANOVA and Tukey's test for multiple comparisons of groups. On the other hand, data from total protein production, Trypan blue assay, and VEGF, Col-1, and FGF-2 expression had a non-normal distribution and were analyzed statistically by the Kruskal-Wallis and Mann–Whitney nonparametric tests. A significance level of 5% was set for all analyses.

Results

Data from cell metabolism, total protein production, and cell counting according to the energy doses (J/cm^2) used to irradiate the HaCaT cells are presented in Table 2.

Greater metabolic activity compared to the non-irradiated controls was observed when the HaCaT cells were irradiated with energy doses of 0.5, 1.5, and 3 J/cm^2, without statistically significant difference among them. When energy doses of 5 and 7 J/cm^2 were used, cell metabolism was similar to that of the control groups (no irradiation).

Regarding total protein production, irradiation of the HaCaT cells with 1.5 J/cm^2 resulted in statistically lower values ($p<0.05$) than those of the control group, while for all other energy doses experimental and control groups presented statistically similar values ($p>0.05$).

All energy doses caused an increase of cell counts, since the number of viable cells (Trypan blue assay) in the irradiated groups was significantly larger compared to the non-irradiated control groups. Among the doses, the greatest biostimulatory effect was observed when energy doses of 0.5, 3, and 5 J/cm^2 were used, without a statistically significant difference among them.

Regarding cell morphology, none of the energy doses used in the study produced negative morphological alterations or death of the keratinocyte culture (Fig. 1). On the other hand, in the positive control group, in which a 0.029% hydrogen peroxide solution was used, only residual cytoplasmic membrane of death cells was observed on the glass substrate (Fig. 1).

Irradiation of keratinocytes in vitro promoted an increase of VEGF and Col-1 expression (Table 3). For VEGF, this increase was observed with all energy doses, but was more remarkable with 0.5 and 1.5 J/cm^2 doses. For Col-1, the best result was obtained with 1.5 J/cm^2, while irradiation with 7 J/cm^2 decreased the expression of this protein. FGF-2 expression, however, was not altered by the different energy doses used in the present study.

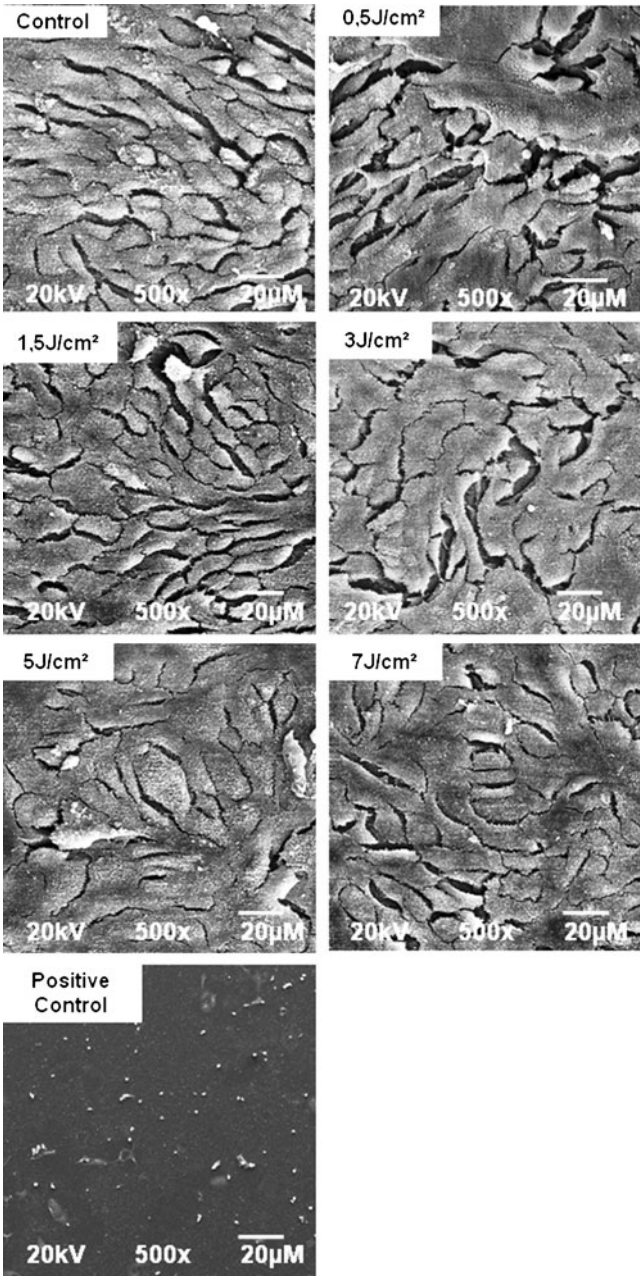

Fig. 1 SEM micrographs showing the morphology of cultured epithelial cells subjected or not to LLLT at different energy doses and treated with hydrogen peroxide (positive control group). Note that in none of the irradiated groups was there variation in the morphology and number of keratinocytes adhered to the glass substrate. All irradiated groups showed cells with no morphological changes when compared to the negative control group. In these images, a number of cells with wide cytoplasm are near to confluence. In the positive control group (0.029% hydrogen peroxide), only fragments of death cells remained attached to the glass substrate. SEM, Original magnification ×500

Discussion

Recent studies have demonstrated that LLLT is capable of promoting proliferation and increasing gene expression and protein production of cells in addition to attenuating

Table 3 Expression of VEGF, Col-1, and FGF-2 by keratinocytes subjected to LLLT using different energy doses (J/cm^2)

Irradiation dose (J/cm^2)	Target genes		
	VEGF	Col-1	FGF-2
0 (control)	1.000 (1.000–1.000) a	1.000 (1.000–1.000) ac	1.000 (1.000–1.000) a
0.5	1.304 (1.211–1.633) bc	1.275 (0.893–1.659) ac	1.204 (1.007–1.388) a
1.5	1.943 (1.468–2.485) b	2.216 (1.890–2.566) b	2.135 (1.429–2.522) a
3	1.238 (0.994–1.662) ab	1.647 (1.406–1.851) ab	1.248 (0.875–1.596) a
5	1.079 (1.031–1.115) ac	1.762 (1.684–1.823) ab	1.017 (0.894–1.181) a
7	1.196 (1.036–1.441) ab	0.826 (0.694–1.113) c	0.780 (0.670–0.973) a

*Values are medians (percentile 25–percentile 75), n=4. For each protein expressed, values followed by the same letters in columns do not differ significantly (Mann–Whitney test, p>0.05).

inflammatory processes and accelerating tissue healing when used in the treatment of oral alterations [2–4]. In the present study, the irradiation of keratinocyte culture (HaCaT) with an InGaAsP diode laser (λ=780) using specific parameters promoted an increase in cell number with all energy doses. Nevertheless, doses of 0.5, 3.0, and 5.0 J/cm^2 were more effective in promoting an increase of the number of viable keratinocytes.

Eduardo et al. [17] evaluated the effect of LLLT (λ= 780 nm) on epithelial cell culture using energy doses of 3 and 5 J/cm^2 delivered by a device with output power of 40 mW and observed an increase of cell metabolism (MTT assay) for both energy doses. These parameters were also used in the present study. The energy dose of 5 J/cm^2 seemed to be more effective in increasing cell metabolism in both investigations. On the other hand, Grossman et al. [29] also obtained positive biostimulation of human epithelial cells after irradiation with 0.5 J/cm^2, particularly when compared to doses of 1 and 1.5 J/cm^2. In the same way as observed in the present study, the doses used by Eduardo et al. [17] and Grossman et al. [29] were effective in causing biostimulation of cells; however, overall, considering all protocols used, doses from 0.5 to 3 J/cm^2 were the most effective in biostimulating cultured human keratinocytes (HaCaT).

The increase in cell metabolism could have resulted from an increase in cell proliferation. To analyze the possible relationship between the cell metabolism and cell proliferation, normalization of the results of SDH activity and total protein production by cell number was carried out, revealing that protein production was indeed correlated with the increase of cell number. However, the same correlation was not observed for SDH activity, as the cells showed an increased metabolic activity even without a significant increase in their number.

The mechanism of LLLT responsible for inducing cell proliferation has been widely evaluated [5–17]. Some authors have demonstrated that action of LLLT on the cells is mediated by the absorption of radiation by the cytochrome c oxidase enzyme, which participates of the oxidative respiration cascade. This enzyme would be responsible for the absorption and transference of energy to other intracellular molecules, activating several biochemical cascades, which, in turn, would have different effects on the cells [30]. This hypothesis is based on the results of studies that revealed an increase in the production of this enzyme after irradiation [30, 31]. Other authors have suggested that the stimulation of cell proliferation by LLLT could be attributed to the activation of signaling pathways, such as the mitogen-activated protein kinase (MAPK) pathway, which is associated with an increase of the receptors involved in these pathways [10, 32]. Corroborating this hypothesis, there are also studies associating the activation of cell proliferation by LLLT with the activation of the PI3K/Akt pathways, which controls several intracellular signaling pathways, such as regulation of gene expression [33].

The positive effect of LLLT on the increase of the proliferation and metabolism of epithelial cells could explain the results of in vivo studies, which have shown an increase in epithelial healing after LLLT using different parameters [1, 2]. It has also been demonstrated that LLLT is capable of acting on the attenuation of inflammatory processes, proliferation of epithelial and connective tissue cells, and tissue remodeling by collagen production; all these effects correspond to events involved in tissue repair [25, 34]. In the present study, despite the increase of the respiratory cell metabolism, no difference was observed in total protein production among the irradiated groups or between them and the control groups. In spite of the lack of statistical significance in total protein production, the evaluation of growth factor and Col-1 gene expression revealed that parameters used in the present study were capable of increasing gene expression in keratinocyte culture. Therefore, the result of total protein production after irradiation could be derived from an early or late evaluation of the cells in vitro, and these proteins could have not been translated up to this moment, or the translated proteins could have exerted their function and had been degraded by post-translational regulation systems [35]. Further research is necessary to evaluate gene and protein expression of these cells when subjected to preset LLLT parameters using other post-irradiation periods.

SEM analysis of irradiated human keratinocytes (HaCaT) revealed that LLLT at different energy doses did not promote significant cellular morphological alterations, demonstrating that none of the irradiation protocols produced deleterious effects to the cells when compared to the control group. The absence of negative effects of LLLT on epithelial cell morphology can be confirmed by comparison of these experimental groups to the positive control group in which a 0.029% hydrogen peroxide solution was used. In this positive control, the HaCaT cells detached from the glass substrate, on which only fragments of death cells were observed.

Several studies have demonstrated that LLLT can stimulate the expression of growth factors and other genes in different cell types [9, 36]. Saygun et al. [36] demonstrated the occurrence of an increase in the expression of basic fibroblast growth factor (bFGF/FGF-2) in fibroblast culture after LLLT at 2 J/cm^2. However, in the present study, the irradiation of keratinocytes did not cause changes in the expression of this growth factor, regardless of the energy dose. This difference in the results could be related to the cell type and/or the wavelength used in each study; while Gaygun et al. [36] irradiated fibroblast culture with a 685-nm diode laser, in the present study, cultured keratinocytes were irradiated with a 780-nm diode laser. In a recent study, Damante et al. [9] observed an increase in bFGF expression in fibroblast culture after irradiation with a LLL (λ=780 nm) at 3 and 5 J/cm^2 energy doses. However, there was no increase in keratinocyte growth factor (KGF) expression in the groups of irradiated cells.

The present study revealed the occurrence of a significant increase in the expression of VEGF and Col-1, which are intimately related to healing events, participating directly in neovascularization and tissue remodeling [24, 37]. Besides the fact that collagen synthesis is a primary function of mesenchymal cells, such as fibroblasts, several studies have demonstrated the importance of the interaction between fibroblasts and epithelial cells during wound healing. According to these authors, the expression of collagen is important on cell migration and adhesion in the wound and can also stimulate the metabolism of cells of connective tissue [24, 38].

These results can also justify the effect of LLLT on repair and healing processes reported in previous in vitro and in vivo studies [1, 2, 39, 40].

Conclusions

Based on the findings of the present study, it could be demonstrated that (1) LLLT at the preset parameters was capable of stimulating the metabolism of human keratinocytes (HaCaT) in culture as well as the expression of some genes and proteins involved in tissue healing process, and (2) considering the irradiation protocols used in this in vitro study, LLLT at energy doses ranging from 0.5 to 3 J/cm^2 were the most effective in promoting biostimulation of the cultured cells.

Acknowledgements The authors acknowledge the Fundação de Amparo à Pesquisa do Estado de São Paulo—FAPESP (grants: 2009/54722-1 and BP.DR: 2009/ 52326–1) and the Conselho Nacional de Desenvolvimento Científico and Tecnológico -CNPq (grant: 301029/2010-1) for the financial support.

References

1. Chor A, de Azevedo AM, Maiolino A, Nucci M (2004) Successful treatment of oral lesions of chronic lichenoid graft-vs.-host disease by the addition of low-level laser therapy to systemic immunosuppression. Eur J Haematol 72:222–224
2. Abramoff MMF, Lopes NNF, Lopes LF, Lauria L, Guilherme A, Caran EM, Barreto AD, Lee MLM, Petrilli AS (2008) Low-level laser therapy in the prevention and treatment of chemotherapy-induced oral mucositis in young patients. Photomed Laser Surg 26:393–400
3. Vescovi P, Merigo E, Manfredi M, Meleti M, Fornaini C, Bonanini M, Rocca JP, Nammour S (2008) Nd:YAG laser biostimulation in the treatment of bisphosphonate-associated osteonecrosis of the jaw: clinical experience in 28 cases. Photomed Laser Surg 26:37–46
4. Bello-Silva MS, de Freitas PM, Aranha AC, Lage-Marques JL, Simões A, de Paula EC (2010) Low- and high-intensity lasers in the treatment of herpes simplex virus 1 infection. Photomed Laser Surg 28:135–139
5. Marques MM, Pereira AN, Fujihara NA, Nogueira FN, Eduardo CP (2004) Effect of low-power laser irradiation on protein synthesis and ultrastructure of human gingival fibroblasts. Lasers Surg Med 34:260–265
6. Khadra M, Lyngstadaas SP, Haanaes HR, Mustafa K (2005) Determining optimal dose of laser therapy for attachment and proliferation of human oral fibroblasts cultured on titanium implant material. J Biomed Mater Res 73A:55–62
7. Moore P, Ridgway TD, Higbee RG, Howard EW, Lucroy MD (2005) Effect of wavelengths on low-intensity laser irradiation-stimulated cell proliferation in vitro. Lasers Surg Med 36:8–12
8. Hawkins DH, Abrahamse H (2006) The role of lasers fluence in cell viability, proliferation, and membrane integrity of wounded human skin fibroblasts following helium-neon lasers irradiation. Lasers Surg Med 38:74–83
9. Damante CA, De Micheli G, Miyagi SPH, Feist IS, Marques MM (2009) Effect of laser phototherapy on the release of fibroblast growth factors by human gingival fibroblasts. Lasers Med Sci 24:885–891
10. Gao X, Xing D (2009) Molecular mechanisms of cell proliferation induced by low-power laser irradiation. J Biom Sci 16:1–16
11. Oliveira CF, Hebling J, Souza PPC, Sacono NT, Lessa FR, Lizarelli RFZ, Costa CAS (2008) Effect of low-level laser irradiation on odontoblast-like cells. Laser Phys Lett 5:680–685
12. Oliveira CF, Basso FG, Lins EC, Kurachi C, Hebling J, de Souza Costa CA (2010) Increased viability of odontoblast like cells subjected to low-level laser irradiation. Laser Phys 20:1659–1666
13. Oliveira CF, Basso FG, Lins EC, Kurachi C, Hebling J, Bagnato VS, de Souza Costa CA (2011) In vitro effect of low-level laser on odontoblast-like cells. Laser Phys Lett 8:155–163

14. Almeida-Lopes L, Rigau J, Zângaro RA, Guidμgli-Neto J, Jaeger MMM (2001) Comparison of the low-level laser therapy effects on cultured human gingival fibroblasts proliferation using different irradiance and same fluence. Lasers Surg Med 29:179–184
15. Kreisler M, Christoffers AB, Al-Haj H, Willershausen B, d'Hoedt B (2002) Low-level 809-nm diode laser-induced in vitro stimulation of the proliferation of human gingival fibroblasts. Lasers Surg Med 30:365–369
16. Azevedo LH, Eduardo FP, Moreira MS, Eduardo CP, Marques MM (2006) Influence of different power densities of LILT on cultured human fibroblast growth. Lasers Med Sci 21:86–89
17. Eduardo FP, Mehnert DU, Monezi TA, Zezell DM, Schubert MM, Eduardo CP, Marques MM (2007) Cultured epithelial cells response to phototherapy with low-intensity laser. Lasers Surg Med 39:365–372
18. Hamajima S, Hiratsuka K, Kiyama-Kishikawa M, Tagawa T, Kawahara M, Ohta M, Sasahara H, Abiko Y (2003) Effect of low-level laser irradiation on osteoglycin gene expression in osteoblasts. Lasers Med Sci 18:78–82
19. Khadra M, Lyngstadaas SP, Haanæs HR, Mustafa K (2005) Effect of laser therapy on attachment, proliferation and differentiation of human osteoblast-like cells cultured on titanium implant material. Biomaterials 26:3503–3509
20. Fujihara NA, Hiraki KRN, Marques MM (2006) Irradiation at 780 nm increases proliferation rate of osteoblasts independently of dexamethasone presence. Lasers Surg Med 38:332–336
21. Haxsen V, Schikora D, Sommer U, Remppis A, Greten J, Kasperk C (2008) Relevance of laser irradiance threshold in the induction of alkaline phosphatase in human osteoblast cultures. Lasers Med Sci 23:381–384
22. Bouvet-Gerbettaz S, Merigo E, Rocca J, Carle JF, Rochet N (2009) Effects of low-level laser therapy on proliferation and differentiation of murine bone marrow cells into osteoblasts and osteoclasts. Lasers Surg Med 41:291–297
23. Bartold PM, Walsh LJ (2000) Narayanan AS (2000) Molecular and cell biology of gingiva. Periodontol 24:28–55
24. Häkkinen L, Uitto V (2000) Larjava H (2000) Cell biology of gingival wound healing. Periodotol 24:127–152
25. Posten W, Wrone DA, Dover JS, Arndt KA, Silapunt S, Alam M (2005) Low-level laser therapy for wound healing: mechanism and efficacy. Dermatol Surg 31:334–340
26. Mosmann T (1983) Rapid colorimetric assay for cellular growth and survival: application to proliferation and cytotoxicity assays. J Immunol Methods 65:55–63
27. Read SM, Northcote DH (1981) Minimization of variation in the response to different proteins of the Coomassie blue G dye-binding assay for protein. Anal Biochem 116:53–64
28. Wiegand C, Hipler U (2008) Methods for the measurement of cell and tissue compatibility including tissue regeneration process. GMS Krankenhaushygiene Interdisziplinär 3:1863–5245
29. Grossman N, Schneid N, Reuveni H, Halevy S, Lubart R (1998) 780-nm low-power diode laser irradiation stimulates proliferation of keratinocyte cultures: involvement of reactive oxygen species. Lasers Surg Med 22:212–218
30. Karu TI, Pyatibrat LV, Kolyakov SF, Afanasyeva NI (2005) Absorption measurements of a cell monolayer relevant to phototherapy: Reduction of cytochrome c oxidase under near IR radiation. J Photochem Photobiol B 81:98–106
31. Eells JT, Henry MM, Summerfelt P, Wong-Riley MT, Buchmann EV, Kane M, Whelan NT, Whelan HT (2003) Therapeutic photobiomodulation for methanol-induced retinal toxicity. Proc Natl Acad Sci USA 100:3439–3444
32. Schefer G, Oron U, Irintchev A, Wernig A, Halevy O (2001) Skeletal muscle cell activation by low-level laser irradiation: a role for the MAPK/ERK pathway. J Cell Physiol 187:73–80
33. Zhang L, Xing D, Gao X, Wu S (2009) Low-power laser irradiation promotes cell proliferation by activating PI3K/Akt pathway. J Cell Physiol 219:553–562
34. Kirsner R (2009) Wound healing. In: Bolognia J, Jorizzo J, Rapini R (eds) Dermatology. Mosby, Bolognia >
35. Khositseth S, Pisitkun T, Slentz DH, Wang G, Hoffert JD, Knepper MA, Yu M (2011) Quantitative protein and mRNA profiling shows selective post-transcriptional control of protein expression by vasopressin in kidney cells. MCP 10:1–21
36. Saygun I, Karacay S, Serdar M, Ural AU, Sencimen M, Kurtis B (2008) Effects of laser irradiation on the release of basic fibroblast growth factor (bFGF), insulin like growth factor-1 (IGF-1), and receptor of IGF-1 (IGFBP3) from gingival fibroblasts. Lasers Med Sci 23:211–215
37. Bates DO, Jones ROP (2003) The roles of vascular endothelial growth factor in wound healing. IJLEW 2:107–120
38. Werner S, Krieg T, Smola H (2007) Keratinocyte-fibroblast interactions in wound healing. J Invest Dermatol 127:998–1008
39. Peplow PV, Chung T, Baxter GD (2010) Laser photobiomodulation of cell proliferations in culture: a review of human and animal studies. Photomed Laser Surg 28:S30–S40
40. AlGhamdi KM, Kumar A, Moussa NA (2011) Low-level laser therapy: a useful technique for enhancing the proliferation of various cultured cells. Lasers Med. Sci. 28[Ahead of print].

cepof.ifsc.usp.br

Grupo de Óptica / CePOF, Instituto de Física de São Carlos, Universidade de São Paulo
Av. Trabalhador Sancarlense, 400, Centro, CP 369, 13560-970, São Carlos - SP
Telefones: (16) 3373-9810; 3373-9823 - Fax: 3373-9811